

CLEARINGHOUSE FOR FEDERAL SCIENTIFIC AND TECHNICAL INFORMATION CFSTI  
DOCUMENT MANAGEMENT BRANCH 410 11

LIMITATIONS IN REPRODUCTION QUALITY

ACCESSION #

AD 601545  
H 64-11778

- ☒ 1. WE REGRET THAT LEGIBILITY OF THIS DOCUMENT IS IN PART UNSATISFACTORY. REPRODUCTION HAS BEEN MADE FROM BEST AVAILABLE COPY.
- ☒ 2. A PORTION OF THE ORIGINAL DOCUMENT CONTAINS FINE DETAIL WHICH MAY MAKE READING OF PHOTOCOPY DIFFICULT.
- ☐ 3. THE ORIGINAL DOCUMENT CONTAINS COLOR, BUT DISTRIBUTION COPIES ARE AVAILABLE IN BLACK-AND-WHITE REPRODUCTION ONLY.
- ☐ 4. THE INITIAL DISTRIBUTION COPIES CONTAIN COLOR WHICH WILL BE SHOWN IN BLACK-AND-WHITE WHEN IT IS NECESSARY TO REPRINT.
- ☐ 5. LIMITED SUPPLY ON HAND: WHEN EXHAUSTED, DOCUMENT WILL BE AVAILABLE IN MICROFICHE ONLY.
- ☐ 6. LIMITED SUPPLY ON HAND: WHEN EXHAUSTED DOCUMENT WILL NOT BE AVAILABLE.
- ☒ 7. DOCUMENT IS AVAILABLE IN MICROFICHE ONLY.
- ☐ 8. DOCUMENT AVAILABLE ON LOAN FROM CFSTI (TT DOCUMENTS ONLY).
- ☐ 9.

NBS 9 64

PROCESSOR:

*Li*

X

293

FTD-TT- 63-209

601545

716 pg. -- \$12.00

# TRANSLATION

AIRCRAFT ELECTRICAL GENERATORS

By

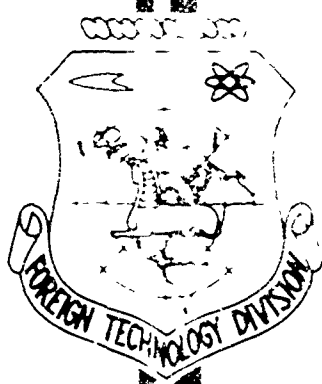
A. I. Bertinov

## FOREIGN TECHNOLOGY DIVISION

AIR FORCE SYSTEMS COMMAND

WRIGHT-PATTERSON AIR FORCE BASE

OHIO





**Best  
Available  
Copy**

# UNEDITED ROUGH DRAFT TRANSLATION

AIRCRAFT ELECTRICAL GENERATORS

BY: A. I. Bertinov

English Pages: 691

THIS TRANSLATION IS A RENDITION OF THE ORIGINAL FOREIGN TEXT WITHOUT ANY ANALYTICAL OR EDITORIAL COMMENT. STATEMENTS OR THEORIES ADVOCATED OR IMPLIED ARE THOSE OF THE SOURCE AND DO NOT NECESSARILY REFLECT THE POSITION OR OPINION OF THE FOREIGN TECHNOLOGY DIVISION.

PREPARED BY:

TRANSLATION DIVISION  
FOREIGN TECHNOLOGY DIVISION  
WP-AFB, OHIO.

FTD-TT- 63-209/1+2

AF-WP-O-MAY 64 83

Date March 20 19

**Aviatsionnyye Elektricheskiye Mashiny**

**A. I. Bertinov**

**AVIATSIONNYYE ELEKTRICHESKIYE GENERATORY**

**Gosudarstvennoye Izdatel'stvo  
Oboronnoy Promyshlennosti  
Moskva 1959  
Pages 1-593**

6-1. 5D-TT-63-209/1+2

## TABLE OF CONTENTS

Preface . . . . .	2
Introduction . . . . .	4
Chapter 1. General Information on Aircraft Electrical Machines . . . . .	11
1.1. Operation Conditions for Aircraft Electrical Machines . . . . .	11
1.2. Basic Requirements for Aircraft Electrical Machines . . . . .	20
1.3. Classification of Aircraft Electrical Machin- ery and Electric-Power Systems . . . . .	22
1.4. Voltage, Frequency, and Number of Phases . .	31
1.5. Losses in Aircraft Electrical Machines . . .	76
1.6. Heating and Cooling of Aircraft Electrical Machines . . . . .	86
Chapter 2. General Information on Aircraft Generators .	133
2.1. Classification of Aircraft Generators . . . .	133
2.2. Technical Specifications and Basic Technical Indices . . . . .	135
2.3. Drives for Direct- and Alternating- Current Aircraft Generators . . . . .	138
2.4. The Problem of Obtaining Constant-Frequency Alternating Current* . . . . .	147
Chapter 3. Alternating-Current Aircraft Generators . .	184
3.1. General Information on Alternating-Current Aircraft Generators . . . . .	184
3.2. Excitation and Selfexcitation of Synchronous Generators . . . . .	196
3.3. Excitation Systems with Stabilization (Com- pounding) . . . . .	213
3.4. Analytical Investigation of Synchronous Gen- erators Allowing for Armature Resistance . .	237
3.5. Characteristics of Aircraft Generators . . .	263
3.6. Single-Phase Synchronous Generators . . . .	285
Chapter 4. Permanent-Magnet Generators . . . . .	305
4.1. General Information on Permanent-Magnet Gen- erators . . . . .	305
4.2. Permanent-Magnet Materials . . . . .	317
4.3. Leakage . . . . .	338
4.4. *Operating Modes of Permanent-Magnet Genera- tors . . . . .	346

This book is a textbook for courses in "Aircraft Electrical Motors and Generators" and "Special Electrical Motors and Generators" given in higher aviation educational institutions, and may prove useful for course or degree projects.

The book discusses general questions of aircraft electrical machinery, the theory of general-purpose and special aircraft generators, analyzes domestic and foreign experience gained in the manufacture of aircraft electrical machinery, and discusses several new circuits.

---

Reviewers: The Department of Aviation and Automotive Equipment of the Moscow Power Institute, Department Chairman, Corresponding Member, Academy of Sciences USSR A.N. Larionov, and Doctor of Technical Sciences Professor M.F. Romanov.

Editor, Candidate of Technical Sciences V.N. Istratov.

Editor-In-Chief, Engineer A.I. Sokolov.

4.5. Design of Permanent-Magnet Generators . . . . .	373
4.6. Voltage Regulation in Permanent-Magnet Generators . . . . .	386
4.7. Elements of the Analytic Theory of Permanent-Magnet Generators* . . . . .	408
Chapter 5. Induction Generators . . . . .	437
5.1. General Information on Induction Generators . . . . .	437
5.2. Fundamentals of Induction-Generator Theory . . . . .	444
5.3. Some Remarks on the Design of Induction Generators . . . . .	458
Chapter 6. Direct-Current Aircraft Generators . . . . .	473
6.1. General Information on Direct-Current Aircraft Generators . . . . .	473
6.2. Armature Reaction . . . . .	502
6.3. Characteristics of Direct-Current Aircraft Generators . . . . .	513
6.4. Direct-Current Commutation . . . . .	536
6.5. The Sliding Contact at High Altitudes . . . . .	560
6.6. Commutating Poles and Compensating Windings . . . . .	569
6.7. Starter-Generators . . . . .	597
Chapter 7. Parallel Operation of Aircraft Generators . . . . .	610
7.1. General Information on Parallel Operation . . . . .	610
7.2. Distribution of Reactance Load . . . . .	614
7.3. Real-Load Distribution . . . . .	624
7.4. Connection for Parallel Operation . . . . .	634
7.5. Parallel Operation of Converters . . . . .	650
7.6. Parallel Operation of Variable-Frequency Generators . . . . .	661
7.7. Parallel Operation of Direct-Current Generators . . . . .	665

This book is a textbook for courses in "Aircraft Electrical Motors and Generators" and "Special Electrical Motors and Generators" given in higher aviation educational institutions, and may prove useful for course or degree projects.

The book discusses general questions of aircraft electrical machinery, the theory of general-purpose and special aircraft generators, analyzes domestic and foreign experience gained in the manufacture of aircraft electrical machinery, and discusses several new circuits.

---

Reviewers: The Department of Aviation and Automotive Equipment of the Moscow Power Institute, Department Chairman, Corresponding Member, Academy of Sciences USSR A.N. Larionov, and Doctor of Technical Sciences Professor M.F. Romanov.

Editor, Candidate of Technical Sciences V.N. Istratov.

Editor-In-Chief, Engineer A.I. Sokolov.

Dedicated to the bright  
memory of my son  
Rolen Bertinov

## PREFACE

The wide application of electric power is one of the most important conditions underlying increased aircraft flight safety and combat efficiency. The degree of electrification of a flying craft is determined in the last analysis by the installed generator capacity, the number of electrified mechanisms, i.e., the number of electric motors, apparatus, instruments, and relays; in this connection, the role and responsibility of aircraft electricians and, in particular, of specialists in aircraft electrical motors and generators has risen considerably.

Aircraft electrical machines have several special features that depend on the conditions under which they are used; thus aircraft electrical machine design presently has the status of an independent field in aircraft electrical engineering.

Quite a number of articles have been published dealing with special topics in the theory and application of aircraft electrical machinery. Certain problems in aircraft electrical machinery are taken up in books on aircraft electrical equipment. Until the present time, however, there has been no book on aircraft electrical machinery and, in particular, a textbook designed specifically for educational institutions that would correspond to the curriculum for a course in "Aircraft Electrical Machinery."

This fact has complicated the author's task, since a considerable number of the topics had to be freshly developed, using as a basis experience gained in this field as well as theoretical and experimental



investigations carried out or participated in by the author.

Lectures given by the author to the students of the Moscow Aviation Institute imeni S. Ordzhonikidze over the 1950-1956 period form the material for the book.

It is assumed that the reader has had the following courses: "Theoretical Fundamentals of Electrical Engineering," "Electrical Motors and Generators," and "Electrical Measurements."

The book consists of two parts. In Part One, we present general information on aircraft electrical machinery and aircraft general-purpose and special generators, while in Part Two we give general information on electrical machinery for aircraft automatic equipment: electric motors, converters, selsyns and amplidynes.

The author wishes to thank the reviewers of this book, Corresponding Member of the Academy of Sciences USSR, Doctor of Technical Sciences Professor A.N. Larionov, Doctor of Technical Sciences Professor G.I. Atabekov, Doctor of Technical Sciences M.F. Romanov, Engineer F.I. Golgofskiy, Candidate of Technical Sciences A.F. Fedoseyev, for making several valuable comments on the manuscript, Engineer A.Ye. Legkova-Bertinova, for the large amount of work done by her in computing the considerable number of graphs and checking many equations, and also Candidate of Technical Sciences V.N. Istratov for undertaking the job of editing the book.

The author requests that all comments and suggestions be sent to: Moscow, I-51, Petrovka, 24, Oborongiz.

## INTRODUCTION

The increased speed, altitude, range, and flight safety of a modern flying craft depends in considerable measure on the level and quality of its electrification. Electrical and radio elements of aircraft equipment provide for reliable brief or extended flights by day or by night at high speeds and altitudes (flight along a radio beam, takeoff and landing in any weather, automatic determination of position, provision of heat during flight, anti-icing measures, etc.).

The special equipment of a flying craft takes the form of a complex set of instruments, apparatus, mechanisms, and machines quite different in operating principle and design.

Such installations and controls may be actuated by muscle power or electrical, hydraulic, pneumatic, mechanical, chemical, or pyrotechnical power sources.

Of all types of energy, electrical energy is the most versatile. It is used to actuate all elements of flying-craft installations and equipment (engine unit, controls, landing gear, devices for communications and illumination, space and spot heating and ventilation, flight and navigation equipment, etc.), while the remaining forms of energy have at best limited special applications.

By using electrical energy, it is possible in practice to automate all operations, increasing their speed, reliability, and accuracy while easing the job of the crew.

The development of aircraft electrical-machinery design is associated with progress in aviation engineering and general electrical-

machine design, and also with the increasing degree of electrification of flying craft..

In 1869, A.N. Lodygin designed a heavier-than-air flying craft with an electric engine, the "Electroplane."

Taking into account the special conditions under which electrical equipment operates on a flying craft, A.N. Lodygin designed a special high-speed electric engine and regulator, and also provided for electrical illumination, thus anticipating the use of household electric lighting (at the end of the Seventies).

P.N. Yablochkov concerned himself with the creation of special storage batteries, which he proposed to use to power electric motors.

During the 1880's, the first vertical takeoff machines appeared; they were powered by surface electric-power sources by means of a cable. The utilization of electric motors was retarded by the lack of economical and small chemical sources of electrical energy.

In 1914, on the eve of the First World War, A.N. Lodygin developed a second design for an electroplane in which the four propellers were rotated by four electric motors. The motors obtained their electric power from a generator driven by a 20-hp internal-combustion motor.

In 1930, V.S. Kulebakin directed the designing of an aircraft driven electrically, while in 1935 A.G. Iosif'yan directed the manufacture of specially designed electric motors to power a vertical-takeoff machine. Owing to unsatisfactory weight characteristics, the electrical drive mechanism had so far not been employed in aviation.

Electrical power was first used on board aircraft for communications and ignition systems, and then for illumination, signaling, heating, and, finally, to furnish electric-drive power and to electrify various installations.

In 1912, the first multiengine bombers were built in Russia, and

the first units consuming electrical power were installed: electrical illumination and heating systems, and a radio installation (on the aircraft "Il'ya Muromets").

In 1912, V.P. Vologdin developed 4000-rpm 1000-cps induction generators of 2 kw capacity for supplying power to the radio equipment of the aircraft "Il'ya Muromets." The generator was belt-driven from the aircraft engine. In addition, V.P. Vologdin developed in 1913 aircraft generators of 500 watts capacity and in 1915 generators delivering 750 watts at a frequency of 1000 cps and a speed of 6000 rpm.

The first aircraft used alternating current at a frequency of 600-1200 cps for the electrical systems, since the basic current-consuming elements of spark-type radio telegraph transmitters required alternating current, while the type of current made no difference as far as illumination and heating were concerned.

The year 1919 saw the conversion of aircraft to the direct-current system with the power furnished by a storage battery and a wind-powered generator delivering 36 watts at 6 v.

Prior to 1929, DC generators delivering no more than 250 watts were in use; the prime movers were wind-driven. It was only in 1934, in connection with the increasing flight speeds, that wind-driven motors were replaced by the main aircraft engine as the prime movers for generators.

Prior to 1936, the 12-v system was used on board aircraft, and maximum generator power was 500 watts. Then owing to the increasing requirements for electric power, generator capacity rose to 1 kw, and the voltage was increased to 24 v. This level was retained up to the beginning of the war in 1939.

As is well known, the first electrical drive units were proposed by A.N. Lodygin for propellers. They received their first practical

application in the starting of aircraft engines.

During the 1925-1926 period, B.A. Talalay succeeded in driving the rotor of a gyroscope by means of a synchronous motor having a speed of 60,000 rpm.

In the period extending from 1926-1929, electrical drive came to be used for boosters, gasoline pumps, oil pumps, in 1930. Retractable landing gear appeared; they were raised and lowered by an electrical-hydraulic drive mechanism (now electrical alone).

Before 1939, aircraft electrical equipment included: generators, storage batteries, ignition system, illumination, heating devices, and monitoring-measurement equipment. Various aircraft employed electrical starters for the aircraft engines, electrical drive mechanisms for landing gear and landing flaps, but the majority of aircraft used pneumatic, hydraulic, or purely mechanical drive systems.

A sudden advance in the development of aircraft electrification came in 1939 with the creation of the Pe-2 dive bomber (V.M. Petlyakov) which for the first time made wide use of electrical mechanisms for landing gear, the stabilizer, landing flaps, and to control radiators, trimmers, supercharger speed, etc.

Before the Second World War, the advantages of the universal application of electric power to basic and auxiliary equipment were not recognized.

Hydraulic or pneumatic systems were preferred for power units; electrical drive units for landing gear and wing flaps were used infrequently on light aircraft. Electrical mechanisms have now replaced hydraulic and pneumatic devices in particular for the reason that damage to any part of an electrical system will in the majority of cases not affect the operation of the entire system, while damage to hydraulic or pneumatic systems will cause a drop in pressure and will

impair operation of the system as a whole.

The Second World War was a turning point in the development of aircraft electrical equipment; at the present time, electrical power is the most important form of energy for aircraft equipment.

In 1932, the installed power of devices consuming electric current on the most highly electrified aircraft amounted to only 5 kw, rising to 30 kw in 1940; it has now reached 100 kw.

The installed capacity of generators on board a four-motor aircraft presently exceeds 100 kw (as against 6 kw in 1940), i.e., there has been a sixteen-fold increase in installed generator capacity over a period of 15 years. There are certain types of aircraft whose installed generator capacity exceeds 250 kw, while current-consuming devices can draw more than 600 kw.

Over the past 15 years, the power of aircraft generators has risen by a factor of 50.

Over 200 electrical machines of 50 different types are installed on a modern four-motor aircraft, including about 30 generators and converters of various powers.

With increasing aircraft size, the relative weight of the electrical equipment and electrical power system has risen. While in a typical two-motor military aircraft (10 tons) the electrical equipment forms 50% of the total weight of all equipment, in a four-motor (32-ton) aircraft, it amounts to 80%, and has an absolute magnitude of 1200 kg. In this case, the relative weight of the electrical power system has risen from 29 to 52% (Table V. 1).

The electrical systems of modern heavy aircraft weigh in excess of 2000 kg, while the electric-power system handles up to 1000 current-consuming devices and is about 100 km long.

Soviet scientists and designers have created electrical machinery

TABLE V. 1

Weight Distribution Among Individual Elements  
of Three Military Aircraft

1 Тип самолета	2 Двухмоторный 10-тонный		3 Четырехмоторный			
	4 16-тонный		5 32-тонный			
6 Вес	абсолют- ный	относи- тельный	абсо- лютный	относи- тельный	абсо- лютный	относи- тельный
	7 кг	8 %	7 кг	8 %	7 кг	8 %
9 Оборудование	576	100	1148	100	1516	100
10 Радио	172	30	286	23,4	254	16,70
11 Приборы	46	8	122	10,6	110	7,25
12 Противобледенитель	45	8	136	11,8	125	8,25
13 Источники электро- энергии	120	20,8	196	17	281	18,8
14 Электросеть	83	14,4	249	21,6	626	41,0
15 Электродвигатель пу- ска	50	8,7	93	6,1	95	6,1
16 Прочее	59	—	66	—	25	—
9 Оборудование	285	100	667	100	1198	100
17 Генераторы	44	15,5	88	13	119	10,0
18 Аккумуляторы	77	27	108	16	37	3,1
19 Электродвигатели	68	24	180	27	275	23,0
20 Электросеть	83	29	249	37,5	626	52,0
21 Вес электрооборудо- вания, относенный к весу оборудова- ния, в %	49,5		58		80	

1) Type of aircraft; 2) 10-ton two-motor; 3) four-motor; 4) 16-ton; 5) 32-ton; 6) weight; 7) absolute, kg; 8) relative, %; 9) equipment; 10) radio; 11) instrument; 12) anti-icing devices; 13) electric-power sources; 14) electric-power network; 15) electric starting motor; 16) other; 17) generators; 18) rechargeable battery; 19) electric motor; 20) electric-power network; 21) weight of electrical equipment relative to total weight of equipment, %.

and alternating-current apparatus of the highest quality, which has facilitated the conversion of aircraft electric systems to alternating

current.

At present, it is necessary to solve important problems in connection with the increased technical level of aircraft electrical-equipment production:

the reliability, high-altitude performance, and durability of all electrical equipment must be increased still more;

electrical machinery, apparatus, instruments, etc., must be made lighter and smaller with an accompanying increase in energy characteristics (efficiency and  $\cos \phi$ );

measures must be taken toward a further increase in the high-altitude and high-speed performance characteristics of electrical equipment;

integrated automation and electrical mechanization of aircraft controls must be introduced;

there should be a widespread introduction of constant-frequency alternating current;

electrical alternating-current drive units that are automatically controlled and regulated must be developed;

new types of aircraft generators, transformers, motors, regulators, etc., must be developed;

there must be increased precision and stability in voltage and frequency regulation;

studies must be carried out of transient, unbalanced, and emergency conditions in aircraft electrical machines, and protection circuits must be improved;

measures must be taken to reduce electrical hazards on board aircraft;

the theory of aircraft electrical machines must be developed, and design methods improved.



## Chapter 1

### GENERAL INFORMATION ON AIRCRAFT ELECTRICAL MACHINES

#### 1.1. OPERATION CONDITIONS FOR AIRCRAFT ELECTRICAL MACHINES

Aircraft electrical machines (AEM) operate under conditions that differ sharply from the operating conditions for general-purpose electrical machines. The basic conditions are:

- a) high-altitude capabilities up to 25 km or more;
- b) sub- and supersonic flying-craft speeds;
- c) increased mechanical loads due to vibration, jolting, and acceleration;
- d) arbitrary spatial orientation;
- e) short service life.

#### High-Altitude Performance

High-altitude conditions are characterized by the parameters of the surrounding air (temperature, density, pressure, humidity, composition, dielectric strength, heat capacity, etc.).

Air temperature is characterized by its height-dependence in accordance with Fig. 1.1, which shows the standard, maximum, and minimum curves for  $t = f(H)$ .

The temperature of undisturbed air taken in drops with increasing flight altitude  $H$  within the troposphere (up to 11 km), then remains constant (to a height of roughly 20 km), increases with  $H > 20$  km, reaching  $0^{\circ}$  at a height of 40 km.

Air temperature depends on altitude, and also on the time of year and location above the earth's surface. The standard international at-

mosphere (SA) is frequently used in calculations; it gives the average values of temperature (Table 1.1).

The relationship between the temperature of the undisturbed air of the standard atmosphere and altitude within the troposphere may be found from the equation

$$t = (15 - 6.5H)^{\circ}\text{C}, \tag{1.1}$$

where H is the altitude, km, and 15° is the initial temperature at sea level at a pressure of 760 mm Hg.

TABLE 1.1  
Standard Atmosphere (SA)

Высо- та H 1	Барометриче- ское давлени P <sub>H</sub>		P <sub>H</sub> = $\frac{P_H}{P_0}$	3 Температура		$\frac{T_H}{T_0}$	4 Объем- ный вес γ <sub>H</sub>	5 Плот- ность ρ <sub>H</sub>	$\frac{\gamma_H}{\gamma_0} = \frac{\rho_H}{\rho_0}$	$\sqrt{\frac{\gamma_H}{\gamma_0}} = \sqrt{\frac{\rho_H}{\rho_0}}$	6 Кинема- тиче- ский коэффи- циент вязкости воздуха γ · 10 <sup>4</sup>	7 Ско- рость звука a <sub>H</sub>	$\frac{\gamma_H}{\gamma_0} = \frac{a_H}{a_0}$
				T <sub>H</sub>	t <sub>H</sub>								
	мм	мм рт. ст.	кг/м <sup>2</sup>		°K	°C		кг/м <sup>3</sup>	кг/м <sup>3</sup>			м <sup>2</sup> /сек	м/сек
-0,5	806,2	10960	1,061	291,25	18,25	1,011	1,285	0,131	1,019	1,024	0,139	342,1	0,965
0	760,0	10332	1,000	288	15,00	1,000	1,225	0,125	1,000	1,000	0,144	340,2	1,000
2	596,2	8105,4	0,784	275	2,0	0,955	1,007	0,1027	0,8215	0,9064	0,1679	332,5	1,165
4	462,2	6284,2	0,608	262	-11,0	0,9097	0,819	0,0835	0,6685	0,81766	0,197	324,5	1,37
6	353,7	4809,5	0,465	249	-24	0,8645	0,6598	0,0673	0,5384	0,73375	0,234	316,3	1,62
8	266,89	3628,4	0,351	236	-37	0,8194	0,5252	0,0536	0,4286	0,6546	0,2799	308,0	1,94
10	198,16	2694,0	0,261	223	-50	0,7743	0,4126	0,0421	0,3367	0,5803	0,339	299,4	2,35
11	169,63	2306,1	0,223	216,5	-56,5	0,7517	0,3638	0,03710	0,2969	0,5449	0,375	295,0	2,6
12	144,87	1969,5	0,191	216,5	-56,5	0,7517	0,3108	0,03169	0,2536	0,5036	0,4386	295,0	3,04
14	105,67	1436,5	0,139	216,5	-56,5	0,7517	0,2266	0,02311	0,18495	0,4370	0,6013	295,0	4,18
15	90,24	1226,9	0,1187	216,5	-56,5	0,7517	0,1935	0,01974	0,15795	0,3974	0,7041	295,0	4,89
16	77,07	1047,8	0,1014	216,5	-56,5	0,7517	0,1653	0,01686	0,1349	0,3673	0,8244	295,0	5,72
18	56,21	764,23	0,074	216,5	-56,5	0,7517	0,1206	0,012296	0,09839	0,3137	1,130	295,0	7,85
20	41,00	557,41	0,054	216,5	-56,5	0,7517	0,08795	0,008968	0,07176	0,2679	1,550	295,0	10,75
22	29,9	405,57	0,0391	216,5	-56,5	0,7517	0,06415	0,006541	0,05234	0,2288	2,125	295,0	14,75
24	21,18	296,54	0,02870	216,5	-56,5	0,7517	0,04679	0,004771	0,03818	0,1954	2,913	295,0	20,35
25	18,63	253,25	0,0245	216,5	-56,5	0,7517	0,03996	0,004075	0,03260	0,1806	3,411	295,0	23,75
26	15,910	216,29	0,0209	216,5	-56,5	0,7517	0,03412	0,00348	0,02785	0,1669	3,994	295,0	27,75
28	11,60	157,76	0,01527	216,5	-56,5	0,7517	0,02489	0,002538	0,02031	0,1425	5,476	295,0	40,1
30	8,464	115,07	0,0111	216,5	-56,5	0,7517	0,01815	0,001851	0,01481	0,1217	7,507	295,0	52,2

1) Altitude, H; 2) barometric pressure p<sub>H</sub>; 3) temperature; 4) weight-volume ratio, γ<sub>H</sub>; 5) density, ρ<sub>H</sub>; 6) kinematic viscosity of air, ν · 10<sup>4</sup>; 7) speed of sound, a<sub>H</sub>; 8) mm Hg; 9) kg/m<sup>2</sup>; 10) kg/m<sup>3</sup>; 11) kg · sec<sup>2</sup>/m<sup>4</sup>; 12) m<sup>2</sup>/sec; 13) m/sec.

At a height H = 11-30 km in the stratosphere (isothermal atmosphere) the air temperature is

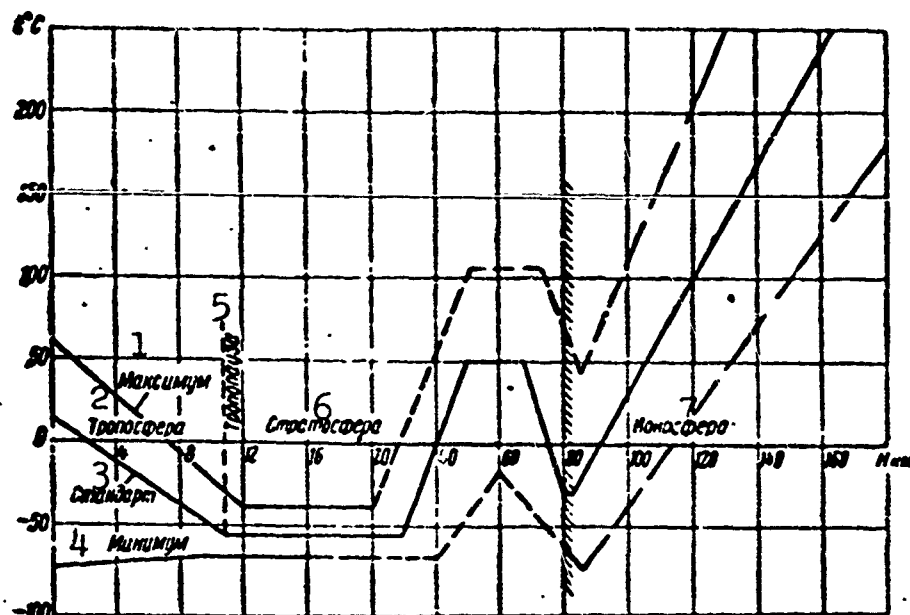


Fig. 1.1. Variation in temperature of undisturbed air stream with height above sea level according to SA. 1) Maximum; 2) troposphere; 3) standard; 4) minimum; 5) tropopause; 6) stratosphere; 7) ionosphere.

$$t = -56,5^{\circ} \text{C} = \text{const.}$$

In designing aircraft electrical machinery, it is necessary to proceed on the basis of the least favorable temperature conditions for undisturbed air. In this case, we use as a basis the maximum standard air temperature, determined by the expressions

$$\text{and } \left. \begin{aligned} t &= (60 - 8,33H)^{\circ} \text{C} & \text{at } H < 12 \text{ km} \\ t &= -40^{\circ} \text{C} & \text{at } H > 12 \text{ km.} \end{aligned} \right\} \quad (1.1a)$$

The air densities with respect to weight ( $\gamma$ ) and mass ( $\rho$ ), which depend on pressure, temperature, and humidity, decrease with height above sea level. The relationship between the relative\* air density and altitude according to the SA (see Table 1.1) may be determined approximately for altitudes up to 11 km from the formula

$$\frac{\rho_H}{\rho_0} = \frac{\gamma_H}{\gamma_0} = \frac{T_H}{T_0} = (1 - 0,0226H)^{4,256} \approx \frac{20-H}{20+H}. \quad (1.2)$$

For altitudes  $H > 11$  km, the formula

$$\frac{\rho_H}{\rho_0} = \frac{\gamma_H}{\gamma_0} \approx 0,3e^{-0,16(H-11)}. \quad (1.2a)$$

may be used; here  $H$  is the altitude, km,  $\gamma_H(\rho_H)$  and  $\gamma_0(\rho_0)$  are the air densities at the altitude and at sea level, respectively,  $\gamma_H^*$  and  $\rho_H^*$  are the relative densities at the altitude  $H$ ; then

$$\rho = \gamma/g, \quad g = 9.81 \text{ m/sec}^2;$$

$$\rho_0 = 0.125 \text{ kg} \cdot \text{sec}^2/\text{m}^4, \quad \gamma_0 = 1.225 \text{ kg/m}^3.$$

The air pressure drops with increasing height above sea level (Table 1.1).

The relative air pressure according to the SA may be found approximately from the formulas

and

$$\left. \begin{aligned} \frac{p_H}{p_0} &= \frac{p_H}{p_0} = (1 - 0.0226H)^{5.256} & \text{at } H \leq 11 \text{ km} \\ \frac{p_H}{p_0} &\approx 170 e^{-0.16(H-11)} & \text{at } H > 11 \text{ km} \end{aligned} \right\} \quad (1.3)$$

where  $p_0 = 760 \text{ mm Hg} = 10,332.3 \text{ kg/m}^2$ .

The relationship among pressure, temperature and air density is established from the gas law

$$\frac{p}{\rho} = gRT.$$

Using Formula (1.2) in the form

$$\frac{p_H}{p_0} = \frac{\gamma_H}{\gamma_0} = \frac{p_H T_0}{p_0 T_H} = \frac{p_H (273 + t_0)}{p_0 (273 + t_H)} = 0.379 \frac{p_H}{273 + t_H}$$

or, taking the values of  $p_0$ ,  $t_0$ , and  $\gamma_0$  from the SA, we can obtain:

and

$$\left. \begin{aligned} p_H &= 0.0473 \frac{p_H}{273 + t_H} \\ \gamma_H &= 0.465 \frac{p_H}{273 + t_H} \end{aligned} \right\} \quad (1.4)$$

where  $p_H$  is the pressure, mm Hg,  $t_H$  is the air temperature at altitude  $H$ , and in accordance with the SA,  $p_0 = 760 \text{ mm Hg}$ , and  $t_0 = 15^\circ\text{C}$ .

The air humidity (relative) may reach 98% at an ambient temperature of  $+20^\circ\text{C}$ .

Air composition. With increasing altitude, the amount of moisture and oxygen in the air decreases, and the concentration of ozone rises.

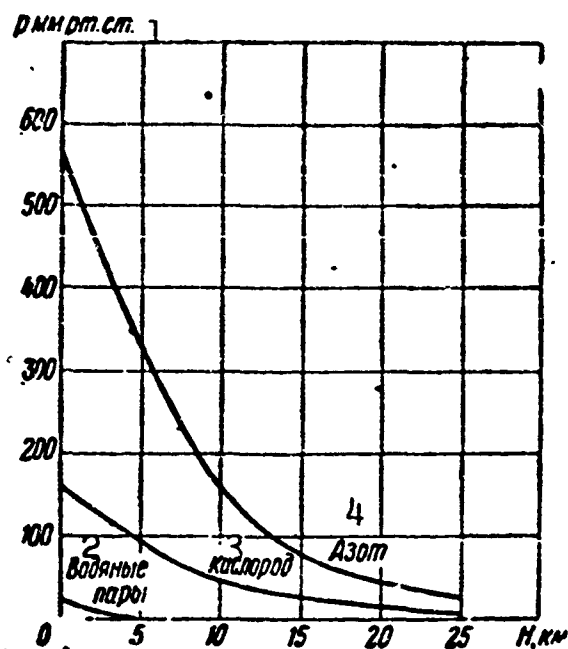


Fig. 1.2. Partial pressures of nitrogen, oxygen, and saturated water vapor as a function of altitude. 1) p, mm Hg; 2) water vapor; 3) oxygen; 4) nitrogen.

Figure 1.2 shows the partial pressures of nitrogen, oxygen, and saturated water vapor as a function of altitude. The amount of ozone at the 20-30 km level is  $(35-40) \cdot 10^{-5} \text{ g/m}^3$ , i.e., greater by a factor of 17-20 than at the earth.

The dielectric strength of air drops as the pressure decreases. At an altitude of 15 km, the dielectric strength of air is roughly 2.5 times less than at sea level. Arc length  $\tau_g$  increases with altitude, and at the 15-km level it nearly doubles for a DC voltage of 24 v.

The curves of Fig. 1.3 show arc time as a function of flight altitude and break current.

The change in parameters of the surrounding air with increasing height has a negative effect on the operation of electrical machines; it decreases cooling efficiency, especially in the stratosphere where the temperature is constant and the air density continues to drop; it impairs commutation conditions, since sparking at sliding contacts and

brush wear increase (under high-altitude conditions, collector sparking can easily change into ring arcing). In addition, the thickening of oil and decrease in structural clearances owing to decreasing temperature can increase the starting counter torque of mechanisms, while increasing ionization raises air conductivity and decreases its electrical strength, which impairs the operation of commutating devices.

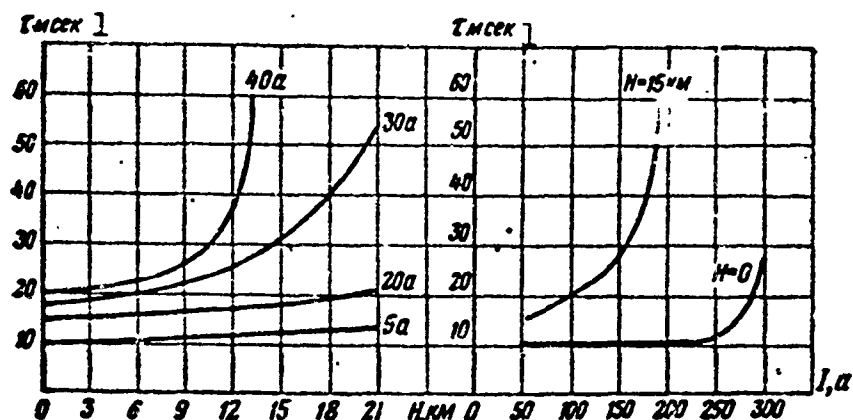


Fig. 1.3. Arc time  $\tau$  as a function of altitude  $h$  and contactor breaking current  $I$  for 125 v DC and an inductive circuit. 1)  $\tau$ , millisecc.

Finally, the high ozone concentration at high altitudes (20-30 km) aids the oxidizing action of the atmosphere on metals and organic materials, and also leads to an increase in air temperature as compared with the SA temperature.

### Flight Speed

As flight speed goes up, the temperature of the air surrounding the flying craft and used to cool electrical machines also increases.

The temperature rise in the boundary layer, in intakes, and within the fuselage of a flying craft is proportional to the square of the flight speed  $v$ , and is independent of the air rarefaction occurring as the craft climbs.

If we assume that the intake air enters the generator duct at a speed equaling the flying-craft speed  $v$ , and leaves at a speed  $v_1$ , the temperature rise of the gas stream owing to its deceleration in the

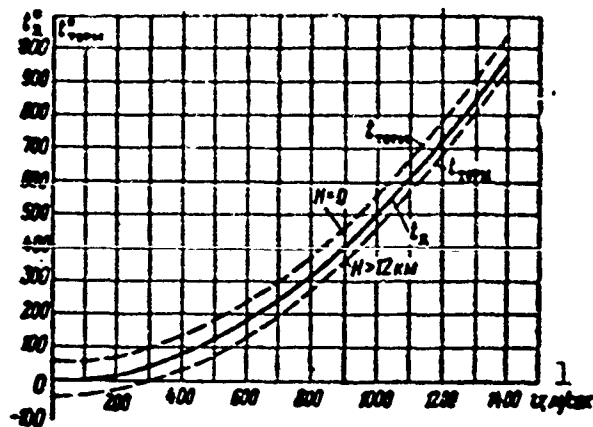


Fig. 1.4. Dynamic temperature rise and impact temperature (dashed line).  $t_d$  and  $t_{torm} = f(v)$  at  $H = 0$  ( $t = 60^\circ\text{C}$ ) and  $H \geq 12$  ( $t = -40^\circ\text{C}$ ).  
1)  $v$ , m/sec.

ventilating system of the electrical machine is determined by the well-known Bernoulli equation:

$$\frac{v_1^2}{2} + \frac{k}{k-1} g R t_1 = \frac{v^2}{2} + \frac{k}{k-1} g R t.$$

then allowing for adiabatic compression, the air temperature will be

$$t_1 = t + \frac{k-1}{2kR} (v^2 - v_1^2) ^\circ\text{C}. \quad (1.5)$$

Thus, the gas-stream temperature will rise by an amount

$$t' = \frac{k-1}{2kR} (v^2 - v_1^2). \quad (1.6)$$

owing to the loss of velocity. For air, the adiabatic coefficient  $k$  is a constant equaling  $k = 1.4$ ; the gas constant  $R = 29.27 \text{ kgm/kg}\cdot\text{degree}$ , and  $g = 9.81 \text{ m/sec}^2$ .

In this case

$$t' = 5 \frac{v^2 - v_1^2}{100^2} ^\circ\text{C}. \quad (1.6a)$$

For complete deceleration of the air stream, i.e., at the critical point where the stream velocity equals zero ( $v_1 = 0$ ),

$$t_x = 5 \left( \frac{v}{100} \right)^2$$

and

$$t_{\text{topm}} = t + 5 \left( \frac{v}{100} \right)^2 \text{°C.} \quad (1.6b)$$

Here  $t_{\text{topm}}$  is the temperature at the critical point, called the impact temperature, and  $t_d$  is the dynamic temperature rise above the temperature of the undisturbed air.

The temperature of the air used to cool electrical machines differs from the impact temperature; it depends on the location of the machine and the method used to cool it. In the general case, if we allow for adiabatic compression, the cooling-air temperature will be below the impact temperature, i.e.,

$$t_{\text{oxa}} = t + \rho_1 \left( \frac{v}{100} \right)^2 < t_{\text{topm}}, \quad (1.6c)$$

where  $v$  is measured in m/sec and  $\rho_1 < 5$ .

For aircraft electrical machinery, we may assume that  $\rho_1 \approx 4.3$ .

In view of (1.1) and (1.6c), we may obtain from the SA:

$$\text{and } \left. \begin{aligned} t_{\text{oxa}} &= 15 - 6.5H + \rho_1 \left( \frac{v}{100} \right)^2 \text{ for } H \leq 11 \text{ km} \\ t_{\text{oxa}} &= -56.5 + \rho_1 \left( \frac{v}{100} \right)^2 \text{ for } H > 11 \text{ km,} \end{aligned} \right\} \quad (1.6d)$$

where  $t$  is the air temperature according to the international standard.

Fig. 1.5. Air temperature as a function of altitude and flight speed ( $M = 0$  and  $M = 2$ ).

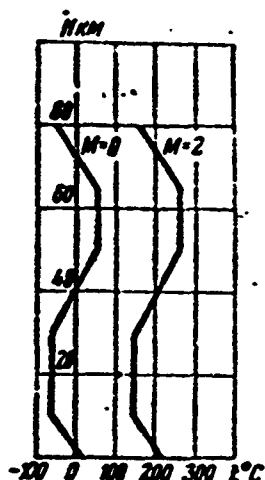


Figure 1.4 gives curves for  $t_d = f(v)$  and  $t_{\text{topm}} = f(v)$ , while Fig. 1.5 shows the air temperature for higher altitudes and flight speeds of  $2M$ .

For flight speeds up to 300 m/sec (1080 km/hr), the cooling-air temperature does not rise by more than 45°C owing to stream deceleration; at a flight speed  $v = 600$  m/sec, however, it reaches 180°C, and at  $v = 900$  m/sec (3240 km/hr), it is 405°C.

It is clear that at flight speeds of  $v > 600$  m/sec, it is impossible to use natural or forced-air cooling for electrical machinery.



## Mechanical Loads

Large mechanical stresses appear in aircraft electrical machines owing to vibration and jolting of the main aircraft engine, and are also caused by acceleration load factors occurring in maneuvering (take-off, landing, and turns), in firing, etc.

The frequency and amplitude of vibrations and jolts are determined by the type of flying craft and the type of main engine. Their magnitudes are normally established in the tactical-technical specifications.

Mechanical loads normally increase with flight speed and reach values of 10 g or more. Vibration frequency fluctuates from 10 to 500 cps.

Mechanical stresses have a substantial effect on electrical-machine design and, in particular, on coupled elements.

## Spatial Orientation

A flying craft and all of the equipment carried by it can occupy any position in space, which also affects electrical-machine design and must be taken into account during design and, in particular, during the choice of bearings.

## Service Life

General-purpose electrical machinery may operate continuously for 10-20 years.

The service life of aircraft electrical machines is considerably less. They should operate without failure and without need for repairs for 500 hr over a three and one-half year period from the day that they leave the factory. The service lives of some aircraft electrical machines may be even lower (for example, generators for delicers, electrical machines for rockets, etc.).

Service life influences the choice of thermal and electrical

loads, which rise as service life decreases; type and size of bearings, and grade of lubricant are also affected.

The permissible winding-insulation temperatures are determined by service life (machine lifetime), as well as by the class (grade) of insulation used.

Insulation service life depends on temperature. Thus, insulation made from organic materials (class A) can serve for 25 years at a temperature of  $100^{\circ}$ , and about 15 min at a temperature of  $200^{\circ}$ .

Insulation service life may be determined from an equation of the type

$$\tau = k_t e^{-0.012 t} \text{ hr},$$

where  $k_t$  is an empirical coefficient;  $t$  is the winding temperature;  $\tau$  is the insulation service life.

For class A insulation, the coefficient  $k_t \approx 72 \cdot 10^7$ , and at  $t = 150^{\circ}$ ,  $\tau = 1200$  hr.

Thus, if we take the service life of aircraft electrical machinery as 500 hr, we can accordingly increase the permissible winding temperature and, consequently, the electrical load as well.

## 1.2. BASIC REQUIREMENTS FOR AIRCRAFT ELECTRICAL MACHINES

Aircraft electrical machines should satisfy the All Union Standards for electrical machinery. In addition, various additional specifications apply to them, necessitated by the peculiarities of the operating conditions. These requirements form the content of the technical plans (TZ) on the basis of which a part is developed and the technical specifications (TT), and the equipment is procured on their basis.

The basic topics covered in the TZ and TT are:

a) uninterrupted operation in any orientation under high-altitude conditions with various accelerations, temperatures, humidities, loads,

and stresses, as is clear from the previous discussion;

b) durability, the degree to which the equipment is selfcontained, and simplicity of servicing;

c) optimum weight and least size;

d) increased mechanical strength;

e) protection against radio interference;

f) protection against penetration of oil, water, or fuel within the electrical machine.

The durability of any device is its ability to continue to operate when damaged. It also provides for resistance of equipment to damage by the automatic connection of parallel or spare equipment.

The degree to which a flying craft is selfcontained indicates its ability to do without airport technical facilities.

The presence of a spare aircraft generator driven by a special motor increases the independence of an aircraft, since it makes it possible to prepare for takeoff while the aircraft engines are not operating.

The requirement of optimum weight and least size is self-evident: every kilogram of excess equipment weight decreases payload and combat ability of a flying craft, while the conditions under which electrical machines are located on aircraft-engine housings, under which they are built into mechanisms, etc., require minimum size.

The problem of minimum electrical-machine weight, however, should be related to power characteristics. A decrease in electrical-machine weight with a simultaneous drop in efficiency may lead to negative results owing to the additional fuel consumption and decrease in lift of the flying craft. It is important to obtain an optimum machine which will give minimum weight for given power characteristics.\*

In aviation, the general tendency of design is to obtain minimum-

weight equipment. Minimum-weight electrical machines do not always result in a flying craft of minimum weight, however. The lower the efficiency of an aircraft generator, the more power that must be taken from the aircraft motor and the greater the weight flow rate of the cooling air. This increases the power (weight) of the aircraft engine and the fuel consumption. Consequently, in calculating the weight of an aviation electrical machine, it is necessary to consider the expenditure of power and fuel on cooling, as well as the power taken from the aircraft engine, i.e., the flying weight must be taken as the basis. In this case, the problem of electrical-machine optimum weight and efficiency will be solved in accordance with the type of flying craft.

### 1.3. CLASSIFICATION OF AIRCRAFT ELECTRICAL MACHINERY AND ELECTRIC-POWER SYSTEMS

There presently is no generally accepted classification of aircraft electrical machinery.

The fields of application and the varieties of aircraft electrical machines are so diverse that they should be classified by basic criteria. Below, we propose a basic classification of aircraft electrical machinery according to function, which will then be given according to the individual types of machines, e.g.:

- a) direct-current and alternating-current generators for supplying the main electrical power system, electrical deicing systems, stand-by and special devices;
- b) single-phase and three-phase transformers and autotransformers;
- c) direct-current and alternating-current motors for continuous, intermittent, and cyclic service in aircraft drive mechanisms;
- d) centralized and individual power-supply converters for gyroscopes, radar, and other systems;

e) control-system amplidynes;

f) special electrical machines for aircraft drive mechanisms, computers and tracking systems (selsyns, magnesyns, fast-response actuating motors, etc.).

Table 1.2 gives the basic aviation electric-power systems, which may be reduced to four groups:

- a) low- and high-voltage direct-current systems;
- b) variable-frequency alternating-current systems;
- c) fixed-frequency alternating-current systems;
- d) mixed or combination systems.

The choice of an electric-power system is determined by the type of flying craft, its function, and the tactical-technical data. Owing to the variety of flying craft, there is no one aircraft electrical power system that is optimum for all cases.

A direct-current system may operate at 30 or 120 v, or at two voltages: 30 and 120 v (Figs. 1.6 and 1.7).

Where two voltages are available, the 30-volt line is used to supply low-power devices and, in particular, for light bulbs whose filaments would have to be so thin to operate from 120 v that they could not withstand vibration.

The 30-v DC system is the most common and most highly developed. It is simple, safe, and satisfies the tactical-technical requirements of small and medium flying craft for altitudes up to 20 km and speeds below 500 m/sec.

For heavy aircraft, requiring more electric power and longer circuits, extending to 75-100 km, this system becomes heavy owing to the excessive weight of conductors. In addition, at high altitudes and flight speeds, the operating reliability of the sliding commutator contact (brushes and commutator) decreases, and it becomes difficult

TABLE 1.2

## Aircraft Electric-Power Systems

1 Системы электро-снабжения	2 Генерирование		3 Распределение		4 Примечание
	5 частота	6 напряжение в	5 частота	6 напряжение в	
8 Постоянно-го тока	8 Постоян-ный ток	30 120 120 30	8 Постоян-ный ток	28,5 — 120 28,5	7 Переменный ток от преобразователя
9 Переменно-постоянного тока	$f = \text{var}$	30 и более 10	11 Постоян-ный и перемен-ный ток	28,5 и более 10	12 Выпрямление части переменного тока переменной частоты
9 Переменно-го тока	$f = \text{var}$	$U = \text{const}$	$f = \text{var}$	$U = \text{const}$	13 Автоматическое поддержание постоянного напряжения
	$f = \text{var}$	$U = \text{var}$	$f = \text{var}$	$U = \text{var}$	14 Автоматическое поддержание $(\frac{U}{f})^n = \text{const}$
	$f = \text{var}$	$U = \text{var}$	$f = \text{var}$	$U = \text{const}$ и $(\frac{U}{f})^n = \text{const}$	15 Применение вольтодобавочного генератора для поддержания $(\frac{U}{f})^n = \text{const}$
	$n = \text{var}$ $f = \text{const}$	$U = \text{const}$	$f = \text{const}$	$U = \text{const}$	16 Преобразователь частоты, муфты, электрические схемы, тормоза
	$n = \text{const}$ $f = \text{const}$	$U = \text{const}$	$f = \text{const}$	$U = \text{const}$	17 Автономная установка
21 Смешанные системы	$f = \text{const}$ , постоян-ный ток	$U = \text{const}$ $U = \text{const}$	$f = \text{const}$ постоян-ный ток	$U = \text{const}$ $U = \text{const}$	18 Автономная установка с генератором постоянного тока от главного привода
	Постоян-ный ток $f = \text{var}$	$U = \text{const}$ $U = \text{const}$	Постоян-ный ток $f = \text{var}$	$U = \text{const}$ $U = \text{const}$	19 Генератор переменного тока и генератор постоянного тока от главного привода
	$f = \text{var}$ $f = \text{const}$	$U = \text{const}$ $U = \text{const}$	$f = \text{var}$ $f = \text{const}$	$U = \text{const}$ $U = \text{const}$	20 Генераторы от главного привода, автономная установка или генератор от главного привода с муфтой

1) Electrical system; 2) generation; 3) distribution; 4) comments; 5) frequency; 6) voltage, v; 7) alternating current from converter; 8) direct current; 9) alternating current; 10) or above; 11) direct and alternating current; 12) part of alternating variable-frequency current rectified; 13) automatic voltage regulation; 14)  $(U/f)^n = \text{const}$  maintained automatically; 15) booster generator used to maintain  $(U/f)^n = \text{const}$ ; 16) frequency converter, couplings, electrical circuits, brakes; 17) independent installation; 18) independent installation with direct-current generator actuated by

TABLE 1.2 (key continued)

main drive; 19) alternating-current generator and direct-current generator actuated by main drive; 20) generators operated from main drive, independent installation or generator driven from main drive with coupling; 21) mixed systems.

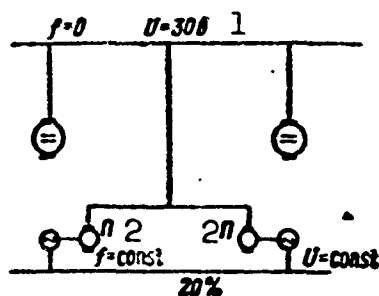


Fig. 1.6. Circuit diagram of 30-v DC electrical system. P) DC-stabilized frequency AC converters, drawing about 20% of generator power. 1) volts; 2) P.

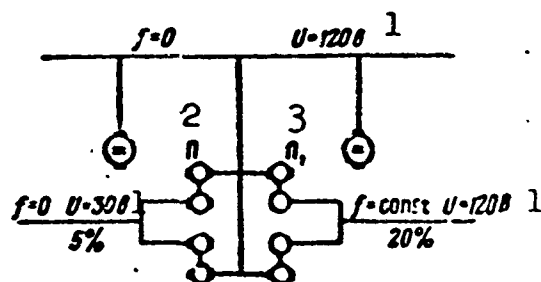


Fig. 1.7. Circuit diagram of 120-v DC electrical system. Converters: P) DC-DC; P<sub>1</sub>) DC-AC. 1) Volts; 2) P; 3) P<sub>1</sub>.

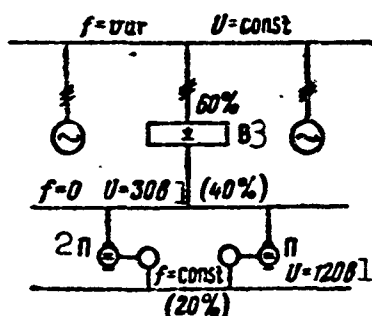


Fig. 1.8. Circuit diagram of AC-DC electrical system. V) Rectifier; P) converters; 1) volts; 2) P; 3) V.

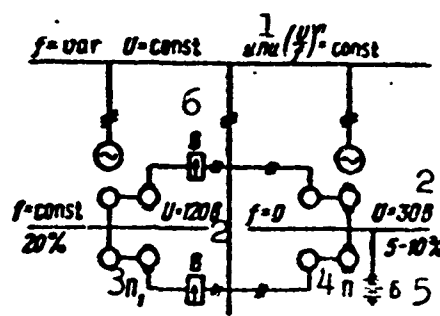


Fig. 1.9. Circuit diagram of variable-frequency electrical system. V) Rectifier; P and P<sub>1</sub>) converters; B) rechargeable battery; 1) or; 2) volts; 3) P<sub>1</sub>; 4) P; 5) B; 6) V.

to cool the commutator.

A 120-v DC system reduces the weight of the conductors by a factor of roughly 4.5 when compared with a 30-v system. This system possesses substantial drawbacks, however:

a) electrical-machine commutation is impaired, especially for low-

power motors whose weight increases;

b) at high speeds, difficulties appear with respect to commutation and regulation of equipment, since arcing time increases owing to the decreasing air density;

c) 120-v rechargeable batteries weigh more than those for 24 v;

d) a 30-v source is required to furnish power to apparatus, instruments, bulbs, etc.

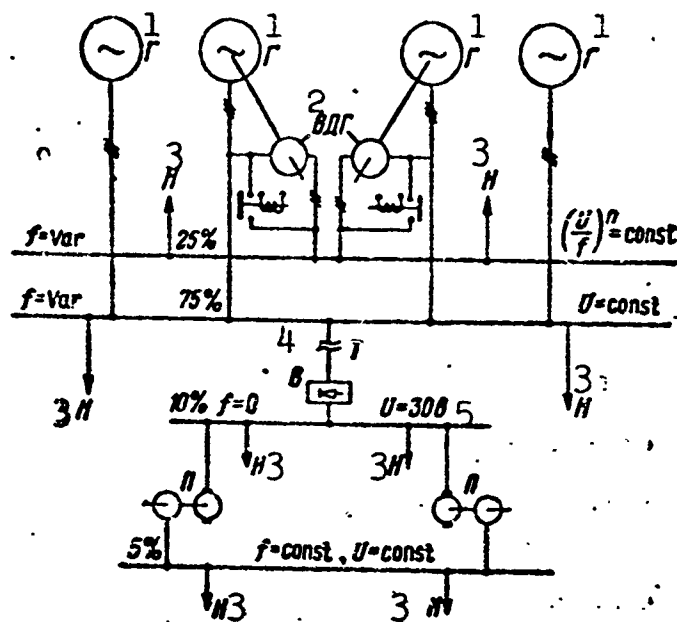


Fig. 1.10. Circuit diagram of combination variable-frequency system. VDG) Booster generators; T) transformer; V) rectifier; P) converter; N) load; 1) G; 2) VDG; 3) N; 4) V; 5) volts.

The system cannot be recommended for use since it is less reliable and has poor high-altitude characteristics.

The availability of two voltages complicates the system but makes it possible to decrease conductor weight.

An AC-DC system consists of variable-frequency AC generators and rectifiers (Fig. 1.8).

A part of the variable-frequency AC power is used directly, and part is rectified by means of semiconductor rectifiers to 28.5 v DC.

The advantage to this system is the possibility of increasing



generator power without a corresponding increase in size, i.e., a decrease in the relative generator weight; there is also a certain decrease in system weight, and it is possible to use the highly developed equipment available for 30 v DC. The utilization of germanium rectifiers makes possible a considerable decrease in rectifier weight while the utilization of silicon rectifier in addition permits solid-state rectifiers to be used at temperatures up to 200°C.

Variable-frequency AC systems may take various forms (see Table 1.2), e.g.:

a) frequency varying with voltage automatically .. intained constant with the aid of a voltage regulator; in this case, the torque of electrical induction motors drops off with increasing frequency and, consequently, motor sizes should be made larger since at maximum frequency it is necessary to provide given starting and maximum torques;

b) system voltage is automatically regulated with frequency variation in accordance with the law  $(U/f)^n = \text{const}$ ; in this case, the torques of induction motors remain nearly unchanged with frequency variation, but other current-consuming devices receive varying voltages, which is not suitable for light bulbs, heating devices, etc. (Fig. 1.9);

c) a mixed system, in which a portion of the energy is distributed at constant voltage  $U = \text{const}$ , while that part of the energy intended to power electric motors is distributed at a voltage that varies in accordance with the law  $(U/f)^n = \text{const}$  (this may be done by means of a booster generator, as shown in Fig. 1.10).

A general drawback to all AC variable-frequency systems is the need for an additional DC electrical system to supply special apparatus: this increases the weights of transformers, motors, capacitors, amplifiers, etc., whose dimensions are determined by the minimum frequency,

and complicates parallel operation.

A constant-frequency AC system with constant voltage is the most suitable for aviation purposes. Constant generator frequency may be obtained by various methods which will be discussed below together with the properties of this system.

Until recently, aircraft basically used 24-30 v DC; under the conditions of ever-increasing power demands, however, such a system no longer satisfies modern aircraft requirements either with respect to the weight of electrical equipment or with respect to reliability, especially for high-speed and high-altitude flights. Thus alternating current came into use.

Three-phase 50-cps AC at 120 v was widely employed in the USSR in 1934 on A.N. Tupolev's mammoth airplane "Maxim Gor'kiy."

The total current drawn by AC and DC current-consuming devices was 31.6 kw. Two three-phase synchronous generators of 3 and 5.5 kva power at 120 v were installed aboard the aircraft together with two DC generators of 3 and 5.8 kw power at 27 v. The generators were driven by special internal-combustion motors at a speed of 3000 rpm.

The basic advantages of using alternating current in aviation are characterized by the following data.

Direct-current aircraft generators of from 3 to 30 kw power rotating at a speed of 4000-9000 rpm have a relative weight of 4-2 kg/kw, while alternating current generators may be built in the 10 to 100 kva power range for speeds of 8000-6000 rpm with relative weights of 1.5-0.75 kg/kva, i.e., they are considerably lighter than direct-current generators.

A comparison of the weights of AC and DC aircraft motors shows that AC motors are two-three times lighter than corresponding DC motors.

TABLE 1.3

Sample Distribution of Electric Power on Modern Aircraft

1 Область применения	Средняя потребляемая мощность % 2	Род тока 3
4 Электронизмерительные и контрольные приборы	1,5	Постоянный 10
5 Освещение	4,0	Безразличен 11
6 Радиоустройства и электроавтоматика	20	Переменный 12
7 Электромеханизмы	20,0	Безразличен 11
8 Электронагрев	50,0	.
9 Разное	4,5	—

1) Field of application; 2) average power drawn, %; 3) type of current; 4) electrical measurement and monitoring instrument; 5) lighting; 6) radio equipment and electrical automatic devices; 7) electrical mechanism; 8) electrical heaters; 9) various; 10) direct; 11) AC or DC; 12) alternating.

Devices consuming electric current may be classified into two groups for aircraft (Table 1.3):

1. Devices running on either type of current — deicing devices, heaters, illumination devices, etc.; they can draw up to 75% of all power.

2. Devices requiring constant-frequency alternating current — communications and radar devices, gyroscope instruments, etc.; they may take about 20% of the total power.

3. Devices requiring constant-voltage direct current — control instruments; they take about 5% of the total power.

Thus, a fixed-frequency alternating-current system will supply about 95% of all the power needs, and only about 5% of the power needs to be converted into direct current, while with a direct-current system, up to 20% of the total power must be converted with the aid of rotating converters which are inefficient and have a high weight-to-power ratio. It is important to note that power drawn by devices re-

quiring alternating current has a tendency to increase, while direct-current needs drop.

The weight of the electrical network may reach 100 kilograms, and is increasing more rapidly than the weight of electrical equipment; on large aircraft, system weight may exceed 50% of the weight of electrical equipment. It thus becomes an urgent necessity to raise the voltage of the aircraft electric system, which is best done by converting to alternating current.

Below we list the advantages and drawbacks to alternating- and direct-current electrical power systems.

#### Advantages in Using a Direct-Current System

1. Simplicity of parallel generator operation — speed regulation is not required.
2. Higher motor starting and overload torques.
3. Economical and simple motor speed control.
4. Less system conductor weight for the same voltage.

#### Drawbacks

1. Limitations on power, speed, voltage, and high-altitude performance.
2. Lower reliability, higher weight, and larger size of apparatus.
3. Higher power conversion (20%).

#### Advantages in the Use of Alternating-Current System

1. Good high-altitude performance owing to the absence of commutators; equipment simplicity and reliability.
2. Higher maximum generator power.
3. Lighter and smaller generators and motors.
4. Possibility of stepping voltage up to 208 v and decreasing network weight.
5. Decrease in interference with radio reception.

6. Less power conversion (5%).

7. Possibility of operation with break in phase.

#### Drawbacks

1. Presence of arrangement for frequency conversion and more complicated parallel-operation apparatus.

2. Reactive power is drawn.

3. Motor speed control is complicated.

#### 1.4. VOLTAGE, FREQUENCY, AND NUMBER OF PHASES

The voltage of an electrical system and generator is determined by: the amount of power supplied, the devices consuming electrical power; the permissible voltage drop in the network; personnel and flying-craft safety; operating reliability under high-altitude conditions; the attempt to decrease transformer and converter power. In addition, it is necessary to allow for the spacing between current-carrying elements, the type of insulation, arc time, and the magnitude of short-circuit currents.

As system power and the length of the electrical network increase, the most efficient voltage also becomes higher. Here we must remember that it is impossible to decrease conductor cross section below some specific size, such as  $0.5 \text{ mm}^2$ , owing to mechanical-strength conditions. Thus, an excessive increase in voltage is undesirable, since in this case conductor cross section will be limited not by current density or permissible voltage drop in the network, but by its mechanical strength.

From the standpoint of personnel safety, DC voltage should not exceed 24 v, and AC voltage, 40 v. Thus, on modern flying craft which as a rule use higher voltages, it is necessary to observe the rules of electrical safety engineering.

The danger of fire due to a stable arc discharge may appear in

TABLE 1.4

Comparison of Conductor Weight for Alternating- and Direct-Current Electrical Systems

Род тока <sup>1</sup>	2 Система электроснабжения	Напряжение <sup>3</sup>	Вес меди % <sup>4</sup>
5 Постоянный	7 Однопроводная система, обратный провод заземлен	27 120	100 22,5
6 Переменный	8 Двухпроводная система 9 Трехпроводная трехфазная система при $\cos \varphi = 0,75$	120 208/120	45,0 30

1) Type of current; 2) electrical system; 3) voltage, v; 4) weight of copper, %; 5) direct; 6) alternating; 7) single-wire system, return conductor grounded; 8) two-wire system; 9) three-wire three-phase system,  $\cos \varphi = 0.75$ .

the presence of a continuing short circuit. Two types of short circuit are possible: a short circuit that interrupts itself following rapid local burning of conductors and structures, or the more dangerous condition of a continuing short circuit resulting from prolonged burning of an arc, leading to welding of the conductors.

The nature of a short-circuit process depends on the magnitude of the current, conductor cross section, and the condition of the contacting surface.

A direct-current arc will burn longer, all other conditions being equal, than an alternating-current arc, especially at high altitudes and higher voltages.

Large short-circuit currents lead to local burning out of conductors, so that arc time does not exceed 0.1-0.3 sec, and if the wire insulation is not combustible, fire hazard is slight. Small short-circuit currents are more dangerous, since arc burning is more stable and continues longer in this case.

Experience has shown that the consequences of short circuits present almost no practical hazards for voltages below 50 v.

At higher voltages, especially with direct current, fire hazard rises, and at voltages above 250 v, a short circuit can eliminate itself only with difficulty.

The voltage value affects the weight of electrical equipment, i.e., an increase in voltage leads to some increase in the weight of generators and motors which is the greater the lower their power. The increase in machinery weight is explained by the decreasing fill factor for the active copper layer owing to an increase in the relative dimensions of insulation and a decrease in conductor cross section.

When the voltage of DC electrical machines is raised, their size and weight rise for powers below 10 kw and drop for powers above 20 kw. This is explained by the fact that in low-power machines, a decrease in commutator weight is not compensated by an increase in machine weight due to the decreasing degree of utilization of the active layer.

The weight of commutating apparatus and fittings (terminals, plugs) decreases, while the weight of storage batteries (of the direct-current system) increases with increasing voltage.

Energy losses in the system drop as the voltage goes up, since the relative importance of voltage drops at contacts and in conductors decreases; in addition, in DC systems, there is a sharp drop in losses at electrical-machine commutators.

In aircraft requiring more than 50 kw, at 30 v the power-system conductor cross section is selected not on the basis of the permissible current density, but from the permissible voltage drop, i.e., the cross section is deliberately increased. Consequently, in this case it is necessary to increase system and generator voltage, which is easily done by converting to alternating current.

Calculations show that for an aircraft with a flying weight of 10 tons, an increase in the voltage above 120 v produces no noticeable

decrease in conductor weight, since 90% of the conductors already have their minimum permissible cross section in terms of mechanical strength. Consequently, in this case it makes no sense to increase system voltage. For a craft with a flying weight of 50 tons, at 120 v about 75% of the wires have the minimum permissible cross section, i.e., in this case it makes sense to increase the voltage still further.

Table 1.4 compares various electrical systems with respect to weight of network copper for constant nominal power, and the same network length and current density.

From the point of view of decreasing network conductor weight, it is advantageous to use 120 v DC. As we have mentioned before, however, difficulties are encountered at high altitudes with direct current of this voltage.

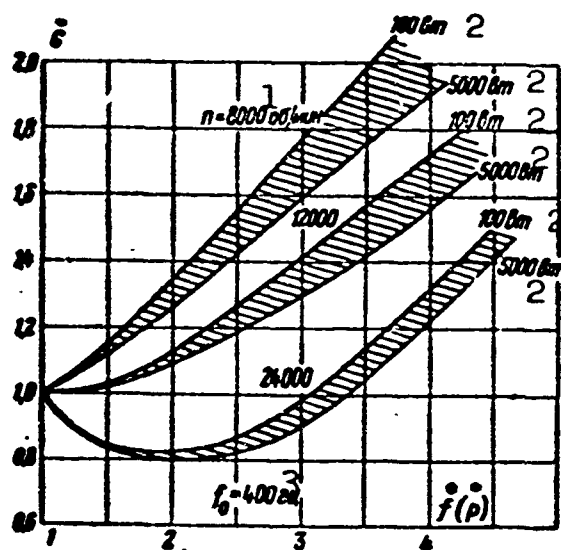


Fig. 1.11. Relative weight of electric motors having various powers as a function of frequency; the weight of the motor at 400 cps is taken as unity. 1) rpm; 2) watts; 3) cps.

For electrical power systems with installed generator capacity of the order of 100-300 kva and about 100 km of conductor, three-phase AC at 208/120 v prove to be optimum, safe, and reliable. Under these conditions, 30 v DC is not optimum, and the system is less reliable owing to the presence of commutators.

With a further increase in aircraft electrical-system power (1000 kva) it is possible that the voltage will be increased to 380/220 v AC.

Thus, in modern aircraft electrical systems we find: direct current at 30 v (across the generator terminals and 28.5 v in the line); three-phase alternating current at 208/120 v (at the generator termi-



nals and 200/115 v in the line) and single-phase alternating current at 120 v (at the generator terminals and 115 v in the line).

It should be noted that the voltage fluctuation in an aircraft network reaches  $\pm 10\%$  with direct current; this is due to the voltage drop in the network as the current varies from 0 to the rated value, by the large variation in cooling-air characteristics, and by imperfection in the voltage regulators.

The modern voltage regulators used in DC systems provide a voltage fluctuation at the generator terminals within limits of 3.5 v (as the load changes from zero to rated value and the temperature ranges from  $+50$  to  $-60^{\circ}\text{C}$  with flights at altitudes up to 20 km).

Modern general-purpose AC aircraft generators with voltage regulators maintain the voltage across their terminals constant to within  $\pm 4\%$ . Generators have recently been developed with regulation systems that maintain the voltage across the terminals constant to within  $\pm 1.5-0.5\%$ .

By decreasing voltage fluctuations at generator terminals, it is possible to compress the range of line-voltage variation and, consequently, to decrease the weight of electrical equipment; a further increase in the precision of generator voltage regulation would lead to instability in parallel operation, however.

The frequency of alternating current and its choice are determined by the requirements of the current-consuming devices; rotational speeds of generators, motors, and mechanisms, energy losses due to eddy currents and hysteresis.

All devices consuming electrical power on board aircraft can be classified into three groups:

a) devices for which the frequency or even the type of current makes no difference (heating and illuminating devices);

b) devices with which it is desirable to use higher frequencies; they include static electromagnetic devices (transformers, magnetic amplifiers, etc.), capacitors, filters, etc.;

c) devices for which it is undesirable to use frequencies above 400 cps: electric motors, the electrical network, etc.

Magnetic amplifiers and transformers are widely employed in radio installations and automatic-control systems; frequencies of 2000 cps or more lead to a reduction in weight and shorter response times in systems using automatic devices.

On the other hand, the majority of modern aircraft electrical mechanisms use intermittently operating electrical motors running at 10,000-12,000 rpm and operating for spans of 6000-8000 rpm. Under such conditions, it is desirable to use four- and six-pole motors ( $2p = 4$  and 6) at a frequency of

$$f = \frac{pn}{60} = \frac{(3 \div 2)(8000 \div 12000)}{60} = 400 \text{ cps.}$$

Restrictions are imposed on further increasing electric-motor speed by the quality of off-the-shelf ball bearings, low reducing-gear efficiency, which drops as the gear ratio goes up, and by increased electromechanical time constant.

Figure 1.11 shows the relative weight of aircraft electric motors as a function of frequency for  $n = 8000, 12,000$ , and  $24,000$  rpm.

Modern aircraft DC generators reach speeds of 10,000-12,000 rpm. Speeds of 15-100-kva salient-pole alternators reach 8000-6000 rpm for machines with six-eight poles, while for nonsalient-pole machines, speeds reach 12,000-24,000 rpm with four or two poles.

Generator speed is limited by the mechanical strength of the rotor; on this basis, nonsalient-pole generators may be constructed for peripheral speeds of up to 200 m/sec, and salient-pole machines

for speeds of up to 70-80 m/sec.

Eight-four-pole generators display good weight and power characteristics in 10-100 kva sizes at speeds of 6000-12,000 rpm, i.e., even at a 400-cps frequency.

### Effect of Frequency Variation on Transformer Size and Losses\*

It is easy to see how frequency variation affects the dimensions of static electromagnetic devices by investigating a transformer.

The electromagnetic power developed by a transformer equals

$$S_e = mEI = 8,88 \frac{f}{400} \frac{B}{10000} S_m S_c \text{ [va]}$$

or

$$\frac{S_e}{S_m S_c} = 8,88 \frac{f}{400} \frac{B}{10000} j \text{ [va/cm}^4\text{]},$$

where

$$mwl = 100 m \omega j q_m = 100 j S_m \text{ [amp]},$$

B and  $S_s$  are the induction in the core and its cross section,  $\text{cm}^2$ ;  $\underline{m}$  and  $\underline{w}$  are the number of phases and the number of turns per phase;  $\underline{j}$  is the current density,  $\text{amp/mm}^2$ ;  $q_m$  is the cross-sectional area of a single conductor,  $\text{cm}^2$ ;  $S_m = mwq_m$  is the total cross-sectional area of copper in the  $\underline{m}$  phases of the winding.

By considering several geometrically similar transformers we see clearly that they are characterized by a proportional change in all linear dimensions and a constant copper fill factor and steel-core cross section.

In the case under consideration, the copper cross section  $S_m$ , the steel cross section  $S_s$ , and the transformer surface P vary in proportion to the square of the linear dimension; the weight (volume) of copper  $G_m$  and of steel  $G_s$ , i.e., the active weight  $G_a$  of the transformer varies in proportion to the third power of the linear dimensions, and the electromagnetic power varies in proportion to the fourth

power of the linear dimensions.

We may thus write  $S_m \equiv S_s \equiv P \equiv \underline{1}^2$ ,

$$G_m = G_c = P \text{ and } S_s = S_m S_c \equiv P^2.$$

In order to simplify the analysis, from this point on we shall use relative units, and quantities corresponding to the initial frequency will carry the subscript "0" and those associated with relative units the asterisk "\*", i.e.,

$$\dot{f} = \frac{f}{f_0}, \quad \dot{B} = \frac{B}{B_0}, \quad \dot{G} = \frac{G}{G_0}, \quad \dot{P} = \frac{P}{P_0}, \quad \dot{P}_c = \frac{P_c}{P_{c0}}, \quad \dot{i} = \frac{i}{i_0} \text{ etc.}$$

In view of this, we may write

$$\dot{S}_s = \frac{S_s}{S_m} = \dot{B} \dot{j} \dot{f} \dot{S}_m \dot{S}_c = \dot{B} \dot{j} \dot{f} \dot{i},$$

whence we determine a transformer linear dimension

$$\dot{i} = \left( \frac{\dot{S}_s}{\dot{B} \dot{j} \dot{f}} \right)^{0.25} = \dot{S}_s^{0.25} (\dot{B} \dot{j} \dot{f})^{-0.25},$$

the surface and cross section

$$\dot{P} = \dot{S}_m = \dot{S}_c = \dot{i}^2 = \dot{S}_s^{0.5} (\dot{B} \dot{j} \dot{f})^{-0.5},$$

as well as the weight

$$\dot{G}_m = \dot{G}_c = \dot{G}_s = \dot{i}^3 = \dot{S}_s^{0.75} (\dot{B} \dot{j} \dot{f})^{-0.75}.$$

Iron losses owing to polarity reversal are determined from the well-known expression

$$P_c = k_c k_{\Sigma c} B^{\alpha} f^{\alpha} G_c \text{ [watts]},$$

or in relative form

$$\dot{P}_c = k_c \dot{B}^{\alpha} \dot{f}^{\alpha} \dot{G}_c.$$

The copper losses in the transformer windings are

$$P_m = k_m k_{\Sigma m} i^2 G_m \text{ [watts]},$$

or in relative form

$$\dot{P}_m = k_m k_{\Sigma m} \dot{i}^2 \dot{G}_m.$$

Here  $k_{v.s}(k_{v.s}^*)$  and  $k_{v.m}(k_{v.m}^*)$  are coefficients that take into account the rise in losses due to eddy-current reactions for the active

steel and winding copper, respectively, and which depend (all other conditions being equal) on the frequency: they may be represented in the approximate form

$$\dot{k}_{s,c} \approx \dot{j}^{a_1} > 1 \text{ and } \dot{k}_{s,u} \approx \dot{j}^{a_2} > 1,$$

where

$$a_1 < 1, \quad a_2 < 1 \text{ and } \dot{j} > 1.$$

If we substitute the values of  $\dot{G}_m^*$  and  $\dot{G}_s^*$  into the expressions for the losses, we obtain, respectively,

$$\dot{P}_c = \dot{S}_e^{0.75} \dot{B}^{a_1 - 0.75} \dot{j}^{-0.75} \dot{j}^{a_1 - 0.75 + a_1},$$

and

$$\dot{P}_u = \dot{S}_e^{0.75} \dot{B}^{-0.75} \dot{j}^{1.25} \dot{j}^{-0.75 + a_2}.$$

Thus, the steel and copper losses are expressed as functions of the electromagnetic power  $\dot{S}_e^*$ , the core induction  $\dot{B}^*$ , the winding current density  $\dot{j}^*$ , and the supply-line frequency  $\dot{f}^*$ .

Using these expressions, we determine the total transformer losses  $\Sigma \dot{P}^*$  and the ratio of the constant losses ( $\dot{P}_s^*$ ) to the variable losses ( $\dot{P}_m^*$ ), i.e.,

$$\Sigma \dot{P} = \frac{\dot{P}_u + \dot{P}_c}{\dot{P}_{u0} + \dot{P}_{c0}} = \dot{P}_s \frac{1 + k_{p0} \dot{k}_p}{1 + k_{p0}}$$

or

$$\Sigma \dot{P} = \frac{1 + k_{p0} \dot{k}_p}{1 + k_{p0}} \dot{P}_s^{0.75} \dot{B}^{-0.75} \dot{j}^{1.25} \dot{j}^{-0.75 + a_2},$$

where

$$k_{p0} = \frac{\dot{P}_{c0}}{\dot{P}_{u0}} \text{ and } \dot{k}_p = \frac{\dot{P}_c}{\dot{P}_u} = \dot{B}^{a_1} \dot{j}^{-2} \dot{j}^{a_1 + a_2 - a_1},$$

— the ratio of transformer constant losses to variable losses.

In the last analysis, transformer relative dimensions with rising frequency are determined by heat-rise conditions. The relative transformer volume changes in proportion to the third power of the linear dimensions, and the relative heat-transfer surface in proportion to

the square of the linear dimensions.

Thus, the specific heat flow, which characterizes transformer heating, will rise in proportion to the first power of the linear dimensions for the constant transformer losses. Actually, the situation is more favorable, since the relative total losses decrease as the frequency goes up and, consequently, the specific heat flow rises less rapidly than the linear dimension  $\frac{*}{l}$  decreases.

The temperature rise of a potted transformer may be characterized in first approximation by the specific heat flow, i.e., the ratio of the sum of the losses to the entire outside surface of the transformer

$$\dot{A}_t = \frac{\Sigma \dot{P}}{\dot{H}} = \frac{1 + k_{p0} k_p}{1 + k_{p0}} \dot{P}_0^{0.25} B^{*-0.25} j^{1.75} f^{-0.25 + \alpha_1}.$$

In order to understand the results obtained, let us consider a specific case; we assume that the transformer electromagnetic power is constant, i.e.,  $\dot{S}_e^* = 1$ , the specific heat flow stays at the same value, i.e., cooling conditions are nearly identical for transformers at all frequencies ( $\dot{A}_t^* = 1$ ), the ratio of the constant losses to the variable losses remains constant, i.e.,  $k_p^* = 1$ , and the thickness and grade of steel as well as conductor dimensions remain unchanged so that  $n' = 1.35$  and  $n'' = 2.0$ .

In view of this, the current density, induction, weight, and losses as functions of frequency will be:

$$\dot{B} = j^{\frac{2}{n'}} f^{\frac{n' + \alpha_1 - \alpha_2}{n'}} \quad \text{or} \quad \dot{B} \approx j f^{-0.675},$$

where we assume that  $k_p^* = 1$  and  $\alpha_1 - \alpha_2 \approx 0$ ;

$$\dot{A}_t = j^{\frac{2.5n'' - 1}{2n''}} f^{\frac{n'' - n' - (n_1 - \alpha_2)}{4n''} + \alpha_2}$$

or

$$\dot{A}_t \approx j^{1.5} f^{-0.0815 + \alpha_2}.$$

By the constancy of the specific heat flow

$$j = f^{\frac{n'' - n' - 4n''a_1 - (a_1 - a_2)}{7n'' - 2}} \quad \text{or} \quad j \approx f^{0,0542 - 0,67a_1}$$

and

$$B = f^{\left(\frac{n'' - n' - 4n''a_1 - (a_1 - a_2)}{7n'' - 2} \cdot \frac{2}{n''} - \frac{n'}{n''}\right)} \quad \text{or} \quad B \approx f^{-(0,021 + 0,67a_1)}$$

Using the values of  $j^*$  and  $B^*$ , we obtain the desired expressions for the transformer weight and losses:

$$\dot{G}_c = \dot{G}_m = \dot{G}_s = (\dot{B} j f)^{-0,75} \approx f^{-0,325 + a_1}$$

$$\Sigma \dot{P} = \dot{P}_m \approx f^{-0,217 + 0,67a_1}$$

Figure 1.12 gives a family of curves corresponding to

$$j, B, \Sigma \dot{P} \text{ and } \dot{G} = \varphi(j).$$

where

$$\dot{A}_1 = 1, \dot{k}_p = 1, \dot{S}_s = 1, n' = 1,35, n'' = 2,0; a_1 \approx a_2 = 0.$$

If we allow for the skin effect ( $a_1 \neq a_2 \neq 0$ ), the induction in the core decreases and the weight rises (dashed lines). The decrease in the exponent  $n''$  (for induction) and the increase in the exponent  $n'$  (for frequency) cause the induction to decrease more rapidly and thus increase the weight.

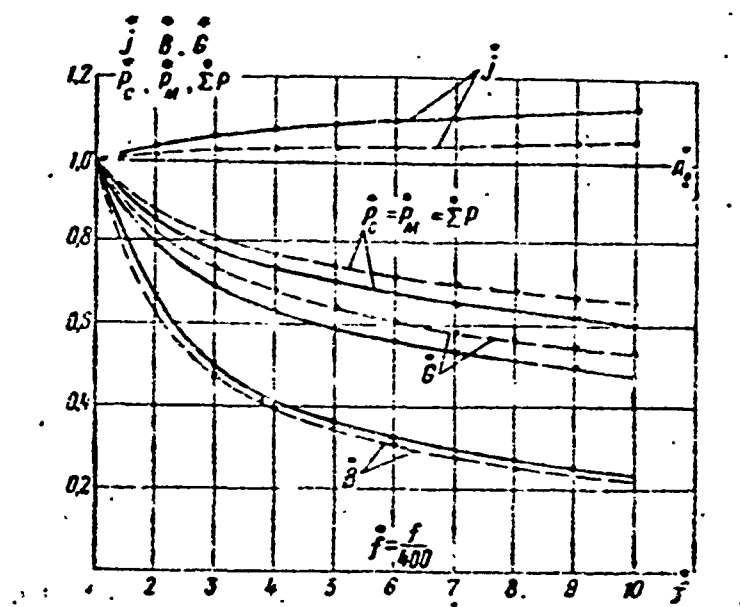


Fig. 1.12. Relative values of weight, induction, current density, and transformer losses as functions of frequency. Solid lines — skin effect not considered, dashed lines — skin effect taken into account.

It follows from what we have said that as the frequency rises, the active transformer weight drops off monotonically, and the degree of decrease depends on the steel grade and signs (the values of  $n'$ ,  $n''$ , and  $\alpha_1$ ).

Experience and more detailed analysis show, however, that the decrease in transformer active weight with increasing frequency occurs only up to some particular frequency after which the transformer active weight begins to rise. This is explained by the increase in additional losses and by the fact that the true cooling surface increases more slowly than the square of the transformer linear dimension. Consequently, an increase in frequency leads to a decrease in transformer weight and an increase in its efficiency; at some particular frequency (above 2000 cps, practically speaking) that depends on transformer design and steel grade and size, the active transformer weight will be at a minimum.

#### Effect of Frequency on the Dimensions of Electrical Machines

If we increase the speed of a generator while keeping the excitation current constant, the induction and the flux in the machine air gap will keep the same values. The voltage, frequency, and electromagnetic power of the generator will rise in proportion to the increase in speed. In order to keep the voltage across the generator terminals constant, it is necessary to decrease the number of armature conductors while keeping the current density unchanged, and to increase the armature cross section in proportion to the speed.

Thus, in the case given, the generator will develop greater power at a higher frequency for the same voltage. In our example, the values of current density in the excitation and armature windings, the line load, and the magnetic-circuit load (magnetic induction) remain unchanged and, consequently, so does the utilization factor  $\sigma = k_0 AB_\delta$ ;



in this case there will be an increase in the specific steel and copper losses. It is possible to increase electromagnetic power and to decrease relative volume and weight by increasing speed, which corresponds to an increase in the armature-emf frequency.

What we have discussed applies in equal degree to DC and AC machines. In machines, we are concerned with increasing the emf frequency in the armature-winding sections.

Clearly, it is not always possible to increase the speed  $n$ , since it is limited by the mechanical strength of machine rotating elements and by the operating efficiency of bearings. If we must keep the speed constant, it is possible to raise the frequency by increasing the number of poles.

If we increase the frequency by increasing the number of poles for a given armature diameter  $D$ , length  $l$ , and speed  $n$  there will be a decrease in the pole spacing and, consequently, in the current per pole, given the same value of induction in the air gap ( $B_\delta = \text{const}$ ); the specific copper and iron losses will rise and the degree to which the active zone is filled with copper will decrease.

Owing to the decrease in the flux per pole, the heights of the center sections of the armature core and yoke will decrease. This in turn will lead to a decrease in the machine outside diameter and an increase in the internal diameter, provided the decrease in the heights of the center portions is not limited by mechanical-strength considerations.

In view of this, we may state that if the speed remains unchanged, an increase in the frequency of synchronous and induction machines can lead to a decrease in the relative volume and weight of the machine only to the limited degree to which it is advantageous to increase the number of poles.

In studying the effect of frequency, we make use of relative magnitudes, indicated by the symbol "\*" while quantities referring to the initial frequency carry the subscript "0". Then the expressions in relative units needed for further analysis will take the following form where  $\dot{S}_e^* = 1$ .

The armature diameter is

$$\dot{D} = \sqrt[3]{\frac{\dot{p}}{\dot{n}\dot{\lambda}}},$$

where  $\dot{\lambda} = \lambda/\lambda_0 = \dot{l}/\dot{\tau}$  is a structural factor.

The pole pitch is

$$\dot{\tau} = \frac{\dot{D}}{\dot{p}} = \sqrt[3]{\frac{1}{\dot{n}\dot{\lambda}\dot{p}^2}} = \sqrt[3]{\frac{1}{\dot{n}\dot{\lambda}\dot{f}\dot{p}}}.$$

The peripheral speed is

$$\dot{v} = \dot{D}\dot{n} = \sqrt[3]{\frac{\dot{n}^2\dot{p}}{\dot{n}\dot{\lambda}}} = \sqrt[3]{\frac{\dot{n}\dot{f}}{\dot{n}\dot{\lambda}}}.$$

The machine length is

$$\dot{l} = \frac{1}{\dot{n}\dot{D}^2} = \sqrt[3]{\frac{\dot{\lambda}^2}{\dot{n}\dot{p}^2}} = \sqrt[3]{\frac{\dot{\lambda}^2}{\dot{n}\dot{f}\dot{p}}}.$$

Armature volume, using the bore diameter, is

$$\dot{L}\dot{\lambda}\dot{l} = \frac{1}{\dot{n}}.$$

where

$$\dot{p} = \frac{p}{p_0}, \quad \dot{n} = \frac{n}{n_0}$$

etc.

Since it is possible to vary the frequency by changing the number of poles or the speed, we shall consider these two methods below.

1. Let  $\dot{p} = \dot{f}$  and  $\dot{n} = 1 = \text{const}$ ; three variations are then possible.

a) The armature diameter and peripheral speed remain unchanged, while the pole pitch varies inversely with the frequency, i.e.,

$$\dot{D} = \dot{v} = 1; \quad \dot{\tau} = \dot{f}^{-1}.$$

In this case the relationships

$$\dot{D}i = i = \frac{1}{f} \text{ and } \dot{\lambda} = \frac{i}{f} = \frac{1}{f^2}.$$

will hold.

b) The armature diameter and peripheral speed increase in proportion to the frequency, while the pole pitch remains unchanged, i.e.,

$$\dot{D} = \dot{v} = f \text{ and } \dot{i} = 1.$$

In this case, the equations

$$\dot{D}i = \frac{1}{f} \text{ and } i = \frac{1}{f^2}.$$

will hold.

c) The armature diameter and peripheral speed increase, while the pole pitch is decreased so that the optimum value of the structural factor remains unchanged, i.e.,

$$\dot{\lambda} = \dot{p} = f, \\ \dot{D} = \dot{v} = \sqrt{\frac{f^{1-\alpha}}{f}} \text{ and } \dot{i} = \sqrt{\frac{1}{f^{2+\alpha}}}.$$

In this case

$$\dot{D}i = \frac{1}{f} \text{ and } i = \sqrt{\frac{1}{f^{2+\alpha}}}.$$

2. Let  $\dot{n} = \dot{f}$  and  $\dot{p} = 1$ ; then three variations also are possible.

a) The peripheral speed remains unchanged, while the armature diameter and pole pitch are decreased in proportion to the increase in frequency, i.e.,  $\dot{v} = 1$  and  $\dot{D} = \dot{\tau} = \dot{f}^{-1}$ .

In this case, it turns out that

$$\dot{D}i = \frac{1}{f}, \quad i = \frac{f}{f} \text{ and } \dot{\lambda} = \frac{f^2}{f}.$$

b) The armature diameter and pole pitch remain unchanged, while the peripheral speed rises in proportion to the frequency, i.e.,

$$\dot{D} = \dot{i} = 1 \text{ and } \dot{v} = f.$$

Consequently,

$$\dot{D}^2 l - l = \dot{l} = \frac{1}{\dot{f}}.$$

c) The diameter and pole pitch are decreased, while the peripheral speed rises in such fashion that the structural factor retains its optimum value, i.e.,

$$\dot{\lambda} = \dot{p} = 1, \quad \dot{D} = \dot{l} = \sqrt[3]{\frac{1}{\dot{f}}}, \quad \dot{v} = \sqrt[3]{\frac{\dot{p}^2}{\dot{f}}},$$

$$\dot{D}^2 l = \frac{1}{\dot{f}} \text{ and } \dot{l} = \sqrt[3]{\frac{1}{\dot{f}}}.$$

During design, we must attempt to ensure that the structural factor will have the optimum value, equaling  $\dot{\lambda} = \dot{p}^{\alpha}$ . Cases may occur, however, in which this cannot be done owing to considerations of mechanical strength or predetermined machine dimensions.

In our future examinations of the effect of frequency on machine dimensions, we shall consider all of the listed methods for varying the frequency.

The basic design equation for electromagnetically excited electrical machines is

$$\frac{D^2 l}{S_p} = \frac{1}{\epsilon n},$$

in which machine volume is determined from bore diameter, and the effect of frequency on electrical-machine size is not reflected.

In order to allow for the effect of frequency on machine size, we use an equation of the form

$$\frac{D^2 l}{S_p} = \frac{k^2}{\epsilon n}, \quad (1.7)$$

which may be considered to be the basic design equation for electrical machinery, determining machine volume from the outside diameter. This last expression accurately reflects the weight and technological peculiarities of an electrical machine, since the weight, installed dimensions, and production tooling are basically determined by machine outside diameter rather than by bore diameter.

It is easily shown that

$$\xi = \frac{D_n}{D} = \frac{a}{p} + \sqrt{1 + b \frac{A \cdot n}{j \cdot \sigma}} \quad (1.8)$$

where

$$a = \frac{\alpha'}{2\pi} \frac{B_\delta}{k_{a.s} B_{c2}} \text{ and } b = \frac{\pi}{15} \frac{10^{-4}}{k_{a.s}}$$

— for external-armature electrical machines;

$$a = \frac{\alpha'}{2\pi} \frac{l}{l_s} \frac{B_\delta}{B_{c1}} k_s; \text{ and } b = \frac{\pi}{15} \frac{10^{-4}}{k_{a.s.v}}$$

— for internal-armature electrical machines;  $S_e$  is the electromagnetic power;  $\sigma = k_o AB_\delta$  is the machine utilization factor;  $A$  and  $j$  are the linear load, amp/cm and current density, amp/mm<sup>2</sup>. For internal-armature machines,  $A$  corresponds to  $A_v = 2\omega_v I_v / \tau$  amp/cm, and  $j = j_v$  is the current density in the excitation winding;  $B_\delta$ ,  $B_{s.ya}$ , and  $B_{s1}$  are the magnetic inductions in the gap and in the armature and yoke cores;  $k_{a.s.ya}$  and  $k_{a.s.v}$  are the utilization factors for the active layer of copper in the armature and excitation winding, respectively;  $k_o$  and  $k_{z.s}$  are the dispersion factor and the steel fill-factor for the armature core;  $\alpha'$  is the design pole span;  $n$  and  $v$  are the angular (rpm) and peripheral (m/sec) speeds;  $D$  and  $l$  are the armature bore diameter and design length;  $D_n$  and  $l_{ya}$  are the machine external diameter and the yoke length ( $l \approx l_{ya}$ ).

The quantities  $a$  and  $b$  as well as the ratio  $A/j$  are nearly constant for any member of a series of electrical machines actually studied. In order to simplify the analysis to come, we use relative quantities and let  $b(A/j) = b_2 \approx \text{const.}$

Allowing for this, the expression for the relative external machine volume will take the form

$$\dot{D}_n^2 j = \frac{D_n^2 l}{D_{n0}^2 l_0} = \frac{\dot{\xi}^2}{\dot{\xi}_0^2} = \frac{\dot{\xi}^2}{\dot{A} \dot{B}_{s1} \dot{n}} \quad (1.9)$$

Since  $n = n_0 \frac{\dot{n}}{\dot{n}_0}$ ,  $v = v_0 \frac{\dot{v}}{\dot{v}_0}$ ,  $p = p_0 \frac{\dot{p}}{\dot{p}_0}$ , etc., the relative value  $\xi^*$  may be represented as

$$\xi = \frac{1}{\dot{p}} \frac{a + p_0 \dot{p} \sqrt{1 + b_2 \frac{n_0}{v_0} \frac{\dot{n}}{\dot{v}}}}{a_0 + p_0 \sqrt{1 + b_{20} \frac{n_0}{v_0}}} \quad (1.10)$$

If  $a = a_0$  and  $b_2 = b_{20}$ ,

$$\xi = \frac{a + p_0 \dot{p} \sqrt{1 + b' \frac{n}{v}}}{\Delta_0 \dot{p}} \quad (1.11)$$

where

$$\Delta_0 = a + p_0 \sqrt{1 + b'}; \quad b' = b_2 \frac{n_0}{v_0}.$$

In the last expression, we substitute the relative frequency  $\dot{f}$  for the relative number of pole pairs  $\dot{p}$ , and make use of the fact that

$$\dot{p} = \frac{\dot{f}}{\dot{n}}, \text{ and } \frac{\dot{n}}{\dot{v}} = \sqrt[3]{\frac{\dot{n}^2 \lambda}{\dot{f}}},$$

we then obtain

$$\xi = \frac{\dot{n}}{\Delta_0} \left( \frac{a}{\dot{f}} + \frac{p_0}{\dot{n}} \sqrt{1 + b' \sqrt[3]{\frac{\dot{n}^2 \lambda}{\dot{f}}}} \right). \quad (1.12)$$

The utilization factor of the apparent specific peripheral force  $\sigma$  basically depends on the power and duty conditions of the machine, the commutation, and overload capability, the cooling system, and class of insulation.

For machines of the same power and type designed for different frequencies, the magnitude of  $\sigma$  depends on the diameter and pole pitch (number of poles), i.e., on the method used to increase the frequency.

If the frequency is increased by an appropriate increase in the number of poles while the speed and diameter are held constant (by means of a decrease in the pole pitch), then the copper fill factor for the active inductor layer ( $k_{a.s.v}$ ) will decrease, leading to a

drop in the excitation magnetizing force; this makes it necessary to decrease  $\sigma$ .

If the frequency is increased by an appropriate increase in speed ( $n$ ) while the number of poles and the peripheral speed are kept constant, the diameter and pole pitch will be decreased.

In this case, there will be a decrease in the value of  $\sigma$  owing to the reduction in the interpole (intertooth) space, which will also lead to a drop in  $k_{a.s.v}$  and excitation magnetizing force.

In the cases considered, the relative value  $\sigma^*$  may (in first approximation) be represented as

$$\sigma \approx e^{-\frac{1}{2}(\frac{p}{2}-1)} = e^{-\frac{1}{2}(\frac{p}{2}-1)} < 1$$

for the first case, and as

$$\sigma \approx e^{-\frac{1}{2}(\frac{1}{2}-1)} = e^{-\frac{1}{2}(\frac{1}{2}-1)} < 1.$$

for the second case.

If the frequency is increased by increasing the number of poles while the speed and pole pitch is kept constant or by increasing the speed while holding the number of poles and the pole pitch constant, the machine utilization factor will rise owing to better utilization of the interpole space (with an increase in the number of poles, since the degree of reduction is decreased) and an improvement in cooling ( $\bar{v}^*$  rises in both cases).

Accordingly, we shall henceforth assume that

$$\sigma \approx e^{\frac{1}{2}(\frac{p}{2}-1)} = e^{\frac{1}{2}(\frac{p}{2}-1)} > 1$$

and  $\sigma^* \approx 1$ .

When the pole pitch is decreased,  $\sigma^*$  decreases, while when  $\bar{v}^*$  increases and  $\tau^*$  is held constant, it will increase.

In view of all this, the expression for the relative machine

volume must be written as

$$\dot{D}_a^2 i = \frac{\dot{n}}{\Delta_0^2} \left( \frac{a}{f} + \frac{p_0}{n} \sqrt{1 + b' \sqrt{\frac{\sigma n^2 \lambda}{\sigma n^2 \lambda}}} \right)^2. \quad (1.13)$$

An analysis of (1.13) shows that:

1) If the frequency is varied while the speed is held constant

$$\dot{n} = \dot{v} = 1,$$

then

$$\dot{D}_a^2 i = \frac{e^{j(j-1)}}{\Lambda_0^2} \left( \frac{a}{f} + p_0 \sqrt{1 + b'} \right)^2 \quad (1.14)$$

and, consequently, it is possible to determine the frequency at which the relative machine volume will be at a minimum, i.e.,

$$f_{\text{opt}} = p_{\text{opt}} = \frac{a}{2\Delta_0 p_0} \left( \sqrt{1 + 8 \frac{\Delta_0 p_0}{a\beta}} - 1 \right). \quad (1.15)$$

The existence of an over-all volume minimum is explained by the fact that as the number of poles is increased (the frequency goes up) the decrease in per-pole flux decreases the height of the armature core (the pole-wheel core), leading to a decrease in the inside diameter. At the same time, there is a decrease in the machine utilization factor and, consequently, an increase in its external volume.

Thus, at a specific value of  $\beta$  there is a frequency (number of poles) for which the machine external volume is at a minimum.

Equation (1.15) was used to plot curves for the relative optimum frequency (number of poles)  $f_{\text{opt}}^* (p_{\text{opt}}^*) = \varphi(\beta)$  for various values of  $\underline{n}$  and  $\underline{v}$  (Fig. 1.13).

The curve of  $p_{\text{opt}}^* = \varphi(\beta)$  at  $n = 6000$  rpm ( $v \approx 50$  m/sec) was plotted for an eight-pole 30-kva aircraft generator. If we assume that this generator has an optimum number of poles at  $n = 6000$  rpm, then  $\beta \approx 0.225$ . The curves for  $n = 12,000$  and  $n = 24,000$  rpm were constructed on the assumption that  $a$ ,  $b$ , and  $A/j$  remain the same, while the peripheral speed equals 50 and 100 m/sec (at  $n = 12,000$  rpm) and 50 and 200 m/sec



(for  $n = 24,000$  rpm).

If we assume that  $\beta = 0.225$ , the optimum frequency will be 520 cps at  $n = 12,000$  ( $v = 50$  m/sec), and 560 cps ( $v = 100$  m/sec); the frequency will be 680 cps at  $n = 24,000$  rpm ( $v = 50$  m/sec) and 750 cps ( $v = 200$  m/sec). Consequently, as the speed goes up ( $n$  and  $v$  increase) the value of the optimum frequency will rise.

Actually  $\beta \neq \text{const}$ , but depends on  $n$  and  $v$  (or  $D$  and  $\tau$ ), i.e., together with the curves of Fig. 1.13, the considerations given characterize only the qualitative aspect of this phenomenon – the increase in optimum frequency with increasing speed. Concrete quantitative relationships in general form can be obtained only with difficulty, and only on the basis of empirical data.

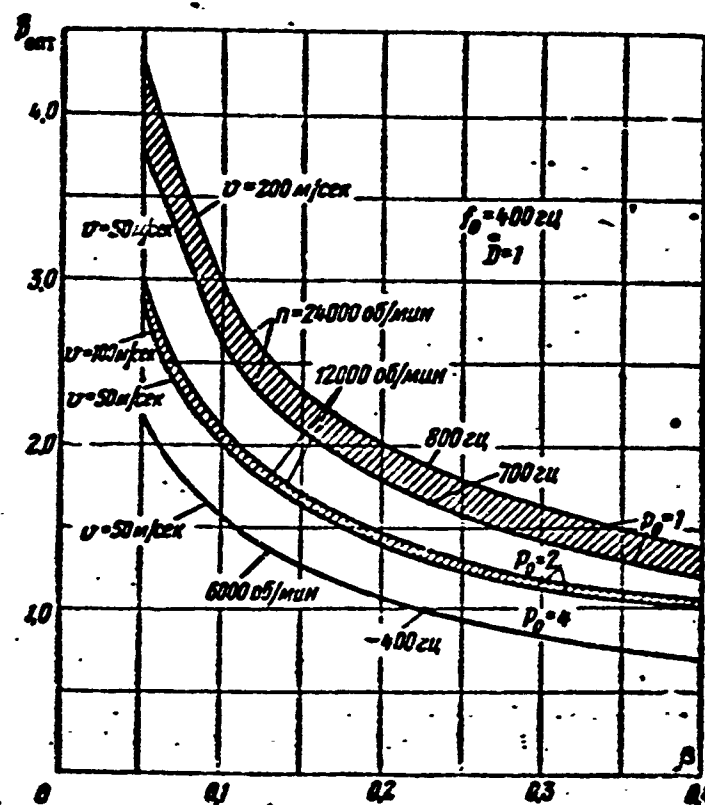


Fig. 1.13. Relative optimum frequency ( $p_{opt}^* = f_{opt}^*$ ) for a synchronous generator as a function of the coefficient  $\beta$ , speed  $n$ , and peripheral speed  $v$ . The reference curve was plotted for  $n = 6000$  rpm,  $v = 50$  m/sec,  $f = 400$  cps, and  $2p_0 = 4$ .

2) If the frequency is increased while the speed remains unchanged ( $\dot{n} = 1$ ) and  $\dot{v} = \dot{f}$  then, by (1.13)

$$\dot{B}_a^2 i \approx \frac{e^{-\frac{1}{2}(\dot{v}-1)}}{\Delta_0^2} \left( \frac{a}{\dot{f}} + p_0 \sqrt{1 + b' \dot{f}^{-1}} \right)^2, \quad (1.16)$$

and the relative machine volume decreases monotonically as the frequency rises until the decrease in armature-core height reaches the limit imposed by mechanical-strength considerations.

3) Where the frequency is raised by increasing the number of poles and the structural-factor variation follows the law  $\dot{\lambda} = \dot{p}^\alpha = \dot{f}^\alpha$ ,

$$\dot{p} = \dot{f}, \dot{n} = 1, \quad \frac{\dot{n}}{\dot{v}} = \sqrt{\frac{\dot{f}}{\dot{f}^{1-\alpha}}}$$

and

$$\dot{B}_a^2 i \approx \frac{1}{\Delta_0^2} \left( \frac{a}{\dot{f}} + p_0 \sqrt{1 + b' \sqrt{\frac{\dot{f}}{\dot{f}^{1-\alpha}}}} \right)^2, \quad (1.17)$$

If we assume that  $\dot{\sigma} \approx 1$  and  $\alpha = 0.5$  (for salient-pole synchronous machines), then

$$\dot{B}_a^2 i \approx \frac{1}{\Delta_0^2} \left( \frac{a}{\dot{f}} + p_0 \sqrt{1 + b' \dot{f}^{-1/2}} \right)^2. \quad (1.17a)$$

4) If we raise the frequency and hold the number of poles and peripheral speed constant, i.e.,  $\dot{n} = \dot{f}$  and  $\dot{v} = 1$ , then

$$\dot{B}_a^2 i \approx \frac{e^{\frac{1}{2}(\dot{v}-1)}}{\Delta_0^2 \dot{f}} (a + p_0 \sqrt{1 + b' \dot{f}})^2 \quad (1.18)$$

and, consequently, it is possible to determine the frequency at which the machine relative volume is at a minimum. Unfortunately, the equation for the optimum frequency takes the form

$$\dot{f} \sqrt{1 + b' \dot{f}} + A_1 \dot{f}^2 + A_2 \dot{f} + A_3 \sqrt{1 + b' \dot{f}} - 1 = 0,$$

i.e., it cannot be solved in the general form.

Here  $A_1$ ,  $A_2$ , and  $A_3$  are constants.

5) If the frequency is raised while the number of poles is held constant and  $\dot{n} = \dot{v} = \dot{f}$ , then

$$\dot{B}_a^2 i \approx \frac{1}{\dot{f}} \approx \frac{1}{\dot{f}}, \quad (1.19)$$

TABLE 1.5

Effect of Various Methods of Changing Frequency on the Size of Electrical Machines (Relative Magnitudes)

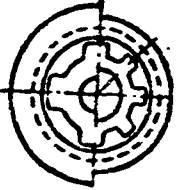
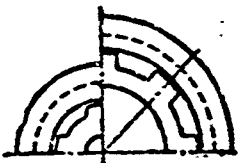
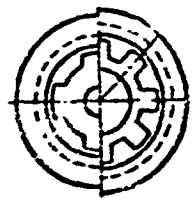
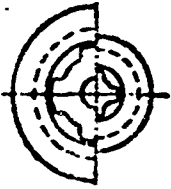


1 Способ изменения частоты	2 Эскиз	$\sigma = AB_1$	$D^2 i = \frac{1}{\sigma n}$	$i = \frac{1}{\sigma n D^2}$ $\lambda = \frac{i}{\tau}$	$k_{a.c.s.} = \frac{S_n}{S_a}$	$D_a^2 i = \frac{n}{\Delta_0^2} \left( \frac{a}{f} + \frac{p_0}{n} \sqrt{1 + b' \frac{n}{v}} \right)^2$
$\dot{p} = \dot{f}$ $\dot{n} = \dot{v} = 1$ $\dot{D} = 1$ и $\dot{\tau} = \frac{1}{f}$ 3		$\sigma = e^{-p(\dot{f}-1)} = e^{-p(\dot{f}-1)} < 1$	$D^2 i = e^{p(\dot{f}-1)} > 1$ при $\dot{f} > 1$ 4	$i = e^{p(\dot{f}-1)}$ $\lambda = \dot{f} e^{p(\dot{f}-1)}$	$k_{a.c.s.} < 1$ $\frac{S_n}{S_a} = 1$	$D_a^2 i = \frac{e^{p(\dot{f}-1)}}{\Delta_0^2} \left( \frac{a}{f} + p_0 \sqrt{1 + b' f^{-1}} \right)^2$
$\dot{p} = \dot{f}$ $\dot{n} = 1$ и $\dot{v} = \dot{f}$ $\dot{D} = \dot{f}$ и $\dot{\tau} = 1$ 3		$\sigma = e^{p(\dot{f}-1)} > 1$	$D^2 i = e^{-p(\dot{f}-1)} < 1$ при $\dot{f} > 1$ 4	$i = \dot{f}^{-2} e^{-p(\dot{f}-1)}$ $\lambda = \dot{f}^{-2} e^{-p(\dot{f}-1)}$ и $\lambda = \dot{f}^{-2} e^{-p(\dot{f}-1)}$	$k_{a.c.s.} > 1$ $\frac{S_n}{S_a} \approx \dot{f}^{-1}$	$D_a^2 i = \frac{e^{-p(\dot{f}-1)}}{\Delta_0^2} \left( \frac{a}{f} + p_0 \sqrt{1 + b' f^{-1}} \right)^2$
$\dot{p} = \dot{f}$ , $\dot{n} = 1$ $\dot{D} = \dot{v} = \sqrt[3]{\frac{\dot{f}-1}{\dot{f}}}$ $\dot{\tau} = \sqrt[3]{\frac{\dot{f}-1}{\dot{f}}}$		$\sigma$ — изменяется мало 5	$D^2 i = \frac{1}{\sigma}$	$i = \sqrt[3]{\frac{\dot{f}-2(1-\sigma)}{\dot{f}}}$ $\lambda = \dot{f}$		$D_a^2 i = \frac{1}{\Delta_0^2} \left( \frac{a}{f} + p_0 \sqrt{1 + b' f^{-1}} \right)^2$ при $\sigma = 0,5$ 4
$\dot{n} = \dot{f}$ $\dot{p} = \dot{v} = 1$ $\dot{D} = \dot{\tau} = \frac{1}{f}$		$\sigma = e^{-p\left(\frac{1}{f}-1\right)} = e^{-p(\dot{f}-1)} < 1$	$D^2 i = \frac{e^{p(\dot{f}-1)}}{f}$	$i = \dot{f} e^{p(\dot{f}-1)}$ $\lambda = \dot{f} e^{p(\dot{f}-1)}$	$k_{a.c.s.} < 1$ $\frac{S_n}{S_a} \approx \dot{f}$	$D_a^2 i = \frac{e^{p(\dot{f}-1)}}{\Delta_0^2 f} \left( a + p_0 \sqrt{1 + b' f^{-1}} \right)^2$
$\dot{n} = \dot{f}$ $\dot{p} = 1$ и $\dot{v} = \dot{f}$ $\dot{D} = \dot{\tau} = 1$		$\sigma \approx 1$	$D^2 i \approx \frac{1}{f}$	$i = \dot{f}^{-1}$ $\lambda = \dot{f}^{-1}$	$k_{a.c.s.} = 1$ $\frac{S_n}{S_a} = 1$	$D_a^2 i \approx \dot{f}^{-1}$

TABLE 1.5 (continued)

1 Способ изменения частоты	2 Эскиз	$\dot{\omega} = \dot{\omega} B_0$	$\dot{D}^2 i = \frac{1}{\dot{\omega} n}$	$\dot{i} = \frac{\dot{\omega}}{\dot{\omega} n \dot{D}^2}$ $\dot{\lambda} = \frac{\dot{i}}{\dot{\omega}}$	$\frac{k_{\text{в.с.с.}}}{S_n} = 1$	$\dot{D}_n^2 i = \frac{\dot{n}}{\Delta_0^2 \dot{\omega}} \left( \frac{a}{f} + \frac{p_0}{n} \sqrt{1 + b' \frac{\dot{n}}{\dot{\omega}}} \right)^2$
$\dot{p} = 1$ $\dot{n} = \frac{f}{\dot{\omega}}$ $\dot{\omega} = \sqrt{\frac{f}{\dot{\omega}}}$ $\dot{b} = \dot{\omega} = \sqrt{\frac{f}{\dot{\omega}}}$		$\dot{\omega} \approx 1$	$\dot{D}^2 i = \frac{1}{\dot{\omega} f}$	$\dot{i} = \sqrt{\frac{f}{\dot{\omega}}}$ $\dot{\lambda} = 1$		$\dot{D}_n^2 i \approx \frac{f^{-1}}{\Delta_0^2 \dot{\omega}} \left( a + p_0 \sqrt{1 + b' f^{1/2} / \dot{\omega}} \right)^2$

In all variations,  $\dot{A} \approx 1$ ,  $\dot{B}_0 \approx 1$ ,  $\dot{S}_m = 1$ ,  $\dot{\Phi}$  and  $\dot{\omega}$  vary so that  $\dot{E} = 1$ .

1) Method of changing frequency; 2) drawing; 3) and; 4) where; 5) varies little.

i.e., the relative machine volume will be inversely proportional to the frequency.

6) For the case in which the frequency is raised by increasing the rotational speed while the structural factor is held constant, i.e.,  $n^* = f^*$ ,  $p^* = 1$ , and  $\lambda^* = p^{\alpha} = 1$ ,

$$D_{\lambda}^2 i = \frac{1}{f \Delta_0^2} (a + p_0 \sqrt{1 + b' f^2})^2. \quad (1.20)$$

If we assume that  $\sigma^* \approx 1$  and  $\alpha \approx 0.5$ ,

$$D_{\lambda}^2 i \approx \frac{1}{\Delta_0^2 f} (a + p_0 \sqrt{1 + b' f^{1/3}})^2. \quad (1.20a)$$

For the sake of clarity, we have summarized in Table 1.5 the equations corresponding to the various ways of changing the frequency.

#### General Comments

1. To each rotational speed  $n$  and to each  $v$  there corresponds an optimum number of poles, which also determines the optimum frequency.

2. For a given rotational speed, the optimum number of poles becomes somewhat larger as the power is increased and, consequently, the optimum frequency also rises somewhat.

3. For the rotational speeds and powers used in aviation, the optimum frequency lies in the 300-500 cps range.

As we know, frequency affects not only machine size but also the iron and copper losses. Below we shall establish the magnitude of this effect.

#### Specific Iron Losses

Iron losses appear owing to variations in the magnitude and direction of the magnetic field. Where the magnetic-field induction is distributed uniformly over the entire cross section of a steel lamination, the specific losses owing to hysteresis and eddy currents are determined from the equation

$$p_c = k_{\text{rex}} \left[ \sigma_r \frac{f}{400} + \sigma_e \left( \frac{f}{400} \right)^2 \right] \left( \frac{B_{cp}}{10^4} \right)^2 \text{ watt/kg}, \quad (1.21)$$

TABLE 1.6

Coefficients for Calculating Iron Losses

1 Марка стали	2 $\rho$ , ohm·mm <sup>2</sup> /m	3 $\sigma_v$ , watt/kg	4 $\sigma_g$ , watt/kg	5 $f = 400$ cps		8 Удельная теплопро- водность $\lambda$ , °C·cm	9 Удельный вес $\gamma_s$ , g/cm <sup>3</sup>
				6 $p_{7.5}$ , watt/kg	7 $p_{10}$ , watt/kg		
10							
334	0,35	0,5	6,50	13,0	23,0		
3340	0,35	0,47	6,90	12,0	21,0		
3340	0,20	0,47	2,24	7,0	12,0	0,25	7,65
10							
344	0,35	0,57	5,70	10,7	19,0		
344	0,20	0,57	1,86	7,2	12,5	0,20	7,55
344	0,15	0,57	1,04	6,8	11,7		
344	0,10	0,57	0,465	6,0	10,5		

Note.  $p_{7.5}$  and  $p_{10}$  are the specific losses respectively for  $B_{sr} = 7500$  gauss and  $B_{sr} = 10,000$  gauss;  $\sigma_v$  and  $\sigma_g$  are obtained by calculation, using the values of  $\Delta$ ,  $\rho$  and  $p_{10}$ .

- 1) Grade of steel; 2)  $\rho$ , ohm·mm<sup>2</sup>/m; 3)  $\sigma_v$ , watt/kg;  
 4)  $\sigma_g$ , watt/kg; 5)  $f = 400$  cps; 6)  $p_{7.5}$ , watt/kg;  
 7)  $p_{10}$ , watt/kg; 8) thermal conductivity, watt/°C·cm;  
 9) specific gravity  $\gamma_s$ , g/cm<sup>3</sup>; 10) Exxx.

where

$$\sigma_g = 26,3 \frac{\Delta^2}{f};$$

$\sigma_g$  and  $\sigma_v$  are constants for the material (Table 1.6);  $\rho$  is the electrical resistivity of the steel, ohm·mm<sup>2</sup>/m;  $\Delta$  is the lamination thickness, mm;  $V_{sr}$  and  $f$  are the peak average induction over the sheet thickness and the frequency;  $k_{mekh}$  is a coefficient allowing for mechanical working of the steel.

From the equation given it follows that

- a) the hysteresis losses are proportional to the first power of the frequency, and do not depend on the thickness of the lamination;  
 b) the losses due to eddy currents are proportional to the frequency and the second power of the lamination thickness;  
 c) iron losses due to hysteresis and eddy currents are propor-

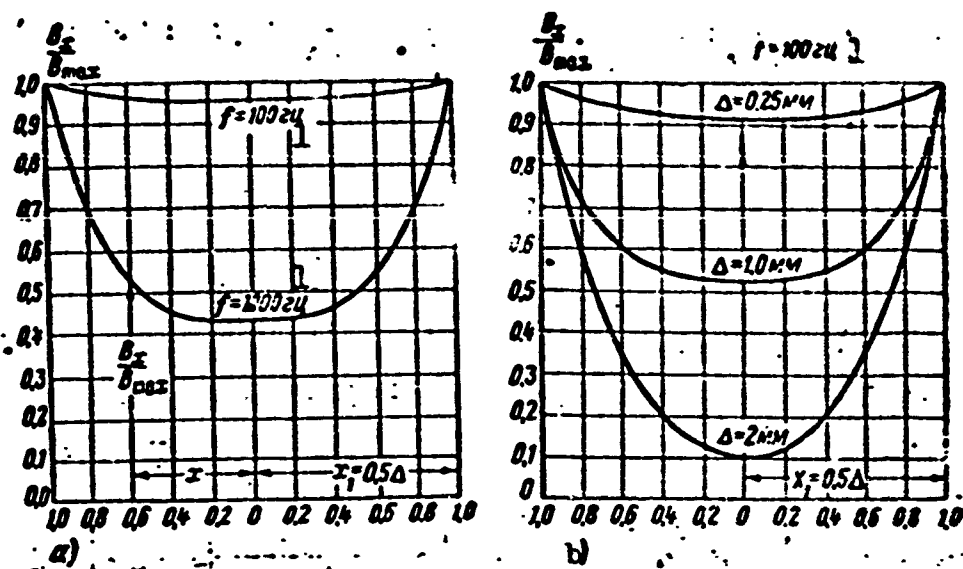


Fig. 1.14. Distribution of the relative magnetic induction over lamination thickness. a)  $f = 100$  and  $1000$  cps; b)  $f = 100$  cps, various lamination thicknesses  $\Delta$  (the induction at the surface of a lamination is taken as unity). 1) cps.

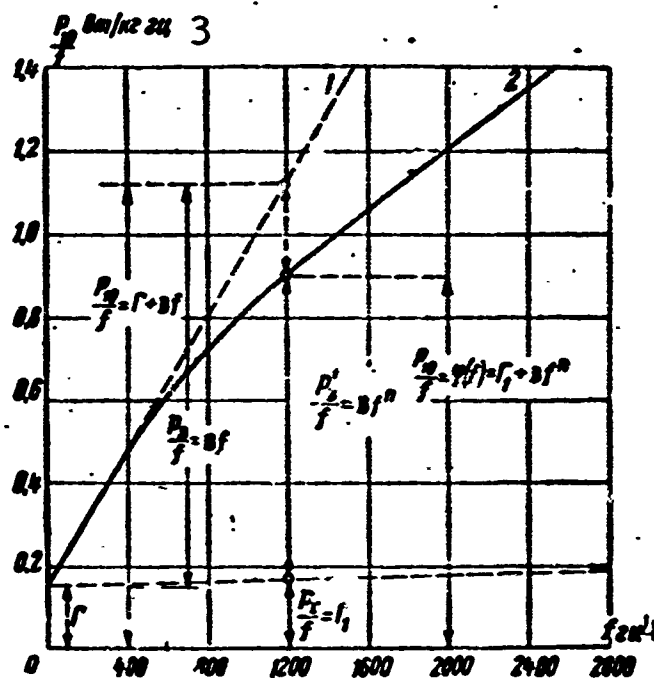


Fig. 1.15. Iron losses over a single cycle (watt/kg·cps) as a function of frequency with  $B = 10,000$  gauss and  $\Delta = 0.35$  mm. 1) Skin effect neglected; 2) skin effect taken into account (experimental data); 3)  $p_{10}/r$ , watt/kg·cps; 4)  $f$ , cps.

tional to the square of the variable-field induction.

With higher frequencies or thicker laminations, it is necessary to

allow for the eddy-current reaction, which causes the magnetic field (induction) to be distributed nonuniformly over the thickness of a steel lamination (Fig. 1.14): the maximum occurs at the lamination edges, with the minimum reached at the center; in addition, the phase difference between the flux and the excitation magnetizing force varies over the lamination thickness.

The eddy-current reaction and, consequently, the degree to which the induction is nonuniform over a lamination thickness is greater the higher the frequency and the thicker the lamination.

If we assume the mean magnetic permeability  $\mu$  to be constant, the relative induction over the thickness of a lamination will be determined by the equation

$$B_x = \frac{B_s}{B_{\max}} = \sqrt{\frac{\operatorname{ch} 2\alpha x + \cos 2\alpha x}{\operatorname{ch} \Delta_1 + \cos \Delta_1}} \quad (1.22)$$

where  $x$  is the distance from the lamination axis to the point at which the value of  $B_x$  is to be determined;

$$\Delta_1 = \alpha \Delta = 4\pi \Delta \sqrt{\frac{\mu}{1000} \frac{f}{400} \frac{1}{\rho}}$$

— is the reduced lamination thickness (an abstract quantity).

Where  $f\Delta^2 \geq 80$ , the nonuniformity of the induction distribution over the lamination thickness must be considered.

The nonuniform distribution of induction over the thickness of steel leads to a decrease in the energy lost to eddy currents, and to an increase in hysteresis losses, as shown in Fig. 1.15.

The decrease in losses due to eddy currents and the increase due to hysteresis may be allowed for with the aid of the reaction coefficients

$$\begin{aligned} k_e &= \frac{3}{\Delta_1} \frac{\operatorname{sh} \Delta_1 - \sin \Delta_1}{\operatorname{ch} \Delta_1 - \cos \Delta_1} < 1, \\ k_r &= \frac{\Delta_1}{2} \frac{\operatorname{sh} \Delta_1 + \sin \Delta_1}{\operatorname{ch} \Delta_1 - \cos \Delta_1} > 1. \end{aligned} \quad (1.23)$$



The coefficients  $k_v$  and  $k_g$  are plotted in Fig. 1.16 as functions of the reduced lamination thickness  $\Delta_1$ ; they differ substantially from unity only where  $\Delta_1 > 2$ .

The specific iron losses owing to magnetic polarity reversal, allowing for eddy-current reaction, are calculated from the formula

$$p_c = k_{\text{max}} \left[ k_r \frac{f}{400} + k_g \left( \frac{f}{400} \right)^2 \right] \left( \frac{B_{cp}}{10^4} \right) [\text{watt/kg}], \quad (1.24)$$

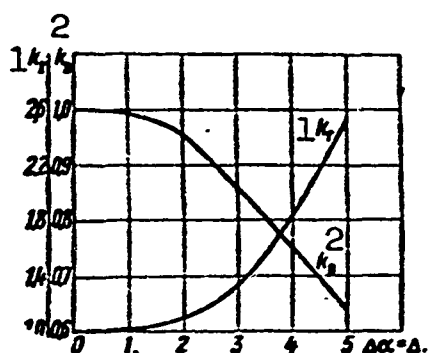


Fig. 1.16. Reaction coefficients  $k_g$  and  $k_v$  as functions of the reduced lamination thickness  $\Delta_1 = \Delta^\alpha$ . When  $\Delta_1 \geq 4$ ,  $k_v = 3/\Delta_1$ ; when  $\Delta_1 \geq 5$ ,  $k_g = 0.5\Delta_1$ . 1)  $k_g$ ; 2)  $k_v$ .

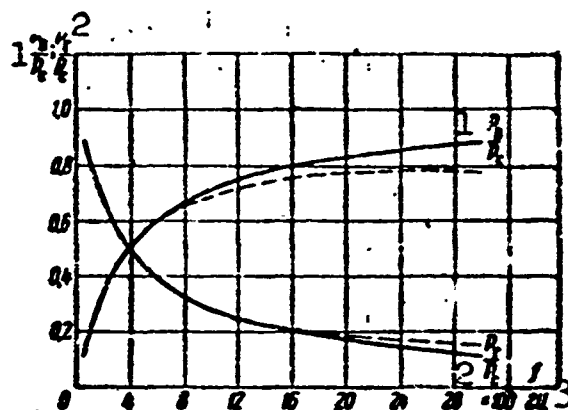


Fig. 1.17. Relative specific hysteresis losses  $p_g/p_s$  and relative specific eddy-current losses  $p_v/p_s$  as a function of frequency, neglecting eddy-current reaction; the dashed line shows the effect of eddy-current reaction. 1)  $p_v/p_s$ ; 2)  $p_g/p_s$ ; 3) cps.

At high frequencies, where the reduced lamination thickness  $\Delta_1 \geq 4$ , the reaction coefficients may be represented in the form

$$\left. \begin{aligned} k_g &= \frac{3}{\Delta_1} = \frac{0.75}{\pi \Delta} \sqrt{\frac{1000 \cdot 400}{\rho} \frac{1}{f}} \\ k_r &= \frac{\Delta_1}{2} = 2\pi \Delta \sqrt{\frac{\rho}{1000 \cdot 400} \frac{f}{1}} \end{aligned} \right\} \quad (1.25)$$

If we substitute into (1.24) the values of  $k_v$  and  $k_g$  from (1.25), we obtain a new expression for the specific iron losses at the higher frequencies and  $\Delta_1 \geq 4$ .

$$p_c = \frac{\Delta}{\sqrt{\rho}} \left( \frac{f}{400} \right)^{1.5} \left( \frac{B_{cp}}{10^4} \right)^2 \gamma_k. \quad (1.26)$$

where

$$\eta_p = 8\pi \left[ \epsilon_r \sqrt{\frac{\mu}{1000}} + \frac{2.5}{10^4} \sqrt{\frac{1000}{\mu}} \right] h_{\text{max}}$$

Thus, when the eddy-current reaction is taken into account and  $\Delta_1 \geq 4$ , the specific iron losses due to hysteresis and eddy currents are proportional to the three-halves power of the frequency and the first power of the lamination thickness.

Figure 1.17 shows the hysteresis and eddy-current losses as functions of frequency; it follows from this that as the frequency goes up, the relative losses due to hysteresis drop.

If it is desired to hold the specific losses constant as the frequency goes up, it is necessary to decrease the induction in the core, allowing for the fact that

$$f^n = \left( \frac{f}{f_0} \right)^{n'} = \left( \frac{B_0}{B} \right)^{n''} = \frac{1}{B^{n''}}$$

so that the new induction, in relative units, will be

$$B = f^{-\frac{1}{n''}}$$

here  $n' = 1.3-1.5$  and  $n'' = 1.8-2.2$ .

Aircraft direct-current machines are normally made with two to ten poles, and run at speeds of  $n = 4000-12,000$  rpm. The magnetic-polarity change frequency in the armature of an aircraft direct-current machine will then reach 600-800 cps, while similar general-purpose machines have magnetic-polarity reversal frequencies of the order of 30-40 cps, i.e., 15-20 times less.

In general-purpose direct-current machines, the specific armature-core losses (steel E11,  $\Delta = 0.5$  mm) equal 2-4 watt/kg, while in aircraft machines of similar power (steel E34,  $\Delta = 0.35$  mm) they reach 50-60 watt/kg.

The specific core losses in alternating-current machines at

frequencies of 400-500 cps are 15-20 times those encountered in general-purpose machines.

### Active Weight and Losses in Armature Core

If we assume that the maximum induction in the armature core  $B_{ya}$  equals the induction in the center section of the armature teeth  $B_{z.sr}$ , the armature core losses may be represented by the equation

$$P_c = p_c G_c = p_{400} \left( \frac{f}{400} \right)^{\alpha} \left( \frac{B_c}{10^4} \right)^{\alpha} G_c \text{ watts} \quad (1.27)$$

where

$$B_c = B_s = B_{acp};$$

$p_{400}$  are the specific core losses  $f_0 = 400$  cps and  $B_s = 10^4$  gauss;  $G_s$  is the weight of active steel in the armature, kg.

The weight of the active armature steel is determined from the expression

$$G_c = D^2 k_c, \quad (1.28)$$

where

$$k_c = \frac{\pi k_{ac} \gamma_c}{4} \left[ \left( \frac{D_n}{D} \right)^2 - \frac{S_n}{S_s} - 1 \right] \quad (1.29)$$

and

$$k_c = \frac{\pi k_{ac} \gamma_c}{4} \left[ 1 - \frac{S_n}{S_s} - \left( \frac{d}{D} \right)^2 \right]. \quad (1.29a)$$

for external-armature and internal-armature machines, respectively.

Here  $D_n$  is the external armature diameter of an internal-pole machine;  $S_{ya} = \pi D^2/4$  is the armature cross section, using the bore diameter;  $S_p = z_p h_p b_p$  is the cross section of all armature slots;  $h_p$  and  $b_p$  are the slot height and width;  $z_p$  is the number of armature slots;  $\underline{l}_s = k_{z.s} \underline{l}$  and  $\gamma_s$  are the length and specific gravity of the armature steel;  $\underline{d}$  is the armature inside diameter for an external-pole machine;  $k_{z.s}$  is the core fill factor.

Allowing for the fact that

$$D^2 l = \frac{S_p}{\pi n}$$

the equation for the weight of steel may be represented as

$$C_c = \frac{S_p k_c}{\pi n} \text{ and } \frac{G_c}{S_p} = \frac{k_c}{\pi n} \quad (1.30)$$

The ratio of the cross section of all armature slots to the cross section of the machine as measured for the bore diameter equals

$$\frac{S_a}{S_p} = \frac{4 S_n}{\pi D^2} = b_1 \frac{A}{j} \frac{n}{v} \quad (1.31)$$

where

$$b_1 = \frac{\pi \cdot 10^{-4}}{15 k_{2.2}} \quad D = \frac{6000 v}{\pi n}$$

and

$$S_n = \frac{S_{M.2}}{k_{2.2}} = \frac{\pi D}{k_{2.2}} \frac{A}{100 j} \quad (1.32)$$

Since  $\frac{a}{D} = \sqrt{1 - b \frac{A}{j} \frac{n}{v} - \frac{a}{p}}$ , we may use the ratio  $D_n/D$  from (1.8) and the ratio  $S_p/S_{ya}$  from (1.31), and obtain on the basis of (1.30)

$$k_c = \frac{\pi k_{2.2} \gamma_c}{4} \left[ \left( \frac{a}{p} + \sqrt{1 + b \frac{A}{j} \frac{n}{v}} \right)^2 - \left( 1 + b_1 \frac{A}{j} \frac{n}{v} \right) \right] \quad (1.33)$$

or

$$k_c = \frac{\pi k_{2.2} \gamma_c}{4} \left[ - \left( \frac{a}{p} - \sqrt{1 - b \frac{A}{j} \frac{n}{v}} \right)^2 + \left( 1 - b_1 \frac{A}{j} \frac{n}{v} \right) \right] \quad (1.33a)$$

for external-armature and internal-armature machines, respectively.

Where  $S_e = 1$ , the weight of active armature steel may be represented in relative units as

$$\dot{G}_c = \frac{k_c}{\pi n} \quad (1.34)$$

taking (1.30) into account.

In investigating actual types of electrical machines, it is possible to assume that  $a$ ,  $b$ , and  $b_1$  remain nearly unchanged. As is clear from (1.30) and (1.34) the speed ( $n$  and  $v$ ), number of poles, and

electromagnetic load have a direct effect on the relative weight of the armature steel.

The frequency does not enter into Expressions (1.30) and (1.34); a change in frequency, however, as we have already said, may be accomplished (in the limiting cases) by increasing either the number of poles or the rotational speed.

With the first method, by increasing the number of poles while holding the speed ( $n$  and  $v$ ) constant, we decrease the height of the armature core (pole wheel) and  $k_s$  and, consequently, the relative weight of steel  $G_s/\dot{S}_e$  as well.

With the second method, where we increase the rotational speed ( $n$  and  $v$ ) while keeping the same number of poles and the same machine diameter,  $k_s$  does not change in value, while the relative weight of armature steel drops in direct proportion to the increase in frequency.

Thus, if in first approximation we assume, to simplify the analysis, that electromagnetic loads  $\sigma^* = \frac{AB}{\delta}$  remain constant when the frequency changes, the frequency variation will have no direct effect on the relative armature steel weight.

The weight of the armature steel varies owing to a change in either the number of poles or the rotational speed. It should be noted that the effect of a change in the number of poles on the relative armature-steel weight is slight, especially when we consider that when the number of poles increases,  $\sigma$  decreases while the height of the armature core cannot go below some specific value owing to mechanical-strength considerations.

Taking (1.27) and (1.30) into account, we may write an expression for the relative armature-steel losses in the general case:

$$\frac{P_c}{S_e} = p_{400} \left( \frac{f}{400} \right)^x \left( \frac{B_c}{10^4} \right)^{x'} \frac{k_c}{sn} \quad (1.35)$$

Taking (1.35) into account, the armature-steel losses in relative units may be represented as

$$\dot{P}_c = \dot{f}^n \dot{B}_c^{\frac{n}{v}} \frac{\dot{k}_c}{\dot{a}^{\frac{n}{v}}}, \quad (1.36)$$

where

$$\dot{k}_c = \frac{a^2 \pm 2ap_0 \dot{p} \sqrt{1 \pm b' \frac{\dot{n}}{\dot{v}} \pm \dot{p}^2 \frac{\dot{n}}{\dot{v}} p_0^2 (b' - b'_1)}}{\dot{p}^2 p_0};$$

here

$$p_0 = a^2 \pm 2ap_0 \sqrt{1 \pm b' \pm p_0^2 (b' - b'_1)};$$

$$b'_1 = b_1 \frac{A}{f} \frac{n_0}{v_0}; \quad b' = b \frac{A}{f} \frac{n_0}{v_0}$$

(the "plus" sign applies to an external armature and the "minus" sign to an internal armature).

Let us clarify the nature of the relationship between  $\dot{G}_s^*$  and  $\dot{P}_s^* = \varphi(\dot{f}^*)$  for the various ways of increasing the frequency.

If  $\dot{p}^* = \dot{f}^*$ ,  $\dot{n}^* = 1$ , and  $\dot{v}^* = 1$ , then

$$\dot{k}_c = \frac{a^2 \pm 2ap_0 \dot{f} \sqrt{1 \pm b' \pm \dot{f}^2 p_0^2 (b' - b'_1)}}{\dot{f}^2 p_0} \approx \dot{f}^{-\alpha_1} < 1.$$

Thus,  $\dot{k}_s^* < 1$  and it will decrease as the frequency goes up, i.e.,

$$\dot{G}_c = e^{-\beta_1 \dot{f}^{-\alpha_1}}; \quad \dot{P}_c = e^{-\beta_1 \dot{f}^{-\alpha_1}} \dot{B}_c^{\frac{n}{v}}. \quad (1.37)$$

If  $\dot{n}^* = 1$ , while  $\dot{v}^* = \dot{p}^* = \dot{f}^*$ , then

$$\dot{k}_c = \frac{a^2 \pm 2ap_0 \dot{f} \sqrt{1 \pm b' \dot{f}^{-1} \pm \dot{f}^2 p_0^2 (b' - b'_1)}}{\dot{f}^2 p_0} \approx \dot{f}^{-\alpha_2}.$$

Consequently  $\dot{k}_s^* < 1$  and it will decrease as the frequency goes up, and what is more, it will increase more rapidly than in the first case, i.e.,  $\alpha_1 < \alpha_2$  and

$$\dot{G}_c = e^{-\beta_1 \dot{f}^{-\alpha_1}};$$

$$\dot{P}_c = e^{-\beta_1 \dot{f}^{-\alpha_1}} \dot{B}_c^{\frac{n}{v}}. \quad (1.37a)$$

If  $\dot{n}^* = \dot{f}^*$ , but  $\dot{v}^* = 1$  and  $\dot{p}^* = 1$ , then

$$\dot{k}_c = \frac{a^2 \pm 2ap_0 \sqrt{1 \pm b' \dot{f} \pm p_0^2 (b' - b'_1) \dot{f}}}{p_0} \approx \dot{f}^{\alpha_3}.$$

Thus  $k_s^* > 1$  where  $f^* > 1$ , and it increases as the frequency goes up, i.e.,

$$G_c = \frac{e^{j(j-1)}}{j^{j-1}} < 1$$

and

$$P_c = e^{j(j-1)} j^{j-1} B_c^{n'}. \quad (1.37b)$$

If  $n^* = v^* = f^*$  and  $p^* = 1$ , then  $k_s^* = 1$  and, consequently, it will not depend on the frequency, i.e.,

$$G_c \approx j^{-1}$$

and

$$P_c = j^{n'-1} B_c^{n'}. \quad (1.37c)$$

Equations (1.36) and (1.37) show that where the induction ( $B_s^*$ ) remains unchanged, the iron losses depend on the frequency and core weight.

If, therefore, the frequency is raised by increasing the number of poles while holding the rotational speed ( $n^*$ ) constant, in first approximation the iron losses will increase in proportion to the  $n'$ -th power of the frequency.

Iron losses rise when the frequency is increased by increasing the rotational speed ( $n^*$ ), and the increase is proportional to the  $(n' - 1)$ -th power of the frequency, i.e., the increase is considerably less than when the speed is held constant.

### Specific Copper Losses

Specific copper losses may be found from the equation

$$p_u = \frac{\rho_t}{\gamma_m} j^2 = k_u j^2 \text{ watt/kg}, \quad (1.38)$$

where  $j$  is the current density, amp/mm<sup>2</sup>;  $\gamma_m$  is the specific gravity of copper, kg/cm<sup>3</sup>;  $\rho_t$  is the copper resistivity, ohm·mm<sup>2</sup>/m;

$$k_u = \frac{\rho_t}{\gamma_m} = \frac{235 + t_m}{129.5}. \quad (1.39)$$

$t_m$  is the temperature of the copper.

Depending on the copper temperature,  $\rho_t$  and  $k_m$  will equal:

$t_m, ^\circ\text{C}$	20	75	100	125	150	175	200	225	250
$\rho_t, 10^{-8}$	17,54	21,3	23,1	24,8	26,5	28,2	30,0	31,7	33,4
$k_m$	1,97	2,39	2,59	2,79	2,97	3,17	3,37	3,56	3,75

Depending on the cooling system, duty cycle, power, and class of insulation, in aircraft electrical machines the current density will be  $j = 8-20 \text{ amp/mm}^2$  in the armature winding, and  $j_v = 5-10 \text{ amp/mm}^2$  in the field winding, i.e., the densities will be 3-4 times greater than for similar general-purpose machines.

Since winding heating and, consequently, the resistivity  $\rho_t$  for aircraft-machine windings is greater than for general-purpose machines, the specific copper losses in aircraft electrical machines will be 10-20 times greater than for similar general-purpose machines. They can reach values of  $p_{m.ya} = 1200 \text{ watt/kg}$  in an armature winding and  $p_{m.v} = 300 \text{ watt/kg}$  in a field winding.

As the data cited imply, specific copper losses considerably exceed specific iron losses. In addition, Equation (1.38) does not allow for the increased losses in conductors carrying alternating current where the skin-effect phenomenon is observed.

If we allow for the skin effect, which increases with increasing frequency, conductor height, and copper cross section in the slot, by introducing the skin-effect coefficient we can represent the specific copper losses as

$$p_m = k_m k_{sk} f^2 \quad (1.40)$$

For a reduced conductor height  $h' \leq 1$

$$k_{sk} = 1 + \frac{9}{k} \left( \frac{b_m}{b_n} \right)^2 \frac{\pi_m - 0,2}{1 + \pi_m^2} h' \left( \frac{f}{400} \right)^2 \quad (1.41)$$



for a rectangular conductor cross section and

$$k_{z.s} = 1 + \frac{5.3}{k} \left( \frac{b_m}{b_p} \right)^2 \frac{n_m - 0.2}{1 + \alpha \delta} d^4 \left( \frac{f}{400} \right)^2 \quad (1.41a)$$

for a circular conductor cross section in the slot.

Here  $b_p$  and  $b_m$  are the slot width and total width of copper in the slot;  $h_m$  is the conductor height, cm;  $n_m$  is the total number of conductors placed one above the other along the slot height;  $\alpha$  and  $\delta$  are the temperature coefficient and the temperature rise;  $d$  is the conductor diameter, cm;

$$k = \frac{l_p}{2l}$$

where  $l_{sr}$  is the average length of the armature winding, cm;  $l$  is the length of the armature, cm.

It follows from the equation given that the additional copper losses are proportional to the square of the frequency.

Thus, an increase in frequency causes an increase in the specific iron losses that is proportional to the  $[n' = (1.3-1.5)]$ -th power of the frequency and additional copper losses that are proportional to the second power of the frequency.

Since an increase in the specific losses can lead to inadmissible heating, it is necessary to diminish such an increase by reducing the core induction and the copper current density and, consequently, the machine dimensions must be increased.

Iron and copper specific losses may be decreased by reducing lamination thickness and increasing its quality, as well as by using conductors of smaller cross section (height). The last method increases the amount of production labor required and decreases the core fill factor  $k_{z.s}$  and the slot fill factor  $k_{z.p}$ , which also entails an increase in machine dimensions.

## Weight of Copper and Losses in Armature Winding

The weight of copper in an armature winding is determined from the expression

$$G_{m.s} = V_{m.s} \gamma_m = m w q_{m.s} l_{cp.s} \gamma_m \text{ kg}, \quad (1.42)$$

where  $m$  and  $w$  are the number of phases and the number of turns in a phase;  $q_{m.s}$  is the cross-sectional area of one conductor,  $\text{cm}^2$ .

In view of the fact that the linear load

$$A = \frac{2m w I}{\pi D} = \frac{100 j V_{m.s}}{\pi D l k} \text{ amp/cm},$$

we obtain

$$G_{m.s} = \pi D l k_{in} \frac{A}{100 j} \text{ kg}, \quad (1.43)$$

i.e., the weight (volume) of the armature copper is proportional to the product of the total armature surface ( $\pi D l$ ) and the linear load, and is inversely proportional to the current density.

If we assume that

$$\pi D l = \frac{\pi S_p}{n_s D} = \frac{\pi^2 S_p}{120 \pi f \sigma} = \frac{\pi^2 S_p}{6000 \sigma v} \text{ cm}^2,$$

the relative weight of copper in an armature winding will equal

$$\frac{G_{m.s}}{S_p} \approx 1.46 \frac{A}{j} \frac{k}{\sigma v} 10^{-7} = \frac{1.46}{10^7 k_s} \frac{k}{j B_s v}, \quad (1.44)$$

where  $v$  is in m/sec,  $j$  is in amp/mm<sup>2</sup>,  $B_s$  is in gauss, and  $\sigma = k_0 A B_s$ .

It is of interest to compare the weights of armature windings (in relative units) for machines designed for different frequencies, i.e., the values of

$$\bar{G}_{m.s} = \frac{A}{j} \frac{k}{\sigma v} = \frac{k}{j B_s v}. \quad (1.45)$$

In order to make an approximate comparison of the weight and dimensions of electrical machines (designed for different frequencies), we here consider the extreme cases in which the ratio  $\lambda = \frac{1}{\tau}$  is not a function of the number of poles, but depends on the method used to

Increase the frequency. Thus, in the general case we can write:

$$\left. \begin{aligned} k &= \frac{i_{cpa}}{2i} = 1 + \frac{\eta}{\lambda} = 1 + \frac{\eta}{\lambda} \\ k &= \frac{i_{cpa}}{i} = \frac{\eta \lambda^{-1} + \lambda_0}{\eta + \lambda_0} \end{aligned} \right\} \quad (1.46)$$

a) For the special case

$$\left. \begin{aligned} k &= 1 + \frac{\eta}{k_\lambda} p^{-\alpha} = 1 + k'_\lambda p^{-\alpha} \\ k &= \frac{k'_\lambda p^{-\alpha} + p_0^\alpha}{k'_\lambda + p_0^\alpha} \end{aligned} \right\} \quad (1.46a)$$

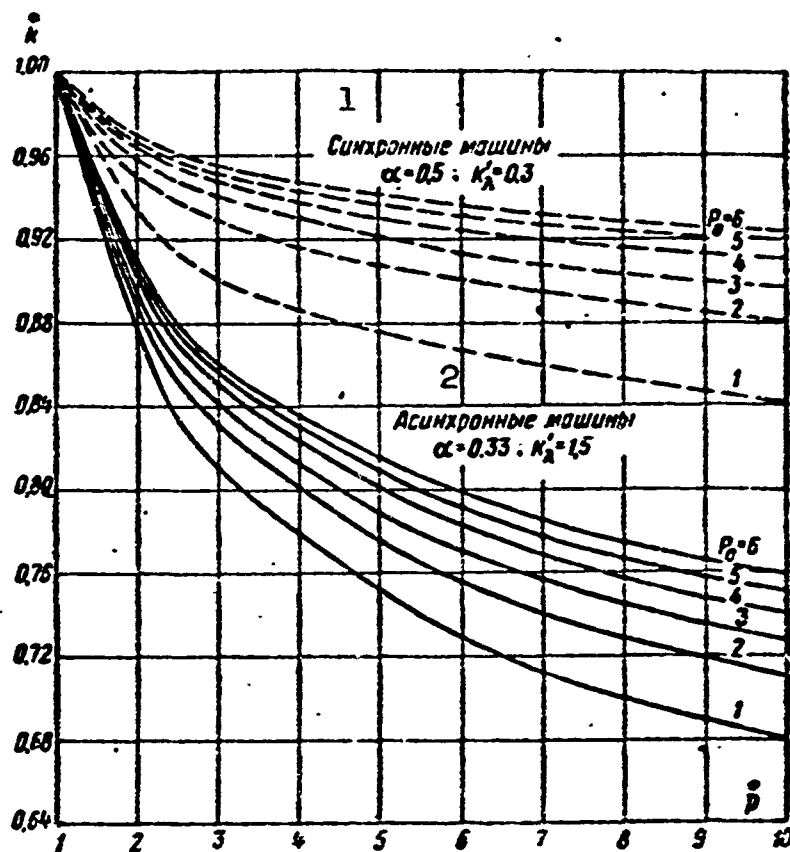


Fig. 1.18. Values of  $k^*$  as a function of the relative number of pole pairs ( $p$ ) for various values of  $p_0$ . 1) Synchronous machines; 2) induction machines.

where  $\lambda$  is determined by the empirical expression  $\lambda = k_\lambda p^\alpha$ ; with sufficient accuracy, we may assume that for synchronous machines

$$\eta = 1.5, k_\lambda \approx 0.5, k'_\lambda \approx 0.3; \alpha \approx 0.5$$

and for induction machines

$$\eta \approx 1.5, k_\lambda = 1.0, k'_\lambda \approx 1.5; \alpha \approx 0.33$$

Figure 1.18 gives a family of curves plotted for synchronous ( $k'_\lambda \approx$

$\approx 0.3$  and  $\alpha \approx 0.5$ ) and induction ( $k'_\lambda \approx 1.5$  and  $\alpha \approx 0.33$ ) machines; the family characterizes the effect of a variation in the number of poles (mean turn length) on the weight of copper in an armature winding.

Certain conclusions may be drawn from Expressions (1.44)-(1.46), e.g.:

a) in terms of the electromagnetic power of a machine, the weight of copper in the armature winding is inversely proportional to the current density, the air-gap induction, and the peripheral speed, and also depends on the number of poles (the value of  $k$ );

b) if the frequency is raised while the values of peripheral speed, current density, and gap induction are held constant, the relative weight of the armature winding will decrease somewhat, since

$$\dot{G}_{a.s} = \dot{k} < 1;$$

c) if the frequency is increased while the pole pitch remains unchanged, i.e., if the peripheral speed is increased ( $\dot{v} = \dot{f}$ ), then

$$G_{a.s} = \frac{\dot{k}}{\dot{f}}.$$

i.e., the relative weight of the armature winding decreases when  $\dot{n} = \dot{f}$  and rises when  $\dot{p} = \dot{f}$ ;

d) if the structural factor is kept constant while the frequency is increased, then  $\dot{G}_m^* < 1$ .

Thus, an increase in frequency leads to a decrease in the relative weight of copper in the armature.

Using (1.40) and (1.43), we may represent the armature-winding losses as

$$P_{a.s} = p_{a.s} G_{a.s} = \frac{p_1 k_{a.s}}{100} \pi D l A_j \text{ watts,} \quad (1.47)$$

while for the heat flow at the armature surface due to losses in the winding it turns out that

$$A_{1.s} = \frac{P_{a.s}}{\pi D l k} = \frac{p_1 k_{a.s}}{100} A_j \text{ watt/cm}^2.$$

In terms of the electromagnetic power of the machine, taking account of (1.44) we find that the armature-winding losses will be

$$\frac{P_{a.s}}{S_2} \approx \frac{1.65}{10^5} \rho_r k k_{a.m} \frac{A f}{a r} = \frac{1.65}{10^5} \frac{\rho_r k^2 k_{a.m}}{k_s} \frac{f}{B_{av}} \text{ watt/kva.} \quad (1.45)$$

The armature-winding losses in relative units occurring upon variation of frequency can be found from (1.40) and (1.46), or from (1.48); they will equal

$$\dot{P}_{a.s} = \dot{k}_{a.m} \dot{k} \frac{\dot{f}}{\dot{B}_{av}}, \quad (1.49)$$

where

$$\dot{k}_{a.m} = \frac{1 + \mu f^2 k^{-1}}{1 + \mu},$$

and

$$\mu = \frac{9 \text{ OR } 5.3}{k_0} \left( \frac{b_m}{b_n} \right)^2 \frac{n_m - 0.2}{1 + a_0} k^4 \left( \frac{f_0}{400} \right)^2.$$

It follows from (1.48) and (1.49) that:

a) in terms of the machine electromagnetic power, the armature-winding losses are directly proportional to the current density and inversely proportional to the air-gap induction and the peripheral speed; they also depend on the number of poles (mean turn length);

b) if we increase the frequency and keep the peripheral speed, current density, and gap induction the same, then  $\dot{k} < 1$  and the relative armature-winding losses  $\dot{P}_{m.ya}^* = \dot{k}_{v.m}^* \dot{k}^*$ , i.e., they vary only slightly;

c) if we increase the frequency while keeping the pole pitch constant ( $\dot{v} = \dot{f}$ ), then  $\dot{k} \geq 1$  and

$$\dot{P}_{a.s} = \frac{\dot{k}_{a.m} \dot{k}}{\dot{f}}.$$

i.e., it decreases as the frequency goes up;

d) if we vary the frequency while keeping the optimum structural factor ( $\dot{\lambda} = \dot{p}^{\alpha}$ ), then

$$\beta_{n.s} \approx \frac{k_{n.s}^2}{\sqrt{j^{1.5}}} < 1$$

or, when  $\alpha = 0.5$ ,

$$\beta_{n.s} \approx \frac{k_{n.s}^2}{j^{1.5}} < 1.$$

Thus, an increase in peripheral speed leads to a decrease in weight and armature-winding losses, while increasing the rotational speed  $n$  has no effect on the weight or armature-winding losses.

#### Weight of Copper and Losses in Field Winding

The weight (volume) of field-winding copper is determined from the equation

$$G_{n.s} = V_{n.s} \gamma_{cu} = 2p w_s l_{cp.s} q_{n.s} \gamma_{cu} \text{ kg.} \quad (1.50)$$

In view of the fact that the magnetizing force for all poles equals

$$F_s = 2p w_s I_s = 200 p w_s q_{n.s} J_s \text{ amp-turns,}$$

while the total cross-sectional area of the field winding is

$$S_{n.s} = 4p w_s q_{n.s} = \frac{2V_{n.s}}{l_{cp.s}} = \frac{2F_s}{100J_s},$$

we obtain an expression for the volume  $V_{m.v}$  and weight  $G_{m.v}$  of the field-winding copper, i.e.,

$$V_{n.s} = \frac{F_s}{100J_s} l_{cp.s} \text{ cm}^3$$

and

$$G_{n.s} = \frac{F_s \gamma_{cu}}{100J_s} l_{cp.s} = \frac{p A_s}{100J_s} l_{cp.s} \gamma_{cu} \text{ kg,} \quad (1.50a)$$

where  $A_v = 2F_v / \pi D$  is the linear load in the excitation circuit, amp/cm.

Thus, the weight (volume) of copper in a field winding is directly proportional to the product of the total excitation magnetizing force and the mean turn length, and is inversely proportional to the current density.

A more detailed analysis shows that if the quantities  $A$ ,  $B_\delta$ , and  $\delta'/\tau$  (the relative air gap) remain unchanged when the frequency varies,

then the total machine excitation magnetizing force under load is inversely proportional to the rotational speed ( $\dot{n}$ ) and directly proportional to the product of the peripheral speed ( $\dot{v}$ ) and the linear load in the excitation circuit ( $\dot{A}_V$ ) and does not depend directly on the frequency; the volume and weight of the field winding are inversely proportional to the peripheral speed of rotation, are directly proportional to the ratio ( $A_V/j_V$ ), and depend on the number of poles so that if we raise the frequency by increasing the number of poles with  $n$  and  $v = \text{const}$ , the total excitation magnetizing force will remain practically unchanged, and the weight of the field winding will decrease owing to a decrease in the mean turn length.

Field-winding losses. The specific field-winding losses are found from (1.38) and do not depend on the frequency. At the same time, the total excitation-winding losses depend on the frequency to the same degree that the weight of the copper does, that is to say we find from (1.38 and 1.50a) that

$$P_{m.s} = p_{m.s} G_{m.s} = \rho_t \frac{j_s F_s}{100} l_{cp.s} = \rho_t \frac{p A_s j_s}{50} l_p K, \quad (1.51)$$

where

$$K = \frac{l_{cp.s}}{2l_p}.$$

In like manner, we can find an expression for the excitation losses per kilovolt-ampere of electromagnetic power:

$$\frac{P_{m.s}}{S_s} = \frac{\rho_t}{\gamma_m} \frac{G_{m.s}}{S_s} j_s^2 \approx \frac{1.64}{10^5} \frac{A_s j_s}{\sigma v} K. \quad (1.52)$$

In relative units, the same expression will take the form

$$\dot{P}_{m.s} = \frac{\dot{A}_s \dot{j}_s}{\dot{\sigma} \dot{v}} \dot{K} = \frac{\dot{A}_s}{\dot{A}} \frac{\dot{j}_s}{\dot{B}_s} \frac{\dot{K}}{\dot{v}}. \quad (1.53)$$

When the frequency is increased, the specific field-winding losses remain unchanged; the relative losses and the relative weight of copper decrease where the number of poles remains constant, and they

TABLE 1.7

Specific Losses, Current Density, and Electromagnetic Loads

1 Типы генераторов	2 <u>Авиационные генераторы</u>		3 <u>Общего применения</u>	
	4 постоянный ток $P_{ном} = 1.5 \div 30 \text{ кВт}$	5 переменный ток 400 гц $S_{ном} = 15 \div 100 \text{ ква}$	6 ток	7 ток 50 гц
8 Удельные потери в $\text{вт/кг}$				
$P_c$	50 ÷ 60	100 ÷ 120	2 ÷ 4	5 ÷ 10
$P_{м.з}$	250 ÷ 1000	250 ÷ 1000		
$P_{м.з}$	150 ÷ 250	150 ÷ 250		
9 Плотность тока в $\text{а/мм}^2$				
$J_a$	10 ÷ 20	10 ÷ 20	3 ÷ 8	3 ÷ 8
$J_b$	5 ÷ 8	5 ÷ 8	2 ÷ 4	2 ÷ 4
10 Линейная нагрузка в $\text{а/см}$	200 ÷ 400	350 ÷ 450	150 ÷ 300	160 ÷ 210
11 Индукция $B_\delta$ в гс	6000 ÷ 7000		6500 ÷ 7500	
12 $n$ в об/мин	4000 ÷ 10 000	8000 ÷ 6000	1500	1500
13 Скорость $v$ в м/сек	50 ÷ 60	50 ÷ 60	30	30

1) Type of generator; 2) aircraft generators; 3) general-purpose machines; 4) direct-current,  $P_{ном} = 1.5-30 \text{ kw}$ ; 5) alternating-current, 400 cps,  $S_{ном} = 15-100 \text{ kva}$ ; 6) direct-current; 7) 50-cps alternating-current; 8) specific losses, watt/kg; 9) current density, amp/mm<sup>2</sup>; 10) linear load, amp/cm; 11) induction  $B_\delta$ , gauss; 12)  $n$ , rpm; 13) speed  $v$ , m/sec.

may even increase where the rotational speed  $n$  is constant (provided that  $\dot{v} = \dot{f} = \dot{p}$ ).

Number of phases. In general-purpose electrical systems, a three-phase alternating-current system with grounded neutral is normally employed. The single-phase alternating-current system is normally used for electrified transportation systems. Modern flying craft use single-phase and three-phase alternating-current systems.



The basic advantages of the single-phase system are.

a) simplification and weight reduction in the distribution network when the single-conductor system is used (the return conductor is the metal frame of the aircraft);

b) a reduction in the weight of transformers, and a decrease in the number of fuses and switches;

c) simplification of protective and switching apparatus.

At the same time, we should assume the following to be drawbacks to this system as compared with a three-phase system:

a) increased weight and reduced efficiency of motors and generators;

b) more complicated starting circuits and reduced motor reliability;

c) an increase in conductor weight when the two-wire system is used;

d) the high vulnerability of the system — damage to a conductor causes the system to fail.

Where a three-phase system is used with a grounded neutral at generators and motors, it is equivalent to a four-wire system, since a metal frame can be considered to be a return conductor of large cross section. In this case, a single-phase load can be connected across either the phase or line voltage. In addition, if one or two conductors are broken, three-phase motors can continue in two-phase or single-phase operation for brief periods of time. Reliability of the electrical power system is increased. A drawback of the three-phase grounded-neutral system is the presence of currents due to phase neutral pulling, which distort the line-voltage form factor.

In view of these difficulties and the several undisputed advantages of three-phase current in alternating-current systems, the three-

phase grounded-neutral system has been adopted.

### 1.5. LOSSES IN AIRCRAFT ELECTRICAL MACHINES

Aircraft electrical machines carry high electrical loads and operate at high speeds and elevated frequencies. This increases the specific losses in electrical and magnetic circuits, as well as losses owing to air friction, losses in sliding contacts and in bearings (Table 1.7).

As we know, losses may be classified as copper losses (armature, commutating-pole, compensating, and field windings)

$$P_m = P_{m.s} + P_{m.l.s} + P_{m.k.o} + P_{m.s'}$$

and as iron losses (armature core, teeth, and additional losses)

$$P_e = P_{e.s} + P_{e.t} + P_{e.a}$$

as mechanical losses (brush friction against the commutator, ventilation losses, and bearing losses)

$$P_{mech} = P_{t.s} + P_g + P_{mech}$$

and as electrical losses at a sliding contact

$$P_{s.k} = I \Delta U_{sk}$$

From the viewpoint of heating, losses may be classified in a somewhat different manner, e.g., armature losses  $P_{ya} = P_{m.ya} + P_s$ , commutator losses  $P_k = P_{t.k} + P_{e.k}$  and inductor losses:

$$P_s = P_{m.s} + P_{m.l.s} + P_{m.k.o}$$

Table 1.8 gives a sample loss distribution for direct- and alternating-current aircraft generators.

The data given show that:

a) in direct-current aircraft machines, 40-50% of all losses occur in the commutator, and 70-80% of all losses are concentrated in the armature and commutator; in general-purpose machines of identical powers, only about 10% of the losses occur in the commutator, and about 60% of the losses are concentrated in the armature and commu-

TABLE 1.8

Sample Loss Distribution (in per cent of total losses)

4 Потери	1 Род тока	2 Постоянный		3 Переменный
	5 Генераторы	6 авиационные	общего 7 применения	8 авиационные
9 В обмотке якоря		27	37	45
10 В обмотке дополнительных полюсов		8	11,5	—
11 В скользящем контакте		23	6	—
12 На возбуждение		11	15	23
13 Из них в обмотке возбуждения		6	—	16
14 В стали якоря		8	13,5	13
15 Механические потери		20	11	8,7
16 Из них на трение щеток		17	3,0	1,1
17 В коллекторе		40	9	—
18 В якоре		35	50	57
19 В коллекторе и якоре		75	59	—
20 К. п. д.		76	83	88

1) Type of current; 2) direct; 3) alternating;  
 4) losses; 5) generator; 6) aircraft; 7) general-purpose; 8) aircraft; 9) in armature winding; 10) in commutating-pole winding; 11) in sliding contact; 12) for excitation; 13) excitation losses in field winding; 14) in armature core; 15) mechanical losses; 16) mechanical losses due to brush friction; 17) in commutator; 18) in armature; 19) in commutator and armature; 20) efficiency.

tator.

b) in alternating-current aircraft machines, 55-60% of all losses are concentrated in the armature, and 15-20% in the field winding, as against 5-8% for direct-current aircraft machines.

Large commutator losses complicate the problem of cooling a machine, especially at high ambient temperatures.

Figure 1.19 gives a sample loss distribution for a 6-kw DC aircraft generator as a function of rotational speed.

An analysis of the data given shows that as generator speed increases:

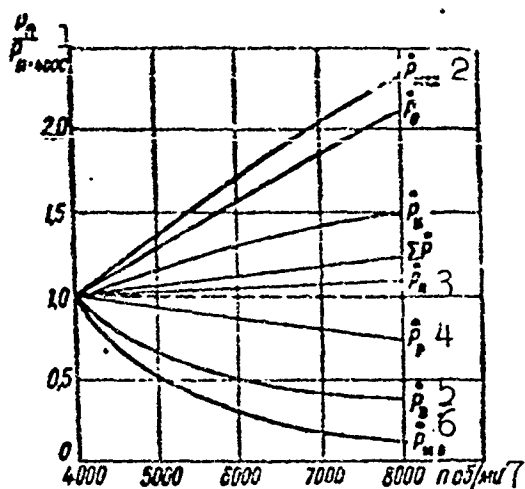


Fig. 1.19. Relative losses in direct-current aircraft generator as a function of rotational speed.  $P_0$  and  $P_{mekh}$  are the no-load and mechanical losses;  $P_{ya}$  and  $\Sigma P$  are the total armature and generator losses;  $P_r$ ,  $P_{m.v}$ , and  $P_v$  are the losses in the regulator, field winding, and in the excitation circuit;  $P_k$  are the commutator losses. 1)  $P_n/P_n = 4000$ ; 2)  $P_{mekh}$ ; 3)  $P_{ya}$ ; 4)  $P_r$ ; 5)  $P_v$ ; 6)  $P_{m.v}$ ; 7)  $P$ , rpm.

a) no-load and mechanical losses rise sharply, in almost linear fashion;

b) the total losses in the machine and the commutator losses rise considerably and also nearly linearly.

c) the total armature losses rise slightly;

d) the field-winding losses drop by a factor of 7.7 when the speed is doubled, while the total losses in the excitation circuit drop by a factor of only 2.7.

It should be noted that losses in the armature winding, in the commutating-pole winding, and the electrical losses at the sliding contact change slightly and can be considered to be independent of rotational speed.

Thus, as the rotational speed increases, the constant losses rise sharply, while the variable losses, which are proportional to the square of the current, tend to decrease. This means that maximum generator efficiency shifts towards higher loads when the rotational speed is increased. Normally, the constant and variable losses are so distributed that maximum efficiency is found in the rated-power zone at minimum speed. At higher rotational speeds and rated currents, consequently, a generator will operate at lowered efficiency. The situation is actually even worse, since a generator frequently operates at less than rated load.

It follows from what we have said that in designing variable-

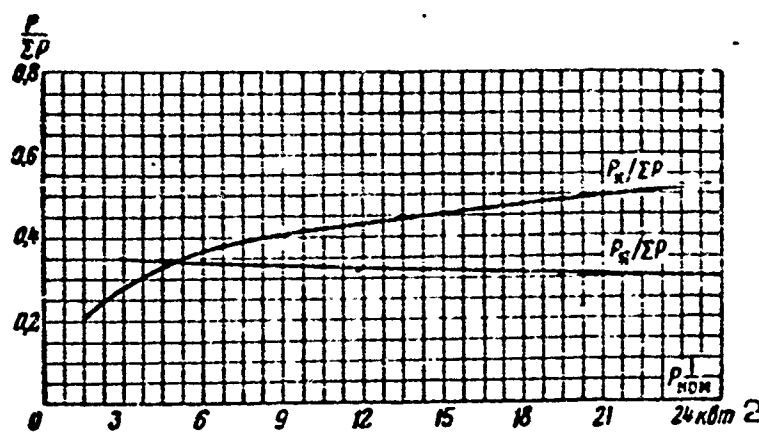


Fig. 1.20. Nature of variation in relative armature losses  $P_{ya}/\Sigma P$  and in relative commutator losses  $P_k/\Sigma P$  as a function of rated power of a DC generator ( $P_{nom}$ ). 1)  $P_{nom}$ ; 2) kW.

speed generators it is necessary to select the electromagnetic loads so that maximum efficiency occurs at a speed that corresponds to the maximum period of rated-load operation.

The main portion of the constant losses is made up of mechanical losses and, in particular, losses due to the friction of brushes against the commutator.

Figure 1.20 shows the relative armature and commutator losses as functions of rated power for aircraft DC generators; it follows from this figure that the relative commutator losses rise as the rated power increases.

Friction losses at the sliding contact might be decreased by taking the radical measure of reducing commutator diameter to a value

$$D_k = (0.7-0.8)D.$$

As has already been shown, the excitation-circuit losses are made up of the field-winding losses  $P_{m.v} = R_v I_v^2$  and the losses in the variable resistance (carbon stack) of the voltage regulator  $P_r = R_r I_v^2$ , i.e.,

$$P_s = UI_s = (R_s + R_r) I_s^2 = P_{s.s} + P_r. \quad (1.54)$$

The way in which the excitation current depends on the load current can be approximated by an expression of the form

$$I_v = I_{v.kh.kh} \left[ 1 + \frac{I_{v.nom} - I_{v.kh.kh}}{I_{v.kh.kh}} \left( \frac{I}{I_{nom}} \right)^k \right], \quad (1.55)$$

where  $I_{v.kh.kh}$  is the no-load excitation current, which does not depend on the load current;  $I_{nom}$  is the rated load current;  $I$  is the actual value of load current;  $I_v$  is the actual value of excitation current corresponding to  $I$ ;  $I_{v.nom}$  is the rated-load excitation current.

The exponent  $k$  ranges from 1.1 to 2.0 depending on the type of machine.

Taking (1.55) into account, it is possible to show that in approximation the losses in the excitation circuit and field winding consist of two components:

$P_{v.kh.kh}$ , which does not depend on the generator load but corresponds to the no-load excitation losses, and  $P_{v.nagr}$ , which depends on the second power of the load; it may also be shown that all generator losses occurring at constant rotational speed can be divided with sufficient accuracy into constant losses, not depending on the magnitude of the load, and equaling

$$P_0 = P_c + P_{mx} + P_{v.kh.kh} = k_0 I_0^0; \quad (1.56)$$

losses depending on the first power of the load and equaling

$$P_1 = P_{s.x} = k_1 I; \quad (1.57)$$

and losses depending on the second power of the load and equaling

$$P_2 = P_{s.s} + P_{s.x.s} + P_{s.x} + P_{s.nagr} = k_2 I^2. \quad (1.58)$$

Taking all of this into account, the total machine losses under surface operating conditions (subscript "0") may be represented as

$$\sum P_0 = k_0 I_0^0 + k_1 I_0 + k_2 I_0^2 = k_0 \left( 1 + \frac{k_1}{k_0} I_0 + \frac{k_2}{k_0} I_0^2 \right). \quad (1.59)$$

or

$$\sum P_0 = P_0 \left( 1 + \frac{P_1}{P_0} + \frac{P_2}{P_0} \right). \quad (1.60)$$

It is clear that the efficiency will be at a maximum when the sum of all losses per unit power is at a minimum, i.e., at the minimum value of the ratio  $\Sigma P/IU$  (with  $U = \text{const}$ ).

Consequently, it is necessary to find the product

$$\frac{d}{dl} \left( \frac{\Sigma P}{I} \right) = \frac{d}{dl} \left( \frac{P_a + P_1 + P_2}{I} \right) = -\frac{k_a}{I^2} + k_2 = 0,$$

and then

$$k_a = k_2 I^2 \text{ or } P_a = P_2. \quad (1.61)$$

Thus, the efficiency reaches its maximum when the load is such that the losses proportional to the square of the current  $P_2 = k_2 I^2$  equal the constant losses  $P_p = k_p$ .

The  $P_1 = k_1 I$  losses, which are proportional to the first power of the current, have no effect on the position of the efficiency maximum.

For a more accurate investigation, it is necessary to take into account the fact that as the load decreases there are also decreases in winding resistances owing to the temperature reduction and in the voltage drop and, consequently, in the loss at the sliding contact.

#### Effect of Cooling-Air Parameters on Loss Magnitude

Iron losses do not depend on cooling-air parameters, i.e., on altitude or flight speed.

Losses in windings, at the sliding contact, and friction losses depend on altitude and flight speed and do not remain constant when cooling-air parameters change: these parameters are temperature, pressure, and composition.

The losses vary in the following way as a function of winding temperature and current:

$$\dot{P}_{mH} = \frac{P_{mH}}{P_{m0}} = \frac{R_{mH}}{R_{m0}} \left( \frac{I_H}{I_0} \right)^2 = \frac{235 + t_{rH}}{235 + t_{r0}} I_H^2. \quad (1.62)$$

where  $R_{mH}$  and  $R_{m0}$  are the winding resistances at currents  $I_H$  and  $I_0$ , respectively;  $\vartheta_H = t_{gH} - t_{kh0}$  and  $\vartheta_0 = t_{g0} - t_{kh0}$  are the winding temperature rises;  $t_{kh0}$  is the "cold" winding temperature;  $t_{gH}$ ,  $t_{g0}$

are the "hot" winding temperatures;  $I^* = I_H/I_0$  is the relative high altitude current.

The subscript "0" indicates surface conditions, the subscript "H" indicates high-altitude conditions.

If winding temperature reaches  $t_{gH} = 250^\circ$  for operation at the altitude H, while  $t_{g0} = 100^\circ$  for operation under surface conditions, the relative winding losses at rated current  $I_H^* = 1$  will rise by

$$\dot{P}_{uH} = \frac{253+250}{235+100} I^2 \approx 1.45 \text{ times.}$$

Thus, for the same value of load current, the change in copper losses is determined by the temperature of the "hot" winding under high-altitude conditions  $t_{gH}$  and under surface conditions  $t_{g0}$ .

Friction losses are made up of cooling losses, sliding-contact losses, and bearing losses.

The bearing losses are small and have little effect on the general picture; we may thus neglect them.

The sliding-contact friction losses  $P_{t.k}$  are considerable, especially in commutator machines, and they increase at high altitudes owing to an increase in the friction coefficient  $\mu$ :

$$P_{t.kH} = P_{t.k0} \frac{\mu_H}{\mu_0} \text{ or } \dot{P}_{t.kH} = \frac{\mu_H}{\mu_0}. \quad (1.63)$$

The ventilation losses  $P_v$  consist of two parts: losses in the fan and ventilating system  $P_{v1}$  and the air-friction losses of rotating machine elements  $P_{v2}$ .

Fan losses depend on the quantity of air by weight driven through the machine and on fan construction. Losses due to air friction at rotating elements depend on the structural characteristics of the machine, the characteristics of the ambient, and the rotor peripheral speed.

Allowing for fan losses, the power spent to move  $Q_v$  m<sup>3</sup>/sec of air at a useful fan pressure of  $h$  mm H<sub>2</sub>O is found from the equation



$$P_{v1} = g \frac{Q_v h}{\eta} = g Q_v \eta g Q_v \frac{v^2}{g} \gamma = G_v v^2 \text{ watts.} \quad (1.64)$$

Here  $h_t = h/\eta = (v^2/g)\gamma$  is the theoretical fan pressure;  $v$  is the peripheral speed (m/sec) taken at the maximum diameter of the fan.

The air weight flow rate  $G_v = Q_v \gamma$  is proportional to the sum of the losses  $\Sigma P$  introduced by the air, and inversely proportional to the permissible temperature rise, i.e.,

$$G_v = \frac{\Sigma P}{t_v} \text{ g/sec,} \quad (1.65)$$

where  $\Sigma P$  is expressed in watts.

$t_v = t_{v.g} - t_{v.kh}$  is the temperature rise in the cooling air, i.e., the difference in the temperatures of the outlet  $t_{v.g}$  and inlet  $t_{v.kh}$  air, normally equal to 30-50°.

Allowing for flight altitude, with  $Q_v = \text{const}$

$$\frac{P_{v1H}}{P_{v1}} = \frac{G_{vH}}{G_v} = \frac{T_H}{T_0} = \frac{T_H}{T_H} \quad (1.66)$$

Losses due to air friction on rotating parts depend on the structural features of the machine and thus cannot be represented by a general equation. As a rule, an equation using empirical coefficients is set up to represent the air-friction losses for each actual machine type.

The friction losses resulting from rotation of a smooth cylinder in atmospheric air can be found from the expression

$$P_{v2} = 1.02 \cdot 10^{-5} M_t n = 705 \left( \frac{n}{1000} \right)^3 \rho_H c_H \int r^2 dt \text{ watts.} \quad (1.67)$$

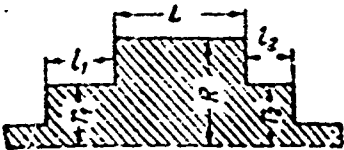

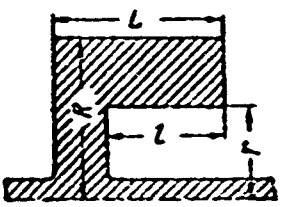
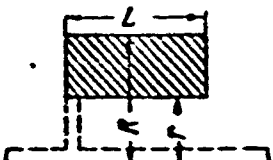
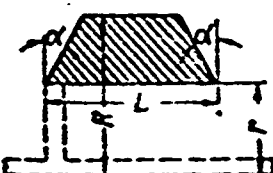
Here  $M_t$  is the frictional moment, g·cm;  $\rho_H$  is the mass density of the air, i.e., the mass per unit volume, from Table 1.1, g·sec<sup>2</sup>/cm<sup>4</sup>;  $c_H$  is the aerodynamic friction coefficient equal to

$$\frac{0.53}{\sqrt{Re}} \text{ and } \frac{0.0286}{\sqrt[4]{Re}},$$

for laminar and turbulent flow, respectively, where the Reynolds number is found from the expression

TABLE 1.9

## Calculation of Air-Friction Losses

1 Вид сечения ротора	2 Геометрический фактор $\int r^4 dl$
	$LR^4 + l_1 r_1^4 + l_2 r_2^4 + 0,4R^5$
	$LR^4 + 0,4R^5$
	$LR^4 \left[ 1 + \frac{l}{L} \left( \frac{r}{R} \right)^4 \right] + 0,4R^5$
	$LR^4 \left[ 1 + \left( \frac{r}{R} \right)^4 \right] + 0,4R^5 \left[ 1 - \left( \frac{r}{R} \right)^5 \right]$
	$LR^4 \left[ 1 - \frac{R-r}{L} \lg \alpha + \left( \frac{r}{R} \right)^4 \right] + \frac{0,4R^5}{\cos \alpha} \left[ 1 - \left( \frac{r}{R} \right)^5 \right]$

1) Shape of rotor cross section; 2) geometrical factor  $\int r^4 dl$ .

$$Re = 2,62 \frac{\pi D^2}{100 \nu_H}$$

$\nu_H$  is the kinetic viscosity of air, i.e., the ratio of the viscosity of the medium to its density.

The critical value of the Reynolds number  $Re_{kr}$  at which laminar boundary flow becomes turbulent is

$$Re_{kr} = 48\,500.$$

The geometrical factor  $\int r^4 dl$  is determined by the form and dimensions of the rotating body (Table 1.9).

Under flight conditions, the magnitude of the friction losses will change owing to variation in the air density  $\rho$  and the electrodynamic friction coefficient  $c$ .

The degree of friction-loss variation under high-altitude conditions may be found from the expression

$$\dot{P}_{v2H} = \frac{P_{v2H}}{P_{v20}} = \frac{P_H}{P_0} \frac{c_H}{c_0} = \dot{P}_H \dot{c}_H \quad (1.68)$$

where  $\dot{P}_H = \dot{\gamma}_H^*$  is found from (1.2) or Table 1.1; and

$$\dot{c}_H = \sqrt{\frac{v_H}{v_0}} = \dot{\gamma}_H^{1/2} \quad \text{for laminar flow;}$$

$$\dot{c}_H = \sqrt[3]{\frac{v_H}{v_0}} = \dot{\gamma}_H^{1/3} \quad \text{for turbulent flow.}$$

The total machine losses owing to cooling will be:

$$P_{v0} = P_{v10} + P_{v20} \quad - \text{ at sea level and}$$

$$P_{vH} = P_{v1H} + P_{v2H} \quad - \text{ at altitude H.}$$

The relative variation in total cooling losses will be

$$\dot{P}_{vH} = \frac{P_{vH}}{P_{v0}} = \dot{\gamma}_H \frac{P_{v10} + P_{v20} \dot{c}_H}{P_{v10} + P_{v20}} \quad (1.69)$$

The electrical brush-contact losses  $P_{e.k_H}$  rise somewhat under high-altitude conditions owing to the increased voltage drop at the sliding contact  $\Delta U$ , which results from impairment of commutation conditions at high altitudes.

The function  $\Delta U = f(H \text{ and } v)$  cannot be evaluated analytically; it can be determined only experimentally for each type of machine and grade of brush.

The constant losses  $P_p$  can be assumed, in first approximation, to be independent of the cooling-air parameters, i.e., of altitude and flight speed since the increase in sliding-contact friction losses is somewhat compensated by the decreased air-friction losses. Thus, in first approximation

$$P_{sH} = P_c + P_{\text{aerom}} + P_{T, \text{a0}} \frac{P_H}{P_0} + P_{\text{aerom}} \frac{235 + t_{rH}}{235 + t_{r0}} + (P_{v10} + P_{v20} \dot{c}_H) \dot{\gamma}_H \approx P_{s0} \quad (1.70)$$

The losses proportional to the first power of the current depend

on the cooling-air parameters. The relative importance of these losses is slight, however, and we do not know the function  $(\Delta U_H / \Delta U_0) = f(H \text{ and } v)$ . In first approximation, we may assume that they do not depend on altitude or flight speed, i.e., when operated at nominal ratings,

$$\dot{P}_{1H} = \dot{P}_{s.H} = \frac{\Delta U_H}{\Delta U_0} \text{ and } P_{1H} \approx P_{1.} = P_1. \quad (1.71)$$

Under high-altitude conditions, the losses proportional to the square of the current may be represented in rated operation, in first approximation, as

$$P_{2H} \approx P_2 \frac{235 + t_{rH}}{235 + t_{r0}}. \quad (1.72)$$

The total losses under high-altitude operating conditions for a current  $\dot{I}_H$ , a speed  $n(f) = \text{const}$ , and a voltage  $U = \text{const}$  will be, in first approximation,

$$\sum P_H \approx P_s + P_1 \dot{I}_H + P_2 \dot{I}_H^2 \frac{235 + t_{rH}}{235 + t_{r0}}. \quad (1.73)$$

Here and above  $P_s$ ,  $P_{m0}$ ,  $P_{v0}$ ,  $P_{t.k0}$ ,  $P_{e.k0}$  are the iron losses, copper losses, ventilating losses, losses owing to brush-contact friction, and electrical losses under surface conditions;

$P_p$ ,  $P_1$ , and  $P_2$  are the constant losses, the losses proportional to  $I$ , and the losses proportional to  $I^2$  under rated operation.

If we still proceed on the basis of the assumption that in climbing to the flight altitude the winding temperature must remain unchanged, then when  $n(f) = \text{const}$  and  $U = \text{const}$ , it is necessary to decrease the current.

Under these conditions, the total losses are found from Equation (1.73) where  $t_{gH} = t_{g0}$ .

## 1.6. HEATING AND COOLING OF AIRCRAFT ELECTRICAL MACHINES

The power developed by an electrical machine is determined basically by the amount of the heat losses that can be removed from the

machine by thermal radiation, convection, and thermal conductivity. In choosing electromagnetic loads, it is necessary to have in mind a rational distribution of heat losses, and to consider the conditions under which they are removed.

In designing a cooling system, it is necessary to distribute the cooling medium so as to ensure that it will be conveyed to the hottest sections.

An electrical machine will be well utilized only if all of its parts are heated uniformly within permissible limits established with an eye to service life and duty cycle.

The sources of thermal energy in an electrical machine are: the magnetic system in which the magnetic induction changes periodically; the electrical system - windings, connections, and sliding contact; surfaces of friction with the cooling medium, sliding contacts, and bearings.

#### Permissible Temperature Limits

The dimensions of an electrical machine of given power are determined in considerable measure by the permissible temperature of individual machine parts, chiefly the windings. The permissible temperatures are in turn conditioned by the type of materials used, the duty cycle and service life of the machine, as well as by the predetermined value of efficiency.

In general electrical-machine design, the maximum permissible temperature of machine parts for continuous operation should not exceed  $130^{\circ}$  with class B insulation or  $105^{\circ}$  for class A insulation. The ambient temperature is here taken to be  $35^{\circ}\text{C}$ .

In the design of aircraft electrical machines, the maximum permissible temperatures may be increased considerably when the shorter service life of electrical machines is taken into account.

The maximum permissible temperature of aircraft electrical machines is limited by: a) the decrease in mechanical and dielectric properties of insulating materials at a high maximum temperature; b) the drop in mechanical and magnetic properties of magnetically soft and magnetically hard materials at temperatures above 150-200°; c) the impairment of mechanical properties of nonferrous and ferrous structural materials at temperatures above 200-250°; d) the decrease in mechanical strength and electrical conductivity of conductor materials; f) [sic] by difficulties encountered in lubricating bearings at temperatures above 150°; g) by the considerable deterioration in the properties of brushes and commutation at temperatures above 200° owing to extreme heating of commutator and brushes, which intensifies ionic processes at the sliding contact, and decreases the contact resistance, which increases the current in a short-circuited section and impairs commutation.

When the temperature changes from -60 to +200°, winding resistance changes by a factor of more than 2.2, which causes considerable fluctuations in voltage, power, and speed, depending on the temperature.

1 Части машины	2 Предельные температуры °C	3 Превышения температур при $t = -40^\circ$
4 Обмотки якоря и возбуждения — изоляция класса А	155	195
5 То же В	175	215
"    С	200	240
6 Коллектор	175+225	215+265
7 Подшипники	150+200	190+240

1) Machine parts; 2) maximum temperatures, °C; 3) temperature rise at  $t = -40^\circ$ ; 4) armature and field windings — class A insulation; 5) the same, class B; 6) commutator; 7) bearings.

Depending on insulation class, lubricant grade, and commutator design, aircraft electrical machines will support the maximum tempera-

tures and temperature rises shown in the table.

As we shall show, the higher the maximum permissible temperatures for machine parts under surface conditions, i.e., the higher the machine thermal load, the lower the altitude at which it will be able to develop rated power at the maximum permissible temperature.

### Thermal Design of an Electrical Machine

The problem of the thermal design of electrical machines consists in determining the temperature rise for individual portions of the machine over the ambient temperature for a given duty cycle.

From the thermal viewpoint, an electrical machine is a complicated system consisting of distributed heat-energy sources (windings and the active iron) separated from each other by boundary layers (insulation).

The thermal calculations represent the most laborious element of electrical-machine design. The simplest machine structure represents a complicated system from the thermal viewpoint. The complexities involved in thermal calculations result from the fact that the thermal process is a multistage and universal phenomenon, and from the difficulties involved in determining the thermal constants (heat capacities, heat-transfer coefficients, and thermal conductivities) of the individual elements. In an electrical machine, the thermal process simultaneously includes free and forced convection, thermal radiation, and thermal conductivity. The heat capacity, heat-transfer coefficient, and thermal conductivity depend on the grade of materials used, design and manufacturing features of the machine, and cooling-medium characteristics (pressure, temperature, the velocity of the air), etc.

The temperature distribution within the volume of each machine element will follow its own laws. The temperature of the same element may take on different values in the radial and axial direction; temperatures in end sections of windings may differ from temperatures in

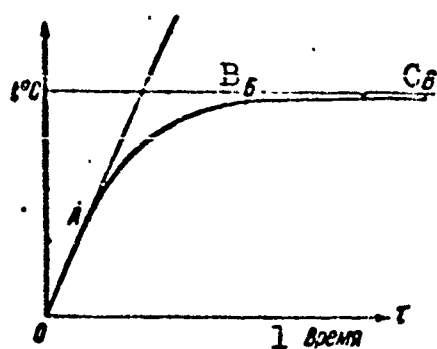


Fig. 1.21. Heating curve for homogeneous body. OA) Adiabatic process; AB) transient heat-transfer; BC) steady-state process. 1) Time.

the active portions, while the temperature of an armature core will be lower at the cooling-medium inlet than at the outlet, etc.

Thus, the concept of "temperature rise" normally refers to average temperatures in the heated body. The ambient temperature is taken to mean the temperature of the air within the room containing the electrical machine, which may be enclosed

or open; for machines using external or internal forced-air cooling, the air temperature at the machine inlet is taken as the cooling-medium temperature.

As is well known, the heating process for a homogeneous body is represented by an exponential curve (Fig. 1.21).

At the beginning of the heating process (section OA) there is a linear rise in body temperature. Consequently, the heating process occurs adiabatically without transfer of heat to the surrounding medium. All thermal losses occurring in the heated body go in their entirety to raise its heat content. The curved portion of the heating curve AB (the "elbow" of the heating curve) corresponds to a transitional heat-transfer regime in which part of the thermal losses go to raise the heat content of the body, and part escapes to the surrounding space. Finally, section BC on the heating curve corresponds to steady-state heat transfer, with all thermal losses delivered to the surrounding space; consequently, the heat content of the body will remain constant.

In general form, thermal processes in an electrical machine correspond to an analytic scheme using distributed constants, which may be represented by a system of differential equations in partial deriva-



tives. The solution of such a system of equations is complicated, and at the present time is not sufficiently reliable, owing to inaccuracy in the initial parameters.

The task can be simplified for all practical purposes by making several assumptions. We shall give the basic assumptions.

1) The temperature of an element is assumed to be constant over its entire volume and equal to some average temperature, i.e., we do not consider the temperature field within a separately considered element of a complex body. This simplification, justified in practice, makes it possible to deal with a heat-flow scheme "with lumped constants," i.e., to represent the thermal process by a system of ordinary linear differential equations of first order. The solution of such a system of equations, however, requires a determination of the roots of the characteristic equation, which, as a rule, is of high order.

2) The temperatures of individual machine sections are taken to be steady-state quantities, with the heating time assumed to be long (operation on section BC) or, conversely, the thermal process is considered to occur so rapidly that there is no heat transfer (adiabatic process) and the temperatures of individual machine sections are taken to rise almost linearly (operation on section OA).

In the first case, temperature calculations reduce to the solution of a system of ordinary linear algebraic equations, while in the second case, they reduce to the calculation of a simple equation for the adiabatic thermal processes occurring in the individual machine elements. If, however, the thermal process occurs rapidly but ends on a section of the exponential curve where there is a point of inflection, it is necessary to solve a system of differential equations in the thermal calculations.

Thermal calculations for aircraft electrical machines operating

under high-altitude and high-speed conditions are also complicated by the fact that the cooling-medium characteristics change continuously, and the laws governing heat transfer to a rarefied gas at high speeds may have special features.

As we know, the temperature of the winding copper equals the mean temperature of the cooling air plus the temperature drop in the insulation and the temperature drop in the boundary layer, i.e., the drop from the winding surface to the cooling air. The temperature drop in the insulation, i.e., the thermal conductivity, is almost independent of the cooling-air characteristics (altitude and flight speed), while the air parameters and nature of the air flow strongly affect the value of the heat-transfer coefficient.

With forced convection, the heat-transfer coefficient may be represented, approximately, by the expression

$$\alpha = \alpha_0 (1 + \xi v) \left( \frac{p}{760} \right)^{\eta} \quad (1.74)$$

where  $\alpha_0$  is the heat-transfer coefficient with  $p_0 = 760$  mm Hg and  $v = 0$ ;  $p$  is the air density, mm Hg;  $\xi$  is a coefficient that characterizes ventilating conditions at the part surface.

Under surface conditions, the air in the air ducts of machines (fixed or rotating) will be characterized by turbulent flow, which ensures a vigorous transfer of heat from the hot machine surfaces.

In high-altitude operation, air density decreases and its kinematic viscosity rises; as a result, the turbulent duct air flow becomes laminar, and in this connection there is a sharp drop in the intensity of heat transfer.

Thus, the increase in machine-element temperature with increasing height is caused not only by a decrease in air density, but also by a change in the nature of the air flow.

The nature of the air flow can change only in stationary ventilating ducts. In internal-armature electrical machines, we speak of the air ducts between the field and commutating-pole windings, while in external-armature machines, we speak of air ducts in the armature. The nature of the air flow in the machine air gap and in rotating air ducts does not change, owing to the artificial turbulence set up in the stream.

Under high-altitude conditions, there is an especially sharp deterioration in the heat-transfer conditions for stationary machine parts. As a result, the hottest areas in a machine may not be the same for high-altitude and surface operation.

Numerous studies have shown that in direct-current machines, temperatures rise more in field windings and especially in commutating-pole windings than in armature windings or in the commutator.

Thus, in designing aircraft electrical machines it is necessary to take special measures to create artificial turbulence in the air flow over stationary machine parts, or else to decrease the thermal load on such elements.

For aircraft machines, we may use an approximate expression for the heat-transfer coefficient, taking the form

$$\alpha \approx \alpha_0 (1 + k \sqrt{v}) \left( \frac{p}{760} \right)^{0.8} \quad (1.75)$$

#### Cooling Systems for Aircraft Electrical Machines

The increased flight speeds and altitudes of modern flying craft require that especial attention be paid to the study of electrical-machine cooling systems.

In order to evaluate such systems it is necessary to take into account: a) system weight and size; b) ease of installation and technical servicing; c) reliability and simplicity; d) the way in which

the system depends on altitude and flight speed; e) system effect on the flying craft from the viewpoint of fuel consumption, decreased lifting capacity and thrust.

The following basic air-cooling systems are in use for aircraft electrical machines:

natural cooling, enclosed or screened electrical machines without forced-air ventilation;

self-cooling, electrical machines with a shaft-mounted fan (Fig. 1.22);

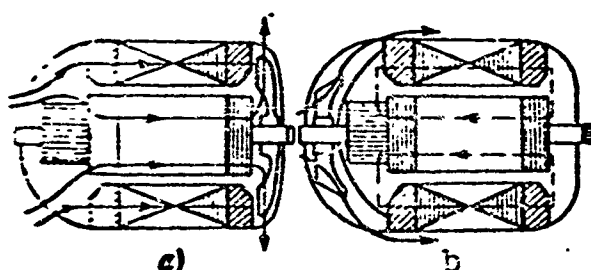


Fig. 1.22. Diagram showing self-cooling. a) Internal axial; b) external axial.

forced-air, independent, or external cooling, electrical machines ventilated by air forced through by the dynamic pressure of the oncoming air stream (Fig. 1.23).

In all systems used to cool aircraft electrical machinery, the altitude and flight-speed cooling characteristics are of considerable interest.

The altitude-speed cooling characteristic of an electrical machine is the name normally given to the relative winding temperature as a function of flight altitude and speed under rated operating conditions, i.e.,

$$t_N = \frac{t_H}{t_0} = f(H \text{ and } v)$$

at rated power, speed, voltage, and power factor. We may also take the

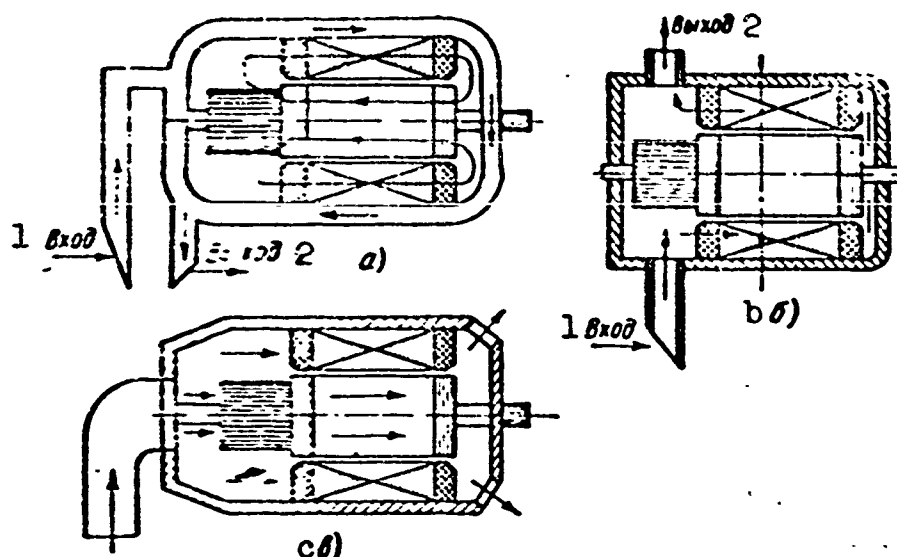


Fig. 1.23. Forced-air cooling systems. a) External axial ventilation; b) internal axial-radial ventilation; c) internal axial ventilation. 1) Inlet; 2) outlet.

relationship

$$\dot{P}_H = \frac{P_H}{P_0} = \varphi(H \text{ and } v)$$

as the altitude-speed cooling characteristic, with the winding temperature, voltage, speed, and  $\cos \varphi$  remaining constant. ( $P$  is the rated power.)

Below we shall examine the enumerated systems for cooling aircraft electrical machines.

Natural cooling is accomplished by the transfer of heat from the surface of a machine owing to heat radiation and free convection. The heat carried off owing to thermal conduction through points of contact of the electrical machine with surrounding objects sometimes reaches a considerable magnitude, but it cannot be calculated, and we shall not consider it here.

The heat transferred by thermal radiation per unit surface may be determined from the equation

$$A_r = 5.7 \left[ \left( \frac{T_k}{100} \right)^4 - \left( \frac{T_v}{100} \right)^4 \right] \text{ watt/m}^2, \quad (1.76)$$

where  $T_k = 273 + t_k$ ,  $^{\circ}\text{K}$ , and  $t_k$ ,  $^{\circ}\text{C}$  is the frame temperature;  $T_v =$

$= 273 + t_v$ , °K and  $t_v$ , °C is the ambient temperature;  $\epsilon$  is a coefficient that characterizes the state of the cooling surface; for electrical machines  $\epsilon = 0.85-0.92$ .

If we assume that the ambient temperature corresponds to the SA for adiabatic deceleration, then if we allow for the variation in air temperature with altitude (in accordance with the SA) and for flight speed, we may represent Eq. (1.76), approximately, in the form

$$A_n \approx 5.4 \left\{ \left( 2.73 + \frac{t_k}{100} \right)^4 - \left[ 2.88 - 0.065H + p_1 \left( \frac{v}{100} \right)^2 \right]^4 \right\} \quad (1.77)$$

for the troposphere, and in the form

$$A_n \approx 5.4 \left\{ \left( 2.73 + \frac{t_k}{100} \right)^4 - \left[ 2.16 + p_1 \left( \frac{v}{100} \right)^2 \right]^4 \right\} \quad (1.78)$$

for the stratosphere. Here  $v$  is the flight speed, m/sec;  $H$  is the flight altitude, km.

Heat transfer due to free convection may be determined per unit surface from the equation

$$A_n \approx 3.48 \sqrt{\frac{p}{v D_n}} \text{ watt/m}^2, \quad (1.79)$$

where  $\vartheta_k = T_k - T_v = t_k - t_v$  is the frame temperature rise;  $p$  is the absolute air pressure, kg/cm<sup>2</sup>;  $D_n$  is the outside diameter of the machine, cm.

If we assume that the ambient temperature corresponds to the SA with adiabatic deceleration, the housing temperature rise with altitude and flight speed taken into account will be

$$\vartheta_n = t_n - 15 + 6.5H - p_1 \left( \frac{v}{100} \right)^2 \text{ at } H \leq 11 \text{ km}$$

and

$$\vartheta_n = t_n + 56.5 - p_1 \left( \frac{v}{100} \right)^2 \text{ at } H > 11 \text{ km}. \quad (1.80)$$

At the maximum free-stream air temperature

$$\vartheta_n = t_n - 60 + 8.33H - p_1 \left( \frac{v}{100} \right)^2 \text{ at } H \leq 12 \text{ km}$$

and

$$\vartheta_k = t_k + 40 - \rho_1 \left( \frac{v}{100} \right)^3 \quad \text{at } H > 12 \text{ km.} \quad (1.81)$$

The relative heat-transfer values for radiation and free convection at high altitudes may be represented in the form

$$\dot{A}_{kH} = \frac{A_{kH}}{A_{k0}} = \frac{\left( 2,73 + \frac{t_{kH}}{100} \right)^4 - \left[ 2,16 + 4,3 \left( \frac{v_H}{103} \right)^2 \right]^4}{\left( 2,73 + \frac{t_{k0}}{100} \right)^4 - 68,8} \quad (1.82)$$

from the SA, at  $v_0 = 0$  and  $H \geq 11$  km,

$$\dot{A}_{kH} = \frac{A_{kH}}{A_{k0}} = (\dot{\vartheta}_{kH})^{5/4} (\dot{p}_H)^{1/2}. \quad (1.83)$$

where  $p_H^* = p_H/p_0$  from (1.3) or Table 1.1;

$$\dot{\vartheta}_{kH} = \frac{\vartheta_{kH}}{\vartheta_{k0}}.$$

The subscript "H" refers to high-altitude conditions, and the subscript "0" to surface conditions.

Where  $\vartheta_k = 0$ , heat transfer by thermal radiation and free convection equals zero. This occurs at flight speeds of:

$$v = 48,5 \sqrt{t_k + 65H - 15} \text{ m/sec at } H \leq 11 \text{ km}$$

and

$$v = 48,5 \sqrt{t_k + 56,5} \text{ m/sec at } H > 11 \text{ km.} \quad (1.84)$$

Figure 1.24 shows the relationships

$$A_H = A_r + A_k = f(H) \quad \text{at } t_k = 60 + 200^\circ \text{ and } v = 0.$$

The data given makes it possible to draw certain conclusions, e.g.:

1) Within the troposphere, heat transfer by thermal radiation and free convection increases, while within the stratosphere, heat transfer by thermal radiation remains constant while heat transfer by free convection falls with increasing altitude and nearly vanishes at an altitude of 20 km; since the relative importance of heat transfer by free convection is slight, however, the total amount of heat transferred is determined by thermal radiation, and is nearly independent

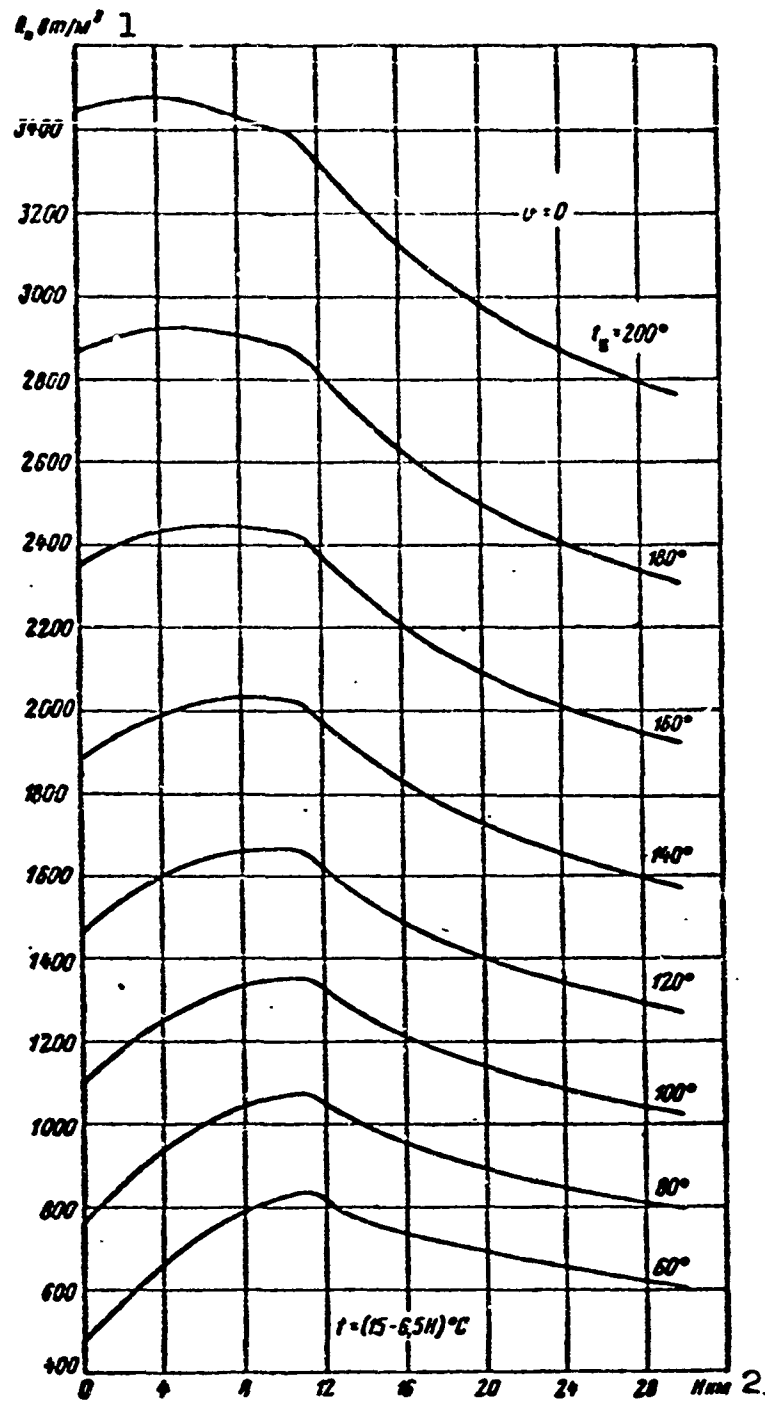


Fig. 1.24. Heat transfer by radiation and free convection as a function of the altitude  $H$  and frame temperature  $t_k$  (neglecting adiabatic compression). 1)  $A_n$ , watt/m<sup>2</sup>; 2)  $H$ , km.

of altitude.

2) The relative heat-transfer value rises more rapidly within the troposphere with increasing altitude the lower the frame temperature. If we assume that heat transfer is the same at sea level and at high



altitudes, then the lower the frame temperature, the higher the permissible flight altitude; thus at  $t_k = 100^\circ$ , it is 27 km, but at  $t_k = 120^\circ$ , it is only 20 km.

3) As the flight speed goes up, the amount of heat transferred by thermal radiation and free convection decreases sharply. At flight speeds greater than 400 m/sec, natural cooling systems are unsuitable.

4) The efficiency of natural cooling is small; the heat transferred per unit area is only 6-15 watt/deg·m<sup>2</sup>, and natural cooling can be recommended only for aircraft electrical machines of less than 100 watts power and for short-time duty at high altitudes, but not for high flight speeds.

High-altitude cooling characteristics. The thermal losses  $\Sigma P$ , that can be removed from the surface  $F$  of an electrical machine by natural cooling are determined from the heat-balance under steady-state conditions, i.e.,

$$\Sigma P = FA = \vartheta_k \Lambda = F \vartheta_k \alpha \text{ watts}, \quad (1.85)$$

where  $\vartheta_k = t_k - t_v$  is the frame temperature rise;  $A = A_1 + A_k = \alpha \vartheta_k$  is the heat transferred from unit surface or the specific heat flows due to radiation and convection, watt/m<sup>2</sup>;  $\Lambda = \Lambda_1 + \Lambda_k$  is the heat transferred from a surface, watt/deg;  $\alpha = \alpha_1 + \alpha_k$  is the heat transfer per unit surface, watt/m<sup>2</sup>·deg.

Since  $A_1$  ( $\Lambda_1$ ,  $\alpha_1$ ) and  $A_k$  ( $\Lambda_k$ ,  $\alpha_k$ ) depend on the condition of the cooling medium, i.e., its temperature  $\underline{t}$ , thermal conductivity  $\lambda_\delta$ , heat capacity  $\underline{c}$ , humidity, etc., the heat loss  $\Sigma P$  that can be removed with natural cooling depends on altitude and flight speed.

The amounts of heat that can be removed from a machine surface on the ground and at high altitudes will differ in accordance with the ratio of the amounts of heat transferred per unit surface, i.e.,

$$\sum \dot{P}_H = \frac{\sum P_H}{\sum P_0} = \frac{\Lambda_{KH} + \Lambda_{KH}}{\Lambda_{K0} + \Lambda_{K0}} = \frac{\Lambda_H}{\Lambda_0} = \dot{A}_H. \quad (1.86)$$

If the ambient temperature rises, the amount of heat transferred to the outside space will decrease and, consequently, in order to maintain frame and winding temperature at the previous level it is necessary to make an appropriate decrease in the amount of heat liberated within the machine.

If the temperatures of frame and windings are identical under ground and high-altitude conditions, the relationship among the various types of losses  $P_p$ ,  $P_1$ , and  $P_2$  will remain nearly unchanged.\* In this case, the relationship between the load current at high altitude and the heat carried off, i.e., in essence, the expression for the natural-cooling altitude characteristic may be determined by using (1.60) and (1.86) from which it follows that

$$\sum P_H = \dot{A}_H \sum P_0, \quad 1 + a_1 \dot{I}_H + a_2 \dot{I}_H^2 = \dot{A}_H (1 + a_1 + a_2) \quad (1.87)$$

and

$$\dot{I}_H^2 + a_{12} \dot{I}_H + [a_2^{-1} - \dot{A}_H (1 + a_{12} + a_2^{-1})] = 0,$$

where  $a_1 = P_1/P_p$ ;  $a_2 = P_2/P_p$ , and  $a_{12} = a_1/a_2 = P_1/P_2$  are the relative heat-loss coefficients.

By solving the quadratic equation for the load current  $\dot{I}_H^*$  we obtain

$$\dot{I}_H = \frac{\dot{I}_H}{\dot{I}_0} = -0,5 a_{12} \pm \sqrt{0,25 a_{12}^2 + \dot{A}_H (1 + a_{12} + a_2^{-1}) - a_2^{-1}}.$$

The current  $\dot{I}_H^*$  will always be less than zero and, consequently, the last equation will take the form

$$\dot{I}_H = \sqrt{0,25 a_{12}^2 + \dot{A}_H (1 + a_{12} + a_2^{-1}) - a_2^{-1}} - 0,5 a_{12} \quad (1.88)$$

where

$$\dot{A}_H = f(H \text{ and } v), \text{ i.e., } \dot{I}_H^* = \varphi(H \text{ and } v)$$

and will represent the altitude characteristic of an electrical machine with natural cooling.

If  $a_1$  is small,  $a_1 \rho \rightarrow 0$  and the expression for the current will be simplified:

$$i_H \approx \sqrt{\frac{\dot{\lambda}_H(1+a_2)-1}{a_2}} = \sqrt{\frac{\dot{\lambda}_H(P_n+P_2)-P_n}{P_2}}. \quad (1.89)$$

The relative heat-transfer value  $\dot{A}_H$  for which the machine will not develop power, i.e., at which its useful load will be zero, is determined from the condition that  $\dot{I}_H^* = 0$ , i.e.:

$$\dot{A}_H = \frac{1}{1+a_1+a_2} = \frac{P_n}{P_n+P_1+P_2} \quad (1.90)$$

or

$$\dot{A}_H \approx \frac{1}{1+a_2} = \frac{P_n}{P_n+P_2}. \quad (1.91)$$

In physical terms this means that losses carried off to the outside space at an altitude  $H$  will equal the constant losses, i.e., the no-load losses and, consequently, the machine cannot develop useful power.

Thus, we have established a relationship between the relative load current  $\dot{I}_H^*$  and the relative amount of heat transferred by radiation and free convection ( $\dot{A}_H^* = \Sigma \dot{P}_H^*$ ). If we know the relative loss coefficients  $a_1$  and  $a_2$ , we can determine the variation in machine load as a function of altitude and flight speed where the winding temperatures are held constant.

Forced-convection cooling - self-cooling or forced cooling - and their efficiencies are determined by the amount of cooling gas, by weight, that passes through the machine in unit time, and by its temperature.

The weight flow rate of a gas may be determined with self-cooling or external forced cooling from the expression

$$G_s = Q\gamma = v_s S \gamma = S \sqrt{2g} \sqrt{h_s \gamma} = S \sqrt{2g} \sqrt{\frac{\Delta h}{R_m} \gamma} \text{ kg/hr}, \quad (1.92)$$

where  $v_s$  and  $\gamma$  are the speed in m/sec and the specific gravity in  $\text{kg/m}^3$

of the cooling gas;

$$h_v = \frac{\gamma}{2g} v_v^2 \quad (1.93)$$

is the dynamic gas pressure at the machine inlet, mm H<sub>2</sub>O;

$$\Delta h = R_x h_v = \frac{R_x}{2g} \gamma v_v^2 \quad (1.94)$$

is the pressure drop in the machine;

$$R_x = \frac{\Delta h}{h_v} = 2g \frac{\Delta h}{\gamma v_v^2} \quad (1.95)$$

is the aerodynamic resistance of the machine, whose numerical value is determined by the shape and dimensions of the air duct; S is the cross-sectional area of the inlet orifice of the machine; Q is the gas volume, m<sup>3</sup>/sec; g = 9.81 m/sec<sup>2</sup> is the gravitational acceleration.

The relative variation in air weight flow rate may be found as a function of altitude from the expression

$$\dot{G}_H = \dot{v}_H \dot{\gamma}_H = \sqrt{\dot{h}_v \dot{\gamma}_H} = \sqrt{\Delta \dot{h}_H \dot{\gamma}_H}, \quad (1.96)$$

where the relative values are

$$\dot{G}_H = \frac{G_H}{G_0}, \quad \dot{v}_H = \frac{v_H}{v_0}; \quad h_{vH} = \frac{h_{vH}}{h_{v0}}; \quad \Delta \dot{h}_H = \frac{\Delta h_H}{\Delta h_0}.$$

The subscript "H" corresponds to operation at altitude H, and the subscript "0" to operation at sea level.

Self-cooling as we have said before, is carried out with the aid of a fan mounted on the shaft of the electrical machine. This cooling system is used in aircraft generators with powers of up to 1-1.5 kw, as well as in aircraft electric motors and converters for almost all power ranges (Fig. 1.25).

The basic drawback inherent in all self-cooling systems lies in the fact that cooling efficiency drops sharply with increasing altitude and flight speed. Another substantial drawback to the self-cooling system lies in the fact that preheated air whose temperature is nearly

independent of altitude may penetrate the machine. In addition, this air may contain oil and fuel vapors.

Let us determine useful power as a function of flight altitude and speed, i.e., let us find the altitude characteristic of a machine using self-cooling.

With self-cooling, the amount of gas by volume that flows through the electrical machine is independent of flight altitude or speed and, consequently, the velocity of the air remains constant, i.e.,

$$v_H = v_0 \text{ and } v_H^* = 1.$$

In this case, it follows from (1.96) that the relative weight flow rate of the cooling gas is directly proportional to the relative specific gravity of the gas, i.e., when  $v_H^* = 1$

$$\left. \begin{aligned} \text{and } \dot{G}_H = \dot{v}_H \dot{\gamma}_H = \dot{\gamma}_H &\approx \frac{20-H}{20+H} \quad (\text{at } H \leq 11 \text{ км}) \\ \dot{G}_H = \dot{\gamma}_H &\approx 0.3e^{-0.16(H-11)} \quad (\text{at } H > 11 \text{ км}). \end{aligned} \right\} \quad (1.97)$$

The air pressure created by a fan on the shaft of an electrical machine is proportional to the square of the rotational speed and to the specific gravity of the air, i.e.,

$$h_{\bullet H} = k_{\bullet} \left( \frac{n}{1000} \right)^2 \dot{\gamma}_H, \quad (1.98)$$

where  $k_{\bullet}$  is a constant corresponding to the air pressure at sea level ( $\gamma_0 = 1.225 \text{ kg/m}^3$  and  $t = 15^\circ\text{C}$ ) with a shaft speed  $n = 1000 \text{ rpm}$ .

The relative air pressure may be represented as a function of flight altitude and the change in fan speed by the equation

$$\dot{h}_{\bullet H} = \frac{h_{\bullet H}}{h_{\bullet 0}} = \dot{n}_H^2 \dot{\gamma}_H, \quad (1.99)$$

where

$$\dot{n}_H = \frac{n_H}{n_0}.$$

With constant shaft speed, the air pressure at the machine inlet

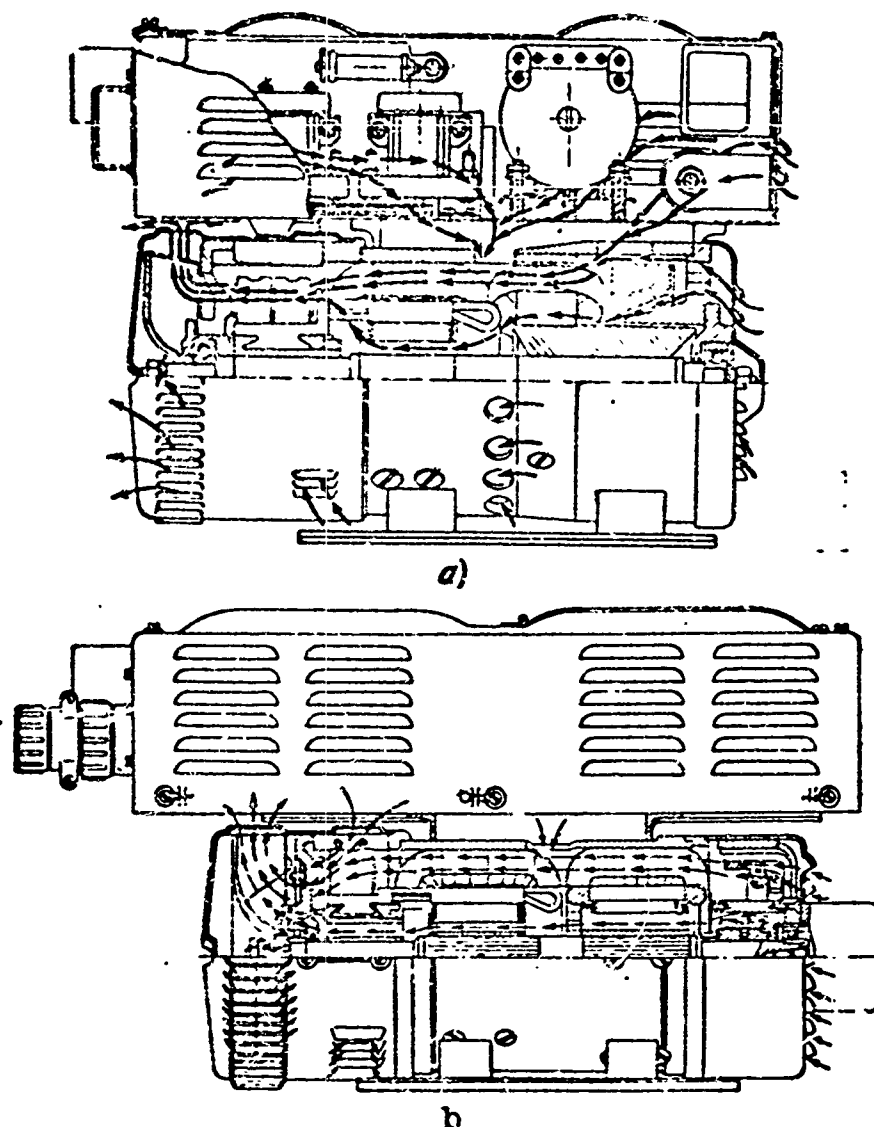


Fig. 1.25. Diagram showing converter self-cooling. a) MA-2500 converter; b) PO-1500 converter.

is proportional to the specific gravity. Allowing for the relative specific gravity of air in accordance with the SA, we obtain

$$\dot{h}_{\bullet H} \approx \dot{n}_H^2 \frac{20-H}{20+H}$$

and

$$\dot{h}_{\bullet H} \approx 0.3 \dot{n}_H^2 e^{-0.16(H-11)} \quad (1.100)$$

for the troposphere and stratosphere, respectively.

Heat losses. As is known, the heat carried off by a cooling gas is

$$\Sigma P = Q c \theta_{\bullet} \text{ [kw]}. \quad (1.101)$$

Since the volumetric heat capacity  $c = c_p \gamma$ , expressed in  $\text{kw} \cdot \text{sec}/^\circ\text{C}$ , is numerically equal to the specific gravity for air, we obtain

$$\sum P = Q \gamma \delta_v = G_s \delta_v. \quad (1.102)$$

The amount of air supplied by a centrifugal fan is proportional to the shaft speed, i.e.,

$$\sum P = \gamma n \delta_v. \quad (1.103)$$

where  $\delta_v = t_{v.g} - t_{v.kh}$  is the temperature rise in the cooling gas.

We may assume in first approximation that the heat absorbed by the cooling air is proportional to the winding temperature rise  $\delta_m$ , i.e., in accordance with (1.102)

$$\sum P \approx G_s \delta_m.$$

where

$$\delta_m = t_m - t_{m.i};$$

$$t_m; t_{m.i}$$

are the temperatures of the winding and the air at the machine inlet, respectively.

Thus, the heat losses carried off by cooling air are proportional to the temperature rise in the machine elements above the inlet-air temperature, to the air specific gravity, and to the fan speed.

The relative amounts of heat removed by the cooling air may be represented as a function of altitude and flight speed by the expression

$$\sum \dot{P}_H = \dot{\gamma}_H \dot{n}_H \dot{\delta}_{m.H}. \quad (1.104)$$

where for the troposphere, the relative values of temperature rise are expressed by the equations

$$\dot{\delta}_{m.H} = \frac{t_{m.H} - 15 - p_1 \left( \frac{v_H}{100} \right)^2 + 6.5 t'}{t_{m.0} - 15 - p_1 \left( \frac{v_0}{100} \right)^2} \quad (1.105a)$$

(with  $\underline{t}$  taken from the SA) and

$$\dot{m}_H = \frac{t_{mH} - 60 - p_1 \left( \frac{v_H}{100} \right)^2 + 8.33H}{t_{m0} - 60 - p_1 \left( \frac{v_0}{100} \right)^2} \quad (1.105b)$$

(with  $t$  at maximum value), where  $t_{mH}$  and  $t_{m0}$  are the winding temperatures.

Formula (1.104) gives a relative heat-loss value that is too low, since it does not allow for natural heat transfer by thermal radiation, free convection, and thermal conduction. Experiments have shown that the relative heat losses are proportional to  $(\gamma_H)^{0.9}$ , i.e., we may assume in approximation that with self-cooling

$$\Sigma \dot{P}_H \approx \dot{\gamma}_H^{0.9} \dot{n}_H \dot{\delta}_{mH} \quad (1.106)$$

It is interesting to determine the relative temperature rise when the relative heat losses removed by the cooling air remain constant.

In this case  $\Sigma \dot{P}_H^* = 1$  and

$$\dot{\delta}_{mH} \approx \frac{\dot{n}_H}{(\dot{\gamma}_H)^{0.9}} \quad (1.107)$$

If we assume winding temperatures  $t_{m0} = t_{mH} = t_m$  and a ground speed  $v_0 = 0$ , then in place of (1.105) we shall have

$$\dot{\delta}_{mH} = 1 + \frac{8.33H - p_1 \left( \frac{v_H}{100} \right)^2}{t_m - 60} \quad (1.108)$$

For the stratosphere, the value 8.33H is replaced by a constant equal to 100 in (1.105) and (1.108). In view of what we have said, taking (1.106) into account, we obtain an expression for the relative heat loss removed by the cooling air:

$$\Sigma \dot{P}_H \approx \left( \frac{20-H}{20+H} \right)^{0.9} \left[ 1 + \frac{8.33H - p_1 \left( \frac{v_H}{100} \right)^2}{\delta_m} \right] \dot{n}_H \quad (1.109)$$

for the troposphere, and

$$\Sigma \dot{P}_H \approx 0.3e^{0.142} \left[ 1 + \frac{100 - p_1 \left( \frac{v_H}{100} \right)^2}{\delta_m} \right] \dot{n}_H \quad (1.109a)$$



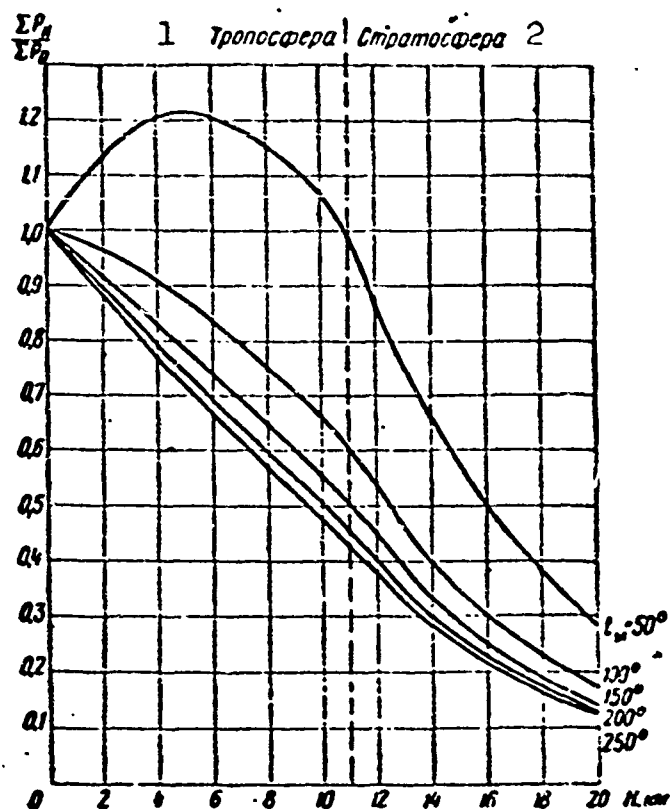


Fig. 1.26. Relative heat losses carried off with self-cooling as a function of altitude. 1) Troposphere; 2) stratosphere.

for the stratosphere (using the maximum temperature in accordance with the SA).

Figure 1.26 shows the relationship  $\Sigma P_H^* = f(H)$  for various winding temperatures  $t_m$  or temperature rises in accordance with the SA with respect to sea level  $\vartheta_m = t_m - 15$ , with the temperature rise due to adiabatic compression neglected.

Equations (1.106) and (1.109) as well as the curves of Fig. 1.25 constructed from these equations give the relative losses in an electrical machine that are carried off by the cooling air provided that the winding temperatures remain constant with changes in altitude and flight speed.

If  $v_H \neq v_0$  or  $t_m \neq \text{const}$ , it is necessary to take the value of  $\Sigma P_{mH}^*$  from (1.105) and (1.106).

The following relationship exists among the losses in an electri-

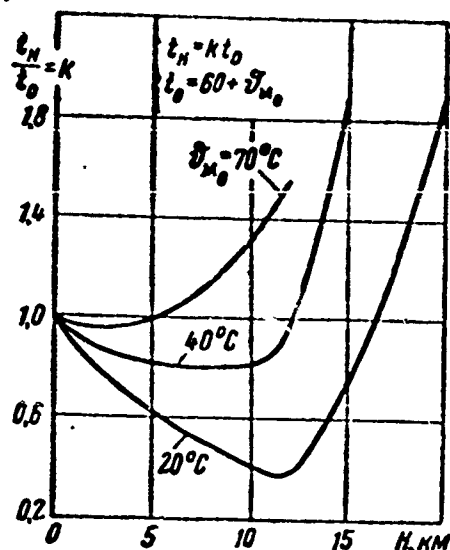


Fig. 1.27. Altitude characteristic for self-cooled aircraft DC electric motor,  $t_H/t_0 = f(H)$  with power held constant and various winding temperature rises under ground conditions,  $\vartheta_{m0} = 20, 40, \text{ and } 70^\circ\text{C}$ .

cal machine, the rated power  $P_{\text{nom}}$ , and the efficiency:

$$\frac{\sum P_H}{P_0} = \frac{P_{\text{nom}_H}}{P_{\text{nom}_0}} \frac{\eta_0}{\eta_H} \frac{1 - \eta_H}{1 - \eta_0}, \quad (1.110)$$

where  $P_{\text{nom}_H}$  and  $P_{\text{nom}_0}$  are the rated powers at a given altitude and at sea level, respectively.

If we assume that the efficiency of an electrical machine at rated power and  $t_{m0} = t_{mH}$  is nearly independent of altitude and flight speed, i.e., that the sum of the losses developed does not change, then

$$\eta_0 = \eta_H$$

and

$$\sum \dot{P}_H = \frac{P_{\text{nom}_H}}{P_{\text{nom}_0}} \dot{P}_{\text{nom}_H}$$

Consequently, Expression (1.106) represents the height and speed characteristic of an electrical self-cooled machine operating with rated load.

Figure 1.27 gives the altitude characteristics for aircraft self-cooled motors for various winding-temperature values.

We may draw the following conclusions from the material presented above:

1) At low flight speeds ( $v < 200 \text{ m/sec}$ ) and constant fan speed, machine temperature begins to fall while the aircraft is climbing and reaches a minimum at some specific flight speed; it then rises sharply, reaching the rated value at some particular altitude. The higher the temperature of the machine (windings, iron) on the ground, the poorer the high-altitude characteristics of the machine. This is explained by

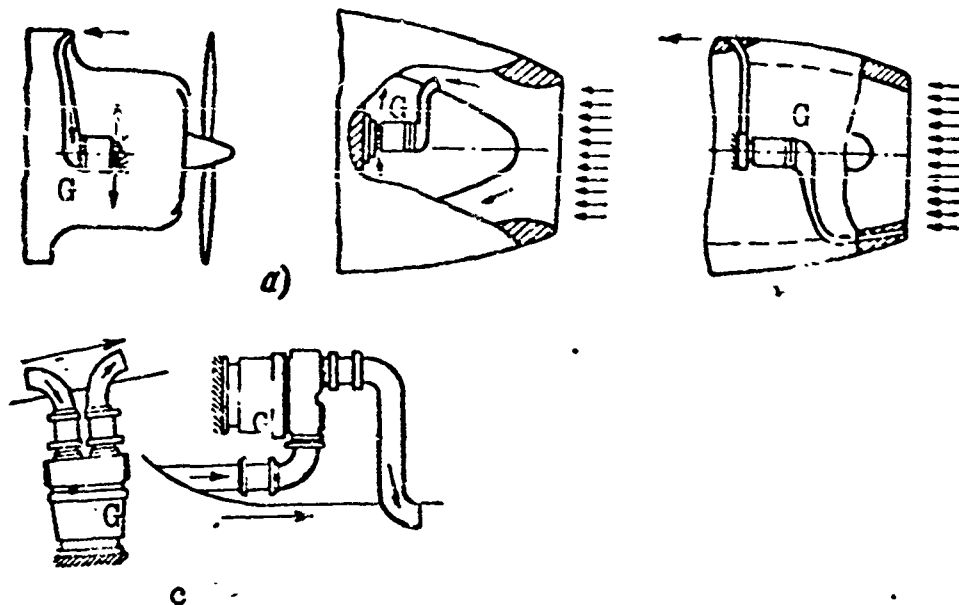


Fig. 1.28. Arrangement of generator and methods of connecting air duct. a) Air released into space under cowl; b) air released behind aircraft-engine cowl; c) connection of air duct; G) generator.

the fact that the relative effect of the temperature drop in the troposphere is weaker the higher the nominal temperature of the machine.

2) The efficiency of a self-cooling system drops sharply with increasing altitude owing to a decrease in the weight flow rate of the air, especially in the stratosphere where the temperature is constant while the air density continues to drop.

3) Self-cooling is unsuitable for high-altitude and high-speed flights ( $v > 300$  m/sec) where the machine is operated continuously, since cooling efficiency drops as a result of the lowered density and increased temperature of the air.

Forced cooling is accomplished by means of the oncoming air stream which arrives at the generator owing to the action of the dynamic head; it is employed for generators having powers above 1.0-1.5 kw.

Figure 1.28 shows the various methods used to connect air ducts and various generator arrangements; Fig. 1.29 shows a forced-air cooling system for an 18-kw generator.

There are two possible types of forced-air cooling.

1) The dynamic pressure at the machine air inlet remains practically constant under all flight conditions.

This may occur when the flight speed rises as the altitude increases. In this case (where  $h_{vH} \approx h_{v0}$ ) the equation

$$\dot{h}_{vH} = \frac{h_{vH}}{h_{v0}} = \frac{\frac{\gamma_H v_H^2}{2g}}{\frac{\gamma_0 v_0^2}{2g}} = \gamma_H \dot{v}_H^2 = 1,$$

will hold, in approximation, for the relative dynamic pressure at the machine inlet and thus

$$\dot{v}_H = \dot{\gamma}_H^{\frac{1}{2}}, \quad (1.111)$$

i.e., the relative velocity  $v_H^*$  of the air entering the machine, depending on the altitude, will rise in inverse proportion to the one-half power of the air density.

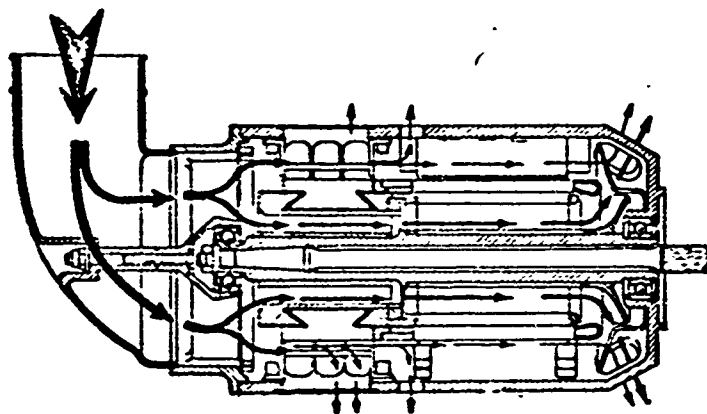


Fig. 1.29. External forced-air cooling of DC aircraft generator.

According to (1.111) the relative weight flow rate of the air equals the square root of the relative specific gravity of the air, since

$$\left. \begin{aligned} \dot{G}_H = \dot{\gamma}_H \dot{v}_H = \frac{\dot{\gamma}_H}{\sqrt{\dot{\gamma}_H}} = \sqrt{\dot{\gamma}_H} &\approx \sqrt{\frac{20-H}{20+H}} \quad (\text{at } H \leq 11 \text{ км}) \\ \dot{G}_H = \sqrt{\dot{\gamma}_H} &\approx 0,545 e^{-0,08(H-11)} \quad (\text{at } H > 11 \text{ км}). \end{aligned} \right\} \quad (1.112)$$

and

2) The flight speed remains almost constant with changes in altitude.

In this case, the velocity of the cooling-system air will remain constant,  $v_H^* = 1$ , and the relative dynamic head will drop as the altitude increases in accordance with the relative specific gravity of the air, i.e.,

$$\dot{h}_{vH} = \dot{\gamma}_H \dot{v}_H^2 = \dot{\gamma}_H \quad (1.113)$$

The relative weight flow rate of the air, as in the self-cooling case, equals the relative specific gravity:

$$\dot{G}_H = \dot{\gamma}_H = \dot{h}_{vH} \approx \frac{20 - H}{20 + H} \quad (1.114)$$

or

$$0.3e^{-0.16(H-1)}$$

Thus, where the dynamic pressure at the generator air intake remains constant, the decrease in air specific gravity with increasing altitude is compensated to some extent by an increase in air velocity. If, however, the flight speed does not depend on altitude, the drop in air density with increasing altitude is not compensated by an increase in flight speed, and the efficiency of a cooling system using external forced air turns out to be the same as that of a system using self-cooling.

The heat losses carried off by the cooling medium are roughly proportional to the weight flow rate of the cooling medium and to the temperature rise in the electrical machine

$$\Sigma P \approx G_m \delta_m \quad (1.115)$$

where  $\delta_m = t_m - t_{v.kh}$  is the winding temperature rise over the inlet-air temperature. The relative heat losses carried off by the cooling air as a function of altitude and flight speed will be

$$\Sigma \dot{P}_H = \dot{G}_H \delta_{mH} \quad (1.116)$$

Taking the value of  $G_H^*$  from (1.96) we can find

$$\Sigma \dot{P}_H = \dot{g}_{mH} \dot{i}_H \dot{v}_H = \dot{g}_{mH} \sqrt{\dot{h}_{vH} \dot{i}_H} = \dot{g}_{mH} \sqrt{\Delta \dot{h}_H \dot{i}_H}. \quad (1.117)$$

For  $\dot{h}_{vH}^* = 1$ , Expression (1.117) will be

$$\Sigma \dot{P}_H = \dot{g}_{mH} \sqrt{\dot{i}_H}. \quad (1.118)$$

Substituting into (1.118) the value of  $\gamma_H^*$  from (1.112) we obtain the relative heat losses at  $t_{mH} = t_{m0} = t_m$  and  $v_0 = 0$ , e.g.:

$$\left. \begin{aligned} \Sigma \dot{P}_H &\approx \sqrt{\frac{20-H}{20+H}} \left[ 1 + \frac{8.33H - p_1 \left( \frac{v_H}{100} \right)^2}{\dot{g}_m} \right] \text{ (at } H < 12 \text{ км),} \\ \Sigma \dot{P}_H &\approx 0.545e^{-0.03(H-11)} \left[ 1 + \frac{100 - p_1 \left( \frac{v_H}{100} \right)^2}{\dot{g}_m} \right] \text{ (at } H > 12 \text{ км),} \end{aligned} \right\} \quad (1.119)$$

where  $\dot{v}_m = t_m - 60^\circ\text{C}$ .

If the calculation is carried out with a temperature corresponding to the SA, it is then necessary to substitute 6.5H and 71.5 for the minuends 8.33H and 100, respectively.

If we take (1.88) and (1.115) into account, it is possible to find the nature of the variation in the relative load current as a function of altitude and flight speed, i.e., the altitude and speed cooling characteristic for an electrical machine with  $t_{mH} = t_{m0} = t_m$

$$\dot{i}_H = \sqrt{0.25a_{12}^2 + \dot{G}_H \dot{g}_H (1 + a_{12} + a_2^{-1}) - a_2^{-1} - 0.5a_{12}}. \quad (1.120)$$

Where  $a_{12} = (a_1/a_2) \rightarrow 0$ , i.e., for small losses that are proportional to the first power of the current,

$$\dot{i}_H = \sqrt{\dot{G}_H \dot{g}_H (1 + a_2^{-1}) - a_2^{-1}}. \quad (1.120a)$$

Expression (1.120) is relatively complicated, and requires a knowledge of the loss coefficients  $a_1$  and  $a_2$ .

The losses  $\Sigma P$  cannot be connected with machine power by any general relationship that is suitable for all types of electrical machines; thus, for example, to make a preliminary determination of the cooling

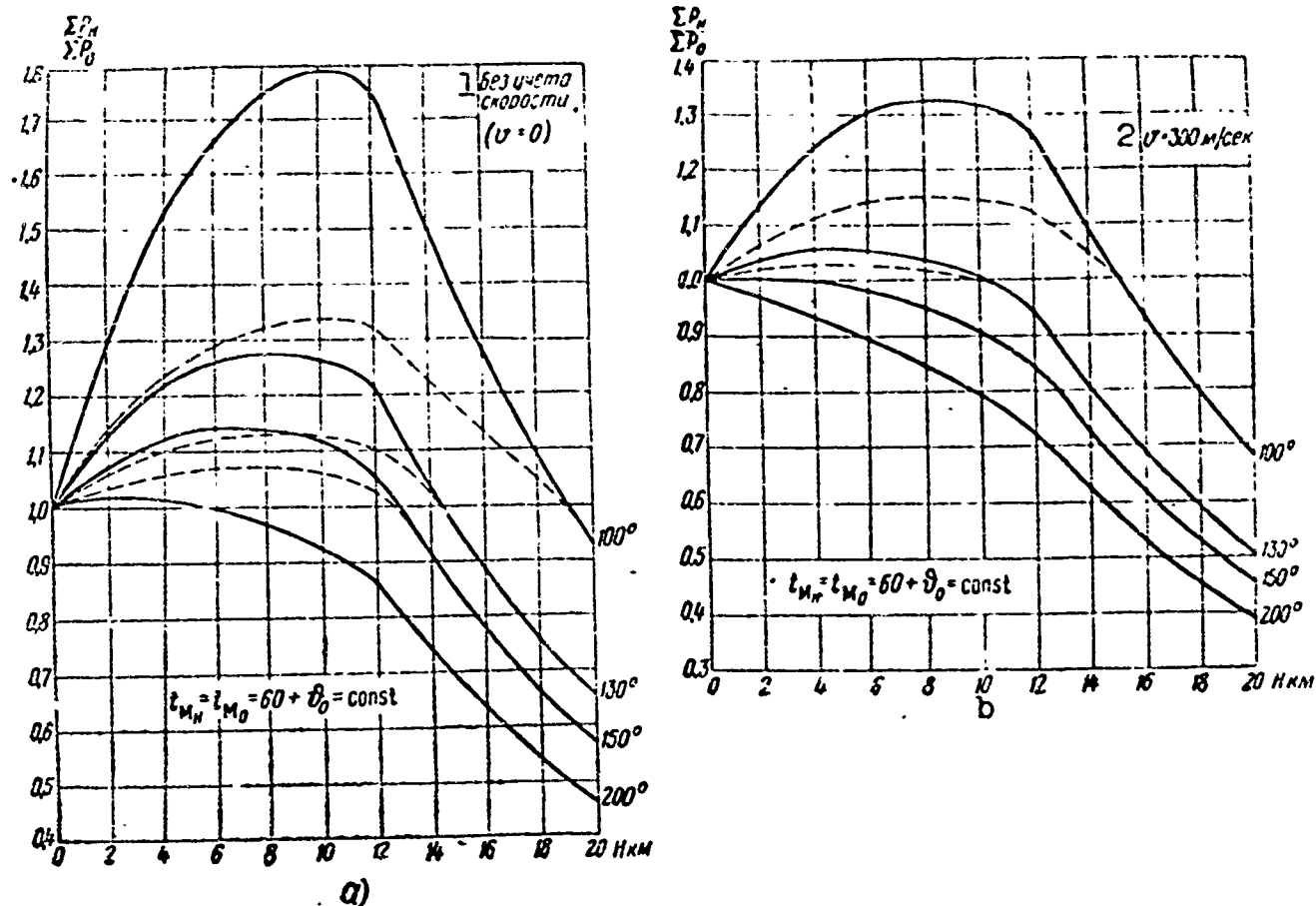


Fig. 1.30. Cooling characteristic of DC aircraft generators for various winding temperatures. The air temperature is taken from the maximum SA value. The dashed curves show the relationship  $\Sigma P^* = f(H)$  for various  $t_m$ , taking (1.121) into account. a) Adiabatic deceleration neglected; b) allowance for adiabatic deceleration of  $v = 300$  m/sec and  $\rho_1 = 4.3$ . 1) Speed neglected ( $v = 0$ ); 2)  $v = 300$  m/sec.

characteristics of aircraft DC generators, the relationship

$$\Sigma \dot{P}_H = \dot{I}_H^\alpha,$$

can be used; here the exponent  $\alpha = 2$  when  $I_H^* > 1$  and  $\alpha = 1$  when  $I_H^* = 0.5-1$ .

In view of what has been said, the altitude and speed cooling characteristic of an aircraft generator may be represented in the form

$$\left. \begin{aligned} \dot{I}_H &= (\dot{\vartheta}_{MH} \dot{G}_H) \quad (\text{at } \dot{I}_H = 0.5-1.0) \\ \dot{I}_H &= \sqrt{\dot{\vartheta}_{MH} \dot{G}_H} \quad (\text{at } \dot{I}_H > 1) \end{aligned} \right\} \quad (1.121)$$

Table 1.10 gives the basic equations for this section, for the

sake of clarity.

Figure 1.30a and b gives the altitude cooling characteristics of aircraft generators for various winding temperatures and flight speeds.

TABLE 1.10

Summary of Formulas Used in Cooling Calculations

	1 Самоохлаждение	2 Продув	
		$\dot{h}_{vH} = 1$	$\dot{h}_{vH} \neq \text{const}$
3 Скорость и объемный расход газа	$v_H = v_0, \dot{v}_H = 1$ $Q_H = Q_0, \dot{Q}_H = 1$	$\dot{v}_H = \frac{1}{\sqrt{\dot{i}_H}} = \dot{Q}_H$	$v_H = v_0, \dot{v}_H = 1$ $Q_H = Q_0, \dot{Q}_H = 1$
4 Весовой расход газа	$\dot{G}_H = \dot{i}_H$	$\dot{G}_H = \sqrt{\dot{i}_H}$	$\dot{G}_H = \dot{i}_H$
5 Давление газа на входе	$\dot{h}_{vH} = \dot{i}_H \dot{n}_H^2$	$\dot{h}_{vH} = 1$	$\dot{h}_{vH} = \dot{i}_H$
6 Тепловые потери	$\Sigma \dot{P}_H = \dot{i}_H^{0.9} \dot{v}_H \dot{n}_H$	$\dot{i}_H \sqrt{\dot{i}_H}$	$\dot{i}_H \dot{i}_H$
7 Ток нагрузки при $t_{mH} = t_{m0}$	$\dot{i}_H = \sqrt{0.25 a_{12}^2 + \Sigma \dot{P}_H (1 + a_{12} + a_2^{-1}) - a_2^{-1} - 0.5 a_{12}}$		
8 при $a_{12} \rightarrow 0$	$\dot{i}_H \approx \sqrt{\Sigma \dot{P}_H (1 + a_2^{-1}) - a_2^{-1}}$		

1) Self-cooling; 2) external forced-air cooling;  
3) gas velocity and volume flow rate; 4) gas weight flow rate; 5) gas pressure at inlet; 6) heat losses; 7) load current when  $t_{mH} = t_{m0}$ ; 8) at.

Basic conclusions: a) air velocity or volume flow rate are independent of flight altitude and speed with self-cooling or external forced-air cooling if the dynamic pressure at the cooling-system inlet (including the external forced-air case) varies in proportion to the specific gravity of the air;

b) the weight flow rate of the air, determining cooling efficiency, is proportional to the specific gravity of the air and the winding temperature rise over the inlet-air temperature. Thus, the weight flow rate of air depends on flight altitude and speed;

c) as flight altitude increases, there is a decrease in the weight



flow rate of the air and, consequently, in cooling efficiency. The decrease in air temperature with increasing altitude that occurs within the troposphere increases cooling efficiency;

d) an increase in flight speed increases air temperature and, consequently, decreases cooling efficiency;

e) the greater the winding temperature rise under surface conditions, the lower the altitude and flight speed at which the windings will reach the maximum permissible temperature, i.e., the poorer the machine cooling characteristics.

Flight efficiency. An essential defect in all forced-air cooling systems using the dynamic pressure of the oncoming air is the increase in the drag of the flying craft caused by distortion of the aerodynamic shape of the flying craft owing to the installation of the intake duct and the loss of power that results when the air flows through the generator cooling system.

Below we determine the power lost owing to the flow of air through the generator cooling ducts.

The magnitude of the internal drag  $R$  is determined by the change in momentum of the air stream, i.e.,

$$R = \frac{G_v}{g} (v_1 - v_2), \quad (1.122)$$

where  $G_v$  is the weight flow rate of the air, kg/sec;  $v_1$  is the air velocity at the inlet, which is nearly equal to the flight velocity  $v$ , m/sec;  $v_2$  is the air velocity at the outlet, m/sec;  $g = 9.81 \text{ m/sec}^2$  is the gravitational acceleration.

As a rule  $v \gg v_2$  and (1.122) may be assumed to equal

$$R \approx \frac{G_v}{g} v \text{ kg.} \quad (1.123)$$

In order to overcome this drag, the aircraft engine must develop additional thrust, i.e., an additional amount of power that may be

found from the equation

$$P_R = Rv \approx \frac{G_s}{g} v^2 \text{ kg} \cdot \text{m/sec} \quad (1.124)$$

or, since  $75g = 735$  and  $1.36 \cdot 735 \approx 1000$ , we find that

$$P_R = \frac{G_s v^2}{735} \text{ hp} = 10 G_s \left( \frac{v}{100} \right)^2 \text{ kw.} \quad (1.125)$$

For a propeller-driven craft, the engine should develop an additional amount of power equal to

$$P_{R_s} = \frac{P_R}{\eta_v} = \frac{10}{\eta_v} G_s \left( \frac{v}{100} \right)^2 \text{ kw,} \quad (1.126)$$

where  $\eta_v$  is the aircraft propeller efficiency, equal to 0.75-0.8 for modern propellers.

The amount of air by weight needed for cooling equals

$$G_s = Q_v = \frac{\Sigma P}{c_p \Delta t_v} = \frac{\Sigma P}{\Delta t_v} \text{ kg/sec,} \quad (1.127)$$

where  $\Sigma P$  is the sum of the losses in the machine that heat the air, kw;  $c_p$  is the specific heat of the air at constant pressure; it equals 1 kw·sec/deg·kg;  $\Delta t_v = t_{v.g} - t_{v.kh}$  is the temperature rise in the cooling air.

If we assume that  $\Delta t_v = 40^\circ\text{C}$ ,  $G_s$  is expressed as

$$G_s = 0.025 \Sigma P \text{ kg/sec.} \quad (1.128)$$

Taking (1.123), (1.125), and (1.127) into account, we obtain a relationship between the internal drag  $R$  and the generator losses, i.e.,

$$R = \frac{\Sigma P}{g} \frac{v}{g} \text{ and } \frac{R}{\Sigma P} = \frac{v}{g^2} \text{ kg/kw,} \quad (1.129)$$

and the relationship between the additional aircraft-engine power losses and the generator losses with external forced-air cooling

$$P_{R_s} = \frac{10 \Sigma P}{\eta_v g^2} \left( \frac{v}{100} \right)^2 \text{ and } \frac{P_{R_s}}{\Sigma P} = \frac{10}{\eta_v g^2} \left( \frac{v}{100} \right)^2. \quad (1.130)$$

Thus, the additional aircraft-engine power losses due to electrical-machine cooling are directly proportional to the square of the flying-craft speed and the sum of the electrical-machine losses, and

inversely proportional to the temperature rise of the air in the electrical machine.

Figure 1.31 gives curves that show aircraft-engine power losses (at  $\eta_v = 1$ ) per kilowatt of electrical-machine loss as a function of flight speed and  $\eta_g$ .

The sum of the losses and the relative electrical-machine losses may be represented in the form

$$\sum P = P_{\text{nom}} \frac{1 - \eta_g}{\eta_g} \text{ and } \frac{\sum P}{P_{\text{nom}}} = \frac{1 - \eta_g}{\eta_g}, \quad (1.131)$$

where  $P_{\text{nom}}$  is the rated generator power, kw;  $\eta_g$  is the generator efficiency.

Taking the value of  $\sum P$  from (1.131)

$$R = \frac{v}{g \theta_s} \frac{1 - \eta_g}{\eta_g} P_{\text{nom}} \text{ kg}$$

and

$$\frac{R}{P_{\text{nom}}} = \frac{v}{g \theta_s} \frac{1 - \eta_g}{\eta_g} \text{ kg/kw.} \quad (1.132)$$

The cooling-air flow rate will then equal

$$G_s = \frac{P_{\text{nom}}}{\theta_s} \frac{1 - \eta_g}{\eta_g} \text{ kg/sec}$$

and

$$\frac{G_s}{P_{\text{nom}}} = \frac{1}{\theta_s} \frac{1 - \eta_g}{\eta_g} \text{ kg/sec} \cdot \text{kw.} \quad (1.133)$$

Substituting the value of  $\sum P$  from (1.131) into Eq. (1.130), we obtain an expression for the relative aircraft-engine power losses as a function of flight speed and generator efficiency (Fig. 1.32):

$$\frac{P_{R_s}}{P_{\text{nom}}} = \frac{10}{\eta_g \theta_s} \left( \frac{v}{100} \right)^2 \frac{1 - \eta_g}{\eta_g} = k_n \left( \frac{v}{100} \right)^2 \frac{1 - \eta_g}{\eta_g}, \quad (1.134)$$

where

$$k_n = \frac{10}{\eta_g \theta_s}.$$

In determining efficiency, the power lost by an aircraft engine

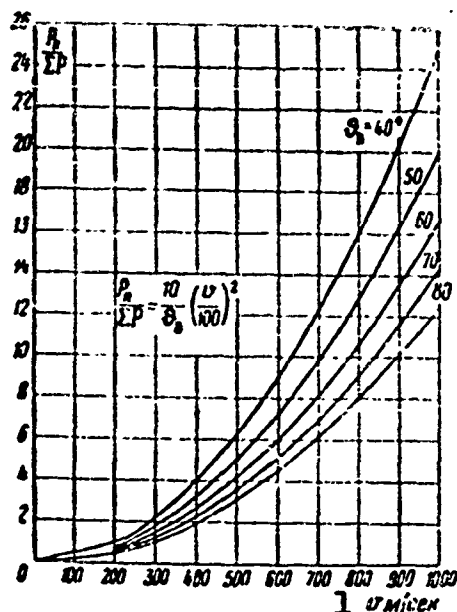


Fig. 1.31. Relative aircraft-engine power losses to electrical-machine cooling for various air temperature rises. 1)  $v$ , m/sec.

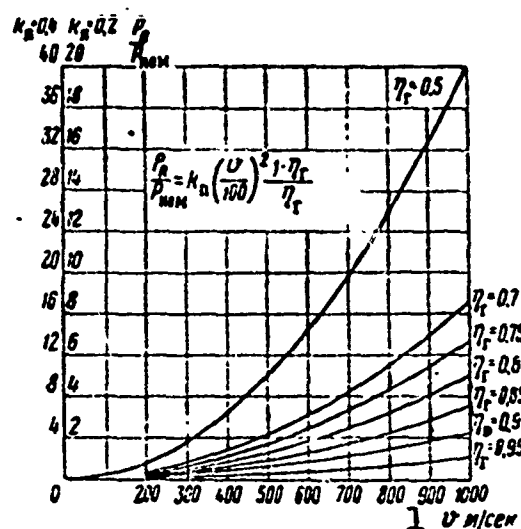


Fig. 1.32. Relative aircraft-engine power losses to electrical-machine cooling as a function of flight speed and generator efficiency. 1)  $v$ , m/sec.

due to electrical-machine cooling should be taken into account. Electrical-machine efficiency is called the flight efficiency when the aircraft-engine losses going to cool the motor are taken into account; the numerical value of this efficiency is determined from the expression

$$\eta_a = \frac{P_{nom}}{P_{nom} + \sum P + P_{R_0}} = \frac{1}{1 + \frac{\sum P}{P_{nom}} + \frac{P_{R_0}}{P_{nom}}} \quad (1.135)$$

Taking (1.131) and (1.134) into account, we obtain after some simple manipulations

$$\eta_a = \frac{\eta_g}{1 + k_p \left( \frac{v}{100} \right)^2 (1 - \eta_g)} \quad (1.136)$$

Equation (1.136) gives a direct relationship between the flight efficiency of an electrical machine and its efficiency and the aircraft flight speed. The value of the coefficient  $k_p$  varies within narrow limits, and for a given series of electrical machines and type of aircraft engine, it will be nearly constant.

Figure 1.33 shows  $\eta_g = f(v)$  for various values of  $\eta_g$  [sic].

Equations (1.135) and (1.136) and the curves of Fig. 1.33 are of considerable interest, since they permit a direct determination of the effect of electrical-machine efficiency on aircraft-engine power loss, and make it possible to find the flight efficiency of a machine. In climbing, the quantity of air by weight decreases and, consequently, there is a corresponding decrease in the power lost by the main engine.

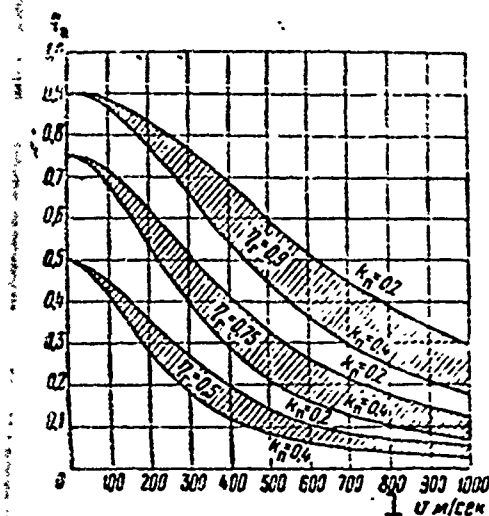


Fig. 1.33. Flight efficiency as a function of speed and generator efficiency.

$$\eta_g = \frac{\eta_r}{1 + k_g \left( \frac{v}{100} \right)^2 (1 - \eta_r)}$$

1)  $v$ , m/sec.

Fuel consumed in overcoming deceleration. In order to overcome the internal drag  $R$  due to deceleration of the air stream in the generator ventilating system, an additional amount of power  $P_R = Rv$  is expended and, consequently, additional fuel is required; its weight will equal

$$G_r = \xi_r P_R t = \xi_r P_R \frac{L}{v} \text{ kg.} \quad (1.137)$$

Here  $t = L/v$  is the duration of the flight, hr;  $L$  and  $v$  are the route length, km, and flight speed, km/hr;  $\xi_r$  is the specific fuel flow rate, kg/kw-hr.

Taking the value of  $P_R$  from (1.134), we obtain

$$G_r = \xi_r P_{nom} k_g \left( \frac{v}{100} \right)^2 \frac{1 - \eta_r}{\eta_r} t \text{ kg.} \quad (1.138)$$

We let  $G_g = g_g P_{nom}$  be the generator weight, where  $g_g = G_g / P_{nom}$  is the relative weight of the generator; then the relative fuel consumption due to generator cooling is

$$\frac{G_r}{G_r} = \frac{\xi_r}{\xi_r} k_n \left( \frac{v}{100} \right)^2 \frac{1 - \eta_r}{\eta_r} t. \quad (1.139)$$

After simple manipulations, allowing for (1.136), we obtain the following expression for the fuel consumed in cooling a generator:

$$G_r = \xi_r P_{nom} \frac{k_n \left( \frac{v}{100} \right)^2}{1 + k_n \left( \frac{v}{100} \right)^2} \frac{1 - \eta_r}{\eta_r} t \text{ kg} \quad (1.140)$$

and

$$\frac{G_r}{P_{nom}} = \xi_r \frac{k_n \left( \frac{v}{100} \right)^2}{1 + k_n \left( \frac{v}{100} \right)^2} \frac{1 - \eta_r}{\eta_r} t \text{ kg/kw.} \quad (1.140a)$$

Where  $v > 600$  m/sec, Relationship (1.140a) is simplified and

$$\frac{G_r}{P_{nom}} \approx \xi_r \frac{1 - \eta_r}{\eta_r} t.$$

Equations (1.138) and (1.140) show that the ordinary or flight efficiencies of a generator have a considerable effect on the additional fuel consumed and, consequently, on the flight and takeoff weights of the flying craft. If generator efficiency is increased, the additional fuel consumption decreases; in this case, however, there will be an increase in the weight of the generator.

It is of interest to determine the permissible increase in generator efficiency, based on keeping the added generator weight resulting from an increase in efficiency equal to the corresponding decrease in additional fuel consumed.

The degree to which generator efficiency  $k_\eta$  can be increased may be found approximately from the condition that the increase in generator weight be compensated by a decrease in the additional fuel consumed due to cooling and power takeoff, by using the expression

$$k_\eta = \frac{\xi_r t}{2 \xi_r \eta_{r1}^2} \left[ 1 + k_n \left( \frac{v}{100} \right)^2 \right]. \quad (1.141)$$

which is meaningful for values of  $t$  such that  $k_\eta > 1$ .

Here the coefficient  $a = 3-4$  shows the relative increase in generator weight for an increase in efficiency  $\Delta\eta_g = \eta_{g2} - \eta_{g1} = 0.01$  within real limits ( $\eta_{g2} > \eta_{g1}$ ).

An analysis of the preceding equations clearly demonstrates the superiority of alternating-current aircraft electrical machines which, as a rule, are more efficient; it is clearly desirable to increase the efficiencies of direct-current aircraft generators in any way possible when they are cooled by the incoming air stream, sometimes even at the expense of some increase in weight. It is also obviously necessary to consider flying-craft function (flight duration and speed) in selecting the utilization factor and power characteristics of electrical machines.

Here we have not considered the change in weight of associated equipment resulting from a change in generator weight and fuel weight, losses due to distortion of flying-craft aerodynamic form caused by the presence of ducts, etc. The considerations given, however, make it possible to establish the boundaries for reasonable utilization of external forced-air cooling and indicate methods for expanding these limits.

Air-cooling systems using the pressure of the oncoming air stream are poorly suited for high-speed or high-altitude flying craft, and new cooling systems for aircraft electrical machines are needed to provide an increase in flight altitude and speed.

#### Ways of Increasing Electrical-Machine Cooling Efficiency

We shall list some ways of increasing the efficiency of electric-machine cooling at high flight speeds and altitudes.

1. The region of applicability of forced-air cooling from the dynamic pressure of the oncoming air stream may be expanded in the following ways:

- a) by decreasing the aerodynamic drag of the cooling system;

b) by increasing the thermal resistance of the insulation, commutator, brushes, soldered joints, lubricant, bearings, etc.;

c) by increasing efficiency through the utilization of magnetic materials with increased magnetic permeability and lower losses; by increasing the quality of core stamping, assembly, and heat treatment, and in some cases by increasing the weight of the machine;

d) by decreasing the amount of cooling air required through an increase in the air temperature excess;

e) by decreasing the cooling-air temperature by spraying water into the air stream at the inlet (in addition, moist air has a somewhat higher heat-transfer coefficient). The amount of water used for cooling is determined by the point at which 100% relative humidity is reached, and the relative water flow rate depends on the inlet-air temperature and its amount. The higher the temperature of the incoming air and the more of it that there is, the lower the degree of utilization of the cooling power of the water. Thus, high-power machines with a relatively large air flow rate in cooling require a larger relative expenditure of water at high speeds for cooling purposes. We may assume to start with that 6-30 kw DC generators and 15-60 kva AC generators require 1-2 kg of water per hour for each kw of generator losses for flights at altitudes of the order of 20 km and at speeds of 650-750 m/sec.

Regulation of the water flow rate requires the presence of a special apparatus;

f) by using air from the cabin pressurizing compressor to cool electrical machines.

The enumerated measures permit an expansion in the region of application of air cooling; they do not, however, eliminate the organic defects in this system (the decreasing weight flow rate of cooling air



with increasing flight altitude, the increasing air temperature and decreasing flight efficiency, i.e., increasing flight weight, occurring with increasing flight speed).

2. Liquid cooling of electrical machines by means of water, oil, aviation fuel, etc., as is well known is more efficient than gas cooling.

The amounts of cooling medium by weight needed to carry off the same amount of waste heat are related in the following manner for water, kerosene, oil, and air — 1:1.92:2.32:4.2. By volume, the quantities are related, respectively, as follows — 1:2.4:2.45:4200.

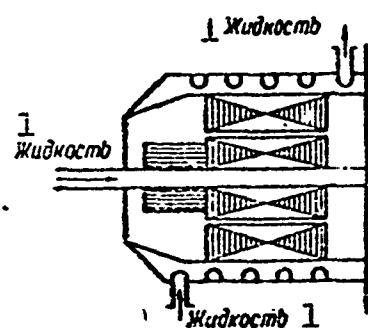


Fig. 1.34. Diagram of liquid-cooled electrical machine.  
1) Liquid.

Thus, as a cooling medium water is roughly twice as efficient as kerosene and four times as efficient as air. The liquid coolant may be applied to the outside surfaces of the machine (which should be shaped appropriately), introduced within the machine with the aid of finned tubes or other devices, and may be brought into the shaft to ducts in the rotating portion of the machine (Fig. 1.34).

With a liquid coolant, very serious difficulties are encountered in cooling the rotating portion of a machine. In DC and AC aircraft electrical machines with rotating armatures, where up to 80% of all losses are concentrated, it is difficult to use a liquid coolant, since it is an extremely complicated matter to supply the coolant through the shaft, especially where kerosene is used.

For stationary-armature electrical AC machines and, in particular, for induction and magnetolectric generators, the liquid-cooling system appears promising. For short-time-duty electrical machines, it is possible to use water or oil without special flow-rate regulating ap-

paratus.

Any possible overconsumption of coolant may be compensated by the reduction in control-apparatus weight. In addition, it is necessary to consider the fact that when a liquid coolant is used, the degree of utilization of the electrical machines is increased, and machine power will rise by 30% or more.

Combined cooling systems exist that supply some fixed weight of air to the interior hollow section of the machine, while a liquid having a negative temperature (ammonia, for example) flows over the outside of the machine. The machine will then be thermally insulated from the outside medium, and will operate reliably under all flight conditions.

3. Cooling of electrical machines by the evaporation of liquid at the interior surface. If a liquid is evaporated at the hot inside surface of an electrical machine, the high latent heat of vaporization and high heat-transfer coefficient will produce efficient cooling.

At atmospheric pressure, the latent heat of vaporization of water is 539 kcal/kg, while the heat-transfer coefficient of boiling water is hundreds of times greater than that of air. As a result, it is only necessary to evaporate about 1.55 kg of water per hour at a machine surface in order to remove 1 kw-hr of waste heat.

Consequently, a 12-kw DC generator with a 75% efficiency, i.e., with losses equaling

$$\sum P = P_{\text{gen}} \frac{1 - \eta_r}{\eta_r} = 12 \frac{0.25}{0.75} = 4 \text{ kw},$$

will require about 6.5 kg of water per hour, and the over-all water consumption will be

$$G_w \approx 1.55 t \sum P \approx 6.2 t \text{ kg},$$

where  $t$  is the length of the flight, hr.

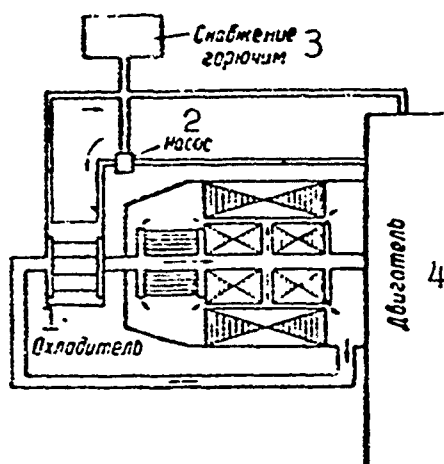


Fig. 1.35. Diagram showing cooling of electrical machine by closed-cycle evaporation. 1) Cooler; 2) pump; 3) fuel supply; 4) engine.

A 12-kw AC generator will have an efficiency of 0.9 where  $\cos \varphi = 0.75$  and, consequently, only 2.1 kg of water will be required for cooling purposes for one hour of operation at full power.

At high flight speeds, the additional weight of cooling water is less than the additional weight of fuel consumed with forced air cooling using external air, i.e., the flight weight of the system will be less than with air cooling.

For short flights it is sensible to supply water continuously in a constant amount corresponding to full generator load, with no special regulating system. Any excess amount of water consumed will weigh less than the equipment used to control the water feed rate. When water evaporation is used for cooling at high altitudes, the temperatures of generator parts decrease, since at low air pressures, the boiling point drops and the latent heat of vaporization increases.

For long flights, it is possible to use a closed sealed cooling system that circulates a constant volume of water; a diagram of such a system is shown in Fig. 1.35.

After vaporization, the water is cooled, condensed in a special device, and again supplied to the machine. In all cases, it is necessary to protect the water against freezing or to use a mixture with a low freezing point.

Water can be supplied to a machine through a hollow shaft or through openings in the frame or in guards.

Cooling by evaporation of water has a favorable effect on sliding-

contact operation, and increases the service life of brushes, rings, and the commutator. Machine rated power may be increased by roughly 30% which to some degree compensates for the increased structural weight of the system as a whole. Such a system tends to be freer from external influences. The evaporator system and water supply may be thermally insulated from the external medium.

Cooling by liquid evaporation is best suited to short flights.

Where this system is employed, it is necessary to solve certain structural problems, to investigate corrosion and the moisture tightness of insulation where a machine is to operate with saturated water vapor.

We should take note of the considerable structural and technological difficulties that appear in the manufacture of devices for supplying water to a machine in view of the relatively low water flow rate and the danger that the small outlet holes may become clogged.

Of considerable interest is a system for external cooling by evaporation, in which the liquid is evaporated not on an inside surface of the machine, but in machine cooling ducts or in an independent water cooler (Fig. 1.36).

The coolant may be supplied to and evaporated in hollows within poles, in ducts in the armature core, in frame ducts, at the commutator surface, etc. In the last case, the system for coolant supply and metering is simplified, and nozzles are eliminated.

A drawback to the external evaporation-cooling system in comparison with the internal system is the higher temperature of the machine, especially at the sliding contact, and a somewhat higher water flow rate.

As an example of the utilization of an internal evaporation-cooling system, let us look at a three-phase 16-kva synchronous gen-

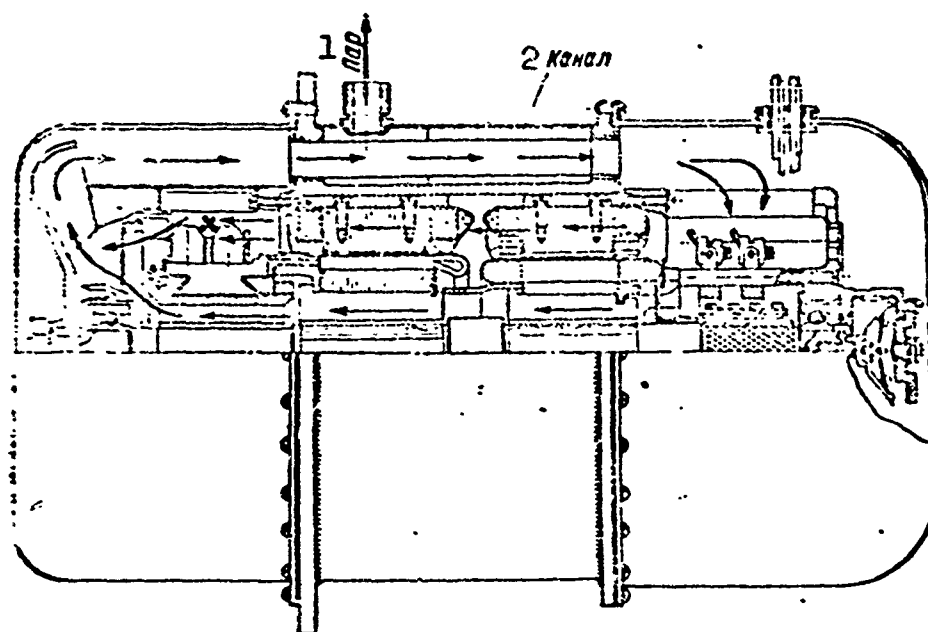


Fig. 1.36. Diagram showing cooling system for aircraft converter using evaporation of water in ducts. 1) Vapor; 2) duct.

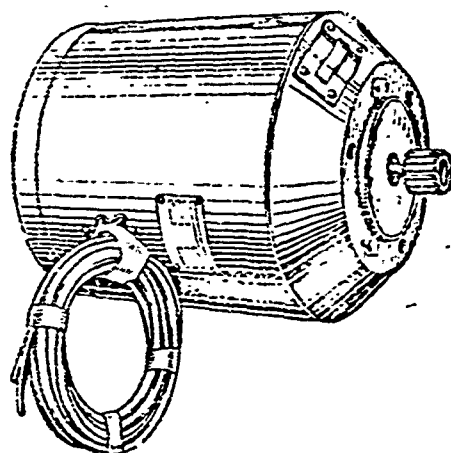


Fig. 1.37. Three-phase generator cooled by the evaporation of water on an interior surface.

erator with a speed of 12,000 rpm, a line voltage of 208 v, with  $\cos \varphi = 0.8$ , and an efficiency  $\eta_g = 0.93$  (Fig. 1.37).

This generator weighs 17.7 kg, and has the following basic external dimensions:  $D_n = 230$  mm and  $L = 320$  mm; the flange diameter is 152 mm, and the diameter under the holes is 127 mm. The water flow rate which amounts to 1.6 kg/hr in rated

operation is regulated by a special valve actuated by a temperature relay installed on the generator.

Water is supplied under pressure to the hollow generator shaft, where it is sprayed onto the inner surface of the machine by four nozzles. The water vapor is carried off through an opening in the generator. The evaporator system and generator water supply are thermally insulated from the surrounding medium. The use of water evaporation cooling makes it possible to increase the rated power of the machine

from 12 to 16 kva, i.e., by 33%.

It is of practical interest to determine the flight speed at which it makes sense to replace an external forced-air cooling system by a system using the evaporation of water at the machine surface. The solution of this problem involves considerable difficulties, and should be carried out separately for each type of flying craft. In order to simplify the problem, we determine the flight speed at which the additional fuel consumed for cooling by external forced air is equal to the water used for evaporation. Here it is assumed that the increase in generator utilization factor with evaporation cooling, the decrease in fuel-tank weight, the elimination of air ducts, etc., compensate the increase in installation weight, including the evaporator system and water supply. If we assume that with evaporation cooling the weight of the equipment rises somewhat, this can be allowed for by a specific coefficient, i.e.,  $\gamma G_t = G_v$ , where  $\gamma > 1$ .

Taking into account what we have said, we can write

$$\gamma \xi_t P_{\text{nom}} k_p \left( \frac{v}{100} \right)^2 \frac{1 - \gamma_r}{\gamma_r} t = 1.55 P_{\text{nom}} \frac{1 - \gamma_r}{\gamma_r}.$$

Solving this equation for the speed  $v$ , we obtain the flight speed at which it is sensible to use evaporation cooling, i.e.,

$$v > \frac{125}{\sqrt{\gamma \xi_t k_p}} \text{ m/sec,}$$

which when  $\xi_t = 0.65$  and  $k_p = 0.25$  yields  $v > 320/\sqrt{\gamma}$ .

If the coefficient  $\gamma = 0.8$  allows for the increase in system weight, the flight speed at which it is sensible to use evaporation cooling will equal 360 m/sec. Calculations for concrete cases show the degree to which the magnitude obtained is correct.

4. Oil cooling of aircraft electrical machines has found ever-increasing application in recent years (Fig. 1.38a and b).

Oil is supplied to and removed from the machine in the direction

of the drive mechanism. In salient-pole AC generators, the oil is supplied alternately through ducts in the generator stator and exciter and then is sent through the generator inductor and the exciter armature. The oil flow rate is constant and does not depend on the generator load.

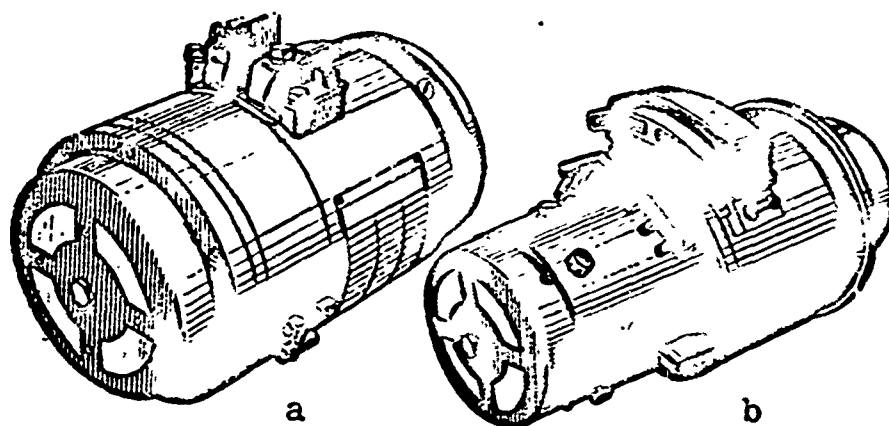


Fig. 1.38. Oil-cooled aircraft generators.  
a) 100-amp 28-v 8000-rpm DC generator weighing 16.3 kg; b) 15-kva 208/120-v 12000-rpm three-phase generator with  $\cos \varphi = 0.75$ , weighing 27.7 kg.

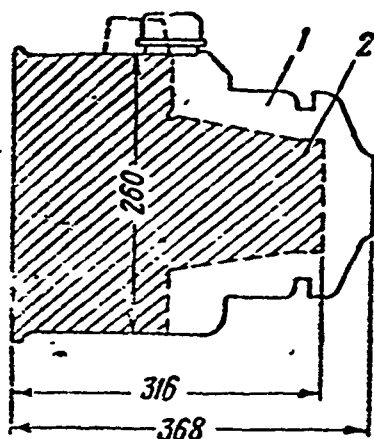


Fig. 1.39. Comparison of three-phase generators with air cooling (1) and oil cooling (2).

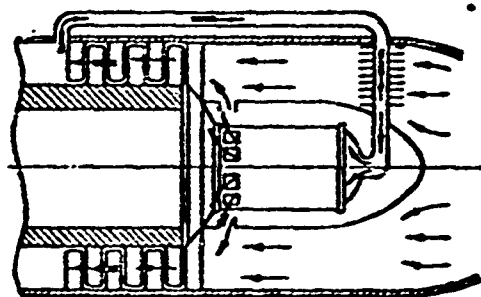


Fig. 1.40. Cooling by means of air taken from TKVRD compressor.

Oil-cooled machines are characterized by the fact that on the drive side, the bearing is located in the drive mechanism itself and, consequently, such machines are made with a single bearing. Oil cooling offers the following advantages.

1) A decrease in machine dimensions (Fig. 1.39) owing to the fact that a 40-60 times smaller cross section is required for the passage of oil than for the passage of air (this makes it possible to decrease the machine diameter), while a decrease in the temperature gradient along the machine length in comparison with air cooling makes it possible to increase the thermal load on the machine.

2) A decrease in power losses owing to deceleration of the air stream, since with oil cooling a smaller amount of air is required to cool the air-oil heat exchangers.

3) Machine power is independent of flight speed and height if the temperature of the incoming oil does not exceed a specific limit ( $150^{\circ}\text{C}$ ). A 40-kva generator with  $\cos \varphi = 0.75$  develops full power at an oil temperature of  $150^{\circ}\text{C}$  and an oil flow rate of 1320 liter/hr.

4) An increase in service life owing to the elimination of "hot spots" in the machine caused by high axial and radial temperature gradients, which also determine the service life. The temperature drop in the oil normally equals several degrees (with air cooling  $\Delta t_v = 40-50^{\circ}\text{C}$ ). In addition, it is possible to provide more reliable oil lubrication of the bearings.

5) Oil-cooled machines are more widely applicable — they are universal. By simply changing the heat exchanger, i.e., by cooling hot cabin air, by evaporation, etc., it is possible to use the same machine under various conditions.

5. Cooling by means of air taken off from a compressor is carried out from an intermediate stage of an axial turbocompressor of a turbojet engine (TKVRD); the air is cooled in an intermediate air or liquid radiator (Fig. 1.40).

The increased air temperature at the compressor output may be compensated by a large weight flow rate, i.e., by an increase in the



stream pressure and velocity. A system with an air-cooled radiator is not as good as external forced-air cooling; a system with a liquid-cooled radiator and, in particular, one using the fuel can operate at high flight speeds and altitudes. Here it is necessary to remember, however, that the draining of air from the TKVRD for generator cooling has a noticeable effect, resulting in decreased thrust and increased fuel consumption.

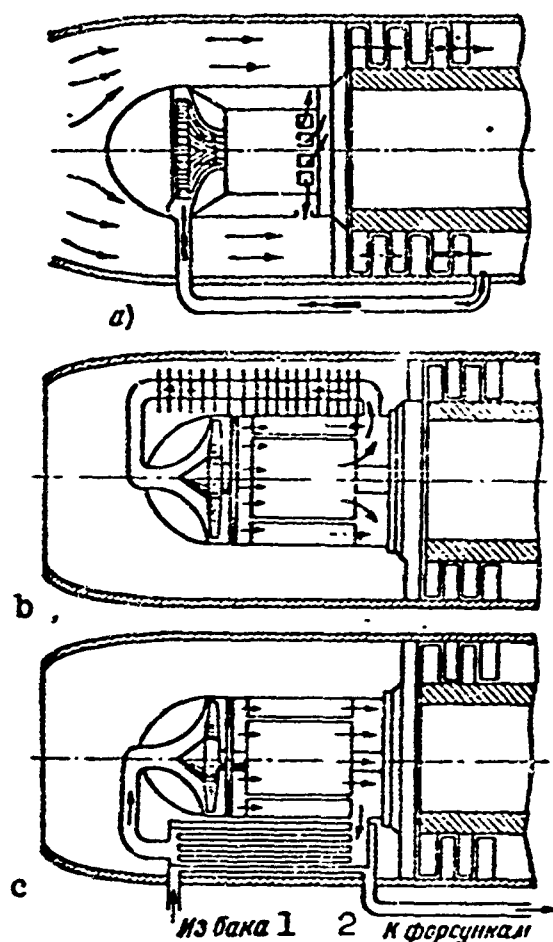


Fig. 1.41. Cooling of air after it has left air turbine. a) Open-cycle system; b) closed-cycle system using intermediate air-cooled radiator; c) closed-cycle system with intermediate fuel- or oil-cooled radiator. 1) From tank; 2) to nozzles.

Figure 1.41 shows a cooling circuit for a generator that takes air from a TKVRD compressor; here the air is cooled in a power air turbine. Compressor air is applied to the air turbine which actuates the

generator and then cools it. In this case, the problems of constant drive speed and generator cooling are solved simultaneously.

Since the temperature of the air at the compressor outlet is high for generator cooling, additional cooling of the air with the aid of a fuel-cooled radiator is needed.

The advantages of this system are independence of cooling-air characteristics, constant rotational speed and lighter generator weight, and the possibility of locating the generator in the most convenient position aboard the flying craft.

A drawback to the system is the low efficiency of the installation. At the input to the air turbine, the working pressure of the air arriving from the compressor fluctuates over a broad range; consequently, in order to keep the generator speed constant, it is necessary to throttle the air, leading to increased losses. In addition, as we have already noted, thrust is lowered and fuel consumption raised when air is bled from the compressor.

Methods exist for increasing cooling efficiency while using a gas power turbine.

In the present work, we mention only certain basic cooling systems to provide a basis for considering an entire group of related systems possessing intermediate properties.

Manu-  
script  
Page  
No.

[Footnote]

13 Here and below, all relative quantities are denoted by the \*.

21 A.I. Bertinov, *Proyektirovaniye samoletnykh elektricheskikh mashin* [Design of Aircraft Electric Machines], Oborongiz [State Press for the Defense Industry], 1953.

37 A.I. Bertinov, Vliyaniye chastoty na razmery i poteri transformatora [Influence of Frequency on Dimensions and Losses of the Transformer], "Elektrotehnika" [Electrical Engineering], Izvestiya VUZ [Bull. Higher Tech. Insts.], 1958, No. 1.

100 Actually, the constant losses decrease somewhat under high-altitude conditions due to a drop in ventilation losses.

Manu-  
script  
Page  
No.

[List of Transliterated Symbols]

- 11 AЭМ = АЕМ = aviatsionnaya elektricheskaya mashina = air-craft electrical machine
- 12 СА = СА = standartnaya atmosfera = standard atmosphere
- 17 д = d = dinamicheskaya dobavka = dynamic rise
- 17 торм = torm = tormozheniye = impact
- 18 охла = okhl = okhlazhdeniye = cooling
- 20 ТЗ = ТЗ = tekhnicheskoye zadaniye = technical plan
- 20 ТТ = ТТ = tekhnicheskkiye trebovaniye = technical specifications
- 25 П = P = preobrazovatel' = converter
- 26 ВДГ = VDG = vol'todobavochnyye generatory = booster generators
- 26 В = V = выпрямитель = rectifier
- 26 Н = N = nagruzka = load
- 26 Г = G = generator = generator
- 37 э = e = elektromagnitnyy = electromagnetic
- 37 с = s = сердечник = core
- 37 м = m = мед' = copper
- 37 а = a = активный = active
- 38 в = v = вихревой = eddy [-current]
- 46 н = n = наружный = external
- 47 з.с = z.s = заполнение сердечника = core fill factor
- 47 а.с.я = a.s.ya = активный слой, якоря = active layer, armature

47	а.с.в = а.с.в = aktivnyy sloy, возбуждение = active layer, excitation [winding]
47	я = ya = yakor' = armature
47	в = v = возбуждение = excitation
50	опт = opt = optimal'nyy = optimum
51	м/сек = m/sec
51	ц = cycles per second
51	об/мин = oborotov v minutu = rpm
55	мех = mekh = mekhanicheskiy = mechanical
55	г = g = gisterezisnyy = hysteresis
55	ср = sr = sredniy = average
55	с = s = stal' = steel, iron
58	ch = cosh
58	sh = sinh
61	з.ср = z.sr = zubtsy, sredniy = teeth, central
61	п = p = paz = slot
67	з.п = z.p = zapolneniye, paz = fill factor, slot
74	ном = nom = nominal'nyy = rated
76	м.д.п = m.d.p. = med', dopolnitel'nyy polyus = copper, commutating pole
76	м.к.о = m.k.o = med', kompensatsionnaya obmotka = copper, compensating winding
76	с.з = s.z = stal', zubtsy = steel, teeth
76	с.д s.d = stal', dopolnitel'naya = iron, additional
76	т.к = t.k = treniye, kollektor = friction, commutator
76	под = pod = podshipnik = bearing
76	э.к = e.k = elektricheskiy, kontaktnyy = electrical, contact
76	щ = shch = shchetka = brush
76	и = i = induktor = inductor
78	р = r = regulyator = regulator
78	к = k = kollektor = commutator

80      в.х.х = v.kh.kh = возбуждение, холостой ход = no-load  
excitation

80      в.ном = v.nom = возбуждение, номинальное = rated-load  
excitation

80      в.нагр = v.nagr = возбуждение, нагрузка = excitation, load

81      г = g = горячий = hot

81      х = kh = холодный = cold

82      в = v = воздух = air (subscript to Q, G)

83      τ = t = трение = friction

84      кр = kr = критический = critical

85      π = p = постоянный = constant

85      подшип = podsh = подшипник = bearing

85      м.в.х = m.v.kh = мед', возбуждение, холостой = copper,  
field-winding, no-load

95      и = i = излучение = radiation

95      к = k = корпус = frame

116      в = v = винт = propeller

117      π = p = потери = losses

119      τ = t = топливо = fuel

119      г = g = генератор = generator

130      ТКВД = ТКВД = турбокомпрессор реактивного двигателя =  
jet-engine turbocompressor

## Chapter 2

### GENERAL INFORMATION ON AIRCRAFT GENERATORS

#### 2.1. CLASSIFICATION OF AIRCRAFT GENERATORS

There are two ways of converting mechanical energy into electrical energy: by the displacement of currents of electricity in a magnetic field, or by the displacement of electric charges in an electric field.

The first method is used in electromagnetic machines, and the second in electrostatic machines. So far, electrostatic machines have been used more in physical laboratories than in engineering. Below we shall consider only electric machines based on the first principle; they are far and away the most common.

Aircraft generators may be classified as follows:

By the type of current:

- a) direct-current generators;
- b) alternating-current generators;
- c) double-current generators.

By function:

- a) generators used to supply the main electrical system;
- b) emergency and stand-by generators;
- c) converter generators;
- d) special-purpose generators.

By operating principle:

- a) synchronous, with electromagnetic excitation; magnetoelectric, excited by permanent magnet; and induction, using electromagnetic or permanent-magnet excitation;

b) induction;  
c) alternating- and direct-current commutator and collector generators.

TABLE 2.1  
Classification and Certain Features of Aircraft Generators

1 рода тока	2 Наименование генераторов	3 Возбуждение	4 Полюсы	5 Система охлаждения	6 Число фаз	7 Частота, Гц	8 Напряжение, В	9 Область применения генераторов	10 Тип привода
Переменный	Синхронные 12	Электромагнитное 13	Внешние или внутренние 14	Самовентилиция, продув 15	3 и 1 3 и 1 16	400 ÷ 1600	208/120 115	Для электросистем и преобразователей 17	18 Авиадвигатель, автономный привод, двигатель постоянного тока
	Магнитоэлектрические 19	Постоянными магнитами 20	Внутренние 21	Самовентилиция 22	1 и 3 16	400 ÷ 6000	208/120 36 и 115 16	Для преобразователей и спецустановок 23	Двигатель постоянного тока, автономный привод 24
	Индукторные 25	Электромагнитное постоянными магнитами 26	Внутренние 27	Самовентилиция, продув 28	1 и 3 16	400 ÷ 6000	115, 60, 30	Для преобразователей и спецустановок 23	Авиадвигатель, двигатель постоянного тока, автономный привод 29
	Асинхронные 30	Переменным током со стороны якоря 31	Внешние 32	Самовентилиция, продув 33	3 и 1 16	400 ÷ 1600	208/120 115	—	—
Постоянный	(Постоянного тока), коллекторные 35	Электромагнитное 13	Внешние 32	Самовентилиция, продув 28	—	—	30	Для электросистем и резерва 36	Авиадвигатель, автономный привод 37
		Постоянными магнитами 20	Внешние 32	Самовентилиция, естественное охлаждение 38	—	—	30	Для питания систем автоматики 39	Двигатель постоянного тока, специальный привод 40

1) Type of current; 2) generator nomenclature; 3) excitation; 4) poles; 5) cooling system; 6) number of phases; 7) frequency, cps; 8) voltage, v; 9) generator region of application; 10) type of drive; 11) alternating; 12) synchronous; 13) electromagnetic; 14) external or internal; 15) selfcooling, forced-air; 16) and; 17) for electric-power systems and converters; 18) aircraft engine, independent drive, direct-current motor; 19) magnetolectric; 20) permanent magnet; 21) internal; 22) selfcooling; 23) for converters and special installation; 24) direct-current motor, independent drive; 25) inductor; 26) permanent-magnet electromagnetic; 27) internal; 28) selfcooling, forced-air; 29) aircraft engine, direct-current motor, independent drive; 30) induction; 31) alternating current from armature side; 32) external; 33) selfcooling, forced air; 34) direct; 35) (direct-current), commutator; 36) for electric-power systems and stand-by purposes; 37) aircraft engine, independent drive; 38) selfcooling, natural cooling; 39) for supplying automatic-device systems; 40) direct-current motor, special drive mechanism.

By nature of drive:

a) generators driven by human muscle power — hand- or foot-

powered;

b) generators driven by a stream of oncoming air ("windmill" driven);

c) generators driven by the main aircraft engine;

d) generators driven by a special engine.

Table 2.1 shows certain features of aircraft generators, requiring no further explanation, in accordance with the classification given.

## 2.2. TECHNICAL SPECIFICATIONS AND BASIC TECHNICAL INDICES

The creation of a new machine normally involves two stages:

a) the design and manufacture of pilot models from TZ;

b) production and delivery of equipment in accordance with the TT.

As a rule, the TT are compiled on the basis of the finished and accepted pilot models, and they are the basic technical document.

The TZ and TT contain: rated characteristics, operating conditions, test and acceptance methods, volume of installation, and certain other data.

Owing to the fact that aircraft technology is developing continuously and rapidly, the specifications for aircraft electrical machines continuously become more demanding with respect to maximum power, variety, and technical and economic characteristics. As a result, the TZ and TT applying to aircraft generators are constantly changed.

Table 2.2 gives examples of some general technical specifications for direct- and alternating-current aircraft generators designed for the main electrical system of a flying craft.

Some technical data for modern general-purpose direct- and alternating-current aircraft generators are given in Table 2.3.

Relative machine weights, characterizing their degree of utilization, are given in Tables 2.4 and 2.5.

Table 2.6, which compares general-purpose and aircraft generators,



TABLE 2.2

## Sample Technical Specifications for General-Purpose Aircraft Generators

1 Генераторы		2 Постоянного тока	3 Переменного тока
4 Высотность в км		21 до 20	
5 Окружающая температура в °C		22 От -60 до +50	
6 Давление в мм рт.ст.		22 От 760 до 43	
7 Относительная влажность		98% <sup>23</sup> при $t = 20^{\circ}\text{C}$	
8 Срок службы		24 500 час. в течение 3 1/2 лет со дня выпуска с завода	
9 Механическая прочность	Вибрация мест крепления, <sup>16</sup> тряска мест крепления	$f = 15$ гц, амплитуда 3,5 мм 25 время 30 мин.	$f = 53$ гц, амплитуда 0,8 мм 26 время 3 час.
10 Перегрузка	По мощности <sup>17</sup>	50%—2 мин. <sup>27</sup>	50%—2 мин.; 90%—5 сек. <sup>28</sup>
	По току <sup>18</sup>	50%—5 мин.; 100%—5 сек. <sup>29</sup>	50%—5 мин.; 100%—5 сек. <sup>30</sup> при $U = 0,9 U_{\text{ном}}$
11 Изоляция обмоток в горячем состоянии	Испытание повышенным напряжением <sup>19</sup>	1000 в при 50 гц—1 мин. <sup>31</sup>	1500 в при 50 гц—1 мин. <sup>32</sup>
	Сопротивление <sup>20</sup>	Более $10^6$ ом при 98% влажности <sup>33</sup>	
Повышение скорости вращения <sup>12</sup>		20% сверх наибольшей скорости в течение 2 мин. <sup>34</sup>	
Коэффициент мощности <sup>13</sup>		— 0,75	
Скорость вращен. в/частота <sup>14</sup>		3800 ÷ 9000 об/мин <sup>35</sup>	400 гц <sup>36</sup>
Напряжение в в <sup>15</sup>		30	208/120

1) Generators; 2) direct-current; 3) alternating-current; 4) altitude, km; 5) ambient temperature, °C; 6) pressure, mm Hg; 7) relative humidity; 8) service life; 9) mechanical strength; 10) overload; 11) winding insulation, hot; 12) speed increase; 13) power factor; 14) rotational speed/frequency; 15) voltage, v; 16) vibration at point of attachment, jolting at point of attachment; 17) power; 18) current; 19) high-voltage test; 20) resistance; 21) up to 20; 22) from xx to xx; 23) at; 24) 500 hr for 3-1/2 years from day of leaving factory; 25)  $f = 15$  cps, amplitude, 3.5 mm, time 30 min; 26)  $f = 53$  cps, amplitude, 0.8 mm, time 3 hr; 27) 50% - 2 min; 28) 50% - 2 min; 90% - 5 sec; 29) 50% - 5 min; 100% - 5 sec; 30) 50% - 5 min; 100% - 5 sec, with  $U = 0.9 U_{\text{ном}}$ ; 31) 1000 v at 50 cps - 1 min; 32) 1500 v at 50 cps - 1 min; 33) above  $10^6$  ohms at 98% humidity; 34) 20% above maximum speed over a 2-min period; 35) 3800-9000 rpm; 36) 400 cps.

TABLE 2.3

## Technical Data for Aircraft Generator

1 Генераторы	2 Постоянного тока	3 Переменного тока
4 Диапазон мощностей $P_{ном}$	14 (0,35÷30) кВт	16 (3÷100) кВа
5 Напряжение в в	15 30	15 208,120
6 Скорость вращения $n$ об/мин	15 3800÷5900 при $P_{ном} < 1,5$ 3800÷9000 при $P_{ном} > 1,5$ 4400÷10000	16 8000 при $S_{ном} < 30$ кВа 6000 при $S_{ном} > 30$ кВа
7 Частота $f$ , гц	—	15 100
8 Система охлаждения	17 Самовентиляция при $P_{ном} < 1,0$ 19 Продув при $P_{ном} > 1,0$	18 Продув
9 Коэффициент мощности	—	0,75
10 Система возбуждения	20 Параллельное или смешанное	21 От возбудителя или самовозбуждение
11 Исполнение	22 Некомпенсированное, компенсированное	23 С внешним или с внутренними полюсами
12 К.п.д.	0,70÷0,80	0,85÷0,95
13 Относительный вес	14 3,7÷2,0 при (3÷30) кВт	15 (2,33÷1,0) при (3÷100) кВа

1) Generator; 2) direct-current; 3) alternating-current; 4) power range  $P_{ном}$ ; 5) voltage, v; 6) speed  $n$ , rpm; 7) frequency  $f$ , cps; 8) cooling system; 9) power factor; 10) excitation system; 11) construction; 12) efficiency; 13) relative weight; 14) kw; 15) at; 16) kva; 17) self-ventilation with  $P_{ном} \leq 1.0$ ; 18) forced-air; 19) forced-air with  $P_{ном} \geq 1.0$ ; 20) parallel or combination; 21) from exciter, or selfexcitation; 22) uncompensated, compensated; 23) with external or internal poles.

TABLE 2.4

## Relative Weight of Direct-Current Generators

$\frac{G_r}{P_{ном}} = f(P_{ном})$										
$P_{ном}$ кВт 1	3	6	9	12	15	18	21	24	27	30
$\frac{G_r}{P_{ном}}$ кг/кВт 2	3,7	3	2,6	2,3	2,25	2,2	2,15	2,1	2,05	2,0

1)  $P_{ном}$ , kw; 2)  $G_g/P_{ном}$ , kg/kw.

TABLE 2.5

## Relative Weight of Alternating-Current Generators

$\frac{G_r}{S_{ном}} = f(S_{ном})$									
$S_{ном}$ 1	3 кВа	3	6	12	18	30	60	75	100
$\frac{G_r}{S_{ном}}$ 2	4 кг/кВт	2,33	1,84	1,67	1,22	1,127	1,15	1,1	1,0

1)  $S_{ном}$ ; 2)  $G_g/S_{ном}$ ; 3) kva; 4) kg/kw.

shows that alternating current aircraft generators are lighter than similar general-purpose generators by more than a factor of 10.

TABLE 2.6

Comparison of General-Purpose and Aircraft Generators

1 Тип генератора	2 Синхронные		3 Постоянного тока	
	общего при- менения	авиацион- ные	общего при- менения	авиацион- ные
6 $P_{ном}$ — мощность в квт (квв)	15	15	25	25
7 $2p$ — число полюсов	4	6	4	8
8 $f$ — частота в гц	50	400	66,7	267
9 $\frac{G_r}{P_{ном}}$ — относительный вес в кг/квт	17,3	1,3	13,2	2
10 Отношение весов	13,3		6,6	

1) Type of generator; 2) synchronous; 3) direct-current; 4) general-purpose; 5) aircraft; 6)  $P_{ном}$  — power, kw (kva); 7)  $2p$  — number of poles; 8)  $f$  — frequency, cps; 9)  $G_r/P_{ном}$  — relative weight, kg/kw; 10) weight ratio.

### 2.3. DRIVES FOR DIRECT- AND ALTERNATING-CURRENT AIRCRAFT GENERATORS

The following basic types of drive may be used:

- a) hand or foot power;
- b) propeller drive;
- c) aircraft-engine drive;
- d) independent drive from special power plant.

Manual drive. Hand- or foot-powered generators are used infrequently for certain aircraft installations powering radio units, lighting, etc., under forced-landing conditions. They are simple in construction and may be made for low powers.

Propeller drive. The first aircraft generators were driven by a propeller ("windmill"), mounted on the generator shaft and rotated by the oncoming air stream during flight. The streamlined generator and

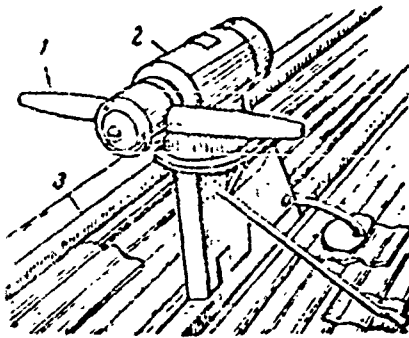


Fig. 2.1. Wind-driven aircraft generator. 1) Wind unit; 2) generator; 3) aircraft wing.

propeller were mounted on the leading edge of the aircraft (Fig. 2.1).

Two types of propellers were used: fixed-pitch or variable-pitch. In the first case, the generator speed depended on the flight speed and the voltage was maintained constant by means of a regulator in the electrical circuit. In the second case, the propeller pitch was automatically changed by means of a centrifugal regulator, and thus the generator speed varied little when the flight speed changed. In the latter case, the generator voltage changed only slightly, and this eliminated the need for using automatic voltage regulators.

At present, such generators are used only on certain trainers and gliders, since they have the following disadvantages:

- a) the possibility that the generator will break away; this creates a hazard to the aircraft and, consequently, decreases its reliability;
- b) the increased drag, especially at high speeds, which impairs the aerodynamic quality of the aircraft;
- c) the need for checking the generator for operating capability under ground conditions;
- d) the limited power and low efficiency of the generator.

Main aircraft-engine drive may take the form of a direct drive with the generator mounted on the main-engine flange (Fig. 2.2a), or a remote drive, with the generator removed to a separate installation and driven with the aid of a flexible shaft (Figs. 2.2b and 2.3).

In the first case, the generator is attached to the aircraft-engine drive box with the aid of a flange.

The structural features are dictated by the location of the generator on the aircraft engine (requirement for minimum weight and size).

The mechanical stresses in the flange material and in the mounting bolts, appearing owing to impact and vibration load factors limit the weight of the generator and its tilting moment (the product of the generator weight by the distance from the flange to its center of gravity) to some specific value. Thus, the external dimensions ( $D_n$  and  $L$ ) of the generator should not exceed specified limits which permit the construction of generators of only limited power.

Thus, with direct drive, the generator is limited in weight, external dimensions (length and diameter), and bending moment at the generator flange.

Such a system, however, gives minimum weight, smallest size, and is reliable and economical.

With remote drive, the limitations on machined diameter and length, as well as on the bending moment, no longer apply, but additional area and weight are required.

The basic drawbacks to main aircraft-engine drive are: variable speed; sharp change in engine speed and nonuniform engine operation; the fact that different engines operate at different speeds; the electrical system is not independent, i.e., the generator depends on the operation of the main engines.

Independent drive arrangements are divided into two groups: semi-independent drives, which require that at least one of the main flying-craft engines be in operation; and independent drives, whose operation is completely independent of the main engines.

The first group includes gas turbines operating on the exhaust gases of the main engines, steam turbines using the heat of the exhaust gases from piston engines, air turbines using air bled from some

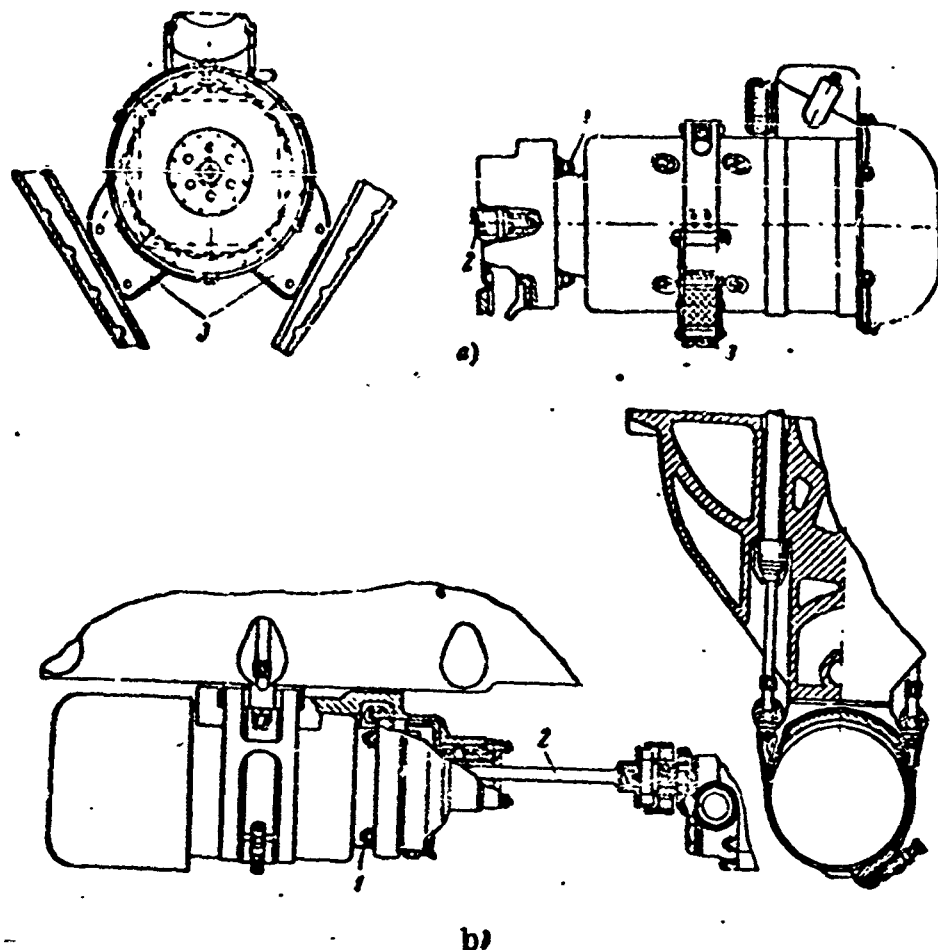


Fig. 2.2. Generator driven from piston aircraft engine. a) Direct drive; b) remote drive. 1) Bolts attaching generator flange to engine; 2) generator drive; 3) rubber pads on which generator rests.

stage of a jet-engine compressor, gas turbines using air taken from a jet-engine compressor together with additional fuel supplied to the turbine.

Gas turbines, operated by the exhaust gases of the main engines, are efficient only at low flight speeds. In addition, the exhaust-gas energy is normally used to power superchargers, and it is therefore inadequate to drive the generators.

Steam turbines are efficient, since they operate with a closed cycle, but this necessitates a steam boiler and condenser, which should have a device to protect it against freezing. All of this makes installations using steam turbines cumbersome.

Air turbines have recently received considerable development for

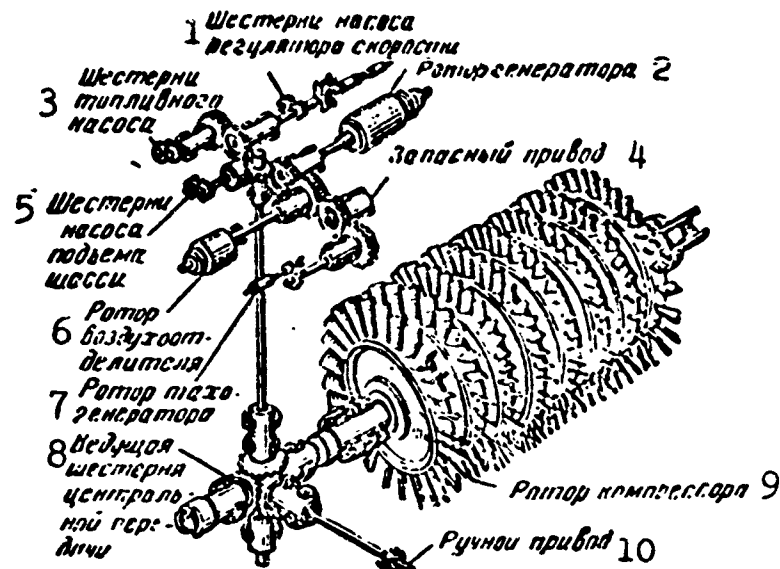


Fig. 2.3. Generator driven by jet engine. 1) Speed-control pump gears; 2) generator rotor; 3) fuel-pump gear; 4) extra drive mechanism; 5) landing-gear-retraction pump gears; 6) rotor of air separator; 7) rotor of tachometer generator; 8) drive gear of central transmission; 9) compressor rotor; 10) manual drive.

generator drive purposes (Fig. 2.4).

Air compressed and heated in a turbojet-engine compressor is supplied to the turbine. The power developed by the turbine depends on the weight flow rate of the air and the temperature drop in the air; the drop is determined by the pressure and temperature of the supply air, and by the turbine efficiency. The air weight flow rate is also determined by the temperature and pressure of the supply air and, in addition, depends on the nozzle cross section.

Owing to the fact that as the altitude increases, the temperature drop in the turbine becomes greater while the air weight flow rate decreases, the power developed by the turbine is nearly independent of flight altitude.

With increasing flight speed, however, the power developed by the turbine increases, and it is necessary to design the turbine for operation while gliding or even for engine operation with the small amount of

gas available when the aircraft is standing on the ground. Thus, at cruising speed it is necessary to decrease the amount of power taken by the turbine artificially by either throttling the air at the tur-

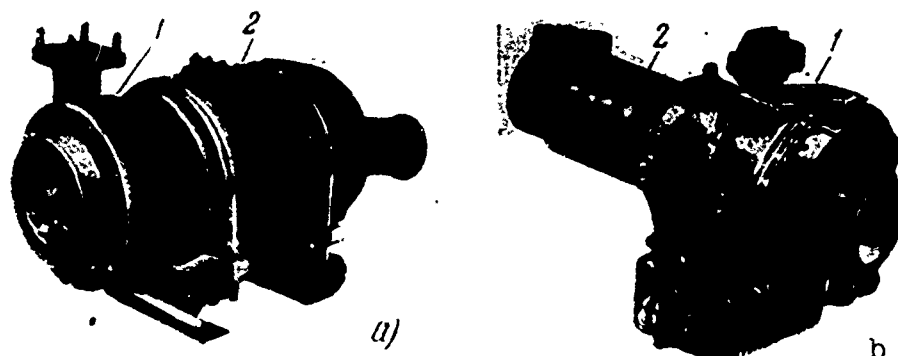


Fig. 2.4. Semi-independent air-turbine generator drive. a and b) Different arrangements. 1) Air turbine; 2) generator.

bine inlet or by changing the nozzle flow cross section (by turning the fixed blades). The first method of turbine control is less efficient but structurally simpler, and the turbine will weigh less. The second method is more efficient but the complex device used to change the nozzle cross section increases the turbine weight; it thus is advantageous when used for high-power turbines.

An advantage of the air turbine is the possibility of using the air handled by the turbine to cool the generator (when the air in the turbine expands, its temperature drops).

The low efficiency (not exceeding 0.6) of the air turbine is a substantial drawback.

Gas turbines differ from air turbines in that a combustion chamber is installed before the nozzle apparatus; fuel supplied additionally is burned here. This decreases the flow rate of the air taken from the compressor for the same turbine shaft power. Such turbines may prove advantageous when used to drive high-power generators.

The advantages of semi-independent drive systems are:

a) the possibility in emergencies of switching the turbine from



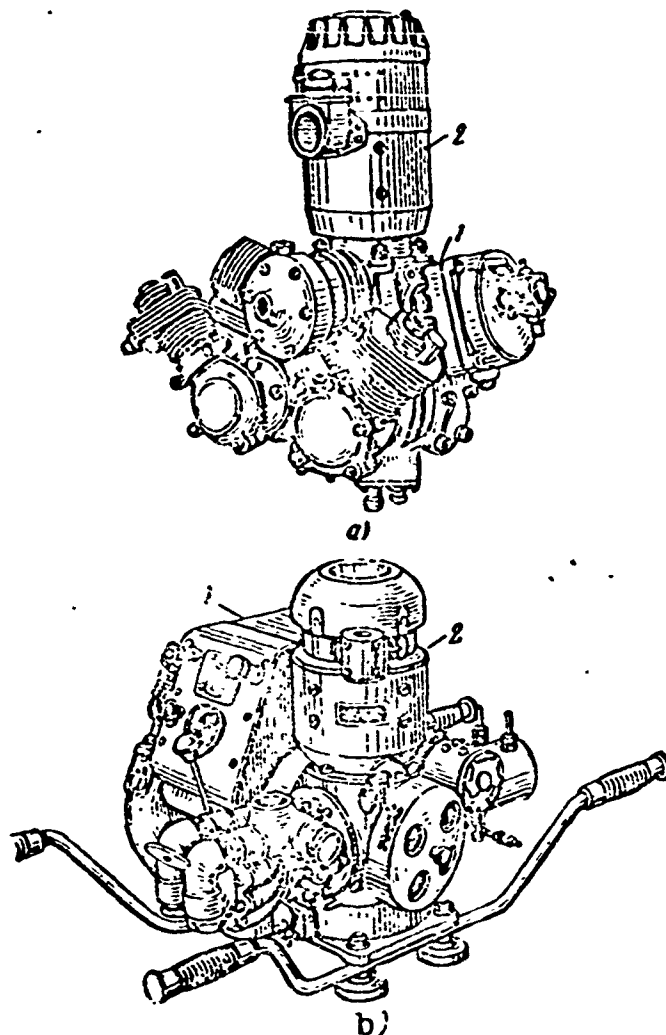


Fig. 2.5. Generator driven independently by internal-combustion motor. a and b) Different arrangements; 1) motor; 2) generator.

one engine to another, which is done by means of a special supply-duct device (common manifold);

b) the possibility of moving the generating unit from the power bay (this is especially important for axial-flow turbojet engines) to the central portion of the aircraft, eliminating the weight of the heavy power conductors (the additional weight of the air ducts is slight, since the air taken from the compressor is also used for cabin supercharging, equipment cooling, etc.);

c) the ease of regulating generator speed, i.e., constant-frequency alternating current can be obtained (a gas-turbine system can hold the speed constant within limits of the order of  $\pm 0.5\%$ );

d) the decrease in the weight of the driven turbogenerator owing to its considerably higher speed.

The second group of independent drive arrangements includes: gasoline-powered internal-combustion engines (Fig. 2.5); air turbines using ram air (Fig. 2.6); and gas turbines with air induction (Fig. 2.7).

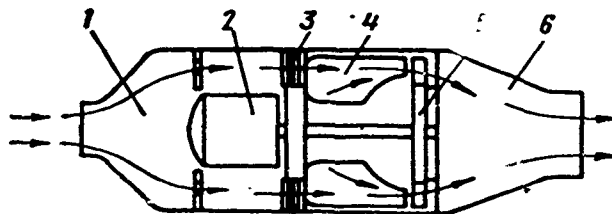


Fig. 2.6. Generator independent gas-turbine drive. 1) Air intake; 2) generator; 3) compressor; 4) combustion chamber; 5) gas turbine; 6) exhaust nozzle.

Independent installations do not depend for their operation on the main aircraft engines, i.e., they may be used while the aircraft is standing on the ground, and under emergency conditions. They possess the same advantages as semi-independent drive arrangements.

They also present substantial drawbacks, however:

a) high weight, large size, and low efficiency of the installation in comparison with generators driven by a main engine;

b) poor high-altitude performance of the units, i.e., additional air-compression devices are needed;

c) the independent engine is less reliable than the main aircraft engine.

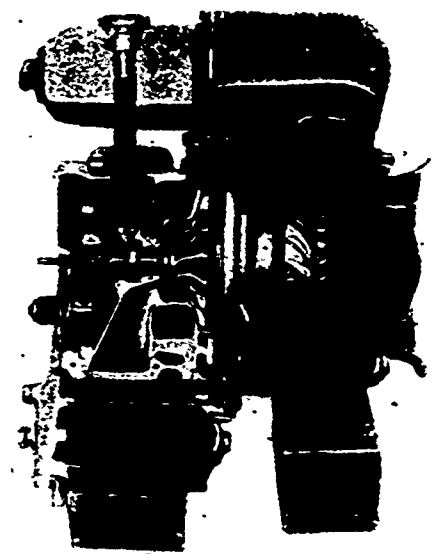


Fig. 2.7. Rover gas turbine.

Owing to these drawbacks, independent drive arrangements are now used only as emergency engines or as sources of electric power and com-

pressed air in starting engines while the aircraft is standing on the ground.

As an example of a high-power independent installation, we have shown a single-stage gas turbine with radial air induction (see Fig. 2.7); at 24,000 rpm, it develops 44 kw of power while the aircraft is standing on the ground and 20 kw when the craft is flying at an altitude of 15 km and a speed of 800 km/hr. While the aircraft is standing on the ground, it requires about 0.86 kg/kw·hr of fuel, and has a dry weight of 52.5 kg.

Fighter craft have used a generator driven by an air turbine (single-stage axial operated by ram air) as an emergency unit.

Two different forms of stand-by alternating-current sources are in use: a) a reserve power-supply unit that moves out into the air stream when an emergency occurs; b) a stand-by power-supply unit installed in a fixed position on the aircraft; when an emergency occurs, a gate opens, and the oncoming air stream strikes the propeller that actuates the generator.

It must be remembered that a reserve alternating-current supply should be provided for various flight speeds, i.e., it is necessary to regulate the speed of the generator propeller and the generator voltage.

Independent installations are presently recommended as auxiliary alternating-current supplies for emergency conditions, for engine starting, and for special purposes.

In addition, in alternating-current electrical systems not using batteries, alternating-current magnetoelectric generators, together with rectifiers, may be used for excitation and for emergency power for relay circuits.

## 2.4. THE PROBLEM OF OBTAINING CONSTANT-FREQUENCY ALTERNATING CURRENT\*

We have already noted that a constant-frequency alternating-current system represents the most desirable choice for the electrical system of a modern flying craft.

The simplest way of obtaining constant-frequency alternating current is to use power plants consisting of a generator driven by a special constant-speed motor. Such installations, however, as we have noted above, are inefficient and are thus employed only in special cases.

If the generators are driven by an aircraft engine, their speed will vary during flight; it thus becomes necessary to manufacture devices to convert the changing aircraft-engine shaft speed into a constant speed for the generator shaft. Two methods may be used to obtain constant frequency where the speed of the prime mover varies: a device may be put between synchronous generator and motor that will keep the speed of the output shaft constant when the speed of the input shaft varies; or alternating current may be generated with varying frequency, corresponding to the motor speed, and the alternating current may then be converted into direct current (for example, in commutator systems).

Where the first method is used to solve the problem, mechanical, electromagnetic, hydraulic, or electromechanical devices may be used.

Table 2.7 shows the basic systems used to obtain constant frequency where the speed of the prime mover varies.

### Mechanical Devices for Obtaining Constant Frequency

If the generator drive uses a multispeed reduction gear, the generator speed will vary within a certain narrow range; the speed fluctuations will be less severe the more stages in the reducing gear.

Where the range of variation in the drive speed is  $n_{\max}/n_{\min} = 2.25$ ,

TABLE 2.7

## Basic Frequency-Conversion Methods

1 Тип преобразователя скорости или частоты	2 Примерный относительный вес	3 К. п. д.	4 Особенности
5 Многоступенчатые механические редукторы и вариаторы	6 Имеют большие габариты и вес	7 К. п. д. редуктора высокий	8 Громоздкий, сложный конструктивно, трудно управляемый, имеют большую инерционность
9 Электромагнитные муфты с плавным изменением передаточного отношения	10 (2÷2.5) кг/квт	11 К. п. д. муфты низкий, и тем ниже, чем больше диапазон изменения скорости	12 Мощность, соответствующая разности скоростей, теряется во вторичной цепи муфты. Усложнен теплосвод у муфты; просты в управлении
13 Электромагнитный тормоз и дифференциал с плавным изменением передаточного отношения	14 Размеры и вес тормоза меньше аналогичной муфты	15 То же, что и для муфты	16 То же, что и для муфты
17 Гидромуфты с плавным изменением передаточного отношения	18 (1÷1.5) кг/квт	19 К. п. д. муфты—85%, К. п. д. системы—75%	20 Требуют сложную гидросистему, хорошо управляемы
21 Электромашинные системы	22 (3.5÷5) кг/квт; имеют большие габариты	23 К. п. д. системы—65% и ниже	24 Требуют коллектор, имеют плохую коммутацию; легко управляемы
25 Электрические системы	26 Имеют большие габариты и вес	27 К. п. д. системы ниже 75%	28 Имеются пути снижения габаритов и повышения к. п. д.

1) Type of speed or frequency converter; 2) approximate relative weight; 3) efficiency; 4) characteristics; 5) multispeed mechanical reduction gears and variable-speed gears; 6) heavy and large; 7) reduction-gear efficiency high; 8) cumbersome, structurally complex, difficult to control, and slow to respond; 9) electromagnetic clutches with continuous variation of gear ratio; 10) (2-2.5) kg/kw; 11) clutch efficiency low, and lower the broader the speed-change range; 12) the power corresponding to the difference in speeds is dissipated in the secondary element of the clutch. Clutch cooling is complicated. They are simple to control; 13) electromagnetic braking and differential with continuously variable gear ratios; 14) the brake is smaller and lighter than an analogous clutch; 15) the same as for a clutch; 16) the same as for a clutch; 17) hydraulic clutches with continuously variable gear ratio; 18) (1-1.5) kg/kw; 19) clutch efficiency, 85%, system efficiency, 75%; 20) requires a complex hydraulic system. Good control characteristics; 21) electromechanical system; 22) (3.5-5) kg/kw, large in size; 23) system efficiency 65% or less; 24) requires commutator, has poor commutator, is easily controlled; 25) electrical system; 26) large and heavy; 27) system efficiency below 75%; 28) ways are available to decrease size and increase efficiency.

the utilization of a two-speed reduction gear makes it possible to maintain the generator shaft speed constant to within  $\pm 17\%$  of the nominal value. This may be done by shifting the reduction-gear transmission at appropriate instants; a four-speed transmission is used.

By increasing the number of reduction-gear speeds, it is possible to gain a considerable increase in generator speed-regulation accuracy. Thus, for example, a three-speed reduction gear from which nine different ratios can be obtained will maintain generator speed constant to within  $\pm 10\%$  of the nominal value.

The application of such multispeed transmissions on board aircraft is limited by the fact that they do not provide for parallel generator operation, since the speeds of the aircraft engines and, consequently, the generator speeds will differ considerably among themselves. In addition, such devices are extremely cumbersome and structurally complicated.

In order to use generators in parallel, it is necessary to employ progressive transmissions with continuously variable gear ratios. Progressive speed regulation may be obtained by using various types of mechanical, electromagnetic, hydraulic, and electromechanical devices - variable-speed drives.

Mechanical versions are divided into friction, gear, inertial, and lever types. The first two types of transmission are continuously operating transmissions, and the last two are impulse types.

Friction variable-speed drives are the most common type. Drives of this type may take different forms:

a) they may involve direct contact with the working elements, with rotation transmitted from the drive shaft to the driven shaft by the direct contact of two gears or with the aid of a third idler gear;

b) planetary gears, in which intermediate rollers execute complex

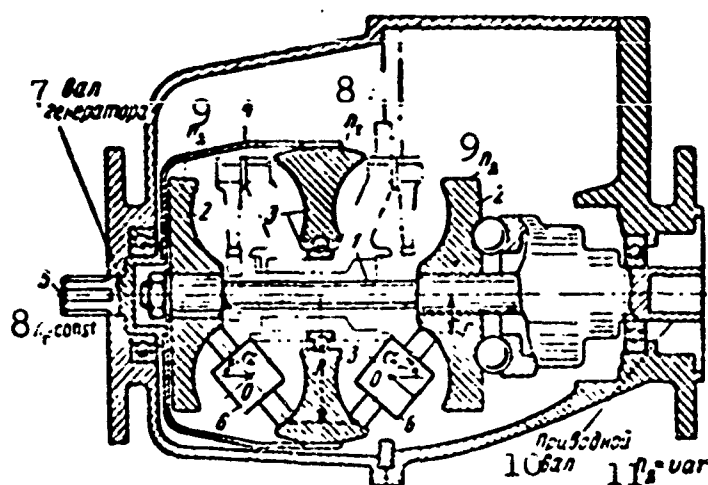


Fig. 2.8. Mechanical friction-type variable-speed drive for 30-kva aircraft generator running at 8000 rpm. 1) Drive shaft; 2 and 3) disks; 4) bushing; 5) generator shaft; 6) rollers; 7) generator shaft; 8)  $n_g$ ; 9)  $n_d$ ; 10) drive shaft; 11)  $n_d = \text{var.}$

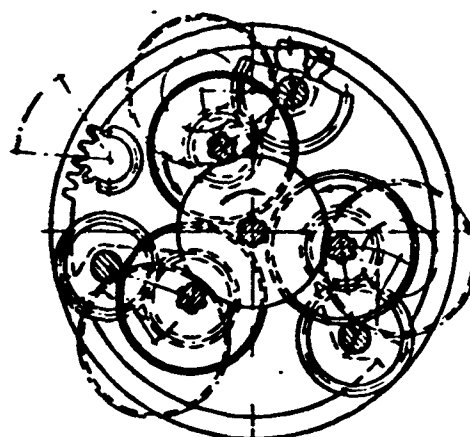
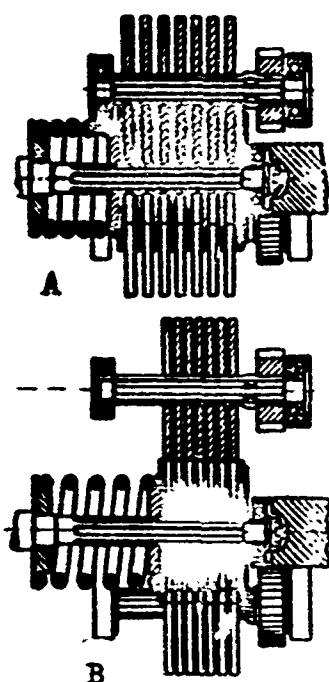


Fig. 2.9. Mechanical variable-speed drive using changing oil viscosity.

motions (transmission with ball satellites).

c) belt transmission, in which the rotation is transmitted by means of a flexible element (flexible belt).

Friction transmissions, as a rule, are relatively inefficient.

Gear-type variable-speed drives are characterized by the absence of slip and, consequently, by high efficiency. Drives of this type may take the following forms:

a) chain drive, in which transmission is accomplished by means of a flexible hinged chain with inserted strips, similar to a V-belt drive, but differing in that a hinged chain is used in place of the

belt, and the pulleys have radial slots;

b) helical-gear drives, in which rotation is transmitted between two helical gears by means of an intermediate helical rotor that can move along its own axis of rotation;

c) planetary-gear drives, in which the gear ratio is regulated by axial displacement of the sun gear, which is engaged with conical planet gears.

Inertial-type variable-speed drives are complex and automatically change their gear ratio as a function of the load on the drive shaft, i.e., they are not suitable for our purposes.

Lever-type variable-speed drives are continuous-operation drives, and since they lack slip elements, they are quite efficient.

As an example, we may take two types of mechanical variable-speed drives manufactured in Great Britain.

One of them (Fig. 2.8) takes the form of a friction variable-speed drive with rollers 6 placed between two drive wheels 2 with semi-toroidal recesses and one driven wheel 3. The wheels 2 are attached to the drive shaft 1. The driven wheel 3 is connected to the shaft by means of bushing 4.

The contact surfaces of the variable-speed drive elements operate as in a deep-groove ballbearing. The speed of the output shaft is held constant by changing the angle of inclination  $\alpha$  of the axis about which the rollers rotate. The speeds are related as  $n_g/n_d = r/R$ .

A device of this type used to drive a 30-kva generator at 8000 rpm measures  $30 \times 40 \times 40 \text{ cm}^3$ . The service life without maintenance is 800 hr.

The second type of variable-speed drive (Fig. 2.9) transmits power by the frictional force in a thin layer of oil that forms between disks on the drive and driven shafts.



The oil carried by the disks to their point of contact is strongly compressed and increases in velocity by a factor of 1000, which increases the friction between the disks. The speed of the output shaft is held constant by changes in the distance between the disk axles.

When used to drive a 30-kva generator, this type of variable-speed drive weighs 20-23 kg.

A general drawback to all mechanical variable-speed drives is the fact that they are cumbersome, structurally complicated, and difficult to control. Since in such devices the gear ratio is changed during operation, it is necessary to apply considerable forces, i.e., the actuating mechanism of the frequency regulator (electric motor, electromagnet, hydraulic cylinder) must have considerable power. As a result, the automatic-control system of an installation using mechanical variable-speed drives is relatively slow-responding.

#### Electromagnetic Clutches

An electromagnetic clutch may be used as a device with a variable gear ratio.

The electromagnetic clutch of Fig. 2.10 consists of two main rotating parts, an armature similar to the rotor of an induction motor, and an inductor, similar to the inductor of a synchronous or direct-current machine.

One of the clutch elements is connected to the engine and is the driving member, while the second element is connected to the generator shaft and is the driven member.

Clearly, an electromagnetic clutch may be made with either external or internal holes. Either the armature or the inductor may be the driving member. The excitation current is applied to the winding through brushes and slip rings.

Operating principle. When the clutch drive element rotates, an

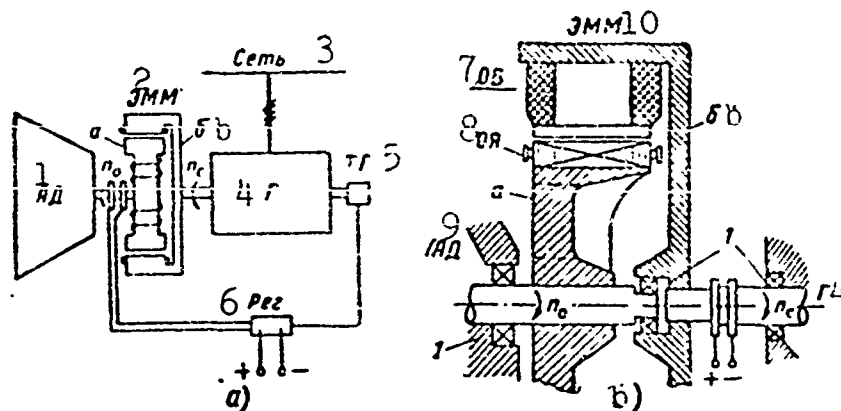


Fig. 2.10. Generator speed-stabilization arrangement using an electromagnetic clutch. a) Wiring diagram; b) structural diagram; AD) aircraft engine; EMM) electromagnetic clutch; a) drive section of EMM; b) driven section of EMM; G) generator; TG) tachometer generator; Reg) regulator; OV) excitation winding; OYA) closed-coil armature winding;  $n_0$  and  $n_s$ ) variable and stabilized speed; 1) AD; 2) EMM; 3) line; 4) G; 5) TG; 6) Reg; 7) OV; 8) OYA; 9) AD; 10) EMM.

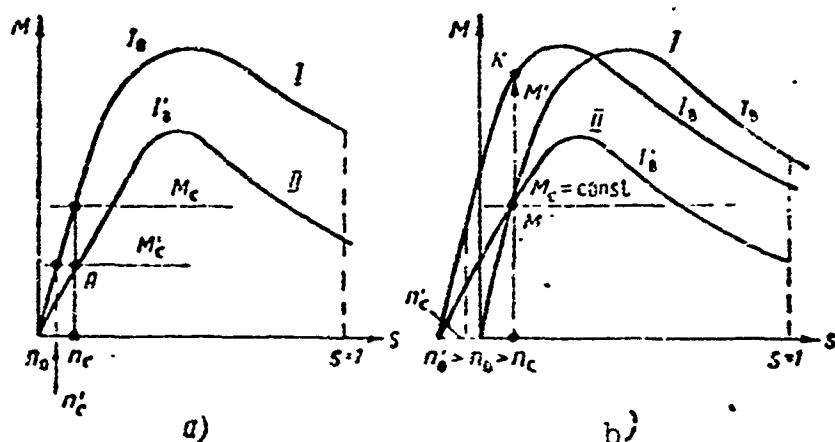


Fig. 2.11. Mechanical characteristics of EMM. a) Decrease in moment of resistance from  $M_s$  to  $M'_s$ ; b) increase in drive-shaft speed from  $n_0$  to  $n'_0$ .

emf with frequency

$$f_0 = \frac{pn}{60}$$

is induced in the armature by the magnetic flux of the inductor; here  $p$  is the number of pairs of holes in the clutch;  $n$  is the speed of the prime mover — of the clutch drive element.

A rotating magnetic field is formed in the closed-coil armature winding; the field interacts with the rotating field of the inductor, causing the armature to rotate at a speed  $n < n_0$ .

Here the frequency of the current in the armature, as in an induction machine, will be

$$f = p \frac{n_0 - n}{60} = f_0 s,$$

where  $s = (n_0 - n)/n$  is the clutch slip.

In an induction machine, the rotating field is formed by a stationary three-phase stator winding supplied with three-phase current; in our case, it is the pole windings, through which direct current flows, that rotate. As in an induction machine, the slip is a function of the load.

Since there are no friction elements in the transmission, such clutches are called electromagnetic slip couplings to distinguish them from electromagnetic friction clutches.

The mechanical characteristics of the couplings are the same as those of an induction machine.

By changing the clutch excitation current (as when the voltage across the terminals of an induction machine is varied) it is possible to change the nature of the mechanical characteristic curve  $M = f(s)$ , as is clear from Fig. 2.11.

The generator may depart from the nominal speed — the speed of the driven clutch shaft  $n_g$  — owing to a change in the active generator load, i.e., a change in the braking moment on the shaft of the clutch driven element, or a change in the speed of the prime mover, and, consequently, in the speed of the clutch driving element.

Let us assume that the moment of resistance (the active load on the generator)  $M_g$  decreases to the value  $M'_g$  (Fig. 2.11a); then if the

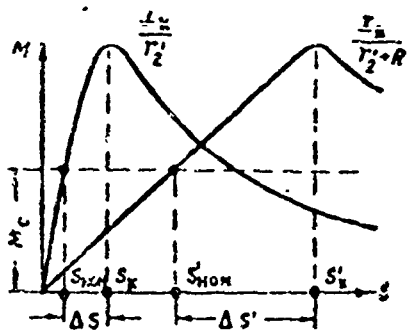


Fig. 2.12. Effective external resistance  $R$  on stable operating range of clutch  $s$ .

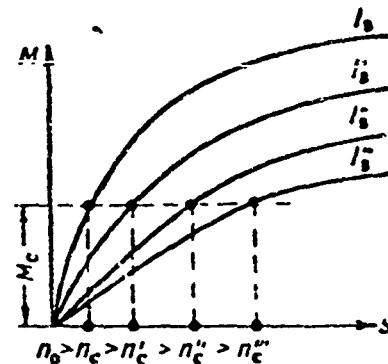


Fig. 2.13. Clutch with armature in form of massive steel ring.

drive speed  $n_0$  remains unchanged, the generator speed will increase to the value  $n'_s$ . For the generator speed to remain unchanged, it is necessary to decrease the clutch excitation current from  $I_v$ , corresponding to the mechanical curve I, to  $I'_v$ , corresponding to the mechanical curve II so that the mechanical curve II will pass through point A (at the intersection of line  $M'_s$  and line  $n_s$ ). The change in excitation current is carried out automatically by an excitation regulator.

Let us next assume that the drive-shaft speed has increased from  $n_0$  to  $n'_0$  (Fig. 2.11b); then the mechanical characteristic curve I, keeping its shape, is moved to the left by  $n'_0 - n_0$ , and the generator speed begins to rise since the moment of resistance  $M_s = \text{const}$ , while the torque  $M$  developed by the clutch rises to a value proportional to the segment  $M' = Kn_s$ . If the excitation current were not regulated, the generator speed would rise from  $n_s$  to  $n'_s$ ; the increase in speed, however, causes the tachometer generator to apply an impulse to the regulator, which decreases the excitation current from  $I_v$  to  $I'_v$ , i.e., the clutch is transferred to curve II, which corresponds to higher drive-element speed and a nominal speed  $n_s$  for the driven element. Thus, by changing the excitation current with the aid of a regulator, it is possible to maintain the speed of the driven clutch element constant, i.e., the generator speed is held constant.

The regulation system responds fairly rapidly.

As we have already noted, the clutch has the same curve for  $M = f(s)$  as an induction motor. The critical slip  $s_k$  corresponding to maximum moment is, as in an induction motor, proportional to the ratio of the active resistance in the armature circuit to the total resistance of the entire circuit, i.e.,

$$s_k = \frac{r_1'}{\sqrt{r_1'^2 + x_k'^2}}. \quad (2.1)$$

For an induction clutch with a normal cage rotor, the critical slip is  $s_k = 0.05-0.2$ , and the appropriate clutch may be used for a narrow range of speed variation, since the stable portion of the characteristic is the region from  $s = 0$  to  $s = s_k$ .

In order to increase the critical slip  $s_k$ , a phase-wound armature with an external resistance  $R$  may be used in the clutch; this does not give the proper effect, however, since the increase in  $s_k$  is accompanied by a simultaneous increase in the nominal slip  $s_{nom}$  (Fig. 2.12), and the stable operating range  $\Delta s$  increases only slightly.

In order to increase the speed-regulation range, it is possible to use the tendency of a current to flow to the outside of a conductor (skin effect), i.e., the property of a conductor of increasing its resistance as the frequency of the current flowing through it rises. The utilization of a clutch making use of the skin effect — a clutch with a deep slot or a clutch with a double squirrel cage — permits stable operation with large slips.

The most favorable characteristic is displayed by a clutch having an armature in the form of a massive steel ring (resembling K.I. Shenfer's massive rotor). As we know, the characteristic curve  $M = f(s)$  for such a clutch will theoretically not have a turning point no matter how large a slip is desired (Fig. 2.13).

For proper utilization of the skin effect, it is necessary to employ relatively high frequencies in the armature. Thus the pole system of such a clutch should be of the interlaced or inductor types (Figs. 2.14 and 2.15, respectively).

In a clutch with an interlaced pole system, the magnetic flux changes from  $+\Phi_{\max}$  to  $-\Phi_{\min}$ . The induction clutch is a parametric machine, in which the magnetic flux changes only from  $+\Phi_{\max}$  to  $+\Phi_{\min}$ , i.e., there is no reversal of sign. Thus, the dimensions of the active section of the first machine are roughly one-half those of the inductor-type machine for exactly the same value of electromagnetic moment. While in a machine with an interlaced pole system any increase in the number of poles is limited by the decreased mechanical strength of the pole pieces (fingers) and by the increase in the leakage flux between them, in a machine using an inductor pole system, there is almost no limit to the increase in the number of poles (teeth).

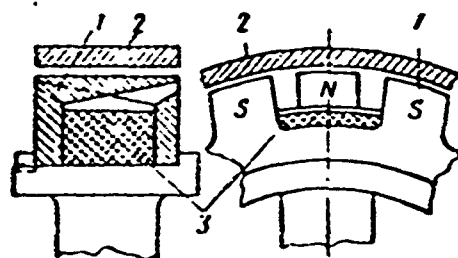


Fig. 2.14. Interlaced pole system. 1) Pole; 2) steel ring; 3) excitation winding.

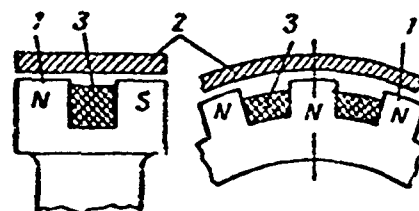


Fig. 2.15. Inductor pole system. 1) Poles; 2) steel ring; 3) excitation winding.

The magnetic-fluid (emulsion) clutch, which has recently found wide application, should also be considered to be an electromagnetic slip clutch with a broad speed-regulation range.

It operates on the following principle. A steel disk or drum coupled with the driving or driven shaft of the clutch rotates in the gap of some magnetic system. The space within this gap is filled with a mixture of oil and iron filings in a specific concentration. In the

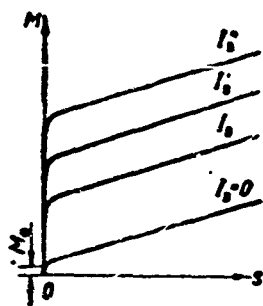


Fig. 2.16. Mechanical characteristic curve for magnetic-fluid clutch.

absence of excitation current, the clutch can transmit only a small torque  $M_s$  (3-10% of the maximum torque) owing to the viscous friction of the disk or drum in the mixture and the friction in the packing devices of the clutch. With excitation current applied, a magnetic flux appears that attracts the iron filings in the mixture, so that they cluster at the disk or drum; the forces with which these particles engage each other increase and, as it were, increase the viscosity of the mixture. As a result, the clutch becomes capable of transmitting large torques, and it is possible to vary clutch slip continuously by changing the excitation current.

The mechanical characteristic curves for such a clutch are shown in Fig. 2.16.

The slope of the curves is determined by the concentration of the working mixture. This type of clutch can also operate with no slip whatsoever where appropriate mixture concentrations and excitation current are chosen. Magnetic-fluid clutches are small in size when compared with electromagnetic (dry) clutches able to transmit the same torque; they are more complicated to operate, however, and have a substantial drawback lying in the fact that their working speeds are limited to 2000-3000 rpm owing to the harmful effect of centrifugal forces on the particles in the working mixture.

In contrast to mechanical variable-speed drives, which are constant-power torque converters, the electromagnetic clutch is a constant-torque power converter. The moment acting on the drive and driven elements under steady-state conditions are precisely the same (electromagnetic), while the speeds differ.

If  $n_0$  is the drive-element speed,  $n_s$  the driven-element speed,

and  $M$  the electromagnetic moment of the clutch, which is independent of the speed, the power applied to the clutch will be  $P_0 = n_0 M$ , and the power taken from the clutch  $P_s = n_s M$ .

The difference in these powers is the clutch slip loss

$$\Delta P = P_0 - P_s = M(n_0 - n_s). \quad (2.2)$$

Consequently, the greater the range of speed variations with the clutch, the higher the losses and the lower the efficiency.

If we let the ratio  $n_{0 \max} / n_{0 \min} = k$ , the minimum clutch efficiency from the viewpoint of slip losses will be

$$\eta_{\min} = \frac{P_s}{P_s + \Delta P_{\max}} = \frac{M n_c}{M n_c + M(n_{0 \max} - n_c)} = \frac{n_c}{n_{0 \max}}. \quad (2.3)$$

In approximation we may assume that  $n_s = n_{0 \min}$  (without considering slip where full excitation current is applied to the clutch, since it will normally equal 3-5%), i.e.,

$$\eta_{\min} \approx \frac{n_{0 \min}}{n_{0 \max}} = \frac{1}{k}. \quad (2.4)$$

i.e., the minimum efficiency of a system using an electromagnetic slip clutch is inversely proportional to the range of speed variation for the drive shaft. For example, where

$$k = \frac{9000}{4000} = 2.25, \quad \eta_{\min} = \frac{1}{k} = 0.445.$$

System efficiency will be still lower, since it is necessary to consider the losses in the generator and the clutch excitation winding.

The considerable amount of power evolved in the clutch as heat complicates cooling of this unit, and this sometimes leads to an increase in size.

Owing to the defects mentioned, electromagnetic slip clutches can be used effectively only in the following cases:

- a) narrow range of speed variation (low-slip operation);
- b) wide range of speed regulation where the load is in the nature



of a fan, for example, in controlling the speed of a wind-tunnel blower (the load moment decreases with increasing slip);

c) wide range of speed control with brief operating periods.

### Electromagnetic Brakes

In addition to electromagnetic clutches, electromagnetic brakes are used to maintain generator speed constant when drive speed varies.

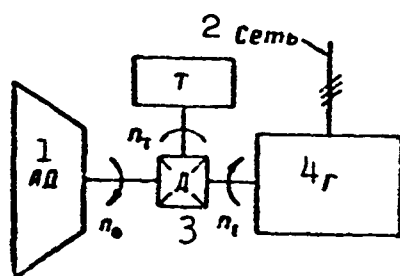


Fig. 2.17. Speed stabilization with the aid of an electromagnetic brake and a differential. D) Mechanical differential dividing the speed and power applied to generator and brake; T) controlled variable-speed electromagnetic brake; 1) AD; 2) line; 3) D; 4) G.

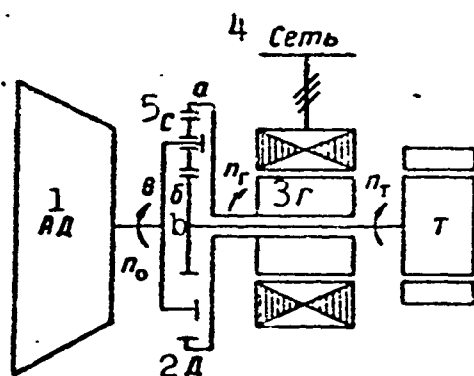


Fig. 2.19. Structural diagram for speed stabilization by an electromagnetic brake and a differential. 1) AD; 2) D; 3) G; 4) line; 5) pinion.

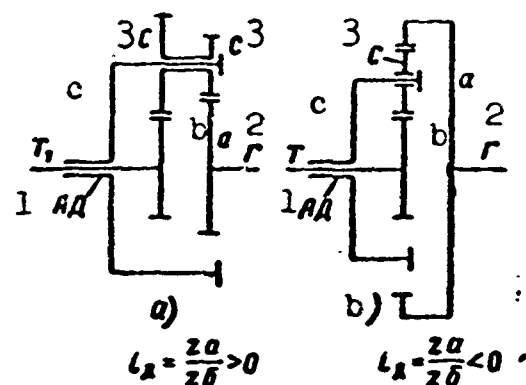


Fig. 2.18. Diagram of mechanical differentials. a) Center gear, constant speed  $n_g$ ; b) center gear, variable speed  $n_T$ ; c) crown runner; s) pinions; 1) AD; 2) G; 3) s.

Figure 2.17 shows an arrangement in which a brake is used for this purpose.

If for a change in the driveshaft speed  $n_0$  there is a corresponding change in the shaft speed of the brake  $n_t$ , i.e., the shaft is braked to some degree, the generator speed  $n_g$  may be held constant.

There are several arrangements of mechanical differentials, but they all

reduce to two groups: those with positive simple-transmission gear

ratios (with the crown runner stopped)  $i_d > 0$  (Fig. 2.18a) and those with negative simple-transmission ratios  $i_d < 0$  (Fig. 2.18b).

Depending on the combination of directions and speeds with which the crown runner and the central gears rotate, various types of differentials may be obtained (dividing, integrating, retarding, accelerating, or idling of the driven shaft).

The differential of Fig. 2.19 is best suited for use with generator drive; here crown runner c is a driven element, and the generator is connected to central gear a and the brake to central gear b.

In this case, all of the differential shafts will rotate in the same direction. The speeds of gears a and b are distributed as a function of the relationship of the resistance moments on these shafts. Thus, where the moments of resistances on gears a and b are equal, they will rotate at the same speed, equal to the speed at which crown runner c rotates. Here pinion S does not rotate about its axis or with respect to the central gears. If gear b is braked more heavily than gear a, the latter will rotate at higher speed, since pinion S will rotate about its axis.

The kinematic relationships for the differential are expressed by the Willys formula

$$i_x = \frac{n_b - n_c}{n_a - n_c}, \quad (2.5)$$

where  $i_d$  is the simple-transmission ratio.

If we let

$$i_x = -\frac{z_a}{z_b} = -i_x',$$

$$n_c = n_0, \quad n_a = n_r \text{ и } n_b = n_r,$$

then

$$n_0(1 + i_x') = n_r i_x' + n_r. \quad (2.6)$$

The force acting on the pinion shaft is distributed equally, and

equal forces act on the teeth of the central gears. Consequently, the torques acting on gears a and b are related as the number of teeth (diameters) of these gears, i.e.,

$$\frac{M_r}{M_t} = \frac{z_a}{z_b} = i_a'. \quad (2.7)$$

From the viewpoint of brake size, it is desirable to increase  $i_a'$ . Actually, if the brake takes the form of an electric machine, the dimensions of the machine armature will be determined by the moment, i.e.

$$D^2 l = \frac{P_a}{n} = M.$$

The choice of  $i_a'$  is determined by the drive speed-variation range and by the maximum brake speed  $n_{t \max}$ .

It follows from (2.7) that the drive speed

$$n_0 = \frac{n_r i_a' + n_t}{1 + i_a'}; \quad (2.8)$$

at maximum brake speed  $n_{t \max}$

$$n_{0\max} = \frac{n_r i_a' + n_{t \max}}{1 + i_a'}; \quad (2.9)$$

at minimum brake speed  $n_{t \min}$

$$n_{0\min} = \frac{n_r i_a' + n_{t \min}}{1 + i_a'}. \quad (2.10)$$

The range of speed variation is

$$k = \frac{n_{0\max}}{n_{0\min}} = \frac{n_r i_a' + n_{t \max}}{n_r i_a' + n_{t \min}}. \quad (2.11)$$

whence the gear ratio or ratio of moments is

$$i_a' = \frac{M_r}{M_t} = \frac{n_{t \max}}{n_r} \frac{1}{k-1} \left[ 1 - k \frac{n_{t \min}}{n_{t \max}} \right]. \quad (2.12)$$

When  $n_{t \min} \rightarrow 0$

$$i_a' \approx \frac{n_{t \max}}{n_r} \frac{1}{k-1}. \quad (2.13)$$

The brake speed is determined from (2.12) and is

$$n_{t \max} = i_a' n_r (k-1) \left[ 1 + \frac{k}{k-1} \frac{n_{t \min}}{n_r i_a'} \right]. \quad (2.14)$$

When  $n_{t \min} \rightarrow 0$

$$n_{r \max} \approx i_a' n_r (k-1) \quad \frac{n_{r \max}}{n_r} \approx i_a' (k-1). \quad (2.15)$$

The maximum power absorbed by the brake, taking (2.14) and the relationship  $M_t = M_g / i_d'$  into account, will equal

$$\left. \begin{aligned} P_{r \max} &= M_r n_{r \max} = M_r n_r (k-1) + \frac{M_r k n_{r \min}}{i_a'} \\ \text{or} \quad \frac{P_{r \max}}{P_r} &= (k-1) \left[ 1 + \frac{k}{k-1} \frac{n_{r \min}}{n_r i_a'} \right] \end{aligned} \right\} \quad (2.16)$$

When  $n_{t \min} \rightarrow 0$

$$\frac{P_{r \max}}{P_r} = k-1. \quad (2.17)$$

Minimum efficiency of the installation from the viewpoint of slip losses in the brake, allowing for (2.16), will be

$$\eta_{r \min} = \frac{P_r}{P_r + P_{r \max}} = \frac{1}{k} \frac{1}{1 + \frac{n_{r \min}}{n_r i_a'}}. \quad (2.18)$$

When  $n_{t \min} \rightarrow 0$

$$\eta_{r \min} \approx \frac{1}{k}, \quad (2.19)$$

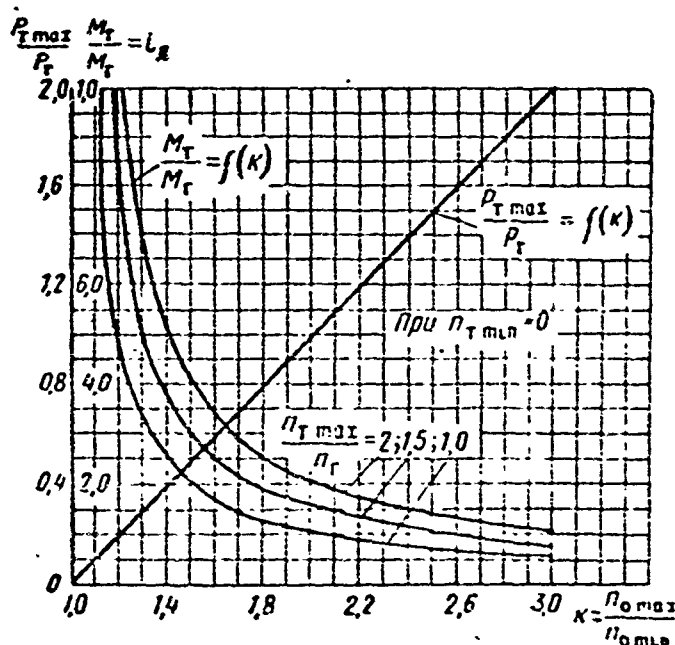


Fig. 2.20. Relative power and moment of brake as a function of speed-variation range.

i.e., it is the same as for an electromagnetic clutch. Thus, an electromagnetic brake and an electromagnetic clutch are equivalent from the viewpoint of losses and efficiency. Figure 2.20 shows the relationships  $1_d' = f(k)$  for  $n_{t \max}/n_g = 2-1$  and  $P_{t \max}/P_g = f(k)$  for  $n_{t \min} \rightarrow 0$ .

Analysis of these curves indicates that it makes sense to use a brake with the range of speed variation for the prime mover small. When  $k = 1.1-1.2$ , the brake will be roughly 15-5 times smaller than a generator and corresponding clutch.

The maximum slip losses in the brake at  $n_{t \max}$  amount to only 10-20% of the generator power. At lower drive speeds ( $n_0 < n_{0 \max}$ ), the losses will be correspondingly lower. Thus, speed may be stabilized with the aid of an electromagnetic brake and mechanical differential where the range of speed variation is small.

When operating with a wide range of speed variation, an electromagnetic brake should be used that has a deep slot, a massive armature (taking the form of a hollow cylinder closed at one end), of the hysteresis or magnetic-fluid type.

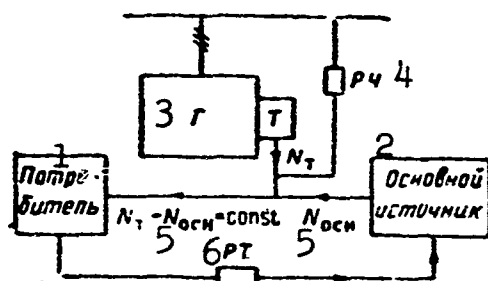


Fig. 2.21. Arrangement for using braking energy. R.Ch.) Frequency regulator; R.T.) regulator for temperature (pressure, etc.). 1) Consuming device; 2) basic source; 3) G; 4) R.Ch.; 5) osn; 6) R.T.

It is also possible to use a phase-wound armature with leads to an external circuit. In this case, brake speed is controlled by changing the resistance in the external circuit of the armature.

Thus, an electromagnetic brake is smaller than an electromagnetic clutch especially where the range of variation in the drive speed is small.

In installations using electromagnetic clutches and brakes, it is possible to decrease the slip losses (increase the efficiency) by in-

troducing additional step-type control, using mechanical drive-speed shifting or by changing the number of poles in a synchronous generator by switching.

In addition, installations using a brake can be made more efficient by using the brake as an additional energy source in any constantly operating system on board the aircraft, using the circuit of Fig. 2.21.

Such systems may include:

a) the heating system of the flying craft. In this case, the braking element is an electrical alternating-current generator supplying several sections of the heating system. By switching several sections from this brake so that they are supplied by the main source, it is possible to control the brake speed;

b) the supercharging system of a pressurized cabin or the generator cooling system. In this case, the braking element is a compressor in which the air flow rate is automatically varied by the alternating-current line frequency regulator;

c) a fuel or hydraulic system. In this case, the braking element is a pump in which the flow rate is varied automatically by the alternating-current line frequency regulator.

#### Hydraulic Devices

Hydraulic clutches may be of the throttle, turbine, or volume types.

The first two types of clutches involve slip, i.e., they are constant-torque devices, while the third type of hydraulic clutch, the volume type, involves no slip, i.e., it is a torque converter (theoretically a constant-power device).

The throttle-type hydraulic clutch is the simplest in design. It takes the form of a pump of any type, whose pressure and suction cavities are connected together by means of a throttling device; the pump

housing is able to rotate. The pump shaft is the drive shaft of the hydraulic clutch and its housing the driven shaft (or vice versa).

The clutch throttle valve rotates to control the driven-shaft speed. Theoretically, the driven-shaft speed may be controlled over a range extending from zero (with the throttle valve wide open) to the speed of the drive shaft (with the throttle valve completely closed).

Since the moments acting on the pump shaft and its housing are equal, control of speed in this clutch occurs at the expense of a power loss, i.e., a decrease in efficiency. In this connection, it is necessary to solve the problem of removing the heat developed in the clutch at large slips.

The chief drawback to such a clutch is its low efficiency and the difficulties involved in cooling it.

The turbine-type hydraulic clutch takes the form of a centrifugal pump and centrifugal hydraulic motor (turbine) combined into a single structural unit.

The liquid circulates over some loop between the pump and the turbine, with no intervening connecting ducts.

If we neglect losses due to dissipation, external ventilation, and mechanical losses, the torques of the pump and turbine will be equal. Thus, a change in the speed of the pump driven element with respect to the drive element (turbine) will be accompanied by slip losses proportional to the difference in the speeds.

The magnitude of clutch slip depends on the load and the degree to which the working cavity of the clutch is filled with liquid. The speed of the clutch driven element is normally controlled by the variation in the degree to which the working cavity of the clutch is filled; this is done by means of a valve that controls the supply of oil to the clutch. Owing to the compactness, relatively low weight,

and small size such clutches have been employed in aircraft engines to power superchargers, and have recently found application in motor vehicles to replace gear boxes.

Throttle and turbine hydraulic clutches have a substantial drawback in their high losses and low efficiency in working at high slips; in this they are similar to electromagnetic clutches and brakes. Volume-type hydraulic clutches are free from this defect.

A volume-type hydraulic clutch is not liable to this drawback. In order to explain the operating principle of hydraulic clutches with continuously variable gear ratios, let us examine the operation of a single element in such a clutch, consisting of two cylinders of which one is a hydraulic pump N and the other a hydraulic motor M.

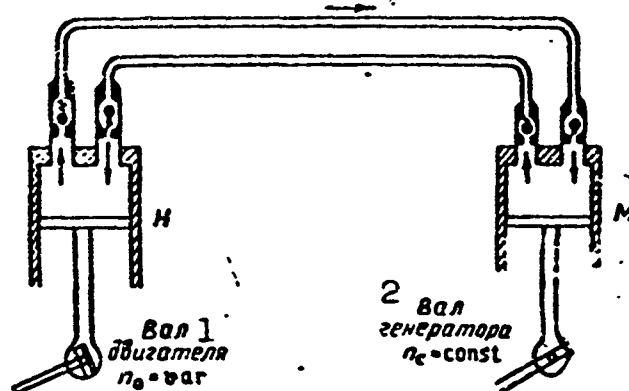


Fig. 2.22. Operating diagram of element in volume-type hydraulic clutch. 1) Motor shaft; 2) generator shaft.

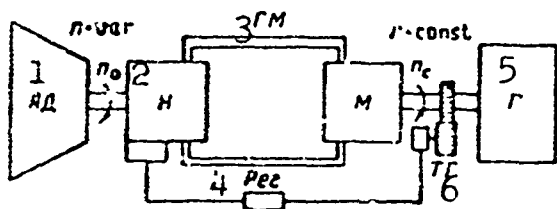


Fig. 2.23. Hydraulic transmission with continuously variable gear ratio. GM) Hydraulic clutch; N) pump; M) motor; TG) tachometer generator; Reg) regulator; 1) AD; 2) N; 3) GM; 4) Reg; 5) G; 6) TG.

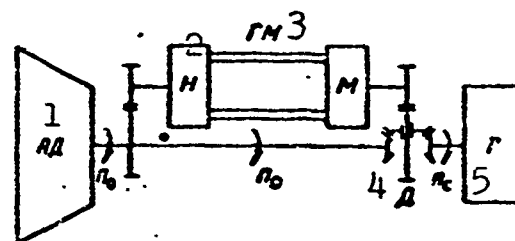


Fig. 2.24. Diagram of hydro-mechanical transmission with differential (D). 1) AD; 2) N; 3) GM; 4) D; 5) G.



As we can see from Fig. 2.22, the piston of the hydraulic pump is fastened to the shaft by means of a cam arrangement that makes it possible to change the eccentricity of the drive cam and thus regulate the piston stroke, i.e., vary the volume of liquid taken in at each pump stroke.

The pump drives a hydraulic motor; the shaft speed of the motor depends on the amount of liquid supplied, i.e., on the throughput  $Q$  of the pump.

If the shaft of the hydraulic pump is connected to the shaft of an aircraft engine that varies in speed, the pump throughput will be determined by the speed  $n$  and the eccentricity  $\epsilon$ , i.e.,  $Q \equiv \epsilon n$ .

It is thus possible to control automatically the amount of eccentricity so that with variable shaft speed the throughput remains constant and, consequently, the hydraulic-motor shaft speed remains constant.

Thus, we obtain a continuous automatic variation in the gear ratio between the motor shaft and the generator shaft by means of the hydraulic clutch. In actuality, the hydraulic clutch has several such cylinders. Such hydraulic clutches are called volume-type clutches owing to the fact that the gear ratio is varied by changing the working volume of liquid handled by the pump in each revolution.

The simplest arrangement for using a direct-action volume hydraulic transmission is shown in Fig. 2.23.

The clutch pump is driven by the aircraft engine, while the clutch motor turns the generator shaft. The pump throughput changes automatically as a function of generator load and aircraft-engine speed.

In this system, all of the power drawn by the generator passes through the hydraulic clutch. The efficiency of such a clutch is

$$\eta_m \approx 0.75.$$

We should note that the most common type of variable-throughput pump — the piston pump — permits speeds of up to 5000-6000 rpm.

In differential hydromechanical systems, the generator is basically driven with the aid of a mechanical transmission, while the hydraulic transmission serves only to hold the generator speed constant.

Thus, if the generator has a speed  $n = 8000$  rpm, and the aircraft engine runs at 3000-8000 rpm, then the hydraulic transmission must add a speed of from 5000 to 0 rpm.

The diagram of a differential hydromechanical transmission is shown in Fig. 2.24. The utilization of such an arrangement with a hydraulic motor rotating in one direction makes it possible to increase the over-all system efficiency by roughly 10-11%, while when a two-direction (reversible) hydraulic motor is used, the increase is roughly 17-18%, owing to the fact that only a portion of the power consumed by the generator passes through the hydraulic clutch, and the absolute losses in it decrease. In such systems, the hydraulic clutches are smaller than direct-acting hydraulic clutches (see Fig. 2.23).

In aviation, we use a special type of volume hydraulic clutch. In it, the power transmitted to the generator is divided without the use of any planetary or differential mechanism; the pump housing and motor housing are structurally integral, and are rotated by the aircraft engine, while the hydraulic-motor rotor turns the generator. The working cavities of the pump and motor are closed with respect to each other and are separated by a distribution-valve device. The pump and hydraulic motor in this clutch are of the piston type, with axial piston displacement (Fig. 2.25).

Drum 2 is connected to the drive shaft (in the hydraulic clutch, the drum is the housing that is turned by a gear). Several ( $z$ ) pistons

of diameter  $d$  are arranged around a circle of diameter  $D$  in the drum. The springs 4 press the pistons against the inclined fixed ring 1.

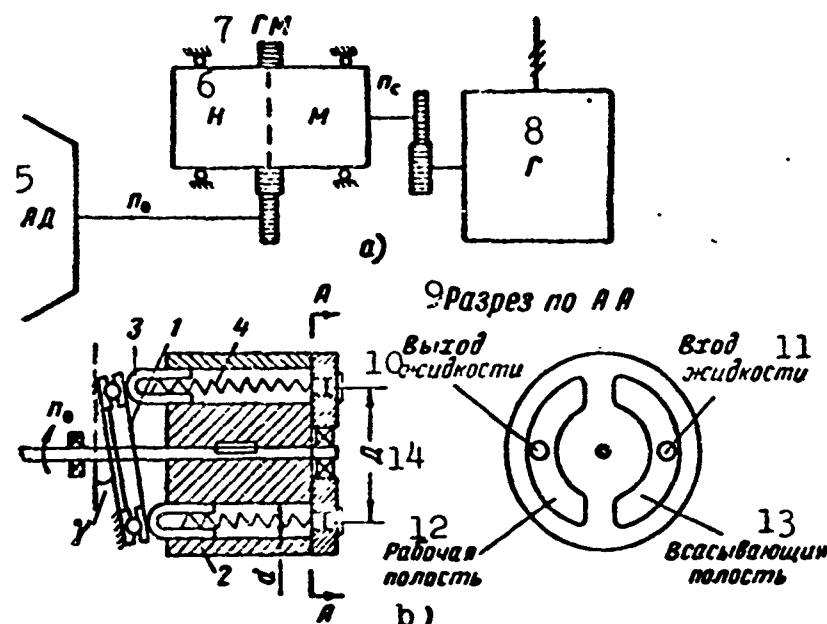


Fig. 2.25. Structural diagram of aircraft hydraulic clutch. a) Diagram; b) principle of hydraulic clutch. 1) Inclined ring; 2) clutch housing; 3) pistons; 4) spring; 5) AD; 6) N; 7) GM; 8) G; 9) section through AA; 10) fluid outlet; 11) fluid inlet; 12) working cavity; 13) intake cavity; 14) D.

When the drum rotates, the pistons slide along the inclined disk and execute a reciprocating motion; at each instant of time, the pistons in one-half of the drum move to the left and take in liquid, while in the other half (shown in Fig. 2.25b) for a given direction of rotation the pistons move to the right, compressing the liquid. In order to decrease the friction of the pistons against the disk, the latter is made in the form of a thrust bearing.

The throughput (discharge) of such a pump will be

$$Q = qn_p \quad (2.20)$$

where

$$qhz = \frac{\pi d^2}{4} D_n \lg \tau_{r,z} \quad (2.21)$$

is the volume of liquid pumped in each revolution.

Thus,

$$Q = \frac{\pi d_n^3}{4} D_n n_n z_n \operatorname{tg} \gamma_n. \quad (2.22)$$

The hydraulic motor is built on the same principle as the pump, but in it the reciprocating motion of the pistons is converted into rotary motion of an inclined ring. The output shaft of the hydraulic motor is connected to the latter.

On the basis of the principle of reciprocity for hydraulic machines, the hydraulic-motor shaft speed will be

$$n_m = \frac{Q}{\frac{\pi d_m^3}{4} D_m z_m \operatorname{tg} \gamma_m}. \quad (2.23)$$

If

$$D_m = D_n, \quad d_m = d_n \text{ и } z_m = z_n,$$

then

$$n_m = n_n \frac{\operatorname{tg} \gamma_n}{\operatorname{tg} \gamma_m}. \quad (2.24)$$

Thus the speed of the inclined disk in the hydraulic motor will be greater than the speed of its drive pump by a factor equaling the ratio of the tangent of the pump-disk angle of inclination to the tangent of the angle of inclination of the hydraulic-motor disk.

Since in the hydraulic clutch described, the pump housing and hydraulic-motor housing are one unit, the speed at which the inclined disk of the hydraulic motor rotates due to the hydraulically-transmitted reciprocating motion of the pistons will be augmented by the pump speed  $n_n$ , i.e.,

$$n_m = n_n \left( 1 + \frac{\operatorname{tg} \gamma_n}{\operatorname{tg} \gamma_m} \right). \quad (2.25)$$

The speed of the hydraulic motor depends on the relationship between the magnitude and direction of the angles of inclination  $\gamma$  for the pump and hydraulic-motor disks.

It follows from (2.25) that if  $\gamma_n = 0$ ,  $n_m = n_n$ , i.e., in this

case the hydraulic motor is rigidly connected to the pump by the fluid in their working surfaces. Circulation of the liquid ceases, and power is transmitted to the generator by purely mechanical means. Some slippage ( $n_m < n_n$ ) is possible owing to leakage.

If  $\gamma_n$  is positive, i.e., the pump disk is inclined to the same side as the hydraulic-motor disk, then the ratio  $\tan \gamma_n / \tan \gamma_m$  will be positive and  $n_m$  will be greater than  $n_n$ . In this case, the pump will supply liquid to the working cavity of the hydraulic motor, and its disk will receive additional rotary motion with respect to the housing.

If  $\gamma_n$  is negative, i.e., the pump disk is inclined in the opposite direction with respect to the hydraulic-motor disk, the ratio  $\tan \gamma_n / \tan \gamma_m$  will be negative, and  $n_m$  will be less than  $n_n$ . In this case, the working and intake cavities of the pump will be interchanged, and the hydraulic-motor disk will receive additional rotary motion owing to displacement of the pistons in the direction opposite to the rotation of the housing.

Thus, by changing the tilt of the pump disk in the hydraulic clutch, it is possible to change the gear ratio continuously; here the clutch hydraulic system itself carries only a portion of the power transmitted to the generator. Such a hydraulic clutch is therefore smaller than when it is used in a direct arrangement.

For cases in which it is difficult to locate the hydromechanical clutch on the engine, however, a purely hydraulic system is used (see Fig. 2.23). Although the weight of the hydraulic units is greater in this system, the heavy power conductor from the power bays to the central bus of the electrical system is replaced by light-weight oil lines.

Figure 2.26 shows a hydromechanical-clutch system with a variable gear ratio made by the Sunstrand Company for a 40-kva generator running

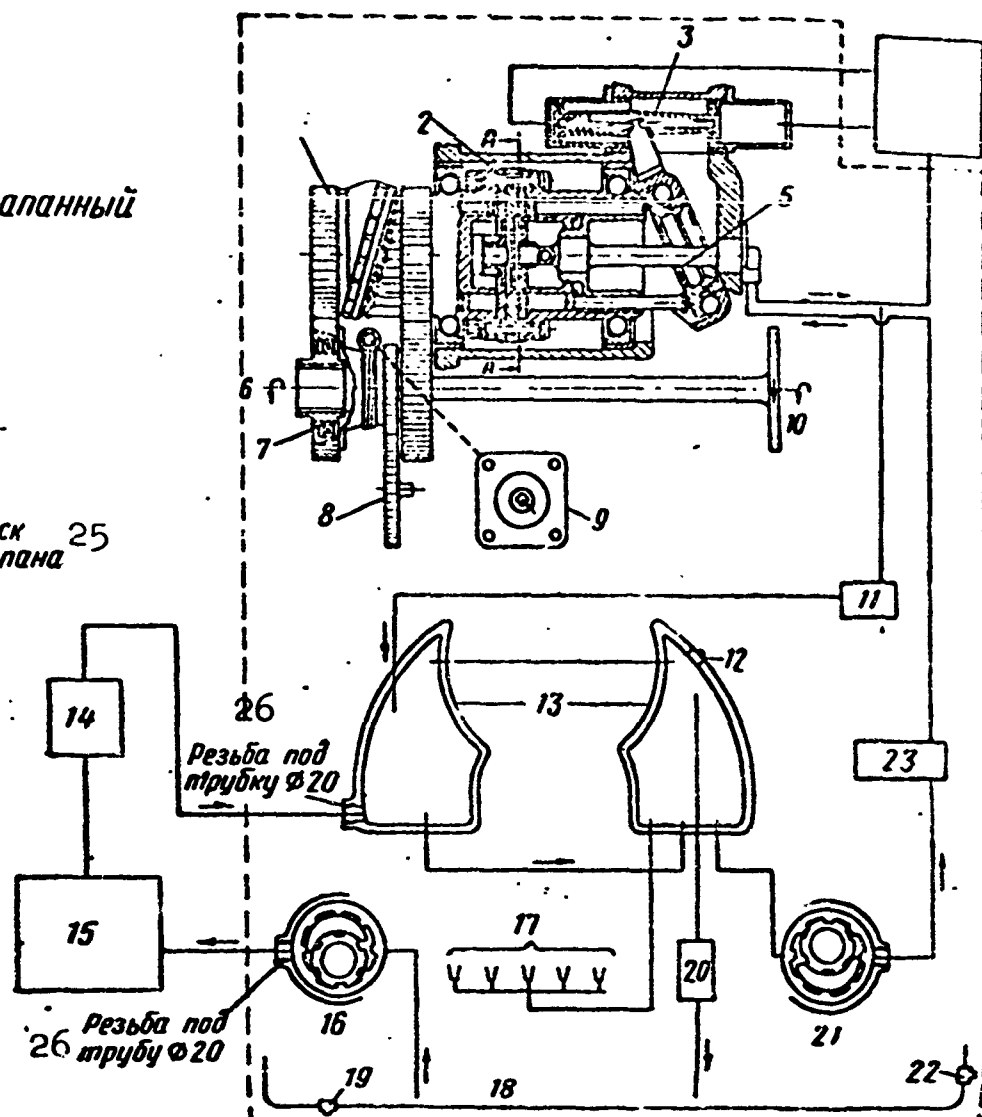
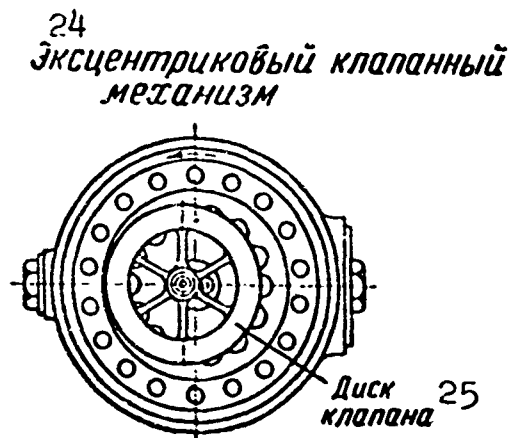


Fig. 2.26. Diagram showing hydraulic-drive system with variable gear ratio. 1) Inclined disk and gear of constant-volume hydraulic motor; 2) rotor and cylinder block; 3) servo piston; 4) control valve; 5) adjustable inclined disk of variable-throughput hydraulic pump; 6) driven shaft, 6000 rpm; 7) clutch; 8) drive for oil pump and pump for working-fluid leakage compensation; 9) tachometer-generator drive; 10) drive shaft, 2400-9000 rpm; 11) protective valve; 12, 19 and 22) plugs; 13) sediment trap (pressure 1.05 atm); 14, 15 and 16) filter, radiator, and pump for lubricating oil; 17) nozzles for lubricating gears, bearings, inclined rings, and other drive parts; 18) sediment trap operating at atmospheric pressure; 20) protective valve for oil pump (1.05 atm); 21) working-fluid leakage-compensation pump; 23) filter; 24) eccentric valve mechanism; 25) valve disk; 26) pipe thread.

at 6000 rpm.

In addition to the hydromechanical clutch (Fig. 2.27) this system contains: a gear-type oil pump and filter for compensation of leakage (pumping) of oil in the hydraulic clutch; it is driven by the hydraulic-clutch drive shaft; a gear pump, radiator, and filter for lubricating

the rotating parts of the clutch; a drain valve maintaining a minimum pressure of  $18 \text{ kg/cm}^2$  for the lines controlling the displacement of the inclined disk; a drain valve in the lubrication system maintaining a minimum pressure of  $1 \text{ kg/cm}^2$ ; an automatic regulator maintaining the speed of the driven shaft constant, and consisting of a tachometer generator, slide valve, and power hydraulic cylinder.

With a change in the drive-shaft speed from 2400 to 9000 rpm, the drive-shaft speed is maintained constant at 6000 rpm, and the angle of inclination of the pump disk changes from  $+24^\circ$  (at maximum gear ratio) to  $-5^\circ 30'$  (at minimum gear ratio).

The cylinder block 2 is driven by the drive shaft with the aid of gears 26 and 27 at a speed that is proportional to the prime mover speed. The right-hand section of the cylinder block is a variable-throughput hydraulic pump in which the stroke of the piston and plungers 25 vary as a function of the angle of inclination of the controllable inclined disk 5. The left-hand side of the cylinder block is a constant-volume hydraulic motor with a disk 1 set at a constant angle. The gear oil pump used to compensate for oil leakage is also driven by the drive shaft; it supplies oil at a mean pressure of 18 atm and keeps the cylindrical spaces between the pistons and plungers (24 and 25) filled with oil at all times. The working pressure of the fluid in the hydraulic clutch is of the order of  $300 \text{ kg/cm}^2$ .

The dry weight of the clutch is 31 kg, its dimensions 760 x 460 mm, and the efficiency 0.75-0.85. A clutch of this type has been used since 1948 on United States aircraft (B-36) and others, and has been adapted for manufacture in Great Britain.

#### Electromechanical Systems

Constant frequency may be obtained by using a combination of several electrical machines (stages). Table 2.8 which shows the basic

TABLE 2.8

## Electromechanical Systems (Stages) for Obtaining Constant-Frequency Current

1 Тип каскада	2 Принципиальная схема каскада	3 Состав каскада (число машин)			7 Скорость машин при оптимальной скорости привода и $k = 2,25$ об/мин*	8 Расчетная мощность машин при генерируемой мощности 30 кВа или $\cos \varphi = 0,75$	9 Минимальный к.п.д. каскада	10 Вес каскада кг	11 Примечание
		4 постоян-ного тока	5 перемен-ного тока	6 выпря-мителей					
12 Прямые схемы		2	1	—	$n_{ГПТ} = 4000 + 9000$ $n_{ДПТ} = n_{СГ} = 6000$	$P_{СГ} = 30 \text{ кВа } 20$ $P_{ДПТ} = 25 \text{ кВт } 21$ $P_{ГПТ} = 32 \text{ кВт } 21$	0,56	130	22 ГПТ—генера-тор постоянного тока ДПТ—двигатель постоян-ного тока СГ—синхрон-ный генератор
		1	1	—	$n_{ГПТ} = 4000 + 9000$ $n_{ОП} = 6000$	$P_{ОП} = 30 \text{ кВа } 20$ $P_{ГПТ} = 26,5 \text{ кВт } 21$	0,65	84	23 ОП—одно-якорный преоб-разователь
13 Диффе-ренци-альные схемы		2	2	—	$n_{ГПТ} = n_{АПЧ} = 3550 + 8000$ $n_{СГ} = n_{ДПТ} = 0 + 6700$	$P_{АПЧ} = 30 \text{ кВа } 20$ $P_{СГ} = 24 \text{ кВа } 20$ $P_{ДПТ} = 16 \text{ кВт } 21$ $P_{ГПТ} = 21 \text{ кВт } 21$	0,59	113	24 АПЧ—асин-хронный преоб-разователь частоты (асинхрон-ная машина двухстороннего питания)
		1	2	—	$n_{ГПТ} = n_{АПЧ} = 3560 + 8000$ $n_{ОП} = 6700$	$P_{АПЧ} = 30 \text{ кВа } 20$ $P_{ОП} = 24 \text{ кВа } 20$ $P_{ГПТ} = 16,5 \text{ кВт } 21$		97	

\*  $k = n_{\max}/n_{\min}$ .



TABLE 2.8 (continued)

1 Тип каскада	2 Принципиальная схема каскада	3 Состав каскада (число машин)			7 Скорость машины при оптимальной скорости привода и $k=2,25$ об/мин	8 Расчетная мощность машины при генерируемой мощности 30 кка/с и $\cos \varphi = 0,75$	9 Минимальный к.п.д. каскада	10 Вес каскада кг	11 Примечание
		4 постоян-ного тока	5 перемен-ного тока	6 выпрями-телей					
Дифференциальные схемы 13		2	2	—	$n_{сг}=n_{гпт}=3550 \div 8000$ $n_{дпт}=n_{апч}=0 \div 6700$	$P_{апч}=30 \text{ кка } 20$ $P_{сг}=18,3 \text{ кка } 20$ $P_{гпт}=16 \text{ кат } 21$ $P_{дпт}=12 \text{ кат } 21$	0,67	109	АПЧ—асинхронный преобразователь частоты (асинхронная машина двухстороннего питания) 24
		1	2	1	$n_{сг}=3550 \div 8000$ $n_{дпт}=n_{апч}=0 \div 6700$	$P_{апч}=30 \text{ кка } 20$ $P_{сг}=32 \text{ кка } 20$ $P_{в}=16 \text{ кат } 21$ $P_{дпт}=12 \text{ кат } 21$	0,72	100	В—кремниевый диодный мост 26
		2	1	—	$n_{гпт}=3550 \div 8000$ $n_{дпт}=4450 \div 0$ $n_{синхр.БМ}=8000$	$P_{дпт}=14 \text{ кат } 21$ $P_{гпт}=18,7 \text{ кат } 21$ $P_{БМ}=30 \text{ кка } 20$	0,65	86	БМ—бифазная машина 27
		1	2	—	$n_{гпт}=4000 \div 9000$ $n_{дпт}=0 \div 10000$ $n_{сг}=6000$	$P_{гпт}=16,5 \text{ кат } 21$ $P_{дпт}=12,5 \text{ кат } 21$ $P_{сг}=30 \text{ кка } 20$	0,58		28 МСД—суммирующий дифференциал
25 Регулятивные схемы		2	2	—	$n_{аг}=n_{дпт}=4000 \div 9000$ $n_{сд}=n_{гпт}=10000$	$P_{аг}=30 \text{ кка } 20$ $P_{сд}=17 \text{ кка } 20$ $P_{гпт}=12,8 \text{ кат } 21$ $P_{дпт}=9,6 \text{ кат } 21$	0,56	90	АГ—асинхронный генератор. Требуется наличие синхронного компенсатора или синхронного генератора в питающей сети 29

TABLE 2.8 (continued)

Тип каскада 1	Принципиальная схема каскада 2	3 Состав каскада (число машин)			Скорость машины при оптимальной скорости привода и $k = 2,25$ об/мин 7	Расчетная мощность машины при генерируемой мощности 30 кВа 8 и $\cos \varphi = 0,75$	Минимальный к.п.д. каскада 9	Вес каскада кг 10	Примечание 11
		4 постоян-ного тока	5 перемен-ного тока	6 выпрями-телей					
Рекупера-тивные схемы		1	1	1	$n_{AG} = n_{ДПТ} = 4000 \div 9000$	$P_{AG} = 30 \text{ кВа } 20$ $P_B = 25 \text{ кВт } 21$ $P_{ДПТ} = 18,7 \text{ кВт } 21$	0,72	64	АГ—асин-хронный гене-ратор. Требуе-т наличия син-хронного ком-пенсатора или синхронного ге-нератора в пи-тающей сети 29
		2	2	—	$n_{CG} = n_{ДПТ} = 4000 \div 9000$ $n_{AD} = n_{ГПТ} = 0 \div 10\,000$	$P_{AD} = 30 \text{ кВа } 20$ $P_{CG} = 58 \text{ кВа } 20$ $P_{ГПТ} = 21 \text{ кВт } 21$ $P_{ДПТ} = 15,7 \text{ кВт } 21$	0,5	111	АД—асин-хронный дви-гатель 30
		1	2	1	$n_{ДПТ} = 4000 \div 9000$ $n_{CG} = 4000$	$P_{CG} = 30 \text{ кВа } 20$ $P_B = 28 \text{ кВт } 21$ $P_{ДПТ} = 21 \text{ кВт } 21$ $P_{ЭММ} = 50 \text{ кВт } 21$	0,54	127	31 В—кремние-вый выпрями-тель ЭММ—элек-тромагнитная муфта 32
		2	1	—	$n_{ДПТ} = 4000 \div 9000$ $n_{ГПТ} = 0 \div 5000$ $n_{синхр.ЭММ} = 4000$	$P_{ГПТ} = 21 \text{ кВт } 21$ $P_{ДПТ} = 15,7 \text{ кВт } 21$ $P_{ЭММ} = 30 \text{ кВа } 20$	0,56	110	
		2	1	—	$n_{ДПТ} = 3600 \div 8100$ $n_{CG} = 6000$ $n_{ГПТ} = 0 \div 11\,000$	$P_{CG} = 30 \text{ кВа } 20$ $P_{ГПТ} = 23 \text{ кВт } 21$ $P_{ДПТ} = 17 \text{ кВт } 21$	0,6	72	33 МРД—разде-ляющий диф-ференциал

TABLE 2.8 (key)

1) Type of stage; 2) basic stage circuit; 3) composition of stage (number of machines); 4) direct current; 5) alternating current; 6) rectifiers; 7) machine speed at optimum drive speed with  $k = 2.25$ , rpm\*; 8) machine design power for generated power of 30 kva with  $\cos \phi = 0.75$ ; 9) minimum stage efficiency; 10) stage weight, kg; 11) notes; 12) direct circuit; 13) differential circuit; 14) GPT; 15) line; 16) DPT; 17) SG; 18) OP; 19) APCh; 20) kva; 21) kw; 22) GPT) direct-current generator; DIT) direct-current motor; SG) synchronous generator; 23) OP) single-armature converter; 24) APCh) induction frequency converter (two-way supply induction machine); 25) regenerative circuit; 26) V) silicon rectifier; 27) BM) double rotating machine; 28) MSD) integrating differential; 29) AG) induction generator. Requires a synchronous compensator or synchronous generator in the supply circuit; 30) AD) induction motor; 31) V) silicon rectifier; 32) EMM) electromagnetic clutch; 33) MRD) dividing differential.

types of stages using direct-current commutator machines also gives approximate values for the powers of the machines used in the stages, their approximate weight, and the efficiency of the system as a whole.

Three types of applications are possible for the stages: direct, differential, and regenerative.

In direct arrangements (1 and 2) all of the power generated by the stage passes through the entire machine. The direct-current generators in circuits 1 and 2 may be replaced by variable-frequency synchronous generators connected to a rectifier.

In differential and regenerative circuits, composition or division of frequencies occurs; this may be done with the aid of: a) an induction machine (one part rotates), b) a double rotating machine (two elements rotate), or c) a mechanical differential (three parts rotate).

In differential circuits (3-8) the power generated by a stage is supplied over two parallel paths that come together again in a special machine that acts as a mixer.

The speed (and power) mixer in differential circuits is an induction frequency converter (APCh) in circuit 3-6, a double rotary machine (BM) in circuit 7, or a mechanical integrating differential

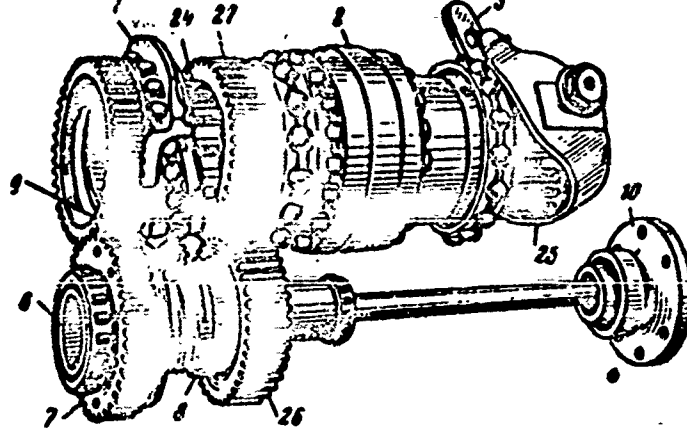


Fig. 2.27. Hydromechanical clutch (housing removed). 24 and 25) Pistons of hydraulic motor and hydraulic pump; 26 and 27) drive gears.

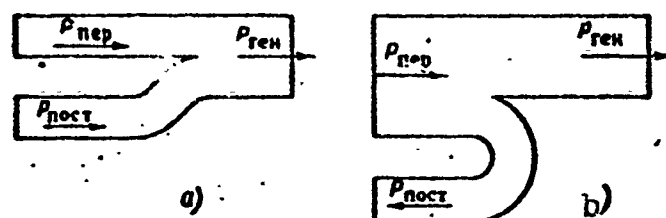


Fig. 2.28. Power diagram for electro-magnetic stages. a) Differential circuits; b) regenerative circuits.

(MSD) in circuit 8.

The power diagram for such stages (with no allowance for losses) is shown in Fig. 2.28a, where

$P_{post}$  is the power passing through the direct-current element;

$P_{per}$  is the power passing through the alternating-current element;

$P_{kask} = P_{gen}$  is the power generated by the stage.

The power  $P_{post}$  changes from zero to the maximum value determined by the range of drive-speed variation, i.e.,

$$P_{post} \approx P_{kask} \left(1 - \frac{1}{k}\right),$$

where

$$k = \frac{n_{rpm \max}}{n_{rpm \min}}.$$

Circuit 6, which uses a solid-state rectifier V has the advantage of permitting the main generating unit V + DPT + APCh to be located

away from the prime mover.

The double rotary machine (BM) in circuit 7 is a synchronous generator in which the "stator" is forced to rotate in a direction opposite to the direction of rotation of the rotor. The frequency of the alternating current taken from the slip rings equals

$$f_{BM} = p \frac{n_{cr} + n_{por}}{60}.$$

A drawback to the double rotary machine is the relative complexity of its construction (it requires two bearing systems, three power slip rings, etc.).

In regenerative circuits (9-14) part of the power taken from the prime mover goes to generate alternating current at constant frequency; the remainder of the power taken off is returned to the engine after several conversions. The power circuit of such stages (with no allowance for losses) is shown in Fig. 2.28b.

Here the maximum power  $P_{post}$  is also determined by the drive-speed variation range, i.e.,

$$P_{post} \approx P_{max} \left(1 - \frac{1}{k}\right).$$

The regenerative circuits 9, 11 and 13 are obtained respectively from the differential circuits 3, 5 and 7 by changing the excitation of the GPT and DPT machine.

In this case, the APCh is operated as an induction generator AG (circuit 9) and as an induction motor (circuit 11), the SG operates as a synchronous motor SD, and the double rotary machine BM as an electromagnetic clutch EMM for which the slip energy is useful.

On this basis, it is possible to use precisely the same stage both as a differential stage over one-half the drive-speed variation range and as a regenerative stage over the other half of the range (two-way regulation). Here it should be possible to change the polarity

for the excitation of one of the direct-current machines smoothly. In addition to returning energy to the prime mover (as in circuits 10 and 12), it is possible to return energy to the direct-current system of the aircraft, if one is used. To do this, it is necessary to install a transformer with a controllable transformation ratio before rectifier V, and to connect the rectifier output to the line. Investigations have shown, however, that the DC line in this case carries considerably greater power than the power developed by the alternating-current stage.

In the presence of variations in the drive-shaft speed or variations in line load, stage frequency is regulated by changing the direct-current motor excitation or the excitation of the generator supplying this motor.

As a rough calculation shows, the relative weight of electromechanical systems is quite high (3-3.5 kg/kva), while their efficiency is relatively low (0.55-0.7). In addition, there are still commutators for one or two machines in the stage, which decreases the reliability of the aircraft power system; thus it is not recommended that they be used for the modern speed range of an aircraft drive. They may find application only for narrow drive-speed ranges.

#### CONCLUSIONS

1. Constant-frequency alternating current is best suited to aircraft power systems.

2. Where the speed of the prime mover varies over a small range, constant generator frequency may be obtained with the aid of an electromagnetic clutch (brake), hydraulic clutch of the turbine (throttle) type, or by electromechanical systems.

3. Where the range of speed variation for the prime mover is large, constant generator shaft speed may be obtained with the aid of

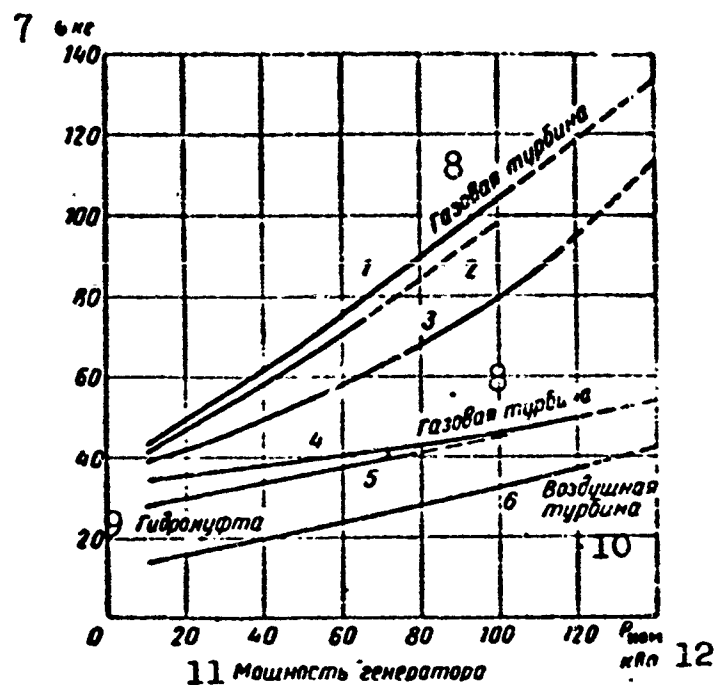


Fig. 2.29. Comparison of weights of several devices used to obtain constant frequency. 1) Air turbine, 24,000 rpm; 2) hydro-mechanical drive, 6000 rpm; 3) gas turbine, 12,000 rpm; 4) unit consisting of air turbine, generator, and regulator; 5) generator with hydromechanical drive; 6) unit consisting of gas turbine, generator, and regulator; 7) G, kg; 8) gas turbine; 9) hydraulic clutch; 10) air turbine; 11) generator power; 12)  $P_{nom}$ , kva.

volume-type hydraulic clutches for which  $\eta \approx 0.85$  and the relative weight equals (1-1.2) kg/kw.

4. Electromagnetic and hydraulic clutches provide for reliable operation of alternating-current generators in parallel and maintain the frequency constant with an accuracy of the order of  $\pm 0.5\%$ .

5. Independent and semi-independent generator drives by means of air or gas turbines running at high speeds are being used on board aircraft. An installation using an air turbine is lighter, and an installation with a gas turbine heavier, than a drive using a hydro-mechanical clutch, but they are more efficient than the latter (Fig. 2.29).

6. The utilization of clutches for speed conversion may also prove useful in systems using direct-current generators. At a constant high speed, the latter will have higher power for the same size, lower relative weight, and better operating characteristics.

7. Electromechanical frequency-conversion systems clearly cannot find application in aviation, since they normally use commutators and are cumbersome.

8. Electrical frequency-conversion systems will be discussed in Part II of the book. As we shall show there, in the light of the latest achievements in the fields of semiconductors and semiconductor triodes, they may also prove suitable for aircraft applications.

Manu-  
script  
Page  
No.

[Footnotes]

147 Paragraph 2.4 was written by the author together with Engineer V.S. Moiziy.

[List of Transliterated Symbols]

135	TЗ = TZ = tekhnicheskoye zadaniye = technical plan
135	ТТ = TT = tekhnicheskiye trebovaniya = technical specifications
137	НОМ = nom = nominal'nyy = rated
137	Г = g = generator = generator
140	Н = n = naruzhnyy = external
150	Д = d = dvigatel' = motor
153	АД = AD = aviatsionnyy dvigatel' = aircraft engine
153	ЭММ = EMM = elektromagnitnaya mufta = electromagnetic clutch
153	ТГ = TG = takhogenerator = tachometer generator
153	Рег = Reg = regul'yator = regulator
153	ОВ = OV = obmotka возбуждениya = field winding



153	ОЯ = ОYa = obmotka yakorya = armature winding
153	c = s = stabilizirovanny = stabilized (subscript to <u>n</u> )
153	c = s = soprotivleniye = resistance (subscript to M)
155	В = v = возбуждениye = excitation
155	к = k = kriticheskiy = critical
160	Д = D = differentsial = differential
160	Г = G = generator = generator
160	Т = T = tormoz = brake
160	С = S = savellit = pinion
161	a, b, c = a, b, c as keyed in Fig. 2.19
162	э = e = elektricheskiy = electrical
164	РЧ = RCh = regulyator chastoty = frequency regulator
164	Р.Т = R.T = regulyator temperatury = temperature regulator
164	осн = osn = osnovnoy = basic
167	Н = n = nasos = pump
167	М = m = motor = motor
167	ГМ = GM = gidravlicheskaya mufta = hydraulic clutch
169	м = m = mufta = clutch
175	ГПТ = GPT = generator postoyannogo toka = direct-current generator
175	ДПТ = DPT = dvigatel' postoyannogo toka = direct-current motor
175	СГ = SG = sinkhronnyy generator = synchronous generator
175	ОП = OP = odnoyakornyy preobrazovatel' = single-armature converter
176	АПЧ = APCh = asinkhronnyy preobrazovatel' chastoty = induction frequency converter
176	В = V = выпряmitel' = rectifier
176	БМ = BM = birotativnaya mashina = double-rotating machine
176	МСД = MSD = summiruyushchiy differentsial = integrating differential

176 АГ = AG = asinkhronnyy generator = induction generator  
177 АД = AD = asinkhronnyy dvigatel' = induction motor  
177 МРД = MRD = razdelyayushchiy differentsial = dividing differential = dividing differential  
179 пер = per = peremenny = alternating  
179 пост = post = postoyanny = direct  
179 как = kask = kaskad = stage  
179 ген = gen = generiruyemy = generated  
179 прив = priv = privodnoy = drive  
180 ст = st = stator = stator  
180 рор = rot = rotor = rotor

## Chapter 3

### ALTERNATING-CURRENT AIRCRAFT GENERATORS

#### 3.1. GENERAL INFORMATION ON ALTERNATING-CURRENT AIRCRAFT GENERATORS

Alternating-current generators may fundamentally be classified in accordance with Table 2.1.

The first three types of generators are of practical importance in aviation. Electromagnetically or magnetically excited synchronous generators are used in single-phase and three-phase models for 208/120 v on the main line and for 36 and 120 v for converters. Inductor-type synchronous generators are used chiefly in the single-phase version for 120 v.

TABLE 3.1

Three-Phase 400-cps Generator Series

1. Мощность $S_{\text{ном}}$ кВА/кВт	15/11,25	30/22,5	45/33,75	60/45	80/60	100/75
2. Скорость $n$ об/мин	8000			6000		
3. Число полюсов $2p$	6			8		
4. К.в.д. $\eta$	0,85	0,88	0,90	0,92	0,94	0,95
5. Вес $G$ , кг	20	30	42	54	70	90

1) Power  $S_{\text{ном}}$  kva/kw; 2) speed  $n$ , rpm; 3) number of poles  $2p$ ; 4) efficiency  $\eta$ ; 5) weight  $G$ , kg.

A three-phase 400-cps generator series used for main aircraft electrical systems can be represented in the form of Table 3.1.

This series has a power factor of  $\cos \varphi = 0.75$ ; air-blast cooling by the oncoming air stream is used; permissible overloads are 150% for two min at 208 v and 200% (current overload) for 5 sec at 187 v.

The series of 400 cps generators for conversion may be represented by the following series of powers:

1	0,05	0,1	0,175	0,25	0,5	0,75
Мощность $S_{nom}$ кВа	1,0	1,5	3,0	4,5	6,0	10

1) Power  $S_{nom}$ , kva.

The generators in this series are three- or single-phase ( $m = 3$  or 1) and have power factors of  $\cos \varphi = 0.6-0.9$  depending on the region of application.

Depending on the number of phases and the region of application, the voltage will normally equal 208/120, 36, or 120 v; cooling is by selfventilation.

The generator weights and efficiencies have been adjusted for operation at an altitude of 15 km. With increased altitude, generator efficiency drops and generator weight increases.

For powers up to 1.5 kva, inductor, magnetoelectric, and synchronous generators are used. For powers of 3 kva or above, synchronous generators using electromagnetic excitation are used.

#### Synchronous Electromagnetically-Excited Generators

Choice of a type of synchronous generator. In low-power and low-voltage machines, it is possible to use synchronous generators with internal or external poles of the direct-current machine type.

Generators intended for the basic electrical system (with powers up to 30 kva) and generators used to form converters (with powers up to 10 kw) may be made with either internal or external poles. Generators for powers of 30 kva or more are normally made with internal poles.

Synchronous machines with external poles offer the following advantages at low powers:

a) increased area for installation of the field winding for the same armature diameter;

- b) improved rotor construction, since it is difficult to mount rotating poles and field windings on small-diameter machines;
- c) the magnetic system may simultaneously serve as the machine frame;
- d) existing direct-current machine models can be used;
- e) improved conditions for cooling-air passage in motor-generators, since as a rule the motor and generator are made with the same number of poles and identical armature diameters;
- f) simplified control systems for converters owing to the fact that the field winding is more accessible.

At the same time, such machines also possess substantial disadvantages:

a) the need for taking off alternating current through slip rings, which considerably increases the structural length of the machine and the losses, especially at low voltages (in three-phase machines with a grounded neutral, four slip rings are used): the presence of the sliding contact in the alternating-current circuit leads to an increase in the phase "voltage skewing" and is an obstacle to any increase in the accuracy of voltage regulation, since the voltage drop across the contact may not remain the same, but may vary in time;

b) in order to increase the voltage-regulation accuracy, it is important for the magnetic circuit to have minimum hysteresis since machines with external poles will always have a longer path for the lines of force in the plain section of steel, which reduces the possibility of precise regulation;

c) the losses developing in the rotor (armature) as a rule considerably exceed the losses in the stator (inductor), i.e.,

$$P_{a2} + P_{\sigma} + P_{\Sigma} > P_{a1}.$$

It is difficult, however, to remove heat from the rotor surface at

high altitudes and flight speeds;

d) for the same outside diameter, which is the dimension of greatest interest, the armature size will be less for external-pole machines and, consequently, the utilization factor for such machines will be lower.

In fact, in internal- and external-pole machines, the outside diameter is determined by the following equations, respectively:

$$D_{n1} = D_1 \left( 1 + \frac{\gamma_1}{p} \right) ; D_{n2} = D_2 \left( 1 + \frac{\gamma_2}{p} \right), \quad (3.1)$$

where

$$\gamma_1 = \frac{h_p + h_{ya}}{\tau} \pi \quad \text{и} \quad \gamma_2 = \frac{h_m + h_{ya} + b}{\tau} \pi, \quad (3.2)$$

$h_p$ ,  $h_{ya}$ , and  $h_m$  are the heights of the slot, yoke, and (magnet) pole, respectively.

The subscript "1" indicates internal-pole machines, and the subscript "2" external-pole machines.

As a consequence, where the outside diameters of machines are identical, i.e.,  $D_{n1} = D_{n2}$ , we find from (3.1) and (3.2) that

$$D_1 \left( 1 + \frac{\gamma_1}{p} \right) = D_2 \left( 1 + \frac{\gamma_2}{p} \right) \quad (3.3)$$

while the ratio

$$k_D = \frac{D_1}{D_2} = \frac{\gamma_2 + p}{\gamma_1 + p}. \quad (3.4)$$

If we take as approximate values for the coefficients  $\gamma_1 \approx 1.2$ -1.25 and  $\gamma_2 \approx 2.5$ -2.8, depending on the number of poles the ratio of the armature diameter for an internal-pole machine ( $D_1$ ) to the diameter in an external-pole machine ( $D_2$ ) will equal roughly

$2p$	4	6	8	10
$k_D = \frac{D_1}{D_2}$	1.40	1.30	1.25	1.2

Thus given the same outside machine diameter, the diameter of the armature for an internal-pole generator will be greater and, consequently, its power will increase, all other conditions being equal.

This fact nearly nullifies the advantages listed for external-pole electrical machines.

Generators for the main electrical power system, normally of 30 kva power or more, are best made with internal poles. For converters, the choice of generator type is determined by the actual application conditions (power, number of phases, regulation circuit, etc.), and a separate selection should be made for each special case.

At high peripheral speeds ( $v > 50$  m/sec), it is difficult to install internal poles. In this case, synchronous nonsalient-pole machines may be used; in such machines, the field winding is laid in slots and fastened securely with wedges and circular bands.

Peripheral speeds of synchronous nonsalient-pole machines may reach 200 m/sec where the rotor is made of 30 KhGSA steel rod.

At peripheral speeds of less than 100 m/sec, the rotor may be made from sheet steel; even at these speeds, however, it is frequently sensible to use a plain rotor. Increased mechanical losses (friction losses) at high rotary speeds do not lead to a sharp drop in generator efficiency, since at high flight speeds the air density drops.

Where aircraft generators are driven by special air or gas turbines, they normally are made in two- or four-pole form, i.e., they run at 12,000-24,000 rpm, using nonsalient-pole construction.

#### Design Features and Fundamentals of Aircraft Synchronous Generators

Aircraft synchronous generators differ from general-purpose generators in: a) short service life — 500 hr, rather than 10-20

years; b) frequency (speed of rotation) - 400 cps, rather than 50; c) cooling-system intensity, air blasting by the oncoming air stream, evaporation of liquid on an interior surface, cooling by means of a liquid at a positive or negative temperature, etc.; d) increased electrical ( $A$  and  $j$ ) and thermal ( $A_t$ ) loads; e) certain structural elements. At the same time, the magnetic loads ( $B_\delta$  and  $B_s$ ) and the general structural assembly remain nearly unchanged.

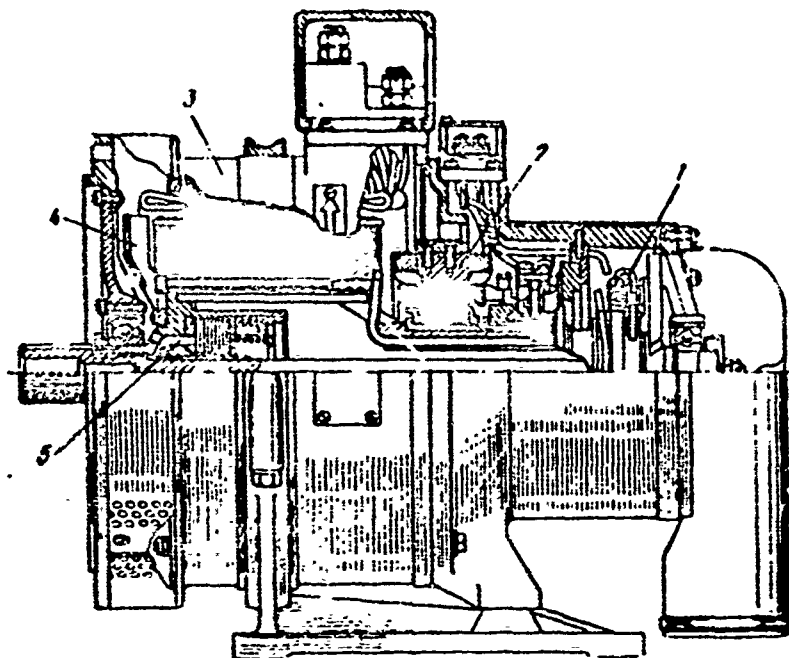


Fig. 3.1. Three-phase 30-kva, 400-800-cps 4000-8000-rpm aircraft salient-pole synchronous generator. 1) Slip rings and brushes; 2) exciter; 3) generator; 4) fan; 5) built-in clutch.

As we have already mentioned, aircraft generators have less than one-tenth the weight of general-purpose generators, and are 20-25% lighter than direct-current aircraft generators, and are considerably more efficient.

Both salient-pole and nonsalient-pole synchronous generators are used for aircraft purposes.

Salient-pole generators are made with external or internal armatures. Figures 3.1-3.3 show the structural make-up of a three-phase salient-pole aircraft machine with an external armature.

Figures 3.4-3.7 show the general structural make-up of an aircraft generator with an internal armature. The generator of Fig. 3.5 uses three slip rings with no neutral lead. The generator of Figs. 3.6 and 3.7 are provided with a neutral lead.



Generators with internal salient poles normally use an exciter located on the generator shaft and slip rings placed beyond the exciter (see Fig. 3.1) or located between the generator and exciter (see Fig. 3.2).

The exciter and slip rings are located on the side opposite the drive mechanism. If the excitation circuit is supplied from an external direct-current source, no exciter is used, and the axial dimensions of the machine are decreased considerably. The generator frame is flange-mounted to the drive motor. The generator flexible shaft is attached to the prime-mover shaft with the aid of the splined end of the flexible shaft (see Fig. 3.2).

The generator flexible shaft is connected to the hollow rotor bushing either by a cone or by splines (see Fig. 3.2).

In generators using internal salient poles, it is important to mount securely the poles and field windings located on the poles. In generators with external poles, it is important to mount securely the end section of the armature windings by means of rings taking the form of hollow cylinders slipped over the end section of the winding or by means of wire wrappings (the first method is more reliable, although more expensive and more complicated from the production viewpoint). The hollow rotor bus ring which carries either the poles with field winding, or the armature core with armature winding, is supported on two ball bearings. In order to improve rotor cooling and to permit operation in the absence of an air blast (at lower power) a fan is installed on the rotor shaft; its diameter is approximately equal to that of the rotor.

The armature winding is normally of the two-layer type with short pitch and continuous class A or B flexible insulation. The end sections are bent into a cone. The armature slots are half-open or

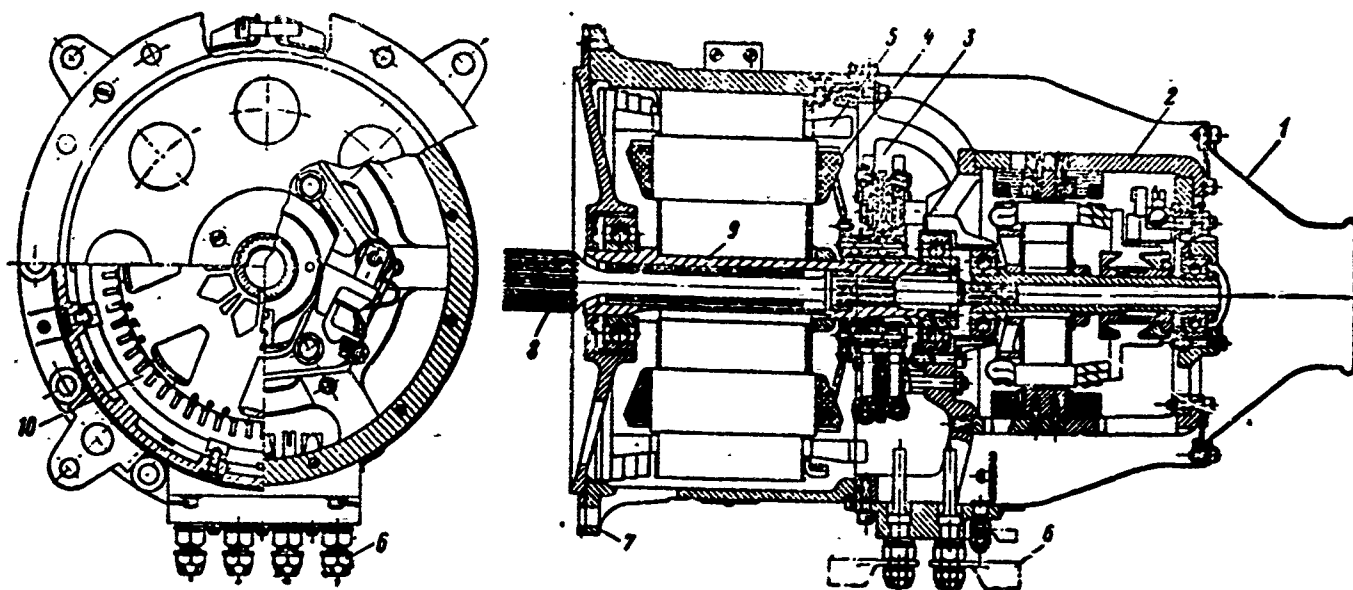


Fig. 3.2. Three-phase salient-pole direct-current synchronous generator, 40 kva power, 400 cps frequency, 6000 rpm. 1) Air duct; 2) exciter; 3) slip rings and brushes; 4) field winding; 5) armature winding; 6) lead terminals; 7) flange; 8) flexible shaft; 9) hollow shaft (rotor bushing); 10) armature core.

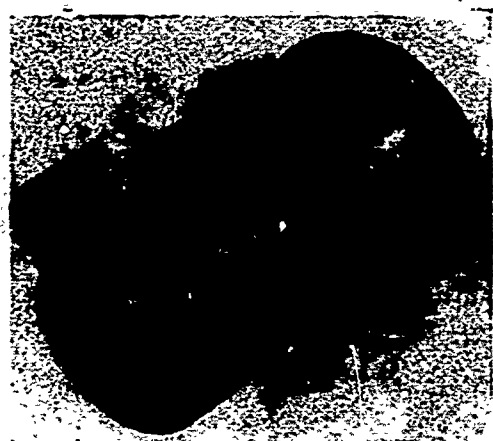


Fig. 3.3. Over-all view of three-phase aircraft generator with external armature.

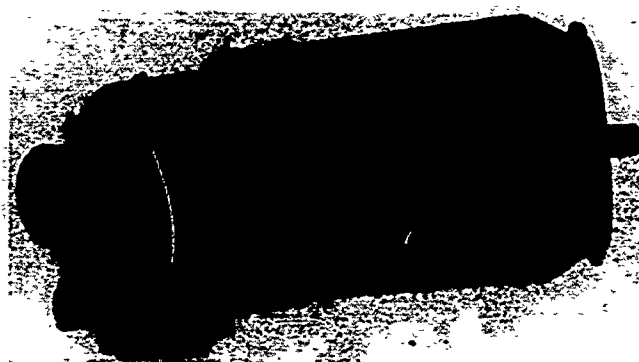


Fig. 3.4. Over-all view of three-phase aircraft generator with internal armature.

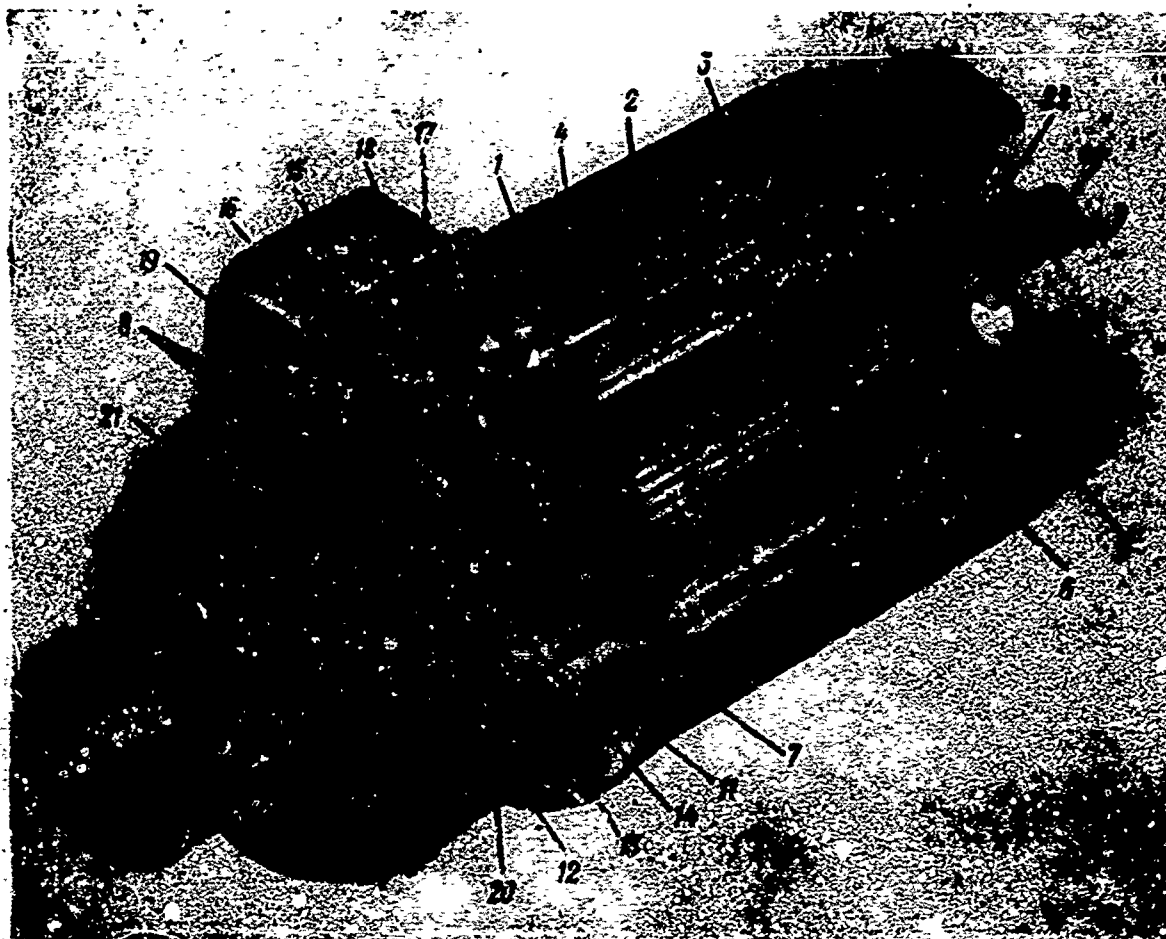


Fig. 3.5. Construction of three-phase salient-pole variable-frequency aircraft generator with internal armature. 1) Frame; 2) pole; 3) field winding; 4) damping element; 5) protective ring; 6) armature; 7) boss; 8) slip ring; 9) hollow shaft; 10) flexible shaft; 11) guard; 12) brush holder; 13) brushes; 14) spiral spring; 15) bus; 16) panel for leads; 17) lead box; 18) cover; 19) connector; 20) protective ribbon; 21) end piece; 22) nut on prime-mover end.



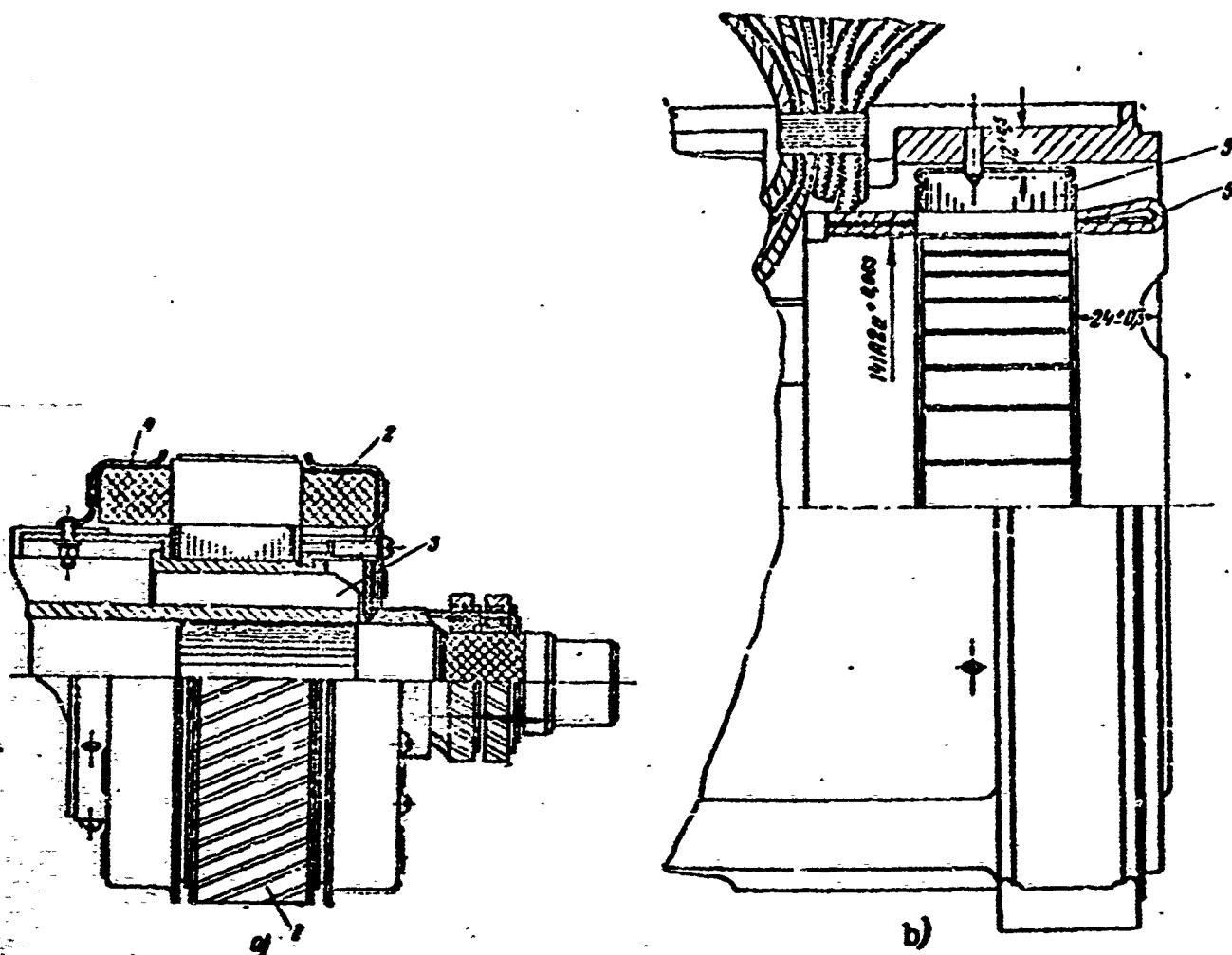


Fig. 3.8. Rotor and stator for three-phase nonsalient-pole aircraft generator, 5.5 kva power. a) Rotor; b) stator. 1) Rotor force; 2) bands; 3) rotor bushing; 4) field winding; 5) armature core; 6) armature winding.

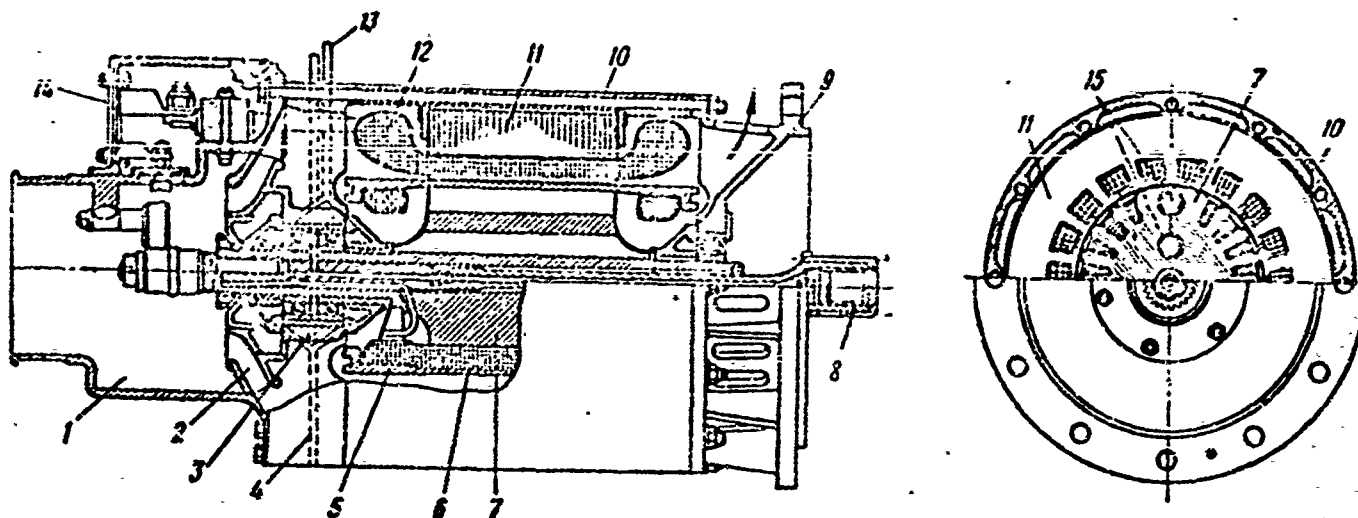


Fig. 3.9. Air-cooled three-phase salient-pole aircraft generator. 1) Air duct; 2) fan; 3) bearings; 4) oil outlet; 5) band; 6) rotor winding; 7) rotor core; 8) flexible shaft; 9) flange piece; 10) stator frame; 11) armature core; 12) armature winding; 13) oil inlet; 14) lead box; 15) air passages.

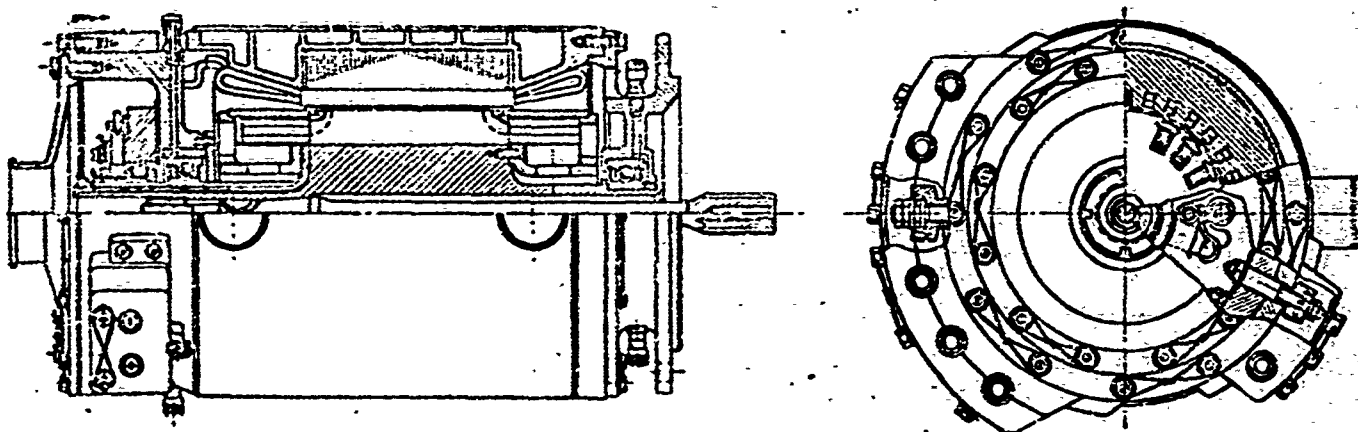


Fig. 3.10. Liquid- and air-cooled three-phase nonsalient-pole aircraft generator, 50 kva, 208/120 v, 500 cps, 30,000 rpm,  $\cos \varphi = 0.85$ .

open.

Figure 3.8 shows the construction of a nonsalient-pole three-phase generator used in an aircraft converter set.

The rotor is laminated. The bands are solid. The armature winding is of the two-layer type with short pitch. Air cooling is used.

Figures 3.9 and 3.10 show one possible design for a two-pole aircraft synchronous generator of 50 kva power using a solid rotor.

In designing a generator, we try to obtain minimum weight and size while providing the required strength. We shall not consider structural details here.

### 3.2. EXCITATION AND SELFEXCITATION OF SYNCHRONOUS GENERATORS

The operation of modern direct- and alternating-current generators is based on the utilization of time-constant magnetic excitation fields. This system is widely employed owing to the simplicity and convenience of inducing direct and alternating currents by means of time-constant magnetic fields.

Electrical currents can also be induced with the aid of variable magnetic (or electrical, in electrostatic machines) excitation fields; this is a more complicated matter, however, since it is necessary to insure that the motion of the current-carrying conductors and the variation in the magnetic field remain synchronized and in phase.

Thus, if we have an alternating-current circuit containing a resistance  $R$ , inductance  $L$ , and capacitance  $C$ , by changing the arrangement of the elements of this circuit, i.e., the system  $L$  and  $C$ , in special cases it may prove possible to excite electrical currents without changing the resistance, i.e., without using commutation to change alternating current into direct current. Where the alternating-current circuit does not contain capacitance, selfexcitation without

commutation is impossible.

Selfexcitation is possible in a circuit containing R, L and C if the natural resonance of the system is used and L or C are periodically changed in connection with this resonance.

As an example of selfexcitation in an alternating-current circuit, we may cite the selfexcitation of a selfcontained induction generator connected across an appropriate capacitance.

If the system is linear, the selfexcitation process continues until the insulation breaks down or the power of the prime mover turning the variable inductance proves inadequate. As we know, steady-state conditions cannot obtain in a linear system and, consequently, it cannot be used as a current generator. In order to obtain stable selfexcitation, as in the case of constant-field excitation, it is necessary to use the nonlinearity of the magnetization curve for steel.

Selfexcitation due to variation in circuit constants (L or C) is called parametric excitation and generators built on this principle are called parametric generators. The theory of parametric excitation and parametric machines is due to the Soviet physicists Mandel'shtam and Papaleksi.

As yet, parametric generators have not found application in aviation, and thus we shall henceforth consider only excitation and selfexcitation systems using time-constant fields.

Synchronous generators may be classified by method of excitation into two main groups: generators with separate excitation and selfexcited generators.

A separate excitation system is a system in which the magnetizing force (n.s.) for excitation is independent of the generator operating regime.



An excitation system is called dependent or a selfexcitation system if the n.s. for excitation depends on the operating regime of the generator.

In the first case, an external (separate) direct-source current is needed to supply the generator excitation circuit; in the second case, there is no need for a separate direct-current source.

Separate-excitation systems do not require remanent magnetism in synchronous generators, while with selfexcitation systems, it is necessary.

The basic excitation systems for synchronous machines are the following.

#### Separate-excitation systems

a) excitation from a separate direct-current source – the aircraft electrical system for a converter;

b) excitation from a direct-current generator – an exciter located on the generator shaft (single-stage or two-stage excitation system).

#### Dependent-excitation (selfexcitation) systems

a) permanent-magnet excitation;

b) generator excitation from its own alternating-current system through a rectifier;

c) excitation from an integral (combined) exciter.

Sometimes the excitation systems of synchronous generators are provided with partial or complete selfregulation of the excitation in a manner similar to that used with direct-current with compound excitation. Such excitation or selfexcitation systems are called compound systems.

#### Compound excitation and selfexcitation systems

a) excitation and compounding from exciter;

b) selfexcitation and compounding from rectifier;

c) selfexcitation and compounding from integral exciter.

Below we shall discuss various excitation and selfexcitation systems for synchronous generators.

### Synchronous machines with separate exciters

Separate excitation of a synchronous generator may be accomplished by various methods: from the aircraft direct-current electrical system, from a special direct-current generator, or from a rechargeable battery.

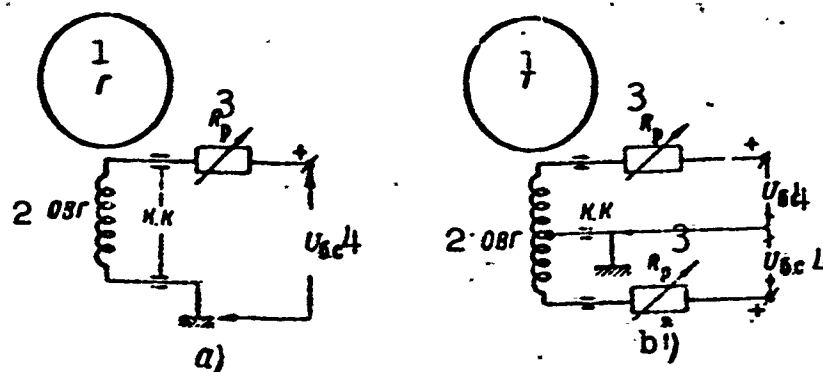


Fig. 3.11. Separate excitation of generators from aircraft power system. a) With one voltage regulator; b) with two regulators operated in parallel. OVG) Generator field winding;  $R_p$ ) regulator resistance; K.K.) slip rings;  $U_{b.s}$ ) aircraft power-system voltage; 1) G; 2) OVG; 3)  $R_p$ ; 4)  $U_{b.s}$ .

Alternating-current generators used in a converter set normally draw power for the excitation circuit from the main aircraft direct-current system. Figure 3.11 shows circuits used to excite alternating-current generators from a separate direct-current source.

Here the generator voltage is regulated by varying the resistance in the generator excitation circuit. A drawback to the system is the relatively high regulation power together with the considerable rate of the regulators owing to the need to change the relatively large generator excitation current. In addition, this system

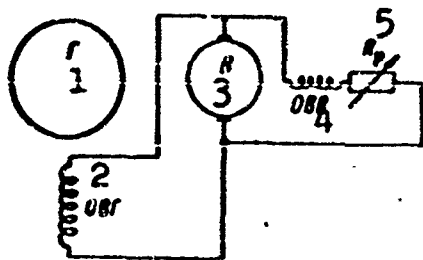


Fig. 3.12. Separate excitation from exciter (single-stage excitation system). V) Exciter; OVV) exciter field winding; 1) G; 2) OVG; 3) V; 4) OVV; 5)  $R_r$ .

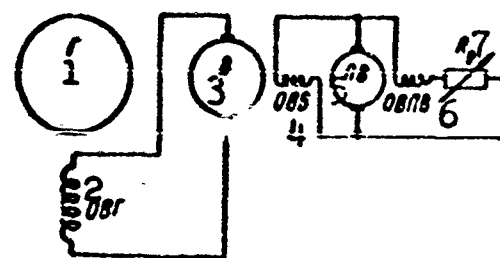


Fig. 3.13. Separate excitation from exciter (two-stage excitation system). PV) Pilot exciter; OVPV) excitation winding of pilot exciter; 1) G; 2) OVG; 3) V; 4) OVV; 5) PV; 6) OVPV; 7)  $R_r$ .

is not selfcontained, since it depends on the external direct-current source and is thus less reliable. For generators of the order of 50 kva power, it is necessary to use a design employing two voltage regulators and three slip rings on the rotor (Fig. 3.11b).

Excitation of a synchronous machine from an exciter (Figs. 3.12 and 3.13) located on the generator shaft is the most common method used in modern general-purpose synchronous machines; in essence, they are two-machine combinations consisting of an alternating-current machine and exciters — direct-current generators. The exciter draws its power (4-10%) from the power of the alternating-current machine, providing a selfcontained excitation system. The drawback is the considerable increase in machine size and weight (for low powers, exciter dimensions are of the same order as the generator dimensions).

Exciters are made with parallel or compound excitation with or without compensation.

An exciter is less reliable structurally than a generator. About 80% of all failures involving low- or medium-power generators normally occur as a result of damage to the exciter, and only 20% owing to generator damage, i.e., the degree of reliability of an

installation is in the last analysis determined by the reliability of the exciter, resulting in a manyfold reduction in over-all reliability.

In addition, we still have the commutator sliding contact with all of its inherent disadvantages at high altitudes and flight speeds. Thus, exciters for aircraft generators should be of especially reliable design, and should provide stable and sensitive excitation of the alternating-current generators under all possible operating conditions.

Fast-responding excitation systems, i.e., systems that rapidly restore voltage across the generator terminals following a change in operating conditions are especially important in starting engines of comparable power, in short circuits, and in order to increase operating stability in parallel. It is determined by the exciter voltage reserve, and by its ceiling voltage and the voltage rate of rise.

The ceiling excitation voltage is the name given to the ratio of the maximum exciter voltage at zero voltage-regulator resistance to the nominal voltage. It is not specified by any standard, and normally it equals 1.5-2.0.

The higher the voltage reserve required, the higher the exciter power and the larger its dimensions. Thus, if the nominal exciter power equals

$$P_{\text{B.NOM}} = U_{\text{NOM}} I_{\text{B.NOM}} = \frac{U_{\text{NOM}}^2}{R_{\text{B}}} = 1 \text{ kW}$$

and the exciter reserve (ceiling) equals 2, the exciter power should be quadruple the rated power, i.e.,

$$2U_{\text{NOM}} \cdot 2I_{\text{B.NOM}} = \frac{(2U_{\text{NOM}})^2}{R_{\text{B}}} = 4P_{\text{B.NOM}} = 4 \text{ kW}$$

The voltage rise rate is the name given to the time required

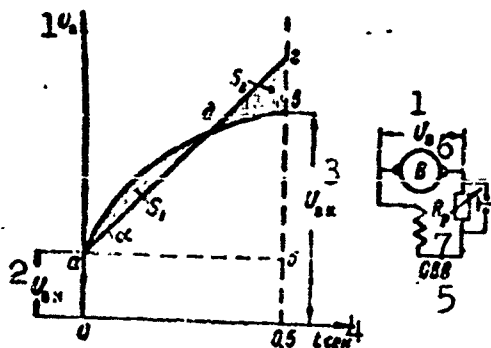


Fig. 3.14. Determining the voltage rise rate for an exciter.  $U_{v.n}$  and  $U_{v.k}$ ) Exciter voltage before and after sudden removal of regulator resistance  $R_r$ .  
 1)  $U_v$ ; 2)  $U_{v.n}$ ; 3)  $U_{v.k}$ ;  
 4)  $t$ , sec; 5)  $OVV$ ; 6)  $V$ ;  
 7)  $R_r$ .

for a predetermined voltage level to be reached when the excitation current is changed abruptly.

Figure 3.14 shows the nature of the exciter voltage rise  $U_v$  after the regulator resistance  $R_r$  has been short-circuited, i.e., following an abrupt change in exciter field current.

If we draw line  $ad$  at an angle  $\alpha$  so that  $ab = 0.5$  sec, the area of triangle  $abd$  will equal the area of  $aecd$ , i.e.,  $S_1 = S_2$ , and in this case the

nominal exciter rise rate will, according to the standard (GOST 183-55), be determined by the ratio of the segments  $bd/ab$ , i.e., by the tangent of the slope angle of line  $ad$ . The time corresponding to segment  $ab$  equals 0.5 sec. The magnitude of segment  $bd$  is expressed in fractions of the nominal exciter voltage.

The nominal excitation increase rate for general-purpose exciters lies in the range

$$\frac{dU_v}{dt} = \frac{bz}{ab} = 1.0 \div 2.0.$$

High-speed exciters for synchronous low-power generators have a ratio

$$\frac{dU_v}{dt} \approx 3 \text{ and higher}$$

Generator voltage can be regulated by changing the resistance in the exciter excitation circuit, or by changing the resistance in the generator excitation circuit.

In the latter case, the regulation power is roughly ten times that of the first case, since the exciter excitation current is

roughly one-tenth of the generator excitation current. In view of this, voltage regulation is carried out by changing the exciter excitation current.

In high-power machines (general-purpose) a two-stage system of excitation is sometimes used (Fig. 3.12b). The drawback to this system is the presence of two exciters on the machine shaft — the exciter and the pilot exciter. The system does, however, increase the voltage rise rate, decrease the control current (power), and eliminate the danger of magnetic reversal in the exciter, which can occur with sudden generator short circuits.

Here we must keep in mind stable operation of the excitation system under all synchronous-generator operating conditions: from no-load conditions (operation on the initial section of the magnetization curve) to overload conditions.

Excitation stability can be increased by shifting excitation regulation from the pilot-exciter circuit to the exciter circuit; in this case, the voltage across the exciter terminals will be constant; this, however, removes one of the important advantages of two-stage regulation — the decreased regulation power.

#### Synchronous machines with selfexcitation

Permanent-magnet excitation. As we have already mentioned, selfexcitation systems include those in which the excitation magnetizing force depends on generator operating regime. By this definition, permanent-magnet excitation should be classified among the selfexcitation systems, since the magnetizing force of the magnets decreases with increasing longitudinal component of the armature magnetizing force. Without going into the theory of synchronous machines using permanent-magnet excitation, which will be treated separately, we only note that the basic advantages of this excitation

system are: a) absence of an exciter and, consequently, of a sliding-contact commutator; b) simplicity, reliability, and independence of the excitation system; c) good high-altitude performance, better high-altitude efficiency, and in some cases as we shall show in Chapter 4, lower generator weight.

Generator excitation from an internal alternating-current line is possible where a solid-state, mechanical, or electronic rectifier is used.

In this case, the generator has an ordinarily accepted design and is distinguished only by the fact that the field winding is supplied with direct current from an internal alternating-current line through a rectifier and, consequently, there is no exciter. The generator voltage is held constant with the aid of a regulator operating in the excitation circuit.

Figure 3.15 shows four excitation circuits for three-phase synchronous generators. Circuit a is used where the direct-current excitation voltage corresponds to the alternating-current line voltage and magnitude. Where it is desirable to have the excitation voltage differ considerably from the alternating-current line voltage, a transformer (circuit b) may be used, or a second additional three-phase winding may be placed into the armature slots of the generator; this winding is intended only to supply the field circuit through a rectifier (circuit c) or, finally, a tap may be made from a part of the winding of each armature phase in order to supply the excitation circuit through a rectifier (circuit d).

Let us examine certain advantages and disadvantages to the circuits shown. The maximum power taken from the line for excitation  $P_{s.v}$  will in the general case (Fig. 3.15b) be

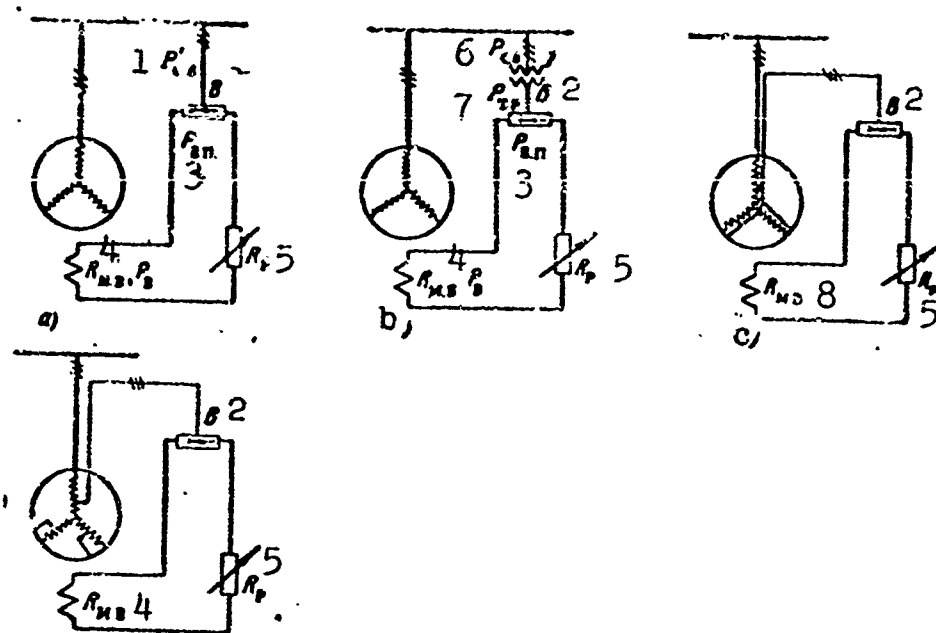


Fig. 3.15. Selfexcitation circuits for synchronous generators. V) Rectifier; T) transformer;  $R_r$ ) regulator resistance;  $R_{m.v}$ ) excitation-winding resistance; 1)  $P'_{s.v}$ ; 2) V; 3)  $P_{v.p}$ ; 4)  $R_{m.v}$ ,  $P_v$ ; 5)  $R_r$ ; 6)  $P_{s.v}$ ; 7)  $P_{t.r}$ ; 8)  $R_{m.v}$ .

$$P'_{c.s} = \frac{P_{tr}}{\eta_{tr} \cos \varphi_{tr}} = \frac{P_{s.v}}{\eta_{s.v} \cos \varphi_{tr}} = \frac{P_s}{\eta_{s.v} \eta_{tr} \cos \varphi_{tr}} \quad (3.5)$$

Here  $P_{v.p} = P_v / \eta_v$  is the rectifier output power (direct-current excitation), equal to the maximum excitation power in the absence of additional resistances in the excitation-winding circuit;  $P_{tr} = P_{v.p} / \eta_{v.p} = P_v / \eta_{v.p} \eta_v$  is the transformer power;  $P_v = R_v I_v^2$  are the losses in the excitation winding under rated conditions;  $\eta_v$ ,  $\eta_{v.p}$ , and  $\eta_{tr}$  are the efficiencies of the excitation circuit (up to the rectifier), the rectifier, and the transformer, respectively.

We shall assume that the excitation-circuit power factor before the transformer (for the line in the absence of a transformer) equals unity. For circuits a, c, and d, which do not contain transformers, we shall have in place of (3.5)

$$P'_{c.s} = \frac{P_{s.v}}{\eta_{s.v}} = \frac{P_s}{\eta_{s.v}} \quad (3.6)$$

The design generator power  $P_{g.r}$  should be considered to be the



amount of power expended on excitation, i.e.,

$$P_{c.p} = P_r + P_{c.s} = P_r \left( 1 + \frac{P_{c.s}}{P_r} \right) = k_p P_r \quad (3.7)$$

where  $k_r = P_{g.r}/P_g = 1 + (P_{s.v}/P_g)$  is the rise factor for the design generator power in comparison with its nominal value ( $P_g$ ). Circuits a, b, and d are equivalent with respect to the design generator power. Circuit b, which has a transformer, has a higher design power and, consequently, leads to a larger generator.

For circuit b the factor  $k'_r$  equals

$$k'_r = 1 + \frac{P_s}{P_r \gamma_{s.s} \alpha \gamma_{tp} \cos \varphi_{tp}} \quad (3.8)$$

while for all the remaining circuits it equals

$$k_p = 1 + \frac{P_s}{P_r \gamma_{s.s}} \quad (3.8a)$$

The complete copper cross section in the generator armature slots is identical for circuits a, c, and d, and is less than that for circuit b in the ratio  $k_r:k'_r < 1$ .

The copper cross section for the auxiliary winding  $S_{m.v}$  in circuit c equals

$$S_{m.s} = S_{m.r} \frac{P'_{c.s}}{P_r} = S_{m.r} \frac{P_s}{P_r \gamma_{s.s} \alpha}, \quad (3.9)$$

where

$$S_{m.r} = 2\pi r \frac{I_r}{j} = \frac{A \pi D}{j} = 2\pi r \frac{P_r}{U_r j} \quad (3.10)$$

is the total copper cross section for the generator calculated using a nominal generator power  $P_g = mU_g I_g$ ;  $A = 2\pi w_g I_g / \pi D$  is the linear load.

Here we assume that the current density and winding factor of the basic and auxiliary windings are the same. The total copper cross section in the armature windings is

$$S_{m.s} = S_{m.r} + S_{m.s} = S_{m.r} k_p$$

where

$$k_p = 1 + \frac{S_{m.s}}{S_{m.r}} = 1 + \frac{P'_{c.s}}{P_r} \quad (3.11)$$

In circuit a, the total copper cross section for the armature winding, if we take (3.10) and (3.11) into account will equal

$$S_{m.s} = \frac{2\pi r P_{r.p}}{U_r J} = S_{m.r} k_p \quad (3.12)$$

In circuit d, a part of the winding for each phase from the neutral point to the tap should have a larger cross section than the portion from the tap to the phase output. If the rated load current of the generator is  $I_g$ , an additional excitation current equal to

$$I_s = I_r \frac{P'_{c.s}}{P_r} \frac{U_r}{U_s} \quad (3.13)$$

will flow from the neutral point to the tap.

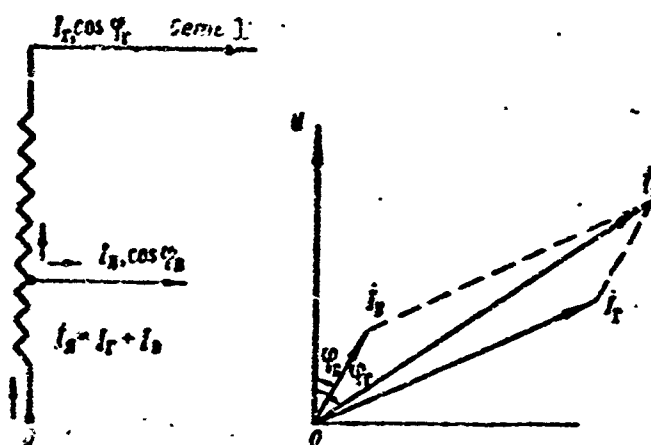


Fig. 3.16. Current distribution in circuit with tap. 1) Line.

The alternating current  $I_v$  is added vectorially to the load current  $I_g$  (Fig. 3.16). Consequently, the scalar resultant current flowing through the phase section from the neutral point to the tap will equal

$$I_s = I_r \sqrt{1 + \left(\frac{I_g}{I_r}\right)^2 + 2 \frac{I_g}{I_r} \cos(\varphi_r - \varphi_g)} \quad (3.14)$$

Here  $\cos \varphi_v$  and  $\cos \varphi_g$  are the power factors for the excitation and load circuits, respectively.

If we take  $\cos \varphi_v = 0.95$  and  $\cos \varphi_g = 0.75$ , then  $\cos(\varphi_g - \varphi_v) \approx 0.92$ , and with an accuracy sufficient for practical purposes, Expression (3.14) may be written as

$$I_s = I_r + I_s = I_r \left( 1 + \frac{P'_{c.s}}{P_r} \frac{U_r}{U_s} \right). \quad (3.15)$$

The cross section of the armature conductors in the section under consideration should be increased in the ratio

$$\frac{S_{u.s}}{S_{u.r}} = \frac{I_s}{I_r} = 1 + \frac{P'_{c.s}}{P_r} \frac{U_r}{U_s}. \quad (3.16)$$

If we assume that  $P'_{s.v} = 0.05P_g$ , while  $U_g = 4U_v$ , the copper cross section should be multiplied by a factor of 1.2. Thus, in circuit d it is desirable to form the armature winding from conductors of larger cross section from the neutral point to the tap and of smaller cross section from the tap to the phase output. The total armature copper cross section will then remain the same as that in circuits a and c.

Practically speaking, generator dimensions will be identical for circuits b and c, since the increase in armature copper cross section in circuit b is compensated by a drop in the slot fill factor in circuit c owing to the presence of two windings in the armature slots.

Comparing circuits b, c and d, we note that the drawback to circuit b is the presence of a transformer and increased general losses owing to the additional losses from the transformers; it does, however, make use of a standard generator. The advantage to circuits c and d are the absence of a transformer and associated losses. These circuits, however, require structural modifications in the armature winding of the generator, which is undesirable and represents a drawback to these circuits.

Circuits c and d cannot be used in practice for synchronous

machines with external poles, since it would be necessary in this case to double the number of slip rings. A substantial disadvantage to circuit d is the presence of electrical coupling between the generator winding and the excitation circuit.

Taking what has been said into account, let us select one of the circuits shown. As we know, several conditions must be satisfied for selfexcitation of a synchronous machine, namely: a) the machine should possess remanent magnetism; b) the resistance in the excitation circuit should be below the critical value; c) the speed of the machine should be above the critical value; d) the current flowing in the excitation circuit should be so directed that it reinforces the remanent-magnetism field.

The resistance in the excitation circuit consists of the excitation-winding resistance  $R_{m.v}$ , the regulator resistance  $R_r$ , and the rectifier resistance  $R_{vypr}$ , i.e.,

$$R_s = R_{m.v} + R_r + R_{vypr} \quad (3.17)$$

With selfexcitation of a machine, the regulator resistance is made as small as possible. During the selfexcitation process,  $R_{m.v} + R_r = \text{const}$ , while the rectifier resistance is a variable that depends on the applied voltage and the current flowing through it; thus,  $R_{vypr}$  will be large at low voltages (small currents) such as occur at the beginning of the selfexcitation process, while it will be small at the end of the selfexcitation process, where the voltage (current) rises. In this connection, at the initial instant of generator selfexcitation, when the residual voltage is small, the excitation resistance will be greater than critical, and selfexcitation will not occur.

Figure 3.17 gives the no-load curve 1 for the generator and the volt-ampere curve 2 for the excitation circuit, which is nonlinear

owing to the nonlinearity of the rectifier resistance. Selfexcitation cannot occur on section OA, since the volt-ampere curve for excitation lies above the no-load curve.

Thus, a substantial disadvantage to this excitation system is the fact that natural selfexcitation is impossible owing to the large rectifier resistance at the initial instant of selfexcitation.

Special measures must be taken to increase the residual flux in order to provide selfexcitation, such as the introduction of additional voltage into the excitation circuit, a decrease in the rectifier resistance at the initial selfexcitation instant, etc.

As investigations have shown, regardless of the selfexcitation system used, the residual flux of a machine excited through a rectifier should be greater than the natural remanent flux of ordinary machines, and this must be taken into consideration when a generator magnetic circuit is designed.

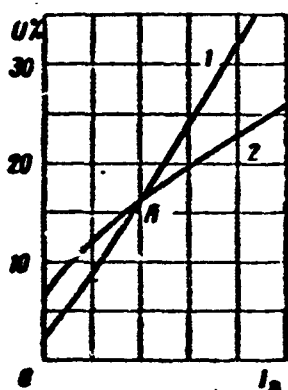


Fig. 3.17. Initial section of no-load curve 1 and excitation volt-ampere curve 2.

We shall indicate several methods for obtaining selfexcitation.

1) In order to increase the residual voltage, part of the magnetic flux path is made from solid magnetic steel, or a special heat-treated sleeve or pole is used (Fig. 3.18).

One possible design is shown in Fig. 3.19. The arrangement shown provides for selfexcitation, but complicates generator construction

and increases its axial length and weight. The utilization of magnetic inserts located under the pole, or of sleeves of magnetic material will also provide selfexcitation; here, however, there is a considerable increase in the reluctance presented to the main flux,

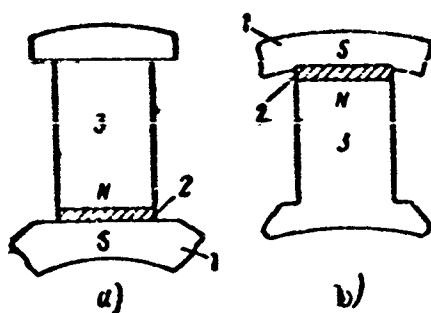


Fig. 3.18. Arrangement of magnetic inserts in machine with internal (a) and external (b) poles. 1) Pole piece; 2) permanent magnet; 3) pole core.

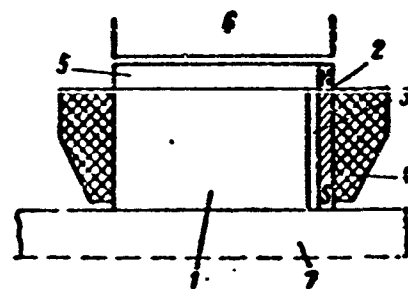


Fig. 3.19. Location of permanent magnet for increasing remanent flux. 1) Pole core; 2) permanent magnet; 3) nonmagnetic insert; 4) field winding; 5) pole piece; 6) stator; 7) bushing.

which leads to an increase in the excitation magnetizing force required. As a result, the dimensions of the generator and rectifier are increased and, in addition, efficiency drops. Thus, for example, in a four-pole 50-cps 10-kva generator, in order to increase the residual voltage from 2.3 to 12.7%, it is necessary to use a 20-mm thick insert of YeKhZ chrome steel ( $B_r = 9500-9000$  gauss and  $H_c = 55-60$  oersteds).

A permanent magnet to be used in generator selfexcitation should be made from a magnetically hard alloy with a high remanent induction  $B_r$ , a relatively small coercive force  $H_c$  and, consequently, a relatively high magnetic permeability (permeance)  $\mu \approx 0.5 (B_r/H_c)$ . These conditions are satisfied by chromium and tungsten steels for which  $B_r = 8500-10,000$  gauss,  $H_c = 60-40$  oersted, and  $\mu = 70-125$ .

If we assume that at the initial instant of selfexcitation, the voltage across the generator terminals is created solely by a permanent magnet, we can then determine in approximation the height of the permanent magnet from the equation

$$h_m = \frac{F_0}{H_m} \frac{U_{ost}}{U_n} \text{ cM.} \quad (3.18)$$

Here

$$F_0 = 0.8 k_s k_\delta B_\delta \quad (3.19)$$

is the magnetizing force for one pole under no-load conditions at rated voltage:  $U_{ost}$  and  $U_n$  are the residual and normal voltages of the machine;  $k_s = F_0/F_\delta = 1.2-1.4$  is a coefficient that takes into account the reluctance of the machine magnetic circuit (with the exception of the air gap);  $k_\delta$  is an air-gap coefficient;  $\delta$  is the length of the air gap, cm;  $B_\delta$  is the no-load air-gap induction at rated voltage;  $H_m = kH_c$  is the magnetic field strength of the permanent magnet (for chromium and tungsten steels, which are recommended, we may take  $H_m \approx 0.95H_c$  for inductions  $B_m < 3000$  gauss).

Thus, for chromium and tungsten steels we may assume in approximation that the ratio  $U_{ost}:U_n = 0.1$ , and we find that

$$h_m \approx 2.5 \frac{F_0}{1000} \text{ cM.} \quad (3.20)$$

The cross section of the permanent magnet is taken to equal the cross section of the pole; the induction in the magnet will then not exceed, as a rule, 1000 gauss.

2. Selfexcitation of a generator at the initial instant may be brought about by connecting into the excitation circuit an additional external voltage which is later taken out of the circuit. As the source of the additional voltage we may use: a rechargeable battery, a stepped transformer or a series transformer, or a potential regulator. This, however, complicates the excitation circuit, reduces the electrical-system reliability, and increases the weight of the installation; thus, this method cannot be recommended for aircraft applications.

The utilization of a series transformer may prove desirable if it is used simultaneously for compounding purposes.

3. At the initial instant, the rectifier resistance may be decreased by disconnecting a portion of the series-connected rectifier elements. When this is done, a higher alternating-current voltage will appear across the remaining part of the rectifier, and the rectifier resistance will drop owing to the decreased number of series-connected elements and owing to the decrease in the resistance of the remaining elements (caused by the increase in voltage). This method of solving the problem is dangerous, since it may lead to rectifier failure. Where the rectifier service life is short (500 hr), however, an improvement in quality by this method may prove desirable.

4. In circuits using stabilizing transformers, selfexcitation can be used successfully if one, or preferably two, phases of the series transformer are briefly short-circuited. The voltage relay forming the short circuit should operate perfectly in order to avoid transformer failure.

### 3.3. EXCITATION SYSTEMS WITH STABILIZATION (COMPOUNDING)

For normal operation of devices consuming electric power, it is necessary to keep the line voltage nearly independent of the magnitude and nature of the load. Especially great line-voltage fluctuations occur when induction motors are started directly, if their power is of the same order as the generator power. Voltage fluctuation causes overheating and underheating of radio tubes and light bulbs, changes the operating conditions of motors, etc. In aircraft electrical systems, the voltage across the generator terminals should be held to within  $\pm 2\%$  of the rated value under all possible operating-condition variations.

As a rule, the voltage is held constant with the aid of special voltage regulators: vibrator-type carbon, magnetic, electronic, or



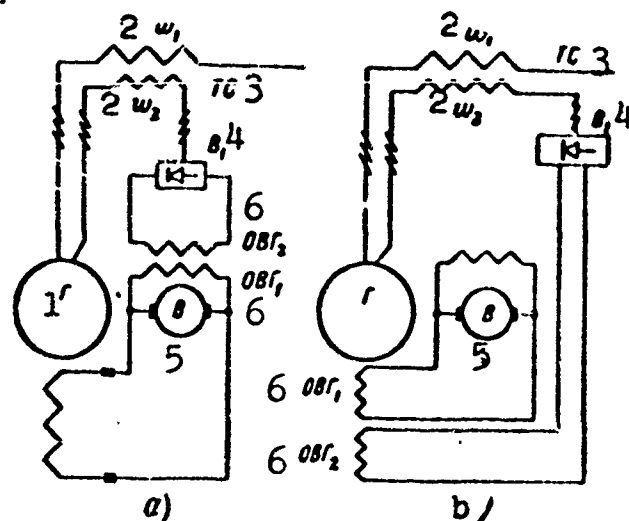


Fig. 3.20. Voltage stabilization with exciter used for excitation. a) Compound exciter field winding; b) compound generator field winding; 1) G; 2)  $w_x$ ; 3) TS; 4)  $V_1$ ; 5) V; 6)  $OVG_x$ .

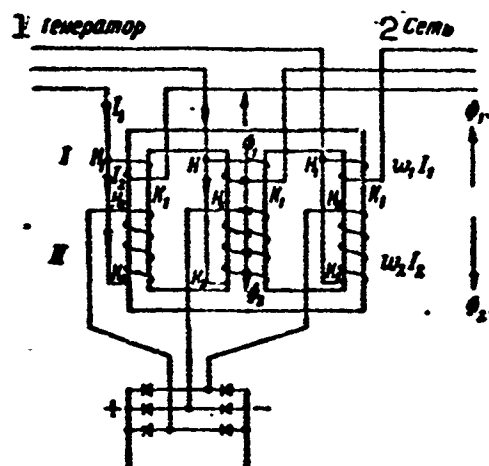


Fig. 3.21. Double-winding TS stabilizing transformer. 1) Generator; 2) line.

combination regulators that maintain the necessary voltage level; such devices are not considered in this course. We shall mention only the arrangement and operation of machines and machine systems that have the property of automatic voltage selfregulation.

#### Voltage Stabilization With Excitation From an Exciter

Figure 3.20 shows a separate-excitation circuit in which the exciter field winding is supplied from an internal alternating-current line through a three-phase rectifier.

In order to obtain the effect of automatic voltage selfregulation, a rectifier is connected into the alternating-current line through a three-phase two-winding current transformer, which is called

a stabilizing transformer (TS).

Figure 3.21 shows the wiring diagram for a two-winding three-phase stabilizing transformer where the directions of the windings are the same for each phase.

The primary winding of the stabilizing transformer is connected in series with the generator armature so that the beginning of the winding is connected to the generator and the end to the line. Here the beginnings of the secondaries are connected to the rectifier and the ends run to the appropriate (main or additional) leads of the armature winding, depending on the type of selfexcitation circuit. With the connections shown for the windings, their magnetizing forces will be in opposition and, consequently, the resultant transformer flux and the emf in the secondary will be proportional to the difference in the winding magnetizing forces, i.e.,

$$\Phi = \frac{F_1 - F_2}{R_m} ; E \equiv F_1 - F_2.$$

Under no-load conditions, where there is no current  $I_1$  in the transformer primary, the no-load excitation current  $I_{20}$  will flow in the secondary.

Under these conditions, the TS secondary operates as a reactance coil (reactor) connected in series with the electrifier, and drops the voltage across its terminals to an amount

$$\dot{U}_{\text{drop}} = \dot{U}_0 - I_{20} Z_{2\sigma}.$$

Under no-load conditions, the flux  $\Phi_0$  in the TS is determined by the magnetizing force  $I_{20} w_2$  of the secondary; it induces a small emf in the primary of the TS.

At some load current  $I'_1$ , for which the magnetizing forces of the primary and secondary are equal, i.e.,  $I'_1 w_1 = I_2 w_2$ , the flux in the TS will equal zero, since the magnetizing forces due to the wind-

ings will cancel. Under such conditions, the inductive reactance of the TS secondary will nearly be zero and the voltage across the rectifier terminals will increase to the generator voltage

$$U_{\text{out}} \approx U_r - I_2 R_2 \approx U_r.$$

If the load current increases, the magnetizing force due to the primary will exceed that of the secondary, and a flux  $F$  will appear in the stabilizing transformer; this flux will induce an additional emf in the secondary. At the same time, the voltage applied directly to the rectifier from the line through the secondary, acting as a reactance coil, will decrease, since when a flux appears in the TS, its impedance rises. Under such conditions, the TS operates as a booster transformer.

Thus, a voltage that depends on the load current appears across the output terminals of the TS to which the rectifier is connected. It is clear that a change in the phase of the load current (power factor) is not handled by the TS, and this is one of the drawbacks to this system of voltage stabilization.

Figure 3.20b shows a voltage-stabilization circuit that differs from the one just discussed in that the field winding of the generator is split into two sections. One of them is powered by an exciter that provides the necessary no-load excitation, and its magnetizing force is independent of the generator operating conditions; the second winding, drawing its power from the alternating-current line through a rectifier, develops a magnetizing force that is proportional to the load current, i.e., it depends on the generator operating conditions. Under no-load generator conditions, as in circuit a, the excitation magnetizing force is formed by winding  $OVG_1$  and, to some degree, by winding  $OVG_2$ . The excitation current in winding  $OVG_2$  is small, since the large reactance of the stabilization-transformer secondary is con-

nected between the rectifier and the alternating-current source. When there is a load on the generator, the armature current flows around the TS primary, and the latter no longer acts as a reactor, but as a stabilizing booster transformer. The inductive reactance of the TS secondary falls and the emf induced in it, which adds vectorially with the line voltage, increases the voltage across the rectifier and, consequently, the excitation current in winding OVG<sub>2</sub>. This is the way in which the stabilizing action of the transformer appears.

Comparing circuits a and b we note that:

- a) the power of the exciter in circuit b is roughly half that of the exciter in circuit a;
- b) the powers of the rectifier and stabilization transformer in circuit a are roughly one-fifth to one-tenth those of circuit b;
- c) for a generator with internal rotating holes, circuit b requires four slip rings as against two for circuit a, which causes the machine to be lengthier and heavier.

The circuits shown in Fig. 3.20 provide voltage stabilization together with reliable selfexcitation.

#### Voltage Stabilization with Rectifier Excitation

Figure 3.22 shows four voltage-stabilization circuits using three-phase stabilization transformers with two or three windings.

Circuits a, b, and c, using two-winding transformers, differ solely in the method used for connecting the ends of the TS secondary to the alternating-current source: in circuit a, they are connected to the generator armature-winding leads, in circuit b, to the leads of the auxiliary armature winding, and in circuit c, to taps on the generator armature winding. In circuits b and c, the nominal excitation voltage does not depend on the nominal generator voltage.

The arrangement and operation of a two-winding stabilization

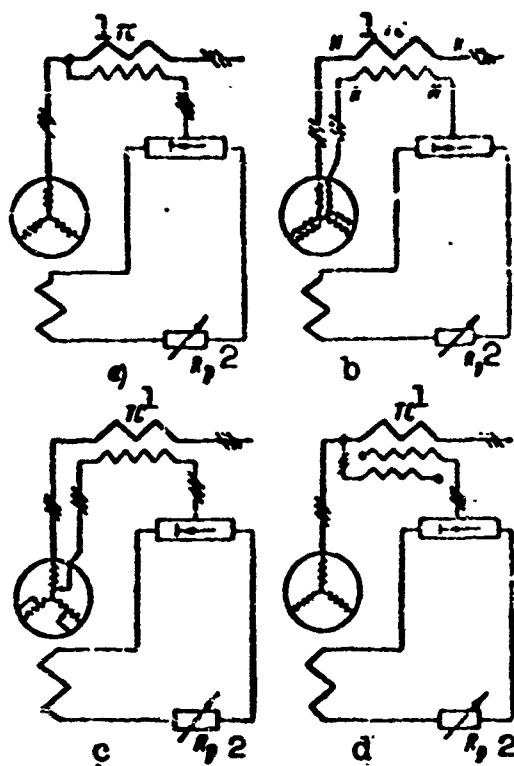


Fig. 3.22. Voltage-stabilization circuit with rectifier selfexcitation. 1) TS; 2)  $R_r$ .

transformer have already been discussed. In voltage-stabilization circuit d, a three-winding stabilization transformer is used, which combines on one core a two-winding stabilization transformer and a three-winding voltage transformer; one of the windings is connected in series with the armature winding as a current-transformer primary; the second is connected in parallel to the armature winding as the primary of a voltage transformer; the third winding, connected to the rectifier, acts as the secondary for both primaries.

Figure 3.23 shows the way in which the windings are arranged on the core.

When there is no load on the generator, the three-winding TS works as an ordinary two-winding voltage transformer. At this time, the minimum voltage will appear across the excitation winding, corresponding to no-load current. When the generator is under load, the transformer flux rises under the influence of the series-winding mag-

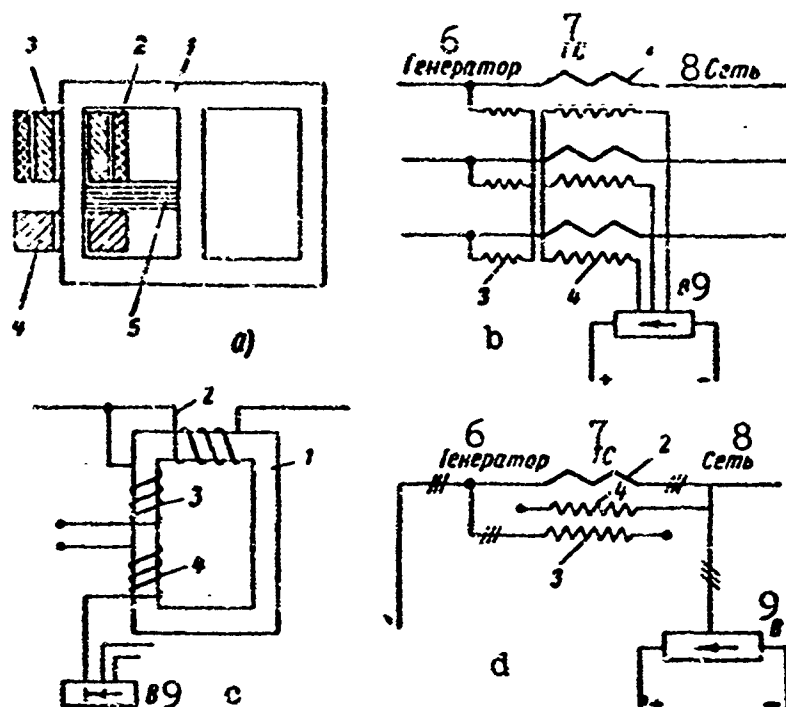


Fig. 3.23. Three-winding stabilization transformer. a) Arrangement of windings; b) wiring diagram; c and d) conventional designations for three-winding transformer. 1) Transformer core; 2) current-transformer primary; 3) voltage-transformer primary; 4) secondary; 5) magnetic shunt; 6) generator; 7) TS; 8) line; 9) V.

netizing force. As a result, there is an increase in the emf induced in the transformer secondary; this emf is proportional (with the transformer unsaturated) to the load current, i.e., as the load current increases, the magnetizing force due to the excitation winding rises, as is necessary to stabilize the generator voltage.

As we can see from Fig. 3.23, the voltage primary of the TS is not concentric with the secondary as is normally the case, but it is higher on the transformer core. In addition, there is a magnetic shunt consisting of steel laminations located between them. The magnetic shunt between the voltage primary and secondary makes it possible (by varying the dispersion flux) to establish the required voltage at the rectifier input when there is no load on the generator. By increasing the dispersion flux (increasing the thickness of the magnetic shunt),

we can decrease the emf induced in the TS secondary.

### Voltage Stabilization with Excitation Taken from an Integral Exciter

Figure 3.24a shows an excitation circuit in which the magnetic circuits of the synchronous-generator and exciter armatures, as well as their primary windings, are combined.

This system provides a decrease in the axial dimensions of the machine and permits some voltage stabilization (selfregulation). As investigations of such an aircraft generator, constructed in accordance with a proposal of the author and with his participation, have shown, however, there are substantial drawbacks: it is difficult and sometimes impossible to obtain a symmetric exciter armature winding (and as a result impermissible sparking occurs at the collector); the external characteristic curve for the exciter drops off sharply.

Below we discuss the basic features of this system and possible ways to improve it.

A single-armature double-current synchronous generator is a synchronous generator with an integral exciter and two independent armature windings. A single machine structure combines an alternating-current generator and a direct-current generator – the exciter, designed to supply the alternating-current generator excitation circuit. The armature winding of the alternating-current generator, which is connected to slip rings, and the armature winding of the direct-current generator (the exciter), which is connected to a commutator, are located in exactly the same slots.

The machine is normally made with fixed external poles and a rotating armature. Machine selfexcitation is provided by residual magnetism. Single-armature double-current generators are always made without commutating poles and are built only for low-power machines.

A single-armature double-current generator has the advantages of

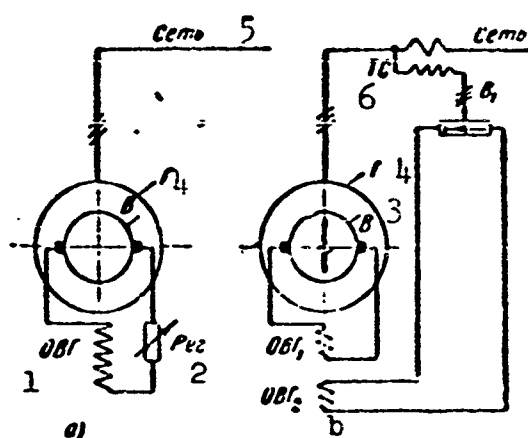


Fig. 3.24. Excitation from integral exciter. a) Standard circuit; b) compound circuit; G) generator; V) exciter; Reg) regulator; V<sub>1</sub>) rectifier; TS) stabilization transformer. 1) OVG; 2) Reg; 3) V; 4) G; 5) line; 6) TS.

decreased weight and smaller axial machine dimensions owing to the utilization of a common magnetic system (see Fig. 3.6).

A substantial drawback to the single-armature double-current generator is the sharply dropping external alternating-current generator characteristic curve observed even with a purely resistive load.

The sharp drop in generator voltage with increasing load current results from the fact that the longitudinal component of the alternating-current armature magnetizing force reduces the main machine flux and, consequently, the emf and voltage for the generator and exciter armature windings. A decrease in the voltage across the exciter terminals and, consequently, in the excitation current lead to an additional reduction in the main machine flux, i.e., to an additional decrease in the emf and voltage for the alternating-current generator armature. Thus, the alternating-current generator voltage drops under the influence of:

- a) the voltage drop across the armature resistance;
- b) the reduction in main flux caused by the magnetizing forces of



the exciter and generator armatures;

c) the additional decrease in main flux due to the decreased exciter voltage resulting from the effect of the armature magnetizing force on the main field.

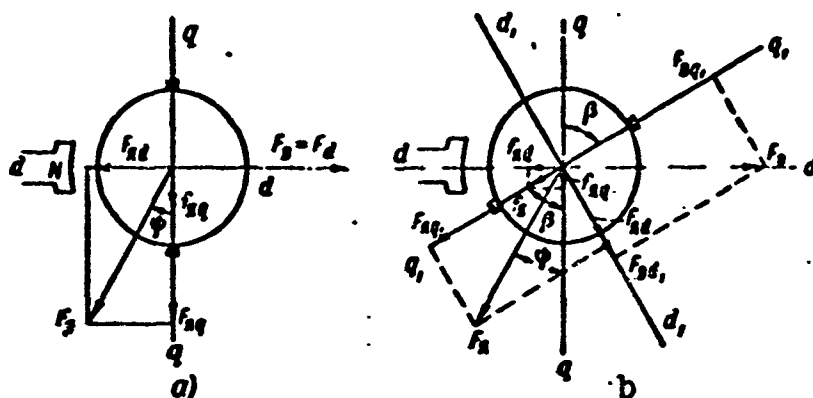


Fig. 3.25. Diagram showing magnetizing forces of generator and exciter armatures. a) With brushes at neutral position; b) brushes shifted.

When the generator terminals are short-circuited, the main flux drops to zero. In this case, the machine loses excitation, and the generator short-circuit current decreases to an amount determined by the residual magnetism.

The external characteristic curve for a single-armature double-current generator is similar to that for a direct-current machine with shunt excitation. The progressive reduction in main flux that occurs when the load increases due to the decreased excitation flux causes the machine to have an external characteristic curve that drops away steeply. In order to increase the stability of the external characteristic curve, it is necessary to increase the excitation current with increasing load. This may be done by:

a) shifting the brushes from the geometrically neutral position in the direction of armature rotation;

b) using two independent excitation windings supplied, respectively, from transverse and longitudinal excitation brushes;

- c) using two independent excitation windings supplied, respectively, from the exciter and from the alternating-current line through a stabilizing transformer and rectifier (compound circuit, Fig. 3.24b);
- d) properly arranging an additional compensator.

Shifting brushes in the direction of rotation. Figure 3.25 shows diagrams for the magnetizing forces of a double-current two-pole machine with the brushes in the neutral position and shifted in the direction of rotation.

If we assume that the load on an alternating-current generator remains constant, the longitudinal and transverse components of the generator-armature magnetizing force, as well as the angular displacement of the current vector (magnetizing force) with respect to the voltage vector (the angle  $\psi$ ) will be constant, and will not depend on the excitation-brush positions.

Depending on the nature of the load — the power factor — the longitudinal component  $F_{ya d}$  of the armature magnetizing force will weaken or reinforce the main machine field  $F_v$ . In the case under consideration, when  $\cos \varphi$  lags, the magnetizing force  $F_{ya d}$  will weaken the main field (Fig. 3.25a).

As we know, the transverse component  $F_{ya q}$  of the armature magnetizing force distorts and somewhat weakens the main field.

With the brusher at the neutral plane, there is no longitudinal magnetizing-force component  $f_{ya d}$  due to the exciter armature, and the longitudinal component  $f_{ya q}$ , which equals the maximum exciter-armature magnetizing force, distorts and somewhat weakens the main machine field. The magnetizing force  $f_{ya}$  of the exciter armature is roughly one-tenth to one-twentieth the magnetizing force  $F_{ya}$  due to the generator armature, and its effect is frequently neglected.

If we move the exciter brushes through an angle  $\beta$  in the direc-

tion of armature rotation, as shown in Fig. 3.25b, we find that: a) the direction and magnitude of the magnetizing-force vector for the generator armature remains unchanged; b) the direction of the exciter-armature magnetizing force  $f_{ya}$  changes, since the axis of the magnetizing force for the exciter armature, which is rigidly coupled to the brush axis, moves in the direction of armature rotation, also through the angle  $\beta$ ; c) the magnitude of the excitation current and, consequently, the magnetizing force  $f_{ya}$  will also vary owing to the fact that the voltage across the excitation-winding terminals can vary in the general case; d) a longitudinal excitation-armature magnetizing force appears and there is a decrease in the magnitude of the transverse component.

By projecting the magnetizing force  $f_{ya}$  due to the exciter armature on the fixed pole axes  $dd$  and  $qq$ , we obtain the longitudinal component  $f_{ya d}$  and the transverse component  $f_{ya q}$  of the magnetizing force due to the exciter armature. The first component (Fig. 3.25b) will weaken the main machine field; as we have already mentioned, however, the effect of the exciter-armature magnetizing force is slight.

The emf in the exciter armature winding, induced by the magnetizing force due to the pole windings,  $F_v$ , decreases owing to the fact that the magnitude of the emf in the exciter armature is determined by the longitudinal component of the pole-winding magnetizing force  $F_v d_1$ , and its magnitude drops as the brush-shift angle increases, and equals zero at  $\beta = 90^\circ$ .

At the same time, an additional emf is induced in the exciter armature winding by the magnetizing force  $F_{ya d_1}$  due to the generator armature; this quantity is proportional to the load, and to some degree cancels the decrease in pole-winding magnetizing force. To determine the magnitude of the magnetizing forces due to the pole and gen-

erator-armature windings, which induce the emf in the exciter armature, we project  $F_v$  and  $F_{ya}$  onto the brush axis  $q_1q_1$  and the axis  $d_1d_1$ .

It is clear that where there is a definite relationship between the armature magnetizing force and the excitation winding magnetizing force, it is possible to obtain a condition that must be satisfied for the generator voltage to remain nearly constant under load variations. When the load power factor varies, the angle of rotation of the brushes should also change. By moving the brushes, we reduce the flux linkage between the exciter-armature winding and the field due to the pole-excitation winding and increase the flux linkage with the generator-armature field. As a result, the excitation magnetizing force of the exciter increases when the angle  $\beta$  changes to some specific value.

A single-armature double-current synchronous generator with two field windings is set up and connected as shown in Fig. 3.26.

In contrast to a single-armature double-current generator with a single excitation winding, the machine under consideration uses a double set of brushes, one normal set on the transverse axis and a second additional set on the longitudinal axis of the pole; there are two field windings — one supplied by the transverse brushes and a second supplied by the longitudinal brushes; the main poles are split in order to reduce the field in the commutation zone of the longitudinal brushes.

Operating principle. As we know, when the armature of a direct-current machine is rotated under no-load conditions in a longitudinal field, an emf is induced in its winding; the maximum emf occurs on the transverse pole axis  $qq$  (here the brushes are located on the longitudinal pole axis; they may be arbitrarily located on the transverse pole axis, however).

If there is a load on the machine, the transverse armature current will appear, the armature winding will rotate in two fields, and two emf's will be induced in it; one of them will have a maximum on the transverse-brush axis, owing to the longitudinal field, and the second additional emf will have a maximum on the pole axis and owing to the transverse armature field. If the brushes are set on the longitudinal pole axis, an emf will appear across their terminals that is proportional to the flux at the transverse machine axis and, consequently, is proportional to the load current. In a single-armature

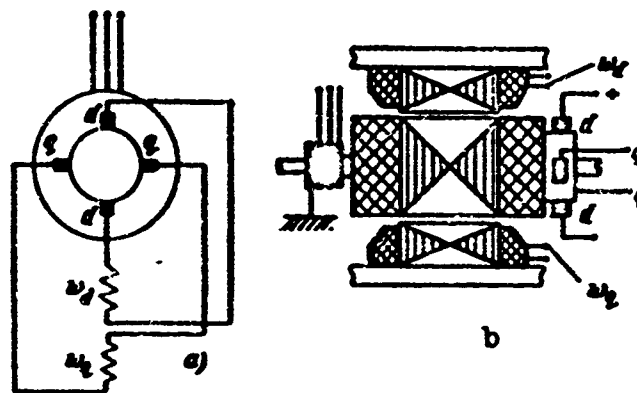


Fig. 3.26. Single-armature double-current generator with two field windings. a) Field-winding connections; b) structural diagram.

double-current generator, the transverse armature field is formed by two components: the transverse field due to the alternating-current generator and the exciter transverse field. Thus, the magnetizing force due to the excitation windings fed by the transverse brushes is supplemented by the magnetizing force of the excitation windings fed by the longitudinal brushes; this quantity is proportional to the load and, consequently, maintains the generator voltage at roughly the same value.

In order to clarify the physical basis for this phenomenon, we have given in Fig. 3.27 a diagram showing the machine magnetizing forces in the presence of an inductive load.

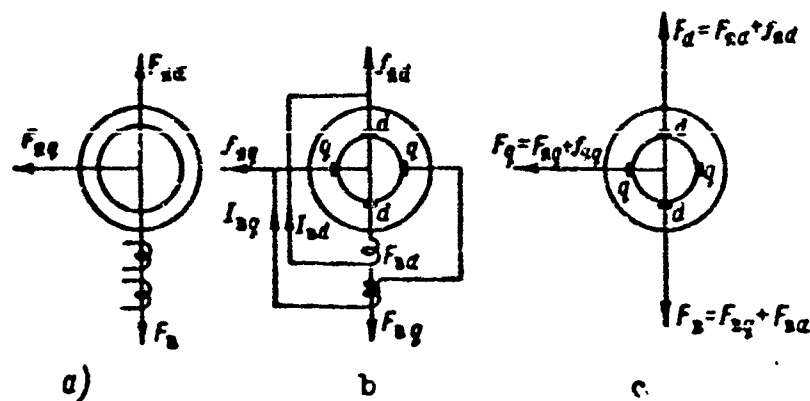


Fig. 3.27. Magnetizing-force diagram for single-armature double-current generator with two field windings. a) Generator-armature magnetizing force; b) exciter-armature magnetizing force; c) magnetizing forces due to generator and exciter armatures.

Here diagram a shows the magnetizing forces due to the alternating-current generator, i.e., the excitation magnetizing force  $F_v$  directed along the longitudinal pole axis; the transverse magnetizing-force component  $F_{ya\ q}$  due to the generator armature and the longitudinal magnetizing-force component  $F_{ya\ d}$  due to the generator armature are opposite in direction to the magnetizing force due to the excitation winding.

Diagram b shows the magnetizing forces due to the direct-current exciter with the double set of brushes; here  $f_{ya\ q}$  is the transverse magnetizing-force component of the exciter armature due to the current  $I_{ya\ q} = I_v\ q$ ; this is the current that flows in the transverse armature circuit. Where the armature is drum-wound, the brushes  $qq$  are located structurally on the longitudinal pole axis;  $f_{ya\ d}$  is the longitudinal magnetizing-force component of the exciter armature due to the current  $I_{ya\ d} = I_v\ d$  flowing in the longitudinal armature circuit.

The complete magnetizing-force picture shown in diagram c is obtained by combining diagrams a and b.

The magnitudes of the exciter transverse current  $I_v\ q$  and trans-

verse magnetizing force  $f_{ya\ q}$  are determined by the resultant longitudinal field of the machine when the brushes are at the geometric neutral plane. The exciter longitudinal current  $I_{ya\ d}$  and longitudinal magnetizing force  $f_{ya\ d}$  are determined by the resultant machine transverse field; the excitation current from the longitudinal brushes  $I_{v\ d}$  increases as the load increases (the transverse armature reaction increases), while the excitation current from the transverse brushes  $I_{v\ q}$  drops under the influence of the load, since the longitudinal field decreases.

When the alternating-current generator is running without load, the transverse armature field is nearly zero, since the transverse exciter-armature magnetizing-force component is small and may be neglected. Consequently, the main excitation field is determined by the magnetizing force due to one excitation winding connected to the transverse brushes of the exciter.

When the generator winding is connected to a composite load an armature reaction appears that weakens the main field but simultaneously induces an emf and a current in the longitudinal armature circuit, which supplies the additional excitation winding. Thus, where the armature magnetizing force and the excitation-winding magnetizing force bear a specific relationship to each other, it is possible for the reinforcing and bucking fields to cancel, and the voltage across the generator terminals will remain nearly constant under load variations.

The drawbacks to this system involve design and production difficulties in making the second set of brushes, especially where more than four poles are used; increased losses at the collector and deterioration of collector cooling; lack of access to the collector; and the fact that the generator voltage depends on the power factor.

Excitation systems not making use of sliding contacts make it possible to eliminate one major drawback to all of the systems enumerated for the excitation or selfexcitation of classical synchronous machines, i.e., the presence of a sliding brush contact.

New systems have recently been proposed for exciting classical machines without sliding contacts, both in the USSR and abroad. In 1955, a French patent was published describing a selfexcitation system for a synchronous machine that did not make use of brushes. This system differs from the selfexcitation systems discussed in that the "slip rings-brushes" unit on the generator shaft is replaced by a rotating transformer excited from the alternating-current line. The secondary voltage, doubled in frequency, is rectified by a dry rectifier located on the shaft of the generator and applied to the generator field winding (Fig. 3.28).

The absence of a sliding contact improves servicing, increases the high-altitude performance characteristic, service life, and operating reliability, eliminates radio interference, and reduces the weight and cost of the machine. At the same time, the system possesses all of the defects of selfexcitation systems (high regulation power, difficulty of selfexcitation) and, in addition, results in increased axial dimensions and structural complications for the machine. By combining the regulation system and the rotating transformer, it is possible to reduce the weight and size of the system (for example, the control winding can be placed in the stator slots).

In 1955, the author suggested two new systems, shown in Figs. 3.29 and 3.30a.

The selfexcitation circuit shown in Fig. 3.29, in contrast to that of Fig. 3.28, uses a synchronous exciter in place of the rotating transformer, i.e., it employs a synchronous three-phase machine whose



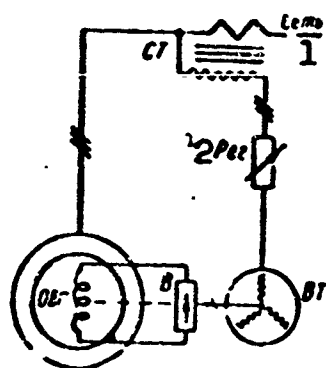


Fig. 3.28. Selfexcitation system without sliding contact using rotating transformer VT and rotating rectifier V. OVG) Generator field winding; Reg) voltage regulator; ST) double-winding stabilizing transformer. 1) Line; 2) Reg.

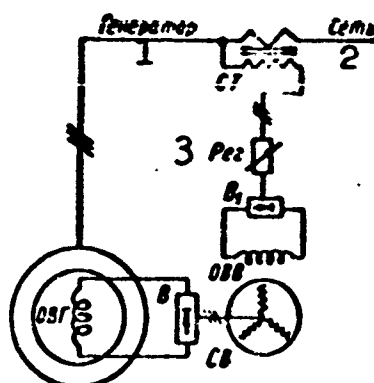


Fig. 3.29. Selfexcitation system without sliding contact using synchronous exciter SV and rotating rectifier V. OVG) Synchronous-exciter excitation winding;  $V_1$ ) rectifier. 1) Generator; 2) line; 3) Reg.

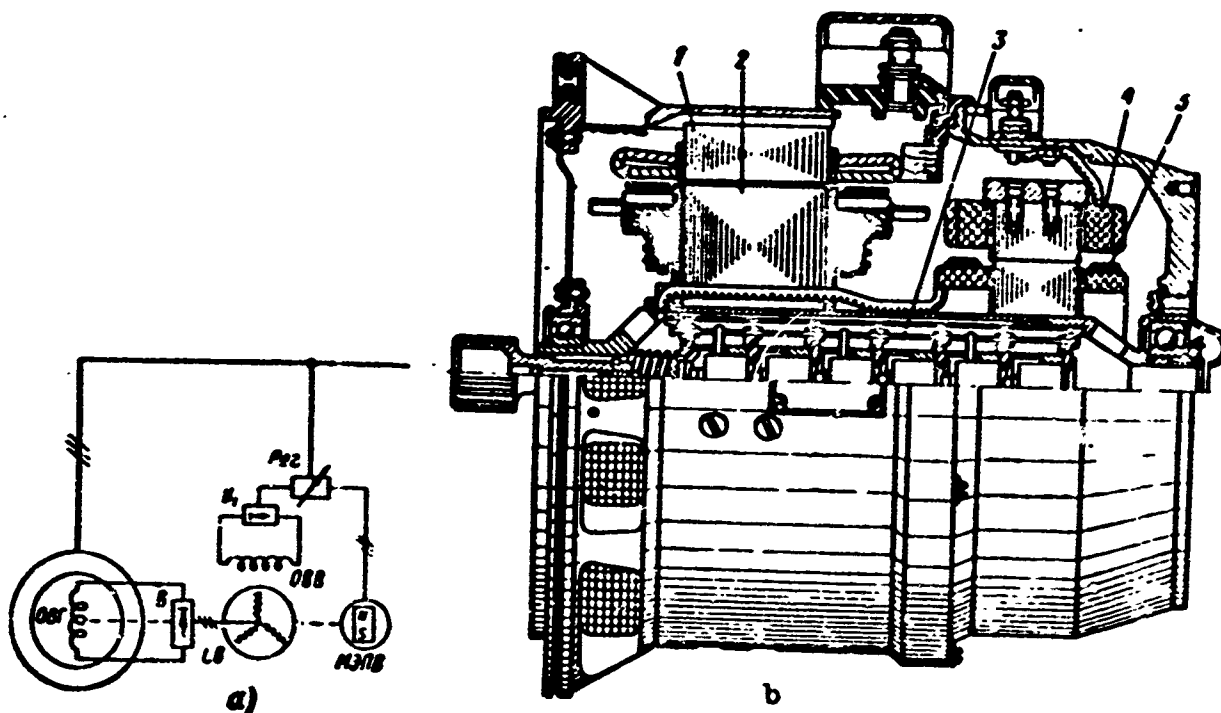


Fig. 3.30. Generator without sliding contact. a) Independent excitation system using synchronous exciter,  $\overline{\text{MEPV}}$  magnetoelectric pilot exciter, and rotating rectifier V; b) construction of generator. 1 and 2) Generator stator and rotor; 3) rotating rectifier; 4 and 5) stator and armature of three-phase exciter.

excitation circuit is supplied from the alternating-current line through a rectifier V. The advantages of this circuit in comparison

with the French system include a voltage-regulation power requirement roughly one-tenth that of the French circuit, since with our circuit the excitation power of the synchronous exciter is regulated rather than the excitation power of the synchronous generator; a considerable decrease in the dimensions of the regulator and stabilization transformer (TS); an improvement in generator operating conditions and a decrease in its power, since the selfexcitation circuit draws considerably less total power (and especially reactive power) from the generator circuit; and the possibility of providing more reliable selfexcitation by increasing the residual voltage in the synchronous exciter.

An autonomous independent excitation system is shown in Fig. 3.30; it differs from the circuit of Fig. 3.29 in that the synchronous-exciter field winding is supplied from a three-phase magnetoelectric generator located on the shaft of the machine. With respect to inde-

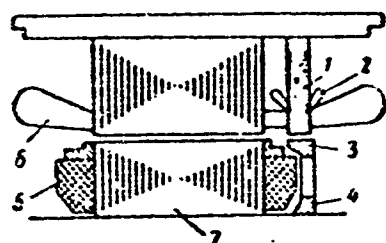


Fig. 3.31. Structural diagram of compensated synchronous generator. 1 and 2) Core (stator) and armature winding of alternating-current exciter; 3) steel exciter ring (rotor); 4) aluminum exciter spider; 5 and 6) excitation winding and armature winding of generator; 7) generator poles.

pendence, power regulation, and reliability of selfexcitation this system is similar to a system with a direct-current exciter, but offers several advantages over the latter system, since there is no sliding commutator contact.

The presence of a magnetoelectric synchronous pilot exciter complicates the design of the entire installation to some degree. It is necessary to remember, however, that the power and dimensions involved are slight and, in addition, the pilot exciter can work at a higher frequency (1000-1600 cps), thus de-

creasing not only the pilot-exciter dimensions but also the dimensions of the magnetic regulator, where used.

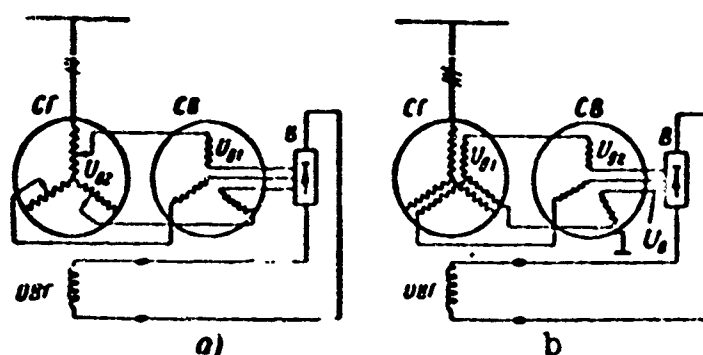


Fig. 3.32. Compensated-generator connections. SG) Generator; SV) synchronous exciter; V) rectifier; OVG) generator field winding. 1)  $U_v$ .

This system can be recommended for high-power aircraft generators and for high speeds where a sliding contact is especially undesirable.

Further modifications of the systems of Figs. 3.29 and 3.30 are possible in accordance with the systems discussed previously.

The general drawback to all excitation and selfexcitation systems not using sliding contacts is the presence of a dry rectifier carrying the full generator excitation power on the shaft (or within a hollow shaft) of the machine. This drawback can be minimized, however, if silicon rectifiers are used; modern silicon rectifiers can deliver about 200 watts from each cubic centimeter, and they operate reliably at a temperature of  $200^{\circ}\text{C}$ . Thus, a silicon rectifier with a volume of up to  $10\text{ cm}^3$  must be placed within the hollow shaft of a 50-100 kva aircraft generator, which is perfectly possible from the structural viewpoint.

Compensated synchronous generator. Voltage transformer-compounded systems react to a change in load current, but are not affected by the phase.

Figure 3.31 shows a system produced in 1948 at the suggestion of the author; it reacts to a change in the magnitude and phase of the load current. The distinguishing characteristic of this compensated synchronous machine is the presence of an integral alternating-current

exciter consisting of an exciter stator built up of laminations and thus resembling a generator stator core; an exciter rotor; and an exciter winding resembling a generator armature winding and located in the exciter-armature slots.

As Fig. 3.31 shows, the generator armature winding is also laid in the exciter-armature slots. The exciter-armature winding may be connected to taps on the generator-armature winding (Fig. 3.32a) or to a special excitation winding laid in the generator-armature slots (Fig. 3.32b).

Operating principle. When the generator is running without load, the voltage across the excitation-winding terminals will correspond to the voltage across the generator armature-winding taps, to which the terminals are connected, or to the voltage across the special armature winding. It is clear that the magnitude of this voltage should be so selected that the generator will develop the rated voltage. In this case, the exciter will not operate and the generator will draw self-excitation from its own circuit. In this mode of operation, the exciter-armature winding will represent an inductive reactance connected in series with the excitation circuit.

If there is a load on the generator, a current will flow through the armature winding that will form a rotating armature-reaction field in the magnetic systems of the generator and exciter. The armature-reaction field induces an emf in the exciter winding that is proportional to the armature current (provided the magnetic circuit is weakly saturated); the phase corresponds strictly to that of the armature magnetizing force. Thus, the magnitude of the excitation-winding voltage equals the geometric sum of the vector corresponding to the portion of the generator armature voltage  $U_{v1}$  that is nearly independent of the load, and the vector corresponding to the exciter armature voltage  $U_{v2}$ ,

which is proportional to the load current (Fig. 3.33a).

The direction of the vector for the voltage  $U_v$  in the excitation winding will be determined by the nature of the load.

With a purely resistive load ( $\cos \psi = 1$ ) the magnetizing-force axis for the armature will be shifted by 90 electrical degrees with respect to the axis. The exciter voltage vector will be shifted by about the same angle with respect to the generator voltage vector.

With a purely reactive load (inductive or capacitive), with the axes of the armature and pole magnetizing forces coinciding, the excitation-voltage vector will add algebraically with the armature-voltage vector with an inductive load and will subtract with a capacitive load (Fig. 3.33b).

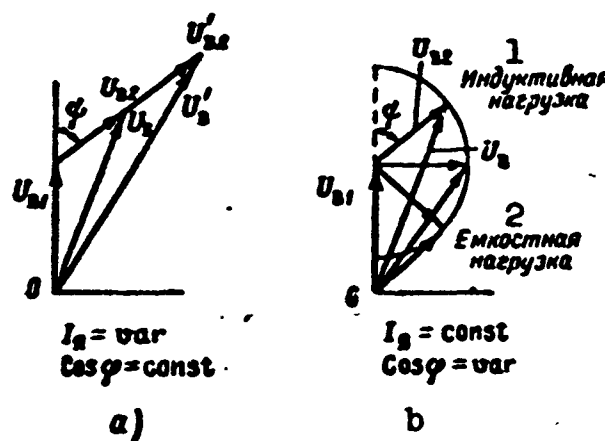


Fig. 3.33. Voltage diagrams for compensated generator. 1) Inductive load; 2) capacitive load.

Thus, the exciter voltage proves to be a function of the magnitude and phase of the load, and the machine is capable of voltage self-regulation.

Tests of a 15-kva aircraft generator made in accordance with the circuit shown have indicated that the generator reacts to changes in the magnitude and nature of the load, and at constant rotational speed holds the voltage constant to within  $\pm 3\%$ . At the same time, it does not react to variations in speed or winding temperature, which have a

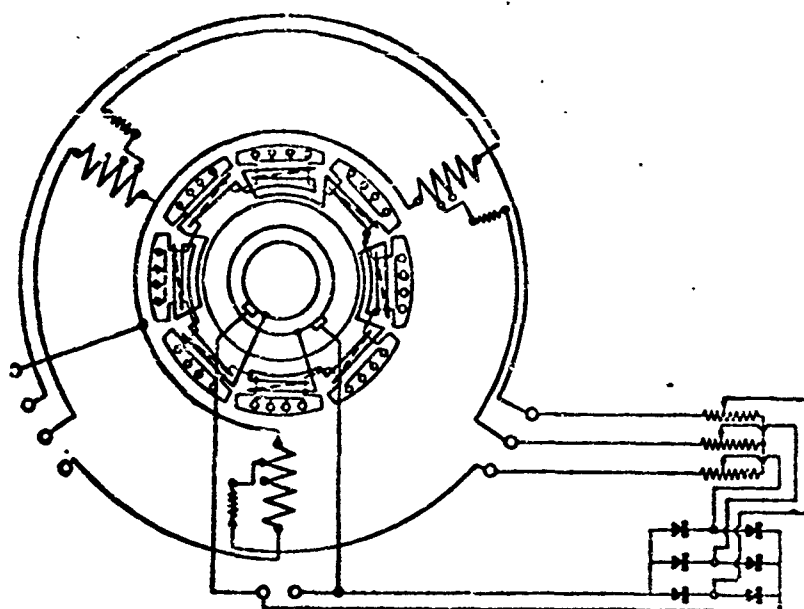


Fig. 3.34. Working connection diagram for compensated aircraft generator, 15 kva, 6000 rpm, 400 cps, 208/120 v.

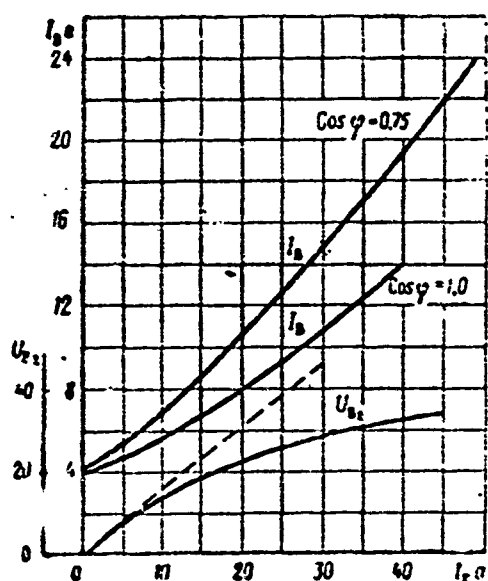


Fig. 3.35. Regulation curves and alternating-current exciter voltage  $U_{v2}$  as a function of load current (experimental data; magnetic circuit of exciter oversaturated).

substantial influence on the generator voltage.

Compensated synchronous generators have an advantage over selfexcitation systems using three-winding compounding transformers in that they do not lose excitation when the generator terminals are short-circuited.

The built-in alternating-current exciter is small in size; the dimensions are determined by the difference in the loaded and no-load generator excitation powers. Combination voltage-stabilization

systems are possible using exciters built into the stator and installed on the generator shaft.

Compensated synchronous generators may find application when high voltage-stabilization accuracy is not required.

Figures 3.34 and 3.35 show connection diagrams for a compensated aircraft synchronous generator of 15 kva power, and its regulation curves  $I_V = f(I_g)$ .

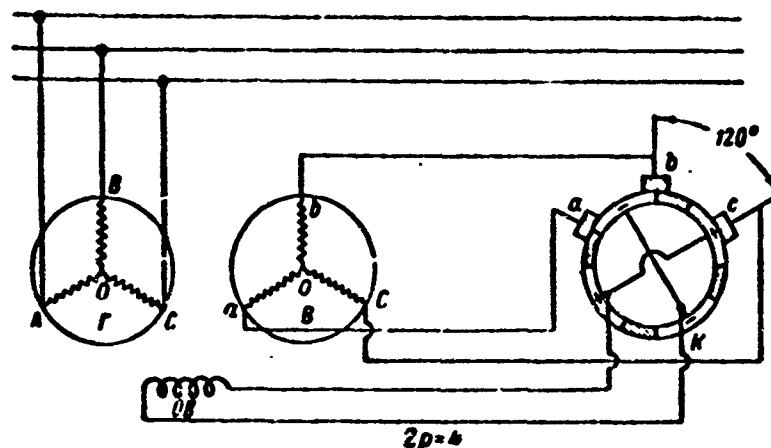


Fig. 3.36. Basic circuit of synchronous generator with mechanical rectifier..

A synchronous generator with mechanical rectifier is made with internal rotating salient poles and a stationary armature. Two three-phase windings are laid through the same armature slots: the generator winding G and the winding V used to supply the excitation circuit.

The mechanical rectifier converts the alternating current of winding V into direct current, which is applied to the excitation winding located on the generator poles. It consists of the stationary brushes a, b, and c spaced 120 electrical degrees apart and fastened to the frame, and the rotating commutator K located on the generator shaft. The commutator consists of  $2p$  active (current-carrying) sectors and  $2p$  insulating (non-current-carrying) sectors, as shown in Fig. 3.36.

Current from the three-phase winding V reaches the rotating commutator of rectifier K through the fixed brushes a, b, and c. Rectified current from the commutator is applied to the rotating excitation winding, which is rigidly connected to the commutator.

A three-phase three-winding stabilization transformer is used for automatic voltage regulation.

The synchronous generator with the mechanical rectifier (which is really an inverted commutator) is lighter in weight and shorter along the axis. This machine is essentially a single-armature double-current generator with two alternating-current windings and the collector replaced by an inverted commutator.

Synchronous machines with mechanical rectifiers are employed for generators of up to 100 kva power at 50 cps, and may be used for aviation purposes.

### 3.4. ANALYTICAL INVESTIGATION OF SYNCHRONOUS GENERATORS ALLOWING FOR ARMATURE RESISTANCE

Modified voltage diagram. In studying synchronous machines, it is customary to neglect the armature-winding resistance. As we shall show below, this cannot be done in studying miniature and low-power synchronous machines. In considering the armature resistance, it is con-

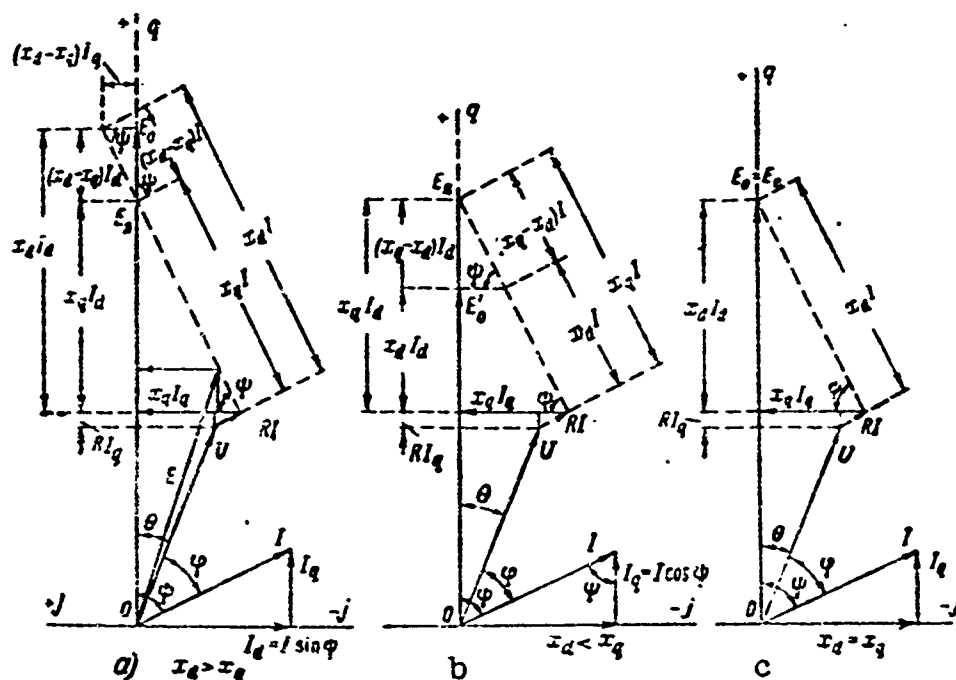


Fig. 3.37. Vector diagrams for synchronous-machine voltage.

venient to use the relative parameters for synchronous machines and modified voltage diagrams constructed with the new parameters taken into account. In order to make the essential nature of the problem



clear, we have given voltage diagrams in absolute and relative units.

Figure 3.37 shows vector voltage diagrams for a synchronous generator with a composite load and lagging current.

Figures 3.37a and 3.37b apply to salient-pole generators with  $x_d > x_q$  and  $x_d < x_q$ , while Fig. 3.37c applies to a nonsalient-pole synchronous generator.

Figure 3.38 gives analogous vector voltage diagrams in relative units. Going from the vector diagrams of Fig. 3.37 to the vector diagrams of Fig. 3.38, expressed in relative units, the angles  $\varphi$ ,  $\theta$ , and  $\psi$ , as well as the armature current remain unchanged. In this case, the parameters will equal, in relative units,

$$\left. \begin{aligned} \dot{x}_d &= \frac{x_d}{x_{nom}} = x_d \frac{I_{nom}}{U_{nom}} \\ \dot{x}_q &= \frac{x_q}{x_{nom}} = x_q \frac{I_{nom}}{U_{nom}} \\ \dot{R} &= \frac{R}{x_{nom}} = R \frac{I_{nom}}{U_{nom}} \end{aligned} \right\} \quad (3.21)$$

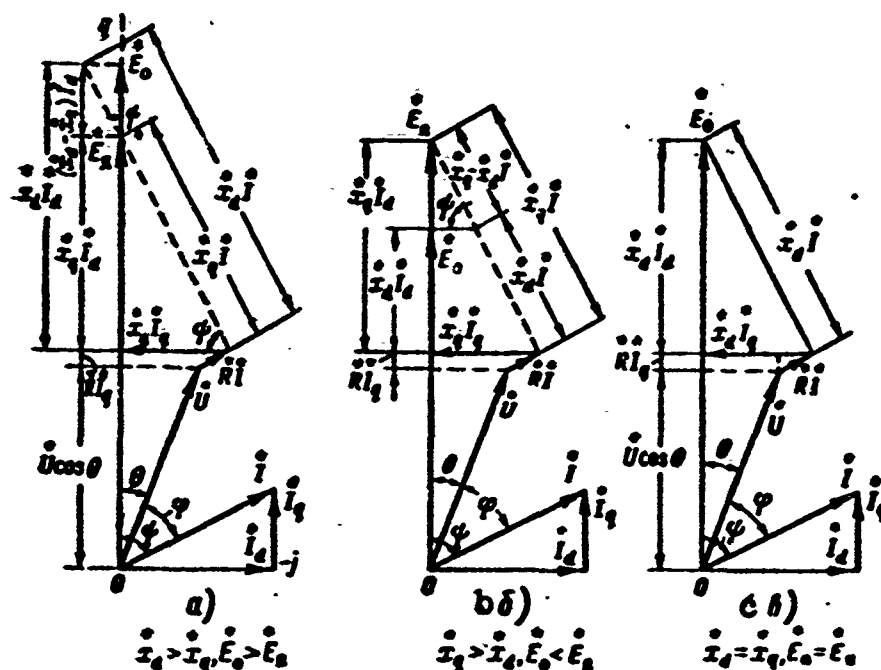


Fig. 3.38. Vector diagrams for synchronous-machine voltage in relative units.

In addition, we introduce the notation

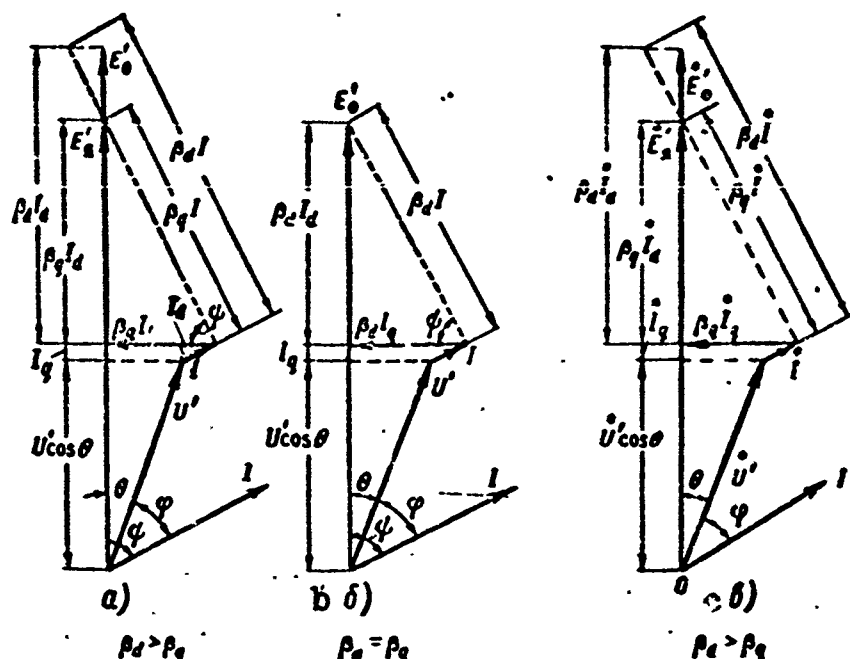


Fig. 3.39. Modified vector voltage diagrams for synchronous machine in absolute and relative units.

$$\dot{U} = \frac{U}{U_{\text{nom}}}, \quad \dot{E}_{01} = \frac{E_0}{U_{\text{nom}}}, \quad \dot{E}_0 = \frac{E_0}{U}, \quad \dot{E}_{a1} = \frac{E_a}{U_{\text{nom}}}, \quad \dot{I} = \frac{I}{I_{\text{nom}}}. \quad (3.22)$$

In studying synchronous machines, taking into account the armature resistance, we use the modified voltage diagrams shown in Fig. 3.39 corresponding to Figs. 3.37 and 3.38.

The following notation is used in the vector diagrams of Fig.

3.39:

the relative synchronous inductance along the longitudinal and transverse axes of the machine is

$$\beta_d = \frac{x_d}{R} = \frac{\dot{x}_d}{\dot{R}}, \quad \beta_q = \frac{x_q}{R} = \frac{\dot{x}_q}{\dot{R}}, \quad (3.23)$$

the magnetic-system unbalance is

$$k = \frac{\beta_d}{\beta_q} = \frac{x_d}{x_q} = \frac{\dot{x}_d}{\dot{x}_q} \quad (3.23a)$$

and

$$\dot{E}_0 = \frac{E_0}{R}, \quad \dot{E}_a = \frac{E_a}{R}, \quad \dot{E}_0 = \frac{\dot{E}_0}{\dot{R}}, \quad \dot{E}_a = \frac{\dot{E}_a}{\dot{R}}; \quad U' = \frac{U}{R}. \quad (3.23b)$$

Taking the modified substitution diagrams into account, it is pos-

sible to write the basic equations for a synchronous generator, allowing for the armature resistance.

### Armature current

The complex armature current and the absolute value of the armature current for a synchronous machine equal

$$I = I_q - jI_d \text{ and } I = \sqrt{I_q^2 + I_d^2}. \quad (3.24)$$

On the basis of the diagram of Fig. 3.39a, the equilibrium equations will be

$$\left. \begin{aligned} I_d \beta_d + I_q + U' \cos \theta &= E'_q \\ -I_q \beta_d + I_d + U' \sin \theta &= 0. \end{aligned} \right\} \quad (3.25)$$

Solving the two last equations simultaneously and taking (3.23b) into account, we are able to obtain a general expression for the longitudinal and transverse armature currents of a synchronous machine

$$\begin{aligned} \pm I_d &= \frac{U' (E'_q \beta_d - I_q \cos \theta - k \sin \theta)}{k + \beta_d^2} = \\ &= \frac{U' E'_q - \cos \theta - k \beta_d^{-1} \sin \theta}{\beta_d} \quad (3.26) \end{aligned}$$

and

$$I_q = k \frac{U' (E'_q - \cos \theta) \beta_d^{-1} + \sin \theta}{1 + k \beta_d^{-2}}, \quad (3.27)$$

where

$$E'_q = \frac{E_q}{U'} = \frac{E_q}{U}.$$

The "plus" sign on  $I_d$  corresponds to a lagging current (inductive load), while the "minus" sign indicates a leading current (capacitive load).

If we neglect the armature resistance ( $R = 0$ ), then

$$\beta_d = \infty \text{ and } U' / \beta_d = U / x_d.$$

In this case, Eqs. (3.26) and (3.27) will be

$$\pm I_d = U' \beta_d^{-1} (E'_q - \cos \theta) = \frac{U}{x_d} (E'_q - \cos \theta) \quad (3.28)$$

and

$$I_q = k U' \beta_d^{-1} \sin \theta = k \frac{U}{x_d} \sin \theta. \quad (3.29)$$

For synchronous machines with nonsalient poles,  $\beta_d = \beta_q$  and  $k = 1$ , i.e.,

$$\pm I_d = U' \beta_d^{-1} \frac{\dot{E}_0 - \cos \theta - \beta_d^{-1} \sin \theta}{1 + \beta_d^{-2}} \quad (3.30)$$

and

$$I_q = U' \beta_d^{-1} \frac{(\dot{E}_0 - \cos \theta) \beta_d^{-1} + \sin \theta}{1 + \beta_d^{-2}}. \quad (3.31)$$

Substituting into (3.24) the currents  $I_d$  and  $I_q$  from (3.26) and (3.27), and also allowing for the fact that

$$\cos^2 \theta = 0.5(1 + \cos 2\theta) \text{ and } \sin^2 \theta = 0.5(1 - \cos 2\theta),$$

following simple manipulations, we obtain a general expression for the absolute value of the armature current:

$$I = \frac{U' \beta_d^{-1}}{1 + k \beta_d^{-2}} \sqrt{\dot{E}_0^2 (1 + k^2 \beta_d^{-2}) - 2 \dot{E}_0 [(1 + k^2 \beta_d^{-2}) \cos \theta - k \beta_d^{-1} \times \\ \times (k-1) \sin \theta] - (k-1) [0.5(k+1) \cos 2\theta + k \beta_d^{-1} \sin 2\theta] + \\ + 0.5(k^2 + 1) + k^2 \beta_d^{-2}}. \quad (3.32)$$

For nonsalient-pole machines,  $k = 1$ , and Eq. (3.32) for the armature current will be considerably simplified:

$$I = \frac{U' \beta_d^{-1}}{\sqrt{1 + \beta_d^{-2}}} \sqrt{1 + \dot{E}_0^2 - 2 \dot{E}_0 \cos \theta}. \quad (3.33)$$

If we neglect the armature resistance ( $R = 0$ ), then the armature current with  $k \neq 1$  and  $k = 1$  will be, respectively,

$$I' = U' \beta_d^{-1} \sqrt{\dot{E}_0^2 - 2 \dot{E}_0 \cos \theta - 0.5(k^2 - 1) \cos 2\theta + 0.5(1 + k^2)} \quad (3.34)$$

and

$$I' = U' \beta_d^{-1} \sqrt{1 + \dot{E}_0^2 - 2 \dot{E}_0 \cos \theta}. \quad (3.34a)$$

Let us consider the ultimate operating mode for a synchronous ma-

chine — a steady-state symmetric short circuit across the generator terminals, with  $U = 0$  and  $\dot{E}_0 = E_0/U = \infty$ .

In this case, the longitudinal and transverse short-circuit current components, as well as their ratio will equal, respectively, from (3.26) and (3.27)

$$I_{dx} = \frac{E_0 \beta_d^{-1}}{1 + k \beta_d^{-2}}, \quad (3.35)$$

$$I_{qx} = \frac{k E_0 \beta_d^{-1}}{1 + k \beta_d^{-2}}, \quad (3.36)$$

$$\frac{I_{dx}}{I_{qx}} = \frac{1}{k} = \frac{\beta_q}{\beta_d} = \frac{x_q}{x_d} = \frac{x_q}{x_d}. \quad (3.37)$$

After  $U'$  has been introduced under the radical in Expression (3.32) the expressions for the steady-state symmetric short-circuit current will take the following form:

in the general case, where  $k \neq 1$  and  $R \neq 0$

$$I_x = E_0 \beta_d^{-1} \frac{\sqrt{1 + k^2 \beta_d^{-2}}}{1 + k \beta_d^{-2}} = E_0 \frac{\sqrt{k^2 + \beta_d^2}}{k + \beta_d^2}; \quad (3.38)$$

when  $k = 1$  and  $R \neq 0$ , we find from (3.38) that

$$I_x = \frac{E_0}{k} \frac{1}{\sqrt{1 + \beta_d^2}} = \frac{E_0}{\sqrt{1 + \beta_d^2}}. \quad (3.39)$$

If we neglect the armature resistance, then regardless of the type of synchronous machine ( $k \neq 1$  or  $k = 1$ ) the short-circuit current will be

$$I_x = \frac{E_0}{k} = \frac{E_0}{x_d}. \quad (3.40)$$

Equation (3.38) which represents the short-circuit characteristic for a salient-pole synchronous machine allowing for the armature resistance, may be changed as follows:

$$\begin{aligned} I_x &= \frac{E_0}{x_d} \frac{\sqrt{1 + k^2 \beta_d^{-2}}}{1 + k \beta_d^{-2}} \frac{I_{nom}}{U_{nom}} \frac{U_{nom}}{I_{nom}} = \frac{E_0}{x_d} I_{nom} \frac{\sqrt{1 + k^2 \beta_d^{-2}}}{1 + k \beta_d^{-2}} = \\ &= E_0 I_{nom} k_x \end{aligned} \quad (3.41)$$

and

$$\dot{I}_x = \frac{I_x}{I_{\text{NOM}}} = \frac{\dot{E}_{01}}{x_d} \frac{\sqrt{1+k^2\beta_d^2}}{1+k\beta_d^2} = \frac{\dot{E}_{01}}{\dot{R}} \frac{\sqrt{k^2+\beta_d^2}}{k+\beta_d^2} = \dot{E}_{01} k_x, \quad (3.42)$$

where

$$x_d = x_d' \frac{U_{\text{NOM}}}{I_{\text{NOM}}}, \quad \dot{E}_{01} = \frac{E_0}{U_{\text{NOM}}}$$

and

$$k_x = \frac{\dot{I}_x}{\dot{E}_{01}} = \frac{1}{x_d} \frac{\sqrt{1+k^2\beta_d^2}}{1+k\beta_d^2} = \frac{1}{\dot{R}} \frac{\sqrt{k^2+\beta_d^2}}{k+\beta_d^2} = \text{tg } \alpha_x \quad (3.43)$$

is the slope tangent for the reduced relative short-circuit characteristic.

In the linear section of the no-load characteristic

$$E_0 = k_0 I_s = I_s \text{ or } \dot{E}_{01} = k_0 \dot{I}_s \frac{I_{s,\text{NOM}}}{U_{\text{NOM}}} = \dot{I}_s,$$

and

$$k_0 = \frac{5k_\phi w_p}{k_s 10^8} \frac{\text{at}}{\delta'} f w_p = \text{tg } \alpha_0 \quad (3.44)$$

is the slope tangent for the no-load characteristic curve;  $w_v$  is the number of field-winding turns per pole;  $k_s$  is a coefficient that allows for the magnetic reluctance of the iron in the magnetic circuit;  $I_v^* = I_v / I_{v,\text{nom}}$  and  $I_{v,\text{nom}}$  are the relative and nominal excitation currents;  $k_f$  is a form factor.

The effect of the armature resistance on the short-circuit current (see Fig. 3.40) may be found by taking the ratio of the current  $I_k$  obtained from (3.38) allowing for the resistance to the current  $I'_k$  obtained by using (3.40) and neglecting the resistance, i.e.,

$$\frac{I_k}{I'_k} = \frac{\sqrt{1+k^2\beta_d^2}}{1+k\beta_d^2} = \beta_d \frac{\sqrt{k^2+\beta_d^2}}{k+\beta_d^2} \quad (3.45)$$

for salient poles;

$$\frac{I_k}{I'_k} = \frac{1}{\sqrt{1+\beta_d^2}} = \frac{\beta_k}{\sqrt{1+\beta_d^2}} = \frac{1}{\beta'} \quad (3.46)$$

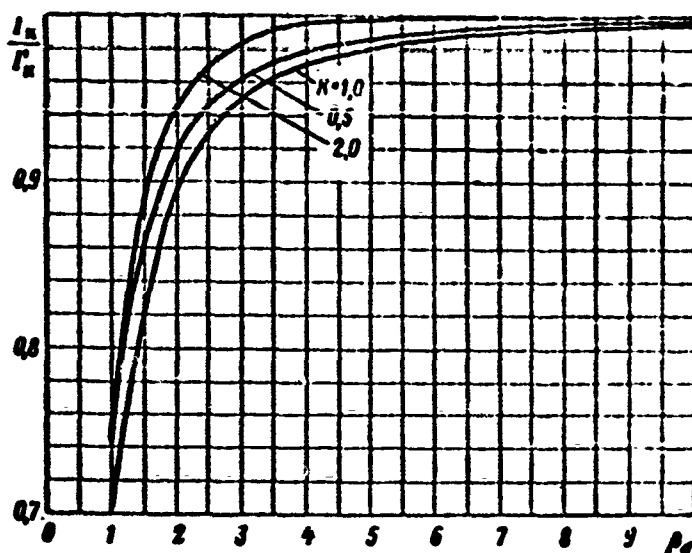


Fig. 3.40. Effect of armature resistance on the steady-state short-circuit current as a function of  $\beta_d$ .

for nonsalient poles.

The effect of magnetic-system unbalance on the magnitude of the steady-state symmetric short-circuit current is found from the derivative of Eq. (3.38) with respect to  $k$  with

$$E'_0 = \text{const and } \beta_d = \text{const},$$

i.e.,

$$\frac{dI_k}{dk} = \frac{d}{dk} \left| \frac{E'_0 \sqrt{1+k^2\beta_d^2}}{\beta_d \sqrt{1+\beta_d^2}} \right| = 0.$$

The solution to the last equation leads to the equation  $k = 1$ . Consequently, the short-circuit current is at a minimum for given values of  $E'_0$  and  $\beta_d$  for nonsalient-pole synchronous machines. Equation (3.39) corresponding to  $I_k$  at  $k = 1$ , gives the minimum short-circuit current.

Taking the ratio of the current  $I_k$  from (3.38) to the current  $I_{k \min}$  from (3.39) we obtain an equation that shows the way in which  $I_k / I_{k \min} = f(k)$  depends on  $\beta_d$ , i.e., allows for the effect of magnetic-system unbalance (type of salient pole) on the short-circuit current:

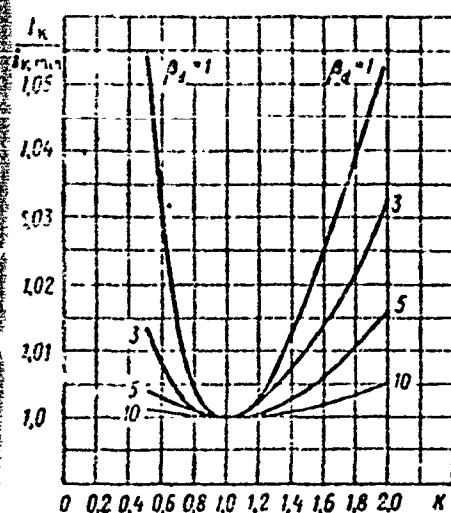


Fig. 3.41. Effect of magnetic unbalance on steady-state short-circuit current.

$$\frac{I_k}{I_{k \min}} = \frac{V(k^2 + \beta_d^2)(1 + \beta_d^2)}{k + \beta_d^2} > 1. \quad (3.47)$$

When  $\beta_d \rightarrow \infty$ , the ratio  $I_k/I_{k \min} \rightarrow 1$  for any real value of  $k$  (Fig. 3.41).

An analysis of the functions shown in Figs. 3.40 and 3.41 shows that:

a) the short-circuit current depends on the armature resistance  $R$  when  $\beta_d < 5$  and is nearly independent of it when  $\beta_d > 10$ ;

b) the magnetic unbalance has a noticeable effect on the short-circuit current where  $\beta_d < 5$  and has practically no effect when  $\beta_d > 5$ ;

c) the value obtained for the current  $I_k$  when the magnetic unbalance is neglected turns out to be too low.

We use (3.38) to find the magnitude of the armature resistance

$$R = \frac{E_0}{I_{k \beta_d}} \frac{V \sqrt{1 + k^2 \beta_d^{-2}}}{1 + k \beta_d^{-2}} = \frac{E_0}{I_k} \frac{V \sqrt{k^2 + \beta_d^2}}{k + \beta_d^2} \quad (3.48)$$

and in relative units

$$\dot{R} = R \frac{I_{\text{nom}}}{U_{\text{nom}}} = \frac{\dot{E}_{01}}{\dot{I}_k} \frac{V \sqrt{k^2 + \beta_d^2}}{k + \beta_d^2}, \quad (3.49)$$

where  $\dot{I}_k = I_k/I_{\text{nom}}$  represents the number of times the steady-state symmetric short-circuit current exceeds the rated current;  $\dot{E}_{01} = E_0/U_{\text{nom}}$  represents the number of times the no-load emf exceeds the rated voltage.

#### No-Load Electromotive Force

The expression for the no-load emf  $E_0$ , corresponding to excitation with a load  $I_{V, \Omega}$ , is found by using the relative parameters ( $\beta_d$  and  $k$ ). To do this, we change the first equation of (3.25), allowing



for the fact that

$$I_d = I \sin \psi = I \sin (\varphi \pm \theta) \quad \text{and} \quad I_q = I \cos \psi = I \cos (\varphi \pm \theta)$$

(here the "plus" sign refers to the generator mode of operation for the synchronous machine, and the "minus" sign to motor operation), i.e.,

$$E_0 = U' \cos \theta \pm \beta_d I_d + I_q = U' \cos \theta + I [\beta_d \sin (\varphi \pm \theta) \pm \cos (\varphi \pm \theta)]. \quad (3.50)$$

Remembering that

$$\cos (\varphi \pm \theta) = \cos \varphi \cos \theta \mp \sin \varphi \sin \theta$$

and

$$\sin (\varphi \pm \theta) = \sin \varphi \cos \theta \pm \cos \varphi \sin \theta,$$

we can represent the last expression in the following form:

$$E_0 = [U' \pm I (\beta_d \sin \varphi \pm \cos \varphi)] \cos \theta + I (\beta_d \cos \varphi \mp \sin \varphi) \sin \theta. \quad (3.51)$$

$$E_0 = I \left\{ \left[ \frac{U'}{I} \pm (\beta_d \sin \varphi \pm \cos \varphi) \right] \cos \theta + (\beta_d \cos \varphi \mp \sin \varphi) \sin \theta \right\}. \quad (3.51a)$$

Letting the relative load inductance be

$$\beta_d = \frac{x_n}{R_n} = \frac{\dot{x}_n}{\dot{R}_n}, \quad (3.52)$$

and the relative load resistance

$$\beta = \frac{R_n}{R} = \frac{\dot{R}_n}{\dot{R}}, \quad (3.53)$$

taking the armature-winding resistance as unity, we are able to obtain an expression for the absolute value of the load impedance and power factor

$$z_{\text{nom}} = \frac{U_{\text{nom}}}{I_{\text{nom}}} = R_n \sqrt{1 + \beta_n^2}, \quad (3.54)$$

$$\cos \varphi = \frac{R_n}{z_{\text{nom}}} = \dot{R}_n = \frac{1}{\sqrt{1 + \beta_n^2}}.$$

as well as for

$$\sin \varphi = \frac{x_n}{z_{nom}} = \frac{\dot{x}_n}{\dot{z}_{nom}} = \frac{\beta_n}{\sqrt{1 + \beta_n^2}} \quad (3.55)$$

and

$$\lg \varphi = \frac{x_n}{R_n} = \frac{\dot{x}_n}{\dot{R}_n} = \beta_n,$$

where  $R_n(\dot{R}_n)$  and  $x_n(\dot{x}_n)$  are the resistive and reactive components of the load impedance  $z_{nom}$ .

Taking these last expressions into account, we are able to obtain the ratio

$$\frac{U'}{I} = \frac{z}{R} = \frac{R_n}{R} \sqrt{1 + \beta_n^2} = \frac{\beta}{\cos \varphi}. \quad (3.56)$$

The load current will then equal

$$I = U' \frac{\cos \varphi}{\beta}. \quad (3.56a)$$

Representing (3.56) and (3.56a) in the form

$$\left. \begin{aligned} \frac{U'}{I} &= \frac{z}{R} = \frac{\beta_d}{\beta_n} \frac{1}{\cos \varphi} \\ I &= U' \frac{\beta_n}{\beta_d} \cos \varphi \end{aligned} \right\} \quad (3.57)$$

and

where

$$\beta_{dn} = \frac{x_d}{R_n} = \frac{\dot{x}_d}{\dot{R}_n} \text{ and } \frac{\beta_d}{\beta_n} = \frac{x_d R_n}{R x_d} = \delta,$$

we obtain a new expression for the emf from (3.51):

$$E_0 = U \delta \cos \varphi \left\{ \left[ \frac{\beta}{\cos \varphi} \pm (\beta_d \sin \varphi \pm \cos \varphi) \right] \cos \theta + \right. \\ \left. + (\beta_d \cos \varphi \mp \sin \varphi) \sin \theta \right\}. \quad (3.58)$$

In (3.58) the unknowns are  $\cos \theta$  and  $\sin \theta$ , which are found easily by using the diagram of Fig. 3.39 and the trigonometric relationships given earlier.

It follows from the diagrams that

$$U' \sin \theta = \beta_d I_d \mp I_d = I [\beta_d \cos (\varphi + \theta) \mp \sin (\varphi + \theta)] = \\ = I [(\beta_d \cos \varphi \mp \sin \varphi) \cos \theta - (\beta_d \sin \varphi \pm \cos \varphi) \sin \theta] \quad (3.59)$$

or, in the generator mode,

$$[U' + I(\beta_d \sin \varphi + \cos \varphi)] \sin \theta = I(\beta_d \cos \varphi - \sin \varphi) \cos \theta. \quad (3.60)$$

On the basis of (3.60) we are able to write the following very important expressions:

the tangent of the internal working phase-shift angle  $\theta$  is

$$\operatorname{tg} \theta = \frac{\beta_d \cos \varphi - \sin \varphi}{\frac{U'}{I} + \beta_d \sin \varphi + \cos \varphi}$$

or, allowing for (3.57) and substituting  $k$  and  $\beta_d$  for  $\beta_q$

$$\operatorname{tg} \theta = \frac{\cos \varphi (\beta_d - k \operatorname{tg} \varphi)}{\frac{k \beta_d}{\cos \varphi} + \cos \varphi (k + \beta_d \operatorname{tg} \varphi)}; \quad (3.61)$$

the cosine of the working phase-shift angle  $\theta$  is

$$\cos \theta = \frac{\frac{k}{\cos \varphi} + \frac{\cos \varphi}{\beta_d} (k + \beta_d \operatorname{tg} \varphi)}{\sqrt{\left(\frac{k}{\cos \varphi}\right)^2 + \frac{2k}{\beta_d} (k + \beta_d \operatorname{tg} \varphi) + \frac{k^2 + \beta_d^2}{\beta_d^2}}}; \quad (3.62)$$

the sine of the working phase-shift angle  $\theta$  is

$$\sin \theta = \frac{\frac{\cos \varphi}{\beta_d} (\beta_d - k \operatorname{tg} \varphi)}{\sqrt{\left(\frac{k}{\cos \varphi}\right)^2 + \frac{2k}{\beta_d} (k + \beta_d \operatorname{tg} \varphi) + \frac{k^2 + \beta_d^2}{\beta_d^2}}}. \quad (3.63)$$

Substituting the values of  $\cos \theta$  and  $\sin \theta$  from (3.62) and (3.63) into (3.58), we obtain an expression for the emf  $E_0$  expressed in terms of the new relative machine parameters, i.e.,

$$E_0 = U \frac{1 + 2 \frac{\beta_d}{\beta_d} \cos \varphi \left( \frac{1+k}{2k} \sin \varphi + \frac{\cos \varphi}{\beta_d} \right) + \left( \frac{\beta_d}{\beta_d} \cos \varphi \right)^2 \left( \frac{1}{\beta_d^2} + \frac{1}{k^2} \right)}{\sqrt{1 + 2 \frac{\beta_d}{\beta_d} \cos \varphi \left( \frac{\sin \varphi}{k} + \frac{\cos \varphi}{\beta_d} \right) + \left( \frac{\beta_d}{\beta_d} \cos \varphi \right)^2 \left( \frac{1}{\beta_d^2} + \frac{1}{k^2} \right)}}. \quad (3.64)$$

As a rule, we are interested in the variation in generator voltage as a function of the load, i.e., the external machine characteristic. It is clear that this magnitude is the reciprocal of  $E_0$ , and it takes the form of an expression for the family of external characteristics

$$\Delta U = \frac{U'}{E_0} = \frac{U}{E_0} = \frac{\sqrt{1 + \left(\frac{\cos \varphi}{\delta}\right)^2 \left(1 + 2k + \frac{\beta_d^2}{k^2}\right) + \frac{\beta_d}{\delta} \frac{\sin 2\varphi}{k}}}{1 + \left(\frac{\cos \varphi}{\delta}\right)^2 \left(1 + 2k + \frac{\beta_d^2}{k^2}\right) + \frac{\beta_d}{\delta} \frac{1+k}{2k} \sin 2\varphi} \quad (3.65)$$

We have thus obtained a general expression for the external characteristics of a salient-pole synchronous machine that allows for the resistance, i.e.,

$$\Delta U = U/E_0 = f(\delta \text{ and } \varphi),$$

where  $\delta = R_n/R = \frac{R_n^*}{R^*}$  characterizes the relative load magnitude.

For nonsalient-pole synchronous machines  $k = 1$  and Expression (3.65) will be

$$\Delta U = \frac{1}{\sqrt{1 + \left(\frac{\cos \varphi}{\delta}\right)^2 (1 + 2k + \frac{\beta_d^2}{k^2}) + \frac{\beta_d}{\delta} \sin 2\varphi}} \quad (3.66)$$

If we neglect the active armature resistance ( $R = 0$ ,  $\beta_d = \infty$ , and  $\beta_d/\delta = \beta_{dn}$ ), we obtain from (3.65)

$$\Delta U = \frac{\sqrt{1 + \beta_{dn} \frac{\sin 2\varphi}{k} + \left(\frac{\beta_{dn}}{k} \cos \varphi\right)^2}}{1 + \beta_{dn} \frac{1+k}{2k} \sin 2\varphi + \frac{\beta_{dn}^2}{k} \cos^2 \varphi} \quad (3.67)$$

where  $k \neq 1$ , and from (3.66)

$$\Delta U = \frac{1}{\sqrt{1 + \beta_{dn} \sin 2\varphi + (\beta_{dn} \cos \varphi)^2}} \quad (3.68)$$

where  $k = 1$ ; here

$$\beta_{dn} = \frac{x_d}{R_a} = \frac{x_d^*}{R_a^*}$$

Equations (3.65)-(3.68), expressed in the relative parameters  $\beta$ ,  $\delta$ , and  $k$ , may be represented in a different form:

instead of  $\Delta U$  according to (3.65):

$$\Delta U = \frac{\sqrt{1 + \dot{R}^2 + \dot{x}_q^2 + 2(\dot{R} \cos \varphi + \dot{x}_q \sin \varphi)}}{1 + \dot{R}^2 + \dot{x}_d \dot{x}_q + 2(\dot{R} \cos \varphi + \dot{x}_q \sin \varphi)} \quad (3.65a)$$

instead of  $\Delta U$  according to (3.66):

$$\Delta U = \frac{1}{\sqrt{1 + \dot{x}_d^2 + \dot{x}_q^2 + 2(\dot{x}_d \cos \varphi + \dot{x}_q \sin \varphi)}} \quad (3.66a)$$

Finally, instead of  $\Delta U$  according to (3.67):

$$\Delta U = \frac{\sqrt{1 + \dot{x}_q^2 + 2\dot{x}_q \sin \varphi}}{1 + \dot{x}_d \dot{x}_q + 2\dot{x}_q \sin \varphi} \quad (3.67a)$$

and instead of  $\Delta U$  according to (3.68):

$$\Delta U = 1/\sqrt{1 + \dot{x}_d^2 + 2\dot{x}_d \sin \varphi} \quad (3.68a)$$

It should be noted that if we find the extremum of Expression (3.65) with respect to  $k$  we will find that the voltage drop is at a maximum or  $\Delta U$  is at a minimum (all other conditions being equal) when  $k = 1$ , i.e., the minimum value of  $\Delta U$  is found from (3.66). This means that if we plot the external characteristics for a salient-pole synchronous machine using Expression (3.66), which is intended for a non-salient-pole machine, the results obtained will be too high, i.e., there is a certain safety factor involved in the calculations.

The external characteristics for a nonsalient-pole synchronous machine may be represented in relative coordinates  $\Delta U = U/E_0$  and  $I_{k1} = I/I_k$ . To obtain an analytical expression for the external characteristics in relative coordinates it is necessary to represent (3.66) in the form

$$1 = \frac{U^2}{E_0^2} + \left( \frac{U \cos \varphi}{E_0} \right)^2 (1 + \beta_d^2) + 2 \frac{U^2 \cos \varphi}{E_0^2} (\cos \varphi + \beta_d \sin \varphi).$$

Since, by (3.39) and (3.57)

$$I_{a1} = \frac{I}{I_k} = \frac{U \cos \varphi}{E_0} \sqrt{1 + \beta_d^2} = \Delta U \frac{\cos \varphi}{1} \sqrt{1 + \beta_d^2}.$$

we can obtain an equation for the family of ellipses

$$1 = \Delta U^2 + I_{a1}^2 + 2 \Delta U I_{a1} \frac{\cos \varphi + \beta_d \sin \varphi}{\sqrt{1 + \beta_d^2}} \quad (3.69)$$

The ellipse axes, inclined to the  $\Delta U$  and  $I_{k1}$  axes at an angle of  $45^\circ$ , are represented by the equations

$$a = \frac{1}{\sqrt{1 - \frac{\sin \varphi + \beta_d^{-1} \cos \varphi}{\sqrt{1 + \beta_d^2}}}} \text{ and } b = \frac{1}{\sqrt{1 + \frac{\sin \varphi + \beta_d^{-1} \cos \varphi}{\sqrt{1 + \beta_d^2}}}} \quad (3.70)$$

If we use the fact that

$$\operatorname{tg} \beta = \beta_d = \frac{x_d}{R}, \quad \cos \beta = \frac{1}{\sqrt{1 + \beta_d^2}} \text{ and } \sin \beta = \frac{\beta_d}{\sqrt{1 + \beta_d^2}},$$

following simple manipulations, Expressions (3.69) and (3.70) can be represented in the form

$$1 = \Delta U^2 + I_{n1}^2 + 2\Delta U I_{n1} \cos(\varphi - \beta) \quad (3.71)$$

and

$$\left. \begin{aligned} a &= \sqrt{1 - \cos(\varphi - \beta)}; \\ b &= \sqrt{1 + \cos(\varphi - \beta)}. \end{aligned} \right\} \quad (3.72)$$

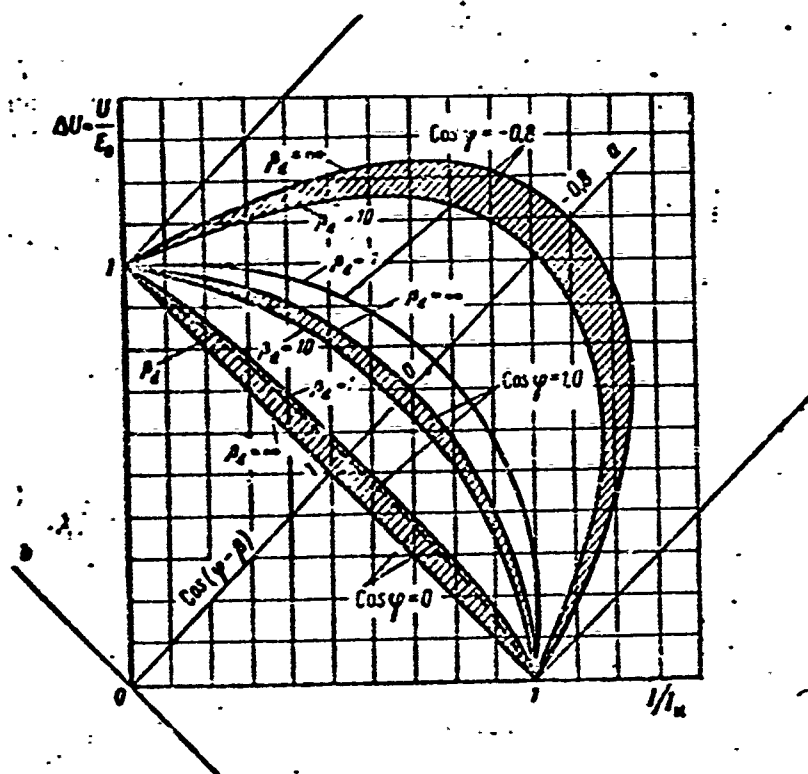


Fig. 3.42. External characteristics for synchronous machine in relative units with constant excitation and  $\cos \varphi$  unchanged.

Analysis of (3.69) and (3.70) has shown that when

$$2\Delta U I_{n1} \frac{\sin \varphi + \beta_d^{-1} \cos \varphi}{\sqrt{1 + \beta_d^2}} = 0 \text{ or } \beta_d = -\operatorname{ctg} \varphi$$

the ellipses become circles with the equations

$$1 = \Delta U^2 + I_{a1}^2; a = b = 1 \quad (3.73)$$

while when

$$\frac{\sin \varphi + \beta_d^{-1} \cos \varphi}{\sqrt{1 - \beta_d^{-2}}} = \pm 1$$

the ellipses become line segments with equations of the type

$$1 = \Delta U^2 + I_{a1}^2 + 2\Delta U I_{a1}, \quad a = \infty, \quad b = \frac{1}{\sqrt{2}}; \quad (3.74)$$

$$1 = \Delta U^2 + I_{a1}^2 - 2\Delta U I_{a1}, \quad a = \frac{1}{\sqrt{2}}, \quad b = \infty. \quad (3.75)$$

Figure 3.42 shows external characteristic curves plotted in relative coordinates for various values of  $\beta_d$  and  $\cos \varphi$ .

### Electrical Power

In the general case, the electrical power of a synchronous machine is expressed by the product of the complex current  $\dot{I} = I_q - jI_d$  and the complex conjugate\* of the voltage  $\dot{U} = U \cos \theta - jU \sin \theta$ , i.e.,

$$S_e = m \dot{U} \dot{I}^* = mU \{ (I_q \cos \theta + I_d \sin \theta) - j(I_d \cos \theta - I_q \sin \theta) \}, \quad (3.76)$$

where

$$P_e = mU (I_q \cos \theta + I_d \sin \theta) \quad (3.77)$$

is the in-phase electrical-power component, and

$$Q_e = mU (I_d \cos \theta - I_q \sin \theta) \quad (3.78)$$

is the reactive electrical-power component.

The same expressions can also be obtained directly from the expression for the in-phase and reactive components of the electrical power of a synchronous machine if we take account of the fact that

$$I_d = I \sin \phi; \quad I_q = I \cos \phi.$$

Substituting the values of  $I_d$  and  $I_q$  from (3.26) and (3.27) into Expressions (3.77) and (3.78), we are able to obtain after simple manipulations expressions for the in-phase and reactive electrical-power components of a salient-pole synchronous machine, allowing for the resistance of the armature winding

$$P_r = A_1 \left[ \dot{E}_0 (\sin \theta + k\beta_d^{-1} \cos \theta) + \frac{k-1}{2} \sin 2\theta - k\beta_d^{-1} \right] \quad (3.79)$$

and

$$Q_r = A_1 \left[ \dot{E}_0 (\cos \theta - k\beta_d^{-1} \sin \theta) + \frac{k-1}{2} \cos 2\theta - \frac{k+1}{2} \right], \quad (3.80)$$

where

$$A = \frac{mU^2}{R\beta_d} \cdot \gamma = \frac{1}{1 + k\beta_d^{-2}}.$$

As (3.79) implies, the active component of the electrical power contains constant, sinusoidal, and cosinusoidal components of the fundamental frequency, as well as a sinusoidal component at the first harmonic.

The reactive component of the electrical power, according to (3.80), contains constant, cosinusoidal, and sinusoidal components of the fundamental frequency as well as a cosinusoidal component at the first harmonic.

If we neglect the armature-winding resistance and make use of the fact that in this case  $\beta_d = \infty$  and  $\gamma = 1$ , we are able to obtain in place of (3.79) and (3.80)

$$P_r = A \left[ \dot{E}_0 \sin \theta + 0.5(k-1) \sin 2\theta \right] \quad (3.81)$$

and

$$Q_r = A \left[ \dot{E}_0 \cos \theta + 0.5(k-1) \cos 2\theta - 0.5(k+1) \right]. \quad (3.82)$$

In contrast to the in-phase electrical-power component, even at  $R = 0$  the reactive component contains a constant component equaling  $-0.5(k+1)(mU^2/R\beta_d)$ .

Equations (3.79)-(3.82) are considerably simplified for nonsalient-pole synchronous machines for which  $k = 1$  and, consequently,  $\beta_d = \beta_q$  and  $x_d = x_q$ . In this case, the in-phase and reactive components of the electrical power, allowing for  $R$ , will be

$$P_r = A_1 \left[ \dot{E}_0 (\sin \theta + \beta_d^{-1} \cos \theta) - \beta_d^{-1} \right] \quad (3.83)$$



and

$$Q_r = A\gamma_1 [\dot{E}_0(\cos\theta - \beta_d^{-1}\sin\theta) - 1], \quad (3.84)$$

where

$$\gamma_1 = \frac{1}{1 + \beta_d^{-2}}.$$

Where the armature-winding resistance equals zero, the same electrical-power components will be

$$P_r' = A\dot{E}_0 \sin\theta = \frac{mE_0U}{x_d} \sin\theta. \quad (3.85)$$

and

$$Q_r' = A(E_0 \cos\theta - 1) = \frac{mE_0U}{x_d} \cos\theta - \frac{mU^2}{x_d}. \quad (3.86)$$

Figure 3.43 shows the function  $P_r/A = f(\theta)$  for various values of  $\beta_d$  with  $\dot{E}_0 = 1$  and  $A = \text{const.}$

The curves of Fig. 3.43 show that when the armature-winding resistance is taken into account, the amplitude of the electrical power decreases (the decrease is greater the smaller  $\beta_d$ ) while there is a decrease in the critical internal phase-shift angle  $\theta_{\max}$ , i.e., the angle at which the power is at a maximum (the decrease is greater the smaller  $\beta_d$ ).

The maximum in-phase electrical power for a nonsalient-pole synchronous machine is determined by the maximum of Expression (3.83), i.e., by the expression

$$\frac{dP_r}{d\theta} = \frac{d}{d\theta} [A\gamma_1 [\dot{E}_0(\sin\theta_{\max} + \beta_d^{-1}\cos\theta_{\max}) - \beta_d^{-1}]] = 0,$$

from which it follows that the critical angle for the internal phase shift is found as

$$\theta_{\max} = \text{arctg } \beta_d. \quad (3.87)$$

It has thus been established that the maximum electrical power for a nonsalient-pole machine, allowing for R, will occur for an in-

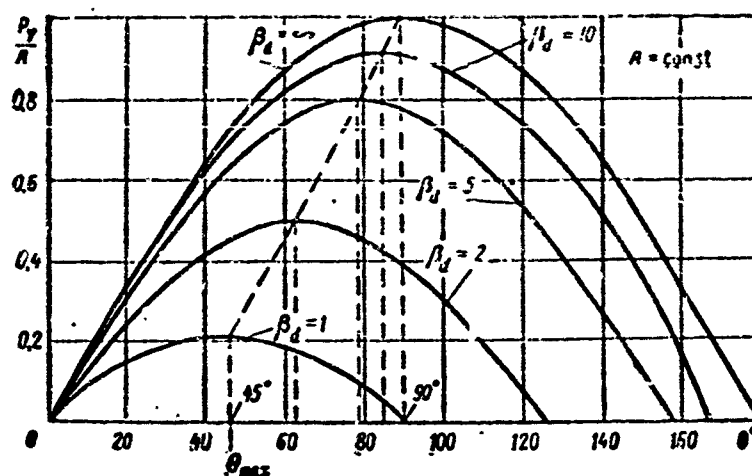


Fig. 3.43. Variation in the electrical power of a nonsalient-pole synchronous machine as a function of the working angle  $\theta$ .

ternal phase-shift angle  $\theta_{\max} = \arctan \beta_d = f(\beta_d)$ , and not at  $\theta'_{\max} = \pi/2$  as in the  $R = 0$  case.

The maximum in-phase electrical power will then equal

$$P_{\varphi \max} = \frac{A I_1}{\beta_d} (\dot{E}_0 \sqrt{1 + \beta_d^2} - 1). \quad (3.88)$$

Since when  $R = 0$ ,  $\theta_{\max} = \pi/2$ , in accordance with (3.85) the maximum in-phase electrical power, neglecting  $R$ , will be

$$P'_{\varphi \max} = A \dot{E}_0 = \frac{\pi E_0 U}{x_d}. \quad (3.89)$$

The ratio of the maximums for the in-phase electrical power with and without allowance for  $R$  will clearly be determined by the expression

$$k_{\varphi \max} = \frac{P_{\varphi \max}}{P'_{\varphi \max}} = \frac{I_1}{\beta_d} (\sqrt{1 + \beta_d^2} - \dot{E}_0^{-1}). \quad (3.90)$$

Figure 3.44 shows the functions  $k_{\varphi \max} = f(\beta_d)$  for values of  $\dot{E}_0^*$  and  $\theta_{\max} = \varphi(\beta_d)$ .

The curves show that for  $\beta_d < 10$ , the peak value  $P_{\varphi \max}$  and the angle  $\theta_{\max}$  (allowing for  $R$ ) depart considerably from the values  $P'_{\varphi \max}$  and  $\theta'_{\max}$  (corresponding to  $R = 0$ ).

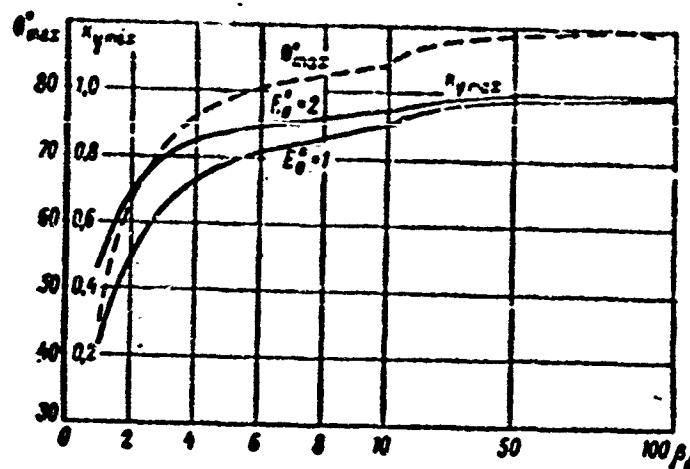


Fig. 3.44. Effect of armature resistance on maximum value of electrical power and critical internal phase-shift angle for a nonsalient-pole synchronous machine.

### Electromagnetic Power

The electromagnetic power of a synchronous machine, i.e., the power of the rotating field, may be defined as the product of the complex current and the complex conjugate of the fictitious emf  $E_{ya}$  (see Fig. 3.37).

For nonsalient-pole synchronous machines, if we do not consider the saturation of the magnetic-circuit iron, the fictitious emf equals the actual emf, i.e.,  $E_{ya} = E_0$ .

In salient-pole synchronous machines,  $E_{ya} > E_0$  and the fictitious emf may be represented by the equation

$$\left. \begin{aligned} E_s &= E_0 - I_d(x_d - x_q) \\ E'_s &= E'_0 - I_d(\beta_d - \beta_q) \end{aligned} \right\} \quad (3.91)$$

When  $\beta_d(x_d) > \beta_q(x_q)$ , which is normally the case,  $E'_{ya}(E_{ya}) < E'_0(E_0)$ , while when  $\beta_d(x_d) < \beta_q(x_q)$ , conversely,  $E'_{ya}(E_{ya}) > E'_0(E_0)$ .

In view of what we have said, the electromagnetic power may be written in the form

$$\begin{aligned} S_e &= m i \hat{E}_s R = m R (I_q - j I_d) \left[ E'_0 - I_d \beta_d \frac{k-1}{k} \right] = \\ &= m R \left[ I_q (E'_0 - I_d \beta_d \frac{k-1}{k}) - j I_d (E'_0 - I_d \beta_d \frac{k-1}{k}) \right]. \end{aligned} \quad (3.92)$$

where

$$P_{\psi} = m R I_d \left( E_0 - I_d \beta_d \frac{k-1}{k} \right) \quad (3.93)$$

is the in-phase electromagnetic-power component,

$$Q_{\psi} = m R I_d \left( E_0 - I_d \beta_d \frac{k-1}{k} \right) \quad (3.94)$$

is the reactive electromagnetic-power component.

An equation for  $P_{\psi}$  may be obtained if we take into account the fact that the electromagnetic power equals the electrical power plus the losses in the armature winding.

Substituting the values of  $I_d$  and  $I_q$  from (3.26) and (3.27) into (3.93) and (3.94), we obtain the following expressions for the in-phase and reactive components of the electromagnetic power for a salient-pole synchronous machine, allowing for the armature-winding resistance:

$$P_{\psi} = A \gamma^2 \left( \sin \theta + \frac{\dot{E}_0 - \cos \theta}{\beta_d} \right) \left[ \dot{E}_0 \left( 1 + \frac{k^2}{\beta_d^2} \right) + (k-1) \left( \cos \theta + \frac{k}{\beta_d} \sin \theta \right) \right] \quad (3.95)$$

and

$$Q_{\psi} = A \gamma^2 \left[ \dot{E}_0 \left( 1 + \frac{k}{\beta_d^2} \right) \left( \dot{E}_0 - \cos \theta - \frac{k}{\beta_d} \sin \theta \right) - \frac{k-1}{k} \left( \dot{E}_0 - \cos \theta - \frac{k}{\beta_d} \sin \theta \right)^2 \right] \quad (3.96)$$

where

$$A = \frac{m U^2}{R \beta_d}; \quad \gamma = \frac{1}{1 + k \beta_d^2}.$$

If we neglect the armature-winding resistance, then in analogy with (3.81) and (3.82) we find that

$$P'_{\psi} = A \left[ \dot{E}_0 \sin \theta + 0.5(k-1) \sin 2\theta \right], \quad (3.97)$$

i.e.,  $P'_{\psi} = P'_{\phi}$  and

$$Q'_{\psi} = \frac{A}{k} \left[ \dot{E}_0^2 + \dot{E}_0 (k-2) \cos \theta - \right]$$

$$-0.5(k-1)\cos 2\theta - 0.5(k-1)]. \quad (3.98)$$

For nonsalient-pole synchronous machines, where  $k = 1$ ,  $\beta_d = \beta_q$ , and  $x_d = x_q$ , these last equations, as in the electrical-power case, are considerably simplified.

Thus, the electromagnetic power equals

$$S_\psi = (I_\psi - jI_d) E_0 R_m = m R I_\psi E_0' - j m R I_d E_0'. \quad (3.99)$$

The expanded values for the in-phase and reactive components of the electromagnetic power, allowing for the armature resistance, will equal, respectively,

$$P_\psi = A_{\gamma_1} \dot{E}_0 \left( \sin \theta + \frac{\dot{E}_0 - \cos \theta}{\beta_d} \right) \quad (3.100)$$

and

$$Q_\psi = A_{\gamma_1} \dot{E}_0 \left( \dot{E}_0 - \cos \theta - \frac{\sin \theta}{\beta_d} \right), \quad (3.101)$$

where

$$\gamma_1 = \frac{1}{1 + \beta_d^{-2}}.$$

When  $R = 0$ , the same expressions will equal

$$P_\psi = A \dot{E}_0 \sin \theta = \frac{m U E_0}{x_d} \sin \theta = P_\psi^*, \quad (3.102)$$

$$Q_\psi = A \dot{E}_0 (\dot{E}_0 - \cos \theta) = \frac{m E_0^2}{x_d} - \frac{m E_0 U}{x_d} \cos \theta. \quad (3.103)$$

The maximum value for the in-phase electromagnetic power of a nonsalient-pole synchronous machine may be found by taking the derivative of Expression (3.100) with respect to  $\theta$  and setting it equal to zero, i.e.,

$$\frac{dP_\psi}{d\theta} = \frac{d}{d\theta} \left[ A_{\gamma_1} \dot{E}_0 \left( \sin \theta_{1\max} + \frac{\dot{E}_0 - \cos \theta_{1\max}}{\beta_d} \right) \right] = 0.$$

After simple manipulations, we find that the critical internal phase-shift angle for which the in-phase electromagnetic power is at a maximum will equal

$$\theta_{1\max} = \pi - \arctg \beta_d = \pi - \theta_{\max}, \quad (3.104)$$

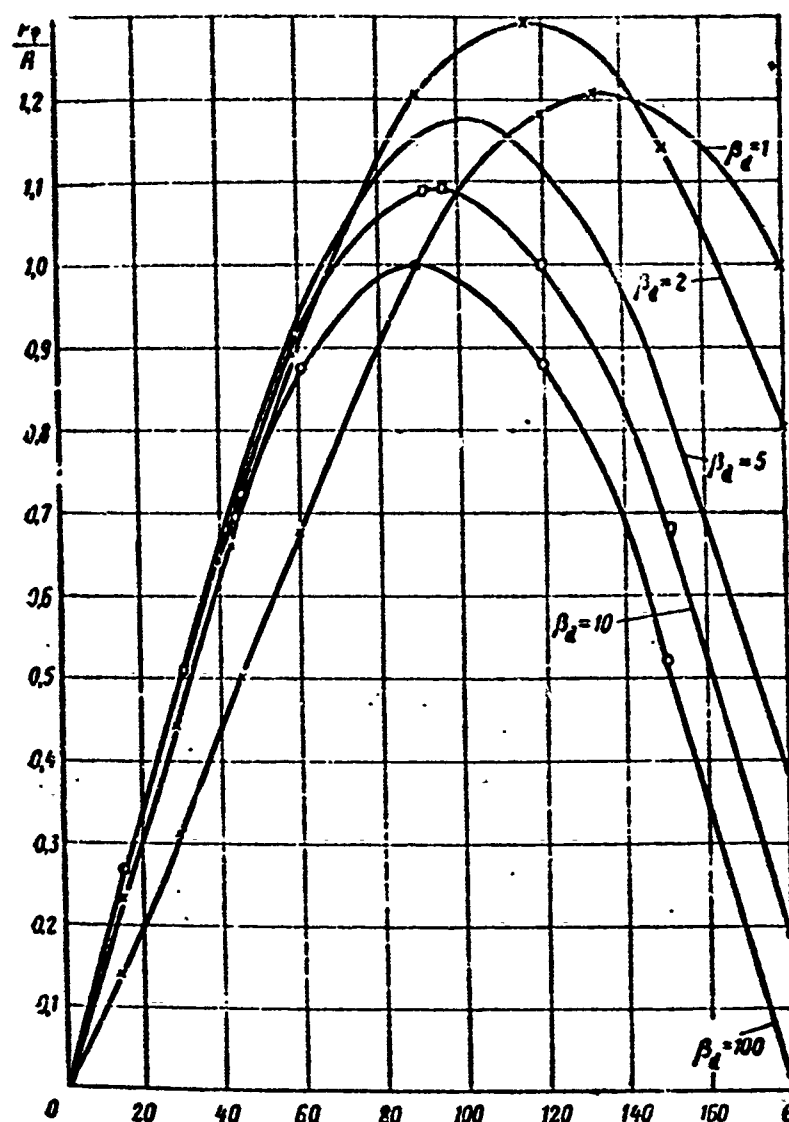


Fig. 3.45. Variation in the electromagnetic power of a nonsalient-pole synchronous machine as a function of the angle  $\theta$ .

where  $\theta_{\max} = \arctan \beta_d$  is the internal phase-shift angle corresponding to the maximum electrical power according to (3.87).

The maximum in-phase electromagnetic power is found from the expression

$$P_{\phi \max} = A \gamma_{11} \beta_d^{-1} [\dot{E}_0^2 + \dot{E}_0 \sqrt{1 + \beta_d^2}]. \quad (3.105)$$

The ratio of the maximum values for the in-phase electromagnetic power when  $R$  is considered and when it is neglected will equal

$$k_{\phi \max} = \frac{P_{\phi \max}}{P_{\phi \max}'} = \frac{\beta_d}{1 + \beta_d^2} (\dot{E}_0 + \sqrt{1 + \beta_d^2}). \quad (3.106)$$

Figure 3.45 shows the function  $P_e/A = f(\theta)$  for various values of

$\beta_d$ , while Fig. 3.46 gives  $\theta_{lmax} = \varphi(\beta_d)$  and  $k_{vmax} = f(\beta_d)$  and also, for the sake of comparison,

$$k_{\varphi max} : \frac{P_{\varphi max}}{P_{\varphi max}} = \frac{k_{\varphi max}}{k_{\varphi max}}.$$

Here the ratio of the maximum in-phase electromagnetic power to the maximum in-phase electrical power for a nonsalient-pole synchronous machine will equal

$$\frac{P_{\varphi max}}{P_{\varphi max}} = \frac{\dot{E}_0 \sqrt{1 + \beta_d^2} + 1}{\dot{E}_0 \sqrt{1 + \beta_d^2} - 1}. \quad (3.107)$$

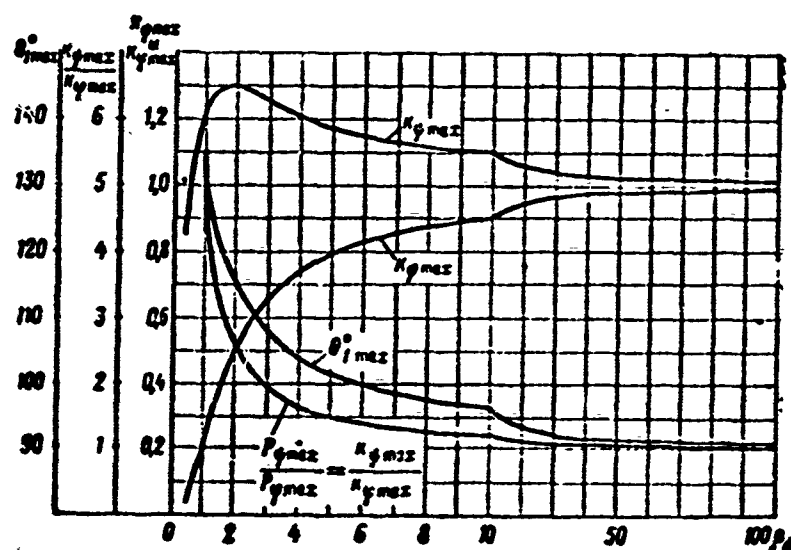


Fig. 3.46. The same as Fig. 3.44, but for electromagnetic power.

Looking at Figs. 3.43-3.45, we see that the maximum electrical power  $P_{\varphi max}$  developed by a generator and the critical internal phase-shift angle  $\theta_{max}$  decreases as the relative inductance  $\beta_d$  decreases. Thus, when  $\beta_d = 1$ ,  $P_{\varphi max} = 0.25$  and  $\theta_{max} = 45^\circ$  as against values of  $P_{\varphi max} = 1$  and  $\theta_{max} = 90^\circ$  for the case in which the energy dissipated in the armature winding is neglected.

The maximum electromagnetic power  $P_{vmax}$  and the critical internal phase-shift angle  $\theta_{lmax}$  rise as the relative inductance  $\beta_d$  decreases.

For the case in which the energy dissipated in the armature winding is neglected,  $P_{vmax} = P_{\varphi max} = 1$  and  $\theta_{max} = \theta_{lmax} = 90^\circ$ .

The maximum electrical power  $P_{\psi \max}$  with  $\beta_d < 1.8$  begins to decrease owing to a sharp drop in the electrical power; when  $\beta_d < 1.8$ , it drops faster than the armature-winding losses rise, and as a result the electromagnetic power, which equals their sum, decreases.

### Parametric Power

In the absence of excitation ( $\dot{E}_0 = 0$ ), the equations for the electrical and electromagnetic powers of salient-pole synchronous machines and their relative values will equal, respectively,

$$P_{\psi} = P_{\psi n} = A \gamma [0.5(k-1) \sin 2\theta - k\beta_d^{-1}], \quad (3.108)$$

$$P_{\psi} = P_{\psi n} = A \gamma^2 \frac{(k-1)^2}{2\beta_d} \left[ 1 + \frac{1 - k\beta_d^{-2}}{(k-1)\beta_d^{-1}} \sin 2\theta - \frac{k+1}{k-1} \cos 2\theta \right], \quad (3.109)$$

where

$$A = \frac{mU^2}{R\beta_d}; \quad \gamma = \frac{1}{1 + k\beta_d^{-2}}.$$

When  $R = 0$ , since in this case  $\gamma = 1$  and  $\beta_d = \infty$ , the same expressions will be:

$$P'_{\psi n} = P'_{\psi n} = A \frac{k-1}{2} \sin 2\theta = \frac{mU^2 k-1}{x_d} \frac{\sin 2\theta}{2}. \quad (3.110)$$

If we allow for the armature resistance  $R$ , an additional constant component with a negative sign will be introduced into the expression for the electrical power, while constant and harmonic components at the first harmonic will be introduced into the expression for the electromagnetic power.

The presence of a constant component with a negative sign in the expression for the electrical power means that under no-load conditions for a parametric synchronous generator, where  $\theta = 0$ , in addition to the reactive current used to form the magnetic field, wattful current will also be drawn from the line to cover the losses in the armature copper caused by the flow of no-load current.

To find the maximum parametric power (moment), we must find the



maximum of Expression (3.109), i.e., we must set the derivative

$$\frac{dP_{\phi s}}{d\theta} = \frac{d}{d\theta} \left[ B \left[ 1 + \frac{1 - k\beta_d^{-2}}{(k-1)\beta_d^{-1}} \sin 2\theta - \frac{k+1}{k-1} \cos 2\theta \right] \right] = 0.$$

equal to zero.

Here B is the constant from Expression (3.109).

Solving this equation, we obtain the value of the angle  $\theta_{pmax}$  at which maximum parametric power is reached; in this case

$$\operatorname{tg} 2\theta_{smax} = -\frac{\beta_d^2 - k}{(k+1)\beta_d}$$

and

$$\theta_{smax} = 0.5 \operatorname{arc} \operatorname{tg} \left[ -\frac{\beta_d^2 - k}{(k+1)\beta_d} \right]. \quad (3.110)$$

Making use of the fact that

$$\cos 2\theta_{smax} = \frac{(k+1)\beta_d}{\sqrt{(k+1)\beta_d^2 + (\beta_d^2 - k)^2}}$$

and

$$\sin 2\theta_{smax} = \frac{-(\beta_d^2 - k)}{\sqrt{(k+1)\beta_d^2 + (\beta_d^2 - k)^2}},$$

we can use (3.109) to obtain an expression for the maximum parametric power in the form

$$P_{\phi smax} = A_1^2 \frac{k-1}{2} \left[ (k-1)\beta_d^{-1} - \sqrt{1 + (k^2+1)\beta_d^{-2} + k^2\beta_d^{-4}} \right]. \quad (3.112)$$

If we neglect the energy dissipated in the armature winding, then  $R = 0$ ,  $\beta_d = \infty$ ,  $\gamma = 1$ , and it follows from (3.112) that

$$P_{\phi smax} = -A \frac{k-1}{2} = -\frac{mU^2}{x_d} \frac{k-1}{2}. \quad (3.113)$$

The effect of the armature resistance on the maximum parametric power is determined by the relationship

$$k_{\phi s} = \frac{P_{\phi smax}}{P_{\phi smax}^0} = \frac{1}{2} \left[ (k-1)\beta_d^{-1} - \sqrt{1 + (k^2+1)\beta_d^{-2} + k^2\beta_d^{-4}} \right]. \quad (3.114)$$

Analysis of (3.109)-(3.114) shows that a salient-pole synchronous machine without excitation can develop an electromagnetic power (torque) in the motor and generator modes; the internal shift angle

$\theta_{\text{pmax}}$ , i.e., the angle between the transverse rotor axis and the external-voltage vector at which the machine develops maximum electromagnetic power, equals  $\pm 45^\circ$  where no energy is dissipated in the armature winding and is less than  $\pm 45^\circ$  when we take the armature resistance into account; the maximum electromagnetic power for a synchronous machine without excitation, allowing for  $R$ , is lower the smaller  $\beta_d$ .

Thus, in unexcited operation, the effect of the armature-winding resistance results in some drop in the maximum power (torque) and the limiting angle for stable operation of the machine.

### 3.5. CHARACTERISTICS OF AIRCRAFT GENERATORS

The properties of electrical machines are described by characteristics, which normally give the graphical relationships among the fundamental quantities. Fundamental alternating- and direct-current machine quantities include:  $U$ , the voltage;  $I$ , the load-current;  $I_v$ , the excitation current;  $n$ , the speed;  $\beta$ , the angle by which the brushes are shifted away from the neutral plane for direct-current machines, and the power factor ( $\cos \varphi$ ) for alternating-current machines.

The relationship among the fundamental quantities may be represented by an equation of the form

$$f(U, I, I_v, n, \beta) = 0 \text{ or } f(U, I, I_v, n, \varphi) = 0. \quad (3.115)$$

In machines with commutating poles, the brushes are normally set at the neutral plane and, consequently, the brush shift angle away from the neutral plane is  $\beta = 0$ .

For machines without commutating poles, the brushes may be shifted away from the neutral plane by a fixed angle, i.e.,  $\beta = \text{const}$ .

Thus, Eq. (3.115) will take the form

$$f(U, I, I_v, n) = 0. \quad (3.116)$$

for all direct-current machines in which the brush position is fixed and for all alternating-currents in which  $\cos \varphi = \text{const}$ .

In general-purpose generators, the speed is normally held constant, i.e.,  $n = \text{const}$  and (3.116) will be

$$f(U, I, I_0) = 0. \quad (3.117)$$

Expression (3.117) is the equation of a surface, and is called the fundamental characteristic equation for a generator.

For a motor, the line voltage is normally constant. In this case, (3.116) will be

$$f(I, I_0, n) = 0, \quad (3.118)$$

i.e., Expression (3.118) is the fundamental characteristic equation for a motor.

We may use (3.117) to obtain a series of generator characteristics, including:

the no-load characteristic

$$E = U_0 = f(I_0) \text{ or } \Phi = \varphi(I_0) \text{ at } I = 0,$$

i.e., the magnetization curve, providing that the excitation current  $I_v$  does not flow through the armature winding;

the short-circuit characteristic

$$I = f(I_v) \text{ at } U = 0;$$

the load characteristic

$$U = f(I_v) \text{ at } I = \text{const};$$

the external characteristic

$$U = f(I) \text{ at } R_v = \text{const or } I_v = \text{const};$$

the regulation characteristic

$$I_v = f(I) \text{ at } U = \text{const}.$$

As we know, all the remaining characteristics may be constructed from the no-load and short-circuit characteristics, i.e., they are fundamental in this sense. The external and regulation characteristics determine the operating properties of the generator.

The shapes of the characteristic curves are affected by the sys-

tem of excitation used for the machine, and thus the characteristics are investigated with reference to each type of machine excitation. The characteristics of aircraft generators operating at constant speed do not differ, for all practical purposes, from the similar characteristics for general-purpose generators.

Henceforth, we shall consider only certain features of aircraft-generator characteristics.

In contrast to general-purpose generators, aircraft generators are sometimes operated at varying speeds. In this case, the appropriate characteristics are plotted for each speed. As a rule, the characteristics are found for three speeds: maximum, rated, and minimum.

#### No-Load Characteristic

$$E = f(I_v) \text{ at } R_n = \infty, I = 0, \text{ and } n = \text{const.}$$

This characteristic determines the magnetic properties of the machine, and is the same as the magnetic characteristic for an independently excited machine.

The emf induced in the armature winding, as we know, equals

$$E = k_E n \Phi \cdot \omega, \quad (3.119)$$

$$k_E = \frac{p}{15} k_f k_o 10^{-3},$$

where  $\omega$  is the number of phase turns;  $k_f$  is the field curve form factor;  $k_o$  is a winding factor.

With the rated voltage unchanged, aircraft machines operate with low saturation at high speeds, but even at the maximum speed, where the saturation is greatest, it is normally somewhat less than in general-purpose machines. The limitation on the saturation of aircraft-generator magnetic circuits is caused by the need:

- a) to decrease machine size, leading to a decrease in the space available for the excitation winding;
- b) to limit the maximum excitation current when a vibrator volt-

age regulator is used;

e) to limit the excitation-winding losses when a carbon regulator is used.

These considerations limit the magnitude of the excitation magnetizing force  $F_v$ , i.e., the size of excitation winding that may be installed on the machine poles; it is thus necessary to decrease the saturation somewhat.

As a rule, at the lowest speed  $n_{\min}$ , the machine operates on a "knee" on the magnetization curve, which corresponds to the average saturation level.

The effect of speed on the no-load characteristic. If the excitation current and, consequently, the flux  $\phi$  do not depend on the speed, the no-load emf will be directly proportional to the speed.

This will occur when the generator field winding is supplied from a constant or regulated direct-current source. In this case, the magnetic flux in the air gap and the magnetic-system saturation will remain constant.

If the excitation current is supplied by an exciter installed on the generator shaft, its magnitude will in turn depend on the speed (in the absence of a voltage regulator). Thus, with independent exciter excitation

$$I_{a.s.} = \frac{U_{e.s.}}{R_{e.s.}} = \text{const}; U_e \equiv \pi;$$

with parallel exciter excitation

$$I_{a.s.} = \frac{U_{e.s.}}{R_{e.s.}} = f(n) \text{ and } U \equiv n^\alpha, \text{ where } \alpha > 1.$$

Thus, with independent exciter excitation and no regulator, the generator emf is proportional to the square of the speed  $E \equiv n^2$ , while with parallel excitation

$$E \equiv n^{2+\alpha_1}, \text{ where } \alpha_1 < 1.$$

In this case, the magnetic flux and magnetic-system saturation will increase as the speed rises (this case is of no practical importance).

If a regulator is used to hold the voltage constant across the generator terminals when a variable speed is involved, as the speed rises, the excitation current and the magnetic flux in the machine air gap will drop.

As we have already noted, generators operating with variable speeds have a family of no-load characteristics, each corresponding to its own speed (Fig. 3.47a). It is possible, however, to represent the entire family of characteristic curves by one reduced curve. To do this, we use the relative form of the no-load characteristic, i.e., we construct the relationship

$$\dot{E} \frac{n_{max}}{n} = f(i_a)$$

or

$$\dot{E} \frac{f_{max}}{f} = \varphi(i_a)$$

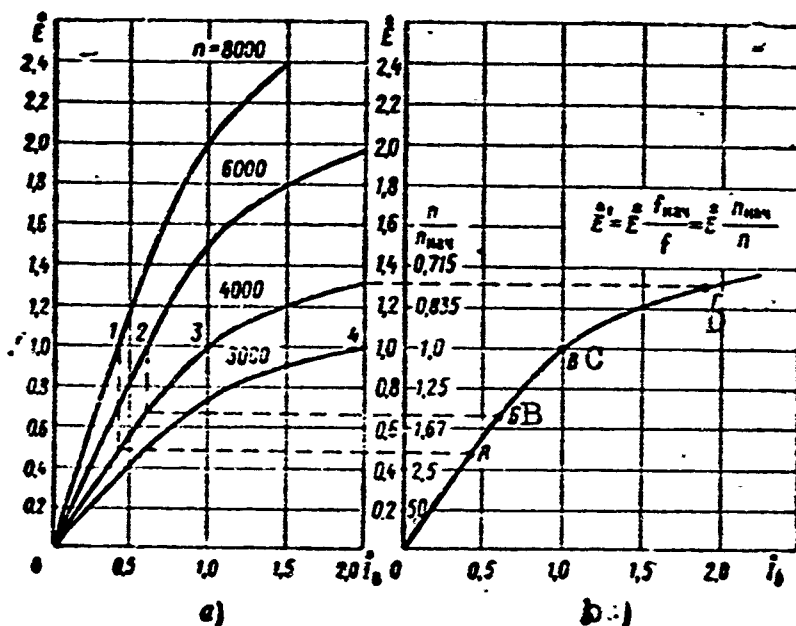


Fig. 3.47. No-load generator curves with varying speeds. a) No-load characteristics in relative units; b) reduced no-load characteristic in relative units.

instead of

$$\dot{E} = f(i_v).$$

where  $\dot{E} = E/U_{\text{nom}}$  and  $i_v = I_v/I_{v.\text{nom}}$ , in relative units.

In this case, in place of the family of no-load curves (Fig. 3.47a), we will have only one curve (Fig. 3.47b), corresponding to the initial frequency at which the nominal voltage corresponds to point C.

Any value may be taken for the initial frequency; it is convenient, however, to use the initial speed for which the rated power of the machine is determined.

If the generator voltage remains unchanged at high speed, the operating point corresponding to the rated voltage will be shifted downward toward the origin away from point C; when the speed drops, it shifts upward along the curve, as we can see from Fig. 3.47b. Curve 3, corresponding to the initial speed, can be considered to be the initial relative characteristic that does not depend on the speed, i.e.,

$$\dot{E} = \dot{E}(n_{\text{mach}}/n) = f(i_v).$$

If the rated voltage remains constant when the speed changes, the nominal voltage at the initial speed  $n_{\text{mach}} = 4000$  rpm ( $n_{\text{mach}}:n = 1$ ) will correspond to point C, since at the initial speed, the characteristic  $\dot{E}(n_{\text{mach}}/n)$  will coincide with the characteristic  $\dot{E}$ . The rated voltage at  $n = 8000$  rpm ( $n_{\text{mach}}:n = 0.5$ ) corresponds to point A, which is located below point C, while the nominal voltage at  $n_{\text{min}} = 3000$  rpm ( $n_{\text{mach}}:n = 1.33$ ) corresponds to point D, located above point C.

Thus, when the speed changes from  $n_{\text{max}}$  to  $n_{\text{min}}$ , the point corresponding to the nominal voltage moves along the curve from A to D.

All statements applying to the no-load curve, and given in the general course on electrical machines, are also applicable in the given case although it is necessary to remember that the location of the nominal-voltage point on the curve depends on the speed.

Thus, when  $n = 2n_{nach}$ , the excitation current corresponding to the rated voltage amounts to 42% of the current at  $n_{nach}$  (point A), while at half voltage, the current drops to 20% of the rated value.

When the speed decreases, the excitation current rises sharply owing to the increased magnetic-system saturation, and when  $n = 0.75n_{nach}$ , at rated voltage it amounts to 195% of the current at  $n_{nach}$  (point D).

The curve for  $\dot{E}' = f(\dot{I}_V)$  clearly shows the relationship between the excitation magnetizing force and the speed where the voltage is held constant.

An analysis of the machine magnetization curve (Fig. 3.48) is carried out with the aid of several coefficients.

The magnetic-circuit coefficient, which is defined as the ratio of the no-load magnetizing force at a point corresponding to  $U_{nom}$  or  $E_{nom}$  to the magnetic potential difference across the air gap, i.e.,

$$k_s = \frac{F_0}{U_g} = \frac{U_i + U_{cr}}{U_i} = 1 + \frac{U_{cr}}{U_i} = 1.1 + 1.4. \quad (3.120)$$

It characterizes the distribution of no-load excitation magnetizing force between the air gap  $U_g$  and the iron  $U_{st}$ .

The relative magnetic-saturation coefficient, which is defined as the ratio of the voltage  $U_a$  (the y-axis segment on Fig. 3.48 cut off by the tangent to point A, corresponding to the nominal voltage) to the nominal voltage

$$k_{o.n} = \frac{U_a}{U_{nom}} = 0.5 + 0.6 \quad (3.121)$$

$k_{o.n} = 0$  in the absence of saturation, and it approaches one under strong saturation.

The magnetic-saturation coefficient, which is defined as the ratio of the relative change in excitation current ( $\Delta \dot{I}'_V = \Delta \dot{I}'_V / \dot{I}'_V$ ) to the relative change in voltage; ( $\Delta \dot{U}' = \Delta \dot{U}' / \dot{U}'$ ) at the nominal point,



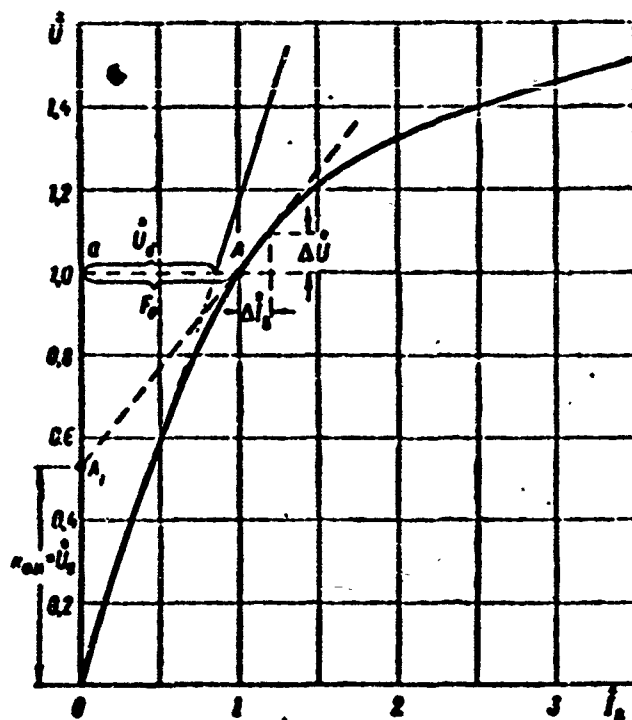


Fig. 3.48. Analysis of no-load curve.

i.e., at  $U_{nom}$  and  $n_{nom}$ , and

$$k_s = \frac{\Delta \dot{I}_s}{\Delta \dot{U}} = \frac{\Delta \dot{I}_s U}{\Delta \dot{U} I_s} \approx 2 \div 2.5. \quad (3.122)$$

Figure 3.48 may be used to establish the relationship between the relative magnetic-saturation coefficient  $k_{o.n}$  and the magnetic-saturation coefficient  $k_n$  in the form

$$\left. \begin{aligned} k_{o.n} &= 1 - \frac{1}{k_n} = \frac{k_n - 1}{k_n} \\ \text{and} \quad k_n &= \frac{1}{1 - k_{o.n}} \end{aligned} \right\} \quad (3.123)$$

This last expression shows that there is a constant relationship between  $k_n$  and  $k_{o.n}$  and, consequently, in order to analyze the magnetization curve only two indices need be used, namely: the magnetic-circuit coefficient  $k_s$  and the relative magnetic-saturation coefficient  $k_{o.n}$ .

We recall that  $k_s$  does not characterize circuit saturation, but

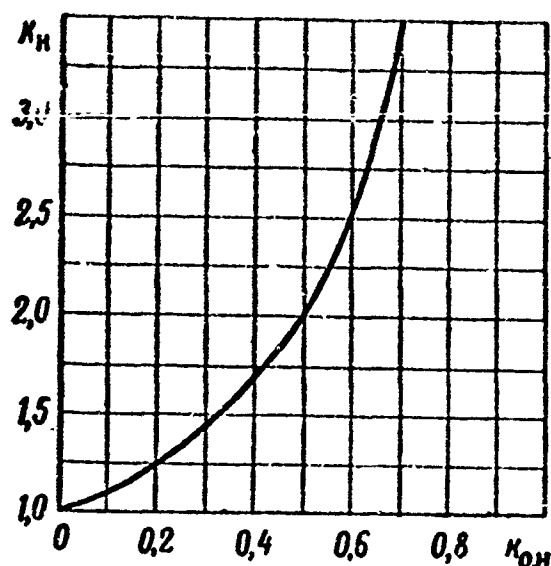


Fig. 3.49. Relationship between magnetic-saturation coefficient  $k_n$  and relative magnetic-saturation coefficient  $k_{o.n}$ .

only indicates the relationship between the magnetizing forces expended on forcing the flux through the steel and the air.

If the saturation curve is expressed in relative form, then  $k_{o.n}$  and  $k_n$  characterize the tangent slope at the point taken as the initial point, i.e., the point with the coordinates (1, 1), and the magnitude of  $k_{o.n}$  is read directly from the y-axis (segment  $OA_1$ ). The magnetic-saturation coefficient is in this case defined as the ratio

$$k_n = \frac{1}{1 - k_{o.n}} = \frac{1}{1 - OA_1} = \frac{1}{A_1a}.$$

Figure 3.49 shows the function  $k_n = f(k_{o.n})$ .

#### Short-Circuit Characteristic

$$I = f(I_v) \text{ at } z = 0, U = 0 \text{ and } n = \text{const.}$$

Vector diagrams corresponding to steady-state symmetric short-circuiting of a synchronous machine are shown in Fig. 3.50 for a single phase, with and without an allowance for the armature resistance; the figure is selfexplanatory.

The excitation short-circuit magnetizing force  $F_k$  is used to com-

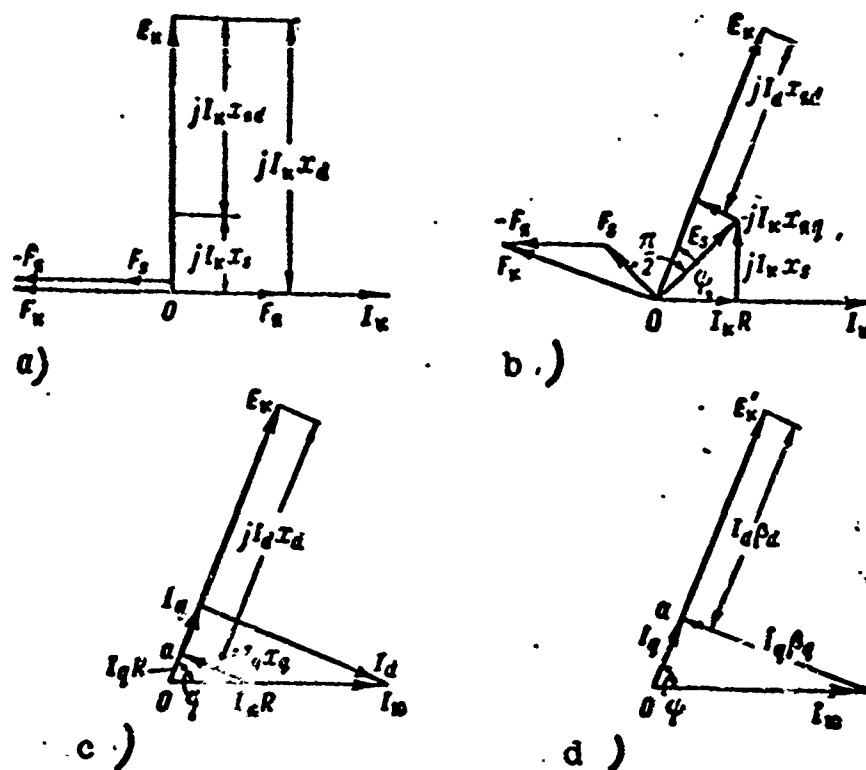


Fig. 3.50. Vector diagrams for steady-state short-circuiting of synchronous salient-pole machine. a) Armature resistance neglected; b) with allowance for armature resistance; c) with allowance for armature resistance and synchronous reactances used in longitudinal ( $x_d$ ) and transverse ( $x_q$ ) axes; d) the same, relative parameters.

compensate for the armature-reaction magnetizing force  $F_{ya}$  and the magnetic drop  $F_s$  due to the flux that induces the emf  $E_s$ , which compensates completely for the voltage drop across the armature winding,

$$E_s = I_k z_k = I_k \sqrt{R^2 + x_s^2}, \text{ i.e.,}$$

$$\vec{F}_s = \vec{F}_a + \vec{F}_r. \quad (3.124)$$

The steady-state short-circuit current is made up of two components:

longitudinal

$$I_d = I_k \sin \phi = I_k \frac{l_q x_q}{l_k R} = I_q \beta_q \quad (3.125)$$

and transverse

$$I_q = I_k \cos \phi = I_k \frac{R}{x_q} = \frac{I_d}{\beta_q}, \quad (3.126)$$

where, from the diagram of Fig. 3.50,

$$\sin \psi = \frac{I_q x_q}{I_x R} = \frac{I_q}{I_x} \beta_q.$$

Since, from the vector diagram, segment  $\overline{Oa}$  equals

$$\overline{Oa} = R I_x \cos \psi = I_q R$$

we take the value of  $I_q$  from (3.126) and obtain an expression for the emf  $E_k$  in the following form:

$$E_k = I_d x_d + I_q R = I_d x_d + R I_d \frac{R}{x_q} = I_d \frac{R^2 + x_d x_q}{x_q} \quad (3.127)$$

or

$$E'_k = I_d \beta_d + I_q = I_d \frac{k + \beta_d^2}{\beta_d}.$$

Taking (3.126) and (3.127) into account, the new expressions for  $I_d$  and  $I_q$  will be

$$I_d = \frac{E_k}{x_d + \frac{R^2}{x_q}} = \frac{E'_k}{(k + \beta_d^2) \beta_d^{-1}} \quad (3.128)$$

and

$$I_q = \frac{E_k}{R + \frac{x_d x_q}{R}} = \frac{E'_k}{(k + \beta_d^2) k^{-1}} \quad (3.129)$$

where

$$k = \frac{\beta_d}{\beta_q} = \frac{x_d}{x_q}, \quad E'_k = \frac{E_k}{R}.$$

On the basis of the preceding equations, the short-circuit current will equal

$$\vec{I}_x = I_q - j I_d = E_k \frac{R - j x_q}{R^2 + x_d x_q} = E'_k \frac{k - j \beta_d}{k + \beta_d^2}, \quad (3.130)$$

so that the absolute value will be

$$I_x = E_k \frac{\sqrt{R^2 + x_q^2}}{R^2 + x_d x_q} = E'_k \frac{\sqrt{k^2 + \beta_d^2}}{k + \beta_d^2}. \quad (3.131)$$

The short-circuit characteristic is the relationship between the armature current and the excitation current. If we neglect the iron

saturation or we use the straight-line section of the no-load characteristic, the emf will be a linear function of the excitation current, i.e.,

$$E = k M I_s = 2\pi f M I_s = \rho I_s$$

and

$$E' = \frac{M}{R} I_s = 2\pi f T I_s = \rho' I_s$$

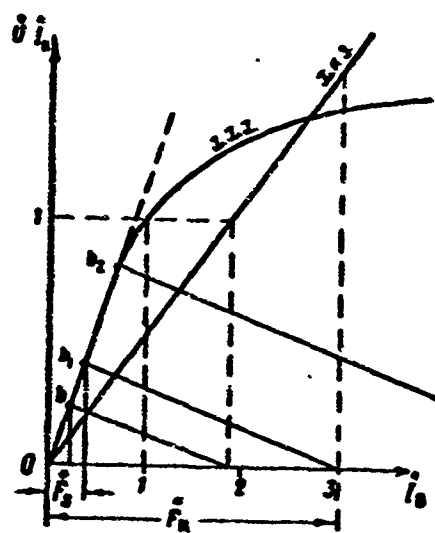


Fig. 3.51. Short-circuit characteristic.

In this case

$$I_k = \rho I_s \frac{\sqrt{R^2 + x_d^2}}{R^2 + x_d x_q} = \rho' I_s \frac{\sqrt{k^2 + \beta_d^2}}{k + \beta_d^2} \quad (3.132)$$

where  $\rho' = \rho/R$ .

This last equation corresponds to a straight line which is also the short-circuit characteristic for constant speed and the conditions assumed. If we also consider the saturation, which is involved only for short-circuit currents exceeding

the nominal current by several times, the short-circuit characteristic (kh.k.z.), like the curve for the no-load characteristic (kh.kh.kh.) will take the form shown in Fig. 3.51.

Let us recall that a decrease in the synchronous induction on the longitudinal axis  $x_d(\beta_d)$  increases the value of  $I_k$  for the same value of  $I_v(I'_v)$  with an increase in saturation. The short-circuit characteristic remains linear as long as the vertex of the reactive triangle (point b, Fig. 3.51) remains on the linear section of the magnetization curve. With a further increase in excitation current, the vertex of the reactive triangle moves above point  $b_2$  and the short-circuit characteristic will no longer be linear.

If we neglect the armature-winding resistance, as is normally

done for medium- and high-power synchronous machines, then

$$I_x = I_d = \frac{E_x}{x_d} = \frac{E_d}{x_d}; \quad I_q = 0. \quad (3.133)$$

The effect of the armature resistance on the short-circuit current has been discussed in §4 of this chapter. Here we need only note that when  $\beta_d > 5$ , the armature-winding resistance may be neglected. In aircraft tachometer synchronous generators,  $\beta \leq 5$ , and the resistance has a noticeable effect on the short-circuit current.

Effective speed on the short-circuit characteristic. Since  $E = 2\pi f M_d I_v$ ,  $x_d = 2\pi f L_d$ ,  $x_q = 2\pi f L_q$ , and

$$\beta_d = 2\pi f \frac{L_d}{R} = 2\pi f T_d,$$

Expression (3.131) is represented in the form

$$\left. \begin{aligned} I_x &= 2\pi M I_v \frac{\sqrt{\left(\frac{R}{f}\right)^2 + (2\pi L_q)^2}}{\left(\frac{R}{f}\right)^2 + (2\pi)^2 L_d L_q} \\ \text{or} \quad I_x &= 2\pi T I_v \frac{\sqrt{\left(\frac{k}{f}\right)^2 + (2\pi T_d)^2}}{\frac{k}{f^2} + (2\pi T_d)^2} \end{aligned} \right\} \quad (3.134)$$

where  $T = M/R$ ,  $T_d = L_d/R$ .

With high frequencies and a low resistance

$$\frac{R}{f} \ll 2\pi L_q, \quad \left(\frac{R}{f}\right)^2 \ll (2\pi)^2 L_d L_q, \quad \frac{k}{f} \ll 2\pi T_d$$

and the current  $I_k$  is independent of the speed (frequency).

At low frequencies and high values of  $R$ , the short-circuit current depends on the speed (frequency), and drops when it decreases.

In aircraft electrical systems, synchronous generators can operate with frequencies varying over the range  $f_2/f_1 = 2.0-2.5$ .

The effect of frequency variation on the short-circuit current may be determined by using the relationship

$$\frac{I_{k2}}{I_{k1}} = \frac{E_{k2}}{E_{k1}} \frac{k + \beta_{d1}^2}{k + \beta_{d2}^2} \sqrt{\frac{k^2 + \beta_{d2}^2}{k^2 + \beta_{d1}^2}}$$

which, provided that  $f_2/f_1 = \bar{f}$  and

$$\frac{I_{k2}}{I_{k1}} = \frac{x_{d2}}{x_{d1}} = \frac{f_2}{f_1} = \bar{f}, \quad \frac{E'_{k2}}{E'_{k1}} = \frac{E_{k2}}{E_{k1}} = \bar{f},$$

may be written as

$$\frac{I_{k2}}{I_{k1}} = \frac{k + \beta_{d1}^2}{k\bar{f}^2 + \beta_{d1}^2} \sqrt{\frac{k^2\bar{f}^2 + \beta_{d1}^2}{k^2 + \beta_{d1}^2}} \quad (3.135)$$

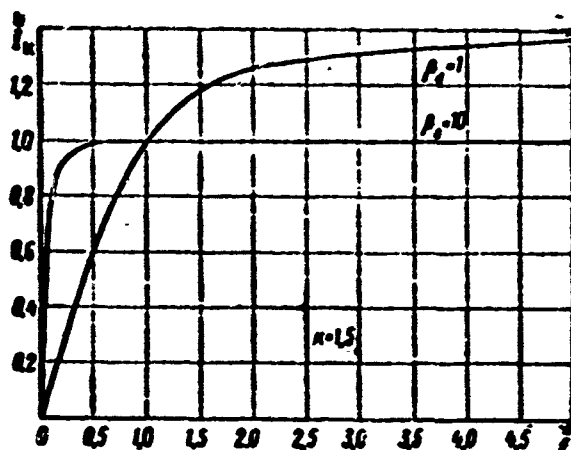


Fig. 3.52. Relative steady-state short-circuit current as a function of frequency.

Here:

$I_{k1}$  and  $\beta_{d1}$  are the short-circuit current and the relative inductance at the initial frequency  $f_1$ ;

$I_{k2}$  and  $\beta_{d2}$  are the same quantities at the changed frequency  $f_2$ .

When  $\bar{f} = (f_2/f_1) \rightarrow 0$ , the ratio  $I_{k2}/I_{k1}$  also approaches zero; when  $\bar{f} = 1$ , it approaches  $I_{k2}/I_{k1} = 1$ ; when  $\bar{f} \rightarrow \infty$ , the ratio is frequency-independent, i.e.,

$$\frac{I_{k2}}{I_{k1}} = \frac{k + \beta_{d1}^2}{k + \beta_{d2}^2}$$

Figure 3.52 gives the function  $\bar{I}_k = I_{k2}/I_{k1} = \varphi(\bar{f})$  for different values of the parameter  $\beta_d$  with  $k = 1.5$ .

If the frequency drops to half the nominal value, there will be

no decrease in the short-circuit current when  $\beta_d \geq 10$ , while where  $\beta_d = 1$ , there will be a decrease to 60% of the rated value.

If the frequency reaches twice the nominal value, there will be no change in the short-circuit current where  $\beta_d \geq 5$ . At the same time, it will increase roughly to 1.25 times the rated value when  $\beta_d = 1$ .

The short-circuit characteristic for synchronous generators intended to supply the main aircraft electrical-system line is frequency-independent over the normal range of frequency variation, since  $\beta_d > 5$  for these generators. For tachometer generators, where  $\beta_d$  may be less than five, and the frequency may change by more than a factor of two, the short-circuit characteristic does depend on frequency.

As we know, the short-circuit ratio (o.k.z.), which characterizes the steady-state short-circuit current, equals

$$\text{o. k. z.} = \frac{I_{k0}}{I_{\text{nom}}} = \frac{F_0}{F_{k.\text{nom}}} = \dot{I}_{k0} \quad (3.136)$$

where  $F_0$  is the no-load excitation magnetizing force with rated voltage across the armature winding;  $F_{k.\text{nom}}$  is the short-circuit excitation magnetizing force with rated current in the armature winding;  $I_{k0}$  is the short-circuit current for a magnetizing force  $F_0$ ;  $I_{\text{nom}}$  is the rated current.

The o.k.z. represents the number of times that the short-circuit current exceeds the rated current with no-load excitation. If we make use of the fact that when  $R = 0$ ,  $I_{k0} = U_{\text{nom}}/x_d$ , Expression (3.136) may be represented in the following form:

$$\text{o. k. z.} = \frac{I_{k0}}{I_{\text{nom}}} = \frac{\frac{U_{\text{nom}}}{x_d}}{I_{\text{nom}}} = \frac{1}{\frac{x_d}{U_{\text{nom}}}} = \dot{I}_{k0} \quad (3.137)$$

Thus, the o.k.z. equals the reciprocal of the unsaturated inductive reactance of the machine in relative units.

The o.k.z. is one important quantity characterizing the operation



TABLE 3.2

Short-Circuit Ratio for Various Types of Synchronous Machines

1 Общего применения					2 Авиационные машины	
3 неявнополюсные		4 явнополюсные			8 явнополюсные с успокоительной обмоткой	9 неявнополюсные
$2p=2$	$2p=4$	5 без успокоительной обмотки	6 с успокоительной обмоткой	7 конденсаторы		
0,5÷0,7	0,8÷1,0	0,8÷1,4	0,3÷1,4	0,4÷0,6	0,5÷0,7	0,6÷0,8

1) General-purpose; 2) aircraft machine; 3) non-salient-pole; 4) salient-pole; 5) no damper winding; 6) with damper winding; 7) condensers; 8) salient-pole with damper winding; 9) nonsalient-pole.

of a synchronous machine. Table 3.2 gives values of the o.k.z. for various types of synchronous machines.

The larger the o.k.z. and, consequently, the lower the value of  $x_d$ , the less effect the armature reaction has on machine operation. A machine with a large o.k.z. will have an external characteristic whose slope is lower, i.e., there will be less voltage variation, and it will have good overload capacity, and will be more stable in parallel operation. Thus, from the viewpoint of synchronous-machine operating characteristics, it is desirable to increase the o.k.z.

The magnitude of the o.k.z. is determined chiefly by the air-gap dimensions, since 75-85% of the excitation no-load magnetizing force  $F_0 = 0.8\delta'B_\delta k_s$  goes to force the flux through the machine air gap. When the air gap is increased, not only  $F_0$  increases, but also the short-circuit excitation magnetizing force  $F_{k.nom}$ , although the latter increases far less than  $F_0$ , and the o.k.z. thus increases.

If we assume that the machine is not saturated (Fig. 3.53), it is easy to establish the relationship between the air-gap dimensions and the magnitude of the o.k.z.

Using the notation of Fig. 3.53a, we may write

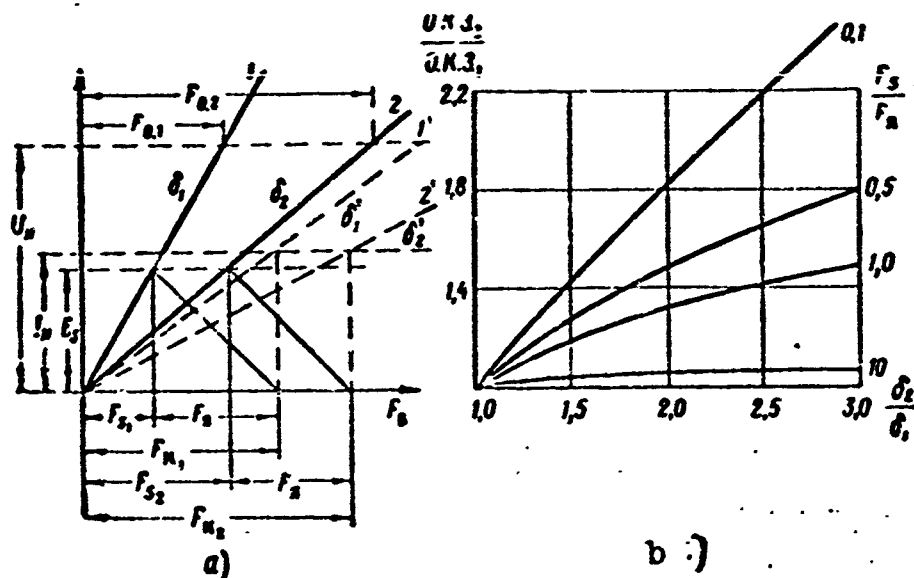


Fig. 3.53. Relationship between o.k.z. and air-gap dimensions. a: 1 and 2) No-load characteristics for gap  $\delta_1$  and  $\delta_2$ ; 1' and 2') short-circuit characteristics for gap  $\delta_1$  and  $\delta_2$ ; b) o.k.z. as a function of air-gap size for various values of  $F_s/F_{ya}$ .

$$(o. k. z.)_1 = \frac{F_{01}}{F_{s1}} = \frac{0.88_1 B_1 t_s}{F_{s1} + F_s} = \frac{1}{x_{s1}} = i_{s01} \quad (3.138)$$

For the same machine, but with an increased gap  $\delta_2$ , we obtain

$$(o. k. z.)_2 = \frac{F_{02}}{F_{s2}} = \frac{0.88_2 B_2 t_s}{F_{s2} + F_s} = \frac{1}{x_{s2}} = i_{s02} \quad (3.139)$$

The relative increase in the o.k.z. due to an increase in the air gap is found from the ratio of (3.138) to (3.139), i.e.,

$$\frac{(o. k. z.)_2}{(o. k. z.)_1} = \frac{\delta_2' F_{s1} + F_s}{\delta_1' F_{s2} + F_s}.$$

It follows from Fig. 3.53a that

$$\frac{F_{s2}}{F_{s1}} = \frac{F_{02}}{F_{01}} = \frac{\delta_2'}{\delta_1'} = \frac{\delta_2}{\delta_1};$$

and then

$$\frac{(o. k. z.)_2}{(o. k. z.)_1} = \frac{\delta_2}{\delta_1} \frac{1 + \frac{F_{s1}}{F_s}}{1 + \frac{F_{s2}}{F_s} \frac{\delta_2}{\delta_1}} < \frac{\delta_2}{\delta_1}. \quad (3.140)$$

In deriving Eq. (3.140) we assume that the reactive triangle ( $F_s$

and  $F_{ya}$ ) remained unchanged and moved parallel to itself. If we assume that  $F_{sl}/F_{ya} = 0.5$ , then when the design air gap is doubled,  $\delta_2/\delta_1 = 2$ , the o.k.z. will increase only by a factor of 1.5, while where  $F_{sl}/F_{ya} = 1$ , the increase factor will be only  $4/3$ .

The larger the ratio  $F_{sl}/F_{ya}$ , the less the o.k.z. will rise as the air gap increases.

Figure 3.53b shows the function  $(\text{o.k.z.})_2/(\text{o.k.z.})_1 = f(\delta_2/\delta_1)$  for various values of the parameter  $F_{sl}/F_{ya} = 0.1-1.0$ .

As the machine air gap increases, it is also desirable to increase the size, weight, and cost of the machine for considerations of cooling and decreasing the added losses. The power of a synchronous machine is normally limited by the excitation winding, and when the air gap increases, the excitation magnetizing force rises and, consequently, there is an increase in the volume and weight of the copper, and of the necessary cross section of the winding space. All of this leads to increased size and cost for the machine. In designing aircraft synchronous generators, the smallest possible air gap is normally selected that will provide the necessary overload handling capability for the machine. The size of the voltage variation is of secondary importance, since automatic voltage regulation is provided.

### Load Characteristic

$$U = f(I_V) \text{ or } \dot{U} = \varphi(\dot{I}_V) \text{ at } I = \text{const.}$$

As we know, the load characteristic is of greatest interest with an inductive load, i.e.,

$$U = f(I_V) \text{ at } \cos \varphi = 0 \text{ and } I = \text{const.}$$

If we know the no-load, short-circuit, and load characteristics for  $\cos \varphi = 0$ , it is possible to find the reactive triangle and, consequently, the synchronous inductance on the longitudinal axis  $x_d$  and the leakage inductance  $x_s$ .



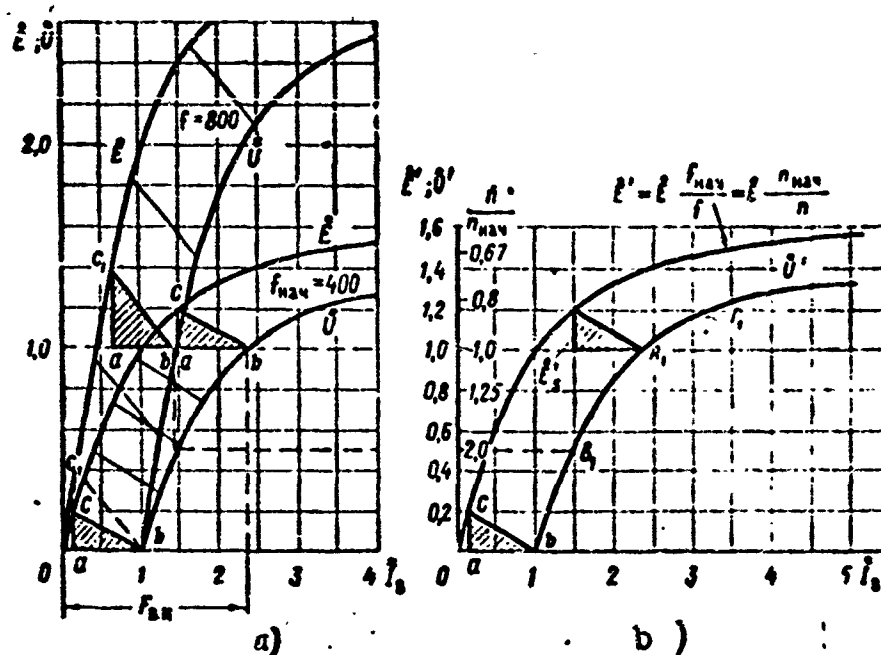


Fig. 3.55. Load characteristics. a) At frequency  $\underline{f}$  and  $2f$ ; b) reduced load characteristic.

frequency and we thus construct a reduced load characteristic (similar to the reduced no-load characteristic), i.e., the function

$$\dot{U}' = \dot{U} \frac{f_{nach}}{f} = \dot{U} \frac{n_{nach}}{n} = \varphi(\dot{I}_s) \text{ at } I = \text{const and } \cos \varphi = 0.$$

In plotting the reduced inductive load characteristic, it is necessary to take account of the fact that the altitude of the reactive triangle, which represents the voltage drop due to leakage fluxes, must be represented in the scale of the reduced voltage, i.e.,

$$\dot{E}_s' = \dot{E}_s \frac{f_{nach}}{f} = \dot{I}_s \frac{f_{nach}}{f}.$$

In this case, when the reduced reactive triangle moves so that its vertex  $\underline{c}$  slides along the reduced no-load characteristic, vertex  $\underline{b}$  describes the reduced load characteristic (Fig. 3.55b). Point  $A_1$  corresponds to rated voltage at rated load and the initial frequency. If we double the speed, the rated-voltage point  $A_1$  will begin to move downward toward the origin and will occupy a position corresponding to the speed  $n/n_{nach} = 2$  (point  $B_1$ ). If, however, the speed is dropped to 0.8 of the initial speed, the rated-voltage point will move upward and

occupy position  $D_1$ , corresponding to a speed  $n/n_{\text{mach}} = 0.6$ . Thus, the curve  $B_1A_1D_1$  is the reduced load characteristic, and is applicable to any speed.

### External Characteristic

$$U = f(I) \text{ at } I_v = \text{const}, \cos \varphi = \text{const}, \text{ and } n = \text{const}.$$

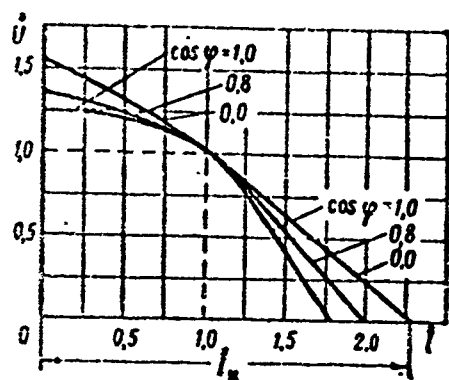


Fig. 3.56. External characteristics in relative units as a function of  $\cos \varphi$ .

Figure 3.56 gives external characteristics for a synchronous generator plotted in relative units for various power factors. The change in voltage across the generator terminals with the magnitude and nature of the load is caused by the effect of the armature reaction and the voltage drop across the resistances and reactances due to the armature-winding dissipation.

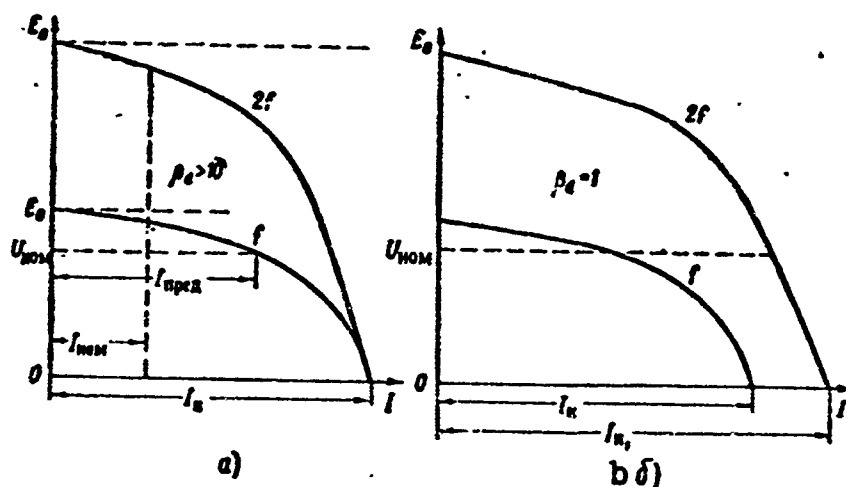


Fig. 3.57. External characteristics for different frequencies  $f$  and  $2f$ . a)  $\beta_d > 10$ ; b)  $\beta_d = 1$ ;  $I_{\text{pred}}$ ) maximum load current at rated voltage.

The rigidity of the external characteristic for synchronous machines, which is determined by the tangent of the slope angle at the x-axis, is considerably less than for similar direct-current machines with parallel excitation.

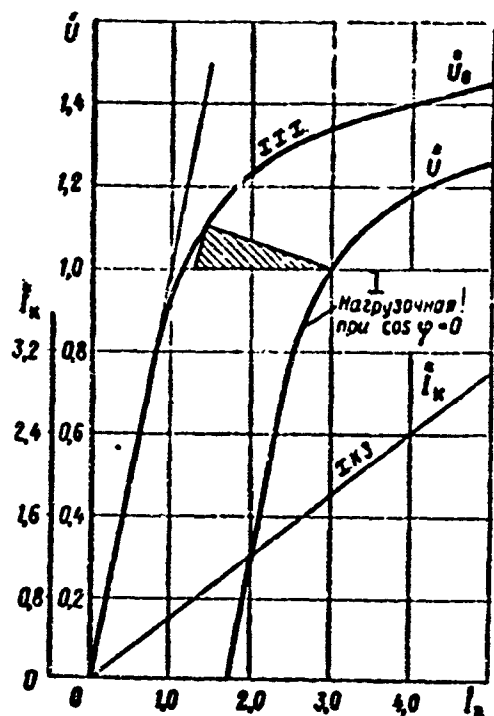


Fig. 3.58. Characteristics for three-phase synchronous aircraft generator, 40 kva, 6000 rpm, 400 cps,  $\cos \varphi = 0.75$ .  
1) Load curve,  $\cos \varphi = 0$ .

In synchronous machines, the voltage increase occurring with a drop in the inductive load ( $\cos \varphi = 0.8$ ) reaches 50%, while in direct-current machines, it does not exceed 15%. This is explained by the fact that the armature magnetizing force in direct-current machines, with the brushes located at the geometric neutral plane, does not buck the main excitation field very much, while in alternating-current machines, the effect of the armature reaction is large, and is greater the lower  $\cos \varphi$ . Considering all of this, we note that all other conditions being equal, in direct-current

machines the magnitude of the excitation magnetizing force and, consequently, the weight of the field winding will be greater than for direct-current machines.

Effect of speed on the external characteristic. When the speed increases, the armature emf rises in proportion to  $n$ , and the initial point (at  $I = 0$ ) for the external characteristic moves upward along the y-axis. The new emf value will be  $E_{02} = E_{01}(f_2/f_1)$ . It is assumed that the excitation current does not depend on the speed.

The point at which the characteristic bends ( $U = 0$ ), corresponding to the short-circuit current, remains unchanged at high values of  $\beta_d$ , while at small values of  $\beta_d$ , it moves to the right along the x-axis. Figure 3.57 shows the way in which the external characteristics change with a speed variation of  $n_2:n_1 = 2:1$  for machines with  $\beta_d > 10$  and  $\beta_d = 1$ .

If the ratio  $U/f = \text{const}$  remains unchanged when the frequency varies, the magnetic load on the machine will remain unchanged, and the relative change in voltage will not depend on frequency. In this case, it is possible to plot a reduced external characteristic that does not depend on the generator speed, in the form of the function

$$\dot{U}' = \dot{U} \frac{f_{\text{ннч}}}{f} = \dot{U} \frac{n_{\text{ннч}}}{n} = \varphi(I)$$

for various values of the parameter  $\cos \varphi$ , as we have done previously for the reduced no-load and load characteristics. If, however, the voltage across the generator terminals remains constant when the speed (frequency) changes, the degree of magnetic-system saturation will drop as the speed goes up and, consequently, the external characteristic will depend on the frequency, and will have to be plotted for each actual value of the frequency.

To conclude, we have shown the characteristics of a 40-kva three-phase synchronous aircraft generator in Fig. 3.58.

### 3.6. SINGLE-PHASE SYNCHRONOUS GENERATORS

Single-phase current is used in special cases: in aviation, railway transportation, high-frequency induction heating; in agriculture, for household appliances, etc. The basic advantage to single-phase current is the reduced number of wires, which is especially important in aviation. In aviation, single-phase synchronous generators are used chiefly in direct-alternating current converters.

The theory of single-phase machines is used to analyze unbalanced or single-phase operating modes for multiphase machines (phase failure, unbalanced short circuit, etc.), and in this respect, it is rather general in nature.

#### Construction

Single-phase synchronous generators are similar in construction



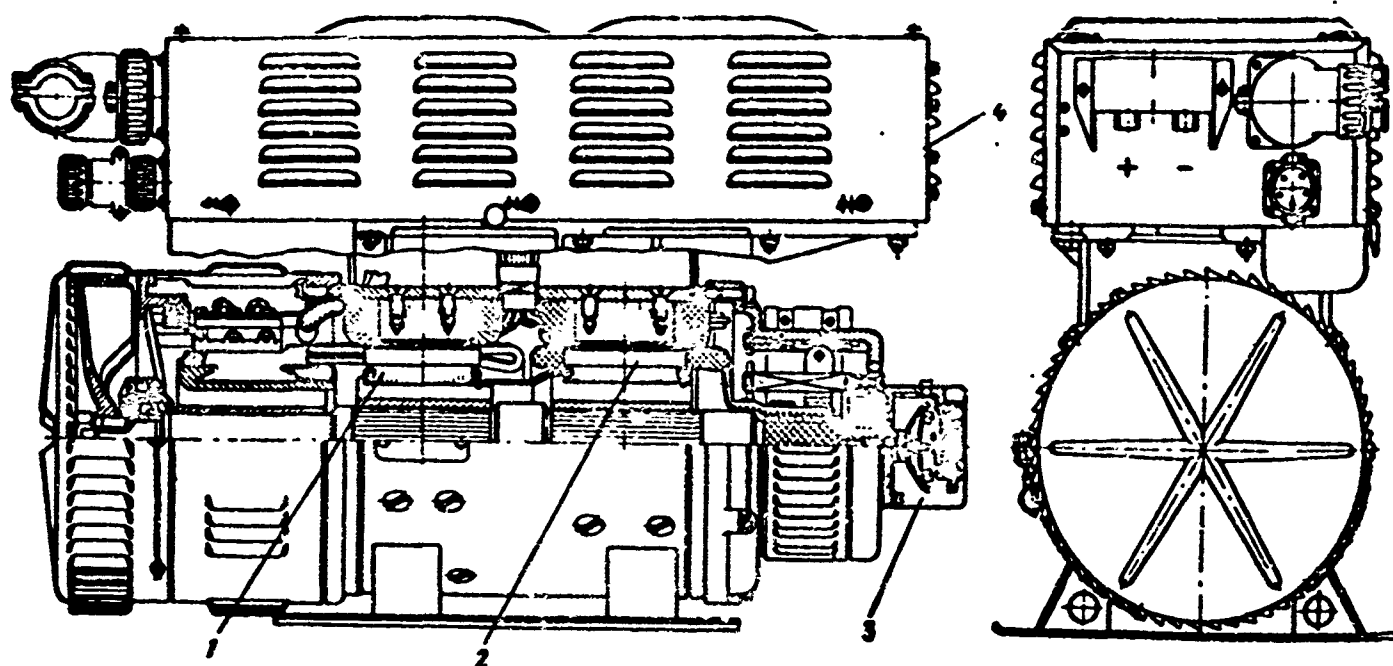


Fig. 3.59. Direct-current aircraft converter. Output: single-phase alternating current at 400 cps, 4500 va power, 115 v,  $\cos \varphi = 0.9$ ,  $n = 8000$  rpm. 1) Direct-current motor; 2) single-phase generator; 3) centrifugal switch; 4) control apparatus.

to three-phase machines in the salient-pole or nonsalient-pole versions. Single-phase salient-pole generators are made with either internal rotating poles, or with external stationary poles, as in the case of direct-current machines.

Figure 3.59 shows the construction of an aircraft converter using a single-phase six-pole synchronous generator with external poles, 4500 va power, 115 v, 400 cps.

The armature is similar to the armature of a three-phase machine, but it has a single-phase (one- or two-layer) winding that occupies about 70% of the region surrounding the armature surface. Thus, about 1/3 of the slots do not carry the winding.

Three-phase machines are frequently used as single-phase machines, with only two of the three phases employed. Figure 3.60 shows a diagram of a single-phase armature winding for a single-phase aircraft generator.

It is pointless to make further use of the armature surface for

placement of the winding, since there is only a slight gain in power for a considerable increase in the weight of the copper. The slots not filled with the winding may be used as axial ventilation ducts.

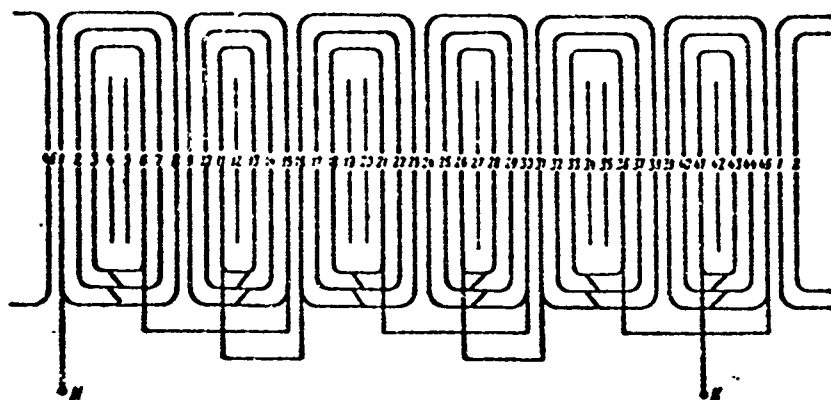


Fig. 3.60. Winding of six-pole single-phase aircraft generator (number of slots,  $z_p = 45$ , of which  $6 \cdot 6 = 36$  are filled).

The pole system of a single-phase machine is similar to that of a three-phase machine, with the exception of the short-circuited damper winding, whose purpose and peculiarities are explained below.

#### Utilization of Three-Phase Machine in Single-Phase Operation

Voltage. Two connections are possible for the armature windings:

a) two phases connected in series; one phase not used; in this case, two-thirds of the armature surface is used, and the voltage across the terminals of the single-phase machine will equal the line voltage of the three-phase machine;

b) all three phases connected in series. In this case, 100% of the armature surface is used, and the voltage across the terminals of the single-phase machine will equal twice the per-phase voltage of the three-phase machine.

Thus, when all three phases are used, 50% more copper is used in the armature, and the voltage rises by only 15.6%. Figure 3.61 shows possible connections for a three-phase winding for single-phase operation.

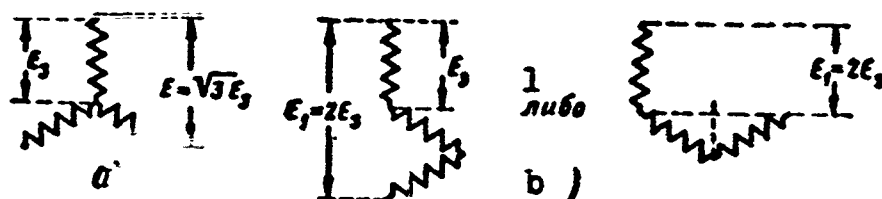


Fig. 3. Possible connections of three-phase winding for single-phase operation. a) Two phases connected in series; b) three phases connected in series;  $E_1$ ) emf across terminals of single-phase machine;  $E_3$ ) phase emf for three-phase machine; 1) or.

**Power.** The degree of utilization of a three-phase machine employed as a single-phase machine depends on the machine operating mode. Where a three-phase machine is used as a single-phase machine, we may keep either the current or the losses in the armature winding unchanged. In the first case, the power of the single-phase machine, with the flux and armature current constant, and two-thirds of the armature surface filled by the winding, is determined from the following relationships:

on the basis of Fig. 3.61, the single-phase power delivered is

$$S_1 = E_1 I = \sqrt{3} E_3 I;$$

and the three-phase power delivered is

$$S_3 = 3 E_3 I;$$

the ratio of the powers is

$$\frac{S_1}{S_3} = \frac{\sqrt{3}}{2} = 0.58.$$

i.e., the degree of utilization of a three-phase model operated as a single-phase machine is 58% when the current in the armature winding remains unchanged.

In the second case, the armature losses are constant and, consequently, the armature current may increase considerably. Using the condition that the losses in the armature winding remain equal, we obtain a new current in single-phase operation, i.e.,

$$P_{a1} = P_{a3} \text{ or } 2I_1^2 R = 3I_3^2 R,$$

and the ratio of the currents for the various armature-copper losses will then be

$$\frac{I_1}{I_3} = \sqrt{1.5} = 1.225.$$

The ratio of the powers in the single-phase ( $P_1$ ) and three-phase ( $P_3$ ) modes with two-thirds of the armature surface used, where

$$S_1 = E_1 I_1 = \sqrt{3} E_3 \cdot 1.225 I_3 \approx 2.13 E_3 I_3$$

and

$$S_3 = 3 E_1 I_1,$$

will clearly equal

$$\frac{S_1}{S_3} = \frac{2.13}{3} = 0.707,$$

i.e., the degree of utilization of a three-phase model used as a single-phase machine will be 70% where the armature-winding losses remain unchanged.

For low-voltage synchronous machines the temperature drop in the insulation is small, and the copper temperature is determined by the total armature losses. Consequently, in this case the degree of utilization of a three-phase machine in single-phase operation equals about 70%. In high-voltage machines, the temperature drop in the insulation is considerable, and thus its degree of utilization in single-phase operation is somewhat lower, lying in the

$$S_1 = (0.7-0.58) S_3$$

range.

When all three phases of the armature winding are used, and the armature current is kept unchanged ( $I_1 = I_3 = I$ ), the power developed by the machine in single-phase and three-phase operation will equal

$$S_1 = E_1 I_1 = 2 E_3 I \text{ and } S_3 = 3 E_3 I.$$

In this case the power ratio will be

$$S_1/S_3 = 2/3 \approx 0.67,$$

which is 15.5% ( $0.67/0.58 = 1.155$ ) greater than in the case in which only two armature-winding phases are used.

Where three phases are used, the armature current cannot increase, since in this case the losses in the windings would be the same for the single- and three-phase versions. Thus, where three phases are used, the machine utilization with respect to power rises by 15.5%, while the weight of copper increases by 50%.

If we proceed on the basis of the fact that the number of gaps utilized in the single-phase machine amounts in general to a fraction  $\gamma$  of the total number of slots, the total number of turns (conductors) in the armature will equal

$$w_{s1} = \gamma m w_s \text{ or } N_{s1} = \gamma N_{s2} \quad (3.141)$$

Provided that the losses in the armature of the single- and three-phase machines are identical, the current in the single-phase machine will be determined by the equation

$$I_1 = \frac{I_2}{\sqrt{\gamma}}. \quad (3.142)$$

Taking (3.141) and (3.142) into account, the linear load on the single phase synchronous machine is found in the form

$$A_1 = \frac{2I_1 w_1}{\pi D} = \frac{2mI_2 w_2}{\pi D} \sqrt{\gamma} = A_2 \sqrt{\gamma}. \quad (3.143)$$

Thus, the line load on a single-phase machine in terms of the entire armature perimeter is reduced by the factor  $\sqrt{\gamma}$ .

In this case, the linear load per tooth carrying the winding increases by a factor of  $1/\sqrt{\gamma}$ , i.e.,

$$A'_1 = \frac{I_{s1}}{z_s} = \frac{I_{s2}}{z_s \sqrt{\gamma}} = \frac{A_2}{\sqrt{\gamma}}, \quad (3.144)$$

where the subscript "p" refers to a slot.

The diameter and length of the armature for a single-phase machine is found from the basic design equation

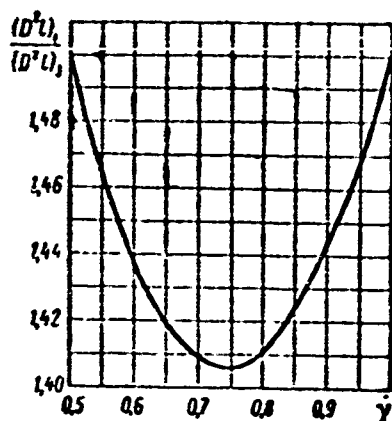


Fig. 3.62. Relative armature volume for single-phase synchronous generator as a function of the degree to which the winding fills the armature with losses in the armature winding of the single- and three-phase machine held the same.

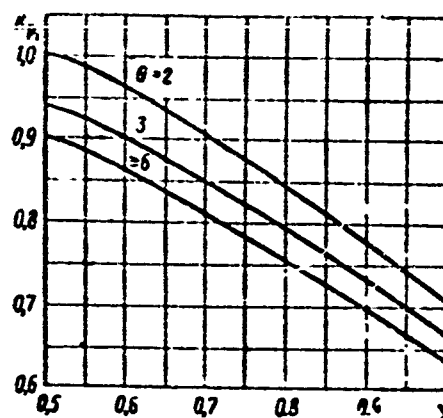


Fig. 3.63. Distribution factor for single-phase winding.

$$D = \sqrt[3]{\frac{S_e}{\pi \lambda \sigma_1}} \quad \text{or} \quad D^2 l = \frac{S_e}{\pi \sigma_1}.$$

Here  $S_e$  is the electromagnetic power, va;  $\lambda = l/D$  is the ratio of the armature length to the armature diameter;  $\sigma_1 = 1.65 k_f k_{01} \alpha B_\delta A_1 10^{-9}$  differs from the corresponding value for a three-phase machine in the size of the winding factor  $k_{01}$  and in the linear load.

The relative volume of a single-phase machine armature is greater than that for a three-phase armature, all other conditions remaining equal, by the ratio

$$\frac{(D^2 l)_1}{(D^2 l)_3} = \frac{\sigma_3}{\sigma_1} = \frac{k_{p3}}{k_{p1}} \frac{A_3}{A_1} = \frac{k_{p3}}{k_{p1}} \frac{1}{\sqrt{3}}.$$

Since the distribution coefficients for the single-phase and three-phase windings may be represented in the form

$$k_{p1} = \frac{\sin 90\gamma}{\gamma \sin \frac{90}{\theta}},$$

$$k_{p3} = \frac{1}{2q \sin \frac{30}{q}} = \frac{1.5}{\theta \sin \frac{90}{\theta}},$$

where  $\theta = m\alpha$  is the number of slots per pole, while the ratio of the distribution coefficients may be represented as

$$\frac{k_{p2}}{k_{p1}} = \frac{1.5\gamma}{\sin 90\gamma}.$$

it can be found that

$$\frac{(D^2I)_1}{(D^2I)_2} = \frac{1.5\sqrt{1}}{\sin 90\gamma} > 1.$$

Figure 3.62 shows the degree to which the armature volume increases for a single-phase machine as a function of  $\gamma$ , while Fig. 3.63 shows the function  $k_{p1} = f(\gamma)$  for various values of  $\theta$ .

It follows from Fig. 3.62 that where the armature-winding losses are unchanged, the minimum armature volume for a single-phase machine will occur at  $\gamma = 0.75$ .

Thus, when  $\gamma$  is increased above 0.75, an increase in the weights of the armature and copper will result.

### Armature Reaction

We shall henceforth consider only the basic space wave for the armature magnetizing-force curve.

When current flows through a single-phase armature winding, it forms in the machine air gap a sinusoidal distribution of the magnetizing force, fixed in space, and pulsating in time in accordance with a sine law. At the same time, the field due to the excitation magnetizing force rotates in space. Thus, the problem of the armature reaction for a single-phase machine reduces to establishing the relationship between the pulsating armature magnetizing force and the rotating pole magnetizing force.

The solution to this problem involves decomposing the pulsating armature field into two fields each with half the amplitude, rotating in phase in opposite directions at the same speed.

The equation for the pulsating space wave of the armature-winding

magnetizing force, formed by the first time harmonic of the current may be represented as the sum of two rotating fields

$$F_x = F_{a1} \sin \omega t \cos x \frac{\pi}{\tau} = \frac{F_{a1}}{2} \sin \left( \omega t - x \frac{\pi}{\tau} \right) + \frac{F_{a1}}{2} \sin \left( \omega t + x \frac{\pi}{\tau} \right). \quad (3.145)$$

Here the field  $F_{ya1}/2 \sin (\omega t - x(\pi/\tau))$ , rotating synchronously, forms the armature reaction for the single-phase machine.

It is stationary with respect to the pole winding, as in the case of the armature reaction of a multiphase machine. The field rotating in the opposite direction

$$\frac{F_{a1}}{2} \sin \left( \omega t + x \frac{\pi}{\tau} \right)$$

induces into the pole system an emf and a current at twice the frequency, as in the case of the emf and currents in a short-circuited transformer secondary.

As a rule, in order to eliminate (quench) the reverse field, damper windings are used at the poles, and only the synchronous field is considered, as is done for multiphase machines. In this case, the armature magnetizing-force amplitude will equal

$$F_a = \frac{F_{a1}}{2} = 0.45 \frac{I_1 w_1}{p} k_{01}. \quad (3.146)$$

Clearly, the sum of the two oppositely rotating fields will yield a pulsating field that is initially stationary in space (time-varying).

#### Opposing Synchronous Armature Field in Single-Phase Machine

The opposing synchronous field, rotating with doubled speed with respect to the pole system, induces emf's and currents at twice the frequency in the field winding, pole iron, and damper windings. In accordance with Lenz' law, these currents will form a flux directed counter to the opposing field, thus reducing its magnitude.

If the machine is of the salient-pole type, the double-frequency field in the excitation winding and pole steel decreases the opposing



armature field only when its axis coincides with the longitudinal axis of the machine, i.e., with the pole axis. When the axes of the armature and excitation-winding opposing fields are  $\pi/2$  apart, the bucking effect of the excitation-winding fields vanishes, and the effect of the pole-iron fields decreases considerably. Thus, the opposing armature field pulsates in time as it rotates.

With nonsalient-pole machines, the effect of the fields on the pole-steel currents does not depend on the position of the armature opposing field and their time pulsations will be reduced.

Eddy currents at twice the frequency in the iron and the excitation winding increase losses, reduce machine efficiency, and raise the temperature of the machine, especially that of the pole surfaces. In addition, the alternating currents flowing in the excitation circuit impair exciter commutation, where used.

When the excitation winding is opened, overvoltages appear owing to the large number of turns that may reach 20 or 30 times the excitation voltage, which may cause the excitation-winding insulation to break down.

#### Shape of the Armature Voltage Curve

The armature opposing field will cause an alternating-current component at the double frequency,  $I_{per}$ , to be added to the direct excitation current  $I_{v.post}$ . Both of these currents will form the resultant excitation current.

The instantaneous value of the resultant pulsating excitation-winding will equal (Fig. 3.64a)

$$i_s = I_{s.nocr} + \sqrt{2} I_{sep} \sin 2\omega t. \quad (3.147)$$

The actual value of the pulsating excitation-winding current will be

$$I_s = \sqrt{I_{s.nocr}^2 + I_{sep}^2}. \quad (3.148)$$

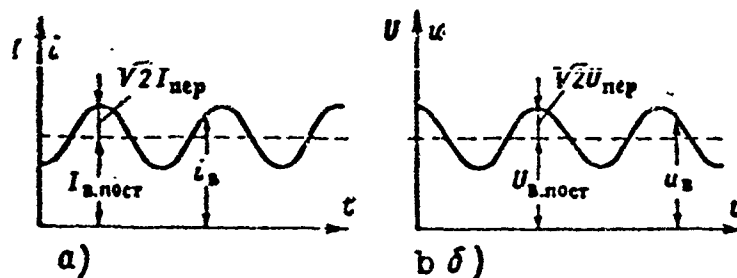


Fig. 3.64. Currents and voltages in excitation winding in the presence of a synchronous opposing field. a) Current curve; b) voltage curve.

In like manner, we also find the voltage across the terminals of the excitation winding (Fig. 3.64b)

$$U_s = \sqrt{U_{nocr}^2 + U_{nep}^2} \quad (3.149)$$

The losses in the excitation winding are determined, in this case, by the equation

$$P_s R_s = (I_{nocr}^2 + I_{nep}^2) R_s \quad (3.150)$$

They are greater than the losses due to the direct current by a factor of

$$\left(\frac{I_s}{I_{nocr}}\right)^2 = 1 + \left(\frac{I_{nep}}{I_{nocr}}\right)^2 \text{ times.}$$

No load. Under no-load conditions, a direct current  $I_{v.post}$  flows in the excitation winding, while a sinusoidal emf is induced in the armature winding. There is no double-frequency current in the excitation winding.

Load. In a multiphase system, the power developed by the generator will be constant, while in a single-phase machine, the power will pulsate at double the line frequency, as does the current flowing in the machine.

In a single-phase machine, the armature current reacts on the rotating inductor field only by means of the alternating fields; as a result, higher harmonics appear in the pole system; if odd harmonics appear in the armature, even harmonics will appear in the excitation

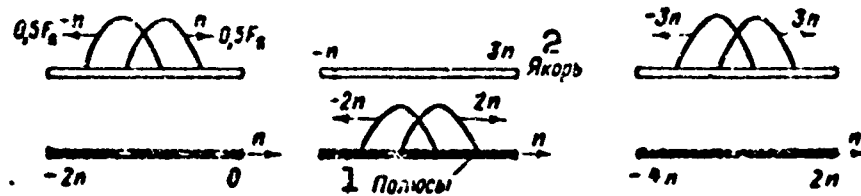


Fig. 3.65. Diagram showing even harmonics induced in excitation circuit and odd harmonics induced in armature circuit. 1) Poles; 2) armature.

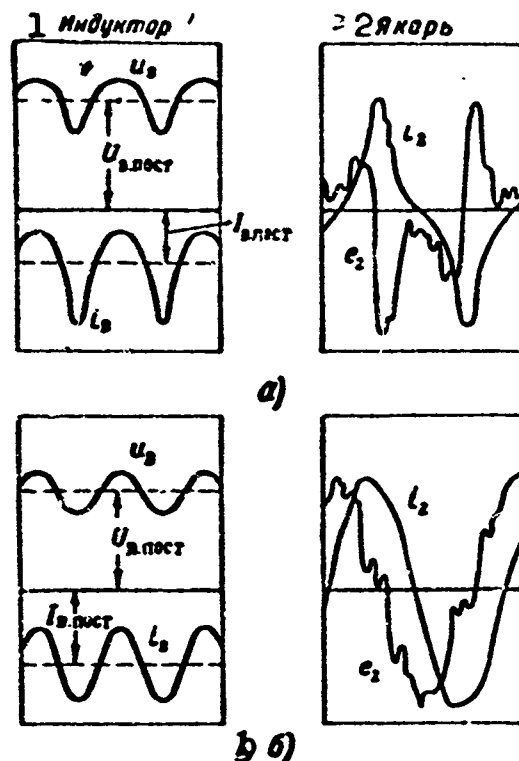


Fig. 3.66. Current and voltage curves in excitation and armature circuits for two-pole short circuiting of nonsalient-pole single-phase synchronous machine with laminated-steel rotor. a) No damper winding; b) rotor with transverse damper winding. 1) Inductor; 2) armature.

circuit.

In fact, the opposing armature field forms in the pole system a single-phase alternating field at twice the frequency that is stationary with respect to the pole system. The single-phase field of the pole system may be split into two rotating fields each with half the amplitude, one rotating in the direction of rotation of the poles, and

the other going in the opposite direction. Both fields appear to have twice the synchronous speed with respect to the poles, i.e., the rotor field has a speed relative to the armature of  $2n + n = 3n$ .

Figure 3.65 shows a diagram of the higher harmonics induced in the stator and rotor circuits. The triple-frequency emf's and currents of the armature induce the fourth harmonics of the emf and current into the pole system, and the latter in turn induce fifth harmonics of the emf and current into the armature, etc.

As a result, the emf curve for the armature departs sharply from sinusoidal shape owing to the superposition of the higher harmonics. The emf and current curves are more distorted the greater the relative armature current. With a short circuit, the current-curve distortion is at its greatest. Allowing for all of this, single-phase machines normally employ special short-circuited low-resistance windings located in the longitudinal pole axis. These windings, called damper windings, are designed to eliminate the armature opposing fields. They free the excitation winding from the first-harmonic currents.

Figure 3.66 shows voltage and current curves for a single-phase machine with a damper winding and without a damper winding.

Thus, the opposing rotating armature field causes an increase in losses, reducing efficiency (by several percent); it leads to a distortion in the voltage-curve shape and to overvoltages in the excitation winding (when it is opened).

#### Voltage Vector Diagram

When a damper winding is used, the vector diagram for a single-phase machine is similar to that of a multiphase machine. A standard method is used to allow for the armature reaction, depending on whether salient or nonsalient poles are used. It must be remembered that the resistance and inductive reactance of a single-phase winding are larger

than the corresponding quantities for a multiphase machine. This increase is due to the effect of remnants of the double-frequency opposing synchronous field.

In plotting a vector diagram for a single-phase machine, it is necessary to allow for the inductive reactance of the opposing phase movement  $x_2$ , which is included in the leakage inductance. Thus, the internal machine emf is determined by the equation

$$E = \sqrt{(U \cos \varphi + RI)^2 + (U \sin \varphi + x_s I + x_2 I)^2} \quad (3.151)$$

Consequently, a single-phase machine should have a somewhat larger magnetic flux than an analogous three-phase machine.

#### Damper Windings

There are two basic designs for short-circuited damper windings which are generally made in accordance with the Dolivo-Dobrovolskiy "squirrel cage" design (Fig. 3.67).

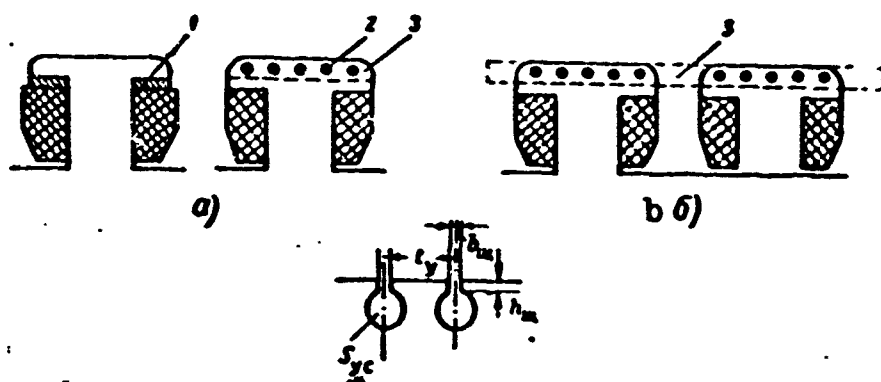


Fig. 3.67. Basic types of damper elements. a) Incomplete; b) complete; 1) short-circuited turn; 2) rods of the element; 3) connecting arcs.

Incomplete squirrel cages (Fig. 3.67a) are placed only on the longitudinal machine axis at the poles, and are not connected together electrically. A variation of the incomplete damper winding has a short-circuited turn located under the pole piece. These elements eliminate only the longitudinal component of the opposing field.

Complete squirrel cages (Fig. 3.67b) are located at the poles and

are connected together by shorting rings. These elements are better, since they eliminate both the longitudinal and transverse components of the opposing field.

It is possible to use combination damper windings consisting of open- or short-circuited elements and a turn under the pole piece.

In single-phase machines, complete damper windings are normally used.

Where damper windings are used, the pole pieces should be laminated, so that the damping eddy currents flow only in the damper winding, and do not cause additional losses in the pole piece.

The resistance of the damper winding should be as small as possible in order to decrease losses in the winding owing to the double-frequency currents, which flow constantly.

In addition, the resistance should be considerably less than the inductive reactance of the unit, so that the currents remain at an angle of  $\pi/2$  away from the induced emf's and, consequently, the flux due to them will be  $180^\circ$  out of phase with the armature opposing flux.

The impedance of the unit  $z_u$  should be small so that the currents carried by it will be adequate to compensate the armature opposing field and so that the excitation winding will be freed from double-frequency currents, which is possible provided that  $R_v \ll z_v$ .

This entails the requirement for the least possible resistance and the limitation on the impedance of the damper winding, i.e., the limitation on dissipation.

Several recommendations may be made regarding the design of damper windings.

1. The tooth pitch  $t_u$  for a damper winding should equal roughly the tooth pitch of the armature winding  $t_1$  in order to decrease losses, i.e.,

$$t_y \approx t_1 = \frac{\pi D}{z}$$

where  $z$  is the number of armature slots.

Consequently, the total number of damper-winding rods should equal the number of armature slots required for the complete pole arc of the machine, i.e.,  $N_u = \alpha z$  ( $\alpha$  is the pole coverage factor).

In synchronous motors, where the damping unit is designed for induction starting, the tooth pitch  $t_u$  should differ by 10-15% from  $t_1$  in order to avoid the phenomenon of "sticking."

2. The slot dimensions for the damper winding are normally dictated by the rod cross section; the rod is normally made of uninsulated ground copper. The slots and, consequently, the winding must be placed as close as possible to the air gap — at the surface of the pole piece.

In aircraft generators, the number of slots (rods) per pole varies normally from 3 to 7. It is preferable to use an odd number of slots per pole. In order to decrease the reactance of the unit, the height of the slot opening crosspiece  $h_{shch}$  should be as small as possible (0.2-0.3 mm), and the width of the opening as large as possible with respect to the size of the rod. The width of the damper-winding slot opening is limited by the increase in the air-gap factor  $k_g$  and the rise in the pulsating losses at the pole surface and in the armature teeth. If the pole pieces are beveled one tooth division, there is a sharp decrease in the tooth harmonics. It is recommended that the end rods of a damping unit be placed as close as possible to the edges of the pole piece.

3. Depending on the type of damper winding and the machine characteristics, the current in the damper winding will be determined by the following equations:

a) Complete short-circuited winding. The currents in a rod and in

the shorting ring equal, respectively,

$$I_{y,c} \approx 0,83 \frac{M_y}{e} [\text{amp}]; I_{y,r} \approx 0,26 A_c [\text{amp}]. \quad (3.152)$$

b) Incomplete short-circuited winding. In this case, the currents are not uniformly distributed, and there is a minimum at the pole axis and a maximum at the edges of the pole piece. The currents in the edge and center rods will be, respectively,

$$\left. \begin{aligned} I_{y,up} &= 1,26 \frac{M_y}{e} [\text{amp}] \\ I_{y,cp} &= 0,46 I_{y,up} [\text{amp}]. \end{aligned} \right\} \quad (3.153)$$

The current in the short-circuited turn may be found, in approximation, from the equation

$$I \approx 0,2 \tau A [\text{amp}]. \quad (3.154)$$

Where combination damper windings are used (a cage at the pole plus a turn under the pole piece or a complete cage plus a turn under the pole piece) the current in the rods (connecting rings) will decrease, depending on the relationship between the dimensions of the cage and the turn owing to the fact that the turn under the pole piece is less effective than a cage on the pole piece.

4. The current density in the damper winding of a single-phase machine is selected with an allowance for the operating mode, cooling system, and energy losses in the winding, since current flows continuously through the winding during operation.

Owing to space limitations, increased current densities are allowed in aircraft single-phase generators; thus for selfcooled generators

$$j_u = (15-20) \text{ amp/mm},$$

and for generators cooled by forced air

$$j_u = (20-25) \text{ amp/mm}.$$



Finally, in general-purpose machines

$$j_u = (5-10) \text{ amp/mm.}$$

5. The cross section for rods and connecting arcs may be found by dividing the corresponding current by the permissible current density.

As a rule, the total rod cross section for a damper winding amounts to (20-30)% of the total armature-winding cross section, while the connecting-arc cross section is about 45% of the rod cross section for each pole, i.e.,

$$\sum S_{y,c} = N_y S_{y,c} = (0,2 + 0,3) \sum S_a = (0,2 + 0,3) 2w S_{a,a}$$

or

$$S_{y,c} = \frac{0,4 + 0,6}{N_y} w S_{a,a}. \quad (3.155)$$

The rod cross section for each pole will then equal

$$\frac{\sum S_{y,c}}{2p} = (0,2 + 0,3) \frac{A_c}{j_c},$$

while the connecting-arc cross section will be

$$S_{y,a} = (0,4 + 0,5) \frac{N_y}{2p} S_{y,c} = (0,4 + 0,5) \frac{\sum S_{y,c}}{2p}. \quad (3.156)$$

6. The degree to which the opposing field is canceled may be found approximately from the equation

$$k_{ms} = \frac{10^6 \lambda_p}{\tau^2 + t_y \lambda_p}, \quad (3.157)$$

where  $\lambda_p = 0.66 + (h_{shch}/b_{shch})$  (for the circular slots of Fig. 3.67).

It follows from (3.157) that the opposing field will be canceled out more the smaller the air gap  $\delta$ , the tooth pitch  $t_u$ , and the leakage conductance of the slot  $\lambda_p$ .

In nonsalient-pole machines, a damper winding is formed by means of a system of wedges and side retaining rings (caps) that lock in the wedges.

Occasionally, copper strips are placed under the wedges, and a cylindrical copper jumper under the retaining rings; thus, a short-

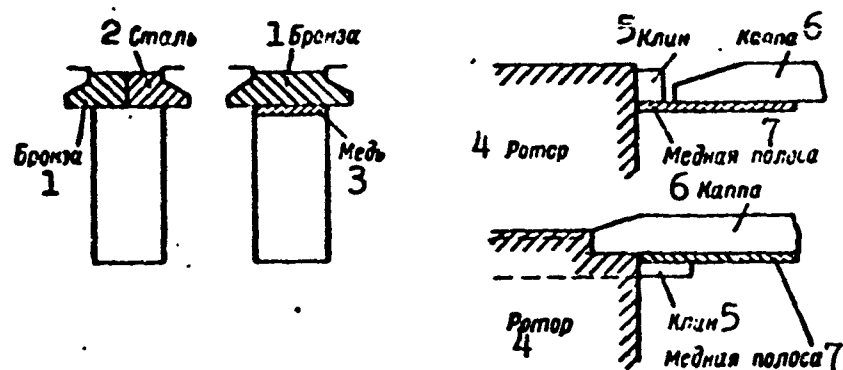


Fig. 3.68. Damper cages for nonsalient-pole machines. 1) Bronze; 2) steel; 3) copper; 4) rotor; 5) wedge; 6) cap; 7) copper strip.

circuiting cage is formed on the rotor under the wedges and caps. Specially formed slots in the central teeth (poles) of the rotor may be used to form the damper cage; copper rods are laid in the slots. Contact between the rods is completed through the rotor faces, as is clear from Fig. 3.68.

The effect of dampers on a single-phase nonsalient-pole generator is characterized by the experimental data of Table 3.3.

TABLE 3.3

Effect of Dampers on Additional Losses and Temperature of Pole Pieces

1 Мощность квд	2 Полюсный наконечник	3 Без успокоителей		4 С успокоителями	
		5 Добавочные потери %	6 Температура наконечника °C	5 Добавочные потери	6 Температура наконечника °C
750	7 Спаяной	3,75	95	0,8	34
1000	8 .	3,00	122	0,5	37
1000	Шихтованный	3,80	150	0,3	18

1) Power, kva; 2) pole piece; 3) no damper; 4) with dampers; 5) additional losses, %; 6) pole-piece temperature, °C; 7) solid; 8) laminated.

Analysis of the data given shows that the use of dampers with a solid (forged) rotor causes a drop in the additional losses by a factor of 4.75-6, and a threefold decrease in the pole-piece temperature. If a laminated rotor is used in place of the solid rotor, there will

be a further decrease in the additional losses and in the pole-piece temperature. The use of steel laminations in place of the forging increases the additional losses and pole-piece temperature rise in the absence of the dampers.

Thus, where a damper winding is used, it is best to employ a laminated rotor, and a solid rotor should be used in the absence of a damper.

In conclusion, we should note that the majority of aircraft DC-AC converters are of the single-phase type. The series of aircraft converters uses various types of single-phase synchronous generators: classical machines with electromagnetic excitation, inductor generators, and permanent-magnet generators.

These generators are driven by direct-current motors that are manufactured together with the generators in a single housing.

Manu-  
script  
Page  
No.

[Footnote]

252 From this point on, we shall depart from the generally accepted notation, and use the symbol " $\wedge$ " for the complex conjugate, in order to avoid confusion with the notation for relative quantities.

[List of Transliterated Symbols]

184	nom = nom = nominal'nyy = rated
186	m = m = med' = copper
186	c = s = stal' = steel (iron)
186	mex = mekh = mekhanicheskiy = mechanical
187	n = n = naruzhnyy = outside
187	n = p = paz = slot
187	y = ya = yarmo = yoke

187  $\pi = p = \text{polyus} = \text{pole}$

197  $\text{H.c} = \text{n.s} = \text{namagnichivayuchshaya sila} = \text{magnetizing force}$

199  $\text{OBF} = \text{OVG} = \text{obmotka возбuzhdeniya generatora} = \text{generator field winding}$

199  $p = r = \text{regulyator} = \text{regulator}$

199  $\Gamma = G = \text{generator} = \text{generator}$

199  $\text{S.c} = \text{b.s} = \text{bortset'} = \text{on-board line}$

199  $\text{K.K} = \text{K.K} = \text{kontaktryye kol'tsa} = \text{slip rings}$

200  $\text{B} = \text{v} = \text{vozbuditel'} = \text{exciter}$

200  $\text{OBB} = \text{OVV} = \text{obmotka возбuzhdeniya vozbuditelya} = \text{exciter field winding}$

200  $\text{PB} = \text{PV} = \text{podvozbuditel'} = \text{pilot exciter}$

200  $\text{OBPB} = \text{OVPV} = \text{obmotka возбuzhdeniya podvozbuditelya} = \text{pilot exciter excitation winding}$

202  $\text{H} = \text{n} = \text{nachal'nyy} = \text{initial}$

202  $\text{K} = \text{k} = \text{konechnyy} = \text{final}$

202  $\text{ГОСТ} = \text{GOST} = \text{Gosudarstvennyy obshchesoyuznyy standart} = \text{State All-Union Standard}$

202  $a, b, c, d = a, b, c, d \text{ as in Fig. 3.14}$

204  $\text{c.B} = \text{s.v} = \text{set'}, \text{vozбuzhdeniye} = \text{line, excitation}$

205  $\text{T} = \text{T} = \text{transformator} = \text{transformer}$

205  $\text{M.B} = \text{m.v} = \text{med'}, \text{vozбuzhdeniye} = \text{copper, excitation}$

205  $\text{B.п} = \text{v.p} = \text{vypryamitel'}, \text{postoyannyy} = \text{rectifier, direct-current}$

205  $\text{M.B} = \text{m.v} = \text{med'}, \text{vozбuzhdeniye} = \text{copper, excitation}$

205  $\text{tp} = \text{tr} = \text{transformator} = \text{transformer}$

205  $\text{r.p} = \text{g.r} = \text{generator, raschetnyy} = \text{generator, design}$

206  $p = r = \text{raschetnyy} = \text{design}$

206  $\text{M.B} = \text{m.v} = \text{med'}, \text{vspomogatel'nyy} = \text{copper, auxiliary}$

209  $\text{выпр} = \text{vypr} = \text{vypryamitel'} = \text{rectifier}$

212  $\text{ост} = \text{ost} = \text{ostatochnyy} = \text{residual}$

212	н = n = normal'nyy = normal
212	м = m = magnit = magnet
214	ТС = TS = transformator, stabiliziruyushchiy = stabilizing transformer
230	CB = SV = sinkhronnyy vozbuditel' = synchronous exciter
230	рег = Reg = <i>рег</i> = regul'yator = regulator
230	МЕНБ = MEPV = magnitoelektricheskiy podvozbuditel' = magneto-electric pilot exciter
232	ГГ = SG = sinkhronnyy generator = synchronous generator
236	K = K = kollektor = commutator
242	к = k = korotkogo zamykaniya = short-circuit
245	В.Н = v.n = vozbuzhdeniye, nagruzka = excitation, load
246	Н = n = nagruzka = load
261	п = p = parametricheskiy = parametric
265	ф = f = forma = form
265	о = o = obmotka = winding
266	В.В = v.v = vozbuzhdeniye vozbuditelya = exciter excitation
267	нач = nach = nachal'nyy = initial
269	ст = st = stator = stator
269	о.н = o.n = otnositel'noye nasyshcheniye = relative saturation
274	х.к.з = kh.k.z = kharakteristika korotkogo zamykaniya = short-circuit characteristic
274	х.х.х = kh.kh.kh = kharakteristika kholostogo khoda = no-load characteristic
277	о.к.з = o.k.z = otnosheniye korotkogo zamykaniya = short-circuit ratio
283	пред = pred = predel'nyy = maximum
291	э = e = elektromagnitnyy = electromagnetic
294	пер = per = peremennyy = alternating
294	пост = post = postoyannyy = direct
298	у = u = uspokoitel'nyy = damping

298 ш = shch = shchel' = slot  
298 с = s = sterzhen' = rod  
301 к = k = kol'tso = ring  
301 кр = kr = kraynyy = edge  
301 ср = sr = sredniy = middle  
302 загл = zagl = zaglusheniye = cancelation  
302 д = d = duga = arc

## Chapter 4

### PERMANENT-MAGNET GENERATORS

#### 4.1. GENERAL INFORMATION ON PERMANENT-MAGNET GENERATORS

Permanent-magnet machines are those excited by permanent magnets. The past years have seen an expansion in the field of application of permanent magnets; this has been facilitated by the considerable successes of the Soviet school of light metallurgy (work of A.S. Zaymovskiy, V.G. Lifshits, V.S. Meskin, B.Ye. Somin, A.N. Denisov, etc.), which has developed high-coercion alloys for permanent magnets.

The properties of permanent magnets have been greatly improved over the past 30 years. In comparison with specimens produced in 1920, the specific magnetic energy has been increased by a factor of 20. There has been a significant rise in the stability of magnets with respect to the influence of service time, temperature variations, impact and vibration loads, and the effect of extraneous magnetic fields.

Permanent magnets are finding ever-wider application in various branches of science and technology as sources of magnetizing force (in electrical machines, instruments, and apparatus), as direction indicators, and also in the formation of attractive forces (hoist magnets, separators, etc.). As an example, permanent-magnet high-frequency synchronous generators have been built with powers of the order of 100 kva. Aircraft DC-AC converters are also frequently made with permanent-magnet generators.

Over a certain power range, permanent-magnet generators are lighter and smaller than machines using electromagnetic excitation;

this is due to the elimination of the exciter. As a result, the problem of commutation is eliminated; this is especially important under high-altitude and high-speed flight conditions, and it is in this connection that permanent-magnet generators play a significant role in aviation.

The advantages of permanent-magnet machines increase as the frequency rises; the field of application of high frequencies is continually broadening. A frequency of 200 cps is used in general electrical-machine design for high-speed electric drive mechanisms (electrical tools), 400-1600 cps for aviation and marine service, and frequencies above 1600 cps in the ball-bearing industry, where there are induction motors running at 120,000 rpm or more, as well as in electrometallurgy.

Permanent-magnet generators differ widely in structural design, depending on function, power, way in which the magnetic system operates, and the type of material used.

Despite the fact that permanent magnets have been known for more than 2000 years, the theory of ferromagnetism has been less thoroughly studied than other fields of science, owing to its complexity. Thus although electrical machines using permanent magnets have been made since 1856, design procedures are less advanced than those for machines using electromagnetic excitation. The accuracy of calculations for electromagnetically excited machines ranges from 1 to 2%, while design accuracy for permanent-magnet machines is about 10%.

As a consequence of the variety of structural designs for magnetic systems, and the presence of a complex relationship between permanent-magnet characteristics and their shape, size, and the type of magnetic material used, there does not exist at the present time a unified design method for magnetic systems using permanent magnets analogous to that used for electromagnetically excited machines.



Existing design methods are either empirical (i.e., the optimum magnetic system is determined by the method of successive approximation, while the initial dimensions are, to a great degree, selected arbitrarily), or are based on design coefficients obtained experimentally that have limited application.

The most complete theory of permanent-magnet electrical machines has been given by the Soviet school of electrical-machine designers at the All-Union Electrical Engineering Institute imeni Lenin by A.I. Kanter, A.N. Larionov, and T.G. Soroker, as well as in publications by Ye.N. Razumovskiy, A.M. Senkevich, G.N. Senilov, etc.

The first to use permanent magnets in the USSR were Academician K.I. Shenfer, who used them for pyrometers, and Academician V.S. Kulebakin, who used them in a magneto.

#### Advantages of permanent-magnet machines

a) high operating reliability, structural simplicity and ease of servicing owing to the absence of sliding contacts and brushes, rotating windings and exciter, and the fact that the machine is independent of direct-current sources;

b) high efficiency and low machine temperature rise owing to the absence of losses in excitation and at sliding contacts; thus, for example, a general-purpose 15 kw 220 v synchronous generator has an efficiency  $\eta = 82.5\%$ , while a permanent-magnet generator has an efficiency of 91%;

c) the fact that the magnetic flux across the air gap does not depend on the machine rotational speed or temperature (up to  $100^{\circ}$ );

d) absence of sparking contacts producing radio interference;

e) lower cost, weight, and size (absence of sliding contacts, field windings, and exciter) in low-power and high-frequency machines.

### Drawbacks to permanent-magnet machines

- a) lack of a direct method of voltage regulation;
- b) increased cost, weight, and size for medium-power machines;
- c) relatively low maximum machine power (permanent-magnet generators are built for up to 100 kva power).

### Magnet Operation

If we magnetize a closed magnetic system such as a ring of constant cross section, the process of magnetization is assumed to end when saturation sets in, corresponding to an induction  $B_s$  in the magnetic conductor (Fig. 4.1).

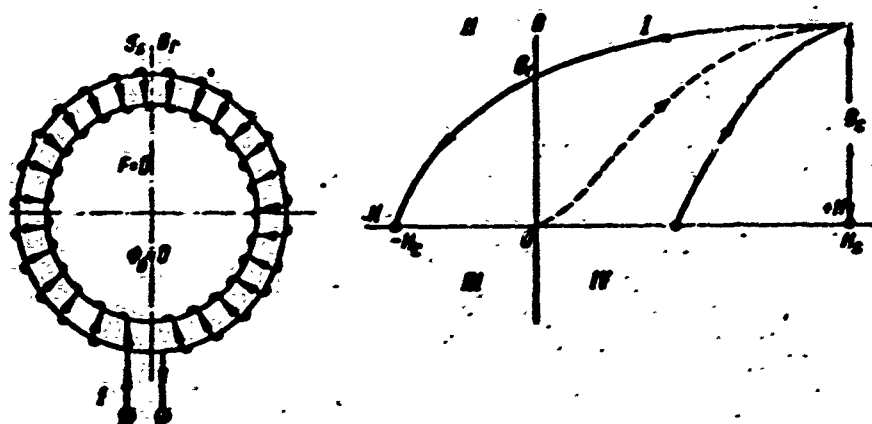


Fig. 4.1. Magnetization of a closed ring to saturation.

If we gradually decrease the current in the magnetizing winding, i.e., decrease the field strength (n.s.) to zero, the induction in the magnetic conductor will drop to the value of the residual induction  $B_r$ , which is a most important characteristic of a magnet. The magnet thus obtained is neutral, since it does not develop a magnetizing force, and cannot serve as a source of magnetic energy. A magnet in closed condition cannot supply energy to external space, although it does possess a residual induction  $B_r$  and a residual flux  $\Phi_r = SB_r$  (like a short-circuited electrical circuit of a generator, in which the armature current flows, but the power delivered by the generator to the

external circuit is zero).

In a closed ring of magnetic material, the lines of force complete their circuit only within the loop. Outside the magnetic material there is no field, i.e., there is no leakage flux  $\Phi_0$ , and the magnetic condition of the ring is determined by the points  $B_r$  and  $H = 0$  on the magnet diagram (this actually is true for an ideal closed magnetic circuit, but in practice the induction is close to the value of  $B_r$ , and the field strength is nearly zero).

The magnetizing force due to a closed magnet and its magnetic flux are determined by the well-known relationships

$$\left. \begin{aligned} \Phi &= S_m B = \frac{F_c}{R_m} = F_c \Lambda_m \\ \text{and} \quad F_c &= \Phi R_m = \frac{\Phi}{\Lambda_m} \end{aligned} \right\} \quad (4.1)$$

where  $F_c = 0.8 h_m H_c$  is the magnetizing force due to the magnet, and is analogous to the emf of an electrical element;  $R_m$  and  $\Lambda_m$  are, respectively, the internal magnetic reluctance and the internal permeance of the magnet;  $H_c$  is the coercive force (specific magnetizing force);  $h_m$  is the length of the magnet along the magnetization path.

Equations (4.1) for the magnetic circuit are analogous to the corresponding equations for an electrical circuit, where the flux  $\Phi$  corresponds to the current  $I$ , and the magnetizing force  $F_c$  corresponds to the emf  $E$ . This analogy breaks down, since in the electric circuit, the current is directly proportional to the emf acting in the circuit, at constant temperature, while the magnetic flux is not proportional to the magnetizing force as a consequence of the phenomenon of saturation ( $\mu \neq \text{const}$ ) and leakage.

If we cut the ring (Fig. 4.2) and form the air gap  $\delta$ , as shown in Fig. 4.2b, polarity appears on the surface of the magnet, chiefly near

the gap surface.

When this happens, together with the basic flux in the air  $\Phi_\delta$ , there also appears a leakage flux  $\Phi_\sigma$ , which will be concentrated chiefly about the air gap, when the gap is small.

In this case, the magnet will have a field opposing the basic magnetization; this bucking field is proportional to the field in the air gap. Since the field in the air gap is opposite in sign to the field in the magnet, the induction in the magnet is decreased, and the operating point will move down along the demagnetization curve. Point A, which characterizes the condition of the magnet when  $\delta > 0$ , lies on the demagnetization curve, i.e., on the external hysteresis curve in the second quadrant, and is characterized by the quantities  $\Phi_a < \Phi_r$ ,  $B_a < B_r$  and  $H_a > 0$ .

If we increase the air gap still more (Fig. 4.2c), the leakage field will increase, and the useful flux in the air gap will drop; the working point that characterizes the magnetic condition of the ring in the neutral condition will shift still further down along the demagnetization curve.

Now the magnet flux will pass through a large air gap, i.e., the reluctance of the magnetic path rises and, consequently, the magnetic flux and induction in the magnet drop to the values  $\Phi_{a1} < \Phi_a$  and  $B_{a1} < B_a$  (point  $A_1$  on Fig. 4.2c).

The value B of the induction in the open magnet is determined by the magnet dimensions and the size of the air gap (by the permeance or reluctance). If we assume that the leakage flux  $\Phi_\sigma$  is constant and traverses the entire magnet core, then  $\Phi = \Phi_\delta + \Phi_\sigma$  and

$$F_c = F_m + F = R_m(\Phi_\delta + \Phi_\sigma) + R_\delta \Phi_\delta = \frac{\Phi_\delta}{\Lambda_m} + \frac{\Phi_\delta}{\Lambda_\delta}, \quad (4.2)$$

where

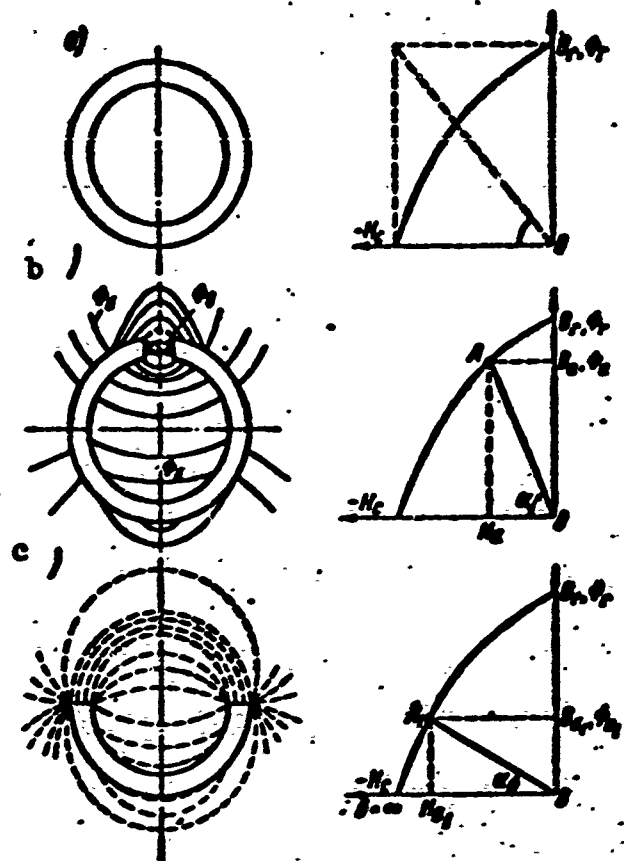


Fig. 4.2. Fluxes and demagnetization curve for ring magnet with various air gaps. a) Magnet closed,  $\delta = 0$  and  $\Phi_\sigma = 0$ ; b) magnet open,  $\delta$  is small,  $\Phi_\sigma$  is small; c)  $\delta$  is large,  $\Phi_\sigma$  is large.

$$\left. \begin{aligned} F_m &= 0,8h_m H_m = R_m \Phi = \frac{\Phi}{\Lambda_m} \\ F &= 0,8h_\delta H = R_\delta \Phi_\delta = \frac{\Phi_\delta}{\Lambda_\delta} \end{aligned} \right\} \quad (4.3)$$

The total magnetizing force developed by the magnet consists of two parts:  $F_m$ , corresponding to the drop  $R_m \Phi$  in magnetic potential in the magnet (i.e., the magnetizing force used to overcome the internal reluctance  $R_m$  of the magnet) and  $F$ , corresponding to the drop in magnetic potential due to the reluctance of the air gap  $R_\delta \Phi_\delta$  (i.e., the magnetizing force used to overcome the external reluctance of the magnet  $R_\delta$ ).

In the case given, the magnet is no longer neutral, but develops

a free magnetizing force  $F$  in the external loop in order to maintain the magnetic flux  $\Phi_0$  in the air gap.

The free magnetizing force  $F$ , multiplied by the magnetic flux  $\Phi_0$  of the air gap gives the external magnetic energy  $A$  of the magnet available for use; then

$$A = BH/8\pi \text{ erg/cm}^3.$$

Thus, the permanent magnet becomes a source of magnetizing force and magnetic energy for the portion of the magnetic circuit lying outside the magnet.

If we enlarge the air gap, the induction in the magnet will drop, and the magnetizing force developed by the magnet in external space (in the air gap) will rise.

The position of point A on the demagnetization curve and, consequently, the values of  $B$  and  $H$  depend on the air-gap permeance; the smaller the gap and the higher the permeance, the higher  $B$  and the smaller  $H$  (point A goes toward  $B_r$ ), and, conversely, when the air-gap permeance decreases,  $H$  rises and  $B$  falls (point A goes toward  $H_c$ ).

Here the external magnet energy will change, reaching a maximum at some definite value of the induction in the magnet  $B_{\max}$ .

Figure 4.3 gives curves for  $A = f(B)$  and  $A = f(H)$ . At point  $A_m$  the magnet (neglecting leakage) will develop the maximum specific energy

$$A_{\max} = (BH)_{\max}/8\pi \text{ erg/cm}^3.$$

Magnetic reversal line. If a magnetic system consisting of a magnet and external reluctance — an air gap — operates at point A on the magnet demagnetization curve (Fig. 4.5a), the application of an external magnetizing force may increase the induction in the magnet. In this case, however, as we know, the magnetization process will not take place in accordance with the external curve  $AB_r$ , but in accordance

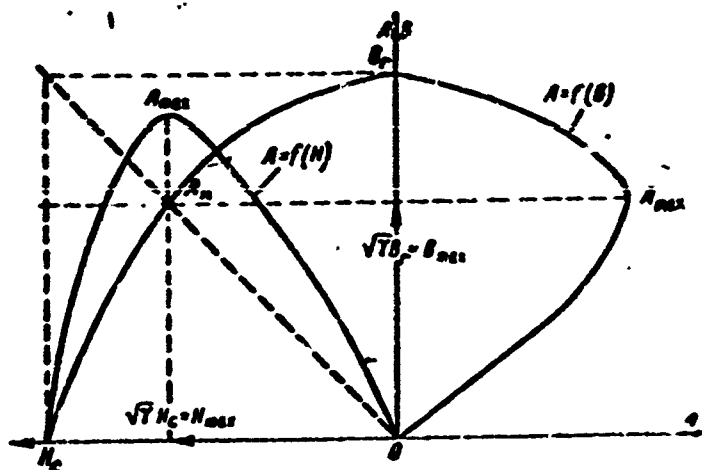


Fig. 4.3. Magnet energy curves, neglecting leakage,  $A = f(B)$  and  $A = f(H)$ .

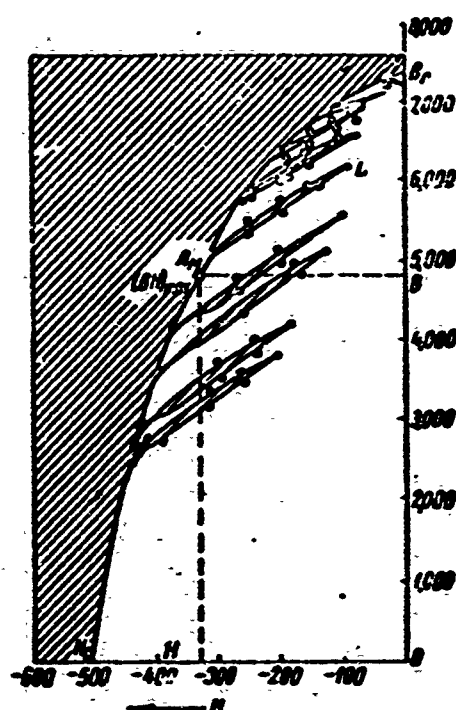


Fig. 4.4. Demagnetization curve for Alnico alloy, and secondary hysteresis loops.

with the secondary hysteresis curve  $AL$ , which always lies below  $AB_r$ ; it is called the magnetic-reversal line. By changing the interval  $H(I)$ , it is possible to obtain a family of secondary loops — reversal curves (Fig. 4.4).

Return curves take the form of narrow sloping sharp open loops. With sufficient accuracy for practical purposes, they may be replaced by a single central straight magnetic-reversal line.

If the field strength is changed many times, but the limits of the interval  $\Delta H$  are not violated, the condition

of the magnet will be determined stably by the reversal line  $AL$ . Thus, the properties of the magnet are reversible and, consequently, the magnet has been stabilized. The same result may be obtained by changing the reluctance of the external loop.

If within a device a closed body is magnetized to saturation induction, and the magnetizing current is then turned off, the induction

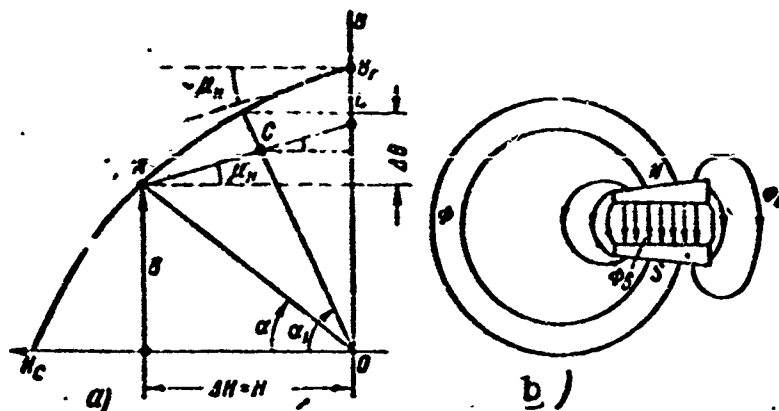


Fig. 4.5. Operation of magnet on reversal line. a) Diagram for magnet; OA) external-loop reluctance without pole pieces ( $R_\delta$ ); OC) external-loop reluctance with pole pieces ( $R_{\delta_1}$ ); b) ring magnet with pole pieces.

$B_r$  remaining within the magnet after this may be considered to be residual, if we neglect the reluctance of the device used to complete the magnetic loop. If we then remove the magnet from the magnetizing device, owing to the demagnetizing effect of the ends, the induction in the magnet will drop to B (point A, Fig. 4.5). If we now again place the magnet in the device, the induction will begin to increase (since the external reluctance is reduced to zero), but the point A will move not toward  $B_r$ , but toward L, i.e., it will move along the reversal line.

A similar picture is obtained when we examine Fig. 4.5b, which shows a permanent magnet with pole pieces (fittings).

A magnet without pole pieces operates at point A, while a magnet with pole pieces operates at point C on the reversal line. Here  $\tan \alpha$  characterizes the permeance of the external air-gap circuit in the absence of pole pieces, and  $\tan \alpha_1$  the permeance of the external circuit with allowance for the pole pieces. Clearly,

$$\tan \alpha_1 > \tan \alpha \quad \text{and} \quad R_\delta > R_{\delta_1}.$$

The reversal coefficient is introduced to account for the phe-



phenomenon of magnetic reversal; it equals the tangent of the slope angle of the reversal line:

$$\operatorname{tg} \mu_H = \frac{\Delta B}{\Delta H} = \frac{dB}{H} = \mu'_v = \lambda_v, \quad (4.4)$$

or the relative reversal coefficient is used; it is defined as

$$\operatorname{tg} \mu = \mu'_v \frac{H_c}{B_r} = \frac{\mu'_v}{\mu_r} = \mu'_v = \lambda_v, \quad (4.5)$$

$$\mu_r = B_r/H_c$$

where  $\mu'_v$  is called the reversible permeability, and  $\mu_v$  the relative reversible permeability.

Thus, in the presence of a changing magnetic field or magnetic reluctance, a magnet does not operate on the demagnetization curve, but on the magnetic-reversal line.

The location of each reversal curve is determined by the position of the initial point A on the external hysteresis curve (the so-called point of departure), the stabilization interval  $\Delta H$ , and the reversible permeability  $\mu'_v$ .

The reversal coefficient (reversible permeability) varies as a function of the induction, decreasing when the induction increases; here the reversal curves become flatter with respect to the H axis, and the area enclosed by them decreases.

Consequently,  $\mu'_v = f(B)$ , i.e., it is a variable. This variation, however, is slight (especially in the magnet's working region); thus, the reversal lines may be considered to be nearly parallel to each other, and  $\mu'_v$  taken as constant and equal to the value obtained for the point that corresponds to the maximum magnet energy (in this case,  $\mu'_v$  is a constant for the magnetic material).

We may assume in first approximation that the slope of the line drawn through the center of a minor hysteresis loop (the slope of the reversal line) equals the slope of the tangent to the main demagnetiza-

tion curve at the initial point  $B_r$  (see Fig. 4.5).

Values of reversible permeability:

for iron-nickel-aluminum alloys:

$$\mu'_v = \operatorname{tg} \mu_H = 4-6;$$

for steels:

$$\text{carbon } \mu'_v = 130-60;$$

$$\text{chrome } \mu'_v = 40-25;$$

$$\text{tungsten } \mu'_v = 44-24;$$

for alloys:

$$\text{Alni (AN) } \mu'_v \approx 3.5-4.0;$$

$$\text{Alnisi (ANK) } \mu'_v \approx 1.2-1.4;$$

$$\text{Alnico (ANKO) } \mu'_v \approx 3.5 \text{ (see §4.2).}$$

The new magnetic materials (alloys) have lower reversible permeabilities, i.e., their reversal curves are flatter.

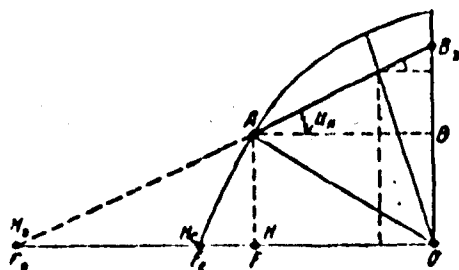


Fig. 4.6. Diagram for magnet operating on reversal line neglecting leakage.

In conclusion, we should note that a magnet operating on the reversal line is stable in the presence of external demagnetizing fields if the field strength of the external demagnetizing field does not exceed the field strength at the point of departure of the reversal line — point

We shall agree to call the point  $B_v$  at which the reversal line intersects the B axis the residual reversal induction, and the point  $H_v$  at which the reversal line intersects the H axis, the apparent reversal field strength (Fig. 4.6).

The concept of apparent field strength applies only to reversible magnets operating on the reversal line (stabilized magnets). The point  $B_v$  actually exists as the end of the stabilization interval, while the point  $H_v$  is fictitious. Clearly,  $\tan \mu_H = B_v/H_v = \mu'_v$ . The reversal

curve may be represented by the equation

$$B = B_s - \mu_0' H. \quad (4.6)$$

#### 4.2. PERMANENT-MAGNET MATERIALS

All magnetic materials may be classified into two groups: soft magnetic materials, which have high permeability, low coercive force, and small magnetic-reversal losses; and hard magnetic materials, having low permeability, high coercive force, and considerable magnetic-reversal losses.

In this chapter, we shall consider only hard magnetic materials.

##### Hard Magnetic Materials

The hard magnetic materials include ferromagnetic alloys possessing high values of residual induction  $B_r$  and coercive force  $H_c$ . They are used as permanent magnets — sources of a permanent magnetic field.

Hard magnetic materials may be divided into five main groups:

- 1) carbon alloy steels;
- 2) magnetic alloys based on the ternary system;
- 3) cold- or hot-worked magnetic alloys;
- 4) magnets compacted from powders, metalloceramic, and sintered alloys;
- 5) magnetic alloys with added precious metals.

Carbon alloy steels. Prior to 1932, martempered carbon alloy steels were used for permanent magnets.

Depending on their chemical composition, these steels were classified as simple carbon, tungsten, chrome, or cobalt steels.

Possessing high residual induction, they have low coercive force and, consequently, develop little magnetic energy.

A substantial drawback to plain carbon steels is the considerable impairment of magnetic properties with age and under the influence of temperature variations, external magnetic fields, and shocks.

Carbon alloy steels, using tungsten, chromium, molybdenum, and cobalt as alloying additives, have better and more stable magnetic properties.

The best alloy steel is cobalt steel containing up to 40% cobalt ( $H_c = 250$  oersteds,  $B_r = 11,500$  gauss).

Cobalt steel has a substantial disadvantage in the scarcity and high cost of cobalt.

Ternary-system alloys. In 1931, a magnetic alloy called alni ( $H_c = 600$  oersteds,  $B_r = 7000$  gauss) was discovered; it is based on the ternary iron-nickel-aluminum system.

Alni alloy has roughly three times the specific magnetic energy of the best cobalt steel, and is considerably less expensive, since it is cast from more plentiful materials.

A substantial drawback to alni alloy is its great mechanical hardness and brittleness; it can be neither machined nor forged. Alni parts are produced by casting and subsequent precision grinding. All holes in the parts must be made during casting.

A further improvement in the iron-nickel-aluminum alloy was gained by using alloying additives or by replacing the cobalt with copper and silicon. Thus alnico and alnisi alloys were created.

All the magnetic materials discussed above are isotropic, i.e., their magnetic properties are identical in that they do not depend on the direction of the magnetizing field.

Isotropic materials are convenient to use; they impose no limitations on magnetic-circuit design.

It was discovered in 1938 that if alni and alnico alloys were cooled in a strong permanent magnetic field ( $H = 1500$  oersteds) from a temperature above the Curie point ( $1300^\circ$ ) they would become magnetically anisotropic, i.e., their magnetic properties would depend on the

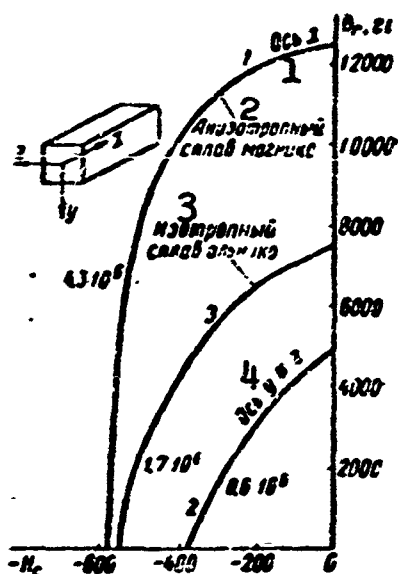


Fig. 4.7. Demagnetization curve for anisotropic alloy of the magnico type and isotropic alnico alloy. 1)  $\underline{x}$  axis; 2) anisotropic magnico alloy; 3) isotropic alnico alloy; 4)  $\underline{y}$  and  $\underline{z}$  axes.

direction of the magnetizing field.

In anisotropic magnetic alloys, the residual induction in the direction of magnetization is roughly doubled following thermomagnetic treatment, with a slight increase in coercive force.

Thermomagnetic treatment produces the best results with magnetic alloys with composition Fe-Al-Ni-Co-Cu-Ti, where the nominal specific energy is increased to  $5.5 \times 10^6$  erg/cm<sup>3</sup> (this exceeds the maximum specific magnetic energy of alni and alnico magnetically isotropic alloys by a factor of three or four).

Figure 4.7 gives demagnetization curves for an anisotropic alloy of the magnico type, as well as for the isotropic alnico alloy.

Curve 1 corresponds to the properties along the magnetization ( $\underline{x}$ ) axis, and curve 2 to the  $\underline{y}$  and  $\underline{z}$  axes, perpendicular to the main  $\underline{x}$  axis. Curve 3 corresponds to the magnetic properties of the same alloy in the isotropic state (alnico), i.e., prior to thermomagnetic treatment.

It is interesting to note that the alloys also become anisotropic with respect to electrical resistance following thermomagnetic treatment, i.e., this type of treatment is not purely magnetic in nature.

Plastic magnetic alloys. The utilization of permanent magnets has been hampered by the low specific magnetic energies of the mechanical alloys suitable for machining; the complexity of the manufacturing process for parts made from metal alloys possessing high specific mag-

netic energies (of the alnico type) is a consequence of their great hardness and brittleness.

Recently, high-coercion plastic magnetic alloys have become common: iron-nickel-copper, iron-cobalt-vanadium, iron-cobalt-molybdenum, etc.; these materials can be cold- and hot-worked.

Powder metallurgy magnets. As we know, when soft magnetic materials are ground up, their coercive force rises monotonically as the particle size decreases. Thus, parts made from powders, even from soft magnetic materials (iron-nickel alloy) become magnetically hard when the particles are sufficiently small in size.

When magnetically hard materials of the alni or alnico type are powdered, the opposite effect is observed: the coercive force decreases as the particles are reduced in size. Magnets made from powdered alnico, however, have good magnetic properties. Alnico, made by powder-metallurgy methods, can be used to make magnets of complex shapes and small size by compacting; this yields products that are low in cost and made with a high degree of precision.

Magnetic materials made by compacting and rolling and containing various proportions of powdered ferric oxide ( $\text{Fe}_3\text{O}_4$ ) and cobalt ferrite ( $\text{CoOFe}_2\text{O}_4$ ), have good magnetic properties following thermomagnetic treatment, with  $B_r = 4000$  gauss,  $H_c = 600$  oersteds, and  $(BH)_{\max} = 1.5 \times 10^6$ .

It is important to take note of the low specific gravity ( $3.5 \text{ g/cm}^3$ ) and high electrical resistance of these magnetic materials.

Permanent magnets made from compacted materials may be given any shape without machining, which is economical in mass production.

Magnetic alloys with added precious metals possess high coercive force, as can be seen from Table 4.1. The alloys, however, being very expensive, are used only in special cases.

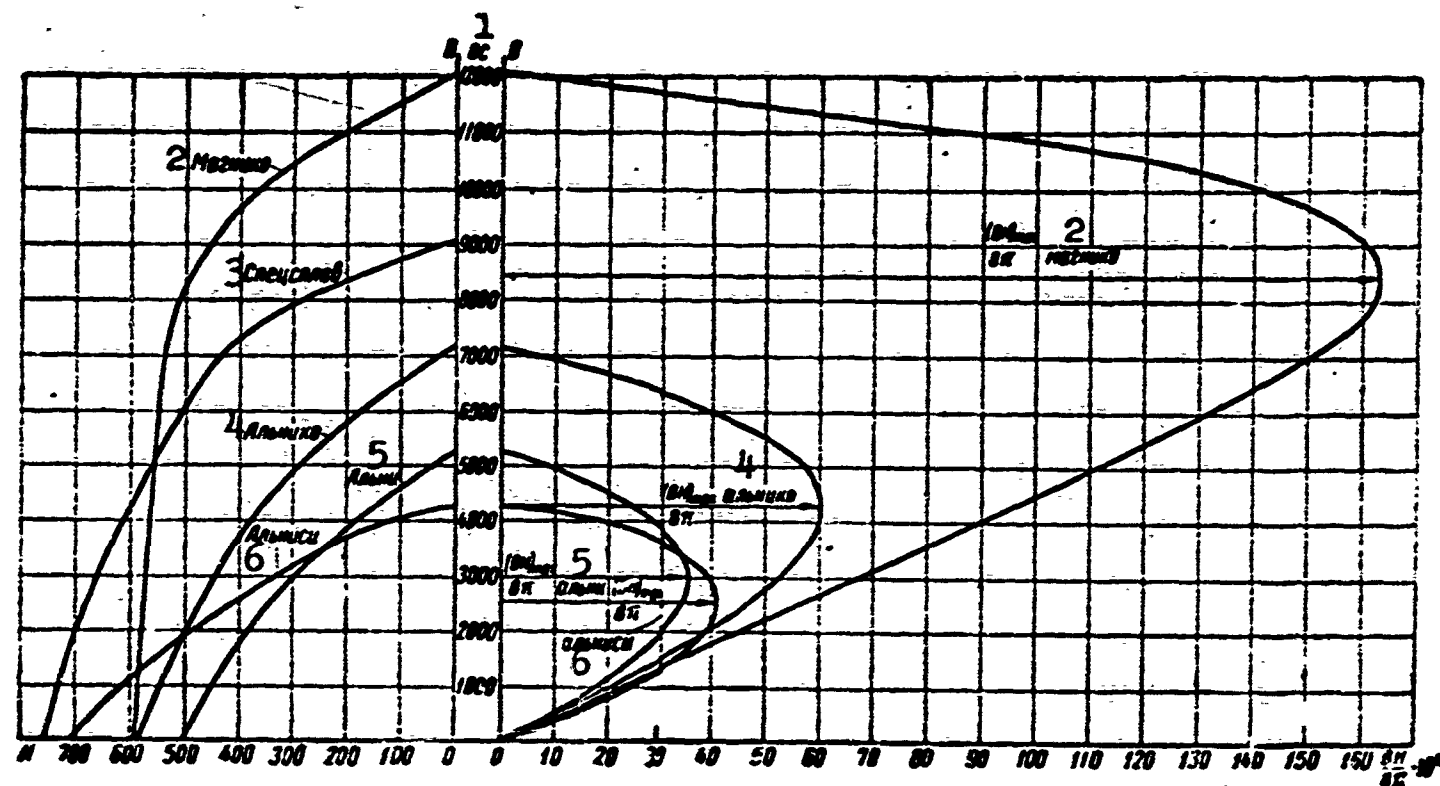


Fig. 4.8. Demagnetization curves for certain permanent-magnet alloys.  
1) Gauss; 2) magnico; 3) special alloy; 4) alnico; 5) alni; 6) alnisi.

TABLE 4.1

## Properties of Magnetic Materials

1 Химический состав в % (балласт Fe)												
3%	4 Наименование	C	W	Cr	Co	Al	Ni	Mn	Cu	Ti	Mo	Va
1	0,65% С-сталь	0,65	—	—	—	—	—	0,85	—	—	—	—
2	1% С	1,0	—	—	—	—	—	0,5	—	—	—	—
3	5% W	0,7	5	—	—	—	—	—	—	—	—	—
4	6% W	0,7	6	0,5	—	—	—	0,5	—	—	—	—
5	1% Cr	0,6	—	0,9	—	—	—	0,45	—	—	—	—
6	2% Cr	0,9	—	2,15	—	—	—	—	—	—	—	—
7	3,5% Cr	1,0	—	3,5	—	—	—	0,5	—	—	—	—
8	6,0% Cr	1,1	—	6,0	—	—	—	0,4	—	—	—	—
9	9% Co	0,9	1,25	5,0	9	—	—	—	—	—	—	—
10	17% Co	0,7	8,25	2,5	17	—	—	—	—	—	—	—
11	36% Co	0,8	3,75	5,75	36	—	—	—	—	—	—	—
12	40% Co	0,7	5,0	4,25	40	—	—	—	—	—	—	—
13	Кобальтхромистая сталь	1,0	—	9	16	—	—	0,3	—	—	—	—
14	КС-магнитная сталь	0,9	7	3,5	36	—	—	—	—	—	—	—
15	Альинико IA	—	—	—	5	12	22,5	—	—	—	—	—
16	IB	—	—	—	5	12	21	—	—	—	—	—
17	IC	—	—	—	5	12	19,5	—	—	—	—	—
18	IIA	—	—	—	12,5	10	18	—	6	—	—	—
19	IIB	—	—	—	12,5	10	17	—	6	—	—	—
20	IIC	—	—	—	12,5	10	16	—	6	—	—	—
21	IIIA	—	—	—	—	12	26	—	—	—	—	—
22	IIIB	—	—	—	—	12	25	—	—	—	—	—
23	IIIC	—	—	—	—	12	24	—	—	—	—	—

2 Магнитные свойства											
$B_r$	$H_c$	$A_{max}$	$B_m$	$A_c$	$\tau$	$\sqrt{\tau}$	$H_m$	$\frac{B_r}{H_c}$	$\frac{B_m}{B_r}$	$\frac{H_m}{H_c}$	Удельный вес г/см <sup>3</sup>
10	42	0,18	6,5	0,42	0,428	0,654	27,7	238	0,65	0,66	7,84
9,0	51	0,2	5,9	0,459	0,436	0,66	33,9	176,5	0,655	0,665	7,8
10,5	70	0,33	7,0	0,735	0,449	0,67	47,2	150	0,665	0,675	8,1
9,5	74	0,33	6,5	0,703	0,47	0,686	50,75	128,5	0,685	0,686	8,15
9,5	52	0,23	6,5	0,495	0,465	0,682	35,4	182,5	0,685	0,682	7,8
9,3	60	0,26	6,3	0,557	0,467	0,683	41,3	155	0,677	0,688	7,8
9,5	66	0,29	6,5	0,627	0,462	0,68	44,6	144	0,685	0,677	7,78
9,5	74	0,3	6,2	0,703	0,427	0,654	48,4	128,5	0,653	0,653	7,78
7,8	122	0,41	5,1	0,952	0,431	0,657	80,5	64	0,654	0,66	7,92
9,0	170	0,61	5,9	1,53	0,399	0,632	103,3	53	0,655	0,608	8,37
9,6	228	0,93	6,3	2,19	0,425	0,652	147,5	42,1	0,656	0,647	8,2
10	242	1,03	6,5	2,42	0,426	0,653	158,5	41,4	0,65	0,655	8,2
—	—	—	—	—	—	—	—	—	—	—	—
10	230	0,9	—	2,3	0,391	0,625	—	43,5	—	—	—
0,66	540	1,4	4,1	3,57	0,392	0,626	342	12,2	0,621	0,632	6,9
7,1	450	1,4	4,7	3,19	0,438	0,662	298	15,8	0,662	0,662	6,9
7,6	400	1,4	5,2	3,04	0,461	0,679	269,5	19,0	0,685	0,674	6,9
7,0	630	1,6	4,2	4,4	0,364	0,603	382	11,1	0,6	0,607	7,09
7,5	560	1,6	4,6	4,2	0,381	0,617	348	13,4	0,613	0,621	7,09
8,0	425	1,6	5,5	3,4	0,470	0,686	291	18,8	0,687	0,685	7,09
6,5	560	1,35	4,0	3,64	0,371	0,609	338	11,6	0,615	0,605	6,9
7,0	470	1,35	4,5	3,29	0,410	0,64	300	14,9	0,643	0,639	6,9
7,5	400	1,35	5,0	3,00	0,450	0,671	270	18,75	0,666	0,675	6,9





Table 4.1 and Fig. 4.8 give the basic properties and demagnetization curves for the basic permanent-magnet materials.

### Magnetizing Permanent Magnets

The methods used to magnetize permanent magnets and the devices employed for this purpose are determined by the design of the element and the shape of the magnet. Magnetization may be carried out with direct or alternating current by means of special electromagnets (outside machines), armature windings, or a special auxiliary winding placed over the poles or body of the machine.

Synchronous-machine rotors of the "spider" type are magnetized on special devices that take the form of very strong electromagnets with special movable pole pieces that correspond to the shape of the magnets to be magnetized.

In order to bring the magnetic field into the saturated condition, the magnetizing field strength should theoretically be infinite. When  $H_s \geq 5H_c$ , however, the residual induction and coercive force of the magnetic material change little as the magnetizing field increases.

When the magnetizing field is stronger than  $H_s < 5H_c$ , the magnetic properties of the magnetic material are greatly impaired.

It must be remembered that if the magnet is not of uniform cross section, it is possible that certain sections of the magnet will be undermagnetized, impairing the magnetic properties of the magnet as a whole.

The magnetizing force of an instrument is absorbed chiefly by the magnet, since the instrument core normally has little reluctance, and

$$H_s = \frac{1.25Iw}{h_m},$$

where  $w$  and  $I$  are the number of turns and the current in the coil of the instrument;  $h_m$  is the length of the magnet along the magnetization

path.

In order to obtain reliable magnetization it is necessary that

$$\bar{F}_s \geq 6\bar{F}_c \quad \text{and} \quad \bar{H}_s \geq 6\bar{H}_c.$$

### Stability of Permanent Magnets

The term "stability" is understood as the ability of the magnet to keep the magnetic flux constant under certain conditions that affect it.

The initial magnetic properties of a permanent magnet may change under the influence of several internal or external factors. The internal factors determine the structural (metallurgical) stability, and the external factors determine the magnetic stability of the magnet.

If the magnetic properties (flux) change owing to a variation in the internal structure of the material — disorientation of the crystals — the structural stability of the magnet is upset; in this case, it is possible to restore the magnetic properties only by subjecting the material of the magnet to heat treatment again.

If a change in magnetic properties occurs owing to external influences, the magnetic stability of the magnet is upset; in this case, the magnetic properties of the material can be reestablished by a new magnetization. Below we shall consider the external factor.

External factors influencing magnet demagnetization are: temperature change, mechanical jolting, field reversal, and changing magnetic-circuit reluctance.

Effect of temperature variation. Temperature has an effect on the magnetic condition of a ferromagnetic substance. The temperature dependence of the ferromagnetic properties of a substance is explained by changes in molecular motion.

Temperature changes in the  $-100$  to  $+300^\circ$  range are of practical significance for electrical machines and instruments. Consequently, it

is necessary to consider only temperatures that do not lead to a disturbance in magnet structural stability or irreversible changes in magnetic properties.

Reversible and irreversible changes (residual deformations) in the magnetic properties of a magnet are observed with temperature variations.

The magnetic properties of a magnet, i.e., the values of  $B_r$ ,  $H_c$ , and the energy BH are impaired when the temperature rises, and are improved when the temperature drops. As a rule, a magnet is magnetized at temperatures of the order of  $15-20^\circ$ . If it is then cooled to a temperature of the order of  $-100^\circ$ , the residual induction  $B_r$  and the magnetic flux in the air gap  $\Phi_g$  rise slightly; the magnet, however, nearly recovers its initial magnetic properties as soon as the temperature is raised to  $15-20^\circ$ , i.e., the improvement in magnetic properties with lowered temperature is reversible.

When the temperature of the magnet rises in comparison to the temperature at which magnetization was carried out, an irreversible impairment of the magnetic properties of the material is observed over the first 3-5 cycles of temperature rise when a sort of temperature stabilization sets in — the magnet has been formed. Reversible changes in magnetic properties take place during succeeding temperature-elevation cycles.

Figure 4.9 gives a demagnetization curve for alnico steel at temperatures of 25 and  $450^\circ$ . Curve 1 corresponds to the initial magnetic properties at  $25^\circ$ . Curve 2 corresponds to the magnetic properties at  $25^\circ$  following 3-4 applications of a temperature of  $450^\circ$ . Thus, the hatched region between curves 1 and 2 corresponds to irreversible loss in magnetic properties under the influence of the  $450^\circ$  temperature. Curve 3 gives the magnetic properties at  $450^\circ$ . The region between

curves 2 and 3 corresponds to reversible changes in magnetic properties occurring with magnet temperature variation from 25 to 450°.

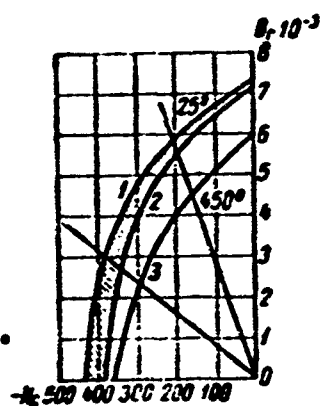


Fig. 4.9. Temperature forming of a magnet.

Investigations have shown that the degree of irreversible impairment in magnet magnetic properties, for a given size, depends on the limiting temperature: the impairment is greater the higher the temperature; the dimensions of the magnet – the slope of the permeability line – effect the value of the flux in the air gap for a given temperature.

Repeated magnetization restores the magnetic properties of a magnet, while if it is subjected to heat treatment, all of what we have said earlier again applies.

Depending on the temperature and type of magnetic material, the following changes in residual induction are observed:

1 Повышение температуры до:	2 Снижение величины $B_r$	
	3 полное	4 необратимое
100°	0,5-2,5%	0,2-0,75%
200°	2-6%	1-3%

1) Temperature increased to:  
2) decrease in value of  $B_r$ ; 3)  
total; 4) irreversible.

Anisotropic materials show less reaction to temperature variations than do isotropic materials, and their flux loss is less.

After a magnet has been subjected to temperature forming, its magnetic properties bear an inverse relationship to temperature changes (within limits imposed by the maximum forming temperature).

The magnetic field strength may be found as a function of temperature for  $t = (-60 \text{ to } +100)^\circ\text{C}$  by using the following equation:

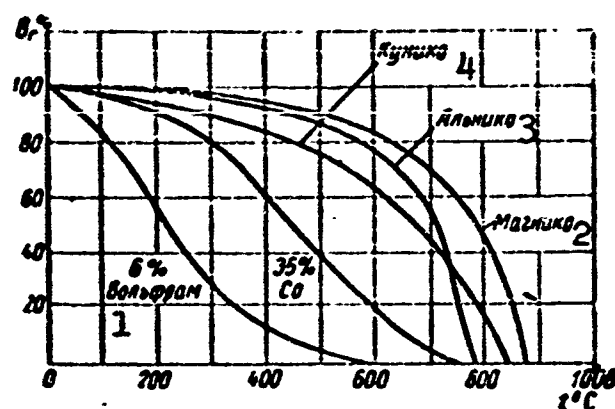


Fig. 4.10. Residual inductions of various alloys as a function of temperature. 1) Tungsten; 2) magnico; 3) alnico; 4) cunico.

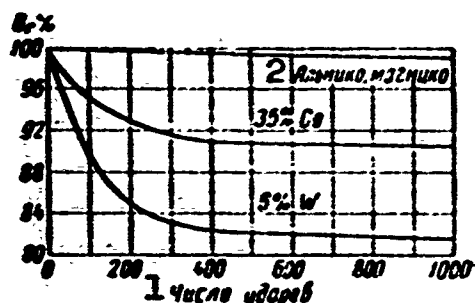


Fig. 4.11. Residual induction as a function of number of shocks. 1) Number of shocks; 2) alnico, magnico.

$$H_t = H_0(1 - at - bt^2),$$

where  $H_0$  is the field strength at  $t = 0$ ;  $a$  and  $b$  are constants that depend on the type of magnetic material and its dimensions.

The change in magnet flux may be determined, in approximation, from the equation

$$\Phi_t = \Phi_{15}[1 - \alpha(t - 15)],$$

where  $\alpha = 0.00017$  to  $0.00025$  per  $^{\circ}\text{C}$ .

Figure 4.10 gives curves for  $B_r = f(t)$  for various materials used in permanent magnets.

In many cases, for example, in tachometer generators, instruments for measuring power, etc. where it is necessary to have a constant flux in the air gap, it is necessary to carry out temperature forming of the magnet in the magnetic system roughly five times at a temperature somewhat exceeding the maximum temperature to be encountered under service conditions. This eliminates irreversible changes in magnet magnetic properties.

Magnetic-system temperature forming is still important when expansion and contraction of the metal in the magnetic circuit causes the permeance to change, i.e., there may be a variation in the slope of the permeance line and the flux in the air gap. For present-day magnets, the maximum permissible temperature is 300°C.

Effect of mechanical jolting. Under the influence of jolts (shocks and vibration), permanent magnets suffer impairment of the initial magnetic properties, since certain of the domains in the direction of the magnetizing field are disoriented.

The degree of demagnetization caused by jolting depends basically on the coercive force. The magnitude of the coercive force characterizes the stability with which the domains keep the directions that they have been given during magnetization.

Magnetic steels and alloys with low coercive forces experience considerable demagnetization under the influence of mechanical shocks, while alloys of the alnico type (with high  $H_c$ ) are relatively stable.

Tests for magnetic stability during jarring have been carried out by dropping magnetized specimens from a height of 1 meter onto a wood floor (Fig. 4.11).

The way in which  $B_r$  depends on the number of shocks varies monotonically in accordance with an exponential function. After 1000 shocks, the residual induction of alnico dropped roughly by 0.5%, while for tungsten steel,  $B_r$  dropped by 18%.

During shock testing of alnico, several specimens showed cracks, while some fractured. This indicates that the physical properties of alnico limit its utilization under impact-load conditions more than does the decrease in magnetic properties.

Experience gained in the utilization aboard aircraft of permanent-magnet machines made from alnico, alnisi, and alni alloys have shown

that the magnetic properties of the magnets do not deteriorate under vibration.

As a rule, magnets are not stabilized with respect to mechanical shocks and vibration, since modern high-coercion alloys are sufficiently stable in this respect.

Effect of tension and compression on magnetic alloys. As a rule, machining and plastic deformation is carried out after the internal crystals of the magnetic alloy have been given their magnetic orientation.

As experiments have shown, the magnetic properties of soft and hard magnetic materials depend on tension and compression due to external forces. The coercive force and residual induction lies under tension. This improvement in magnetic properties is reversible, i.e., after the tensile forces have been removed, the magnetic properties of the materials are restored to the original levels.

Effect of external magnetic fields. The variation in magnetic induction under the influence of external fields may be taken into account by using the demagnetization curve for the magnet, if we know the effective strength of the external field. Here it is necessary to allow for the fact that the field of the permanent magnet affects the external magnetic field, and thus the determination of the effective external field presents well-known difficulties. The field of the permanent magnet causes the strength of the external field acting on the magnet to depart from its true initial value.

Figure 4.12a shows the magnetization curve for a magnet and the line OR that corresponds to the permeance of the magnetic-circuit air gap. The point at which the line OR intersects the  $B_r H_c$  curve (point R) determines the magnitude of the magnetic induction in the magnet.

If an additional constant external demagnetizing magnetic field



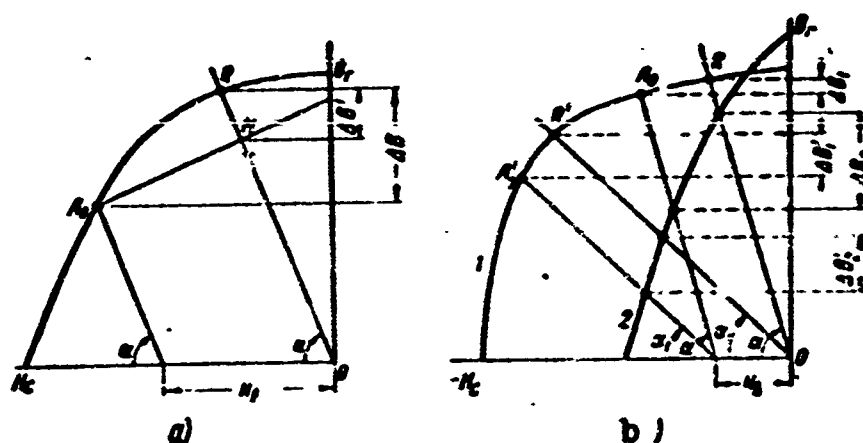


Fig. 4.12. Effect of external field  $H_v$  on magnitude of  $B$  depending on permeance of magnetic circuit (slope of line  $OR$ ) and type of magnetic alloy (curves 1 and 2).

of strength  $H_v$  is acting, line  $OR$  will be shifted parallel to itself to the left by an amount  $H_v$ , while point  $R$  will shift downward along the  $B_r H_c$  curve to point  $A_0$ . In this case, the induction in the magnet will drop by an amount  $\Delta B$ . After the external field has been removed, point  $A_0$  returns to line  $OR$ , not along the demagnetization curve but along a minor hysteresis loop to point  $M$ . In this case, the magnetic induction in the magnet drops by an amount  $\Delta B'$ , which represents the irreversible induction (flux) loss.

Subsequent applications of an external field of the same strength will produce a further slight drop in magnetic induction, since several of the early minor hysteresis loops do not come together but approach stability conditions asymptotically. After several repetitions of the cycle (5-6) the minor loops begin to coincide, and there is no further change in the induction.

The magnetic properties of the magnet may be restored by again magnetizing the magnet to saturation.

The same phenomenon is also observed when alternating external magnetic fields of the same strength are applied.

A 50-cps alternating field yields practically the same results as

far as the change in  $B$  is concerned as a (5-6)-fold application of a constant magnetic field of the same strength.

The reversible and irreversible changes in magnetic flux in a magnet caused by external magnetic fields also depend on the magnetic-circuit reluctance and the type of magnetic material. Precisely the same value of demagnetizing field  $H_v$  will produce differing induction drops in the magnet, depending on whether the magnet operates with a large ( $\Delta B'_1$ ) or small ( $\Delta B_1$ ) external reluctance (Fig. 4.12b).

The shape of the demagnetization curve, i.e., the type of material, also affects the magnitude of  $B$  for a given value of demagnetizing field ( $\Delta B_1$  and  $\Delta B_2$ ) and ( $\Delta B'_1$  and  $\Delta B'_2$ ).

Effect of high-frequency external magnetic fields. Experiments have shown that the metal materials used in permanent magnets are capable of shielding themselves against the effects of high-frequency external transient fields.

If a permanent magnet is subjected to prolonged high-frequency pulses of an external magnetic field, demagnetization will be observed.

The magnet will be demagnetized by each pulse in turn up to about 15 oscillations, and then a new magnetic condition will be established in the magnet; it will be maintained despite the continuing action of an external high-frequency magnetic field. It has been established that the degree of magnet demagnetization is greater the higher the coercive force of the material.

In materials with low values of  $H_c$ , electromagnetic shielding limits the penetration of external magnetic fields within the magnet, and such materials are in a good position with respect to demagnetization.

Magnets may be shielded by applying a thin layer of material with high permeance to the surface of the magnet; this is effective, for example, when the entire surface of the magnet is covered with a thin

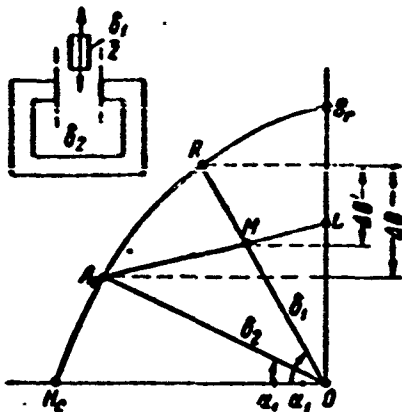


Fig. 4.13. Effect of variation in reluctance on magnetic properties.

layer of copper.

A magnet is frequently shielded against the action of external fields with the aid of a magnetic shunt, which damps the external magnetic field (this method is used in many sensitive instruments).

Effect of variation in reluctance. The magnetic flux in the air gap may change also owing to variations in the reluctance of the magnetic circuit.

In practice, a variation in  $R_\delta$  results from a change in the size  $\delta$  of the air gap in the magnetic circuit. This may happen as a result of expansion and contraction of steel sections, shocks, and also occurs frequently under normal service conditions of the device itself (lifting magnets).

Let us assume that under operating conditions, a strip of soft steel is periodically brought into and out of the air gap; in this case, the air gap will be either  $\delta_1$  or  $\delta_2$  (Fig. 4.13).

Let us magnetize the device with the steel strip in the air gap. In this case, line OR and point R on the  $B_r H_c$  curve will characterize the magnetic condition of the device.

The first time the steel strip is removed from the air gap, the gap size will increase to  $\delta_2$ , and the working point will shift along the  $B_r H_c$  curve to position  $A_0$ . Line  $OA_0$  and point  $A_0$  now correspond to the new magnetic condition of the device, i.e., the magnetic induction has decreased by the amount  $\Delta B$ .

If we now return the plate to its initial position, i.e., decrease the air gap to the initial value at  $\delta_1$ , point  $A_0$  will move to point M by way of a minor hysteresis loop. As the gap subsequently alternates

between  $\delta_1$  and  $\delta_2$ , the working point will move along the line  $A_0M$ .

The effect of external reluctance on the magnetic properties of a circuit with a permanent magnet depends on the shape of the demagnetization curve (Fig. 4.14). For example, in a device having an external magnetic-circuit reluctance that is low (small  $\delta$ ) vanadium steel with 6% W will develop more energy than alnico alloy (line OE), i.e., the external magnetic-circuit reluctance has not been properly selected.

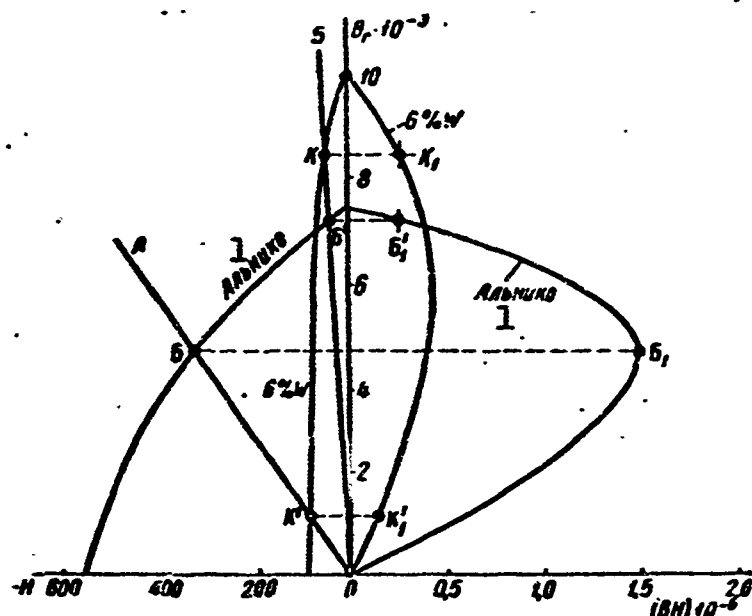


Fig. 4.14. Effect of external magnetic-circuit reluctance on specific energy developed by various alloys. 1) Alnico.

An increase in the air gap causes a sharp drop in the induction and external-circuit energy in a circuit with vanadium steel, while in a circuit using alnico, the drop in induction is accompanied by an increase in external-circuit energy (line OA).

#### Magnet Stabilization

In order to increase the stability of permanent-magnet properties, they are normally subjected to an aging process — stabilization.

Magnet stabilization may be carried out by applying a constant or alternating external demagnetizing field that is stronger than the strongest field that can possibly appear during service, or by demag-

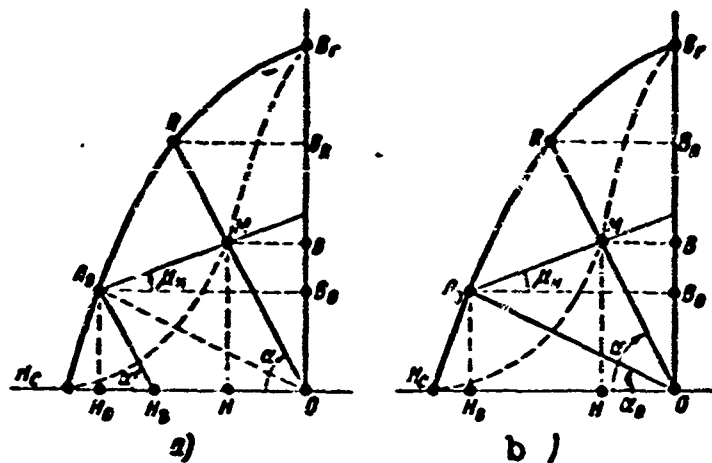


Fig. 4.15. Magnet stabilization. a) By external field  $H_v$ ; b) by opening magnetic circuit ("by air"). The dashed lines indicate the position of the working point on the reversal line, depending on the degree of magnet stabilization.

netizing the magnet in air under the influence of the free poles of the magnet itself (open-circuit stabilization).

Figure 4.15 gives demagnetization curves for the first and second cases (a and b).

Here line  $OR$  is the permeance line for the magnet in a closed circuit, after the magnetizing field has been removed.

In order to stabilize the magnet, we make use in case a of a field strength  $H_v$ , which corresponds to point  $A_0$  with coordinates  $B_0$  and  $H_0$  on the demagnetization curve or line  $H_v A_0$ , parallel to line  $OR$ . After the stabilizing field has been removed, point  $A_0$  moves along a minor hysteresis loop, and the system working point becomes point  $M$  (with coordinates  $B$  and  $H$ ), which is located below point  $R$ .

The difference  $(B_R - B)$  is proportional to the loss in air-gap flux due to stabilization of the magnet.

To stabilize the magnet in case b, it is taken out of the magnetizing apparatus without shunting the poles. The magnetic-circuit reluctance rises and point  $R$  moves to point  $A_0$  which corresponds to

the reluctance of the open magnetic circuit - of the free magnet (line  $OA_0$ ).

After the magnet has been placed into the system, point  $A_0$  moves to point M. If the system operates with a constant air gap and there is no secondary-circuit reaction in it, point M will be the working point of the magnet.

Air stabilization is not recommended where magnetic materials with low values of  $B_r$  and  $H_c$  are to be used, since in this case there is a considerable drop in the efficiency of the magnet.

The slope of the free-magnet permeance line  $OA_0$  may be found by plotting the field pattern for the free magnet and determining the mean permeance of the external air gap.

In the interests of obtaining a stable voltage across generator terminals, it is recommended that a magnet be stabilized within the machine, using a sudden short-circuit current. This is especially sensible with large values of transient reactance  $x'_d$  (low values of short-circuit current).

The degree of magnet stabilization  $k_s$  is defined as the ratio  $H_v/H$  with stabilization by external magnetic field and as the ratio  $\tan \alpha / \tan \alpha_0$  with open-circuit stabilization. The higher the degree of stabilization, i.e., the higher the relative initial demagnetizing field, the more stable the magnet will be under all external influences. The amount by which the degree of stabilization can be increased is limited, however, since magnet efficiency decreases, i.e., the magnet becomes larger.

It is of interest to establish a relationship between the coordinates of the working point M ( $H$ ,  $B$ ) and the point of departure for the reversal line  $A_0$  ( $H_0$ ,  $B_0$ ) on the demagnetization curve.

Using the notation of Fig. 4.15a, the induction at the working

point M may be represented as

$$B = B_0 + (H_0 - H)\mu'_v. \quad (4.7)$$

The expression for the field strength H is somewhat more complicated.

Since  $\tan \alpha = B/H = B_0/(H_0 - H_v)$ , we may use (4.7) where  $k_s = H_v/H$  to obtain

$$\begin{aligned} H &= \frac{B}{\mu'_v} = \frac{B_0 + \mu'_v(H_0 - H)}{B_0} (H_0 - H_v) = \\ &= (H_0 - Hk_c) \left[ 1 + \frac{\mu'_v}{B_0} (H_0 - H) \right] \end{aligned}$$

or, rewriting the last expression for H, we obtain a quadratic equation of the form

$$H^2 - H \frac{(1+k_c)(B_0 + \mu'_v H_0)}{\mu'_v k_c} + \frac{H_0(B_0 + \mu'_v H_0)}{\mu'_v k_c} = 0,$$

whose solution gives the unknown field strength:

$$H = \frac{B_0 + \mu'_v H_0}{2\mu'_v k_c} \left[ (1+k_c) \pm \sqrt{(1+k_c)^2 - \frac{4\mu'_v k_c H_0}{B_0 + \mu'_v H_0}} \right]. \quad (4.8)$$

Only the "minus" sign is meaningful in Formula (4.8). If we substitute the value of H from (4.8) into (4.7), we then obtain

$$B = \frac{B_0 + \mu'_v H_0}{2\mu'_v k_c} \left[ 2\mu'_v k_c - (1+k_c) + \sqrt{(1+k_c)^2 - \frac{4\mu'_v k_c H_0}{B_0 + \mu'_v H_0}} \right]. \quad (4.9)$$

Eqs. (4.7) and (4.8) are used in practice, however.

By moving point  $A_0$  along the  $B_r H_c$  curve, we may use (4.7) and (4.8) to construct the demagnetization curve along which the working point M moves (dashed curves in Fig. 4.15) provided that  $k_s$  and  $\mu'_v$  remain unchanged.

Let us find the equation of the working demagnetization curve for case b, using the notation of Fig. 4.15b.

The induction at the working point B is found from Expression (4.7); in view of the fact that

$$\lg \alpha = \frac{B_0}{H_0}, \quad \lg \alpha = \frac{B}{H}, \quad \frac{\lg \alpha}{\lg \alpha_0} = k_c, \text{ i.e.,}$$

$$H = \frac{B_0 + \mu'_s(H_0 - H)}{\lg \alpha} = \frac{B_0 + \mu'_s(H_0 - H)}{k_c \lg \alpha_0} = \frac{H_0}{B_0} \frac{B_0 + \mu'_s(H_0 - H)}{k_c},$$

the field strength  $H$  is found as

$$H = \frac{H_0(B_0 + \mu'_s H_0)}{\mu'_s H_0 + k_c B_0}. \quad (4.10)$$

If we substitute the value of  $H$  from (4.10) into (4.7) we then obtain

$$B = \frac{B_0 H_0 (\mu'_s + k_c - 1) + k_c B_0^2}{\mu'_s H_0 + k_c B_0}. \quad (4.11)$$

We thus obtain the desired relationships

$$H \text{ and } B = f(H_0, B_0) \text{ for } \mu'_s \text{ and } k_s = \text{const.}$$

In like manner, for case a we may use (4.7) and (4.10) to plot the working demagnetization curve.

#### 4.3. LEAKAGE

The primary-circuit leakage flux in machines using electromagnetic excitation becomes quite large, especially for salient-pole synchronous machines using internal poles and direct-current machines with commutating poles. In aircraft machines, which are relatively low in power and have high linear loads, the leakage flux reaches even greater values.

Considerable difficulties are encountered in calculating leakage fluxes, since the leakage paths are complicated. This makes it necessary to use empirical formulas.

In designing permanent-magnet machines it is assumed that the entire leakage flux  $\Phi_c$  is concentrated at the ends of the magnets, and that there is a parallel working flux  $\Phi_\delta$  in the air gap; in this case, the flux will remain constant and will equal the sum of the fluxes  $\Phi = \Phi_\delta + \Phi_c$  (actually, the flux  $\Phi$  will be found only in the neutral section of the magnet, and it will decrease as we approach the poles).



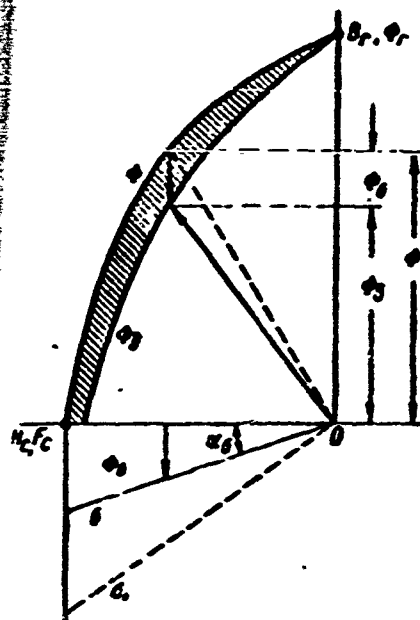


Fig. 4.16. Characteristic curve of magnet with allowance for leakage.  $\Phi$ ) Flux in neutral section of magnet;  $\Phi_g$ ) flux in air gap;  $\Phi_\sigma$ ) leakage flux.

In machines using electromagnetic excitation, in determining the reluctance of the leakage-flux paths, we neglect the pole reluctance in comparison with the air-gap reluctances. In permanent-magnet machines, the pole reluctance cannot be neglected, since  $\mu = 5-8$  in this case, and at the working value of induction,  $\mu = 1.5-3$ , so that the reluctance  $R_m = l_m / \mu S_m$  is quite large.

Taking all of this into account together with the fact that air gaps in permanent-magnet machines are made as small as possible and that the pole height is normally small, we may conclude that the leak-

age factor for permanent-magnet machines is normally not considerable.

Figure 4.16 gives characteristic curves for a magnet, allowing for pole leakage. Here the  $\Phi_\sigma$  term in the magnetizing-force function is represented as a line drawn down from the  $x$  axis at an angle  $\alpha_\sigma$  corresponding to the leakage flux: the flux  $\Phi_\sigma$  is directly proportional to the magnetizing force  $F$ , since the flux path is basically completed through air, and thus equals zero at point 0, where  $F = 0$ .

The tangent of the slope  $\alpha_\sigma$  of the leakage line  $\sigma$  equals the leakage permeance of the magnet

$$\operatorname{tg} \alpha_\sigma = \frac{\Phi_\sigma}{F} = \Lambda_\sigma \quad (4.12)$$

The curve makes it possible to determine the relationship between the magnetizing force at the surface of a pole and the useful flux, if we subtract the ordinates of line  $\sigma$  from the ordinates of curve  $\Phi$ ,

i.e.,

$$\Phi_s = \Phi - \Phi_o.$$

### Determining Pole Leakage Flux

The entire pole leakage flux is divided into two parts: the pole-piece leakage flux  $\Phi_{on}$ , which is an external flux with respect to the magnet; and the leakage flux between the surfaces of the magnet pole core  $\Phi_{om}$ , which is an internal flux with respect to the magnet (Fig. 4.17).

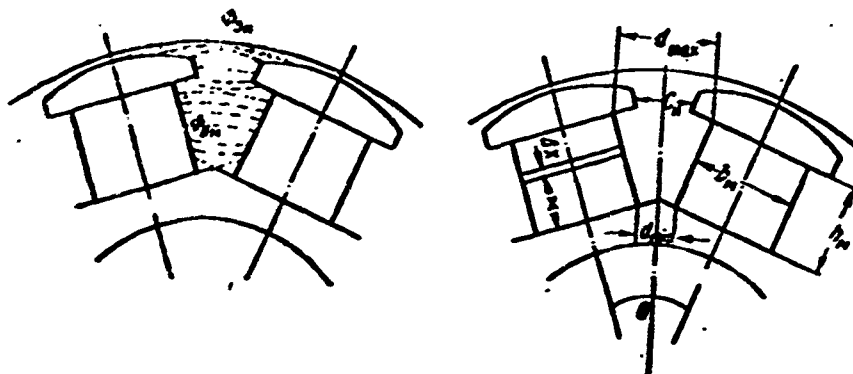


Fig. 4.17. Pole leakage. a) Pole-leakage pattern; b) dimension designations.

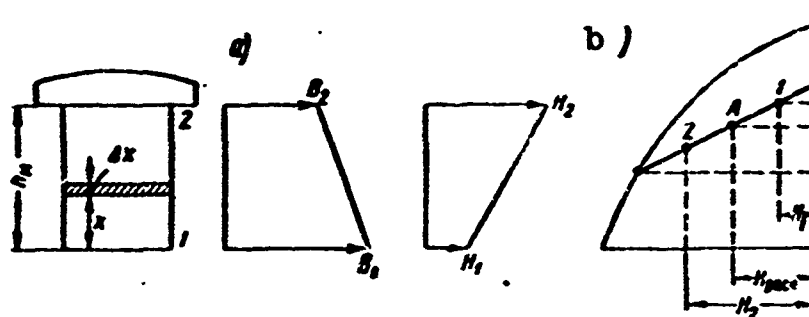


Fig. 4.18. Effect of leakage flux  $\Phi_{om}$  on the distribution of induction. a) Change in induction and field strength along height of magnet; b) determination of design value of field strength  $H_{rasch}$ .

No difficulties are involved in determining  $\Phi_{on}$ , and the calculation is carried out by a method commonly employed in electrical-machine design.

The leakage flux  $\Phi_{om}$  changes the induction in the magnet along

the height of the magnet, and as a result the specific magnetizing force (field strength) developed by the magnet will also vary along the height of the magnet, which complicates design calculations. Under the influence of the leakage flux  $\Phi_{om}$ , the induction decreases along the height of the magnet as we go away from the base of the pole (from the point  $x = 0$  to the point  $x = h_m$ ), while the specific magnetizing force developed by the magnet increases (Fig. 4.18).

In Fig. 4.18b, point 1, corresponding to the base of the magnet ( $x = 0$ ) has an induction  $B_1 > B_2$  and a specific magnetizing force  $A_1 = 0.8H_1 < A_2 = 0.8H_2$ , where  $B_2$  and  $A_2$  are the coordinates of point 2, which correspond to the surface of the pole at the pole piece ( $x = h_m$ ).

If we allow for the fact that the induction is not constant along the height of the magnet, the calculation of the leakage flux for the pole core of a permanent magnet becomes greatly complicated.

Let us note that the induction in the core of an electromagnet also varies along the height of the pole under the influence of  $\Phi_{om}$ , and even more than in the case of permanent magnets. The specific magnetizing force, however, developed by an electromagnet varies less, since the drop in magnetic potential in the pole core is slight, and may be neglected. At the same time, the drop across the high reluctance of a permanent magnet is large and the change in field strength has a substantial effect on  $\Phi_{om}$ .

In order to simplify the calculations for the internal scattering flux, which depends on the distribution of magnetizing force along the length of the magnet, we replace the true leakage flux by an equivalent theoretical flux passing through the entire length of the magnet, as in the case of the leakage flux for the pole pieces.

Thus, the internal leakage flux is also considered to be external, i.e., to originate entirely from the surface of the pole.

The magnitude of the equivalent leakage flux for the pole core is so chosen that the specific magnetizing force corresponding to the equivalent pole flux will now be a constant quantity which when multiplied by the length of the magnet will equal the total magnetizing force of the pole. We thus now proceed on the basis of the theoretical field strength (point A on Fig. 4.18), which equals

$$H_{p2.v} = \frac{1}{h_m} \int_0^{h_m} H_x dx. \quad (4.13)$$

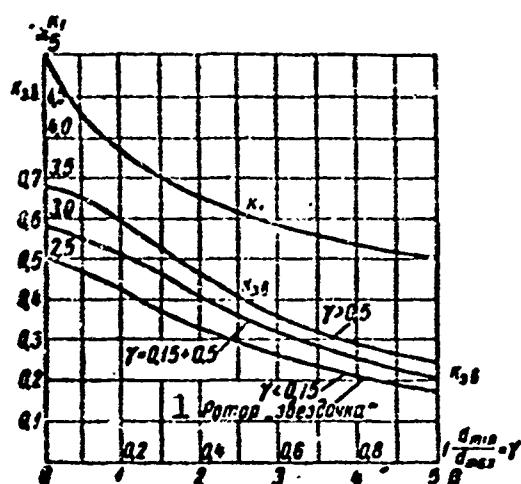


Fig. 4.19. Design coefficients for pole leakage  $k_{z.v} = f(\gamma, \beta)$  and  $k_1 = f(\gamma)$ . 1) "Spider" rotor.

Taking all of this into account and assuming that the cross section and reversal factor along the entire height of the magnet are constant, T.G. Soroker has suggested an expression for calculating the leakage permeance of the poles in permanent-magnet machines; it takes the form

$$\Lambda_{z1} = k_{z.v} \Lambda_{m1} + \Lambda_{n1}. \quad (4.14)$$

where  $\Lambda_{m1} = l_m \lambda_{m1}$  is the leakage permeance of the magnet pole;  $\Lambda_{n1}$  is the

leakage permeance of a pole piece;  $k_{z.v} = f(\gamma, \beta)$  is a coefficient that allows for the decrease in pole permeance caused by the allowance for magnet reluctance;

$$\gamma = \frac{d_{min}}{d_{max}}; \quad \beta = \sqrt{0.8 \frac{h_m \Lambda_{n1}}{\mu_v b_m}}. \quad (4.15)$$

$\mu_v$  is the reversal coefficient;  $\lambda_{m1}$  is the specific leakage permeance of the magnet pole core, found as in the case of electromagnet machines;  $d_{min}$  is the smallest pole separation (at the base);  $d_{max}$  is the maximum pole separation (at the tip of the pole core);  $h_m$  is the height of the magnet.

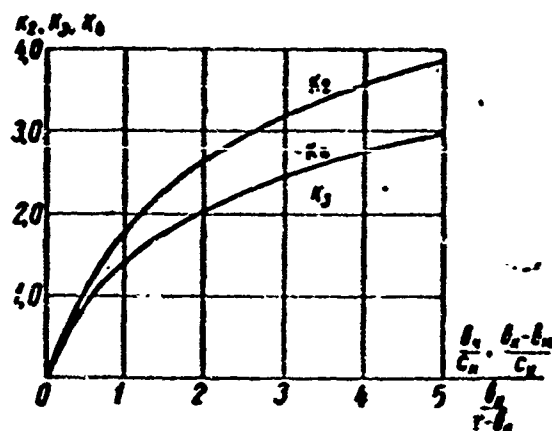


Fig. 4.20. Design coefficients for pole leakage.

$$k_1 = f\left(\frac{b_1}{r - b_1}\right), \quad k_2 = f\left(\frac{b_2}{c_1}\right), \\ k_3 = f\left(\frac{b_1 - b_2}{c_1}\right).$$

The  $k_{z.v}$  function is found from Fig. 4.19 after the value of  $\Lambda_{m1}$  has been determined. For a rotor of the "spider" type the curve corresponding to  $\gamma < 0.15$  is used, and  $\Lambda_{n1} = 0$ .

The leakage permeance of a magnet pole equals

$$\Lambda_{m1} = \lambda_{m1} l_m = h_m \left( \frac{l_m}{d_{max}} k_1 + k_2 \right), \quad (4.16)$$

where  $k_1 = f(\gamma)$  and  $k_2 = f(b_m/d_{max})$ .

For a "spider" type rotor

$$\Lambda_{m1} = \lambda_{m1} l_m = h_m \left( \frac{5l_m}{r - b_1} + k_2 \right), \quad (4.17)$$

where

$$k_2 = f\left(\frac{b_2}{r - b_1}\right).$$

The leakage permeance of the pole pieces is

$$\Lambda_{p1} = 5l_m \frac{b_2}{c_1} + [2h_m + 2l_m - (l_m + l_2)] k_3 + k_4 l_m, \quad (4.18)$$

where  $l_m$  is the length of the magnet core;  $l_2$  is the length of the armature core; and  $l_n$  is the length of a pole piece;

$$k_3 = f\left(\frac{b_2}{c_1}\right); \quad k_4 = f\left(\frac{b_2 - b_1}{c_1}\right).$$

$k_1$ ,  $k_2$ ,  $k_3$ , and  $k_4$  are found from Figs. 4.19 and 4.20.

M.I. Zemlyana used a fluxmeter to determine the influence of the air gap on the leakage flux of a twelve-pole spider-type magnet assembled in the armature with half-closed slots. The results of the investigation showed that the smaller the air gap in permanent-magnet machines, the greater the useful machine flux caused by the increase in total flux and the decrease in leakage flux; at zero gap, the leakage did not equal zero – the leakage flux travels along the magnet faces and in the armature slots.

The leakage flux with zero gap under no-load conditions reached 10% of the total flux, i.e.,  $k_g \approx 1.1$ . When the gap was increased to 0.3 mm, the leakage flux rose to 20% of the total flux  $\Phi$ . A further increase in  $\delta$  to 2 mm raised  $\Phi_g$  to  $0.3\Phi$ ; when  $\delta > 3$  mm,  $\Phi_g$  increased slowly and no longer was proportional to the gap size; it reached  $0.7\Phi$  with the rotor removed (free).

Here we should mention that the total flux  $\Phi$  of the magnet also decreased.

Experience has shown that with the rotor removed, the total flux is roughly halved, and the leakage flux rises to 70% of the total flux, with the useful flux amounting to only 30% of the total flux, while the leakage coefficient reaches the enormous value of 3.34.

#### Effect of Method of Magnetization and Fittings on Magnet Characteristic Curve

If the magnetic circuit consists of several elements (magnet, pole pieces, and armature), there will be three permeances:

- a) the permeance of the free magnet ( $\Lambda_s$ );
- b) the permeance of the magnet together with the pole piece ( $\Lambda'_s$ );
- c) the permeance of the magnet in assembled form ( $\Lambda_0$ ) – in the machine – as shown in Fig. 4.21.

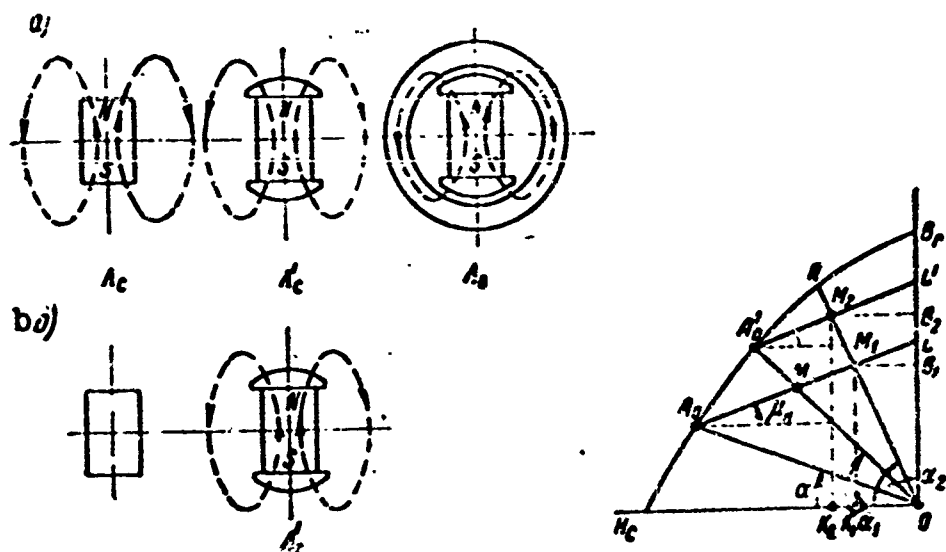


Fig. 4.21. Effect of method of magnetizing in presence of fittings. a) Magnetization outside machine without pole pieces;  $\Lambda_s$ ) free-magnet permeance without fittings (line  $OA_0$ );  $\Lambda'_s$ ) free-magnet permeance with fittings (line  $OM$ , point  $M$  on reversal line  $A_0L$ );  $\Lambda_0$ ) permeance of assembled machine (line  $OR$  or  $M_1$  - the working point); b) magnetization with pole pieces, outside machine;  $\Lambda'_s$ ) permeance of free magnet with fittings (line  $OA'_0$ , point  $A'_0$  - on demagnetization curve:  $M_2$  - working point).

The location of the working point under no-load conditions depends on the method of magnetization. There are two possible ways of magnetizing a magnet - with or without the fittings.

If the magnet is magnetized (Fig. 4.21a) and the pole piece is then attached to it and the inductor placed into the machine in this form,  $A_0$  will be the point of departure for the reversal line  $A_0L$ , and  $M_1$  will be the no-load working point. Moreover,  $\tan \alpha$ ,  $\tan \alpha_1$ , and  $\tan \alpha_2$  refer, respectively, to the permeances of the free magnet, the free magnet with pole pieces, and the magnet as assembled in the machine. Similarly, points  $A_0$ ,  $M$ , and  $M_1$  will correspond to the energy of the free magnet, the energy of the free magnet with pole pieces, and the energy of the magnet as assembled in the machine. If, however, the magnet is magnetized with the pole pieces attached (Fig. 4.21b),  $A'_0$

will be the point of departure for the reversal line  $A'_0L'$ , and  $M_2$  will be the no-load working point.

Since rectangle  $K_2M_2B_2O$  is larger in area than rectangle  $K_1M_1B_1O$ , the magnet energy, which is proportional to the area, will be greater in the second case.

Thus, it is sensible to magnetize the magnet together with the pole pieces, since in this case the point of departure for the reversal line will be raised, and the magnet will have a better weight-to-strength ratio with open-circuit stabilization. Physically, this is explained by the fact that the permeance of the free magnet with pole pieces (fittings) is higher, and the leakage permeance lower, than in the absence of the pole pieces.

#### 4.4.\* OPERATING MODES OF PERMANENT-MAGNET GENERATORS

##### No-Load Conditions

With no load on the generator, the magnetizing force at the pole surface (i.e., the free magnetizing force, is used to overcome the magnetic potential drop across the magnetic circuit (excluding the permanent magnet itself). In the general case, the magnetic-potential drop will equal

$$F_0 = U_\delta + U_{shch} + \sum U_i. \quad (4.19)$$

where  $U_\delta = 0.8\delta'B_\delta$  is the drop across the active air gap;  $U_{shch} = 0.8\delta_{shch}B_{shch}$  is the drop across the inactive air-filled slot;  $\sum U_i = U_z + U_{ya} + U_k + U_j$  is the drop in the magnetically soft steel sections of the magnet circuit;  $U_z$  and  $U_{ya}$  are the drops in the teeth and in the armature core;  $U_k$  and  $U_j$  are the drops in the fingers (pole pieces) and in the pole ring.

The curves for the functions  $\phi = f(F)$  or  $E = \varphi(F)$  are nearly straight lines, since saturation of the magnetic circuit in permanent-magnet machines is normally slight. If the line is taken to be straight,



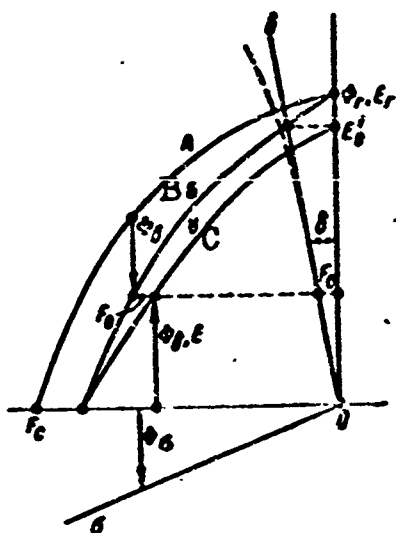


Fig. 4.22. Magnet diagram, no-load conditions.  $O\delta$ ) No-load line;  $O\sigma$ ) leakage line. Curve C is obtained by subtracting the abscissas of curve B and line  $O\delta$ .

and we consider the drop across a slot as part of the total drop in the secondary magnetic circuit,

$$F_0 = 0.8B_1 \left( \delta' + \frac{\sum U_i}{0.8B_1} \right) = 0.8\delta'' B_1. \quad (4.20)$$

Here  $\delta'' = k_0 \delta + 1.25(\sum U_i / B_0)$  cm is the reduced theoretical air gap with allowance for the magnetic-potential drop in the entire magnetic circuit of the machine, with the exception of the permanent magnet;

$$B_1 = \frac{\Phi}{S_1} = \frac{\Phi}{\alpha' \tau} \text{ [gauss]} \quad (4.21)$$

is the maximum induction in the air gap under no-load conditions;

$$\Phi = \frac{E \cdot 10^8}{4k_0 k_{0w} f} \text{ [maxwells]} \quad (4.22)$$

is the useful flux in the air gap that induces the armature emf  $E$ ;

$\alpha' = b' / \tau$  is the calculated pole pitch, which in general will equal

$$\alpha' = \alpha k_\alpha + \frac{4}{\frac{\tau}{\delta} + \frac{6}{1-\alpha} \frac{\delta_{\max}}{\delta}}. \quad (4.23)$$

With the same air gap, i.e.,  $\delta = \delta_{\max}$ ,

$$\alpha' = \alpha + \frac{4}{\frac{\tau}{\delta} + \frac{6}{1-\alpha}}. \quad (4.24)$$

The coefficient  $k_\alpha = f(\delta_{\max} / \delta)$  is found from Table 4.2.

TABLE 4.2

Calculation of Pole Coverage

$\frac{\delta_{\max}}{\delta}$	1.0	1.5	2.0	2.5	3.0
$k_\alpha$	1.0	0.85	0.77	0.71	0.66

In the magnet diagram (Fig. 4.22), the no-load line is represented by line  $O\delta$ , which runs at an angle  $\delta$  to the  $x$  axis. The tangent of the

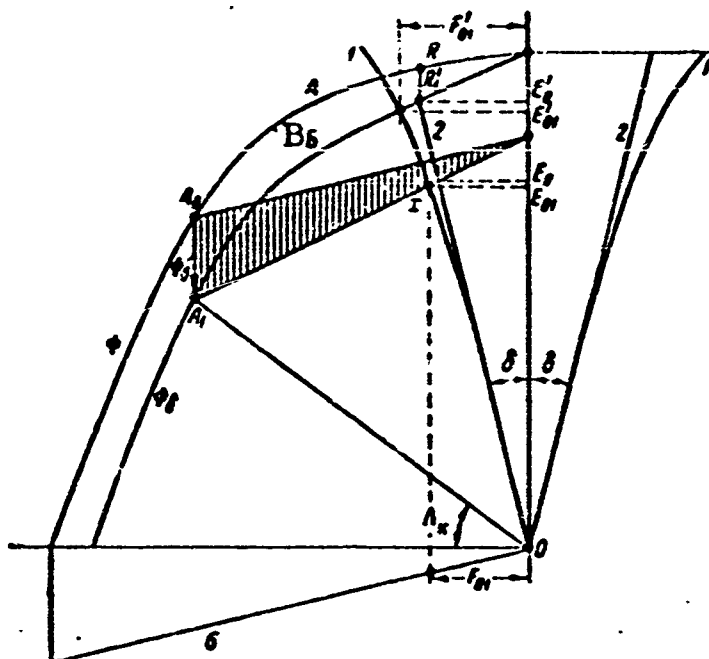


Fig. 4.23. No-load diagram with "air" stabilization. 1) No-load curve allowing for saturation. x) No-load point with operation on reversal line.

slope of the no-load curve equals the design reluctance of the air gap  $R_\delta$ , i.e.,

$$\operatorname{tg} \delta = \frac{F_0}{\Phi_0} = \frac{0.8 \alpha' B_\delta}{S_\delta B_\delta} = 0.8 \frac{\alpha'}{\alpha' \tau l} = R_\delta. \quad (4.25)$$

where  $S_\delta = \alpha' \tau l$  is the design air-gap cross-section area.

The design air-gap reluctance may also be obtained from the expression

$$R_\delta = \frac{l_\delta}{\mu S_\delta} = 0.8 \frac{\alpha'}{\alpha' \tau l}. \quad (4.26)$$

If the rotor is magnetized while in the machine, under no-load conditions the armature will develop an emf corresponding to the ordinate  $OE'_{01}$  (Fig. 4.23); if, however, the rotor is magnetized while outside the machine, the no-load voltage will be determined by the ordinate  $OE_{01}$ . The no-load voltage will drop by an amount  $E'_{01} - E_{01}$  owing to the fact that in the second case, the magnet is stabilized "in air" and operates on the reversal line.

It follows from Fig. 4.23 that when the actual no-load curve (1)

is replaced by the straight line (2) there will be some increase in the no-load emf.

### Operating Mode

When a load is placed on a permanent-magnet machine operating as a generator or a motor, a current appears in the armature, which in general forms direct-axis and quadrature-axis components of the armature-reaction magnetizing force.

The nature of the armature reaction in direct-current machines is determined by the position of the brushes with respect to the neutral plane, while in alternating-current machines, it is determined by the power factor of the load.

In permanent-magnet machines, the phenomenon of armature reaction is basically different in nature than in machines using electromagnetic excitation.

The basic difference lies in the fact that in machines using electromagnetic excitation, the armature reaction is reversible, i.e., it acts only at the instant a current flows in the armature, and it disappears entirely, leaving no residual effect when the load is removed. Thus, an elastic deformation of the magnetic field occurs (with no residual deformations).

In permanent-magnet machines, the armature reaction is irreversible under certain conditions, i.e., when the load is removed (armature current ceases) the magnet turns out to be demagnetized under the influence of the armature reaction that previously had occurred. Consequently, in this case there is a residual inelastic deformation of the magnetic field. In order to avoid residual deformations of the magnetic field, permanent-magnet machines are stabilized, i.e., are subjected to the action of a demagnetizing field whose magnitude exceeds the maximum intensity of a field that may be encountered under service

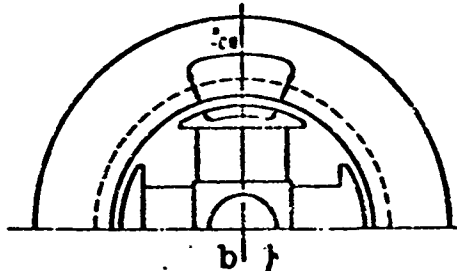
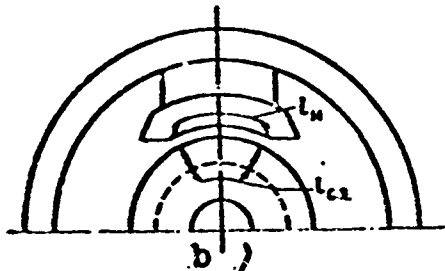
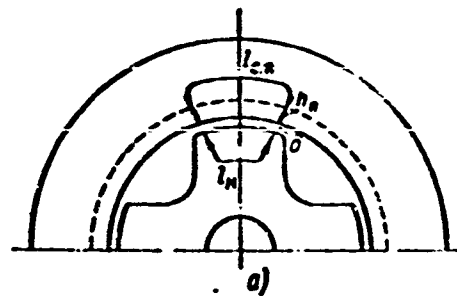
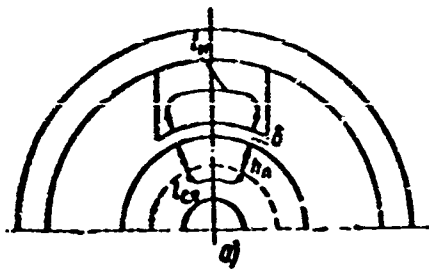


Fig. 4.24. Quadrature-axis armature-reaction field in direct-current permanent-magnet machines. a) Without pole pieces; b) with pole pieces.

Fig. 4.25. Quadrature-axis armature-reaction field in alternating-current permanent-magnet machines. a) Without pole pieces; b) with pole pieces.

conditions.

Let us consider the phenomenon of armature reaction in direct- and alternating-current machines.

Quadrature-axis component of armature reaction. The quadrature-axis armature-reaction flux in electromagnetically excited machines deforms (distorts) the magnetic field in the machine air gap, intensifying magnetization of one half of the pole piece, and reducing magnetization of the other half.

Owing to the phenomenon of saturation, field distortion leads to some decrease in machine flux, which is provided for by a corresponding increase in the excitation magnetizing force.

In permanent-magnet machines whose rotors are made without pole pieces (Figs. 4.24a and 4.25a), the quadrature-axis flux  $\phi_{yaq}$  due to the quadrature-axis component of the armature-reaction magnetizing force will always be less than the same flux in similar machines using

electromagnetic excitation.

This is explained by the fact that in such machines, the reluctance encountered by the quadrature-axis armature-reaction flux is greater than in electromagnetically excited machines. As a matter of fact,

$$\Phi_{aq} = \frac{F_{aq}}{R_q},$$

where  $R_q = R_\delta + R_m + R_{s.ya}$  is the flux-path reluctance for the quadrature axis (for one pole);  $R_\delta$  is the air-gap reluctance;  $R_m$  is the reluctance of the magnet material in the direction perpendicular to the direct-axis field;  $R_{s.ya}$  is the reluctance of the armature teeth and core;  $F_{yaq}$  is the quadrature-axis component of the armature magnetizing force.

The reluctance of the magnet material  $R_m = l_m / \mu S_m$  is large, since the permeability of the magnet material is

$$\mu \approx 0,5 \frac{B_r}{H_c} = 3 + j2,$$

i.e., only 3-12 times more than the permeability of air, and 100-1000 times less than the permeability of the pole-piece steel. At the same time, the reluctance of a soft-steel pole piece in an electromagnetically excited machine is so small that it can always be neglected.

Thus, the quadrature-axis fluxes in electromagnetic and permanent-magnet machines, under identical conditions, will be related as the reluctances

$$\frac{\Phi_{aq}}{\Phi_{aqm}} = 1 + \frac{R_m}{R_\delta + R_{cs}},$$

i.e., the quadrature-axis flux  $\Phi_{yaq}$  due to the quadrature-axis component of the armature-field magnetizing force  $F_{yaq}$  in permanent-magnet machines (without pole pieces) will always be less than the quadrature-axis flux in exactly similar machines using electromagnetic excitation.

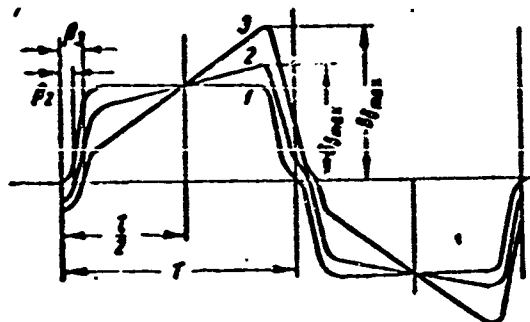


Fig. 4.26. Distortion of field in direct-current machine air gap due to quadrature-axis armature reaction. 1) Curve for field, no-load condition; 2) curve for field under operating conditions, permanent-magnet machine; 3) curve for field under operating conditions, electromagnetically excited machine ( $\beta_3 > \beta_2$ ).

In direct-current permanent-magnet machines, this leads to a situation in which the magnetic field in the air gap is less distorted, i.e., the degree to which the induction maximum increases in the air gap and the displacement of the physical neutral plane  $\beta$  (Fig. 4.26) will be less.

This fact affects machine commutation favorably, and permits some increase in the linear load and pole span, resulting in some reduction in machine size.

In alternating-current permanent-magnet machines, a decrease in the permeance for the quadrature-axis armature-reaction flux leads to a decrease in the quadrature-axis armature-reaction synchronous inductance  $x_{yaq}$ .

If an alternating-current permanent-magnet machine is made with soft-steel pole pieces (Fig. 4.25b) of sufficient height, the quadrature-axis armature reaction will act as in the case of electromagnetically excited synchronous machines. In this case, the armature reaction is taken into account by a standard method.

If the machine is made without pole pieces, with a "spider" type armature (Fig. 4.25a), it is a complicated matter to determine the effect of the quadrature-axis armature reaction, since the permeability of the magnet material is low, and must be taken into account. As investigations have shown, the quadrature-axis armature-reaction field in such machines is small in comparison with the direct-axis field; it magnetizes the magnets in the direction perpendicular to the initial magnetization, and results in almost no change in the main flux or leakage flux.

The quadrature-axis reactance is determined from the well-known expression

$$x_q = x_{s,q} + x_{\sigma}$$

where  $x_{\sigma}$  is the leakage reactance;  $x_{yaq}$  is the armature-reaction quadrature-axis reactance, equal to

$$x_{s,q} = \frac{E}{I} \frac{F_a}{U_a} k_a k'_{z.v} = (x_{s,q})_0 k'_{z.v}. \quad (1.27)$$

Here  $k'_{z.v} \approx \alpha / (1 + 0.25 b_m / \delta' \mu_v)$  is a coefficient that allows for the decrease in the inductance  $x_{yaq}$  owing to the increased reluctance in the quadrature-axis flux path in a machine that has a rotor of the "spider" type, i.e., a rotor without pole pieces.

Direct-axis armature-reaction component. In direct-current machines with brushes located at the neutral plane, there is no direct-axis armature magnetizing-force component. In synchronous machines, it is determined by the well-known expression

$$F_{a,d} = 0.45 m \frac{I_a w_a}{p} k_a$$

In permanent-magnet machines, the effect of the armature direct-axis magnetizing force on the main field depends on the method used to magnetize the magnet.

If magnetization is carried out in the assembled machine, the no-

If the generator is first loaded so that the maximum direct-axis armature-reaction component equals  $F_{ya dk}$ , then by drawing a line parallel to OR, it is possible to obtain point  $A_1$  on the flux line  $\Phi_\delta$  and point  $A_0$  on the demagnetization curve, which represents the point of departure for the reversal line  $A_0L$  (plotted in accordance with the reversal coefficient  $\mu_v$ ).

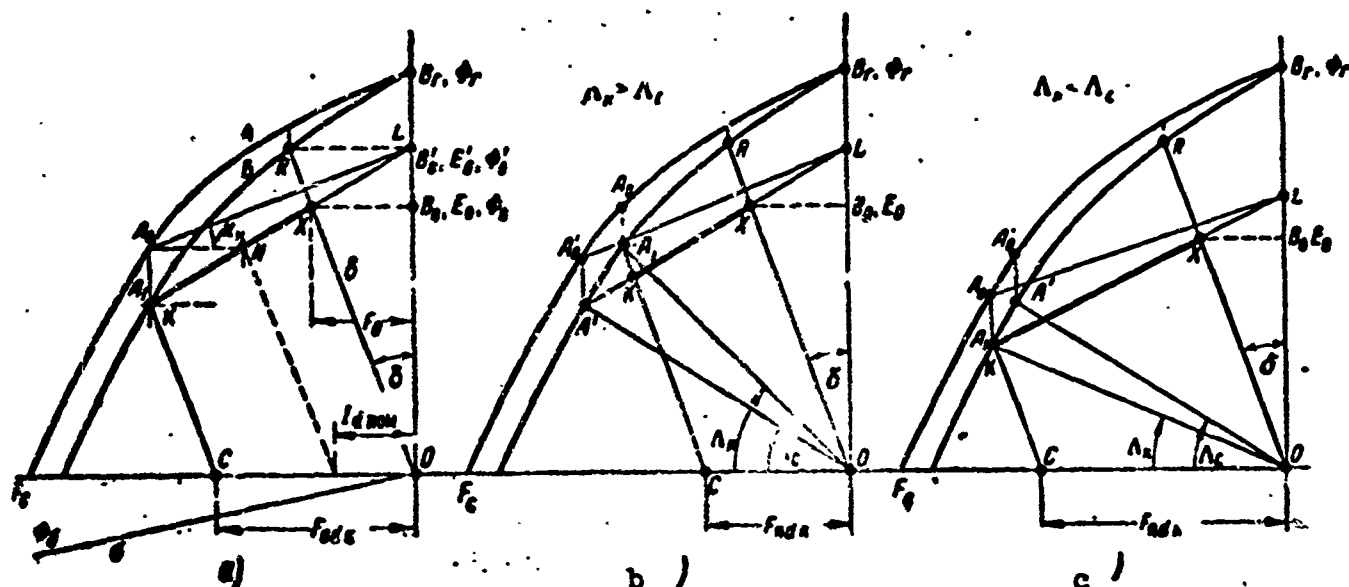


Fig. 4.27. Effect of direct-axis armature reaction, allowing for leakage. a) Magnetization in assembled machine; b) magnetization outside machine ( $\Lambda_s < \Lambda_k$ ); c) the same ( $\Lambda_s > \Lambda_k$ ).

It is clear that the machine voltage under no-load conditions will be lower after the armature reaction  $E_0$  has taken effect than the machine voltage in no-load operation prior to action of the armature



reaction  $E'_0$ , i.e.,  $E'_0 > E_0$ .

Machine operation as a function of load is determined by line  $A_1X$ . Point N corresponds to loading of the machine by the direct-axis current  $I_{d \text{ nom}}$ .

In the case under consideration, where the magnet has been magnetized in assembled form, the armature reaction demagnetizes the machine, i.e., there is inelastic deformation of the magnetic field, and the operating point lies below point R.

If magnetization is performed outside the machine, it is necessary to consider the case in which the permeance of the free magnet is less than the short-circuit permeance and, consequently, the demagnetizing effect of the armature reaction is less than the demagnetizing effect of the free magnet (Fig. 4.27b), as well as the case in which the free-magnet permeance is greater than the short-circuit permeance and, consequently, further demagnetization of the magnet may occur during a short circuit (Fig. 4.27c).

In the first case, where the armature reaction is small, the point of departure for the reversal line will determine the free-magnet permeance (point  $A'_0$ ) which is less than the permeance of the magnet during a short circuit, i.e.,  $\Lambda_s < \Lambda_k$  and, consequently, when the armature current changes from zero to  $I_k$ , the working point will shift along line  $KKh$  away from point  $Kh$ , which corresponds to no-load conditions, to point  $K$ , corresponding to a short circuit. Thus, in the case given, the armature short-circuit reaction will not lead to residual deformation of the pole magnetic flux.

In the second case, where the armature-reaction magnetizing force is high and the magnet permeance during a short circuit is less than the air-gap permeance ( $\Lambda_s > \Lambda_k$ ), the point of departure for the reversal line  $A_0$  determines the magnet permeance during a short circuit.

Consequently, in this case the armature reaction will produce residual deformation of the magnetic field.

If the free-magnet permeance is less than the short-circuit permeance, it makes sense to use a magnetic shunt during installation or disassembly of the magnet in order to increase efficiency. Where  $\Lambda_s > \Lambda_k$ , the magnetic shunt is not used, since the armature reaction results in more severe demagnetization of the magnet than does the demagnetizing effect of the ends of the free magnet.

Magnet curves (see Fig. 4.27) are conveniently represented as shown in Fig. 4.28.

Here line  $kKh$  represents the way in which machine emf depends on armature magnetizing force (current) or represents the reversal line, allowing for the leakage flux and the drop in the magnetic circuit; line  $KA_1$  represents the drop in the magnetic circuit under short-circuit conditions; line  $A_1A_0$  represents the short-circuit leakage flux. Point  $Kh$  on the  $y$  axis corresponds to no load when  $F(I) = 0$ . Point  $K$  corresponds to a short circuit with  $F_{dk}(I_{dk})$ .

In permanent-magnet machines, the direct-axis armature-reaction reactance  $(x_{yad})_{m.e}$  is less than in electromagnetically excited ma-

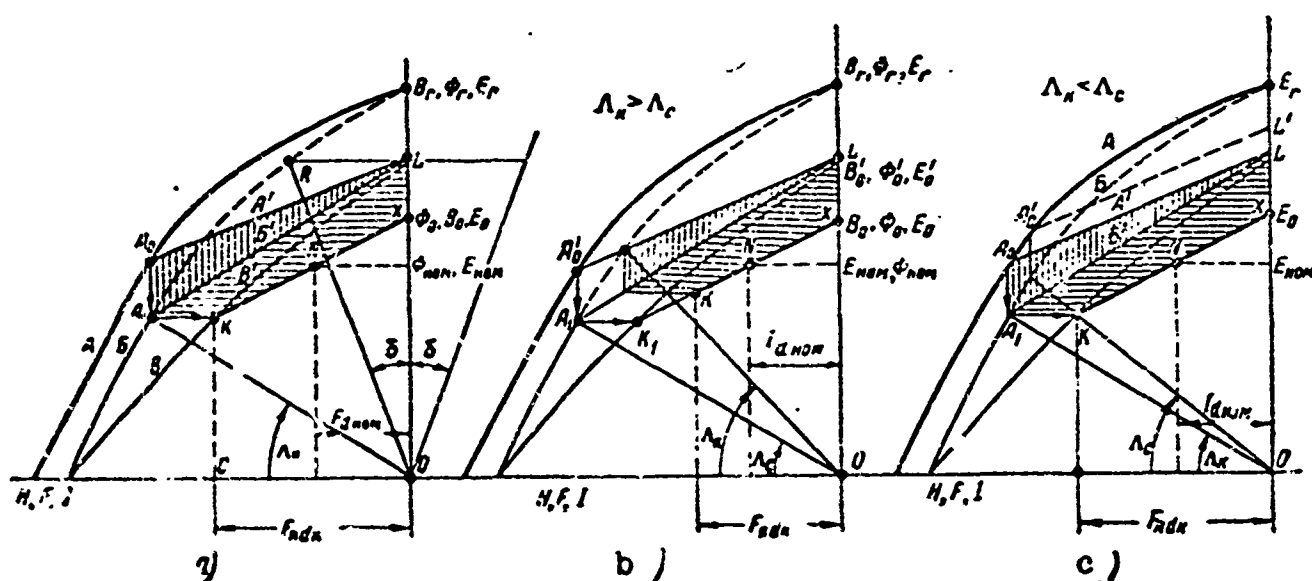


Fig. 4.28. Magnet curves.

chines  $(x_{\text{yad}})_{\text{e.m.}}$ , since the reluctance of the permanent magnet is included in the path  $\Phi_{\text{yad}}$ .

It follows from the equivalence scheme (Fig. 1.59a) that

$$\dot{x}_{\text{ad}} = \dot{\Lambda}_1 \frac{\dot{\Lambda}_m + \dot{\Lambda}_\sigma}{\dot{\Lambda}_m + \dot{\Lambda}_\sigma + \dot{\Lambda}_1} = \dot{x}_1 \frac{\dot{x}_m + \dot{x}_\sigma}{\dot{x}_m + \dot{x}_\sigma + \dot{x}_1}.$$

Thus, in contrast to electromagnetically excited machines, for which  $(\dot{x}_{\text{yad}})_{\text{e.m.}} = \dot{x}_\delta = \dot{\Lambda}_\delta$ , i.e., depends on the air-gap reluctance, the ratio  $(x_{\text{yad}})_{\text{m.e.}}$  also depends on the magnet permeance  $\dot{x}_m = \dot{\Lambda}_m$  and the pole leakage  $\dot{x}_\sigma = \dot{\Lambda}_\sigma$ .

If the ratio  $\dot{x}_\delta / (\dot{x}_\sigma + \dot{x}_m) = 1.19$ , then  $(x_{\text{yad}})_{\text{m.e.}} / (x_{\text{yad}})_{\text{e.m.}} = 0.5 - 0.05$ . As a rule  $(x_{\text{yad}})_{\text{m.e.}}$  decreases faster than  $(x_{\text{yaq}})_{\text{m.e.}}$ , and thus  $(x_{\text{yaq}})_{\text{m.e.}} \geq (x_{\text{yad}})_{\text{m.e.}}$ , while  $(x_{\text{yad}})_{\text{e.m.}} > (x_{\text{yaq}})_{\text{e.m.}}$ .

Complete relative magnet diagram. If we plot the magnet characteristic - the demagnetization curve - in relative coordinates  $\dot{B} = B/B_r$  and  $\dot{H} = H/H_c$ , taking  $B_r$  and  $H_c$  as unity, we are then able to obtain the normal relative characteristic (relative hyperbola), which is suitable for all types of permanent-magnet materials (allowing for a difference in scales for each type of material).

The relative magnet characteristic is approximated by a relative hyperbola.

$$\dot{B} = \frac{1 - \dot{H}}{1 - \frac{\dot{H}}{\dot{B}_s}} = \dot{B}_s \frac{1 - \dot{H}}{\dot{B}_s - \dot{H}},$$

where

$$\dot{B}_s = \frac{B_s}{B_r},$$

$B_s$  is the saturation induction.

The initial quantities taken as unity for the relative diagram are: the induction and flux

$$B_r = 1, \Phi_r = B_r S_m = 1;$$

the emf

$$E_r = 4k_\phi k_0 \omega f \Phi_r \cdot 10^{-8} = 1;$$

the coercive force and magnetizing force

$$H_c = 1, F_c = 0.8 H_c h_m = 1,$$

the armature current

$$I_c = \frac{p F_c}{0.45 m k_d k_0 \omega} = 1.$$

the impedance

$$z_c = \frac{E_r}{I_c} = 1;$$

the reluctance and permeance

$$R_r = \frac{F_c}{\Phi_r} = 1; \Lambda_r = \frac{\Phi_r}{F_c} = 1;$$

the permeability

$$\mu_r = \frac{B_r}{H_c} = 1;$$

the virtual specific magnetic energy

$$A_c = \frac{B_r H_c}{8\pi} = \frac{\Phi_r F_c}{20 V_m} = 1 \text{ erg/cm}^3,$$

where  $V_m = h_m S_m$  is the volume of one pole;

the virtual magnet power

$$S_c = m I_c E_r = \frac{4}{4.5} \frac{k_\phi}{k_d} \frac{\mu \Phi_r}{1000} \frac{F_c}{100} \frac{f}{100} = 1.$$

In the relative magnet diagram, the tangent for the slope of the leakage line equals the relative leakage permeance  $\dot{\Lambda}_\sigma^*$ , i.e.,

$$\text{tg} \dot{\alpha} = \frac{\Phi_\sigma}{\Phi_r} : \frac{F}{F_c} = \frac{H_c}{B_r} \frac{h_m}{b_m} \dot{\Lambda}_\sigma = \frac{\Lambda_\sigma}{\Lambda_r} = \dot{\Lambda}_\sigma, \quad (4.28)$$

while the tangent for the slope of the no-load curve equals the relative calculated air-gap reluctance

$$\text{tg} \dot{\alpha} = \frac{F_0}{F_c} : \frac{\Phi_0}{\Phi_r} = \frac{B_r}{H_c} \frac{S_m}{S_0} \frac{\delta^*}{h_m} = \frac{R_0}{R_r} = \dot{R}_0, \quad (4.29)$$

where  $S_m = b_m l_m$  is the magnet cross-sectional area;  $S_0$  is the theoretical air-gap cross-sectional area;  $h_m$  is the length of the magnet along

the magnetization path (for one pole);  $b_m$  is the width of the magnet;  $l_m$  is the axial length of the magnet,  $\Lambda_{\sigma 1} = \Lambda_{\sigma} / l_m$ .

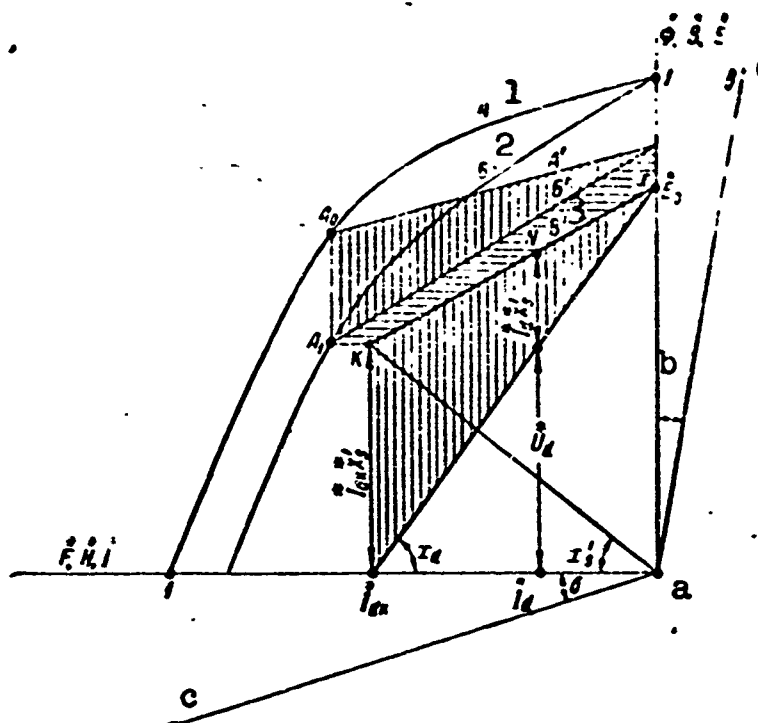


Fig. 4.29. Complete relative magnet diagram. 1) A; 2) B; 3) C'.

Figure 4.29 gives the complete relative magnet diagram for a salient-pole electrical machine without pole pieces (of the "spider" type). On this diagram: A is the demagnetization curve with no allowance for leakage, i.e.,  $\Phi = \varphi(F)$  or  $\Phi^* = \varphi(F^*)$ ; B is the demagnetization curve allowing for leakage, i.e.,  $\Phi_{\delta} = \varphi(F)$  or  $\Phi_{\delta}^* = \varphi(F^*)$ ; C' is the same quantity, allowing for the drop in magnetic potential along the magnetic circuit, i.e., allowing for the no-load curve.

Here and below the symbol "\*" indicates a relative quantity, i.e.,

$$\Phi^* = \frac{\Phi}{\Phi_r}, \quad \Phi_{\delta}^* = \frac{\Phi_{\delta}}{\Phi_r}, \quad F^* = \frac{F}{F_r}, \quad \text{etc.}$$

Point k corresponds to the condition of the magnet under short-circuit conditions provided that the coordinates  $(I_{dk}, E_{dk})$  of point k express, respectively, the direct-axis short-circuit current component and the direct-axis short-circuit emf, equal to

$$E_{dk} = I_{dk} \left( x_s + \frac{R_{ya}^2}{x_s} \right) = I_{dk} x'_s \quad (4.30)$$

with the armature-winding resistance  $R_{ya}$  taken into account or  $E_{dk} \approx I_{dk} x'_s$ , since  $x'_s \approx x_s$ , where  $R_{ya}$  is small.

The quadrature-axis inductance for a current  $I$  may be found directly from the diagram, using the curve for  $\delta$ , as

$$x_{sq} = \frac{E_q}{I} = z_c \operatorname{ctg} \delta k_q k'_{sq} \quad (4.31)$$

since  $\dot{E}_q = k_q k'_{zv} \dot{F}_{ya} \cot \delta$  and  $\dot{I}_{ya} = \dot{F}_{ya}$ .

Line A', drawn at an angle  $\tan \mu$  to the  $\underline{x}$  axis is the reversal line, while B' is the reversal line allowing for leakage.

Line V' is the reversal line allowing for the magnetic potential drop in the external magnetic circuit, and is the internal machine characteristic, i.e., represents the way in which direct-axis machine emf depends on the direct-axis armature-current component; it is obtained by subtracting from the  $\underline{x}$  axis value of line B' the corresponding  $\underline{x}$ -axis values of the no-load curve. If we assume that the machine is not saturated, then line V' will be a straight line.

$\dot{E}_0$  corresponds to the stabilized value of generator emf under no-load conditions, and point  $\dot{I}_{dk}$  to machine short circuiting, when the voltage across the terminals equals zero, and the entire emf is expended in the drop across resistance  $\dot{x}'_s$  due to the current  $\dot{I}_{dk}$ . Thus, line  $\dot{I}_{dk} \dot{E}_0$  is the external generator characteristic for a purely inductive load, i.e.,

$$\dot{U}_d = \dot{E}_d - \dot{I}_d \dot{x}'_s = \varphi(\dot{I}).$$

Thus, for an arbitrary value of direct-axis armature current we can find from the relative diagram:

- a) the longitudinal stator-voltage component  $\dot{U}_d$ ,
- b) the direct-axis voltage drop in the stator winding  $\dot{I}_d \dot{x}'_s$ ,

c) the magnetic potential drop in the magnetic loop - teeth, core, gap -  $\dot{U}_0$ ,

d) the pole leakage flux  $\dot{\Phi}_\sigma$ .

If the machine is somewhat saturated, the curves  $B'$ ,  $V'$ , and  $\dot{I}_{dk} \dot{E}_0$  will be straight lines. In this case, the machine direct-axis reactance may be found from the diagram as

$$x_d = \frac{E_0}{I_{dk}}.$$

In relative form, the direct-axis reactance is expressed in the form

$$\dot{x}_d = \frac{\dot{E}_0}{\dot{I}_{dk}} = \frac{x_d}{z_c} = \lg x_d \quad (4.32)$$

The procedure for plotting a relative diagram for a magnet is as follows:

- using relative units, introduce into the second quadrant the magnetization curve  $A$ , into the third quadrant the leakage line  $\sigma$ , and into the first quadrant, the no-load curve  $\delta$ ;
- plot curves  $B$  and  $V$  in the second quadrant;
- determine the position of point  $k$  at the intersection of curve  $V$  and line  $Ok$ , which runs at an angle  $x'_s$  to the  $x$ -axis; here  $\tan x'_s = x'_s/z_c$  and  $x'_s = E_{dk}/I_{dk}$ ;
- plot lines  $KA_1$  and  $A_1A_0$  and find the point of departure for the reversal line  $A_0$ ;
- plot the reversal line  $A'$  from the value of the reversal coefficient  $\mu_v$ ;
- plot lines  $B'$  and  $V'$ ;
- join  $I_{dk}$  and  $E'_0$  so as to obtain the external machine characteristic for a purely inductive load, i.e., plot the curve representing the function

$$U_d = \varphi(I_d) \text{ for } \cos \varphi = 0.$$

If we know the external characteristic for  $\cos \varphi = 0$ , it is possible to find the function  $U = \varphi(I)$  for a given value of  $\cos \varphi$ .

Let us consider in more detail the equation for the virtual magnet power in view of the fact that

$$S_c = m I_c E_c = \frac{4}{0.45} \frac{k_\phi}{k_d} 10^{-3} (p \Phi_r F_c f) = p \Phi_r F_c f,$$

where  $k_d$  is the direct-axis armature-reaction factor.

Thus, the power developed by a magnet is directly proportional to the residual flux  $p\Phi_r$ , the coercive force  $F_c$ , and the frequency  $f$ .

While in this case the virtual specific energy of the magnet is

$$A_c = \frac{B_r H_c}{8\pi} = \frac{\Phi_r F_c}{20V_m}, \quad (4.33)$$

on the basis of (4.33), the virtual magnet power will be

$$S_c = 0.89 \frac{k_\phi}{k_d} 10^{-6} V_m A_c f = V_m A_c f = A_{c \text{ poln}} f, \quad (4.34)$$

where  $V_m = 2ph_m S_m = 9\pi(k_d/k_\phi)10^6 (S_c/B_r H_c f)$  is the total volume of the magnet;  $A_{c \text{ poln}} = A_c V_m$  is the total virtual energy for the magnet.

Thus, the virtual power developed by a magnet is directly proportional to the total magnet volume  $V_m$ , the virtual specific energy of the magnet  $A_c$ , and the frequency  $f$ , or it is directly proportional to the total virtual magnet energy and the frequency.

The power developed by a permanent-magnet generator is a part of the virtual magnet power, i.e.,

$$S = mUI = BS_c,$$

where

$$B = \frac{mUI}{mE_r I_c} = \frac{UI}{E_0 I_c} \frac{E_0 I_c}{E_r I_c} = B_1 B_2$$

is the utilization factor for the virtual energy of the magnet, and depends on magnet properties ( $\mu_v$ ,  $\gamma$ ), the permissible voltage drop  $\Delta U = U/E_0$ , and  $\cos \varphi$ .



The ratio  $UI/E_0 I_k = \varphi(\Delta U, \cos \varphi)$  is found by using a vector voltage diagram, while the maximum value for  $E_0 I_k / E_r I_c = \varphi_1(\mu_v, \gamma)$  is found from the magnet diagram (either graphically or analytically by approximation to the demagnetization curve).

By using (4.34) it is possible to find the basic dimensions of a permanent-magnet machine

$$D = \sqrt[3]{\frac{S}{\sigma_{m.e} \lambda f}} \quad (4.35)$$

where  $\sigma_{m.e} \approx 3.5 \cdot 10^{-8} B_r H_c k_{z.m}$ ,

$$B_1 \approx \Delta U^2 [\sqrt{\Delta U^{-2} - \cos^2 \varphi} - \sin \varphi] \text{ for } R_s \approx 0; x_s \approx x_g;$$

$$B_{2 \text{ out}} \approx \mu_1 \gamma - 0.5 (\mu_2 - 0.2); \mu_2 = 0.9 - 1.05 \text{ for } \Lambda_s = 4 - 10;$$

$\lambda = l_m / D$  is a structural factor;  $k_{z.m} = S_m / S_{ya}$  is a factor representing the degree to which the rotor cross section is occupied by the magnet.

For a rotor of the "spider" type

$$k_{z.m} = \frac{S_m}{S_r} = \frac{2ph_m h_u}{\frac{\pi D^2}{4}} = 4\alpha \frac{h_u}{D} = 2\alpha p^{\frac{1}{p-1}},$$

where  $\alpha = b_m / \tau$  and  $p < 1$ .

For a rotor with soft-steel pole pieces  $h_p$  high and  $p \geq 2$  (on the basis of the maximum possible magnet cross section)

$$k_{z.m} = \frac{S_{m \max}}{S_r} = \frac{p}{\pi} \left( \frac{D - 2h_p}{D} \right)^2 \operatorname{tg} \frac{90}{p}.$$

An increase in  $p$  causes a decrease in  $k_{z.m}$ , especially when we go from  $p = 2$  to  $p = 3$ . When  $p > 5$ ,  $k_{z.m} \approx \text{const.}$

It follows from the last expression that the power developed by a permanent-magnet machine in first approximation does not depend on the speed, but is determined by the frequency and total energy of the magnet. This distinguishes permanent-magnet machines from electromagnetically excited machines.

## Short-Circuit Conditions

Transient processes in permanent-magnet machines have a considerable effect on their operation under normal conditions, since transient currents may weaken the magnet permanently, and distort the field in the air gap.

The degree of magnet demagnetization, i.e., the point at which the reversal line departs, is determined by the maximum value of the direct-axis armature magnetizing-force component.

In synchronous generators and motors operating in electrical systems of relatively high power, the maximum armature magnetizing force will occur under asynchronous conditions when the line voltage and synchronous-machine emf are  $180^\circ$  out of phase. Asynchronous conditions may occur for a synchronous machine when it drops out of synchronism, or during the process of synchronization (asynchronous starting of synchronous motors, and selfsynchronization of synchronous generators).

The maximum steady current flowing in the internal machine circuit during synchronous operation with small slip may be found from the equation

$$i_{\max} = \frac{E_0 + U}{Z_r + Z_c} \text{ or } I_{d\max} = \frac{E_0 + U}{x_{dr} + x_{dc}},$$

where the subscript "c" refers to line impedances.

The steady short-circuit current across the terminals of a machine with excitation corresponding to  $E_0$  will equal

$$I_k \approx \frac{E_0}{x_{dr}}.$$

Consequently,

$$\frac{I_{d\max}}{I_k} = \frac{E_0 + U}{E_0} \frac{x_{dr}}{x_{dr} + x_{dc}} = \frac{1 + \frac{U}{E_0}}{1 + \frac{x_{dc}}{x_{dr}}}$$

and the maximum direct-axis armature-current component is

$$I_{d \max} = I_k \frac{1 + \frac{U}{E_0}}{1 + \frac{x_{d \epsilon}}{x_{d r}}} \quad (4.36)$$

In parallel operation of  $n$  generators of identical power, assuming that

$$Z_{\epsilon} = \frac{Z_r}{n-1}; \quad x_{d \epsilon} = \frac{x_{d r}}{n-1},$$

it follows from (4.36)

$$\frac{I_{d \max}}{I_k} = \left(1 + \frac{U}{E_0}\right) \frac{n-1}{n}. \quad (4.37)$$

If we assume that  $E_0 = U$ ,

$$\frac{I_{d \max}}{I_k} = 2 \frac{n-1}{n}, \quad (4.38)$$

i.e., when  $n \rightarrow \infty$ , the current multiplier during a transient process approaches  $I_{d \max}/I_k \rightarrow 2$ , while where  $n = 2, 3$ , or  $4$ , the current multiplier will be 1, 1.333, or 1.5, respectively.

Thus, the most dangerous condition from the viewpoint of demagnetizing a synchronous machine (operated as a generator or motor) is operation from a high-power line with the generator emf  $E_0$  vector  $180^\circ$  out of phase with respect to the line voltage  $U$  vector with hyposynchronous conditions.

In direct-current permanent-magnet machines, the maximum direct-axis armature magnetizing-force component will be found with the brushes positioned at the neutral plane, while the maximum quadrature-axis armature magnetizing-force component will occur when the generator is improperly connected for parallel operation, or when a motor is operated under reverse-current conditions.

Influence of nature of short-circuit. The demagnetizing effect of armature magnetizing force during a short circuit depends on the rate at which the short-circuit current rises. Where the armature magnetizing force rises slowly, i.e., when the short-circuited generator turns

over from a stationary position, or when the short circuit is due to a gradual decrease in external-circuit resistance to zero, the short-circuit current and, consequently, its demagnetizing effect as well is determined by the position of the reversal line and the no-load emf that appears following the short circuit.

The instantaneous short-circuit current considerably exceeds the steady short-circuit current, and is determined by the emf existing prior to the short circuit.

In view of all this, the magnet should be stabilized by an instantaneous short circuit; in order to obtain reliable stabilization, at least five short-circuiting operations should be carried out.

The nature of the short circuit has a particularly noticeable effect in the absence of rotor damper circuits.

Together with V.G. Andreyev, the author has conducted investigations into transient processes in single-phase and three-phase permanent-magnet generators using aluminum-lined "spider" type rotors. The generators were stabilized by opening the magnetic circuit, by direct current, by balanced and unbalanced, instantaneous and gradual short circuits. After each stabilization, the generator was again magnetized. In order to discover the effect of secondary damper circuits, investigations were also made in the absence of the aluminum rotor lining.

Figure 4.30 shows the shape of the magnetic field in the air gap under no-load conditions with the magnet stabilized by opening the magnetic circuit, by steady two- and three-phase short-circuit current, by multiple instantaneous short-circuit two- and three-phase currents, and by direct current.

Analysis of the oscillograms given has shown that:

a) the shape of the no-load magnetic-field curve depends on the method used to stabilize the magnet;

b) when the magnet is stabilized by opening the magnetic circuit, the shape of the no-load field is the same as the shape of the no-load field for machines using electromagnetic excitation;

c) when short-circuit current or direct current is used for stabilization, the field curve displays an asymmetric saddle-shaped pattern;

d) maximum demagnetization of the magnet and distortion of the field occurs when direct current is used for stabilization;

e) in addition to direct current, three-phase instantaneous short-circuit current produces high demagnetization and field distortion.

Field irregularity owing to the quadrature-axis armature-reaction field is doubled when steady three-phase short-circuit current is used for stabilization, while it rises by a factor of 3.5 when instantaneous short-circuit current is used for stabilization. The increase in field irregularity when instantaneous short-circuiting is used is explained by the increased dip in the curve, since the instantaneous short-circuit current multiplier is greater than the steady-current multiplier.

Figure 4.31 shows the shape of the field curve with rated current,  $\cos \varphi = 0.96$  and  $\cos \varphi = 0.08$ , and stabilization by opening the magnetic circuit.

Figure 4.32 shows the shape of the field curve for steady two- and three-phase short-circuit currents.

Figure 4.33 gives oscillograms for the emf curve with stabilization by opening of the magnetic circuit and by means of instantaneous three-phase short-circuit current.

The curves show that the emf is nearly sinusoidal in shape, despite the considerable distortion of the magnetic-field curve. We note that the machine tested had a double-layer winding with short pitch

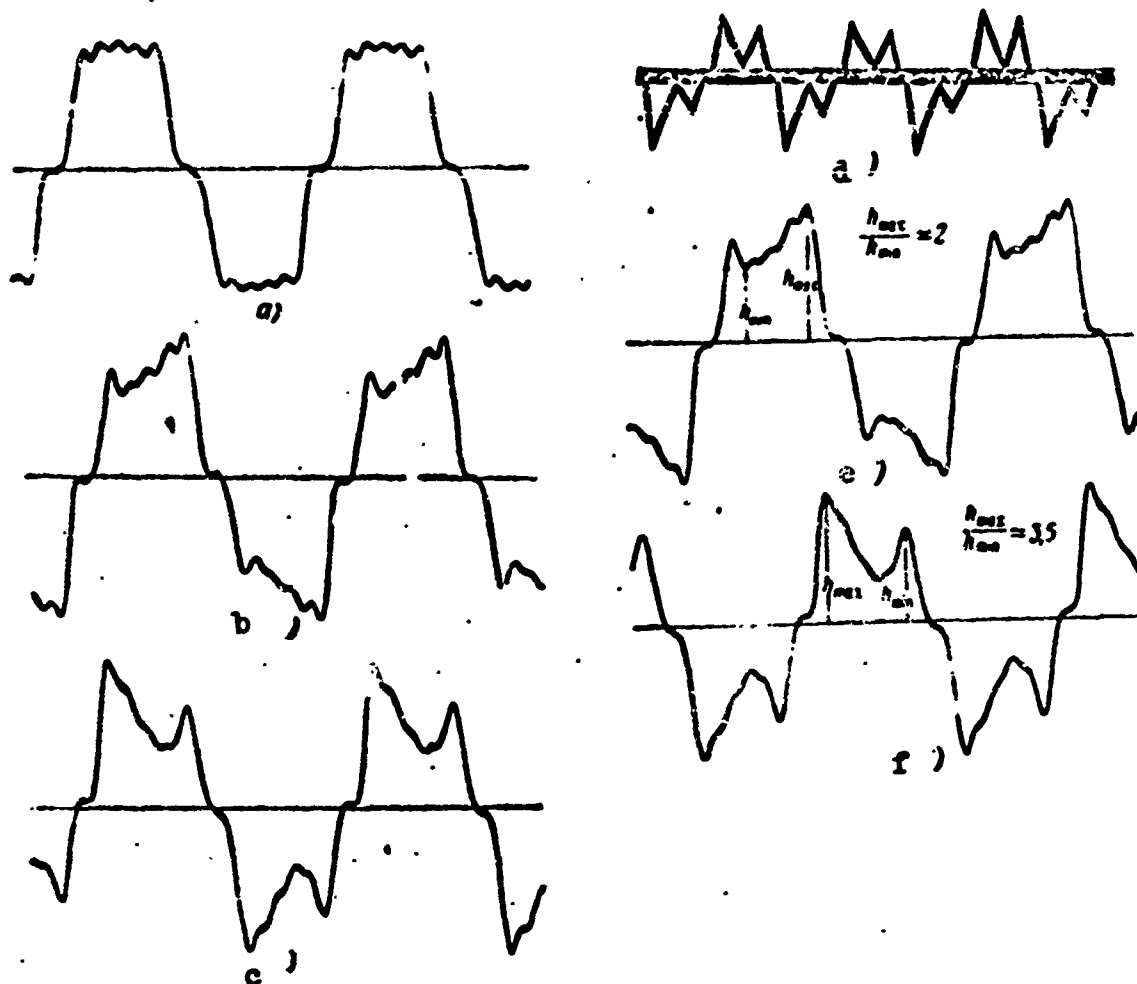


Fig. 4.30. Shape of field in air gap of three-phase permanent-magnet aircraft generator with various stabilization methods. a) "Air" stabilization; b) stabilization by steady two-phase short-circuit current; c) stabilization by instantaneous two-phase short-circuit current; d) stabilization by direct current; e) stabilization by steady three-phase short-circuit current; f) stabilization by instantaneous three-phase short-circuit current.

and a fractional number of slots per pole and phase.

Figure 4.34 gives field curves for stabilization by opening of the magnetic circuit and by instantaneous short-circuit current, as well as the emf curve for single-phase machines following stabilization by instantaneous short-circuit current.

Figure 4.35 shows an oscillogram for instantaneous short circuiting of a three-phase direct-current generator.

The investigations carried out permit us to draw the following conclusions.

1. In order to obtain stable characteristics for permanent-magnet

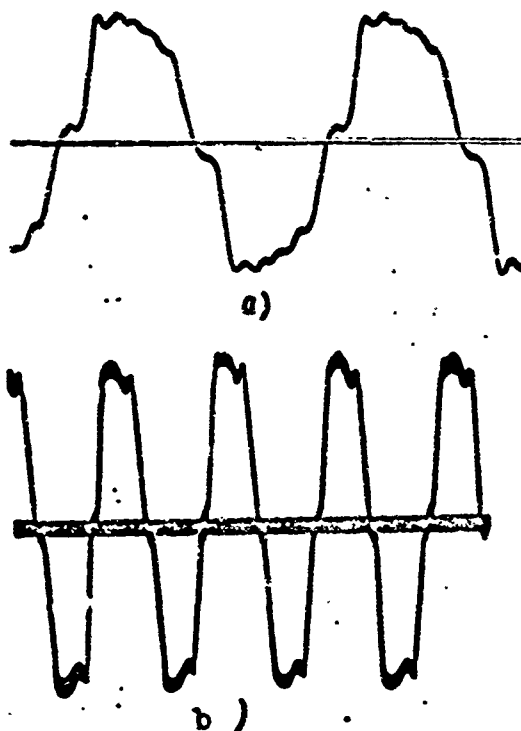


Fig. 4.31. Shape of field curve at rated current following "air" stabilization. a)  $\cos \varphi = 0.96$ ; b)  $\cos \varphi = 0.08$ .

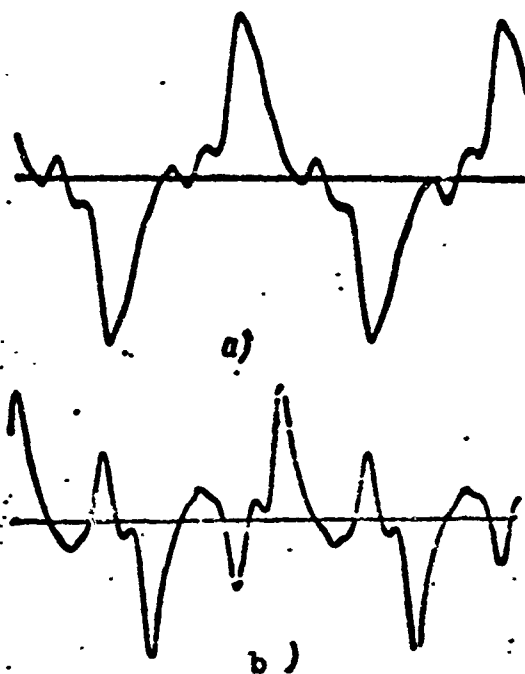


Fig. 4.32. Shape of field curve for steady short-circuit current. a) Two-phase; b) three-phase.

machines, they must (in general) be stabilized under no-load conditions at maximum speed by instantaneous short-circuit current.

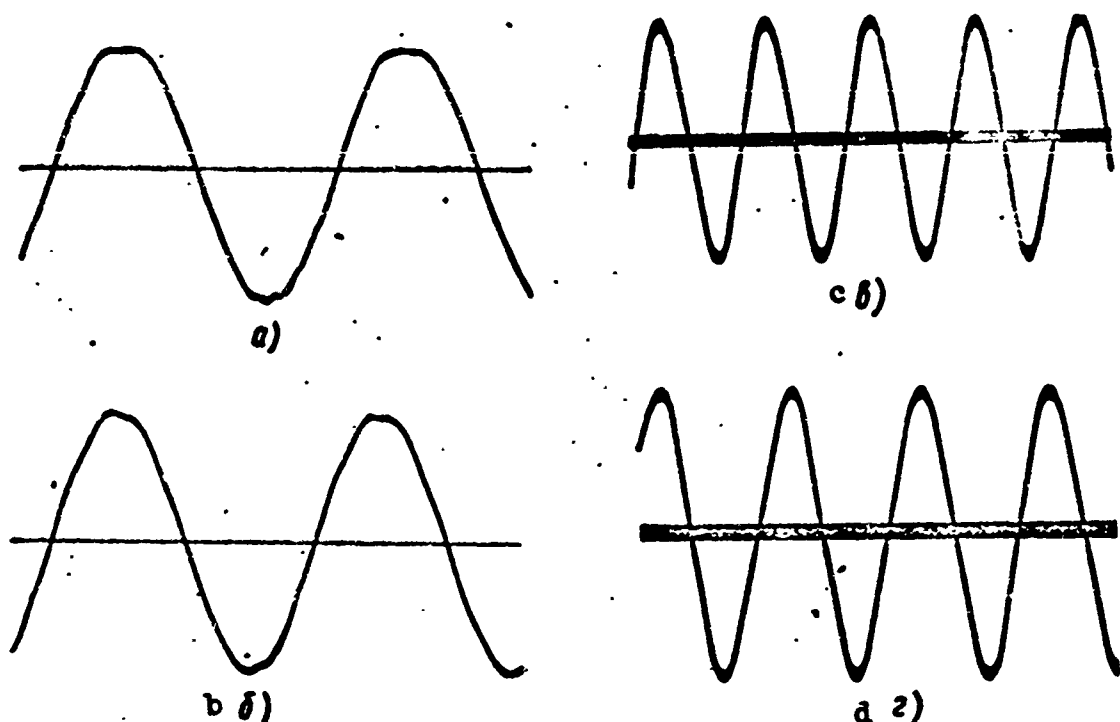


Fig. 4.33. Shape of voltage curves for three-phase permanent-magnet aircraft generator. a) No-load voltage following "air" stabilization; b) no-load voltage with stabilization by instantaneous three-phase short-circuit current; c) voltage at rated current and  $\cos \varphi = 0.96$  ("air" stabilization); d) the same,  $\cos \varphi = 0.08$  ("air" stabilization).

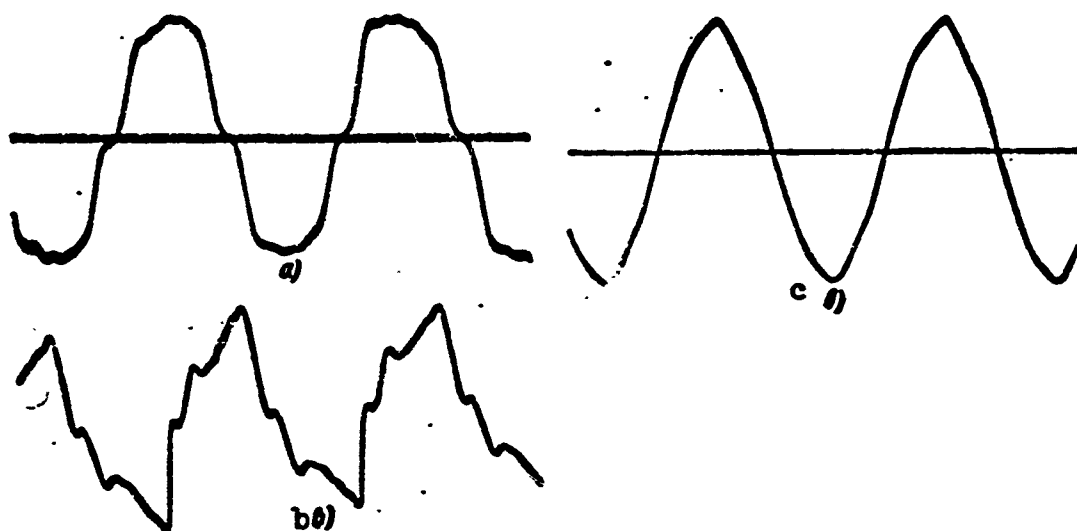


Fig. 4.34. No-load field and voltage curves for single-phase permanent-magnet aircraft generator. a) Field after "air" stabilization; b) field after instantaneous short-circuit current stabilization; c) voltage after instantaneous short-circuit current stabilization.

2. In order to obtain a steady reversal line and maximum short-circuit current (especially for single-phase machines), it is necessary to carry out at least five short-circuiting operations.



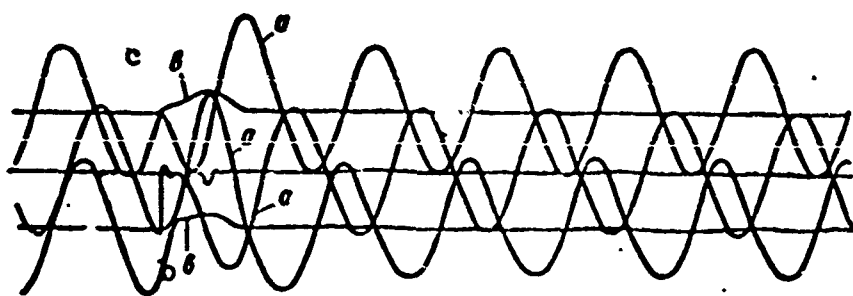


Fig. 4.35. Oscillogram showing instantaneous short-circuit current for three-phase permanent-magnet aircraft generator. a) Armature current after short circuit; b) phase voltages.

3. The "voltage loss" due to stabilization depends on the machine parameters and the efficiency of the rotor damper circuits. For rotors made of alnisi alloy lined with aluminum, the voltage loss is

$$\frac{E_0' - E_0}{E_0'} 100 = 10 \div 20\%$$

when

$$S_{\text{nom}} = 75-500 \text{ watts.}$$

4. In machines using magnets made from alnisi-alnico alloy, the short-circuit permeance is less than the permeance of the open magnetic circuit, and thus they retain their properties when the rotor is disassembled without magnetic shunts.

5. Voltage calibration (decreasing the voltage to the rated value) may be carried out intelligently by applying direct current to the armature winding while the machine rotor is turning.

6. The presence of an aluminum lining decreases the voltage loss by about 2-20% when  $S_{\text{nom}} = 75-500$  watts and, consequently, correspondingly increases machine efficiency.

7. When the rotor carries damper windings, an instantaneous short circuit decreases the no-load voltage in comparison with a slow short circuit by roughly 5-10%. When there are no damper windings, the demagnetization due to an instantaneous asymmetric short circuit is con-

siderably increased.

8. The direct-current short-circuit component disappears rapidly, and the sustained condition sets in after two-three cycles.

The magnitude of the sustained short-circuit current is directly proportional to the residual emf following the first instantaneous short circuit. The amplitude of the instantaneous short-circuit current is low and is determined by the emf prior to the occurrence of the short circuit.

9. The nature of the instantaneous short-circuit process and the quantitative relationships are nearly identical for single- and three-phase machines.

10. The quadrature-axis armature magnetizing-force component acts directly on the ends of the permanent-magnet poles, producing alternate magnetization perpendicular to the main flux. The quadrature-axis alternate magnetization of the pole ends deforms the field curve in the machine air gap. The field distortion remains after the load has been removed, i.e., this phenomenon is irreversible. The distortion is greater the greater the load (armature current). Maximum residual distortion of the magnetic field in the gap occurs when there is a short circuit across the machine terminals in the presence of a capacitive load.

11. In permanent-magnet machines using "spider" type rotors, the quadrature-axis armature-reaction field is smaller in magnitude than in a corresponding electromagnet machine; its effect, however, is considerable from the viewpoint of residual distortion of the air-gap field.

The voltage curve for permanent-magnet generators is nearly sinusoidal when the winding is properly chosen.

#### 4.5. DESIGN OF PERMANENT-MAGNET GENERATORS

Figure 4.36 shows several designs of alternating- and direct-current synchronous permanent-magnet generators.

Synchronous permanent-magnet machines are normally made with internal salient poles. If external fixed salient poles and a rotating armature are used, one of the important advantages of these machines disappears, since in this case a sliding contact is required to take off the alternating-current energy.

In general structural make-up, armature, and armature (stator) winding, synchronous machines excited by permanent magnets or electromagnets are similar. They differ only in rotor construction.

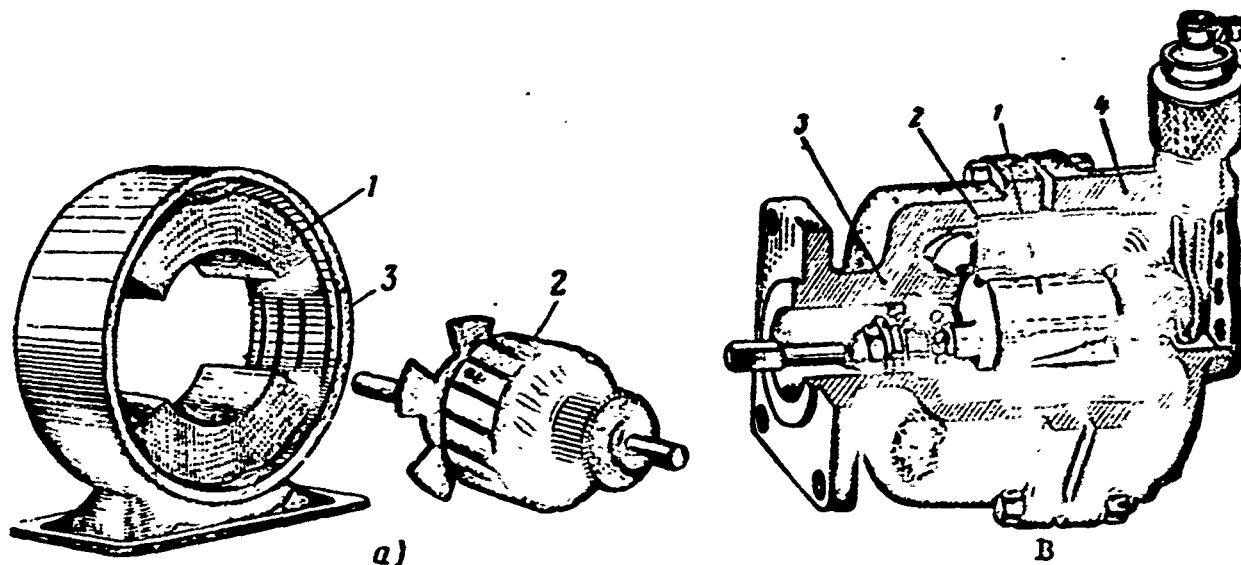


Fig. 4.36. Permanent-magnet machine design. a) Two-pole direct-current generator; b) four-pole type 4UG-1 tachometer generator. 1) Permanent magnet; 2) armature; 3 and 4) frame.

There are three main types of rotors for permanent-magnet machines:

- a) rotors with salient poles of the "spider" type for low-power machines;
- b) rotors of interlaced design for medium-power machines;
- c) rotors of salient-pole construction with soft-steel pole pieces for medium- and high-power machines.

## "Spider" Type Rotors

From the structural and production viewpoints, "spider" type rotors are simplest of all, and offer the following advantages:

- simplicity of structure and production;
- good utilization of the armature volume by the magnet as compared with other types of rotors, providing smaller machine dimensions (Fig. 4.37).

The basic drawbacks are:

- incomplete utilization of the magnet material (Fig. 4.38);
- smaller specific magnetic energy than other types of rotors, owing to the complexity of the spider shape;
- instability of magnetizing-force and emf curves;
- high sensitivity to instantaneous short-circuit current;
- low mechanical strength, limiting the peripheral speed of the rotor;
- limited values of air-gap induction (2000-6000 gauss, depending on type of material used) and limited linear load (short magnetization path).

A "spider" type magnet may take the form of several elements connected in parallel (Fig. 4.38a).

During magnetization, the same magnetizing force is applied to all points on the magnet pole surface, and the flux flowing through the length of the magnet will be greater than where the flux path is shorter. Consequently, the magnet is not magnetized uniformly over its cross section. In addition, the cross-sectional area of the main portion of the rotor is normally made 5-10% greater than the pole cross section, since during operation the flux in the main portion of the rotor is greater than the flux in a pole by the magnitude of the leakage flux; this also obstructs uniform magnetization of the magnet.

Since the spider is magnetized by means of a special apparatus, the induction in the main portion of the rotor decreases during magnetization owing to the leakage flux, which shunts the main field (Fig. 4.38b).

During magnetization of the magnet, the leakage flux may reach a large value, since the permeability of the magnet material is comparable with the permeability of air.

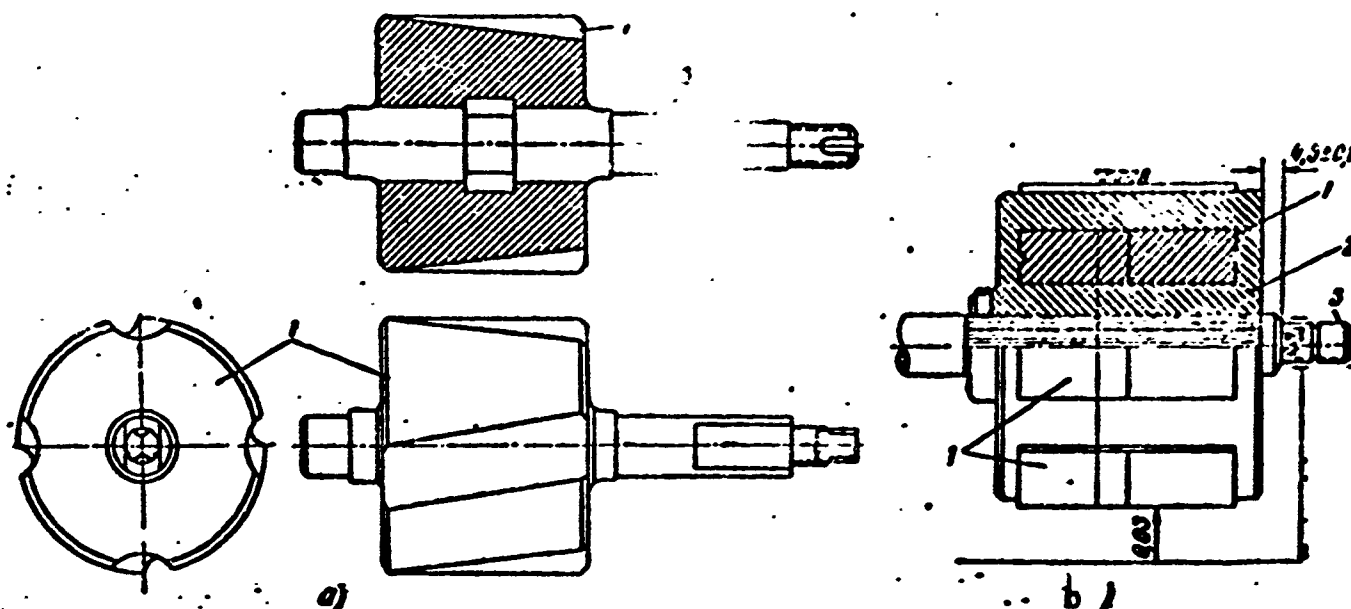


Fig. 4.37. Construction of "spider" type rotors. a) Four-pole rotor for tachometer generator, made from alnico surrounding nonmagnetic shaft; b) six-pole generator rotor enclosed in aluminum. 1) Magnet; 2) aluminum; 3) shaft.

As a result, cases can occur in which the magnetic material of the main part of the rotor not only increases the magnetic energy of the rotor, but decreases the degree of magnetic utilization of the rotor core in the external circuit owing to an increase in the over-all reluctance of the magnetic path. Thus, the rotor drum affects the machine magnetic circuit as a considerable reluctance, rather than as a source of magnetic energy. During operation of the machine, on the other hand, the induction in the basic portion of the rotor is somewhat greater than the induction in a pole core owing to the phenomenon of leakage (Fig. 4.38c).

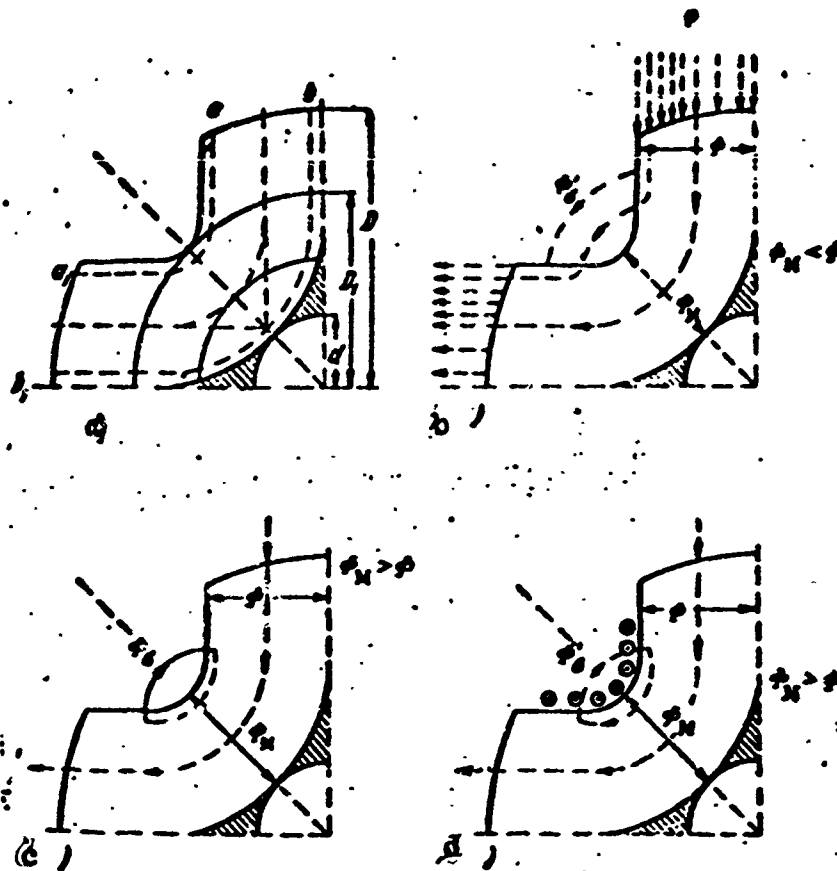


Fig. 4.38. Analysis of "spider" rotor design.  
a) Magnet element  $aa_1$  considerably shorter than  $bb_1$ ; b) induction in neutral plane less during magnetization than at poles ( $\phi_m < \phi$ );  
c) during service, induction in the magnet neutral plane greater than at poles ( $\phi_m > \phi$ );  
d) magnetization of spider by winding located on poles.

This phenomenon may be counteracted by making the main portion of the rotor equal in cross-sectional area to the area of a pole core, and by decreasing the leakage flux during magnetization by appropriate choice of pole sizes. If the spider is magnetized with the aid of a winding on the poles (Fig. 4.38d), this drawback will be removed; this cannot be done for practical reasons in aircraft machines, however.

If rotors of the "spider" type do not have soft-steel pole pieces, distortion of the air-gap field will result, and there will be strong demagnetization of the magnet due to instantaneous short-circuit currents.

The magnetic field formed by the quadrature-axis armature magnetizing-force component  $F_{yaq}$  travels at right angles to the poles; although it has no noticeable effect on the magnitude of the pole flux, it sets up a residual field deformation in the air gap.

When the pole pieces are made of soft steel, the quadrature-axis armature field does not produce residual field deformations, since it travels along the pole piece.

The position of the armature-reaction magnetizing-force axis changes relative to the pole axis, depending on the nature of the load. Consequently, the armature-reaction magnetizing force produces asymmetric demagnetization of the pole ends. As a result, the shape of the field in the gap is distorted as is the machine emf curve, which now depends on the nature of the load.

When an abrupt short circuit occurs, a pole of hard magnetic material with low permeability and high resistivity ( $0.7-0.8 \text{ ohm}\cdot\text{mm}^2/\text{m}$ ) damps the magnetizing force due to the sudden short-circuit current only slightly, and the eddy currents in the pole core will be small in magnitude and will be rapidly attenuated.

As a result, the sudden short-circuit current magnetizing force, which is attenuated very little by pole eddy currents decreases the magnetization of the pole more than would a steady short circuit.

The influence of abrupt short-circuit current may be reduced by forming a damper system on the rotor; this is done by surrounding the rotor with aluminum or coating the surface of the pole with a thin layer of copper.

The presence of a damper system is especially important if we wish to decrease the effect of the reverse field in single-phase machines.

The magnitude of the air-gap induction depends on the condition

for maximum field energy. Thus, if alnisi alloy is employed, the air-gap induction will be  $B_g \leq 2200-2400$  gauss, disregarding dependences on power, frequency, and speed. It can be increased only by changing the type of magnetic alloy used, and this is a drawback to the design.

The length of the magnet is  $h_m = R\rho^{-\gamma}$ ; it determines the magnet magnetizing force  $F_c = 0.8h_m H_c$ , and is normally small, especially where there are a large number of poles and, consequently, the pole pitch  $\tau$  is small. Thus, in order to decrease the effect of armature reaction, the linear load (A) is decreased; this quantity is directly proportional to the armature magnetizing force, since

$$F_a = 0.45k_a A \tau = A,$$

where R is the armature radius and  $\gamma < 1$ .

A decrease in the linear load leads to an increase in machine weight, however.

Thus, in "spider" type rotors, the choice of values for  $B_g$  and A will depend on the type of magnetic alloy employed, which sometimes leads to nonoptimum designs, and limits machine power.

The application of "spider" type rotors is also limited by mechanical-strength conditions — by a peripheral speed of the order of 30 to 45 m/sec.

For an alloy of Fe, Ni, and Al, the breaking stress is 200-300 kg/cm<sup>2</sup>; the permissible stress (for a safety factor of two-three) is of the order of 100 kg/cm<sup>2</sup>. Consequently, rotor diameters should not exceed the following values (for  $v \approx 45$  m/sec):

1) $n, \text{ об/мин}$	3000	6000	8000	12000	24000
$D, \text{ см}$	30	15	10	8	4.5

1) n, rpm.

Figure 4.37 shows the construction of a "spider" type rotor used in aircraft tachometer generators with about 10 va power, and in air-



craft generators with about 1000 va power. In the first case, a four-pole magnet is used, and in the second case a six-pole magnet.

If the magnet is more than 40-50 mm wide, it is assembled from several magnets (Fig. 4.39), since the magnetic properties of the magnet deteriorate in large castings.

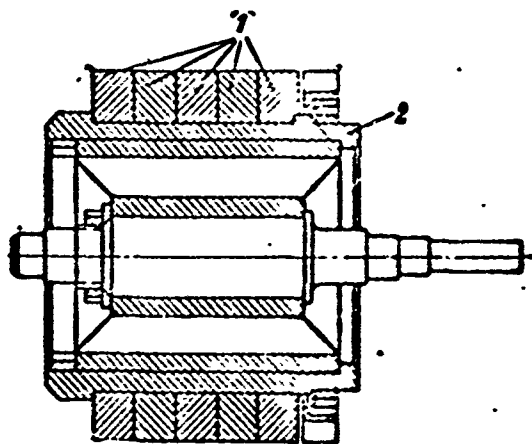


Fig. 4.39. "Spider" type rotor composed of several magnets.  
1) Magnets; 2) nonmagnetic sleeve.

The manufacture of a composite rotor complicates the production process, since the volume of polishing and assembly work is increased. In addition, the magnet pole axes may shift their relative positions. Thus, manufacturers attempt to attain a uniform magnetic structure throughout the entire volume of a casting, and for a large-volume magnet, to use fewer magnets in the assembled rotor where possible. Investigations have shown that covering rotors with aluminum increases magnet efficiency and raises generator power up to 20%, depending on the number of poles and the rated power.

The maximum power of a generator using a "spider" type rotor is determined by the type of material used, the frequency, and the power factor. If modern alloys are employed, at a frequency of 400 cps with  $\cos \varphi = 0.8$ , the maximum power will be 1.5-2 kva, while at a frequency of 1000 cps with  $\cos \varphi = 0.8$ , power may be increased to 3-5 kva.

### "Interlaced" Rotors

Figure 4.40 shows some possible structural configurations for interlaced rotors. An interlaced rotor consists of a cylindrical magnet and two disks of soft steel having projecting poles - "fingers."

One disk and all corresponding poles are of the same polarity,

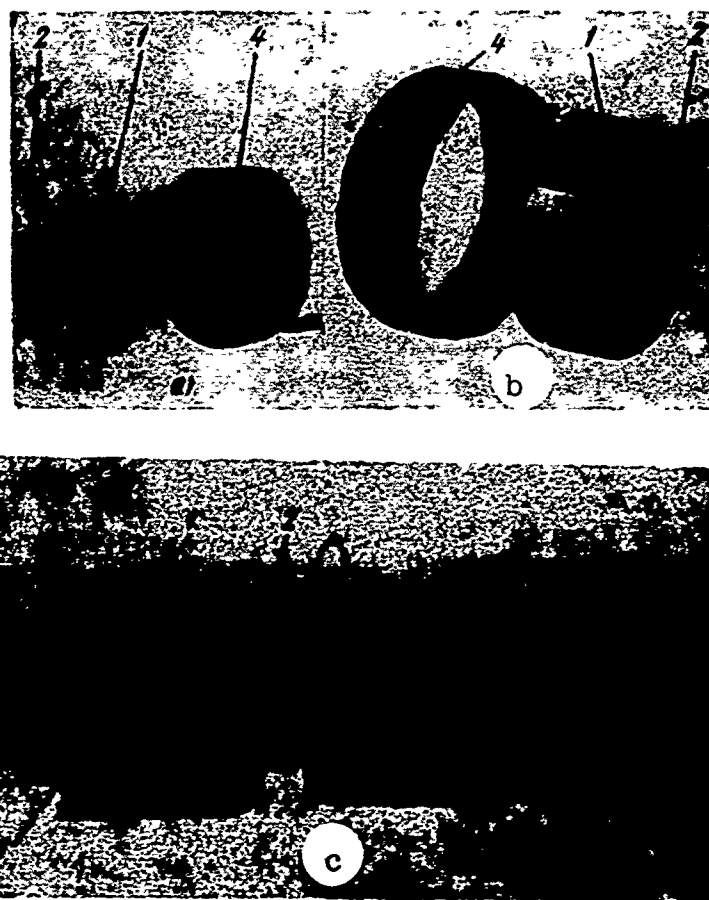


Fig. 4.40. Interlaced rotors. a) Six-pole generator; b) 14-pole generator; c) generator rotor and motor armature for six-pole aircraft converter. 1) Interlaced poles; 2) pole disk; 3) cylindrical magnet; 4) generator armature.

while the other disk is of opposite polarity. After polishing, the magnet is mounted in recesses in the pole disks, and held by the faces.

The shaft is normally made of a nonmagnetic steel, but it may also be made of an ordinary steel if a sleeve of sufficiently thick nonmagnetic material is placed between the shaft and the magnet. Utilization of the shaft or sleeve of nonmagnetic material eliminates the danger

of shunting of the magnet's field.

The interlaced rotor is free from the drawbacks of the "spider" type of rotor, but it is more complicated to produce.

The rotor is magnetized in assembled form. The short cylindrical magnet is magnetized reliably, and the field within it is nearly uniform, which increases the efficiency of the magnet and permits heat-treated alloys to be employed more effectively in the magnetic field.

Soft-steel pole pieces facilitate the formation of eddy currents during transient processes; these currents reliably damp short-circuit impulse currents. Thus, magnet stabilization is determined, for all practical purposes, by steady, rather than impulse short-circuit currents, which also improves the magnet efficiency.

The demagnetizing effect of the armature magnetizing force is less for machines with interlaced rotors than for machines with "spider" rotors for steady conditions as well. This is explained by the effect of leakage for the interlaced poles; it rises as the direct-axis armature magnetizing-force component increases.

In view of what we have said, it proves possible to increase the linear load on a machine with an interlaced rotor.

The air-gap field curve and, consequently, the emf curve as well are stabilized, and their shapes are established by appropriate processing of the pole pieces, as in the case of electromagnetically excited synchronous machines.

The cylindrical magnet can be made more reliably than a spider type, and the mechanical-strength limitations on peripheral speed can be eased considerably.

The magnet of an interlaced rotor is made with a relatively small ratio of magnet length to magnet diameter ( $l/D$ ). It takes the form of a flat cylinder, since the magnet cross section

$$S_m = \frac{\pi d_m^2}{4} \left[ 1 - \left( \frac{d_v}{d_m} \right)^2 \right]$$

is determined by the total magnetic flux due to all poles

$$B_m = \frac{p \Phi_p k_o}{S_m},$$

where  $d_v$  and  $d_m$  are the shaft and magnet diameters;  $\Phi_p$  is the flux due to a single pole;  $k_o$  is the leakage factor;  $B_m$  is the induction in the magnet.

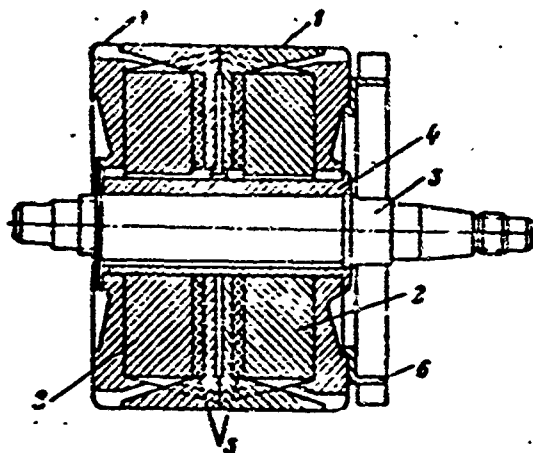


Fig. 4.41. Double Larionov rotor. 1) Interlaced pole; 2) cylindrical magnets; 3) shaft; 4) nonmagnetic sleeve; 5) soft-steel ring; 6) fan.

The length of the magnet is determined by the magnetizing force required to force the flux through the magnetic-circuit reluctance, allowing for the armature reaction.

The peripheral speed of an interlaced rotor may reach values of 100 m/sec. For peripheral speeds of a magnetic cylinder exceeding 50 m/sec, it may be fastened with the aid of a thin hollow steel cylinder of nonmagnetic material similar to the cylinders used to fasten the end portions of windings for nonsalient-pole synchronous machines.

The maximum dimensions of the magnet cylinder limit the maximum machine power for a given frequency.

A.N. Larionov suggested a double interlaced rotor that increases the maximum power of a machine with an interlaced rotor. As Fig. 4.41

shows, the magnets are connected in parallel, and the flux is doubled; it is thus possible to decrease the radial dimensions of the rotor or to increase the power of the machine.

In machines using interlaced rotors, the linear load may be increased to 250 amp/cm, while the air-gap inductance may be raised to 6000-7000 gauss, disregarding the dependence on the kind of alloy employed. The choice of  $A$  and  $B_\delta$  is dictated by the conditions that permit optimum machine dimensions to be obtained, and by the need to satisfy the applicable technical specifications, as in the case of electromagnetic machines.

By increasing  $A$  and  $B_\delta$ , we are able to construct high-power permanent-magnet machines. At frequencies of 500-1000 cps, generators using interlaced rotors may be built with powers of the order of 10-20 kva. Thus, the advantage of the interlaced rotor is a higher degree of magnet utilization, stable magnetizing-force shape, better emf shape, and the possibility of raising the maximum power.

A drawback to interlaced-rotor machines, especially in sizes below 1000 watts, is the fact that the radial machine dimensions are greater. In addition, in such machines, the magnet makes less use of the rotor cross section than in the case of a spider-type rotor; this results in increased size and weight. It should be noted that at high speeds, the ends of the fingers bend, and thus special mountings must be used.

For low-power machines, a decrease in magnet weight does not lead to a decrease in over-all machine weight owing to the need for locating the poles between the starter and the cylinder magnet.

When the frequency is increased (number of poles raised), there is a decrease in the degree of utilization of the rotor cross section by the magnet, i.e., the ratio

$$k_{\text{an}} = \frac{S_n}{S_s} = 2ap^{-1}$$

is reduced for a "spider" type rotor, while for an interlaced rotor, the ratio

$$k_{\text{an}} = \left(\frac{d_n}{D}\right)^2 \left[1 - \left(\frac{d_s}{d_n}\right)^2\right] = 2\lambda k_s \frac{B_s}{B_n}$$

does not depend on the number of poles.

When the frequency is raised, there is a proportional decrease in magnet volume; this gain may be realized entirely with an interlaced rotor by an appropriate reduction in magnet length and, consequently, machine length. Thus, at high frequencies (large number of poles), interlaced-rotor machines can be smaller and lighter (providing better use is then made of the magnet) than "spider" type machines.

#### Rotors with Pole Pieces

Rotors with soft-steel pole pieces are complicated to produce, but they offer several substantial advantages.

A permanent-magnet rotor with pole pieces is similar to an electromagnetic rotor in which the core and field winding (electromagnet) have been replaced by a permanent magnet.

Pole pieces permit increased air-gap induction, sinusoidal distribution of magnet flux over the pole pitch, regulation of the pole leakage flux (for optimum use of the magnet), and damping of the magnetizing-force reaction due to transient currents.

Permanent-magnet machines using pole pieces can attain 100 kva power at 400 cps, and this still does not represent the limit.

Figure 4.42 shows construction of a rotor for which each pole consists of several permanent magnets taking the form of rectangular parallelepipeds.

The soft-steel permanent magnets are attached to the pole ring with the aid of pole pieces also made from soft steel.

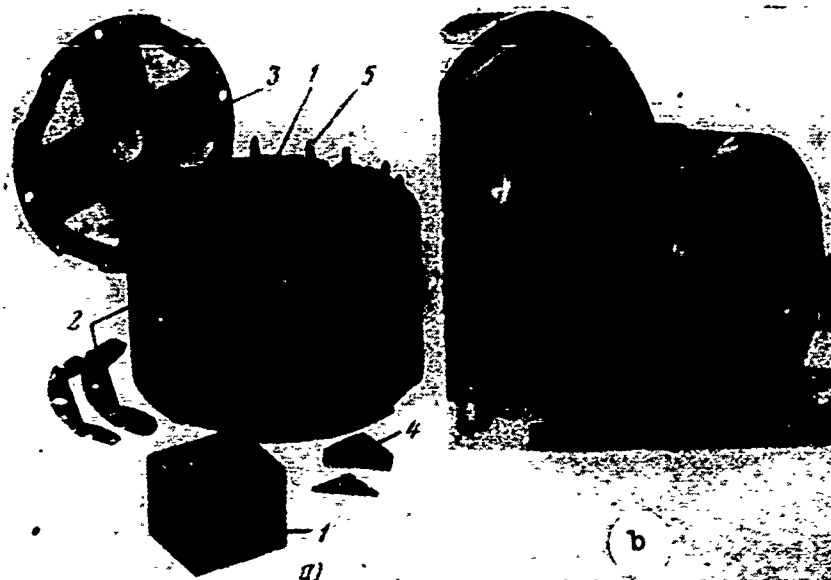


Fig. 4.42. Rotor of 6.3-kva 60-cps four-pole machine. a) Rotor assembly; b) machining of outside diameter. 1) Prism pole magnets; 2) pole pieces specially designed to increase leakage; 3) steel nonmagnetic disk to strengthen rotor; 4) element of rotor yoke; 5) steel rotor mounting screws.

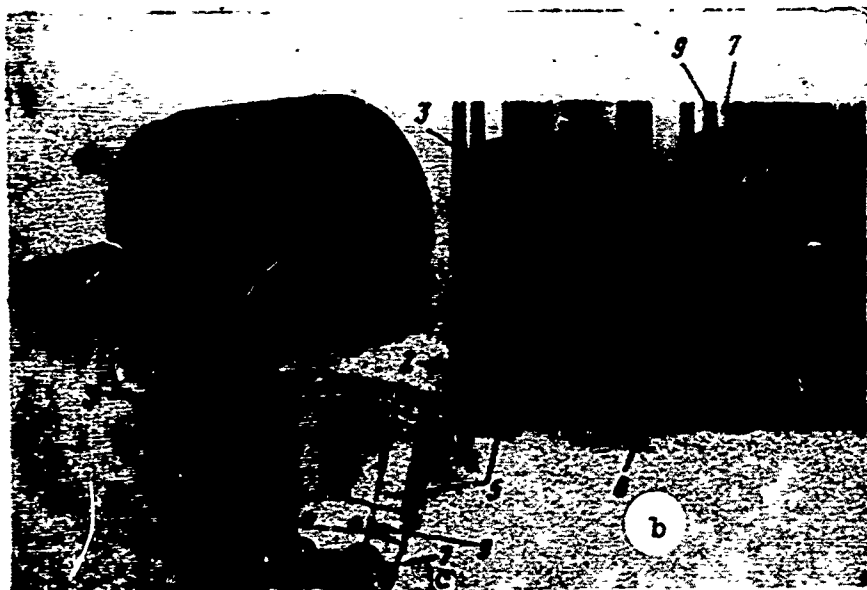


Fig. 4.43. Construction of rotor for 28-pole 75-kva 400-cps permanent-magnet generator. a) General view of rotor; b) rotor assembly; c) magnet mounting. 1) Prism magnet, made from magnico alloy; 2) soft-steel pole piece; 3) steel mounting pins; 4) damper-winding rods; 5) steel nonmagnetic disks forming rotor frame; 6) aluminum covering; 7) steel inside ring; 8) soft-steel rotor yoke; 9) steel mounting pins for elements of rotor yoke.

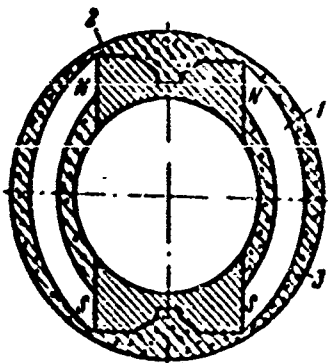


Fig. 4.44. Two-pole rotor with pole pieces. 1) Magnet; 2) pole piece; 3) aluminum covering.

The pole pieces are held tightly against the pole ring with the aid of nonmagnetic-steel bolts.

The pole pieces are made longer than the stator core in order to protect the magnets against unbalanced demagnetization due to the armature reaction. The thickness of the pole pieces, dictated by structural considerations, is normally inadequate to provide damping of

the magnetizing-force reaction due to armature transient currents; thus copper short-circuited turns (loops) are placed on the magnets under the pole pieces, or else a damper winding is used with the pole pieces.

Figure 4.43 shows the construction of a rotor for a three-phase 28-pole 75-kva 400-cps generator, while Fig. 4.44 shows the construction of a two-pole rotor in which the magnets are tangentially magnetized. Soft steel, which fills the space between the poles in the tangential direction serves as the pole piece.

#### 4.6. VOLTAGE REGULATION IN PERMANENT-MAGNET GENERATORS

Voltage regulation and stabilization is an important problem in permanent-magnet machines; its solution presents considerable difficulties and the following approaches may be used:

- 1) decreasing the voltage drop;
- 2) stabilizing the voltage by using capacitors;
- 3) regulating the voltage by means of interpole shunts;
- 4) regulating the voltage by changing the frequency;
- 5) regulating the voltage by means of saturable reactors;
- 6) regulating the voltage by varying the reluctance of the magnetic path.



### Decreasing the Voltage Drop

Two factors are responsible for the voltage drop appearing across the armature-winding terminals when we go from no-load to rated-load conditions while the speed and temperature remain unchanged: the voltage drop in the armature circuit, and the reversible change in air-gap flux due to the armature reaction.

Thus, in order to reduce the voltage drop, it is necessary to decrease the relative armature magnetizing force, i.e., to decrease the direct-axis synchronous impedance of the machine, which is proportional to the armature-reaction magnetizing force  $F_{ya}$ .

To reduce  $F_{ya}$  and, consequently,  $x_d$ , we reduce the linear armature load (decrease the number of turns per phase for the same current) and correspondingly increase the machine air-gap flux. This leads to an increase in the volume of magnet and machine, as well as in the short-circuit ratio, which normally equals one, and in this case rises to 2-3.

Figure 4.45 shows the way in which the relative values of axial length  $l'$ , magnet weight  $G'$ , linear load  $A'$ , number of armature turns  $w'_{ya}$ , emf  $E'_0$ , voltage  $U'$ , power  $P'$ , and efficiency  $\eta'$  depend on the quantity  $\Delta U = U/E_0$  for a permanent-magnet aircraft generator using a spider made from alnisi alloy (the spider diameter remains constant).

Analysis of the curves given shows that when  $\Delta U$  is raised from 0.78 to 0.9, it is necessary to double the axial length of the machine. In order to obtain a value  $\Delta U = 0.95$ , it is necessary to multiply the length (volume) of the magnet by 3.5. Actually, the situation is even worse, since in order to lengthen the magnet, the shaft must be reinforced and the air gap increased, and the generator power must also drop owing to failure to use the optimum magnet geometry.

A further decrease in the voltage drop makes no sense owing to

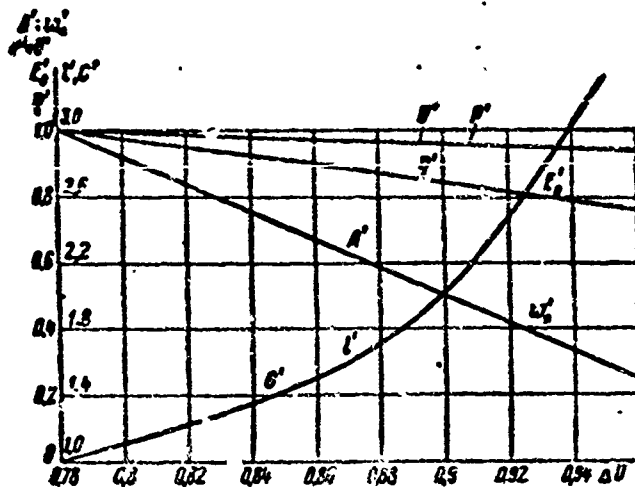


Fig. 4.45. Relative values of size, weight, number of turns in armature winding, linear load, no-load emf, voltage, power, and efficiency as functions of voltage variation.

the excessive increase in machine length.

It should be remembered that generator efficiency will drop in this case, since the increase in surface and mechanical losses in the core will not be compensated by decreased losses in the armature winding.

The method that takes into account speed changes, temperature,  $\cos \varphi$ , and the load gives a relatively high degree of voltage stabilization; its advantage lies in its simplicity and the absence of voltage-regulating devices. This method may be recommended for low-power generators operated with a constant high power factor ( $\cos \varphi \approx 0.9$ ) and over a small load-variation range  $(0.5-1.0)P_{\text{nom}}$ .

As an example, we can cite a 200-wa permanent-magnet generator used to supply central power  $f = 400$  cps; at  $\Delta U \approx 0.95$ , it maintains the voltage constant to within  $\pm 8\%$  under loads varying from zero to rated value, in the presence of temperature fluctuations over the  $-50^\circ$  to  $+60^\circ\text{C}$  range, with a constant value of  $\cos \varphi = 0.6$ . The generator uses a double-length (volume) magnet, and has higher losses than a similar machine for which  $\Delta U \approx 0.85$ .

## Voltage Stabilization by Means of Capacitors

Two types of capacitor stabilizers may be connected into the armature winding of a generator:

a) a series-connected capacitor stabilizer that compensates the complete direct-axis generator reactance (a so-called series stabilizer);

b) a capacitive stabilizer connected in parallel and used to supply the generator with inductive or capacitive magnetizing current, depending on the nature of the load (so-called parallel stabilizer).

Series stabilizer. Figure 4.46a shows various ways of connecting series capacitors into a generator armature circuit: direct capacitor connection (for low-power generators delivering relatively high voltages); connection through unsaturated step-up current transformers (in order to reduce the compensating capacitance); connection through unsaturated step-up current transformers whose secondaries are connected to a delta-connected group of capacitors (the line voltage is applied across the capacitor terminals).

Operation of these circuits is based on the fact that the voltage drop in a generator caused basically by the armature reaction and leakage fluxes is compensated by a capacitance connected in series.

If the capacitance is so selected that the reactance of the capacitor  $x_k$  equals the synchronous generator reactance  $x_g$ , the generator voltage drop will be determined purely by the resistance, which is normally small.

With a load varying from zero to rated value, series-connected capacitors make it possible to stabilize the voltage to within 2% for a constant value of  $\cos \varphi \leq 0.8$ , and to within 5% when  $\cos \varphi = 1.0$ .

Figure 4.46b gives vector voltage diagrams for  $x_k = 0$ ,  $x_k = x_g$ , and  $x_k > x_g$ , with  $x_k$  given for the armature circuit.

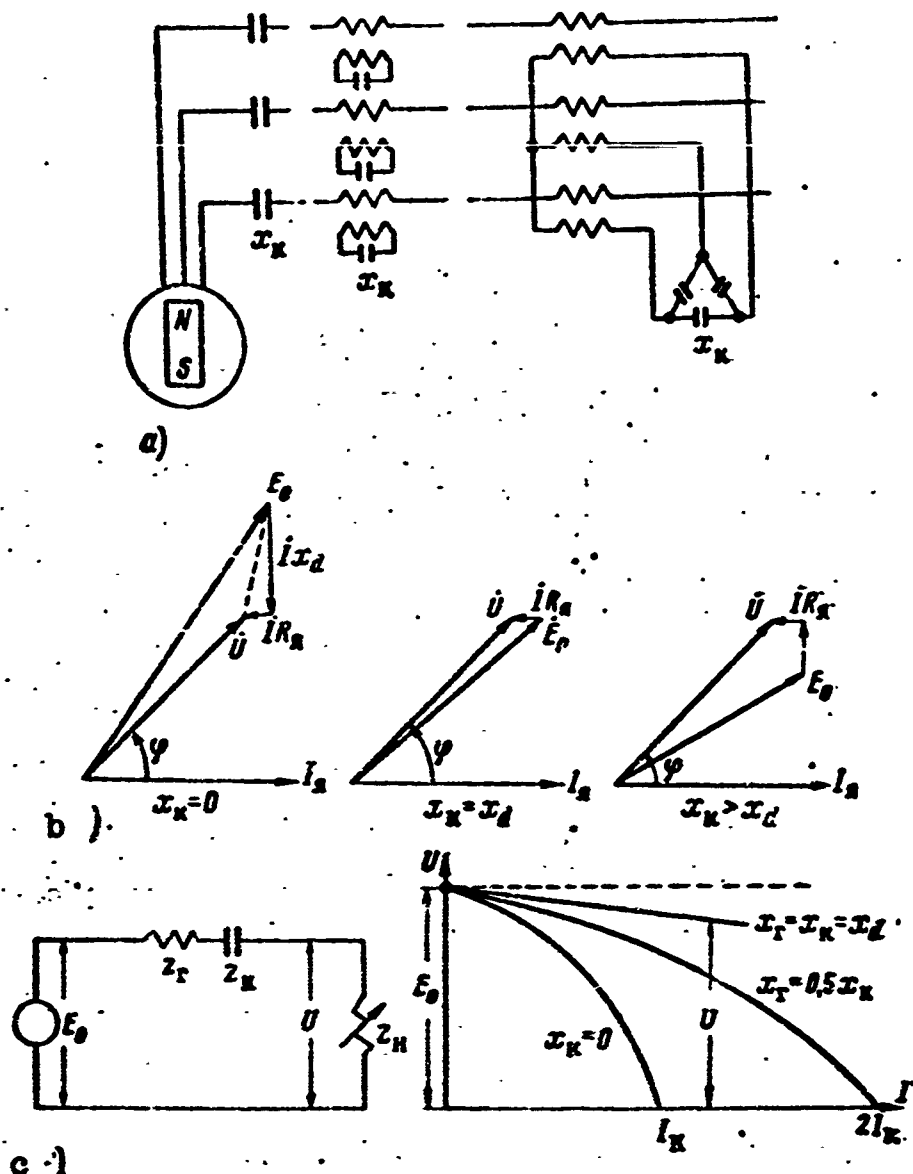


Fig. 4.46. Capacitor connected in series with armature circuit used for voltage stabilization. a) Various capacitor connections; b) vector diagrams for various values of the ratio  $x_k/x_d$ ; c) equivalent circuit and external characteristics.

Figure 4.46c gives the equivalent circuit for series compensation and the external generator characteristic for various capacitances. If the capacitor is brought into resonance with the synchronous reactance of the machine, there will be a considerable reduction in the voltage drop. Complete voltage stabilization, however, can be obtained only provided that there is no saturation ( $x_g = \text{const}$ ) and that the nature of the load remains unchanged ( $\cos \varphi = \text{const}$ ). When  $\cos \varphi$  takes on

other values for the load, the voltage stabilization is impaired, and this is the basic drawback of this method, since there is no measuring device that will directly sense departure of the generator voltage from the rated value. There should be no possibility of transformer saturation, for if this were not the case, sharp increases in current might cause the transformer inductance to vary within wide limits, and resonance phenomena might appear in the transformer-capacitor circuit, destroying any stabilization whatsoever. Small amounts of transformer saturation lead to increased system weight and size, especially where voltage stabilization is required for three-phase permanent-magnet generators.

As experiment and calculation have shown, voltages may be stabilized to within 10% with provision for magnetic-system saturation and variation in  $\cos \varphi$  given a proper choice of capacitances. Here the generator will weight considerably less than when the first voltage-regulation method is used, since the armature reaction compensation increases the utilization factor for the permanent magnet. Large size and high cost represent the basic disadvantages to voltage stabilization of permanent-magnet machines by means of capacitors. Since the capacitor reactance is inversely proportional to frequency, however, high-frequency systems (including aircraft power systems) can make use of capacitors that are considerably smaller and lighter.

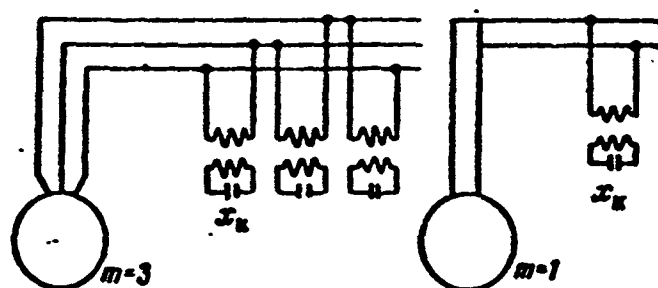


Fig. 4.47. Voltage stabilization by means of capacitors connected in parallel with armature circuit.

Parallel stabilizer. Figure 4.47 shows various ways of connecting capacitors in parallel with a generator armature circuit.

Circuit operation is based on ferroresonance currents. The value of the capacitance and the inductance of the saturated transformer should be such that resonance occurs in the stabilizer circuit under no-load conditions at rated voltage.

With this stabilization method, an inductive or capacitive current is introduced into the armature circuit, depending on the nature of the deviation of generator voltage from the rated value. The stabilizer reacts directly to a voltage deviation from a given level, and it acts directly on the armature circuit.

With this stabilization method, the transformer should be saturated. When the voltage is to be raised, the generator sees the stabilizer as an inductance, when the voltage is to be dropped, the generator sees the stabilizer as a capacitance, while at resonance, the stabilizer appears as a resistive load.

Consequently, this stabilizer represents an additional load on the generator, necessitating an increase in the strength and size of the magnet.

A parallel stabilizer can stabilize output voltage to within roughly 1-2% when  $\cos \varphi = 1$ . For lower values of  $\cos \varphi$ , stabilization accuracy drops to 3-5%. Since the parallel stabilizer reacts to a deviation in stabilizing voltage away from the rated value, it to some degree compensates for temperature variations in generator voltage, and this represents an advantage for this type of stabilizer over the series stabilizer; owing to the nonlinearity of the resistance presented by a parallel stabilizer, the device may distort the shape of the generator curve at high values of inductive current. As far as weight and size are concerned, this stabilizer is somewhat better than

the series stabilizer.

Series or parallel stabilizers cannot be used to stabilize the voltage of permanent-magnet generators supplying main aircraft power systems, since they do not provide the required precise voltage; they may prove useful, however, for purposes of increasing  $\cos \varphi$ , especially at high frequencies and voltages.

#### Voltage Regulation by Interpole Shunts

If a magnetic shunt is placed between the poles, a considerable portion of the armature magnetizing force will be used to form the flux through the shunt. In this case, there will be a considerable decrease in the proportion of the armature magnetizing force available for direct-axis bucking of the magnet magnetizing force.

This method gives positive results for load power factors of  $\cos \varphi = 1$ , since in this case the armature magnetizing force is directed at right angles to the pole axis, while the quadrature-axis armature-reaction flux completes its path almost entirely through the shunt. This method cannot be used with lagging  $\cos \varphi$ .

Thus, the method of interpole-shunt voltage regulation may be used when  $\cos \varphi = 1$ , and when the utilization of capacitors is limited due to their size and cost.

Interpole shunts have not come into use in aircraft direct-current machines.

#### Voltage Regulation by Frequency Variation

Occasionally, the permanent-magnet generators used in aircraft DC-AC converters use a system that regulates the voltage by changing the converter rotation speed. Here it is possible to maintain voltage constant to within  $\pm 4\%$  under loads varying from 0.3 to rated value, under temperature fluctuations ranging from  $-50$  to  $+60^\circ\text{C}$ , and with an unchanged value of  $\cos \varphi = 0.9$  (the frequency fluctuates over a  $\pm 10\%$  range).

## Voltage Regulation by Means of Saturable Reactors

The voltage of permanent-magnet generators may be regulated with sufficient precision by means of saturable reactors connected into the armature circuit.

The voltage across the output terminals of the reactor, equaling

$$U = E_a - I[(R_r + R_a) + j(x_r' + x_a)],$$

is held constant by the varying inductive reactance  $x_d$  of the reactor.

At rated load,  $x_d$  should be at a minimum; in this case, the choke magnetizing current will be at a maximum. As the load decreases, it is necessary to increase  $x_d$  in order to hold the voltage constant; this is done by decreasing the reactor magnetizing current.

The basic drawbacks to this method are the decreased efficiency of magnet utilization owing to the presence of an additional inductance in the armature circuit ( $x_d$ ) which increases machine size and weight; the considerable size and weight of the reactors, and the increased losses in the system when the reactor losses are considered.

## Voltage Regulation by Variation of Magnetic-Circuit Reluctance

In 1951, a proposal was made\* to regulate the flux in permanent-magnet machines by varying the reluctance of the armature core by applying a controlled external field to it.

The regulated permanent-magnet machine differs from the ordinary version only in that there is space for a toroidal magnetizing winding 2 (Fig. 4.48) in slots and on the outside surface of the armature core.

The circuit operates in the following manner. At zero load, the flux in the machine is at its maximum, since there is no armature-reaction magnetizing force, and the magnetizing force due to the magnet is expended solely in the magnetic drop in the external circuit. Under these conditions, the magnetizing force due to the magnetizing winding is at its maximum, since it must increase the armature-core



reluctance to a point at which the increment is equivalent to the effect of the direct-axis armature-reaction component.

In rated operation, the magnetizing force due to the direct-axis armature reaction is nearly at its limiting value (permanent-magnet generators are normally not designed for overload operation) and, consequently, under these conditions the magnetizing force due to the magnetizing winding should be at its minimum, in accordance with the regulator operating cycle (theoretically,  $F_p = 0$ ).

Thus, the regulation system draws minimum power for regulation under working conditions, and maximum power when the generator is running without load, which represents an advantage over ordinary voltage-regulation systems for electrical machines using electromagnetic excitation.

It must be noted that the magnitude of the maximum in-phase power expended for regulation is less (even when the generator is running without load) than that drawn by electromagnetically excited machines, owing to the fact that there is no air gap in the magnetizing flux path. For this same reason, the inductance of the magnetizing winding is higher than the inductance of the field winding in an electromagnetically excited machine.

A regulated permanent-magnet generator delivering 1000 watts of power at 400 cps uses about 3% of rated power for regulation under operating conditions, and about 10% under no-load conditions. With electromagnetic excitation, the same generator would use about 15% of the rated power for excitation under rated conditions.

Precision of voltage stabilization is not limited by generator characteristics, and depends on the type of regulator employed. Thus, series permanent-magnet generators provide a rated voltage constant to within  $\pm 3\%$  under load changes of from 0 to 100%, temperature fluctua-

tions ranging from  $-50$  to  $+60^{\circ}\text{C}$ , and values of  $\cos \varphi = 0.6-1.0$ . The voltage-fluctuation range may even be decreased to  $\pm 0.5\%$ , i.e., this method provides high precision of voltage regulation.

Regulated permanent-magnet generators are heavier than unregulated generators owing to the fact that the generator has greater external diameter (part of each armature slot is occupied by a magnetizing winding), while the height of the armature core increases (the induction within the armature should not exceed 12,000 gauss for the grades of steel normally employed); there is some increase in the volume of the magnet, since regulated machines are made with relative voltage drops of the order of 0.8-0.85, rather than the values of 0.75-0.8 used in unregulated machines.

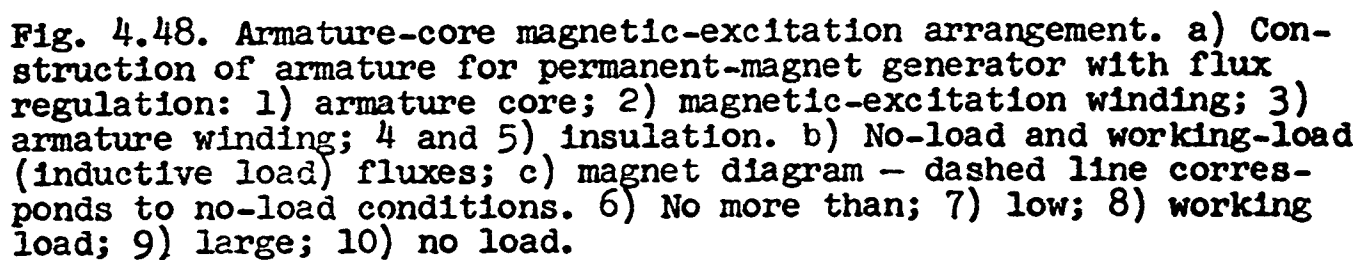
Thus, the weight of a regulated DC-AC converter delivering 1000 va at 400 cps (without control equipment) is increased by roughly 10%, or by 25-30% in terms of the generator weight.

The total weight of the regulated converter, taking into account the weight of all equipment, is increased by about 15%.

As calculations have shown, the relative increase in weight of regulated permanent-magnet generators goes up as the diameter (power) of the machines increases (and is slight with machines having powers of the order of tens of kva).

In order to increase the degree of utilization of regulated permanent-magnet machines, it is possible to use sheet steel with high saturation induction (material of the armko type); this makes it possible to increase the induction in the armature core to 16,000 gauss. In addition, it proves useful to connect capacitors into the armature circuit, especially for machines running at high frequencies and voltages.

Thus, the advantages of this voltage-stabilization system, which



- high voltage-stabilization precision;
- small amount of energy drawn for regulation purposes;
- relatively slight increase in weight of regulated machine;

— good voltage-curve shape.

The regulation characteristics, i.e., the curves representing the relationship between the armature-core excitation magnetizing force

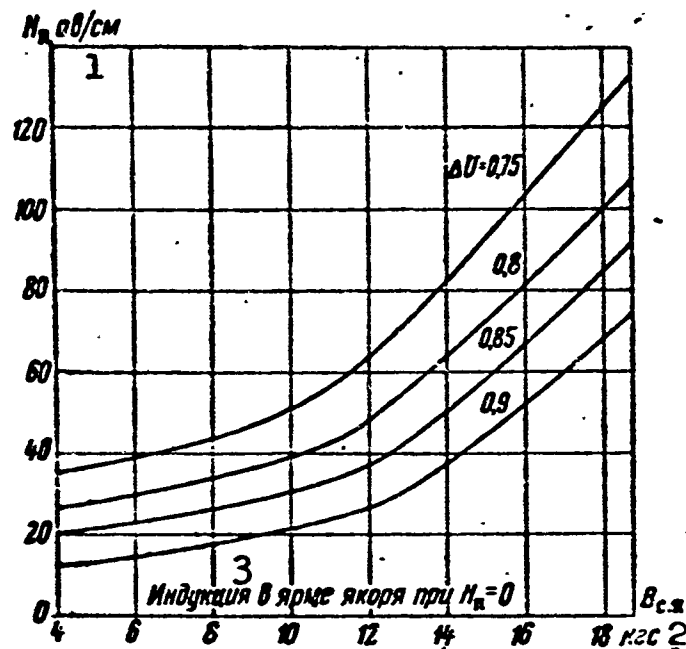


Fig. 4.49. Regulation characteristic curves for aircraft permanent-magnet generators ("spider" type rotor).

$H_p = f(B_{s.ya})$  with respect to  $\Delta U$ .

1)  $H_p$ , ampere-turns/cm; 2) kgs; 3)

induction in armature yoke at  $H_p = 0$ .

and the load current for constant voltage, speed, and power factor

$$F_p = f(I) \text{ for } U = \text{const}, n = \text{const}, \text{ and } \cos \varphi = \text{const},$$

may be found experimentally, or by a graph-analytical method.

The magnitude of the specific excitation magnetizing force  $H_p$ , i.e., the excitation magnetizing force per centimeter of mean armature-core length is determined by the armature-core induction due to the alternating flux  $B_{s.ya}$  and by the range of generator-voltage variation — by the quantity  $\Delta U = U/E_0$ . Figure 4.49 gives values of  $H_p = f(B_{s.ya})$  in terms of  $\Delta U$ ; the values were obtained experimentally.

In order to find  $F_p = f(I)$  it is necessary to have a family of curves representing the simultaneous armature-core magnetization due to the alternating and constant fields — the so-called volt-ampere

characteristics  $B_m = \varphi(H_{ef})$  with respect to  $H_p$  and the complete magnet diagram, constructed with no allowance for the magnetic potential drop in the armature core (Fig. 4.50).

The voltampere characteristics may be found experimentally or calculated analytically. In the latter case, by using the hyperbolic sine to approximate the volt-ampere characteristics, and assuming that, roughly, the induction in the core varies in accordance with the law

$$B = B_s + B_{max} \sin \omega t,$$

we obtain an expression for the instantaneous field strength in the core

$$H = \alpha \operatorname{sh} \beta B = \alpha \operatorname{sh} \beta (B_s + B_{max} \sin \omega t),$$

where  $\alpha$  and  $\beta$  are approximation coefficients equaling, respectively, 0.17 and 0.00045 for E21 steel and 0.0115 and 0.0005 for armko;  $B$  is the total induction in the armature core;  $B_p$  is the constant component of the induction;  $B_{max}$  is the peak value of the alternating induction component.

This last expression may be represented in dimensionless form; the volt-ampere characteristics will then be universal, i.e., they will be suitable for all types of steels

$$h = \operatorname{sh} b = \operatorname{sh} (b_s + b_m \sin \omega t),$$

where

$$h = \frac{H}{\alpha}, \quad b = \beta B, \quad b_s = \beta B_s, \quad \text{и} \quad b_m = \beta B_{max}$$

After appropriate manipulation, the expression for the instantaneous field strength will be

$$h = h_s + \sum_{n=1}^{\infty} h_{2n} \cos 2n\omega t - \sum_{n=1}^{\infty} h_{2n+1} \sin (2n+1)\omega t.$$

where

Fig. 4.50. Universal magnetization curves.

$$h_{2n} = 2J_{2n}(jb_m) \cdot \xi_n,$$

$$h_{2n+1} = 2J_{2n+1}(jb_m) \sqrt{1 + \xi_n^2},$$

$$\xi_n = \frac{h_n}{J_0(jb_m)},$$

the  $J_n$  are  $n$ th-order Bessel functions in the purely imaginary argument  $(jb_m)$ .

In order to determine the true strength of the alternating field in the armature core,  $h_{ef}$ , it is necessary to square the alternating part of the expression for  $h$ , and find its mean value over a cycle.

In view of all this, the true alternating field strength in the armature core can be expressed with the aid of an infinite series whose coefficients are Bessel functions of a purely imaginary argument, i.e.,

$$h_{ef} = 1.41 \sqrt{(1 + \xi^2) \sum_1 [J_{2n+1}(jb_m)]^2 + \xi^2 \sum_1 [J_{2n}(jb_m)]^2}.$$

Using this last expression, we plot on Fig. 4.50 the dimensionless volt-ampere characteristics

$$b_m = \varphi_1(h_{ef}) \text{ for } h_p.$$

If we lay off on the dimensionless volt-ampere characteristics (see Fig. 4.50) the line A'B', corresponding to the internal characteristic AB taken from the relative magnet diagram, and converted to the scale of the volt-ampere characteristics, the ordinate values of the points at which line A'B' intersects the volt-ampere curves will give, in the scale used, the no-load emf for various values of the constant field, i.e.,  $E_0 = f(H_p)$ . Knowing the functions  $E_0 = f(H_p)$  and  $E_0 = f_1(I)$ , we can plot the regulation characteristics

$$H_p = \varphi(I).$$

The procedure used in making the plot is as follows:

- 1) we find  $E_0^*$  from the magnet diagram, disregarding the magnetic

drop in the armature core (§4.7);

2)  $\dot{E}_0$  is brought over from  $E_r$  coordinates to  $b_m$  coordinates;

3) from point A', corresponding to  $\dot{E}_0$  in  $b_m$  coordinates, we draw line A'B' at an angle  $\alpha'_{ad} = \arctan (b_m/h_{ef})$  to the x-axis;

4) we convert the ordinates for the points at which line A'B' intersects  $b_m = \varphi_1(h_{ef})$  from the  $b_m$  scale to the  $E_r$  scale, and obtain the function

$$\dot{E}_0 = f(h_e).$$

If  $\Delta U \geq 0.8$ , then with an armature-core induction of  $B_{s.ya} \approx 10,000$  gauss (for alnico and alnisi alloys), we may assume, initially, a specific excitation magnetizing force of

$$H_p \approx 50 \text{ ampere-turns/cm.}$$

Dimensions of magnetization winding. In determining the dimensions of the magnetizing winding, it is necessary to allow for the fact that the maximum voltage across the winding terminals will amount to about 45% of the line voltage, while the remaining voltage is accounted for by the drop across the voltage regulator. The magnetizing-winding magnetizing force is determined from the expression

$$F_{max} = \pi D_n H_{p,max} \left(1 - \frac{h_e}{L_{ef}}\right) = \pi D_n H_{p,max} \dot{E}_p \text{ ampere-turn (4.39)}$$

where  $H_{p,max}$  is the strength of the constant field in the armature core with no load on the generator, ampere-turns/cm;  $D_n$  and  $h_{ya}$  are the outside diameter and height of the armature core;  $H_p = f(\Delta U)$  is found from Fig. 4.49.

The maximum generator no-load control current  $I_{p,max}$  is determined by the type of regulator used, and should be so selected as to make maximum use of the regulator rectifier.

The number of turns in the magnetization winding is

$$w_n = \frac{F_{max}}{I_{p,max}}.$$



The cross section of the magnetizing winding, if we take (4.39) into account and assume that

$$l_{z.p} \approx 2,2l \left( 1 + \frac{k_p}{l} \right) = 2,2k_p$$

will be

$$S_n = \rho_l \frac{F_{n \max}}{U_{z \max}} l_{z.p} \approx 2,2 \rho_l \Pi_n \frac{H_{n \max}}{U_{z \max}} \xi_D \xi_l \text{ } \mu\text{M}^2, \quad (4.40)$$

where  $\Pi_n = \pi D_n l$  is the outside surface area of the armature core,  $\text{cm}^2$ ,

$$U_{z \max} \approx 0,45 U_n;$$

in first approximation

$$S_n \approx 1,1 \Pi_n \frac{H_{n \max}}{U_{z \max}} 10^{-3} \text{ } \mu\text{M}^2.$$

The magnetization-winding resistance is

$$R_n = \rho_l \frac{l_{z.p} w_n}{S_n} \approx 2,2 \rho_l \Pi_n \frac{H_{n \max}}{I_{z \max} S_n} \xi_D \xi_l; \quad (4.41)$$

in first approximation

$$R_n \approx 5 \Pi_n \frac{H_{n \max}}{I_{z \max} S_n} \cdot 10^{-4} \text{ ohms.}$$

The maximum no-load magnetization-winding losses are

$$P_{n \max} = R_n I_{z \max}^2 \approx 2,2 \rho_l \xi_D \xi_l \Pi_n H_{n \max} I_{z \max} \text{ watts,} \quad (4.42)$$

where

$$I_{z \max} = \frac{I_{n \max}}{S_n} \text{ amp/mm}^2.$$

The maximum specific heat flow due to magnetization-winding losses is

$$a_{n \max} = \frac{P_{n \max}}{\Pi_n} = 2,2 \rho_l \xi_D \xi_l H_{n \max} j_{z \max} \text{ watt/cm}^2$$

and is nearly independent of generator power; it is a constant equaling roughly  $0.20 \text{ watts/cm}^2$  when  $j_{p \max} = 8 \text{ amp/mm}^2$ .

Depending on the type of regulator, it is recommended that the magnetizing-current factor be taken in the range  $k_p = I_{p \max} / I_{p \min} = 4-6$ .

The relative control power, since

$$Dl = \frac{S}{Df\sigma_{m.e}} = S^{1/2} \lambda^{1/2} (f\sigma_{m.e})^{-1/2}$$

will equal

$$\begin{aligned} \frac{P_{n \max}}{S} &= 6.9 \rho_i \xi_D \xi_r H_{n \max} j_{n \max} \frac{\lambda^{1/2} k_D}{S^{1/2} (f\sigma_{m.e})^{1/2}} \approx \\ &\approx 7.0 \rho_i H_{n \max} j_{n \max} \frac{\lambda^{1/2} k_D}{S^{1/2} (f\sigma_{m.e})^{1/2}} \end{aligned} \quad (4.43)$$

where  $k_D = D_n/D$ ,  $\sigma_{m.e} \approx 3.5 \cdot 10^{-8} B_{H_c} B_r k_{z.m}$  is the degree of utilization of the permanent-magnet machine.

In approximation

$$\frac{P_{n \max}}{S} \approx \frac{H_{n \max} j_{n \max}}{DfH_c B_r} = \frac{H_{n \max} j_{n \max}}{S^{1/2} (fH_{cD} B_r k_{z.m})^{1/2}}$$

i.e., the relative control power will in first approximation decrease with increasing armature diameter (machine power), frequency, and specific magnet energy. In addition, it depends on the values of  $\cos \varphi$ ,  $\Delta U$ ,  $p$ ,  $\gamma$ , and  $\mu_v$ , since the machine dimensions in turn depend on these quantities.

The ratio of the total cross-sectional area of the magnetization winding to the total cross-sectional area of the armature winding is determined from the expression

$$\sum S_n = \frac{F_{n \max}}{j_{n \max}} = \frac{\pi D_n \xi_D}{j_{n \max}} H_{n \max} \text{ and } \sum S_a = \frac{\pi D A}{j_a}$$

in the following manner:

$$\frac{\sum S_n}{\sum S_a} = \frac{D_n}{D} \frac{j_a}{j_{n \max}} \frac{H_{n \max}}{A} \left( 1 - \frac{k_n}{D_n} \right). \quad (4.44)$$

The relative magnetizing-winding copper cross section in the armature slots will decrease as the linear load (machine power) rises. In low-power machines, the magnetization winding occupies about half the slot cross section.

Regulation circuits. Voltage regulation and stabilization based on changing the reluctance of the magnetic circuit by saturating the

armature core with a constant flux can be classified as a direct regulation method, since the sensing element of the regulator reacts to a deviation of the generator voltage from a specified level. The regulator is of the static type with a specific permissible static response that depends on how well the regulator characteristics match the "regulation" characteristic of the generator.

$$I_p = f(I) \text{ for } U_g = \text{const and } n = \text{const.}$$

For proper operation of the regulator with minimum static response delay, the working magnetization current-change factor (constant flux) should not exceed a specific magnitude that will be provided by a regulator of a given type for the given load resistance (magnetization-winding resistance). With this method of regulation, the operating peculiarity of the regulators lies in the fact that they operate, for resistive-inductive loads, with considerable generator magnetization-winding inductance, which is considerably more than the inductance of generator field windings for precisely the same power, owing to the absence of a gap in the magnetization flux path.

When this method is used to regulate the voltage of permanent-magnet generators, a regulator with a saturable reactor (an inductor magnetic amplifier) may be used together with a carbon regulator, working in conjunction with the magnetic amplifier.

The first type of regulator represents a direct-acting static regulator whose measuring organ consists of the excitation winding of the saturable reactor, which reacts directly to a departure in regulated voltage from the predetermined value.

The basic generator-regulation circuit may be three-phase or single-phase. The single-phase version, naturally, is used to regulate voltages in single-phase permanent-magnet generators.

The circuit of Fig. 4.51 uses a three-phase saturable reactor DT

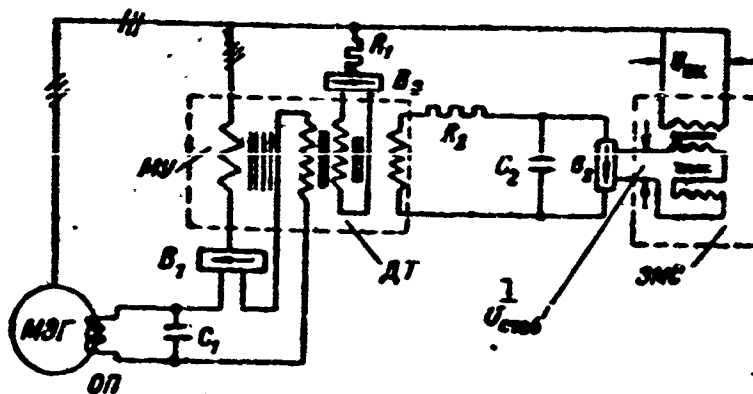


Fig. 4.51. Three-phase voltage-regulation circuit for permanent-magnet generators. OP) Armature-core magnetization winding; MU) three-phase magnetic amplifier;  $V_1$ ,  $V_2$ , and  $V_3$ ) solid-state rectifiers supplying power respectively to magnetization and feedback windings, bias winding, and control winding. 1)  $U_{stab}$ .

whose inductive reactance appears as a variable resistance in the circuit of the generator magnetization winding. This winding is supplied from the generator voltage through the three-phase reactor and the selenium bridge  $V_1$ . The capacitor  $C_1$  at the output of the selenium bridge is used to compensate the considerable inductive reactance of the generator magnetization coil, increasing the gain of the three-phase reactor and circuit sensitivity. The inductive reactance of the choke controls the voltage-measuring organ of the circuit — the magnetizing winding of the three-phase reactor DT, which is supplied from the generator voltage through the full-wave selenium bridge  $V_3$ . The electromagnetic voltage stabilizer EMS is used in the circuit to create the base bias voltage. The ampere-turns of the bias winding, supplied through  $V_2$  from the voltage of the EMS, may be used to set the operating point on the three-phase inductor curve  $I_{dr} = f(I)$ .

We note that with this regulation method, owing to the considerable inductance of the generator magnetization winding, it is necessary to raise the positive feedback coefficient for the three-phase

reactor. The feedback winding of the reactor is connected in series with the generator magnetization winding.

The circuit of Fig. 4.51 was used to test aircraft permanent-magnet generators of 75-1000 va power; their voltages were held constant to within  $\pm 2\%$  (allowing for unbalanced line voltages). Here the weight and size of the regulator corresponded roughly to the weight and size of a regulator designed to regulate voltages of electromagnetically excited generators.

The degree of voltage waveform distortion rises somewhat with increasing magnetizing field strength (when  $H_p \text{ max} > 50$  ampere-turns/cm).

The basic voltage waveform distortion is introduced by the effect of the generator load on the nonlinear resistance of the three-phase reactor and the selenium rectifiers where the apparent regulation power is of considerable magnitude with respect to the rated generator power.

The lower the generator power, the less the regulation power that may be drawn from it, i.e., it is necessary to decrease the generator magnetization current for the same  $F_p$ .

This leads to an increase in the area occupied by the magnetization winding and an increase in machine size, since the pure resistance of the winding should not exceed a specific quantity dictated by the conditions for the optimum saturable-reactor characteristic. The resistive voltage drop across the magnetization winding should be

$$\Delta U_{\text{res}} \leq \frac{U_r}{\sqrt{2}}.$$

Thus for low-power generators (200 va or less), utilization of this method leads to increased generator weight and size.

For high-power generators, considerable regulation power (considerable magnetization current) may be permitted without noticeable

distortion in generator voltage waveform; here the relative regulation power drops with increasing generator power. Thus, it makes the most sense to use this regulation method for generators of 300 va or more power.

Thus, for a generator with a power of about 500 va, maximum apparent control power (no load) is

$$P_{\text{max}} = \sqrt{3} I_a U_a \approx 125 \text{ va}$$

for a wattful regulation power  $P_{\text{p.akt}} = R_p I^2 = 50 \text{ watts}$ , and the magnetization winding occupies 50% of the slot cross section.

In order to decrease voltage unbalance in regulating a three-phase permanent-magnet generator, the best solution is to use the three-phase version, since it sets up a balanced load for the generator. The three-phase circuit weighs somewhat more than the single-phase version, however.

#### 4.7. ELEMENTS OF THE ANALYTIC THEORY OF PERMANENT-MAGNET GENERATORS\*

The theory of circuits with permanent magnets is based on the demagnetization curve, which characterizes a source of magnetizing force, and is called the magnet diagram. It is uniquely determined by: the coercive force  $H_c$ , residual induction  $B_r$ , hysteresis-curve form factor  $\gamma$ , and the reversal coefficient  $\mu_v$ .

The form factor  $\gamma$  is defined as the ratio of the maximum magnetic energy  $A_{\text{max}} = (BH/8\pi)_{\text{max}}$  to the relative magnetic energy  $A_c = B_r H_c / 8\pi$ , i.e.,

$$\gamma = \frac{A_{\text{max}}}{A_c} = \frac{(BH)_{\text{max}}}{B_r H_c} = (\dot{B}\dot{H})_{\text{max}} \quad (4.45)$$

The magnet diagram may be represented in  $B_r$  and  $H_c$  coordinates, in  $\phi_r$  and  $F_c$  coordinates, or in the relative units  $\dot{B} = B/B_r$  and  $\dot{H} = H/H_c$  (see §4.4); here the units of reluctance  $R_r$ , permeance  $\Lambda_r$ , and permeability  $\mu_r$  are the quantities

$$\left. \begin{aligned} R_r &= \frac{F_c}{\Phi_r} = 0,8 \frac{h_m}{S_m} \frac{H_c}{B_r} = R \frac{H_c}{B_r} = \frac{R}{\mu_r} \\ \Lambda_r &= \frac{\Phi_r}{F_c} = 1,25 \frac{S_m}{h_m} \frac{B_r}{H_c} = \Lambda \frac{B_r}{H_c} = \Lambda \mu_r \\ \mu_r &= \frac{B_r}{H_c} \end{aligned} \right\} \quad (4.45)$$

Here

$$K = 0,8 \frac{h_m}{S_m} = 0,8 k_m \quad \text{and} \quad \Lambda = 1,25 \frac{S_m}{h_m} = \frac{1,25}{k_m}$$

are the reluctance and permeance of the space occupied by the magnet (not the magnet material);  $k_m = h_m/S_m$  is the magnet form factor;  $h_m$  and  $S_m$  are the length and cross-sectional area of the magnet.

Here, in relative units, the reluctance and permeance of the external circuit will be

$$\left. \begin{aligned} \dot{K}_s &= \frac{R_s}{R_r} = \frac{\dot{F}}{\dot{\Phi}} = \frac{F}{F_c} \frac{\Phi_r}{\Phi} = \frac{\dot{H}}{\dot{B}} = \frac{1}{S_s} \frac{S_m}{h_m} \mu_r \\ \dot{\Lambda}_s &= \frac{\Lambda_s}{\Lambda_r} = \frac{S_s}{S_m} \frac{k_m}{\mu_r} \end{aligned} \right\} \quad (4.47)$$

where the symbol \* indicates relative quantities.

Here, as we have already noted, regardless of the coordinate system used, the following relationships will hold for the tangent of the slope of line Oδ:

$$\left. \begin{aligned} \text{tg } \delta &= \frac{\dot{F}}{\dot{\Phi}} = \frac{\dot{H}}{\dot{B}} = \frac{\mu_r}{\mu} = \frac{1}{\mu^*} = \dot{K}_s \\ \text{tg } \alpha &= \text{ctg } \delta = \frac{\dot{B}}{\dot{H}} = \frac{\mu}{\mu_r} = \frac{1}{\mu_r} = \dot{\Lambda}_s \end{aligned} \right\} \quad (4.48)$$

where  $\mu^* = \mu/\mu_r$  is the relative permeability of the magnet material.

The magnetizing-force curves for modern permanent-magnet materials may be approximated, with adequate accuracy, by a rectangular hyperbola of the form

$$B = B_r \frac{H_c - H}{H_c - \frac{H}{\mu_r}} = B_r \frac{H_c - H}{H_c - aH} = B_r \frac{1(H_c - H)}{H_c(1 - (2\sqrt{1-\mu_r})H)} \quad (4.49)$$

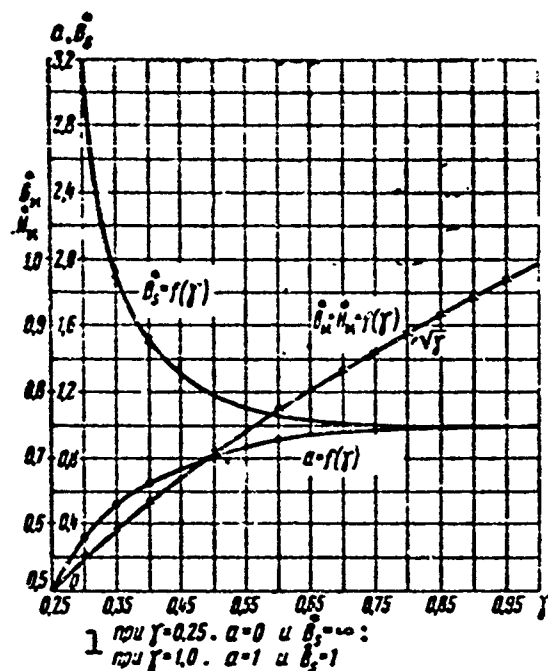


Fig. 4.52. Relative saturation induction (induction and field strength at point  $\hat{B}_{H_{max}}^{**}$ ) as function of curve shape.  
1) For.

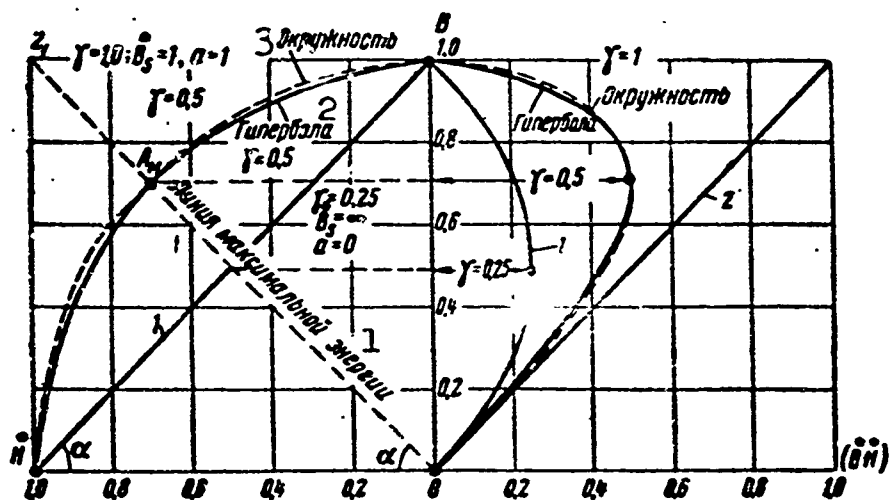


Fig. 4.53. Demagnetization curves in relative units. 1) Maximum-energy line; 2) hyperbola; 3) circle.

or in the relative units

$$\hat{B} = \hat{B}_s \frac{1 - \hat{H}}{\hat{B}_s - \hat{H}} = \frac{1 - \hat{H}}{1 - \alpha \hat{H}} = \frac{\gamma(1 - \hat{H})}{\gamma - (2\sqrt{\gamma} - 1)\hat{H}}. \quad (4.49a)$$

Here  $H(\hat{H})$  is assumed to be positive for demagnetization and



$$a = \frac{1}{\dot{B}_s}, \quad \dot{B} = \frac{B}{B_r}, \quad \dot{H} = \frac{H}{H_c}, \quad \dot{B}_s = \frac{B_s}{B_r} = \frac{1}{2\sqrt{1-\gamma}}.$$

$\gamma = (BH)_{\max} / B_r H_c = (\dot{B}\dot{H})_{\max}$  is the form factor for the demagnetization curve.

Figure 4.52 gives  $\dot{B}_s^*$  and  $\alpha = f(\gamma)$ , as well as  $\dot{B}_m^*$  and  $\dot{H}_m^* = f(\gamma)$  at the point  $(\dot{B}\dot{H})_{\max}$ .

Using (4.49) it is easy to use the parameter  $\gamma$ ,  $\dot{B}_s^*$ , or  $a$  to construct the relative demagnetization curve. Analysis of (4.49) has shown that when  $\gamma = 0.25$ , the rectangular hyperbola degenerates into the straight line

$$\dot{B} = 1 - \dot{H},$$

which corresponds to the least desirable shape for the demagnetization curve as a triangle.

When  $\gamma = 1$ , the hyperbola degenerates to a straight line parallel to the x-axis, i.e.,

$$\dot{B} = 1,$$

which corresponds to ideal permanent-magnet material having a demagnetization curve in the form of a rectangle; in this case, there is no reversal line, since  $\mu_v = (\Delta B / \Delta H) = 0$ .

When  $\gamma = 0.5$ , the equation of the hyperbola takes the form

$$\dot{B} = \frac{1 - \dot{H}}{1 - 0.828\dot{H}};$$

it may be replaced, with accuracy adequate for practical purposes, by a circle (the dashed line of Fig. 4.53), whose form factor also equals 0.5, i.e.,

$$\dot{B} = \sqrt{1 - \dot{H}^2}.$$

Figure 4.53 gives demagnetization curves in relative coordinates; the curves have various form factors.

If we assume that all the possible demagnetization curves lie in the zone between the diagonal 1 and the rectangle 2, the form factor

may theoretically vary from  $\gamma = 0.25$  (for the diagonal) to  $\gamma = 1$  (for curve 2), i.e.,  $0.25 < \gamma < 1$  and, consequently,  $1 < \tilde{B}_s^* < \infty$  and  $1 > a > 0$ .

Modern permanent-magnet materials have form factors in the range  $\gamma = 0.3-0.65$ ; the first value applies to alloys of the alnisi type (ANK), and the second to alloys of the magnico type (ANKO). Consequently, for these materials,  $\tilde{B}_s^* = 3.15-1.06$  and  $a \approx 0.318-0.945$ .

The carbon, chrome, and tungsten steel used earlier had form factors of  $\gamma \approx 0.5$ .

Despite the great variety of applications and structural shapes for magnets, magnetic circuits using permanent magnets may be classified into two basic groups according to operating mode.

The first group includes magnets used in circuits in which the permeance remains unchanged and in which external magnetic fields have no effect. The second group includes magnets used in circuits with varying permeances, and experiencing the effects of external varying magnetic fields.

For magnets working under a constant load — static mode — there are two cases: the magnet is not stabilized and operates on the demagnetization curve and, consequently, is irreversible; or the magnet is stabilized and operates on the reversal line and, consequently, is reversible.

When the magnet works with a changing load — dynamic mode — the magnet will always operate on the reversal line and will be reversible (magnets of permanent-magnet machines).

When complicated permanent-magnet circuits are studied, the following assumptions, justified by experience, are usually made:

a) the magnet is magnetized to saturation and, if it is anisotropic, it is magnetized along the appropriate axes;

b) the fittings are not saturated and, consequently, there is a linear relationship between the magnetizing force and the flux;

c) the magnet has a constant cross section, the flux remains the same along the length of the magnet, and is distributed uniformly over its cross sections; transverse magnetization is neglected (this assumption is correct where the magnet form factor  $k_m < 2$ );

d) the entire magnet leakage flux  $\phi_\sigma$  emanates from the poles, i.e., it appears in parallel with the pole flux  $\phi = \phi_\delta + \phi_\sigma$ , and the leakage factor  $k_\sigma = \phi/\phi_\delta = \text{const}$  along the entire length of the magnet;

e) the permanent magnet is considered as a source of magnetizing force and as a part of the magnetic circuit having a reluctance (permeance)  $R_m(\Lambda_m)$ ;

f) the internal magnet magnetizing force  $F_c$  consists of the magnetizing force  $F$  which it develops at the pole surfaces and the magnetic potential drop in the magnet itself, i.e.,  $F_c = F + R_m\phi$ , where  $\phi$  is the magnetic flux within the magnet, and equals the sum of the flux in the gap  $\phi$  and the leakage flux  $\phi_\sigma$ ;

g) if we do not take the leakage flux into account, the internal magnet magnetizing force  $F_c$ , after the magnetic potential drop in the magnet itself has been subtracted, is expended in overcoming the magnetic potential drop in the external-circuit reluctance (air gaps and magnetically soft sections of the circuit), and to compensate the demagnetizing effect of external fields.

As is well known, there is an electrical analogy for any magnetic circuit. Utilization of equivalent circuits for the magnetic circuits of permanent-magnet machines simplifies the analytical investigation of such machines.

Below we shall consider magnets operating on the reversal line and in the dynamic mode, and we shall not go into the peculiarities of

magnet operation on the demagnetization curve.

### Operation on the Reversal Line

Let us consider the case in which a permanent magnet designed to operate in a magnetic circuit with constant reluctance in the absence of external magnetic fields is first stabilized, either by changing the external permeance (leakage stabilization) or by means of an external demagnetizing field. In this case, the magnet will operate on a minor hysteresis loop having initial point on the main hysteresis curve and intersecting the y-axis (B) at point  $B_v$ .

As a rule, a minor hysteresis loop originating at the main hysteresis curve is replaced by a straight line connecting the initial and terminal points of the minor loop. This line is called the reversal line, and point  $A_0$  is called the point of departure for the reversal line (§4.1).

The position of the reversal line is determined uniquely by the position of the point of departure on the demagnetization curve and the reversal coefficient  $\mu'_v$ .

If we assume that all the reversal lines are parallel, i.e.,  $\mu'_v = \text{const}$ , they should also be parallel to the limiting reversal line, which corresponds to the tangent to the demagnetization curve at point  $B_r$ . Thus, for a preliminary determination of the slope of a reversal line, it may be considered to be tangent to the demagnetization curve at point  $B_r$ , and the slope of the reversal line is determined as the derivative of the equation of the demagnetization curve at point  $B_r$  where  $H = 0$ . If, for example, we approximate the demagnetization curve by a rectangular hyperbola, by differentiation we obtain the following expression:

$$\mu'_v = \frac{B_r - 1}{B_r} = 1 - a = \frac{(V_1 - 1)^2}{1}. \quad (4.50)$$

It is clear that at  $\gamma = 1$ , the reversal coefficient will equal zero, i.e., there is no reversal curve: at  $\gamma = 0.25$ , the reversal coefficient reaches its maximum of unity.

As a rule, the ratio  $\mu_v/\mu_k > 1$ , and in the working zone it equals roughly 3 for anisotropic alloys of the magnico type and 1.1-1.6 for isotropic alloys of the alnico type.

For alloys with low demagnetization-curve form factors ( $\gamma \leq 0.3$ ),  $\mu_v$  approaches the value  $\mu_k$  as found from Expression (4.50). For alloys with large form factors ( $\gamma \geq 0.6$ ), in the working zone  $\mu_v$  exceeds  $\mu_k$  by a factor of 2.5-3.

Figure 4.54 gives equivalent circuits for the magnetic circuit in absolute and relative units, as well as magnetic-circuit hysteresis diagrams for a magnet operating on the reversal line.

In the equivalent circuits, the internal reluctance of the magnet is assumed to be constant. For this purpose, we introduce the concept of the virtual magnetizing force,  $\dot{F}_v^* = F_v/F_c$ ; the magnitude of this quantity is determined by the intersection of the reversal-line continuation with the x-axis. In this case, the working characteristic of the magnetizing-force source takes the form of a straight line, while the permeability and internal reluctance of the magnet are represented by the equations:

$$\mu_r = \frac{\dot{B}}{\dot{H}_B - \dot{H}_0} = \frac{\dot{B}_B}{\dot{H}_B} = \frac{\dot{B}_B}{\dot{H}_B} = \frac{\dot{B}_B}{\dot{H}_B} = \dot{\Lambda}_m$$

— the reversal permeability (internal permeance of the magnet);

$$\dot{R}_m = \frac{R_m}{R_r} = \frac{1}{\mu_r} = \frac{1}{\dot{\Lambda}_m}$$

— the internal reluctance of the magnet.

#### Stabilization by Opening Magnetic Circuit

Figure 4.55 gives a magnetic-circuit diagram corresponding to mag-

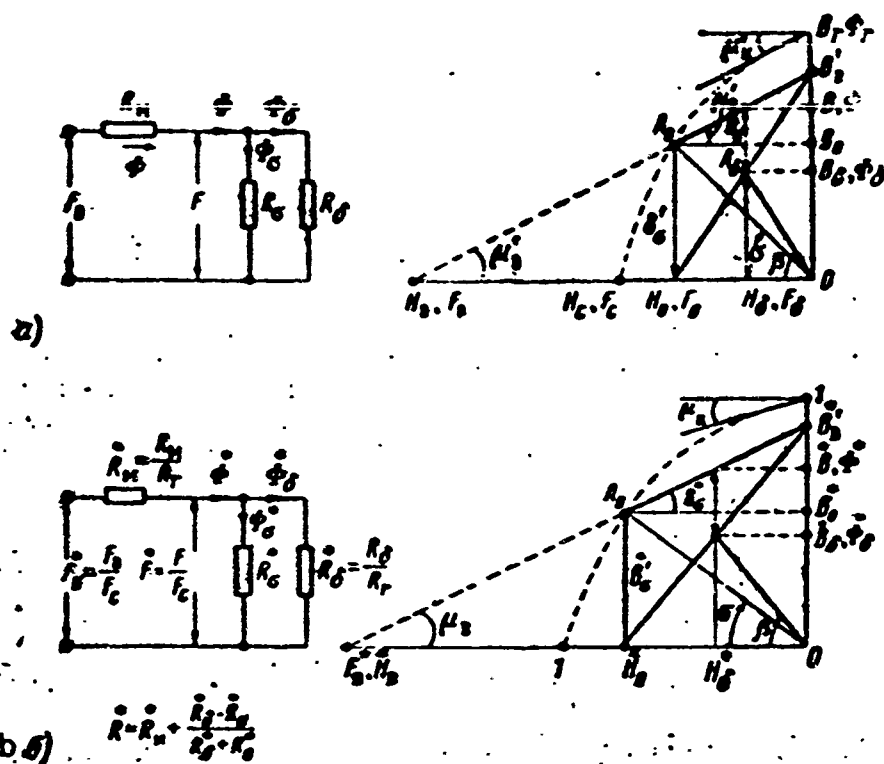


Fig. 4.54. Equivalent circuits and corresponding magnet hysteresis diagrams for magnets operating on reversal line. a) Absolute units; b) relative units.

net operation on a reversal line, allowing for leakage.

Here it has been assumed that at the point of departure of the reversal line, the useful flux is zero ( $\Phi \equiv B_0 = 0$ ), i.e.; at point  $A_0$  the entire magnet flux takes the form of a leakage flux ( $\Phi = \Phi'_0$ ). In practice, this means that magnet stabilization is carried out to a value  $B_0 = B'_0 = H_0 \tan \sigma = H_0 \Lambda_0$ , i.e., the magnet is stabilized by opening the magnetic circuit. Using the notation of Fig. 4.55, we write certain relationships.

The inductions corresponding to the leakage flux are

$$\dot{B}_0 = \dot{B}'_0 = \dot{H}_0 \tan \sigma = \dot{H}_0 \Lambda_0; \quad \dot{B}_s = \dot{H} \tan \sigma = \dot{H} \Lambda_0. \quad (4.51)$$

The virtual inductions corresponding to the slope of the reversal line are

$$\dot{B}_m = \dot{H}_0 \tan \sigma = \dot{H}_0 \Lambda_m = \dot{H}_0 \mu_s; \quad \dot{B}_n = \dot{H} \tan \sigma = \dot{H} \mu_n. \quad (4.52)$$

The useful magnetic induction in the air gap is

$$\dot{B}_i = \dot{B}_s - (\dot{B}_m + \dot{B}_n) =$$

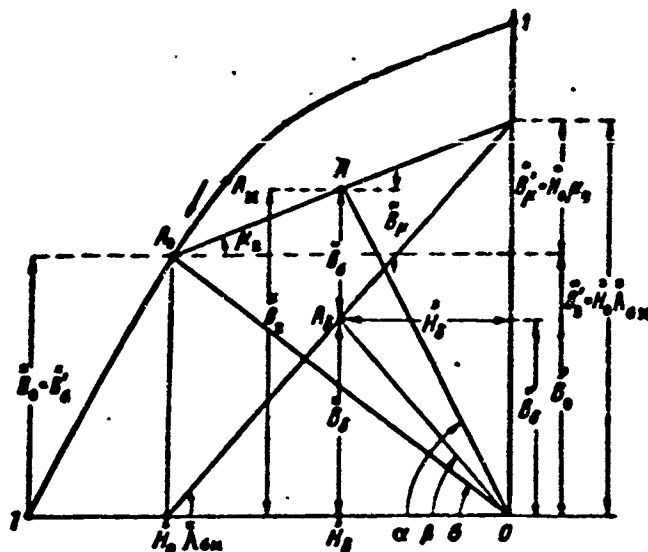


Fig. 4.55. Relative magnet diagram for open-circuit stabilization.

$$= \dot{B}_s - \dot{H}(\dot{\Lambda}_s + \dot{\Lambda}_m) = \dot{B}_s - \dot{H}\dot{\Lambda}_m, \quad (4.53)$$

where the induction  $\dot{B}_v^*$  corresponds to the point at which the reversal line intersects the B axis, i.e., to the maximum induction for an external magnetic reluctance of zero ( $\dot{B}_v^*$  is the induction with the magnetic circuit short-circuited); it will equal

$$\dot{B}_s = \dot{B}_m + \dot{B}_s = \dot{H}_0 \dot{\Lambda}_m = \dot{H}_s \dot{\Lambda}_m. \quad (4.54)$$

Here

$$\begin{aligned} \dot{\Lambda}_m &= \dot{\Lambda}_s + \dot{\Lambda}_m, \\ \dot{H}_s &= \frac{H_s}{H_e} = \dot{H}_0 \frac{\dot{\Lambda}_m}{\dot{\Lambda}_s} = \dot{H}_0 \left(1 + \frac{\dot{\Lambda}_s}{\dot{\Lambda}_m}\right). \end{aligned}$$

$\dot{H}_0$  is the field strength corresponding to the point of departure of the reversal line  $A_0$ , i.e., the field strength for the open magnetic circuit.

If we make use of the value of  $\dot{B}_v^*$  from (4.54), the induction in the air gap can then be represented as

$$\dot{B}_s = (\dot{H}_0 - \dot{H}) \dot{\Lambda}_m + \dot{B}_s \left(1 - \frac{\dot{H}}{\dot{H}_0}\right) = (\dot{H}_0 - \dot{H}) \dot{\Lambda}_m. \quad (4.55)$$

Let us establish the relationship between the coordinates of the

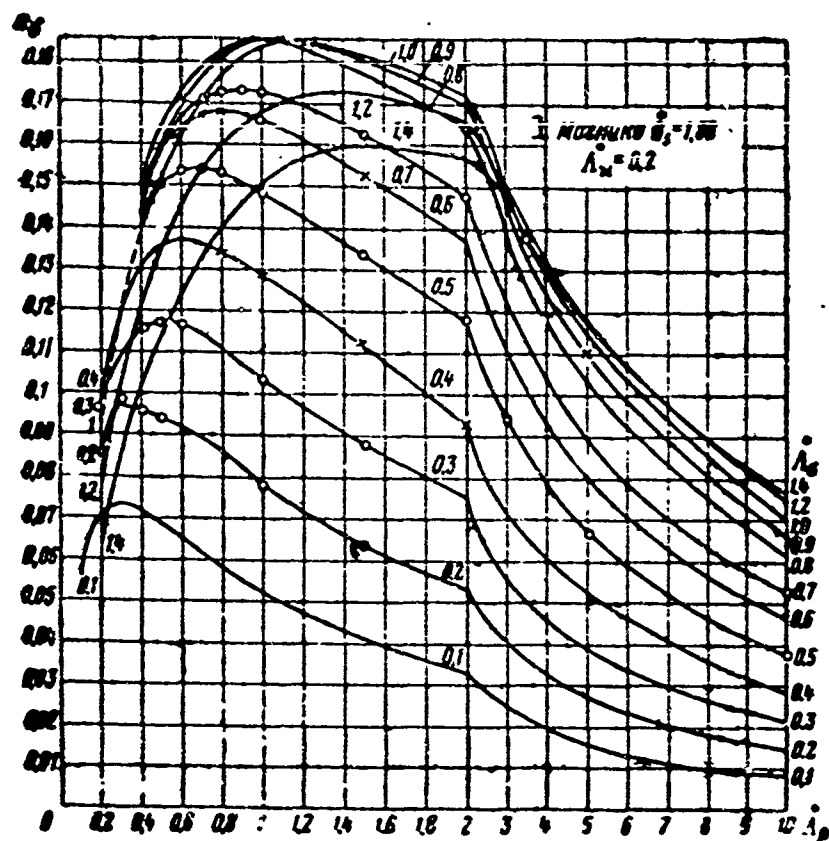


Fig. 4.56. Relative useful energy for alnico alloy as function of external-circuit permeance  $\Lambda_{\beta}^*$  and leakage permeance  $\Lambda_{\sigma}^*$  for reversal coefficient  $\mu_v = 0.2$ . 1) Magnico.

point of departure of the reversal line ( $\vec{B}_0 = \vec{B}'_{\sigma}$  and  $\vec{H}_0$ ) and the coordinates of the useful-energy point ( $\vec{B}_{\delta} = \vec{B}$  and  $\vec{H}_{\delta} = \vec{H}$ ). Since

$$\vec{B}_i = \vec{H}_i \Lambda_{\beta} = (\vec{H} - \vec{H}_{\sigma}) \Lambda_{\beta},$$

then

$$\left. \begin{aligned} \vec{H}_i &= \vec{H}_0 \frac{\Lambda_{\sigma}}{\Lambda_{\beta} + \Lambda_{\sigma}} = \vec{B}_0 \frac{1}{\Lambda_{\sigma}} \frac{\Lambda_{\sigma}}{\Lambda_{\beta} + \Lambda_{\sigma}}, \\ \vec{B}_i &= \vec{H}_i \Lambda_{\beta} = \vec{B}_0 \frac{\Lambda_{\beta}}{\Lambda_{\sigma}} \frac{\Lambda_{\sigma}}{\Lambda_{\beta} + \Lambda_{\sigma}}, \end{aligned} \right\} \quad (4.56)$$

where  $\Lambda_{\beta}$  is the external-circuit permeance.

Allowing for scattering, the expressions for  $\vec{H}_{\delta}$  and  $\vec{B}_{\delta}$ , with the magnet operating on the reversal line, can be found directly from the equivalent circuit of Fig. 4.54.

The useful specific magnetic energy developed by the magnet in



external space, allowing for (4.55), will be

$$a_2 = \frac{A_2}{A_c} = (\dot{B}\dot{H})_2 = \dot{H} \left[ (\dot{H}_0 - \dot{H}) \dot{A}_m + \dot{B}_s \left( 1 - \frac{\dot{H}}{\dot{H}_0} \right) \right] \quad (4.57)$$

or on the basis of (4.56)

$$a_2 = \dot{H}_0^2 \dot{A}_s \left( \frac{\dot{A}_{sm}}{\dot{A}_s + \dot{A}_{sm}} \right)^2 = \dot{B}_s \dot{H}_0 \frac{\dot{A}_s}{\dot{A}_s} \left( \frac{\dot{A}_{sm}}{\dot{A}_s + \dot{A}_{sm}} \right)^2 \quad (4.58)$$

When the demagnetization curve is approximated by a rectangular hyperbola, the x-axis value for the point of departure is found from the expression

$$\dot{H}_s = \frac{\dot{B}_s}{2} \frac{1 + \dot{A}_s}{\dot{A}_s} \left[ 1 - \sqrt{1 - \frac{4\dot{A}_s}{\dot{B}_s(1 + \dot{A}_s)^2}} \right] \quad (4.59)$$

Figure 4.56 shows a plot of the function  $a_\delta = f(\dot{A}_\beta^*)$  for several values of  $\dot{A}_\sigma^*$  for magnico alloy (ANKO4).

In order to find the maximum useful magnetic energy in the air gap, it is necessary to find the partial maximums, computing the partial derivatives with respect to  $\dot{H}^*$  and  $\dot{H}_0^*$ , and approximating the demagnetization curve.

On the assumption that  $\dot{H}_0^* = \text{const}$ , i.e.,  $\dot{B}_s^* = \text{const}$  and  $\dot{A}_\sigma^* = \text{const}$ , we find the field strength  $\dot{H}^*$  for which the magnet develops the maximum useful energy in the air gap while operating on the reversal line at a given value of leakage permeance,  $\dot{H}_\sigma^*$  and  $\dot{H}_0^*$ . On the basis of (4.57)

$$\frac{da_2}{d\dot{H}} = \frac{d}{d\dot{H}} \left[ \dot{A}_m (\dot{H}\dot{H}_0 - \dot{H}^2) + \dot{B}_s \left( \dot{H} - \frac{\dot{H}^2}{\dot{H}_0} \right) \right] = 0.$$

whence

$$\dot{H} = \dot{H}_{s \max} = \frac{\dot{H}_0 (\dot{A}_m \dot{H}_0 + \dot{B}_s)}{2 (\dot{A}_m \dot{H}_0 + \dot{B}_s)} = \frac{\dot{H}_0}{2}.$$

and taking (4.51) into account, we find that

$$a_{i, \max} = (\vec{B} \vec{H})_{i, \max} = \frac{\vec{H}_0}{2} \left( \frac{\vec{H}_0 \vec{\lambda}_u}{2} + \frac{\vec{B}_0}{2} \right) - \frac{\vec{H}_0^2 \vec{\lambda}_{u0}}{4} \quad (4.60)$$

i.e.,

$$a_{i, \max} = \frac{\vec{H}_0 \vec{B}_0}{2} \quad (4.61)$$

since

$$\vec{H}_0 \vec{\lambda}_{u0} = \vec{B}_0$$

Thus, if the point of departure of the reversal line corresponds to the maximum leakage flux, the maximum useful magnetic energy in the air gap will appear during operation at the center of the reversal line, i.e., at the point at which the useful field strength equals half the field strength for the open magnetic circuit and the useful induction equals half the induction for the short-circuited magnetic circuit:

$$\vec{H}_{i, \max} = 0.5 \vec{H}_0; \quad \vec{B}_{i, \max} = 0.5 \vec{B}_0$$

The maximum useful specific energy will then equal

$$A_{i, \max} = A_c \frac{\vec{H}_0 \vec{B}_0}{4} \text{ [erg/cm}^3\text{]}. \quad (4.62)$$

Absolute magnetic-energy maximum. If the leakage permeance, i.e., the quantity  $\vec{\lambda}_0^*$  changes, the point of departure for the reversal line  $A_0(\vec{H}_0^*, \vec{B}'_0)$  will shift along the main demagnetization curve. Each reversal line, i.e., each degree of stabilization, will have its own maximum useful magnetic energy.

In order to determine the optimum useful magnetic energy, i.e., the value of  $\vec{H}_0^*$  for which the optimum useful energy will be developed at the center of the reversal line it is necessary, as in the preceding case, to find the partial derivative of Expression (4.60) with respect to  $\vec{H}_0^*$  in view of the fact that  $\vec{H}_0 = 0.5 \vec{H}_0^*$  and  $\vec{B}'_0 = f(\vec{H}_0^*)$ , i.e.,

$$\frac{da_i}{d\vec{H}_0} = \frac{d}{d\vec{H}_0} \left[ \frac{\vec{H}_0^2 \vec{\lambda}_u}{4} + \vec{B}_0 \frac{\vec{H}_0}{4} \right] =$$

$$-\frac{\dot{H}_0 \dot{\Lambda}_m}{2} + \frac{\dot{B}_s \dot{H}_0}{4 \dot{H}_0} + \frac{\dot{B}_s}{4} = 0$$

and

$$2\dot{\Lambda}_m \dot{H}_0 + \dot{B}_s + \dot{H}_0 \frac{\dot{B}_s}{\dot{H}_0} = 0. \quad (4.63)$$

It is clear that in order to solve Eq. (4.63) it is necessary to approximate the demagnetization curve in accordance with the procedure discussed above, for example, in accordance with (4.49) in the form of a rectangular hyperbola.

In this case, optimum utilization of the magnet will occur at the center of the reversal line, whose position is determined by the quantities  $\dot{H}_{0\max}^*$  and  $\dot{\Lambda}_m^* = \mu_v$ , with  $\dot{H}_{0\max}^* = f(\dot{\Lambda}_m^*, \dot{B}_s^*)$ .

After certain manipulations we obtain

$$\begin{aligned} a_{i\max} &= \frac{\dot{H}_{0\max}^2 \dot{\Lambda}_m}{4} + \dot{B}_s \frac{\dot{H}_{0\max}}{4} = \\ &= \frac{\dot{H}_{0\max} \dot{B}_s - \dot{B}_s (1 - \dot{\Lambda}_m) \dot{H}_{0\max} - \dot{\Lambda}_m \dot{H}_{0\max}^2}{4 \dot{B}_s - \dot{H}_{0\max}} \end{aligned} \quad (4.64)$$

or, assuming that

$$\dot{\Lambda}_m = \frac{\dot{B}_s - 1}{\dot{B}_s},$$

we find

$$a_{i\max} = \frac{\dot{H}_{0\max} \dot{B}_s^2 - \dot{B}_s \dot{H}_{0\max} - (\dot{B}_s - 1) \dot{H}_{0\max}^2}{4 \dot{B}_s \dot{B}_s - \dot{H}_{0\max}}. \quad (4.65)$$

The field strength at the point of departure  $\dot{H}_{0\max}^*$  for which the magnet develops the absolute maximum of useful magnetic energy may be found graphically.

As investigations have shown, Formula (4.65) yields considerable errors, which increase as the value of  $\gamma$  increases. This formula may be used, however, for preliminary calculations in the absence of data on the reversal coefficient. Figure 4.57 gives the functions

$$\dot{H}_{0\max} \dot{B}_{1\max}; a_{1\max} = f(\gamma) \text{ for } \dot{\Lambda}_m = \text{const},$$

obtained by the author by calculation for magnetic alloys employed in practice.

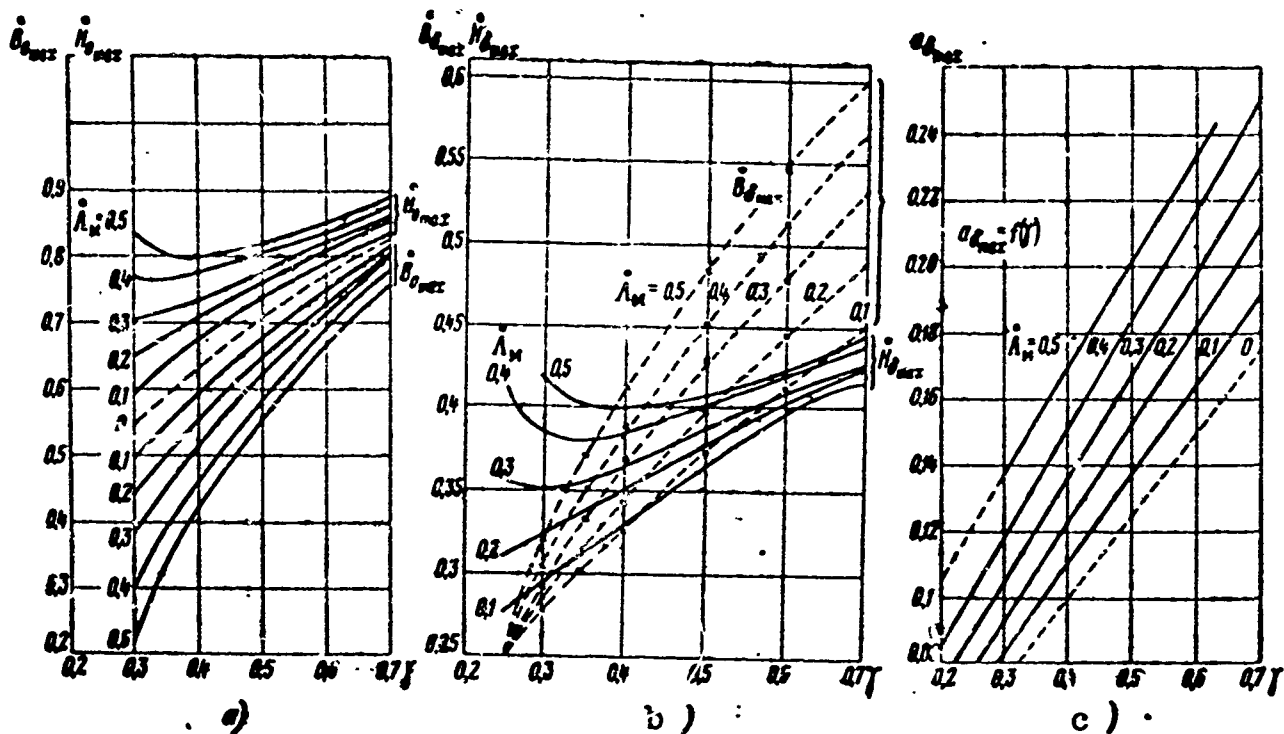


Fig. 4.57. Calculated curves for the absolute maximum of magnetic energy. a) Coordinates of point of departure of reversal line ( $\dot{H}_{0\max}$  and  $\dot{B}_{1\max}$ ); b) coordinates of point of maximum useful energy ( $\dot{H}_{0\max}$  and  $\dot{B}_{1\max}$ ); c) relative maximum energy.

Since it is not possible to solve Eq. (4.63) in a general form suitable for subsequent utilization in (4.64) and (4.65), an approximate equation is used here for the maximum useful energy; it takes the form

$$a_{1\max} \approx (0.25 + 0.16 \dot{\Lambda}_m) \gamma + 0.05 \dot{\Lambda}_m. \quad (4.66)$$

Here the magnet utilization factor will be

$$k_{\max} \approx \frac{a_{1\max}}{\gamma} = \frac{A_{1\max}}{A_c \gamma} = 0.25 + (0.16 + 0.05 \gamma^{-1}) \dot{\Lambda}_m. \quad (4.67)$$

In conclusion, we note that by using triangle, circle, and rectangle approximations it is possible to obtain analytical expressions for all of the quantities of interest to us in a form convenient for the investigation. They agree well, as has been shown by a comparison

of the results obtained with the circle and hyperbola approximations (with  $\gamma = 0.5$ ). This gives us a basis for studying circuits containing permanent magnets, with the appropriate approximation for the magnet diagram used depending on the alloys employed.

Thus, if the operating point is located on the reversal line, at the point of maximum useful magnet energy, and the magnet has been stabilized by opening the magnetic circuit, the following laws will hold for the optimum (absolute maximum) useful energy:

a) the operating point on the demagnetization curve is located below the point  $(\dot{B}\dot{H})_{\max}^{**}$ , i.e.,

$$\dot{H}_{0\max} > \sqrt{\gamma}, \quad \dot{B}_{0\max} < \sqrt{\gamma}$$

and

$$\dot{\Lambda}_m < 1;$$

b) the larger  $\dot{\Lambda}_m^*$ , the larger the ratios

$$\frac{\dot{H}_{0\max}}{\dot{H}_{\max}} > 1 \text{ and } \frac{\dot{B}_{\max}}{\dot{B}_{0\max}} > 1;$$

provided all other conditions remain the same;

c) the leakage factor will always be less than 2 for operation at the optimum useful-energy point, i.e.,

$$k_{\max} < 2.$$

#### General Case of Operation on Reversal Line

Let us study the equivalent circuit for a permanent-magnet machine making the following assumptions in addition to those made earlier.

1. The machine magnetic circuit (Fig. 4.58) consists of the working air gap, secondary-circuit magnetic flux path (armature teeth and core), primary-circuit magnetic flux path (pole piece, pole ring), inactive air slot (between pole and pole ring, between pole and pole piece, between pole ring and magnet), which have the following respec-

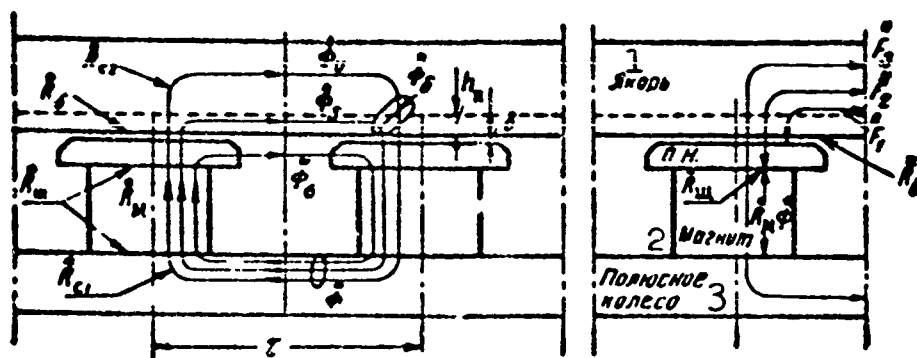


Fig. 4.58. Element of magnetic circuit for salient-pole permanent-magnet machine with pole pieces. The reluctances, fluxes, and magnetizing forces are shown in relative units. 1) Armature; 2) magnet; 3) pole ring.

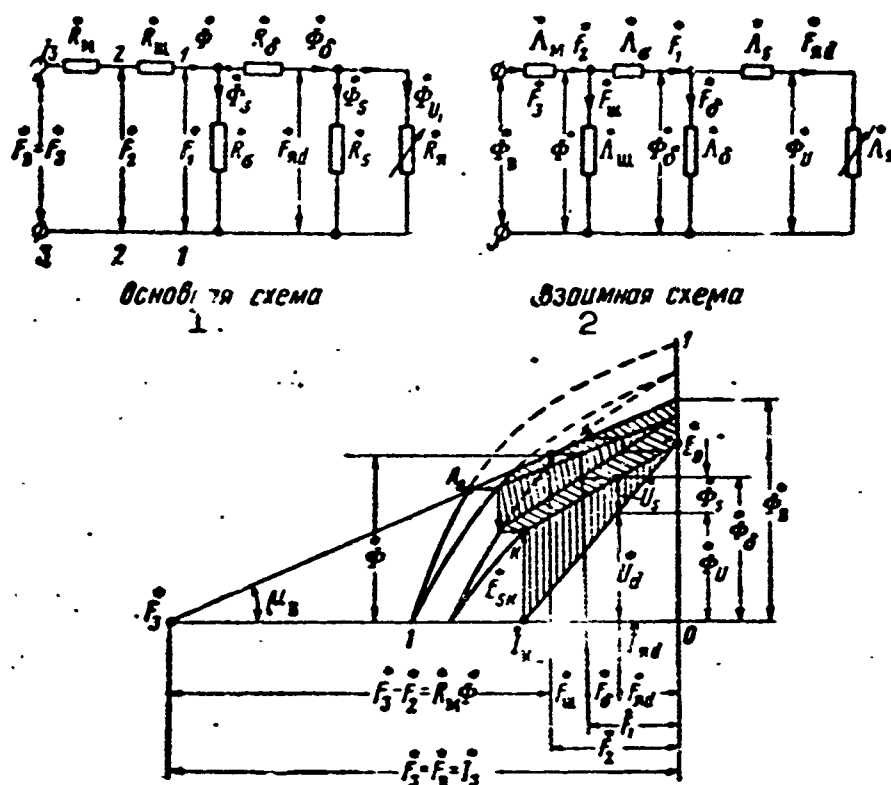


Fig. 4.59. Equivalent circuits and complete magnet diagram in relative units.

For  $F_0$  (internal) and  $I_{kd} E_0$  (external) generator characteristics. 1) Basic circuit; 2) inverse circuit.

tive reluctances (permeances):

$$\dot{\lambda}_1(\dot{\lambda}_1), \dot{K}_2(\dot{\lambda}_2), \dot{K}_3(\dot{\lambda}_3) \text{ and } \dot{K}_m(\dot{\lambda}_m).$$

2. Since the magnetic circuit is not saturated, the reluctances of the magnetically soft steel sections of the secondary magnetic cir-

cuit are included in the reluctance of the air gap, while the reluctance of the magnetically soft steel sections of the primary magnetic circuit are included in the air-slot reluctance.

3. The magnetic flux  $\Phi$  emitted by the surface of a magnet pole is assumed to consist of the useful flux ( $\Phi_U$ ), the primary-circuit (pole) leakage flux  $\Phi_\sigma$ , and the secondary-circuit leakage flux  $\Phi_s$ , i.e.,

$$\Phi = \Phi_U + \Phi_\sigma = \Phi_U + \Phi_s + \Phi_\sigma,$$

where the flux  $\Phi_U$  induces an emf corresponding in magnitude to the voltage across the machine terminals  $U$ , the flux  $\Phi_s$  induces the armature leakage emf, and the flux  $\Phi_\delta = \Phi_U + \Phi_s$  corresponds to the internal emf  $E$  of the machine.

Figure 4.59 gives the equivalent magnetic-circuit diagrams for a salient-pole machine and the complete magnet diagram.

In these circuits,  $\bar{R}_{ya}^*$  is a variable reluctance corresponding to the direct-axis armature-reaction magnetizing-force component;  $\bar{R}_\delta^*$ ,  $\bar{R}_{shch}^*$ , and  $\bar{R}_c^*$  are fixed reluctances offered to the magnetic flux by the air gap, air slot, and magnetically soft steel sections of the circuit;  $\bar{R}_m^*$  is the internal magnet reluctance, which is constant for operation on the reversal line.

The fluxes  $\Phi_\sigma^*$  and  $\Phi_s^*$  shunt the useful flux, increasing  $\Phi^*$  when  $\Phi_U^* = \text{const}$ ; consequently, the reluctances corresponding to these fluxes diminish the over-all reluctance of the equivalent circuit. This means that  $\bar{R}_\sigma^*$  and  $\bar{R}_s^*$  are connected in parallel to the reluctances  $\bar{R}_{shch}^*$ ,  $\bar{R}_\delta^*$ , and  $\bar{R}_c^*$ .

The equivalent circuit considered is suitable for any circuit with permanent magnets and constant or variable circuit parameters. It is clear that if the air-gap reluctance or steel permeability are changed in the system,  $\bar{R}_\delta^*$  or  $\bar{R}_s^*$  will vary.

The equivalent circuit is compiled and corresponding equations

written, depending on the actual object being investigated, with allowance for constant and variable circuit parameters, as well as leakage fluxes.

Below we have given several equations based on the equivalent circuit for the synchronous salient-pole machine.

The reluctance and permeance for the portion of the equivalent circuit to the right of section 1-1 are

$$\dot{R}_1 = \frac{1}{\frac{1}{\dot{R}_s} + \frac{1}{\dot{R}_1 + \frac{\dot{R}_s \dot{R}_2}{\dot{R}_s + \dot{R}_2}}} = \frac{\dot{R} \dot{R}_s}{\dot{R} + \dot{R}_s (\dot{R}_s + \dot{R}_2)}$$

or after substitutions

$$\dot{R}_s = \frac{1}{\dot{\Lambda}_s}, \dot{R}_2 = \frac{1}{\dot{\Lambda}_2}, \dot{R}_1 = \frac{1}{\dot{\Lambda}_1}$$

and after defining  $\dot{\Lambda}_{ya}^* + \dot{\Lambda}_s^* = \dot{\Lambda}_{ya s}^*$ , we obtain

$$\left. \begin{aligned} \dot{R}_1 &= \frac{1}{k_1 [\dot{\Lambda}_s + \dot{\Lambda}_{s s} (1 + \dot{\Lambda}_s \dot{R}_1)]} \\ \dot{\Lambda}_1 &= \frac{1}{\dot{R}_1} = k_1 [\dot{\Lambda}_s + \dot{\Lambda}_{s s} (1 + \dot{\Lambda}_s \dot{R}_1)] \end{aligned} \right\} \quad (4.68)$$

where

$$\begin{aligned} \dot{R} &= \dot{R}_s \dot{R}_1 + \dot{R}_2 \dot{R}_{s s} = \frac{1 + \dot{\Lambda}_s \dot{\Lambda}_{s s}}{\dot{\Lambda}_s \dot{\Lambda}_1} = \frac{1}{k_1 \dot{\Lambda}_s \dot{\Lambda}_1}, \\ k_1 &= \frac{1}{1 + \dot{R}_s \dot{\Lambda}_{s s}}. \end{aligned}$$

The expressions obtained for  $\dot{R}_1^*$  and  $\dot{\Lambda}_1^*$  are suitable for permanent-magnet machines with "spider" type rotors which have no air slots and, consequently, for which there will be no section with a reluctance  $\dot{R}_{shch}^*$  in the equivalent circuit.

In machines with soft-steel pole pieces, the equations become more complicated: it is necessary to determine the reluctance and permeance for the portion of the replacement circuit to the right of sec-



tion 2-2, i.e., we must allow for the relative reluctance (permeance) of the slot. In this case

and

$$\left. \begin{aligned} \dot{R}_2 &= \dot{R}_1 + \dot{R}_m = \dot{R}_m + \frac{\dot{R}\dot{R}_0}{\dot{R} + \dot{R}_0\dot{R}_{ss}} = \frac{1}{k_2[\dot{\Lambda}_0 + \dot{\Lambda}_{ss}(1 + \dot{\Lambda}_0\dot{R}_0)]} \\ \dot{\Lambda}_2 &= \frac{\dot{\Lambda}_1}{1 + \dot{R}_m\dot{\Lambda}_1} = \frac{1}{\dot{R}_2} = k_2[\dot{\Lambda}_0 + \dot{\Lambda}_{ss}(1 + \dot{R}_0\dot{\Lambda}_0)], \end{aligned} \right\} \quad (4.69)$$

where

$$k_2 = \frac{k_1}{1 + \dot{R}_m\dot{\Lambda}_0 + k_1\dot{R}_m\dot{\Lambda}_{ss}}$$

The reluctance (permeance) of the complete equivalent circuit, allowing for the internal magnet reluctance, i.e., at terminals 3-3, is found from the expression

and

$$\left. \begin{aligned} \dot{R}_3 &= \dot{R}_m + \dot{R}_2 + \dot{R}_1 = \frac{1}{k_2[\dot{\Lambda}_0 + \dot{\Lambda}_{ss}(1 + \dot{R}_0\dot{\Lambda}_0)]} \\ \dot{\Lambda}_3 &= \frac{1}{\dot{R}_3} = k_2[\dot{\Lambda}_0 + \dot{\Lambda}_{ss}(1 + \dot{R}_0\dot{\Lambda}_0)], \end{aligned} \right\} \quad (4.70)$$

where

$$k_2 = \frac{k_1}{1 + (\dot{R}_m + \dot{R}_0)\dot{\Lambda}_0 + k_1(\dot{R}_m + \dot{R}_0)\dot{\Lambda}_{ss}}$$

Thus, the reluctance or permeance at any section is expressed, in general, as

$$\left. \begin{aligned} \dot{R}_n &= \frac{1}{k_n[\dot{\Lambda}_0 + \dot{\Lambda}_{ss}(1 + \dot{R}_0\dot{\Lambda}_0)]}; \\ \dot{\Lambda}_n &= k_n[\dot{\Lambda}_0 + \dot{\Lambda}_{ss}(1 + \dot{R}_0\dot{\Lambda}_0)], \end{aligned} \right\} \quad (4.71)$$

where

$$k_n = \frac{1}{(\dot{R}_n + \dot{R}_m)[\dot{\Lambda}_0 + (1 + \dot{R}_0\dot{\Lambda}_0)\dot{\Lambda}_{ss}] + (1 + \dot{R}_0\dot{\Lambda}_{ss})}$$

Fluxes and emf's. The emf's are directly proportional to the corresponding magnetic fluxes; consequently, in the equivalent circuit the flux  $\phi$  in the magnet corresponds to the virtual emf, which equals  $E_{01} = k_E \phi$ , which equals the machine emf under no-load conditions, pro-

vided that there is no primary-circuit leakage flux; the emf induced by the flux in the air gap will be  $E_\delta = k_E \Phi_\delta$ , while the voltage across the machine terminals will be  $U = k_E \Phi_U$ .

Let us determine the fluxes and emf's in the machine, neglecting the voltage drop across the armature resistance.

The total machine magnetic flux is

$$\dot{\Phi} = \dot{\Phi}_\delta + \dot{\Phi}_\sigma = \dot{\Phi}_\delta + \dot{\Phi}_\sigma + \dot{\Phi}_U = \frac{\dot{F}_1}{\dot{R}_1} = \dot{F}_1 \dot{\Lambda}_1. \quad (4.72)$$

Here  $\dot{F}_1$  is the magnetizing force of the poles at the air gap.

The emf corresponding to the total machine flux is

$$\dot{E}_{01} = k_E \dot{\Phi} = k_E \dot{F}_1 \dot{\Lambda}_1. \quad (4.73)$$

The primary-circuit leakage flux is

$$\dot{\Phi}_\sigma = \dot{F}_1 \dot{\Lambda}_\sigma = \dot{\Phi} \frac{\dot{\Lambda}_\sigma}{\dot{\Lambda}_1} = \dot{\Phi} \dot{K}_1 \dot{\Lambda}_\sigma. \quad (4.74)$$

and its relative value is

$$\frac{\dot{\Phi}_\sigma}{\dot{\Phi}} = \frac{\dot{\Lambda}_\sigma}{\dot{\Lambda}_1} = \frac{\dot{\Lambda}_\sigma}{k_1 (\dot{\Lambda}_\sigma + \dot{\Lambda}_{ss} (1 + \dot{K}_1 \dot{\Lambda}_\sigma))}. \quad (4.75)$$

The air-gap flux is

$$\dot{\Phi}_\delta = \dot{\Phi}_U + \dot{\Phi}_\sigma = \dot{\Phi} - \dot{\Phi}_\sigma = \dot{F}_1 (\dot{\Lambda}_1 - \dot{\Lambda}_\sigma) = \dot{F}_1 k_1 \dot{\Lambda}_{ss}. \quad (4.76)$$

The primary-circuit leakage factor  $k_\sigma$  is determined by the ratio of the fluxes:

$$k_\sigma = \frac{\dot{\Phi}_\sigma}{\dot{\Phi}_\delta} = \frac{\dot{\Phi}_\sigma}{\dot{\Phi}} = 1 + \frac{\dot{\Phi}_\sigma}{\dot{\Phi}} = \frac{\dot{\Lambda}_1}{\dot{\Lambda}_1 - \dot{\Lambda}_\sigma} = 1 + \dot{K}_1 \dot{\Lambda}_\sigma + \frac{\dot{\Lambda}_\sigma}{\dot{\Lambda}_{ss}}, \quad (4.77)$$

where

$$\frac{\dot{\Phi}_\sigma}{\dot{\Phi}} = \frac{\dot{\Lambda}_\sigma}{\dot{\Lambda}_1 - \dot{\Lambda}_\sigma} = \frac{\dot{\Lambda}_\sigma}{k_1 \dot{\Lambda}_{ss}} = \frac{\dot{\Lambda}_\sigma (1 + \dot{K}_1 \dot{\Lambda}_{ss})}{\dot{\Lambda}_{ss}}. \quad (4.78)$$

The machine emf induced by the air-gap flux is

$$\dot{E}_\delta = \dot{E}_{01} \frac{\dot{\Phi}_\delta}{\dot{\Phi}} = \frac{\dot{E}_{01}}{k_\sigma} = \dot{E}_{01} \left( 1 - \frac{\dot{\Lambda}_\sigma}{\dot{\Lambda}_1} \right) \quad (4.79)$$

while its relative value is

$$\frac{\dot{E}_2}{\dot{E}_{01}} = 1 - \frac{\dot{\Lambda}_2}{\dot{\Lambda}_1} \quad (4.80)$$

The secondary-circuit (armature) leakage flux will be, by Expressions (4.72) and (4.76)

$$\begin{aligned} \dot{\Phi}_s &= \frac{\dot{F}_{s,el}}{\dot{R}_s} = \frac{\dot{F}_1 - \dot{\Phi}_1 \dot{R}_1}{\dot{R}_s} = \dot{\Phi}_1 \dot{\Lambda}_1 [\dot{R}_1 (1 + \dot{k}_2 \dot{\Lambda}_2) - \dot{R}_s] = \\ &= \dot{F}_1 \dot{\Lambda}_1 [1 - (\dot{\Lambda}_1 - \dot{\Lambda}_2) \dot{k}_2] = \dot{F}_1 \dot{\Lambda}_1 (1 - k_1 k_2 \dot{\Lambda}_{s,el}). \end{aligned} \quad (4.81)$$

The useful flux corresponding to the voltage across the machine terminals will be

$$\dot{\Phi}_U = \dot{\Phi}_1 - \dot{\Phi}_s = \dot{F}_1 k_1 \dot{\Lambda}_2 = \dot{\Phi}_1 k_1 \frac{\dot{\Lambda}_2}{\dot{\Lambda}_1} \quad (4.82)$$

and its relative value is

$$\frac{\dot{\Phi}_U}{\dot{\Phi}_1} = \frac{\dot{\Phi}_U}{\dot{\Phi}_1} = k_1 \frac{\dot{\Lambda}_2}{\dot{\Lambda}_1} \quad (4.83)$$

The voltage across the machine terminals is

$$\dot{U} = \dot{E}_1 \frac{\dot{\Phi}_U}{\dot{\Phi}_1} = \dot{E}_1 \frac{\dot{\Lambda}_2}{\dot{\Lambda}_{s,el}} \quad (4.84)$$

or

$$\dot{U} = \dot{E}_{01} k_1 \frac{\dot{\Lambda}_2}{\dot{\Lambda}_1} = \dot{E}_{01} \frac{\dot{\Lambda}_2}{\dot{\Lambda}_2 + \dot{\Lambda}_{s,el} (1 + \dot{k}_2 \dot{\Lambda}_2)} \quad (4.85)$$

Magnetizing forces and currents. The magnetizing forces are directly proportional to the currents and, consequently, in the equivalent circuit a virtual current  $I_v = I_3$  corresponds to the virtual magnetizing force  $F_v = F_3$ , i.e.,  $F_3 = k_1 I_3$ . Similarly,  $F_2 = k_1 I_2$ ,  $F_1 = k_1 I_1$ , and  $F_{ya d} = k_1 I_{ya d}$ , where the coefficient  $k_1 = 0.45m(w/p)k_0$ .

The armature current is determined below. On the basis of the equivalent circuit (Fig. 4.59) the magnetizing force in section 1-1 is

$$\dot{F}_1 = \dot{F}_2 \frac{\dot{R}_1}{\dot{R}_2} = \dot{F}_2 \frac{\dot{\Lambda}_2}{\dot{\Lambda}_1} = \dot{F}_2 \frac{k_2}{k_1} \quad (4.86)$$

and

$$\frac{\dot{F}_1}{\dot{F}_2} = \frac{F_1}{F_2} = \frac{I_1}{I_2} = \frac{k_2}{k_1} = \frac{1}{1 + (\dot{R}_M + \dot{R}_m)(\dot{\Lambda}_0 + k_1 \dot{\Lambda}_{ss})} \quad (4.87)$$

The magnetizing force in section 2-2 is

$$\dot{F}_2 = \dot{F}_2 \frac{\dot{R}_2}{\dot{R}_2} = \dot{F}_2 \frac{\dot{\Lambda}_2}{\dot{\Lambda}_2} = \dot{F}_2 \frac{k_2}{k_2}$$

and

$$\frac{\dot{F}_2}{\dot{F}_2} = \frac{F_2}{F_2} = \frac{I_2}{I_2} = \frac{k_2}{k_2} = \frac{1 + \dot{R}_m(\dot{\Lambda}_0 + k_1 \dot{\Lambda}_{ss})}{1 + (\dot{R}_M + \dot{R}_m)(\dot{\Lambda}_0 + k_1 \dot{\Lambda}_{ss})} \quad (4.88)$$

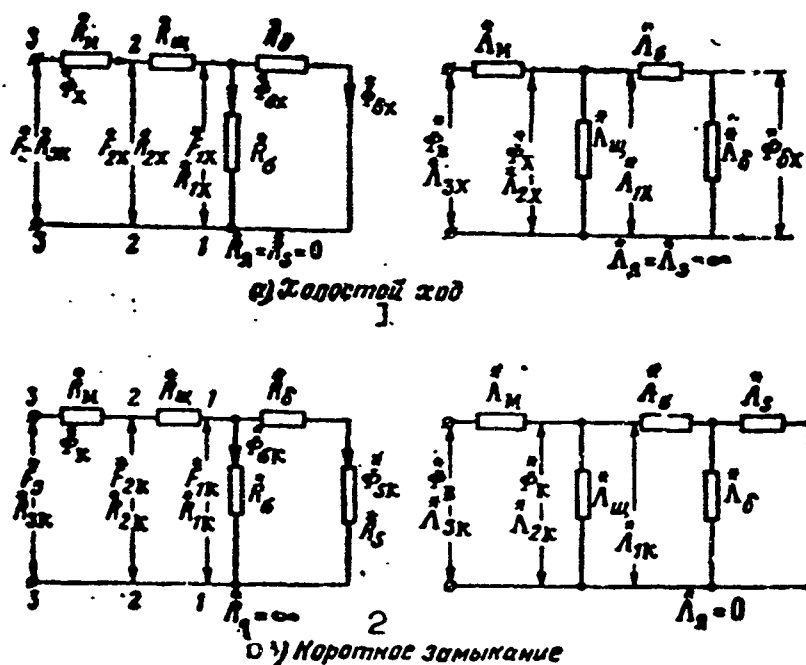


Fig. 4.60. Equivalent circuits corresponding to Fig. 4.59, no-load and short-circuit conditions. 1) No-load; 2) short-circuit.

The ratio of the currents is

$$\frac{I_1}{I_2} = \frac{F_1}{F_2} = \frac{\dot{R}_1}{\dot{R}_2} = \frac{\dot{\Lambda}_2}{\dot{\Lambda}_1} = \frac{k_2}{k_1} = \frac{1}{1 + \dot{R}_m(\dot{\Lambda}_0 + k_1 \dot{\Lambda}_{ss})} \quad (4.89)$$

It is now also easy to find an expression for the current in the armature, since  $F_{ya} = \Phi_s R_s = \Phi_u R_{ya}$

$$\dot{F}_{s,d} = \dot{\Phi}_s \dot{R}_s = \dot{\Phi}_u \dot{R}_{ya}$$

and

$$\begin{aligned} \frac{\dot{F}_{s,d}}{\dot{F}_s} &= \frac{F_{s,d}}{F_s} = \frac{I_{s,d}}{I_s} = \frac{\Phi_u R_{ya}}{\Phi_s R_s} = \\ &= k_1 \frac{\dot{\Lambda}_s}{\dot{\Lambda}_1} = k_2. \end{aligned} \quad (4.90)$$

Thus, the direct-axis armature-current component will be

$$\dot{I}_{s,d} = \dot{I}_s k_2 = \frac{\dot{I}_s}{\dot{R}_m \dot{\Lambda}_s + (1 + R_s \dot{\Lambda}_s)(1 + \dot{R}_m \dot{\Lambda}_s)}. \quad (4.91)$$

Thus, using the equivalent circuit, it is possible to establish the law governing the variation of voltage across the machine terminals and the direct-axis armature-current component when  $\cos \varphi = 0$  and  $R_{ya} = 0$ .

The working regimes of electrical machines are normally analyzed by a method that combines the no-load and short-circuit regimes. This presupposes linearity of the characteristic, which occurs in permanent-magnet machines.

A machine under no-load conditions is characterized by absence of armature current and, consequently, armature reaction and leakage are absent, i.e.,

$$I_s = 0, F_{s,d} = 0, \dot{\Lambda}_s = \frac{1}{\dot{R}_s} = \infty, \dot{\Lambda}_1 = \frac{1}{\dot{R}_1} = \infty.$$

The output terminals of the reluctance circuit are closed, while the inverse circuit, using permeances, has open terminals (Fig. 4.68).

The short-circuited machine is characterized by absence of voltage across the machine terminals, and thus the useful flux  $\Phi_u$  will also disappear, i.e.,

TABLE 4.3

## Plotting External Characteristic

1 Искомые величины	2 Режим	3. Холостого хода	4 Короткого замыкания
5 Проводимости	6 внешней цепи	$\dot{A}_{1x} = \frac{1 + \dot{R}_s \dot{A}_s}{\dot{R}_s}$	$\dot{A}_{1x} = \dot{A}_s + \frac{\dot{A}_s}{1 + \dot{R}_s \dot{A}_s} = \frac{\dot{A}_s + \dot{A}_s (1 + \dot{R}_s \dot{A}_s)}{1 + \dot{R}_s \dot{A}_s}$
	7 в точке отхода	$\dot{A}_{2x} = \frac{1 + \dot{R}_s \dot{A}_s}{\dot{R}_s + \dot{R}_{\Sigma} (1 + \dot{R}_s \dot{A}_s)}$	$\dot{A}_{2x} = \frac{\dot{A}_s + \dot{A}_s (1 + \dot{R}_s \dot{A}_s)}{\dot{R}_{\Sigma} [\dot{A}_s + \dot{A}_s (1 + \dot{R}_s \dot{A}_s)] + (1 + \dot{R}_s \dot{A}_s)}$
	8 полная	$\dot{A}_{3x} = \frac{1 + \dot{R}_s \dot{A}_s}{\dot{R}_s + \dot{R}_{\Sigma \Sigma} (1 + \dot{R}_s \dot{A}_s)}$	$\dot{A}_{3x} = \frac{\dot{A}_s + \dot{A}_s (1 + \dot{R}_s \dot{A}_s)}{\dot{R}_{\Sigma \Sigma} [\dot{A}_s + \dot{A}_s (1 + \dot{R}_s \dot{A}_s)] + (1 + \dot{R}_s \dot{A}_s)}$
9 Коэффициенты		$k_{1x} = k_{2x} = k_{3x} = 0$	$k_{1x} = \frac{1}{1 + \dot{R}_s \dot{A}_s}$
			$k_{2x} = \frac{k_{1x}}{1 + \dot{R}_{\Sigma} \dot{A}_s + k_{1x} \dot{R}_{\Sigma} \dot{A}_s} = \frac{1}{\dot{R}_{\Sigma} \dot{A}_s + (1 + \dot{R}_{\Sigma} \dot{A}_s)(1 + \dot{R}_s \dot{A}_s)}$
10 Магнитные потоки			$k_{3x} = \frac{1}{\dot{R}_{\Sigma \Sigma} \dot{A}_s + (1 + \dot{R}_{\Sigma \Sigma} \dot{A}_s)(1 + \dot{R}_s \dot{A}_s)}$
			$\Phi_x = \dot{F}_{1x} \dot{A}_{1x}$
			$\Phi_{sx} = \dot{F}_{1x} \dot{A}_s = \Phi_x \frac{\dot{A}_s}{\dot{A}_{1x}}$
			$\Phi_{sx} = \dot{F}_{1x} (\dot{A}_{1x} - \dot{A}_s) = \frac{\dot{F}_{1x}}{\dot{R}_s}$
			$\Phi_{sx} = \Phi_x \frac{\dot{A}_s}{\dot{A}_{1x}} = \dot{F}_{1x} \dot{A}_s$
			$\Phi_{sx} = \dot{F}_{1x} \frac{\dot{A}_s}{1 + \dot{R}_s \dot{A}_s} = \dot{F}_{1x} (\dot{A}_{1x} - \dot{A}_s)$
			$\Phi_{sx} = 0$
			$\Phi_{Ux} = 0$

11 B. a. c	$\dot{E}_x = k_E \dot{\Phi}_x - k_E \dot{F}_{1x} \dot{\Lambda}_{1x} - \dot{E}_{01}$ $\dot{E}_{1x} = \dot{E}_x \frac{\dot{\Phi}_{1x}}{\dot{\Phi}_x} - \frac{\dot{E}_x}{1 + \dot{R}_1 \dot{\Lambda}_0} = \dot{E}_0$ $\dot{E}_{2x} = 0$ $U_x = \dot{E}_{1x} - \dot{E}_0$	$\dot{E}_x = k_E \dot{\Phi}_x$ $\dot{E}_{1x} = \dot{E}_x \frac{\dot{\Phi}_{1x}}{\dot{\Phi}_x} = \dot{E}_x \frac{\dot{\Lambda}_0}{(1 + \dot{R}_1 \dot{\Lambda}_0) \dot{\Lambda}_0}$ $\dot{E}_{2x} = \dot{E}_{1x} - \dot{I}_{d2} \dot{x}_2$ $U_x = 0$
12 H. c. u. r. o. m	$\frac{\dot{F}_{1x}}{\dot{F}_{2x}} = \frac{1}{1 + \dot{R}_{m.m} (1 + \dot{R}_1 \dot{\Lambda}_0)} = \frac{k_{2x}}{k_{1x}}$ $\frac{\dot{F}_{1x}}{\dot{F}_{2x}} = \frac{k_{2x}}{k_{1x}} = \frac{1}{1 + \dot{R}_{m.m} (1 + \dot{R}_1 \dot{\Lambda}_0)}$ $\dot{I}_d = 0$	$\frac{\dot{F}_{1x}}{\dot{F}_{2x}} = \frac{\dot{\Lambda}_{2x}}{\dot{\Lambda}_{1x}} = \frac{k_{2x}}{k_{1x}} = \frac{\dot{I}_{1x}}{\dot{I}_{2x}} = \frac{1}{1 + \dot{R}_{m.m} (\dot{\Lambda}_0 + k_{1x} \dot{\Lambda}_0)}$ $\frac{\dot{F}_{1x}}{\dot{F}_{2x}} = \frac{\dot{\Lambda}_{2x}}{\dot{\Lambda}_{1x}} = \frac{k_{2x}}{k_{1x}} = \frac{\dot{I}_{1x}}{\dot{I}_{2x}} = \frac{1}{\dot{R}_{m.m} \dot{\Lambda}_0 + (1 + \dot{R}_1 \dot{\Lambda}_0) (1 + \dot{R}_{m.m} \dot{\Lambda}_0)}$ $\frac{\dot{F}_{1d}}{\dot{F}_{2x}} = \frac{\dot{I}_{d1}}{\dot{I}_{2x}} = k_{2x}$

1) Quantity sought; 2) regime; 3) no-load; 4) short-circuit; 5) permeance; 6) external-circuit; 7) at point of departure; 8) complete; 9) coefficients; 10) magnetic fluxes; 11) emf's; 12) magnetizing forces and currents.

$$U=0, \Phi_v=0 \text{ and } \dot{A}_s = \frac{1}{R_s} = 0.$$

Under these conditions, the output terminals of the reluctance circuit are open, while those of the inverse circuit are closed (Fig. 4.60b).

In view of what has been said, making use of Expressions (4.68) to (4.72) it is possible to write a series of equations that correspond to the no-load and short-circuit regimes of the machine.

On the basis of the no-load regime, we can determine the no-load emf, while the direct-axis short-circuit current is found from the short-circuit conditions; we then can find the external characteristic of the machine. All of the equations have been given in Table 4.3 for the sake of clarity.

Plotting the external characteristic. Figure 4.61 gives a magnet diagram in simplified form. Point  $A_0$  corresponds to the condition of the magnet in its neutral plane under short-circuit conditions. The short-circuit line  $OA_0$  characterizes the permeance (reluctance) of the external (with respect to the magnet) portion of the magnetic flux path, allowing for the armature reaction under short-circuit conditions. The coordinates of the point of departure for the reversal line  $A_0$  (short-circuit regime) are  $\dot{F}_{2k}^*$  and  $\dot{\Phi}_k^*$ .

The slope of line  $OA_0$  with respect to the x-axis is determined by the short-circuit permeance (reluctance) in section 2-2 of the equivalent circuit (see Fig. 4.60), i.e.,

$$\dot{A}_x = \operatorname{tg} \alpha_x = \frac{\dot{\Phi}_x}{\dot{F}_x}; \quad \dot{R}_x = \operatorname{ctg} \alpha_x \quad (4.92)$$

Point Kh corresponds to the condition of the magnet in its neutral plane under no-load conditions. The no-load line OKh characterizes the magnetic permeance (reluctance) of the portion of the magnetic flux



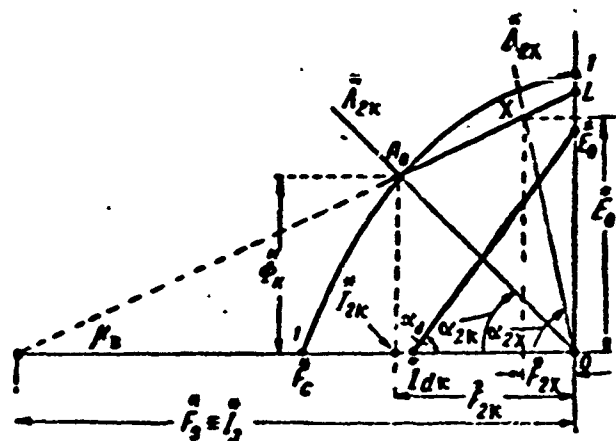


Fig. 4.61.

path external to the magnet under no-load conditions. The coordinates of the no-load point on the reversal line are  $\dot{F}_{2kh}^*$  and  $\dot{\Phi}_{kh}^*$ .

The slope of line OKh with respect to the x-axis is determined by the no-load permeance (reluctance) in section 2-2 of the equivalent circuit, i.e.,

$$\dot{A}_{2x} = \operatorname{tg} \alpha_{2x} = \frac{\dot{\Phi}_x}{\dot{F}_{2x}}; \quad \dot{R}_{2x} = \operatorname{ctg} \alpha_{2x}. \quad (4.93)$$

For a "spider" type rotor,  $\dot{A}_{shch}^* = \infty$  and

$$\dot{A}_{2x} = \dot{A}_{1x}, \quad \dot{A}_{2x} = \dot{A}_{1x}, \quad \dot{R}_{2x} = \dot{R}_{1x} \text{ и } \dot{R}_{2x} = \dot{R}_{1x}.$$

Determining  $\dot{A}_{2k}^*$ , we find the point of departure for the reversal line  $A_0$  and the value of  $\dot{I}_{2k}^*$ . Using the reversal coefficient  $\mu_v$ , we plot the reversal line and then use the value of  $\dot{A}_{2kh}^*$  to find the no-load point Kh and the value of  $\dot{E}_{C1}^*$ .

Knowing  $\dot{E}_{01}^*$  and  $\dot{I}_{2k}^*$ , we find the no-load emf  $\dot{E}_0^*$  and the direct-axis short-circuit current component  $\dot{I}_{dk}^*$ , and by connecting  $\dot{E}_0^*$  and  $\dot{I}_{dk}^*$ , we obtain the external generator characteristic with no intermediate plotting.

- 346 See §4.7.
- 394 The author's proposal was developed and tests of industrial specimens were carried out in cooperation with Engineers V.G. Andreyev and S.R. Mizyurin.
- 408 A.I. Bertinov, Elementy analiticheskoy teorii magnitoelektricheskikh tsepey [Elements of the Analytical Theory of Permanent-Magnet Circuits], Trudy MAI 84 [Reports of the Moscow Aviation Institute, 84], Oborongiz, 1957.

[List of Transliterated Symbols]

- 309 м = m = magnit = magnet
- 315 в = v = vozvrat = reversal
- 335 в = v = vneshniy = external
- 340 н = n = nakonechnik = pole piece
- 340 расч = rasch = raschetnyy = design
- 342 з.в = z.v (zv) = zvezdochka = spider
- 344 с = s = svobodnyy = free
- 346 щ = shch = shchel' = slot
- 346 з = z = zubets = tooth
- 346 я = ya = yakor' = armature
- 346 к = k = kogt' = finger
- 351 с = s = serdechnik = core
- 351 э = e = elektromagnitnyy = electromagnetic
- 35 ном = nom = nominal'nyy = rated
- 354 к = k = korotkogo замыкания = short-circuit (also K)
- 355 Х = Kh = kholostoy = no-load
- 356 м.э = m.e = magnitoelektricheskiy = permanent-magnet
- 357 э.м = e.m = elektromagnitnyy = electromagnetic
- 362 полн = poln = polnyy = total

363 з.н = z.m = zapolneniye, magnit = full factor, magnet  
 363 п = p = polyus = pole  
 382 в = v = val = shaft  
 389 к = k = kondensator = capacitor  
 389 г = g = generator = generator  
 394 д = d = drossel' = reactor  
 399 эф = ef = effektivnyy = effective  
 399 sh = sinh  
 405 дт = dt = drossel' trekhfaznyy = three-phase saturable reactor  
 406 ОП = OP = obmotka podmagnichivaniya = magnetization winding  
 406 МУ = MU = magnitnyy usilitel' = magnetic amplifier  
 406 В = V = vypryamitel' = rectifier  
 406 стаб = stab = stabilizator = stabilizer  
 406 EMC = EMS = elektromagnitnyy stabilizator = electromagnetic stabilizer  
 406 др = dr = drossel' = reactor, inductor  
 406 МЕР = MEG = magnitoelektricheskiy generator = permanent-magnet generator  
 406 вх = vkh = vkhod = input  
 407 акт = akt = aktivnyy = resistive, dissipative, wattful  
 422 и.м = i.m = ispol'zovaniye magnita = utilization of magnet

## Chapter 5

### INDUCTION GENERATORS

#### 5.1. GENERAL INFORMATION ON INDUCTION GENERATORS

Induction generators were invented in 1877 by P.N. Yablochkov and were used to produce high-frequency current at 20-50 kc.

Over the past 25 years, induction high-frequency generators have come into wide use in aviation, electrometallurgy (arc welding, surface hardening, melting, etc.), for high-speed electrical drive mechanisms (textile motors, electric saws, hand electric tools), etc., where frequencies of from 200 to 10,000 cps are used, since in this range mechanical generators offer substantial advantages over electronic oscillators.

The Leningrad "Elektrik" plant makes induction generators for industry of up to 100 kva power at a frequency of 8000 cps. The "Elektrosila" and KhEMZ Plants manufacture induction generators with powers up to 1000 kva at frequencies of about 10,000 cps.

For aircraft, single-phase 400-cps induction generators are used in series MA converters for powers of up to 0.1 to 2.5 kva. Single-phase induction aircraft generators are also made for 20 kva, 900 cps, and 9000 rpm; 500 va, 6000 cps, and 12,000 rpm; 2.5 kva, 5000 cps, and 50,000 rpm; and so forth.

A large number of unusual induction generators having powers from 0.5 to 600 kva and frequencies of from 500 to 60,000 cps were created by V.P. Vologdin, in particular for use in aviation.

Definition. An induction machine is an electrical machine for

which the main magnetic flux at an arbitrary point in the air gap varies solely in magnitude. Otherwise, there would be a periodic change in the flux linked with the armature winding owing to the variation in air-gap permeance. This fact makes it possible to locate the field and armature windings on the stationary part of the machine.

Arrangement. Induction generators are normally used as parts of converters employed to change commercial line-frequency (50-60 cps) alternating current into high-frequency (200-10,000 cps) alternating current, or as parts of converters changing direct current into high-frequency alternating current. The electric drive motor (in the first

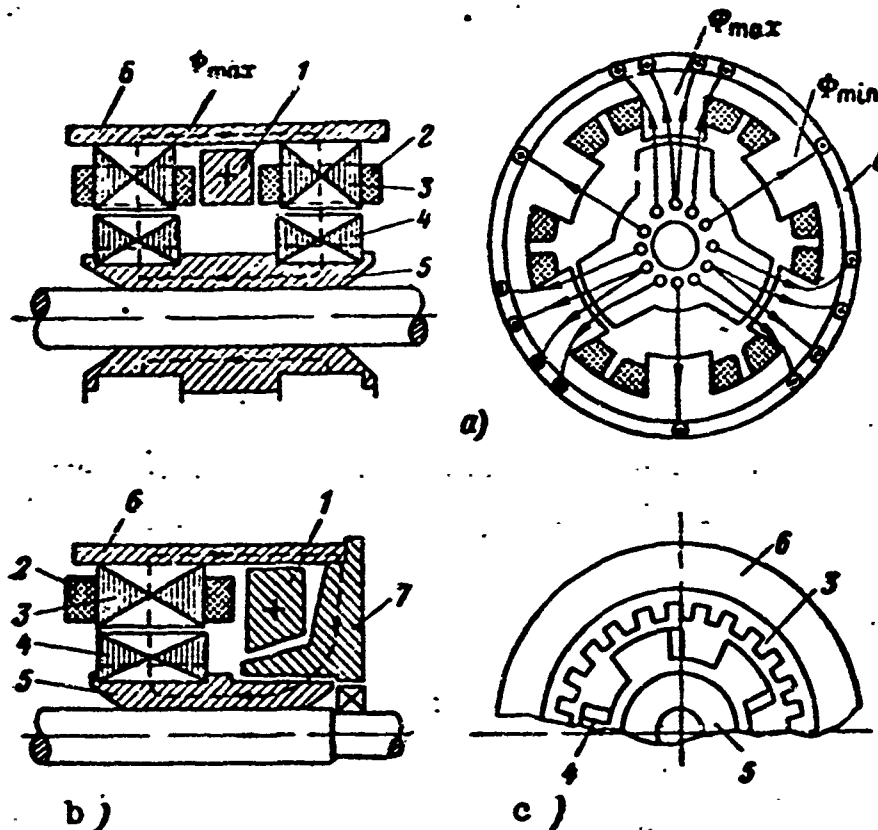


Fig. 5.1. Single-phase homopolar induction generator, 400 cps, 8000 rpm. a) Double-unit construction; b) single-unit construction; c) active zone, three-phase construction, 800 cps, 8000 rpm. 1) Field winding; 2) armature winding; 3) armature teeth and core; 4) rotor teeth and core; 5) rotor sleeve; 6) stator housing; 7) flange.

case, an induction or synchronous motor, and in the second case a direct-current motor) and the induction generator are normally placed in

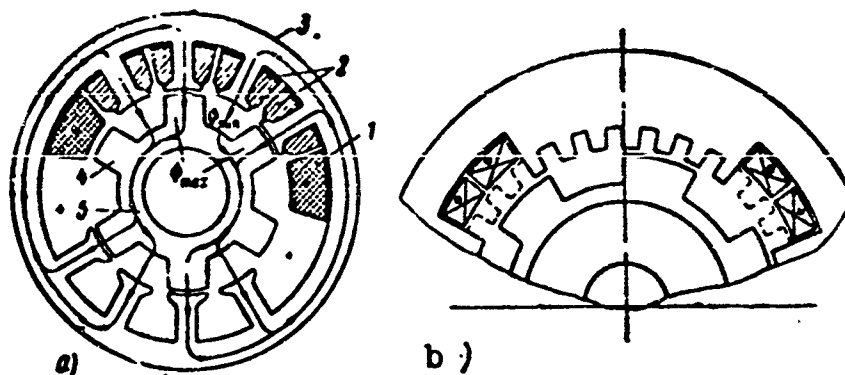


Fig. 5.2. Multipolar induction generator with classical active zone. a) Single-phase, two excitation poles, 800 cps, 8000 rpm; b) three-phase, four excitation poles (designations are the same as in Fig. 5.1).

a common housing, which permits a reduction in the axial dimensions and weight of the converter. Far less frequently, induction generators are driven by internal-combustion or turbine engines.

There are a large number of known structural designs for induction machines.

Figures 5.1-5.3 give transverse and longitudinal sections through two of the main types of induction alternating-current generator that are employed in aviation.

The main magnetic field is excited in the air gap of an induction machine by a winding 1, which is located in all types of induction generators on the stationary part of the machine (together with the armature winding); the field winding carries direct current.

The armature winding (alternating-current winding 2) is also always located in slots in the stationary part of the machine.

The teeth and core of the armature 3 and the teeth and core of the rotor 4 are made from electrical-grade sheet steel 0.35-0.20 mm thick, depending on the frequency. In the design of Fig. 5.1, the rotor teeth and core may also be made massive.

The rotor sleeve 5 and stator housing 6 are normally made from armco steel; in the designs of Figs. 5.2 and 5.3, they are assembled

from sheet steel.

In the single-unit design, the flange 7, which carries the main flux, is also made from armco steel:

In all single-phase induction machines of classical type, the number of rotor poles equals half the number of stator teeth. For a machine of m-phase design, there are twice as many stator tooth units as there are rotor tooth units.

One peculiarity associated with the induction generator is the fact that its frequency is twice as high as that of a synchronous generator having the same number of poles (teeth), i.e.,

$$f = z_2 n / 60 \text{ cps,}$$

where the number of rotor teeth  $z_2$  corresponds to  $p$  rather than to  $2p$ .

Operating principle. The magnetic flux in the air gap is produced by the field winding, which carries direct current (or by permanent magnets). The direction of the magnetic flux is shown in Fig. 5.1. In the double-unit construction, one unit contains only north poles, and the second unit only south poles. In the designs of Figs. 5.2 and 5.3, the field polarity changes, as in the classical consequent-pole machine.

When the rotor turns uniformly, the permeance of the air gap will change periodically, since the number of stator poles (teeth) is 2 or  $2m$  times the number of rotor slots (poles). Consequently, the magnetic flux in the air gap will also change periodically from  $\phi_{\max}$ , when the axes of the rotor and stator teeth coincide, to  $\phi_{\min}$ , when the axes of the rotor and stator teeth differ by the angle  $\pi$  (Fig. 5.4). Thus, the flux in the machine air gap will consist of constant and varying components. The mean flux will equal  $\phi_0 = 0.5 (\phi_{\max} + \phi_{\min})$ , while the variable flux will be  $\phi_1 = 0.5 (\phi_{\max} - \phi_{\min})$ .

The armature winding is permeated by a flux that periodically changes in magnitude as the air-gap permeance changes; consequently,

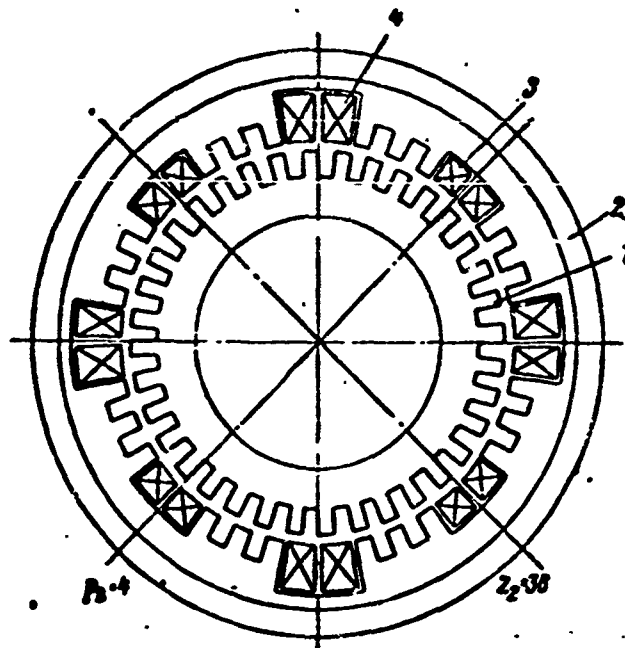


Fig. 5.3. Single-phase multipolar induction generator with tooth-type active zone. Four excitation poles, four armature windings, a frequency  $f = z_2 n / 60 = 36 \cdot 10,000 / 60 = 6000$  cps,  $n = 10,000$  rpm. 1) Rotor; 2) stator; 3) armature winding; 4) field winding.

the changing flux component  $\Phi_1$  induces a varying emf in the armature winding. Thus, with constant magnetizing force and uniform rotor rotation, the machine flux periodically changes in magnitude without changing sign, and induces a varying emf into the secondary winding.

Advantages: a) structural simplicity and reliability – the rotating part of the machine carries neither windings nor sliding contacts, which simplifies production and operation;

b) simplicity and reliability of voltage regulation;

c) possibility of increasing rotational speed up to 100 m/sec or more;

d) higher efficiency owing to the smaller amount of excitation power and the absence of sliding-contact losses.

Disadvantages: a) relatively poor weight/power ratio in these models owing to the fact that the flux changes from  $\Phi_{\max}$  to  $\Phi_{\min}$ ,



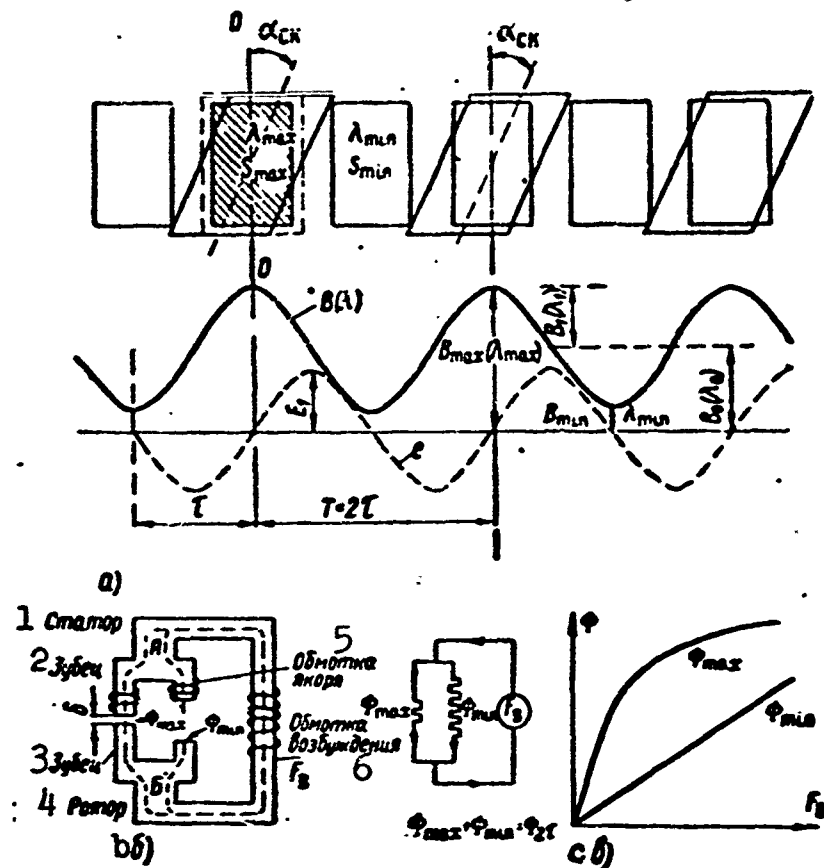


Fig. 5.4. Operating principle of induction generators. a) Field and emf curves; b) equivalent circuit of induction generator; c) fluxes  $\Phi_{max}$  and  $\Phi_{min}$  as functions of excitation magnetizing force  $F_v$ . 1) Stator; 2) tooth; 3) tooth; 4) rotor; 5) armature winding; 6) field winding.

rather than from  $+\Phi$  to  $-\Phi$ ;

b) high reactance, sometimes necessitating capacitive compensation;

c) the shape of the emf curve depends on the magnitude and nature of the load.

Classification. It is desirable to classify induction machines as follows.

In accordance with the spatial arrangement of field windings:

a) Homopolar (ring-type) generators having one field winding whose axis coincides with the machine axis, i.e., the field winding encloses the rotor axis. In such generators, the flux in the rotor

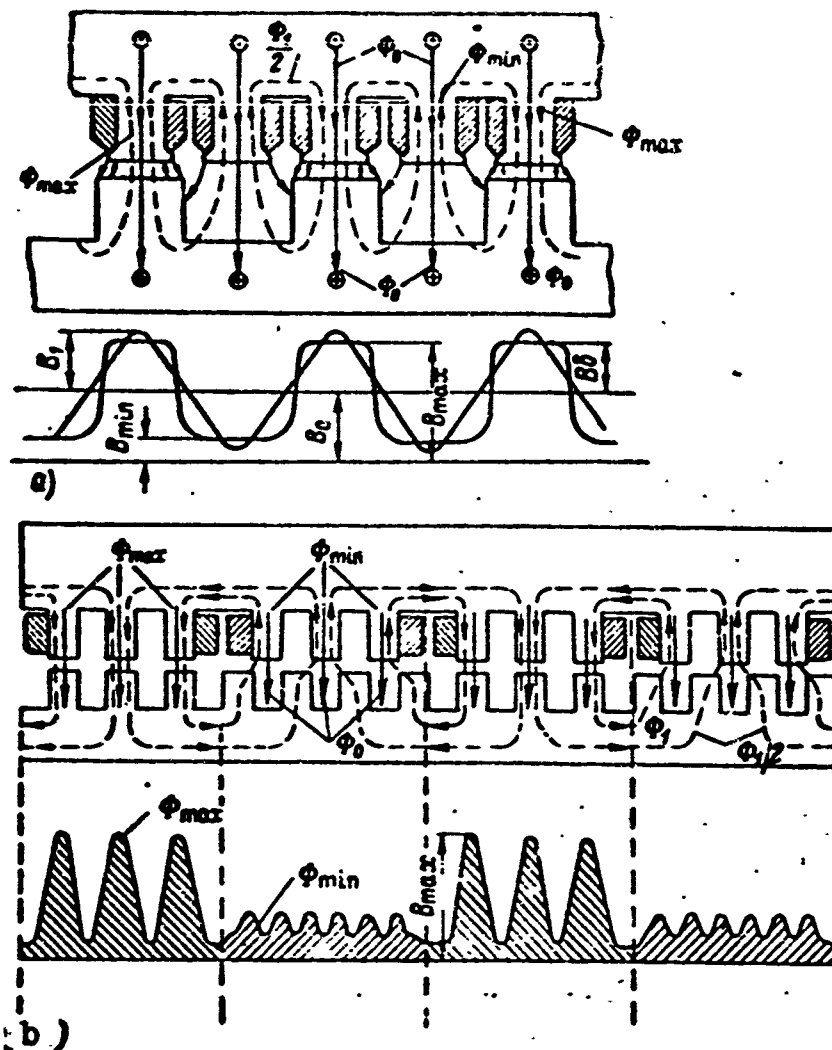


Fig. 5.5. Field pattern in air gap of induction generator. a) Classical active zone; b) tooth-type active zone.

teeth does not change in sign, and the rotor may be made solid (see Fig. 5.1).

b) Multipolar (segmental) generators having  $2p_v$  field windings whose axes are perpendicular to the machine axis, i.e., they do not enclose the rotor axis. This type of induction generator is similar in the arrangement of its magnetic system to a direct-current machine. In generators of this type, the flux in the rotor teeth changes in sign at a frequency of  $f_v = (p_v n / 60)$  and, consequently, the rotor should be assembled from electrical-grade sheet steel (see Figs. 5.2 and 5.3).

According to the structure of the active band:

a) Classical type for which the rotor tooth pitch  $t_2$  equals twice

the stator tooth pitch multiplied by the number of phases, i.e.,

$$t_2 = 2\pi t_1 \text{ and } z_1 = 2\pi z_2.$$

b) Tooth type (see Fig. 5.3), where the rotor tooth pitch equals the stator tooth pitch multiplied by the number of phases, i.e.,

$$t_2 = \pi t_1 \text{ and } z_1 = \pi z_2.$$

c) System with pulsating flux in rotor teeth, where the rotor tooth pitch is roughly equal to the stator tooth pitch. This system makes no sense, and will not be considered here.

Figure 5.5 shows field forms for homopolar induction generators with various active zones.

## 5.2. FUNDAMENTALS OF INDUCTION-GENERATOR THEORY

The working processes for all types of induction machines are similar and thus results obtained for one such machine can be applied to the others.

The induction generator is a salient-pole synchronous machine, and thus the theory of salient-pole synchronous machines can basically be extended to inductor generators, providing that a suitable choice of parameters is made.

If we take the rotor-tooth axis as the machine direct axis and an axis rotated through an angle of  $\pi/2$  with respect to the direct axis as the quadrature axis, the direct-axis and quadrature-axis armature-reaction inductive reactances will then be  $x_{yad}$  and  $x_{yag}$ .

The leakage inductive reactances will be: in the slots, end section, and as a result of higher magnetizing-force harmonics in the gap, we will have  $x_{sd} = x_{sq} = x_s$ .

The effect of armature reaction in an induction generator is similar to the effect of armature reaction in an ordinary synchronous generator, i.e., an inductive load will decrease the main flux while a capacitive load will increase it.

## Permeances and Fluxes in the Air Gap of an Induction Generator

Figure 5.6 shows the pattern of variation in the magnitude of the permeance and the flux (induction) in the air gap (which is proportional to the permeance) for a classical active zone on the assumption

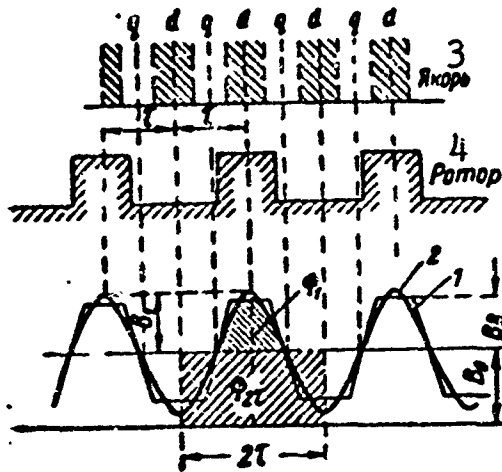


Fig. 5.6. Field curve in air gap of induction generator for closed armature slots. 1) Field curve in gap; 2) first harmonic of field curve;  $\Phi_1$ ) first-harmonic flux;  $\Phi_{2\tau}$ ) flux at double the pole pitch; 3) armature; 4) rotor.

that the reluctance of the steel sections of the magnetic circuit equals zero ( $\mu = \infty$ ); the surface of the stator bore is smooth, i.e.,  $k_g = 1$ ; neither hysteresis nor eddy currents appear in the magnetic circuit; we consider only the first harmonic of the field.

As the rotor turns, the air-gap permeance in an induction generator changes periodically with a period equal to  $2\tau$ , as does the induction, which corresponds to the permeance.

Representing the permeance curve as a harmonic series, we obtain the following

well-known expressions for the air-gap permeance:

$$f(x) = \frac{a_0}{2} + \sum_1^{\infty} a_n \cos nx + \sum_1^{\infty} b_n \sin nx = \lambda_0 + \sum_1^{\infty} \lambda_n \sin n(\alpha - \omega t),$$

where

$$\left. \begin{aligned} a_n &= \frac{2}{\tau} \int_0^{\tau} f(x) \cos nx dx, & b_n &= \frac{2}{\tau} \int_0^{\tau} f(x) \sin nx dx, \\ \lambda_0 &= \frac{1}{\tau} \int_0^{\tau} f(x) dx, \\ \lambda_n &= \sqrt{a_n^2 + b_n^2}, & \operatorname{tg} \alpha &= \frac{a_n}{b_n}. \end{aligned} \right\} \quad (5.1)$$

Since the field winding forms a magnetic field strength that is constant in space and in time over the length of the pole pitch on the

armature surface, the air-gap induction will be proportional to the permeances, i.e.,  $B = F\lambda$  and

$$B_x = B_0 + \sum_1^{\infty} B_n \cos n(\alpha - \omega t), \quad (5.2)$$

where  $B_0 = U_{\delta z} \lambda_0$  and  $B_n = U_{\delta z} \lambda_n$  are the constant components and the  $n$ th harmonic of the induction in the machine air gap;  $U_{\delta z}$  is the magnetic potential drop across the active band (air gap and armature tooth).

The first harmonic of the induction and the first-harmonic flux in the air gap will equal, respectively,

$$\left. \begin{aligned} B_1 &= B_1 \cos(\alpha - \omega t), \\ \Phi_1 &= \frac{2}{\pi} B_1 l \cos(\alpha - \omega t). \end{aligned} \right\} \quad (5.3)$$

We determine the phase no-load emf

$$e = -\frac{d\Phi_1}{dt} = -w \frac{d\Phi_1}{dt} = E_{1m} \sin \omega t,$$

where

$$E_1 = 4k_p k_w \omega \Phi_1 10^{-8}. \quad (5.4)$$

The air-gap permeance (induction) is a complex function of the active-band geometry and depends on the saturation of the magnetic system. To simplify the problem, we assume that the active zone (rotor and stator teeth) is not saturated and that its reluctance is taken into account by means of an appropriate increase in the air gap. In addition, we base the calculations on the excitation magnetizing force corresponding to the active band  $U_{\delta z}$ , which we assume to remain unchanged. Under these conditions, it is possible to construct, as an example, a simplified picture of the field in the air gap, and to determine  $\lambda(B)$  for it. Some simplified field patterns are shown in Fig. 5.7.

The simplest field pattern, consisting of constant  $\lambda_0(B_0)$  and variable  $\lambda_1(B_1)$  components, can be represented by the simple expression

$$\lambda_x = \lambda_0 + \lambda_1 \cos \alpha = \lambda_0 \left( 1 + \frac{\lambda_1}{\lambda_0} \cos \alpha \right), \quad (5.5)$$

where

$$\begin{aligned} \lambda_0 &= 0,5 \lambda_{\max} (1 + \rho), \\ \lambda_1 &= 0,5 \lambda_{\max} (1 - \rho), \\ \lambda_{\max} &= \frac{2\lambda_1}{1 - \rho} = \frac{2\lambda_0}{1 + \rho}, \quad \rho = \frac{\lambda_{\min}}{\lambda_{\max}}. \end{aligned}$$

$\lambda_{\max}$  and  $\lambda_{\min}$  are the permeances of the air gap corresponding to the tooth axis and the axis of the rotor intertooth space, respectively.

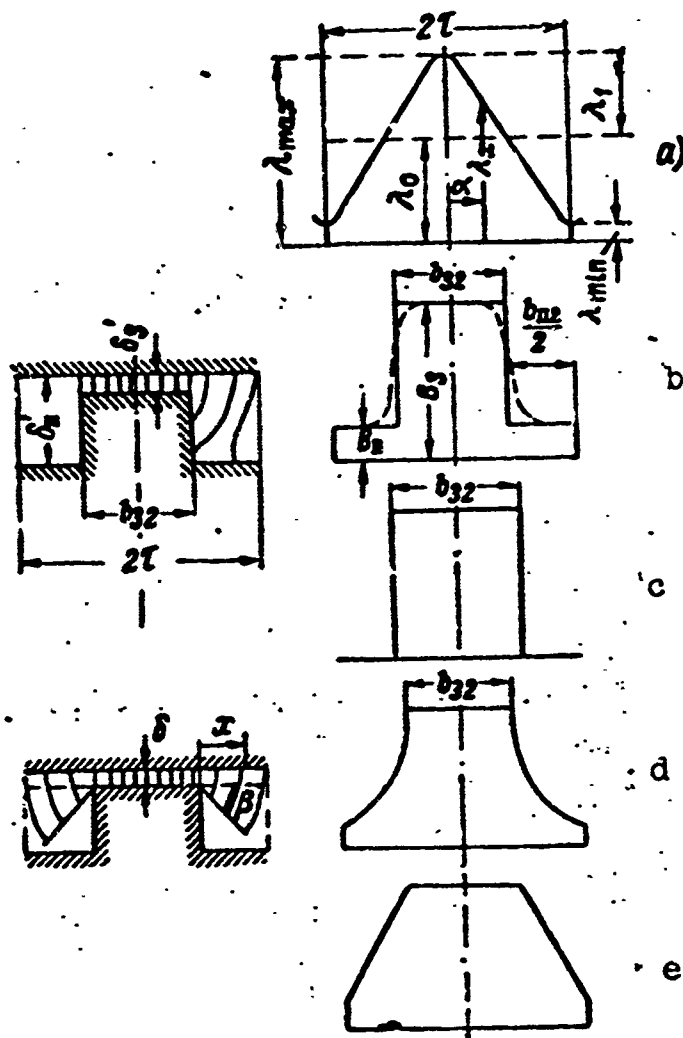


Fig. 5.7. Simplified field patterns for induction generator no-load conditions.  $b_{z2}$ ) Width of rotor tooth;  $b_{p2}$ ) width of rotor slot;  $B_z$ ) maximum induction along rotor-tooth axis;  $B_p$ ) maximum induction along slot axis.

The double pole-pitch flux is

$$\Phi_{21} = B_0 2\tau l_1 = B_{max} (1 + \rho) \tau l_1. \quad (5.6)$$

The first harmonic of the flux going to induce the emf is

$$\Phi_1 = \frac{2}{\pi} B_1 \tau l_1 = \frac{1}{\pi} B_{max} (1 - \rho) \tau l_1. \quad (5.7)$$

The degree of flux utilization is

$$k_1 = \frac{\Phi_1}{\Phi_{21}} = \frac{1}{\pi} \frac{1 - \rho}{1 + \rho} \approx 0.318 \frac{1 - \rho}{1 + \rho}. \quad (5.8)$$

Here the maximum degree of air-gap flux utilization for inducing the emf is only 31.8% at  $\rho = 0$  and only 28.8% at  $\rho = 0.05$  (the usual value).

On the basis of the field shape (Fig. 5.7b), the amplitude of the magnetic-induction first harmonic, considering that

$$B_s = \frac{0.4\pi U_{1s}}{b_s} \quad \text{and} \quad B_n = \frac{0.4\pi U_{1s}}{b_n},$$

will equal

$$B_1 = \frac{2}{\pi} (B_s - B_n) \sin \alpha_1 \frac{\pi}{2} = 0.8 U_{1s} \frac{1 - \rho_1}{b_s} \sin \alpha_1 \frac{\pi}{2} \quad (5.9)$$

while the first harmonic of the flux will be

$$\Phi_1 = \frac{2}{\pi} B_1 \tau l_1 = \frac{1.6}{\pi} U_{1s} \frac{1 - \rho_1}{b_s} \tau l_1 \sin \alpha_1 \frac{\pi}{2}. \quad (5.10)$$

Here

$$\rho_1 = \frac{b_1}{b_s} < 1, \quad \alpha_1 = \frac{b_{n2}}{\tau}. \quad (5.11)$$

The double pole-pitch flux is

$$\begin{aligned} \Phi_{22} &= (B_s B_{n2} + B_n B_{s2}) l = \\ &= 0.4\pi U_{1s} \frac{b_{n2}}{b_s} \left(1 + \rho_1 \frac{b_{n2}}{b_{s2}}\right) l. \end{aligned} \quad (5.12)$$

where

$$\frac{b_{n2}}{b_{s2}} = \frac{2\tau - b_{n2}}{b_{n2}} = \frac{2}{\alpha_1} - 1.$$

The degree of flux utilization is

$$k_1 = \frac{\Phi_1}{\Phi_{22}} = \frac{2}{\pi^2} \frac{\sin \alpha_1 \frac{\pi}{2}}{0.5 \alpha_1 + \frac{\rho_1}{1 - \rho_1}}. \quad (5.13)$$

When  $\alpha_1 = 0.8$  and  $\rho_1 = 0.05$ , the flux utilization is 42.5% of the total air-gap flux, while when  $\alpha_1 = 1$ , it is 36.7%. As the relative rotor-tooth width  $\alpha_1 = b_{z2}/\tau$  increases and the ratio  $\rho_1 = \delta_z/\delta_p$  increases, the degree of flux utilization will drop.

If we assume that the ratio  $\rho_1 = 0$ , we obtain an expression for the field form of Fig. 5.7c.

For the field distribution of Fig. 5.7d, the amplitude of the first-harmonic for the curve can be represented, as N.Ya. Al'per has shown, in terms of the sine and cosine integrals in the form

$$\lambda_1 = \frac{2\pi}{\pi\beta} \sin \alpha_1 + \frac{2}{\pi\beta} \left\{ \cos \gamma \left[ \text{ci}(\pi - \gamma) - \text{ci} \frac{\beta}{\pi} \right] - \sin \alpha_1 \left[ \text{si}(\pi - \gamma) + \text{si} \frac{\beta}{\pi} \right] \right\}, \quad (5.14)$$

where  $\gamma = \alpha_1 - (\delta/\beta\tau)$ ,  $\beta$  is an angle in radians.

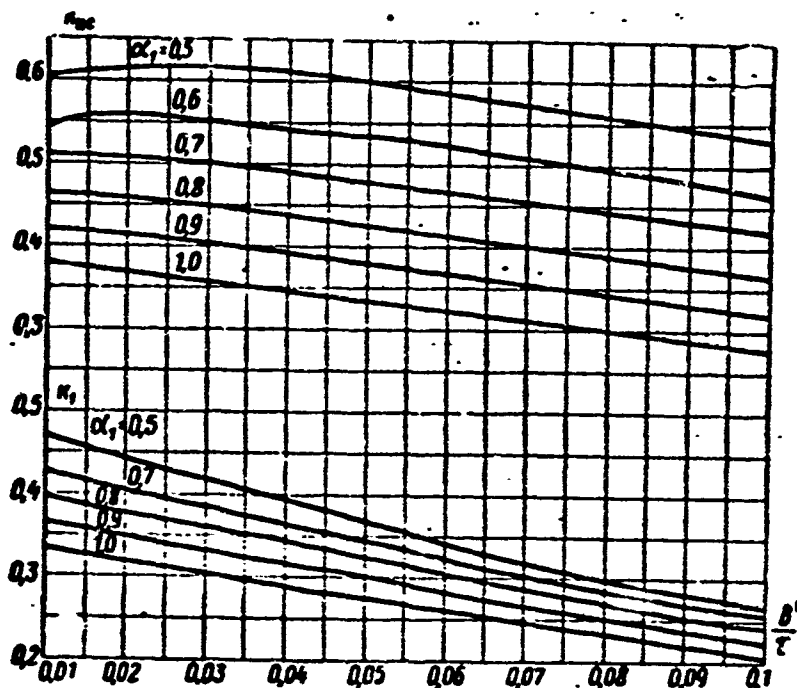


Fig. 5.8. Coefficients for induction-generator magnetic circuit. Degree of flux utilization  $k_1 = f(\alpha_1, \delta'/\tau)$ , degree of utilization of induction generator  $k_{1s} = \varphi(\alpha_1, \delta''/\tau) = k_1 k_m$ .

The first harmonic of the flux is

$$\Phi_1 = \frac{2}{\pi} B_{\tau} l = \frac{2}{\pi} l U_1 \lambda_1. \quad (5.15)$$



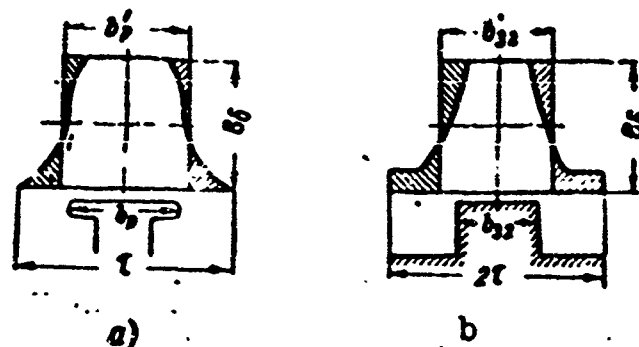


Fig. 5.9. No-load induction distribution coefficient. a) Classical synchronous machine,  $k_m = b'_r/b_r$ ; b) induction generator,  $k_m = b'_{z2}/b_{z2}$ .

The double pole-pitch flux is

$$\Phi_N = B_0 2\tau l = 2\tau l U_0 \lambda_0 \quad (5.16)$$

The degree of flux utilization

$$k_1 = \frac{\Phi_1}{\Phi_N} = \frac{1}{\pi} \frac{\lambda_1}{\lambda_0} = f\left(\alpha_1; \frac{\delta}{\tau}\right) \quad (5.17)$$

is found from the curves of Fig. 5.8.

When  $\alpha_1 = 0.8$  and  $\delta/\tau = 0.05$ , 32.3% of the flux is used.

Thus, the degree of utilization of the flux will turn out to be low if we base the calculation on the field distribution of Fig. 5.7a, and high if we use the distribution of Fig. 5.7b, in comparison with the field of Fig. 5.7d, which resembles the true field.

In conclusion, for induction machines we determine the induction distribution coefficient under no-load conditions,  $k_m$ , which in classical synchronous machines (Fig. 5.9) is found from the equations

$$\Phi = B_0 \tau l = B_0 \tau' l = B_0 b'_p l;$$

$$\alpha' = \frac{b'_p}{\tau} = k_m \frac{b_p}{\tau} = k_m \alpha_1$$

to equal

$$k_m = \frac{b'_p}{b_p} = \frac{\alpha'}{\alpha_1}.$$

In induction generators, it is necessary to proceed on the basis

of the double pole pitch

$$\Phi_{21} = B_0 2\tau l = B_1 2x' \tau l = B_1 b'_{z2} l,$$

i.e.,

$$k_u = \frac{b'_{z2}}{b_{z2}} = 2 \frac{x'}{a_1} = \frac{\Phi_{21}}{B_1 b_{z2} l} = \frac{\Phi_1}{k_1 B_1 b_{z2} l}. \quad (5.18)$$

Thus, the maximum induction in the air gap of an induction generator is

$$B_1 = \frac{\Phi_1}{k_u k_1 b_{z2} l} = \frac{\Phi_1}{k_{us} b_{z2} l} \text{ [gauss]} \quad (5.19)$$

and the magnetic potential drop across the air gap is.

$$U_\delta = 0.8 \delta' B_\delta \text{ ampere-turns}, \quad (5.20)$$

where  $k_{is} = k_1 k_m = 2k_1 (\alpha' / \alpha_1)$  is a coefficient characterizing the degree of utilization of the induction generator, and is found from Fig. 5.8;  $\alpha'$ ,  $b'_{z2}$ , and  $b_{z2}$  are design quantities.

#### Armature Reaction of Induction Generator

The armature reaction of an induction generator is determined as in the case of salient-pole synchronous generators, while the effect of armature magnetizing force on the main machine field will also depend on the magnitude and nature of the load.

In the general case, the armature magnetizing force is split, as is usual, into direct-axis and quadrature-axis components, and the direct- and quadrature-axis armature-reaction fluxes are found by multiplying the magnetizing force by the appropriate permeance. Thus if we consider only the first harmonic of the armature magnetizing force,

$$\left. \begin{aligned} f_{ad} &= F_{ad} \cos(\theta - \omega t), \\ f_{aq} &= F_{aq} \sin(\theta - \omega t), \\ B_{ad} &= f_{ad} \lambda_d, \\ B_{aq} &= f_{aq} \lambda_q, \end{aligned} \right\} \quad (5.21)$$

and

where

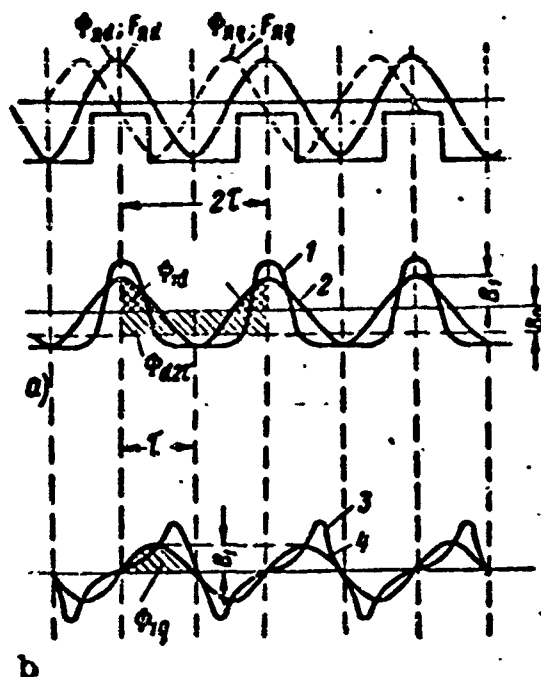


Fig. 5.10. Armature-reaction field curves. a) Direct axis; b) quadrature axis. 1 and 3) Flux curves; 2 and 4) first harmonics of the flux due to direct-axis and quadrature-axis armature magnetizing force;  $\Phi_{2\tau}$ ) double pole-pitch flux due to magnetizing force  $F_{yad}$ ;  $\Phi_{1d}$  and  $\Phi_{1q}$ ) first-harmonic fluxes due to magnetizing forces  $F_{yad}$  and  $F_{yaq}$ .

$$\left. \begin{aligned} F_a &= 0.45m \frac{I_a}{p} \sin \phi \\ F_{ad} &= F_a \sin \phi \\ F_{aq} &= F_a \cos \phi \end{aligned} \right\}$$

(5.22)

and

In order to determine the armature-excitation field reduction coefficients  $k_{1d}$  (direct-axis) and  $k_{1q}$  (quadrature-axis) for the machine, the armature-field curve of Fig. 5.10 is represented in series form and the first harmonics are separated out and set equal to the first harmonic of the excitation field.

Each harmonic of the armature magnetizing force forms an infinite series of harmonics in the gap; we shall consider only the first har-

monic, which is stationary with respect to the excitation magnetizing force and which forms the armature reaction.

The first harmonic of the armature magnetizing force for the direct and quadrature axes forms all possible higher harmonics of the induction. The instantaneous values of the direct- and quadrature-axis inductions due to the first harmonic of the armature magnetizing force will be

$$\left. \begin{aligned} B_{1d} &= F_{1a} \left[ \frac{\lambda_{1d}}{2} + \left( \lambda_{0d} + \frac{\lambda_{2d}}{2} \right) \cos(\theta - \omega t) + \right. \\ &\quad \left. + \frac{1}{2} \sum_2 (\lambda_{n-1} + \lambda_{n+1})_d \cos n(\theta - \omega t) \right] \\ \text{and} \\ B_{1q} &= F_{1a} \left[ \left( \lambda_{0q} - \frac{\lambda_{2q}}{2} \right) \sin(\theta - \omega t) + \right. \\ &\quad \left. + \frac{1}{2} \sum_2 (\lambda_{n-1} - \lambda_{n+1})_q \sin n(\theta - \omega t) \right] \end{aligned} \right\} \quad (5.23)$$

If we confine our examination to the first harmonic, the direct- and quadrature-axis armature-reaction fluxes will be

$$\left. \begin{aligned} \Phi_{1d} &= \frac{2}{\pi} B_{1d} \tau l = \frac{2}{\pi} \tau l F_{1a} \left( \lambda_{0d} + \frac{\lambda_{2d}}{2} \right) \cos(\theta - \omega t), \\ \Phi_{1q} &= \frac{2}{\pi} \tau l F_{1a} \left( \lambda_{0q} - \frac{\lambda_{2q}}{2} \right) \sin(\theta - \omega t), \end{aligned} \right\} \quad (5.24)$$

while the corresponding armature-reaction emf's will be

$$e_{1d} = E_{1d \max} \sin \omega t$$

and

$$e_{1q} = E_{1q \max} \cos \omega t,$$

where

$$\left. \begin{aligned} E_{1d} &= 4 \tau l \omega_s f F_{1a} (\lambda_{0d} + 0.5 \lambda_{2d}) 10^{-8} \text{ V}, \\ E_{1q} &= 4 \tau l \omega_s f F_{1a} (\lambda_{0q} - 0.5 \lambda_{2q}) 10^{-8} \text{ V}. \end{aligned} \right\} \quad (5.25)$$

If the amplitude of the first harmonic of the armature-reaction magnetizing force equals the first harmonic of the excitation magnetiz-

ing force under no-load conditions, i.e., if  $F_{lyad} = U_{\delta z}$ , the reduction coefficients for the direct- and quadrature-axis armature reactions will equal (according to N.Ya. Al'per) (Fig. 5.11)

and

$$\left. \begin{aligned} k_{1d} &= \frac{\Phi_{1d}}{\Phi_1} = \frac{\lambda_{0d} + 0.5\lambda_{2d}}{\lambda_1} \\ k_{1q} &= \frac{\Phi_{1q}}{\Phi_{1d}} = \frac{\lambda_{0q} - 0.5\lambda_{2q}}{\lambda_{0d} + 0.5\lambda_{2d}} \end{aligned} \right\} \quad (5.26)$$

Expression (5.25) has been obtained on the assumption that the permeance of the stator center section and of the rotor is so large as to be negligible. Actually, the magnetic potential drop in the center section can be of the same order of magnitude as that across the air gap. The center-section permeance affects only the direct-axis armature-reaction flux; the quadrature-axis armature-reaction flux is completed outside the stator and rotor supporting sections.

If we let  $\Lambda$  be the permeance of the supporting body and leakage paths divided by the surface area of the stator bore, then

$$\Lambda = \Lambda_c + \Lambda_s \approx \Lambda_c$$

and

$$\Lambda_c = \frac{\Phi_c}{U_c} \frac{1}{2\pi r l}$$

since the leakage permeance  $\Lambda_s$  normally does not exceed several percent of  $\Lambda_s$ .

The potential drop  $U_s$  in the supporting body decreases the emf due to the direct-axis armature reaction, as is provided for in the coefficient

$$k_x = 1 - 1.57 \frac{k_1}{k_{1d}} \left( 1 - \frac{U_{\delta z}}{F_0} \right).$$

The magnetic-circuit coefficient  $k_s = (F_0/U_{\delta z}) = 1 + (U_s/U_{\delta z})$  is found from the no-load curve.

In the beginning of this section, we made the assumption that the armature surface is smooth. If we allow for the presence of the slots,

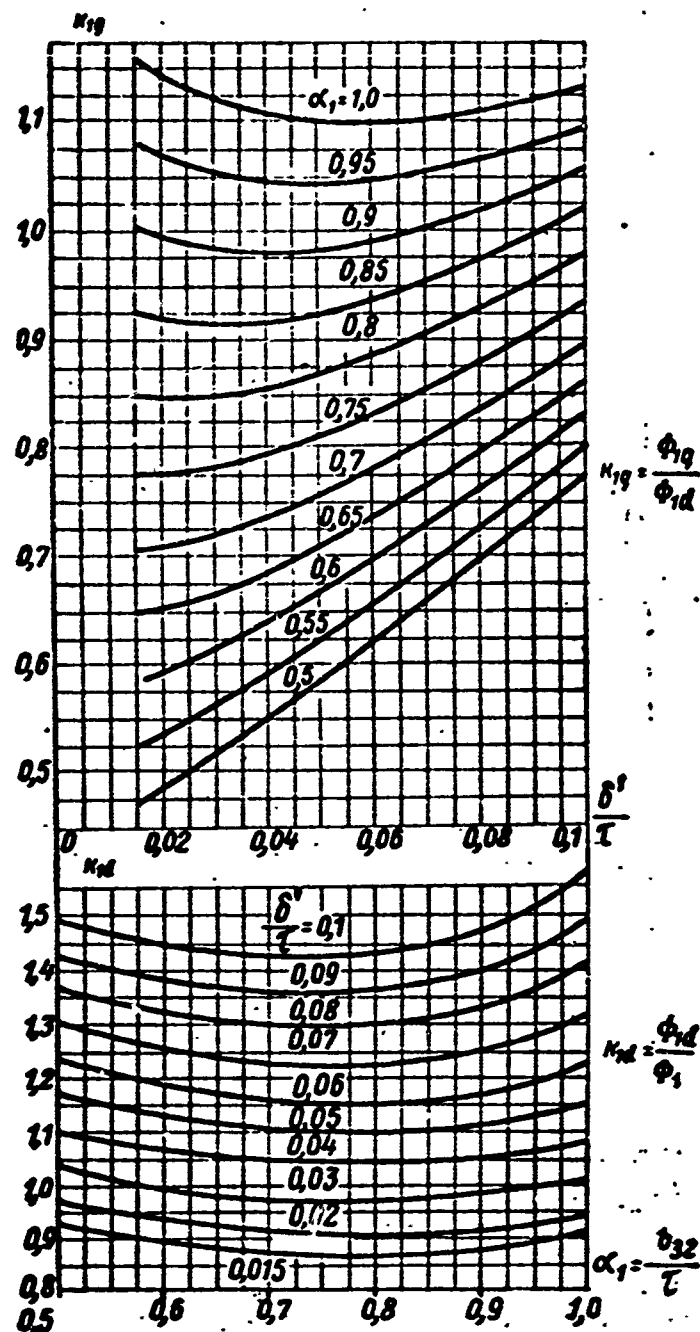


Fig. 5.11. Armature-reaction reduction coefficients.  $k_{1d} = f(\alpha_1, \delta'/\tau)$  - direct axis;  $k_{1q} = f(\alpha_1, \delta'/\tau)$  - quadrature axis.

the direct-axis and quadrature-axis armature-reaction inductive reactance is equal to  $x_{yad} = (E_{yad}/I) \equiv (\phi_{yad}/I)$  and  $x_{yaq} = (E_{yaq}/I) \equiv (\phi_{yaq}/I)$  will decrease in value. The effect of opening the gaps is provided for in the coefficient  $k_{r.p} = f(b_{shch}/\tau)$ , with the values

$b_{shch}/\tau$	0.1	0.2	0.3	0.4
$k_{r.p}$	0.99	0.94	0.86	0.78

## Characteristics of Induction Generators

Figure 5.12 shows the no-load, load, and short-circuit characteristics. It is clear from this figure that the characteristics of in-

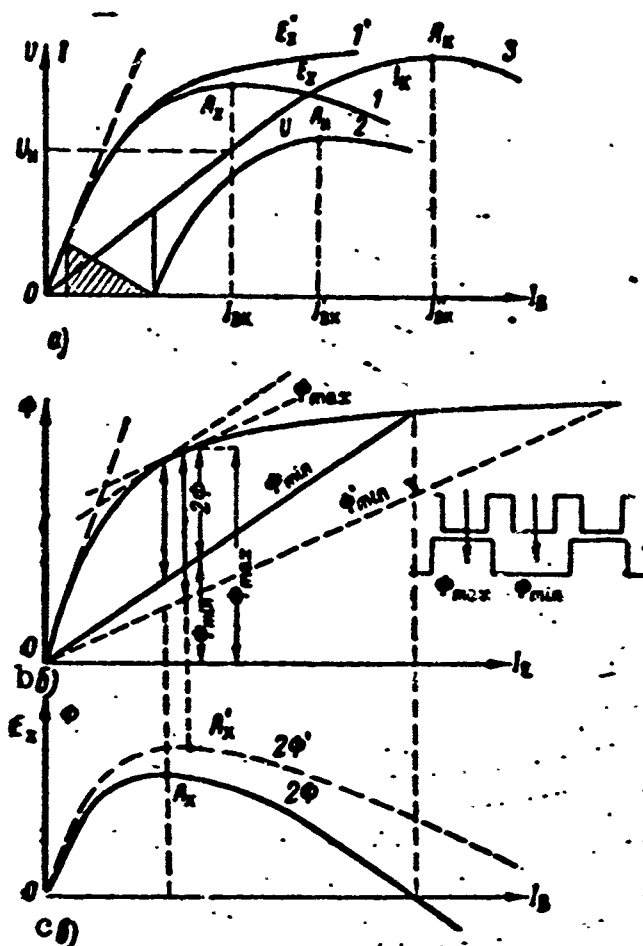


Fig. 5.12. Characteristics of induction generators. 1 and 1') No-load characteristics for induction and synchronous generators; 2) load characteristics; 3) short-circuit characteristic.

Induction generators differ basically from similar characteristics for other electric generators.

As a rule, the no-load curve  $E = f(I_v)$  at  $I = 0$  and the load curve  $U = f(I_v)$  at  $I = \text{const}$  consist of three sections: an initial straight-line section corresponding to the unsaturated condition of the magnetic circuit, where the flux rises steeply in proportion to the excitation magnetizing force; a central curved portion corresponding to mean saturation, where the flux increases noticeably, but not

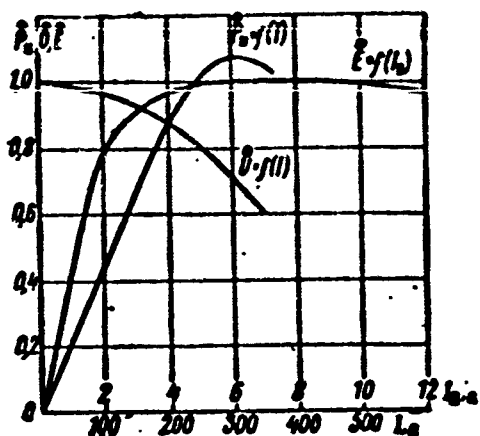


Fig. 5.13. Characteristic of 30 kva, 1200 cps, 12,000 rpm aircraft induction generator,  $m = 1$ .

in proportion to the increase in excitation magnetizing force; and a final straight-line section corresponding to the saturated state of the machine, where the flux rises only slightly in proportion to the excitation magnetizing force (curve 1').

The induction-generator characteristic (curves 1, 2, and 3) have critical points  $A_{kh}$ ,  $A_n$ , and  $A_k$ , where changes in sign occur, i.e., below the points A, an increase in excitation magnetizing force is accompanied by increases in machine flux and emf, while with a further increase in excitation magnetizing force, the machine flux and emf will drop. This is explained in the following manner.

The changing machine flux that induces the emf into the armature winding equals

$$\Phi = 0.5(\Phi_{\max} - \Phi_{\min}).$$

where  $\Phi_{\max}$  and  $\Phi_{\min}$  are the fluxes whose paths are completed, respectively, along the direct (iron) and quadrature (air) machine axes (Fig. 5.12b).

The relationship  $\Phi_{\max} = f(F_v)$ , which has a great deal of influence on the magnetic-circuit saturation, is represented by a curved line, while the relationship  $\Phi_{\min} = f(F_v)$  is represented by a line that is nearly straight; thus with increasing excitation, the varying flux ( $2\Phi$  in Fig. 5.12c) increases below point A in accordance with the curved section of  $\Phi_{\max} = f(F_v)$  and then begins to drop.

If the value of the minimum flux decreases to the value  $\Phi'_{\min}$ , the critical point will move to the right along A'. Consequently, the



larger the ratio  $\phi_{\max}/\phi_{\min} = \lambda_{\max}/\lambda_{\min}$ , the larger the excitation magnetizing force required to reach the critical point.

Thus, in induction machines, the magnetic circuit should be weakly saturated and the ratio  $\lambda_{\max}/\lambda_{\min}$  should be as large as possible. For high saturations, the utilization efficiency of the machine drops and at a certain value of excitation, the voltage may even become equal to zero.

From the physical viewpoint, the bend in the no-load curve may be explained by the fact that the machine direct-axis permeance decreases at high saturations and becomes comparable with the machine quadrature-axis permeance and, consequently, the changing component of the flux, which induces the emf into the armature winding will equal the difference of the machine direct- and quadrature-axis fluxes, which first reaches a maximum (point  $A_{kh}$ ) and then drops rapidly.

Figure 5.13 shows the characteristics of a 30 kva 1200 cps 12,000 rpm single-phase aircraft induction generator.

### 5.3. SOME REMARKS ON THE DESIGN OF INDUCTION GENERATORS

#### Choice of Induction-Generator Type

Manufacturing conditions and power-to-weight ratio considerations make it desirable to design salient-pole synchronous generators for frequencies of up to 500 cps with peripheral speeds of  $v \leq 50$  m/sec and  $\tau = (v/2f) \geq 50$  mm.

Nonsalient-pole synchronous generators, for which each rotor tooth is a pole, may be used for frequencies  $f = (v/2\tau) \leq 1600$  cps with  $v \leq 100$  m/sec and for frequencies of up to 2400 cps with  $v \leq 150$  m/sec and  $\tau \geq 30$  mm.

Consequently, the upper frequency limit for synchronous generators is determined by the minimum pole pitch, which is dictated by structural considerations, manufacturing conditions, and the power-to-weight

ratio.

In induction generators using a tooth-type active zone with  $v \approx 150$  m/sec and a minimum rotor tooth pitch of 1.25 mm, it is possible to obtain a frequency of  $f = 15,000/2 \times 1.25 = 60,000$  cps. A further increase in frequency, however, is limited in induction generators by the minimum armature tooth pitch in machines with a classical active zone and by the minimum rotor-tooth width in machines using a tooth-type active zone.

It is difficult to make a classical active zone for frequencies above 2000-3000 cps, especially where  $m = 3$ ; a tooth-type active zone is therefore used.

The advantages of homopolar generators are: a) the rotor teeth do not change magnetic polarity and thus need not be laminated, which makes it possible to increase the rotor peripheral speed (up to 150 m/sec); the iron losses will drop;

b) the field winding will be smaller and lighter and, consequently, the resistance and losses will be less;

c) single- and multiphase armature windings will be symmetric.

Drawbacks of homopolar generators: a) the excitation flux passing axially along the rotor sleeve and stator yoke increases their cross-sectional area and weight; currents will appear in the bearings and there will be increased leakage through the frame of the electric drive motor (single-frame construction);

b) the moment of inertia of the rotor (owing to the high weight) and the magnetic-field inertia are considerable (the magnetic circuit contains large massive sections);

c) the time constant  $T = L/R$  of the excitation circuit rises, since the field winding has low resistance and high inductance (all of the excitation flux is linked with the entire field winding) leading

to prolongation of transients and possible overvoltages when the load is removed.

Advantages of heteropolar generators: a) size and weight of rotor sleeve and armature core are determined, in the main, by structural considerations, since the number of field poles may be increased and the cross section (weight) of the magnetic circuit decreased;

b) the moment of inertia, magnetic-field inertia, and excitation-circuit time constant are lower than for homopolar machines;

c) there are no axial fluxes, which reduces leakage and is favorable from the viewpoint of bearing and drive-motor operation for single-frame designs.

Drawbacks of heteropolar generators: a) higher losses in the iron and the field winding;

b) need to take special measures in order to obtain symmetric armature windings, especially with a three-phase system;

c) lower permissible rotor peripheral speed ( $v \leq 90$  m/sec);

d) considerable losses in rotor teeth.

#### Geometry of Active Zone

It is recommended that the following quantities be taken as basic: the number of slots per pole and per phase is normally equal to unity ( $q = 1$ ). The total number of slots in the armature per unit (classical active zone) is

$$z_1 = 2mz_2 = \frac{120f}{n} m,$$

where

$$z_2 = 60f/n.$$

The armature tooth and pole pitches are

$$t_1 = \frac{\pi D}{z_1} = \frac{30v}{mz_2 n} = \frac{v}{2mf} \text{ and } \tau = mt_1.$$

If the speed and frequency are given, the tooth and pole pitches,

as well as the number of teeth and armature diameter may be found from the formulas given. It is desirable to use semienclosed armature slots, as this increases machine utilization efficiency, although it results in some manufacturing complications.

The width of a rotor tooth, i.e., the pole width, is

$$b_{z2} = \alpha_1 \tau, \text{ where } \alpha_1 = 0.7-0.8.$$

The width of the space between poles is

$$b_{\alpha} = 2\tau - b_{z2} = \tau(2 - \alpha_1) = (1.3 \div 1.2)\tau.$$

The depth of a rotor slot is

$$h_{\alpha} \geq 0.5\tau; \quad h_{\alpha} \geq 20\delta.$$

The air gap is made as small as possible, allowing for strength and manufacturing considerations, and considering the limitation of surface losses; then  $\delta = 0.2 + (D/500)$  mm.

In order to improve the shape of the voltage curve, the rotor teeth are beveled, which reduces the magnetic coupling between the armature winding and the field winding. We allow for this by means of the bevel factor

$$k_{\text{ex}} = \frac{\sin 0.5\epsilon_{\text{ex}}}{0.5\epsilon_{\text{ex}}},$$

where

$$\epsilon_{\text{ex}} = (0.4 \div 0.65)\tau.$$

### Magnetic Circuit

In induction generators, the magnetic circuit is weakly saturated. Saturation of the magnetic circuit decreases the modulation of the flux in the armature teeth and, consequently, reduces the utilization efficiency of the machine. In addition, a relative increase in the magnetic potential drop across the magnetic-circuit iron distorts the shapes of the field and the machine emf curve, and also makes them more dependent on the nature of the load.

Thus, the choice of the magnetic loads in the iron is of basic importance.

Induction-machine design is frequently based not on the air-gap induction, as is the rule, but on the permissible induction in the armature teeth. If we allow for the magnetic skin effect and the specific iron losses, the armature-tooth induction will drop as the frequency rises. Thus, for a frequency  $f = 400-10,000$  cps, we can initially use the following values of induction for the stator teeth,  $B_{zs}$ :

1 $f$ , cps	400	1000	1600	2400	6000	8000	10 000
2 $B_{zs}$ , gauss	12 000	11 000	10 000	9000	7000	6000	5000
	11 000	10 000	9000	8000	6000	5000	4000

1)  $f$ , cps; 2)  $B_{zs}$ , gauss.

The induction in the magnetic circuit outside the active zone should not exceed roughly  $1.2 B_{zs}$ .

Under no-load conditions, the magnetic potential drop across the air gap is determined from the maximum induction in the air gap, i.e.,

$$B_g = \frac{\Phi_1}{a_1 U_g} \frac{1}{k_{sc}} = \frac{B_{s1}}{K_{sc}}$$

and

$$U_i = 0.88 B_{s1}$$

If the magnetic-circuit coefficient for the active zone is

$$k_{sc} = \frac{U_{s1}}{U_i} = 1 + \frac{U_{s1} + U_{s2}}{U_i} \geq 1.5,$$

it is then necessary to consider saturation of the tooth zone. To do this, we introduce the notion of the equivalent air gap  $\delta'_{ekv} = k_{s1} \delta'$ , which we use to determine the coefficients  $k_1$  and  $k_{1s}$  as well as the flux  $\Phi_{2\tau}$  and the emf  $E \equiv k_1 \Phi_{2\tau} = \Phi_1$ .

Here  $U_{zs}$  and  $U_{zr}$  are the magnetic potential drops across the stator and rotor teeth.

For a homopolar generator, calculations for the magnetic circuit outside the active band are based on the total fluxes:

for the rotor yoke

$$\Phi_{z,p} = \frac{\Phi_1}{k_1} p = \Phi_{z,p};$$

for the stator yoke, allowing for the leakage flux

$$\Phi_{z,c} = \Phi_{z,p} + \Phi_o,$$

where the leakage flux under no-load conditions is

$$\Phi_o = 2\Lambda_o (U_{\delta z} + U_{ya,r}) \approx 0,05\Phi_{z,p}.$$

Here  $U_{\delta z}$  and  $U_{ya,r}$  are the magnetic potential drops across the active band and the rotor yoke.

Owing to the effect of the armature magnetizing force, the air-gap field under load will differ from the no-load field: the main flux will be supplemented by the differential leakage flux  $\Delta\Phi$ , which represents the difference between the total fluxes due to the excitation magnetizing force and the armature magnetizing force for identical values of the flux first harmonics.

It is usual to neglect the differential flux in magnetic-circuit calculations for loaded synchronous machines, but in induction machines  $\Delta\Phi \approx (0.05-0.15)\Phi_{2\tau}$  and it must be taken into account during the calculations.

The approximate differential flux can be determined from the equations

$$\Delta\Phi = F_{a,d} \Delta\Lambda,$$

where  $\Lambda = (\Phi_{z,p}/F_0) = \Phi_1/k_1 F_0$  is the magnetic-circuit no-load permeance;

$F_{a,d} = 0,45m(w_a/l_a/p)k_{1d}$  is the direct-axis armature reaction and  $\xi = 1 - 1.57(k_1/k_{1d})$ .

Allowing for saturation, the permeance  $\Lambda$  is found for an emf somewhat larger than  $E$ , i.e., we let

$$\Delta = \frac{\Phi_{21}}{10(F'_0 - F_0)}$$

where  $F_0$  and  $F'_0$  are found from the no-load curve for  $E_0$  and  $1.1E_0$ , respectively.

Allowing for what we have said, the maximum calculated induction in the air gap under load can be represented as

$$B'_1 = B_1 + \Delta B_1$$

where

$$\Delta B = B_{21} \frac{F_{21} \lambda}{10(F'_0 - F_0)} \text{ and } B_{21} = \frac{\Phi_{21}}{2\lambda}$$

For the magnetic circuit outside the active zone, the calculated fluxes under load will equal, respectively,

$$\begin{aligned}\Phi_{2, p2} &= \Phi_{2, p} + p \Delta \Phi, \\ \Phi_{2, c2} &= \Phi_{2, p2} + \Phi_{21}, \\ \Phi_{21} &= 2\lambda_0 (U_{2, s2} + U_{2, p2} + F_{21}).\end{aligned}$$

#### Parameters of Induction Generators

In view of the fact that the inductive reactances of induction generators are considerably higher than those found in the ordinary type of synchronous machine, the voltage drop across them is considerably greater. Let us compare them, in relative units, for induction and synchronous machines.

The leakage inductive reactance is

$$\dot{x}_{s2} \approx 2.83 \frac{\sum \lambda}{k_{sc} m q k_{0n}^2} \frac{A}{B_1}$$

for induction machines, and

$$\dot{x}_s \approx 2.83 k_\phi \frac{\sum \lambda}{m q k_{0n}^2} \frac{A}{B_1}$$

for synchronous machines. Their ratio is

$$\frac{\dot{x}_{s2}}{\dot{x}_s} = \frac{1}{k_{sc} k_\phi} \frac{k_0}{k_{0n}} \approx (2.0 + 2.2) \frac{k_0}{k_{0n}},$$

since  $k_{1s} \approx 0.5-0.4$  while  $k_f \approx 1.0-1.07$ .

Here  $g$  is the number of slots per pole and per phase;  $\Sigma\lambda$  is the total leakage permeance, determined in the usual way.

Armature-reaction inductive reactance (direct-axis and quadrature-axis

$$\dot{x}_{ad} = 0,45 k_{1d} k_{0d} k_x \frac{A\tau}{U_{1s}} k_p = \frac{3+k_1}{4}$$

for induction machines, and

$$\dot{x}_{ad} = 0,45 k_d k_0 \frac{A\tau}{U_{1s}}$$

for synchronous machines. Their ratio is

$$\frac{\dot{x}_{ad}}{\dot{x}_{ad}} \approx \frac{k_{1d}}{k_d} k_x \frac{k_{0d}}{k_0} \approx (0,85 + 1,5) \frac{k_{0d}}{k_0},$$

since

$$k_{1d} = 0,9 + 1,4, k_d = 0,8 + 0,9, k_x \approx 0,85, k_p = \frac{3+k_1}{4} \approx 1,$$

Similarly

$$\dot{x}_{aq} = 0,45 k_{1q} k_{0q} k_p = \frac{3+k_1}{4} \frac{A\tau}{U_{1s}}$$

for induction machines, and

$$\dot{x}_{aq} = 0,45 k_q k_0 \frac{A\tau}{U_{1s}}$$

for synchronous machines.

Their ratio is

$$\frac{\dot{x}_{aq}}{\dot{x}_{aq}} \approx \frac{k_{1q} k_{0q}}{k_q k_0} \approx 2,0 + 2,4$$

where  $m = 1$  and  $2.25-2.7$  where  $m = 3$ , since

$$k_{1q} = 0,77 + 0,95, k_q = 0,3 + 0,7, \\ \frac{k_{0q}}{k_0} = 0,9 + 0,8 \text{ and } k_p = \frac{3+k_1}{4} \approx 1.$$

Here  $k_{r.p} = f(b_{shch}/\tau)$  is the open-slot coefficient;  $k_g$  is the air-gap coefficient.



## Transient inductive reactance

It follows from the direct-axis transient equivalent circuit that

$$\dot{x}_{d''} = \dot{x}_{d'} + \dot{x}_{d'd} = \dot{x}_{d'} + i\dot{x}_{d''}$$

where

$$i = 1 - 1.57 \frac{k_1}{k_{1d}}$$

For the quadrature axis

$$\dot{x}_{q''} = \dot{x}_{q'}$$

and

$$\dot{x}_{q''} = \dot{x}_{q''} = \dot{x}_{q'} + \dot{x}_{q''}$$

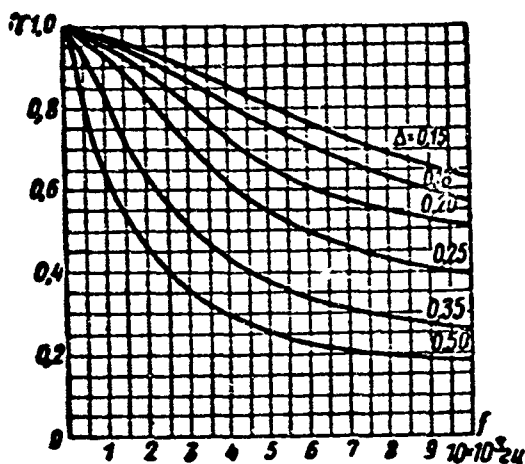


Fig. 5.14. Utilization efficiency for lamination, allowing for magnetic skin effect  $\gamma = \varphi(\Delta; f)$ .

The usual relationships between the reactances are

$$\dot{x}_{d''}/\dot{x}_{d'} = 0.3 + 0.7$$

for induction machines, and

$$\dot{x}_{d''}/\dot{x}_{d'} = 0.1 + .3$$

for synchronous machines.

The negative-sequence inductive reactance is

$$\dot{x}_2 = 0.5(\dot{x}_{d''} + \dot{x}_{q''}) > \dot{x}_2$$

since

$$\dot{x}_{d''} > \dot{x}_{d'} \text{ and } \dot{x}_{q''} > \dot{x}_{q'}$$

The synchronous inductive reactance is

$$\dot{x}_{d''} = \dot{x}_{d'} + \dot{x}_{d''}$$

Where  $m=1$   $\dot{x}_{d''} = \dot{x}_{d'} + \dot{x}_{d''}$

In order to reduce the inductive reactances, induction generators are made with low linear loads and high air inductions, while to reduce the voltage drop, capacitive compensation is frequently provided by connecting a capacitor into the armature circuit.

## Magnetic Skin Effect in Sheet Steel

It was noted in Chapter 1 that when  $f\Delta^2 > 80$ , the phenomenon of

magnetic skin effect in sheet steel must be taken into account. In magnetic-circuit calculations (in determining the field strength) it is necessary to use the maximum induction in the iron, with an allowance for the magnetic skin effect. Since this effect is produced solely by the variable component of the induction, the expression for the maximum induction in the teeth, allowing for the magnetic skin effect and considering only the first harmonic of the flux, will be

$$B'_{\text{a.c}} = \frac{l_1}{b_{\text{ac}} k_{\text{ac}}} \left( B_0 + \frac{B_1}{\gamma} \right) = \frac{l_1 B_0}{b_{\text{ac}} k_{\text{ac}}} \left( 1 + \frac{B_1}{\gamma B_0} \right),$$

where

$$B_0 = \frac{\Phi_1}{2\lambda l} \cdot \frac{1}{k_1}$$

is the constant component of the air-gap induction;

$$B_1 = \frac{\pi}{2} \frac{\Phi_1}{\lambda l}$$

is the amplitude of the variable component of the air-gap induction;

$\gamma = \varphi(\Delta; f)$  is the sheet-steel utilization efficiency from Fig. 5.14.

Thus, the skin-effect phenomenon results in an increase in the magnetic potential drop across the magnetic circuit and an increase in the excitation magnetizing force.

#### Selection of Basic Dimensions

If the size of the diameter is not limited by the peripheral speed or installation conditions, it may be found from the basic design equation

$$D = \sqrt[3]{\frac{S_e}{\pi \lambda c_m}}$$

where  $S_e = S_n(E/U)$  is the electromagnetic power of the generator;  $\lambda = l/D$  is a structural factor;  $c_m = 1.65 k_0 k_{ac} \alpha_1 A F \cdot 10^{-9}$  is the machine utilization factor or the specific tractive effort;  $k_{1g} = f(\alpha_1; \delta'/\tau)$  is the degree of utilization of the induction generator from Fig. 5.8.

For heteropolar machines, where the armature winding does not fill the entire armature surface, it is necessary to multiply  $\sigma_1$  by a factor that allows for the degree to which the armature surface is taken up by the winding.

Let us compare the utilization efficiencies of single- and three-phase induction generators and similar synchronous machines of classical type. For a synchronous machine, the armature volume will be

$$D^2l = \frac{S_a}{n\lambda_s}.$$

For the ratio of the induction-generator armature volume  $(D^2l)_1$  and the armature volume for a similar synchronous machine  $(D^2l)$ , the relationship

$$\frac{(D^2l)_1}{(D^2l)} = \frac{E'_a}{E'} \frac{k_0 k_\phi k_m}{k_{ac} k_{sc}},$$

holds, where

$$\frac{E'_a}{E'} = \frac{E_a}{E} = \sqrt{\frac{(\cos \varphi + \dot{R})^2 + (\sin \varphi + \dot{x}_{sa})^2}{(\cos \varphi + \dot{R})^2 + (\sin \varphi + \dot{x}_s)^2}}$$

is the relative emf for the induction and synchronous generators;  $k_{01}$  and  $k_0$  are winding factors;  $k_m$  is a coefficient that characterizes the utilization efficiency of the synchronous machine when there is a change in the number of phases ( $k_m = 1$  when  $m = 3$  and  $k_m \approx 0.71$  when  $m = 1$ ).

As a rule,  $E'_1 > E'$ , since  $\dot{x}'_{s1} > \dot{x}'_s$ . Consequently, for identical generator powers, the theoretical electromagnetic power of the induction generator will be greater than that of the synchronous machine in the ratio  $E'_1/E' = E_1/E \approx 1.1-1.2$ .

In single- and three-phase homopolar induction generators with classical active zones,  $k_{01} = 1$ . In three-phase synchronous generators with short winding pitch,  $k_0 = k_r \times k_u \approx 0.91$ , while in single-phase machines with diameter winding pitch,  $k_0 = k_r \approx 0.8$ .

Taking the proper value for  $k_m$  and letting  $k_{18} = 0.4-0.5$ , we find that

$$\frac{(D^2)_n}{(D^2)} \approx 2.2 + 2.7 \text{ for } m=3$$

and

$$\frac{(D^2)_n}{D^2} \approx 1.3 + 1.7 \text{ for } m=1.$$

Consequently, it makes sense to use induction generators in the single-phase version. As the frequency increases (with the speed unchanged), the number of poles increases while the pole pitch is reduced; in synchronous machines, this latter fact causes a reduction in the useful volume available between the poles for the field winding. Thus, where the number of poles is greater than 8-10 or where the pole pitch is of the order of 30-35 mm, it is necessary to increase the size of the machine, in view of the reduction in the amount of inter-pole space that is filled with copper. Here the dimensions of a single-phase induction generator of less than 10 kva power may prove less than those of a synchronous generator, since the reduction in pole pitch has almost no effect on the utilization efficiency of the induction machine.

The following preliminary data may be used to select the linear load:

$S_{nom}, \frac{1}{kva}$	0.1+1.0	1+2	2+3	3+6	6+10	10+20	20+50
$A, \frac{2}{a/cm}$	80+150	120+180	160+220	200+250	240+350	300+400	380+420

1) kva; 2) amp/cm.

### Losses and Efficiency

Induction generators are more efficient than similar synchronous machines. The losses are found by means of the usual formulas. The only

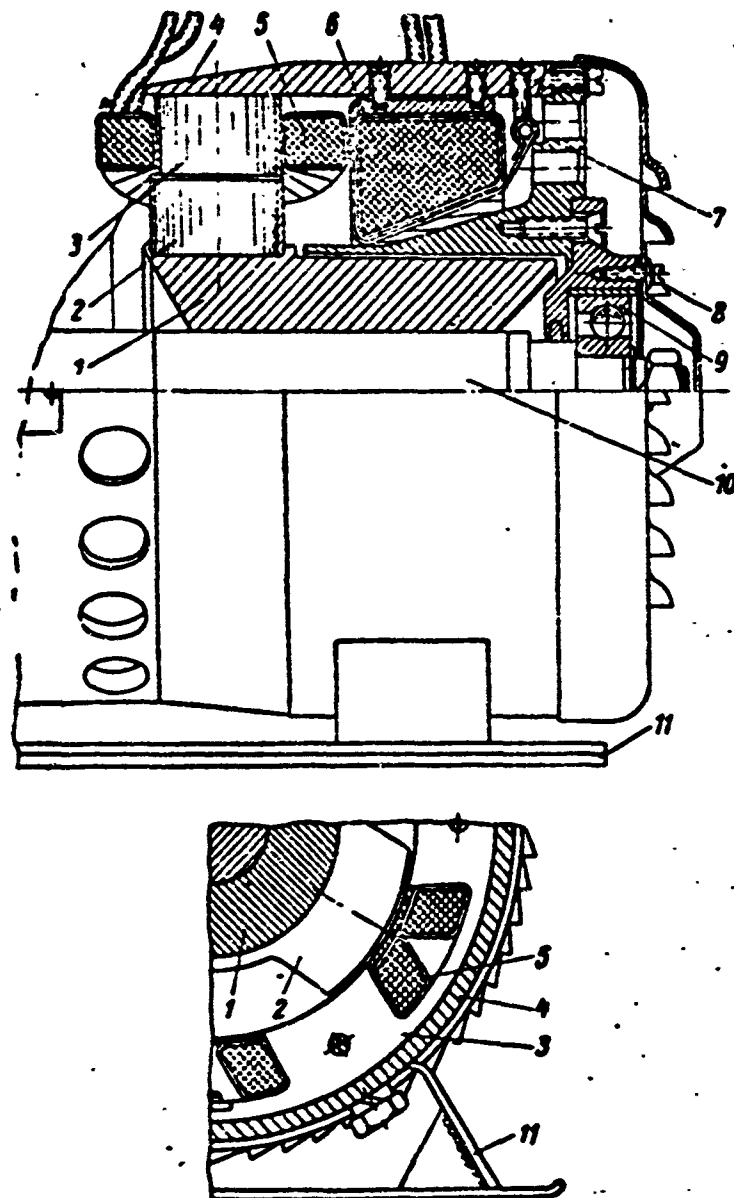


Fig. 5.15. Construction of 2500 va 400 cps 8000 rpm single-unit homopolar single-phase aircraft induction generator. 1) Sleeve; 2) rotor and tooth core; 3) armature and tooth core; 4) frame; 5) armature winding; 6) field winding; 7) flange; 8) cover; 9) bearing; 10) shaft; 11) feet.

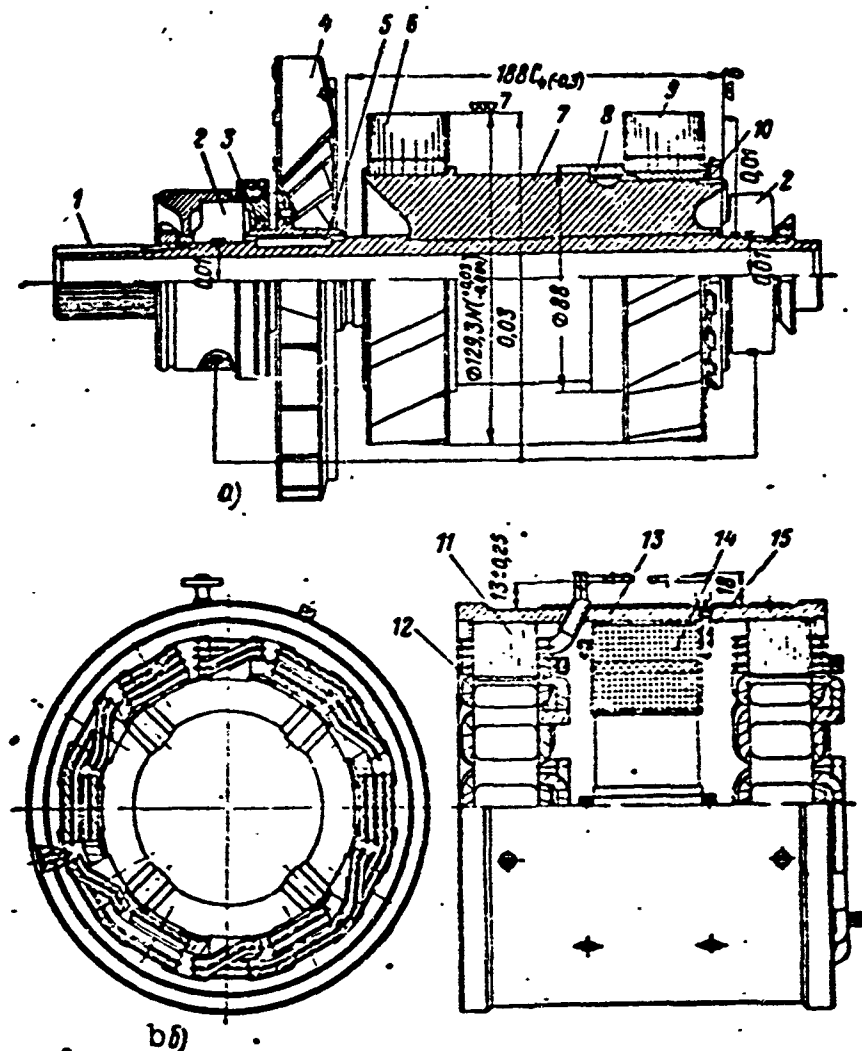


Fig. 5.16. Construction of 30 kva 1200 cps 12,000 rpm double-unit homopolar single-phase aircraft induction generator; a) rotor; b) stator. 1) Shaft; 2) bearing; 3) packing; 4) fan; 5) key; 6) laminated rotor unit; 7) armco rotor sleeve; 8) key; 9) removable rotor unit; 10) nut; 11) laminated stator unit; 12) armature winding; 13) armco stator frame; 14) multilayer field winding; 15) field-winding frame mounting.

exceptions are the losses in the iron of the teeth, where the induction changes only in magnitude, with no change in sign, which affects the magnitude of the hysteresis losses. In the latter case, the specific iron losses can be found in approximation from the equation

$$p_c \approx \sigma_v \left( \Delta \frac{f}{100} \right)^2 + \sigma_g \left[ 1 + a \left( \frac{B_{03}}{10^4} \right)^2 \right] \frac{f}{100} \text{ watt/kg.}$$

The total iron losses are

$$P_c = p_c \left( \frac{B_{12}}{10^4} \right)^2 G_{s1} k_\Delta \text{ watts.}$$

Here  $a \approx 0.5$  is a constant of the material (found empirically);  $k_\Delta = f(\Delta)$  is a technical coefficient;  $\sigma_v = 6.4$  and  $4.8$ ,  $\sigma_g = 3.8$  and  $2.8$  for E3 and E4 steels, respectively;  $B_{03} = \frac{\Phi_1}{k_1 2\pi l} \frac{l_1}{b_{s1} k_{\Delta c}}$  is the constant component of the tooth induction;  $B_{12} = \frac{\Phi_1}{\pi l} \frac{\pi}{2} \frac{l_1}{b_{s1} k_{\Delta c}}$  is the amplitude of the alternating component of the tooth induction.

To conclude, we have shown in Figs. 5.15, 5.16, and 5.17 the construction of single- and two-unit homopolar aircraft induction generators of various powers.

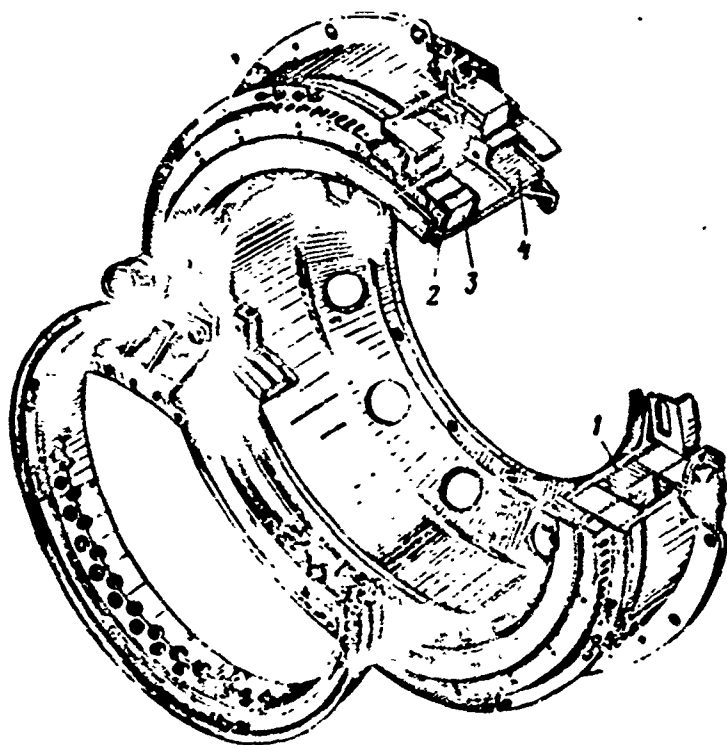


Fig. 5.17. Construction of homopolar two-unit single-phase aircraft induction generator of special design. 1) Field winding; 2) armature winding; 3) armature core; 4) inductor (pole) core.

The Soviet scientists A.Ye. Alekseyev, N.Ya. Al'per, V.P. Vologdin, R.P. Zhezherin, M.M. Krasnoshapka, and M.A. Spitsyn, among others, have made considerable contributions to the development of the theory of the working process and to the development of calculation methods.

Manu-  
script  
Page  
No.

[List of Transliterated Symbols]

437	XЭМЗ = KhEMZ = Khar'kovskiy Elektromashinny Zavod = Khar'-kov Electrical Machinery Plant
442	ск = sk = skos = bevel
443	в = v = возбуждениe = excitation
444	я = ya = yakor' = armature
446	ф = f = forma = form
447	з = z = zubets = tooth
447	п = p = paz = slot
449	ис = is = ispol'zovaniye = utilization
449	м = m = magnit = magnet
450	ср = sr = sredniy = average
453	э = e = elektromagnitnyy = electromagnetic
454	с = s = spinka = supporting body
455	щ = shch = shchel' = slot
455	г.п = r.p = raskrytiye pazov = gap opening
456	н = n = nagruzochnyy = load
456	к = k = korotkogo zamykaniya = short-circuit
456	х = kh = kholostoy = no-load
462	э.с = z.s = zubtsy statora = stator teeth
462	э.р = z.r = zubtsy rotora = rotor teeth
462	экв = ekv = ekvivalentnyy = equivalent
463	я.р = ya.r = yarmo rotora = rotor yoke

463 я.с = ya.s = yarmo statora = stator yoke  
464 и = i = induktivnyy = inductive  
466 ~~24~~ = gts = gertsy = cycles per second  
468 y = u [not identified]  
468 p = r [not identified]  
471 с = s = stal' = steel (iron)  
471 в = v [not identified]  
471 r = g [not identified]



## Chapter 6

### DIRECT-CURRENT AIRCRAFT GENERATORS

#### 6.1. GENERAL INFORMATION ON DIRECT-CURRENT AIRCRAFT GENERATORS

Three basic direct-current generator series have come into use in Soviet aviation: the DSF series, 0.3-1.0 kw power, 12-24 v; the GS self-cooled series, 0.35-1.0 kw power, 27.5 v; the GSR high-speed series using forced cooling, 1.5-18 kw power, 28.5 v.

Table 6.1 gives the basic technical data for these series of direct-current aircraft generators, ranging in power from 0.3-18 kw, while Figs. 6.1, 6.2, and 6.3 illustrate their construction.

An analysis of the data indicates the high technical level of the GSR series of direct-current aircraft generators, which are characterized by structural reliability, good performance up to altitudes of 15 km or more, high speed ( $n = 3800-9000$  rpm), high utilization efficiency (3.7-2.0 kg/kw), and high electromagnetic loads:  $A = 300-450$  amp/cm with  $P_{nom} = 3-30$  kw. The air induction is  $B_\delta = 6000-7000$  gauss, the current density in the armature winding is  $j = 15-20$  amp/mm<sup>2</sup>, in the commutating-pole winding and compensation winding,  $j_{d.p} \approx j_{k.o} = 10-12$  amp/mm<sup>2</sup>, in the field winding,  $j_v = 6-8$  amp/mm<sup>2</sup>, while at the brush contact  $j_{shch} = 20-30$  amp/cm<sup>2</sup> with  $P_{nom} = 3-30$  kw.

At the present time, aircraft use a single-wire direct-current electrical system at 28.5 v, with the negative side grounded.

The utilization of high-voltage direct current (120 or 220 v) reduces the reliability of the electrical system.

TABLE 6.1

## Basic Technical Data for Direct-Current Aircraft Generators

1 Тип генератора	2 Номинальные данные				7 Вес G кг	8 Отно- ситель- ный вес G/P <sub>н</sub> кг/квт	9 Вы- сот- ность H км	10 Расход и давление воздуха дм <sup>3</sup> /сек и мм вод. ст.	11 Габариты		14 Число полюсов		17 Тип щеток
	3 Мощ- ность P <sub>ном</sub> квт	4 На- пря- жение U в	5 Ток I а	6 Скорость n об/мин					12 Ди- аметр D мм	13 Дли- на l мм	15 Ос- нов- ных 2р	16 До- пол- нитель- ных	
20 ДОС	0,3	12	25,0	3,0—3,5	14,5	48,5	5,0	18 Внешний самообдув					
21 ДСФ-500	0,5	24	20,8	2,2—4,5	13,7	27,4	5,0						
21 ДСФ-650	0,65	24	27,1	2,2—6,5			5,0						
21 ДСФ-1000	1,0	24	41,7	4,0—6,0	13,0	13,0	8,0						
22 ГС-350	0,35	27,5	12,7	3,8—5,4	7,6	21,5	12	Внешний самообдув	128	305,5	4	—	ЭГ-8 25
22 ГС-650	0,65	27,5	23,6	3,8—5,4	12,0	18,5	12	18	128	305,5	4	—	ЭГ-8 25
22 ГС-1000	1,0	27,5	37,0	3,8—5,4	14,4	14,4	12		128	305,5	4	—	ЭГ-8 25
23 ГСК-1500	1,5	27,5	54	3,8—5,5	11,7	7,8	15	19 Продув 30/	130	265	4	—	ЭГ-8 25
24 ГСР-3000	3,0	28,5	100	4,0—9,0	11,0	3,67	15	40/			4	4	МГС-726
24 ГСР-6000	6,0	28,5	200	4,0—9,0	18,5	3,08	15	70/260	140	315	4	4	МГС-726
24 ГСР-9000	9,0	28,5	300	4,0—9,0	24,0	2,67	15	95/260	166	386	6	3	МГС-726
24 ГСР-12000	12,0	28,5	400	4,0—9,0	28,0	2,34	15				8	4	МГС-726
24 ГСР-18000	18,0	28,5	600	3,8—9,0	41,5	2,23	15	235/400	198	480	8	4	МГС-926

1) Type of generator; 2) ratings; 3) power  $P_{nom}$ , kw; 4) voltage  $U$ , v; 5) current  $I$ , amp; 6) speed  $n$ , rpm; 7) weight  $G$ , kg; 8) weight-to-power ratio  $G/P_n$ , kg/kw; 9) altitude  $H$ , km; 10) air flow rate and pressure, dm<sup>3</sup>/sec, mm H<sub>2</sub>O; 11) dimensions; 12) diameter  $D$ , mm; 13) length  $l$ , mm; 14) number of poles; 15) main, 2p; 16) commutating; 17) type of brushes; 18) external self-ventilated; 19) forced-air; 20) DOS; 21) DSF-xxx; 22) GS-xxx; 23) GSK-1500; 24) GSR-xxxx; 25) EG-8; 26) MGS-x.

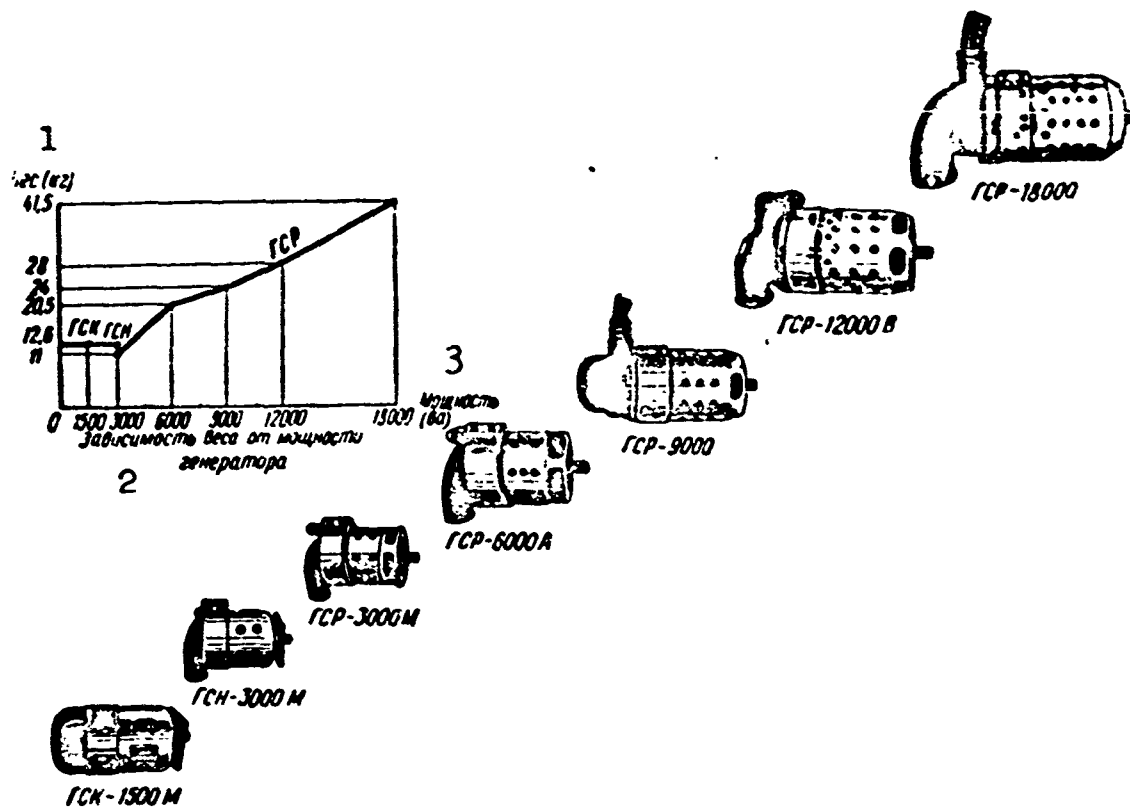


Fig. 6.1. Series GSR direct-current aircraft generators.  
1) Weight (kg); 2) weight as a function of generator power;  
3) power (volt-amperes).

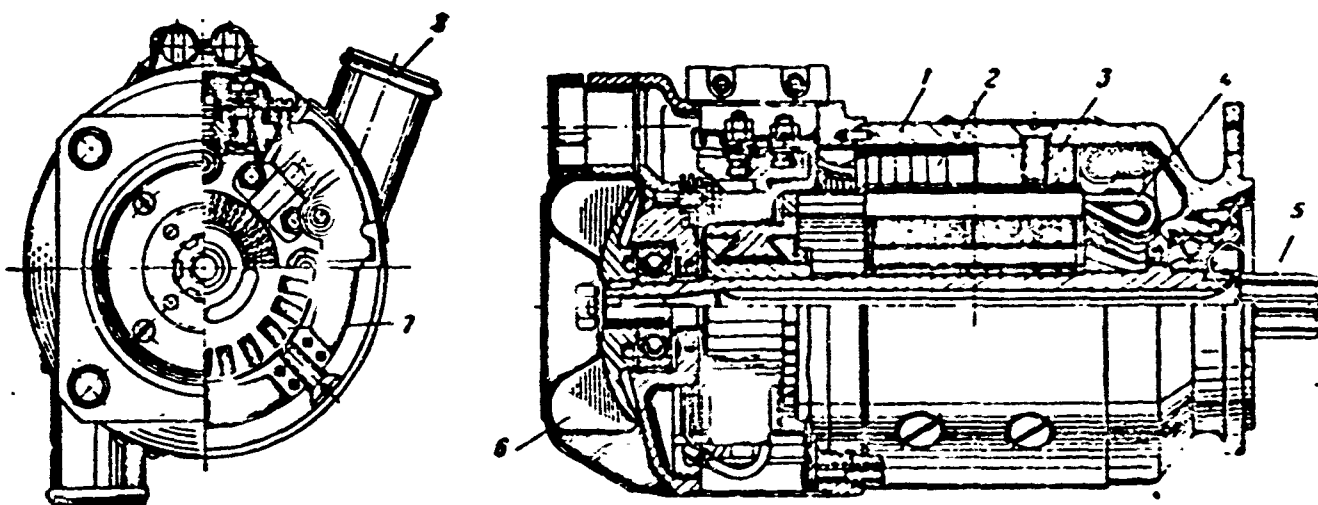


Fig. 6.2. GSK-1500M generator. 1) Frame-monoblock; 2) field winding; 3) pole core; 4) armature winding; 5) shaft; 6) fan; 7) armature; 8) air intake.

### Dimensions of Direct-Current Generators

Effect of rated voltage on dimensions of aircraft generator. As we know, when the voltage increases, the volume and weight of the armature increase, while the volume and weight of the commutator decrease. As a matter of fact, the armature volume may be represented by the

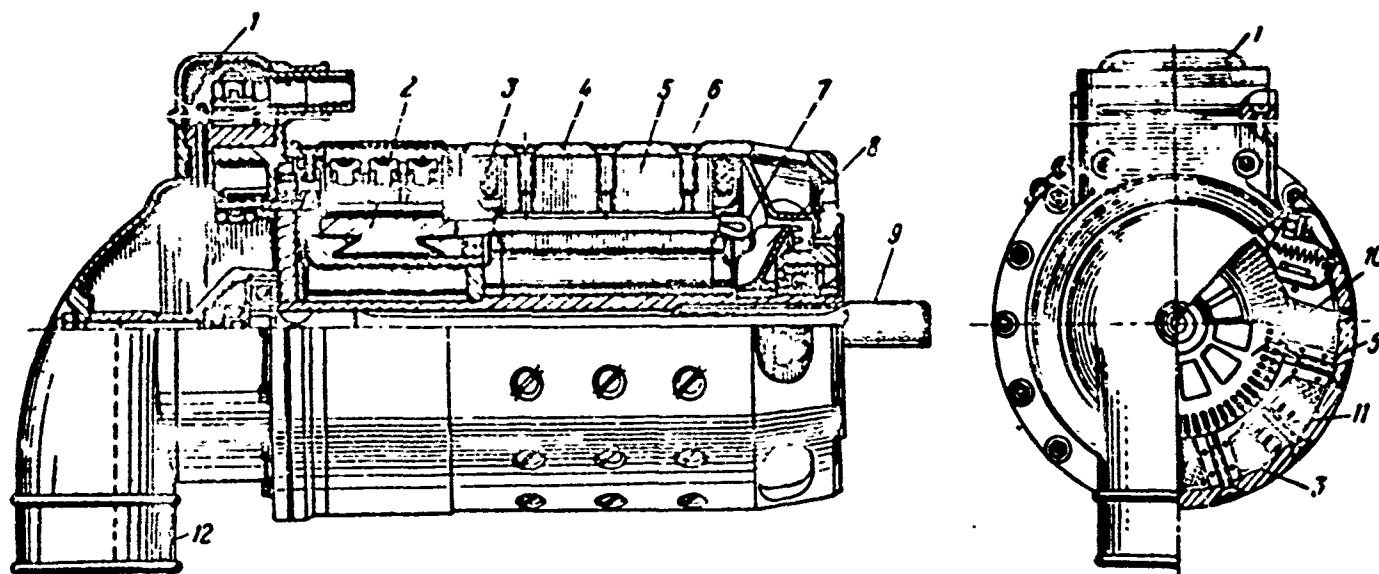


Fig. 6.3. 12 kw generator. 1) lead box; 2) commutator; 3) field winding; 4) housing; 5) pole; 6) pole mounting; 7) armature winding; 8) fan; 9) flexible shaft (spring); 10) armature; 11) commutating pole; 12) air inlet.

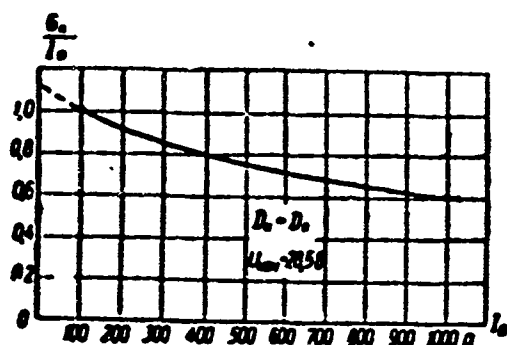


Fig. 6.4. Relative weight of aircraft-generator commutator as function of armature current.

equation

$$D^2 l = \frac{6.1 P_e 10^3}{\pi A B_{\delta, \text{cp}}} \text{ cm}^3, \quad (6.1)$$

where  $D$  and  $l$  are the armature diameter and length, cm;  $P_e$  is the electromagnetic power, kw;  $A$  is the linear load, amp/cm;

$B_{\delta \text{sr}} = \alpha B_{\delta}$  is the mean air-gap induction, gauss.

Even though the rated voltage does not enter into this expression, as this quantity increases, there is a reduction in the current, the total number of armature-winding conductors increases in proportion to the voltage, and there is also an increase in the thickness of the armature-slot insulation. This causes a drop in the slot fill factor  $k_{z.p}$ .

As a result, with  $B_{\delta \text{sr}} = \text{const}$  remaining unchanged, the linear load  $A$  should be decreased, since with the current density unchanged, the cross-sectional area of the armature-winding copper should be decreased for the same slot cross section.

Thus either the machine power will drop with the dimensions remaining unchanged ( $D^2l = \text{const}$ ), or the armature dimensions will increase ( $D^2l = \text{var}$ ) with the electromagnetic load unchanged ( $AB_{\delta sr} = \text{const}$ ).

Thus, as the rated voltage increases, the armature size and weight also increase.

The dimensions of the commutator are basically determined by the magnitude of the rated armature current. Consequently, in first approximation the commutator size and weight will be inversely proportional to the rated voltage. Actually, the relationship  $G_k = f(U_n)$  is affected by: the commutator diameter, reactance voltage, potential difference between neighboring commutator segments, etc.

As the voltage goes up, the decreasing commutator weight tends to compensate for the increased armature weight, although this does not prevent the reactance emf from increasing or remove structural limitations.

Figure 6.4 shows the relative commutator weight as a function of armature current; the curve, plotted from data for existing aircraft machines, represents

$$\frac{G_k}{I_a} = f(I_a).$$

The relative commutator weight for an armature current of 100 amp is taken as unity.

Figure 6.5 gives curves for the total weight of an aircraft direct-current generator as a function of the torque  $P_e/n$  for  $U_{\text{nom}} = 30$  v (curve A) and  $U_{\text{nom}} = 120$  v (curve B), and of the speed for  $U_{\text{nom}} = 30$  v.

The curves are plotted from the empirical formulas

$$G = 14 \left( \frac{P_{\text{nom}}}{n} \right)^{0.67} \text{ kg} \quad (6.2)$$

for generators with rated voltage of  $U_{\text{nom}} = 30$  v, and

$$G = 15,2 \left( \frac{P_{\text{nom}}}{n} \right)^{0,61} \text{ kg} \quad (6.3)$$

for generators with rated voltage of  $U_{\text{nom}} = 120$  v.

An analysis of the curves given indicates that low-power generators ( $P_{\text{nom}}/n < 2$ ) of the 30-v type are lighter than 120-v generators; for medium-power generators ( $P_{\text{nom}}/n = 2-4$ ), the 30-v and 120-v machines weigh nearly the same; for high-power generators ( $P_{\text{nom}}/n > 4$ ), the 30-v generators are heavier than the 120-v machines.

Aircraft direct-current generators are built for up to 30 kw power at initial speeds of 3800 rpm. This means that a change to 120 v would lead to a slight weight reduction for generators of 18 kw or more power, while 9- and 12-kw generators would weigh the same, and there would be an increase in the weight of generators of 6 kw or less.

It is clear that for direct-current aircraft motors, especially low-power machines, there will be a considerable increase in weight if they are changed to 60 or 120 v.

In view of this, we shall consider below only 24-30 v direct-current generators.

Effect of initial speed on generator size. The size and weight of the armature, for a constant utilization efficiency ( $AB_{\text{gr}}$ ) will be inversely proportional to the speed

$$\frac{V_{s1}}{V_{s2}} = \frac{n_2}{n_1}. \quad (6.4)$$

Actually, the machine utilization efficiency, equal to

$$\sigma = 1,65 AB_{\text{gr}} 10^{-3}, \quad (6.5)$$

may increase as the speed goes up, since the cooling ability of the armature surface will increase.

Commutator volume and weight are nearly independent of speed.

If we were to construct a series of aircraft generators using an

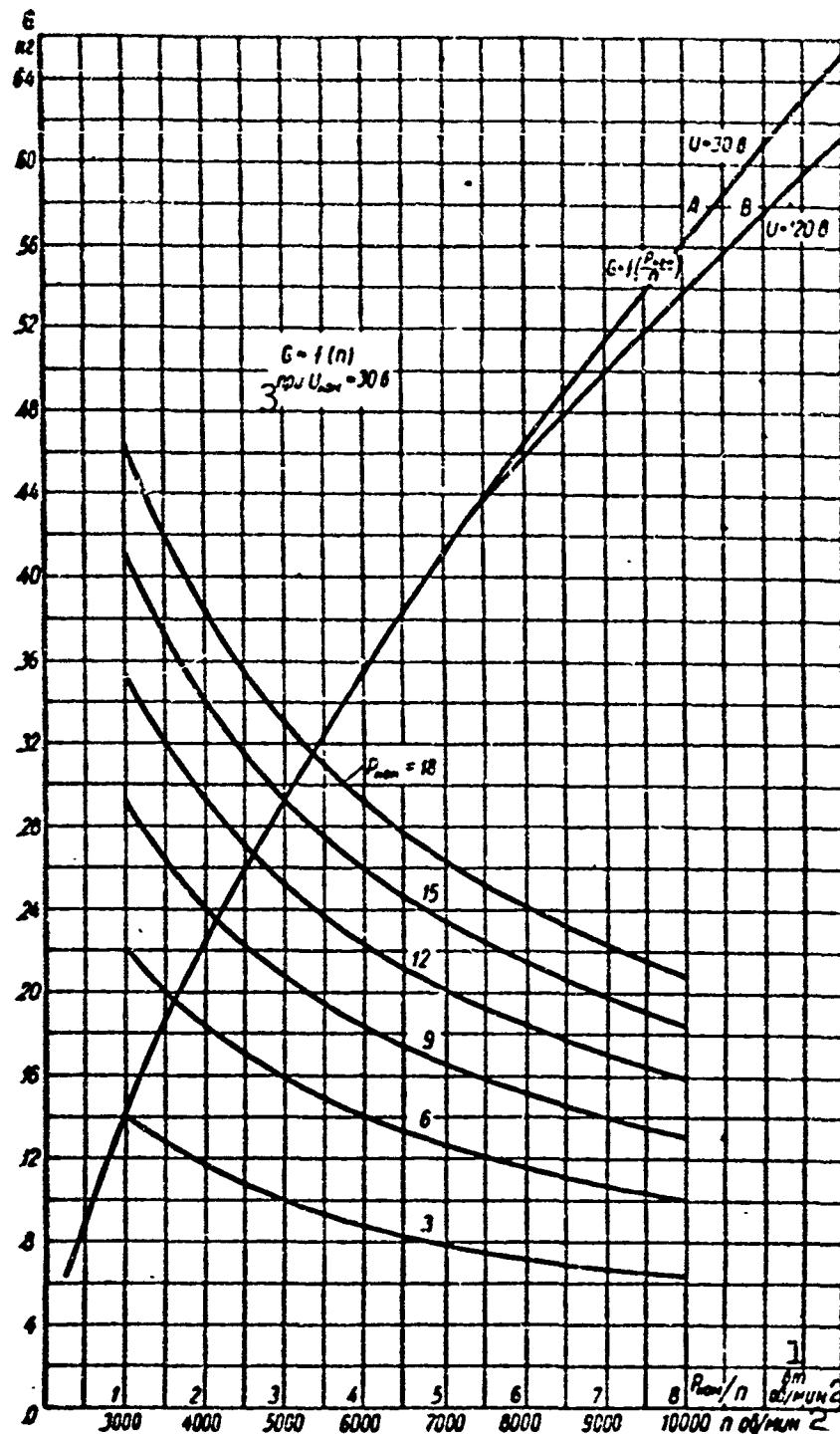


Fig. 6.5. Total weight of aircraft generators as a function of speed and torque. 1) Watts; 2) rpm; 3) for.

initial speed of 4500 rpm rather than 4000 rpm, we should expect a drop in generator weight, considering (6.2), by the ratio

$$\frac{G_1}{G_2} = \left[ \frac{\left( \frac{P_{nom}}{n} \right)_1}{\left( \frac{P_{nom}}{n} \right)_2} \right]^{0.87} = \left( \frac{n_2}{n_1} \right)^{0.87} \approx 1.11.$$

i.e., by about 11%.

From the point of view of mechanical strength of the armature, there are no difficulties involved in increasing the speed to 10,000 rpm; here the commutator dimensions may be determined on the basis of commutation conditions, using the previous peripheral speeds. In this case, generator weight will be reduced by about 13%.

Thus, we can recommend a further increase in initial speed of aircraft generators to 4500-5000 rpm. If we increase generator initial speed to 8000 rpm, there will be a weight reduction by about a factor of 1.65,

$$\frac{G_1}{G_2} = \left( \frac{n_2}{n_1} \right)^{0.67} \approx 1.65,$$

while if the speed is held constant (with the aid of special devices), it is possible to reduce the generator weight sharply or to raise the rated power considerably, to improve operating characteristics, since the machine will operate at constant speed, to reduce excitation power and the dimensions of the voltage-regulation apparatus considerably, and to increase the accuracy of voltage regulation, since the range over which the excitation current varies will be reduced.

Thus in certain cases, we may recommend the utilization of constant-speed clutches for aircraft direct-current generators; such devices provide a rotational speed that is constant to within  $\pm 5\%$ .

### Structural Elements

Structural differences between aircraft generators and machines designed for ground use are caused by installation and cooling conditions, as well as by the attempt to decrease size and weight as much as possible.

For the sake of example, we shall give a brief description of aircraft generators designed for high altitudes and high speeds,



where it is possible to use air cooling.

Figures 6.6, 6.7, 6.8, and 6.9 show the construction of direct-current aircraft generators using the pressure of the oncoming airstream.

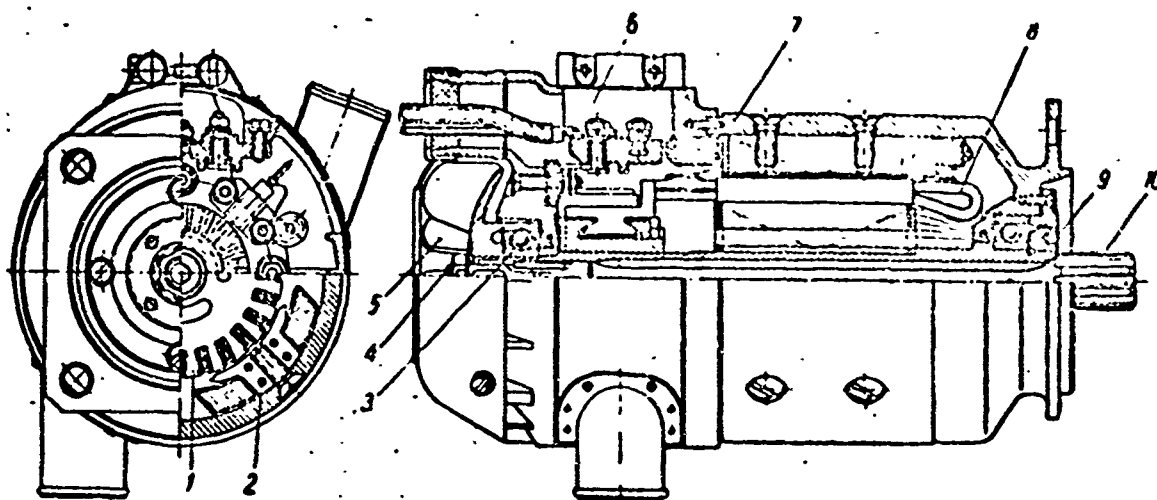


Fig. 6.6. Construction of GSK-1500 M generator, no commutating poles. 1) Armature; 2) pole with winding; 3) bearing; 4) flexible-shaft mounting; 5) fan; 6) terminal box; 7) frame; 8) armature winding; 9) hollow shaft; 10) flexible shaft.

The generators are of the plan type, protected construction, using shunt excitation without compensation. The generators are mounted on the aircraft engine by the flange, and are driven through a reducing gear and a flexible splined shaft. The gland packing of the reducing gear keeps oil from getting into the generator. Type GSK-1500M generators do not use commutating poles, while both GSR-3000 and GSR-6000 generators use a full set of commutating poles, while GSR-9000, GSR-18,000, and GSR-12,000 generators are provided with a half-set of commutating poles. The arrangement of the structure is clear from the figures.

Armature core. The armature-core assembly of a direct-current machine is made up of stamped laminations of electrical-grade steel, insulated from each other and installed perpendicular to the shaft. As a rule, the sheets from which the laminations are stamped are  $\Delta = 0.5$

0.2 mm thick. Steel 0.5 mm thick is used for a magnetic-reversal frequency  $f = 50$  cps; where  $f > 50$  cps but less than 1000 cps,  $\Delta = 0.35$  mm, while when  $f > 1000$  cps, it is desirable to use steel that is of the order of 0.2-0.25 mm thick.

The slots in the armature laminations (in which the coil is wound) are made by single-pass stamping, which ensures good quality and rapid manufacture. Individual slot punches are used only in the manufacture of one-of-a-kind or experimental machines. The armature slots are made half-open or completely open, as a rule with parallel walls. With half-open slots, the armature winding is sometimes placed into the core slots from the end.

The armature core is either press-fitted onto the shaft (GSK-1500 generators) or onto a hollow sleeve - a hollow steel shaft. Final fiber-glass laminate sheets are placed at the ends of the assembly; they are held against the armature assembly by backup washers made from an aluminum alloy. These washers hold the assembly together, so that the steel laminations of the assembly cannot come apart.

Torque is usually transmitted to general-purpose machines with the aid of prismatic keys. In aircraft machines, a knurled surface with no key is used.

Core mounting. The following elements are used to mount the armature core in the axial direction:

- a) press-fitted end washers;
- b) thrust rings, shrink-fitted onto the shaft;
- c) self-locking split thrust rings, installed in circular shaft grooves;
- d) coil holders.

Aluminum backup washers have been used in direct-current aircraft machines.

In medium- and high-power machines, the armature core is provided with axial vents for the cooling air. Radial ventilation ducts are not provided, since the length of an assembly in a direct-current aircraft machine does not exceed 125 mm.

The slots are frequently skewed in the armature core for a distance equal to one or one-half slot pitch. As a rule, the slots are skewed to the left, i.e., the armature slots form a left-hand spiral resembling a left-hand thread.

Figures 6.10 and 6.11 show the normal structural composition of a typical armature in a modern aircraft generator.

Armature winding. The choice of armature-winding type is dictated by the power, voltage, and speed.

In order to make the best possible use of the active band of the machine, it is desirable to have the smallest possible number of parallel circuits, and the maximum conductor cross-sectional area.

Here, however, commutation conditions and temperature-rise considerations limit the current in a circuit to no more than 300 amp in general-purpose machines and 100 amp in aircraft machines.

In aircraft generators of less than 6 kw power, a wave-type armature winding is used, while for 6 kw or more, a lap winding is used.

The basic advantage offered by the lap winding is the forced distribution of current among the circuits, which improves commutation conditions; the drawback to this type of winding is its sensitivity to magnetic-system asymmetry.

In order to prevent equalizing currents from flowing through the brushes, with multipole lap windings and multiple wave windings, several points on the winding that would be at the same potential were the field to be fully symmetric are connected together by low-resistance equalizers.

The equalizers carry a variable current that compensates for pole-flux asymmetry and improves commutation conditions. It is clear that this will be accompanied by some additional heating of the arma-

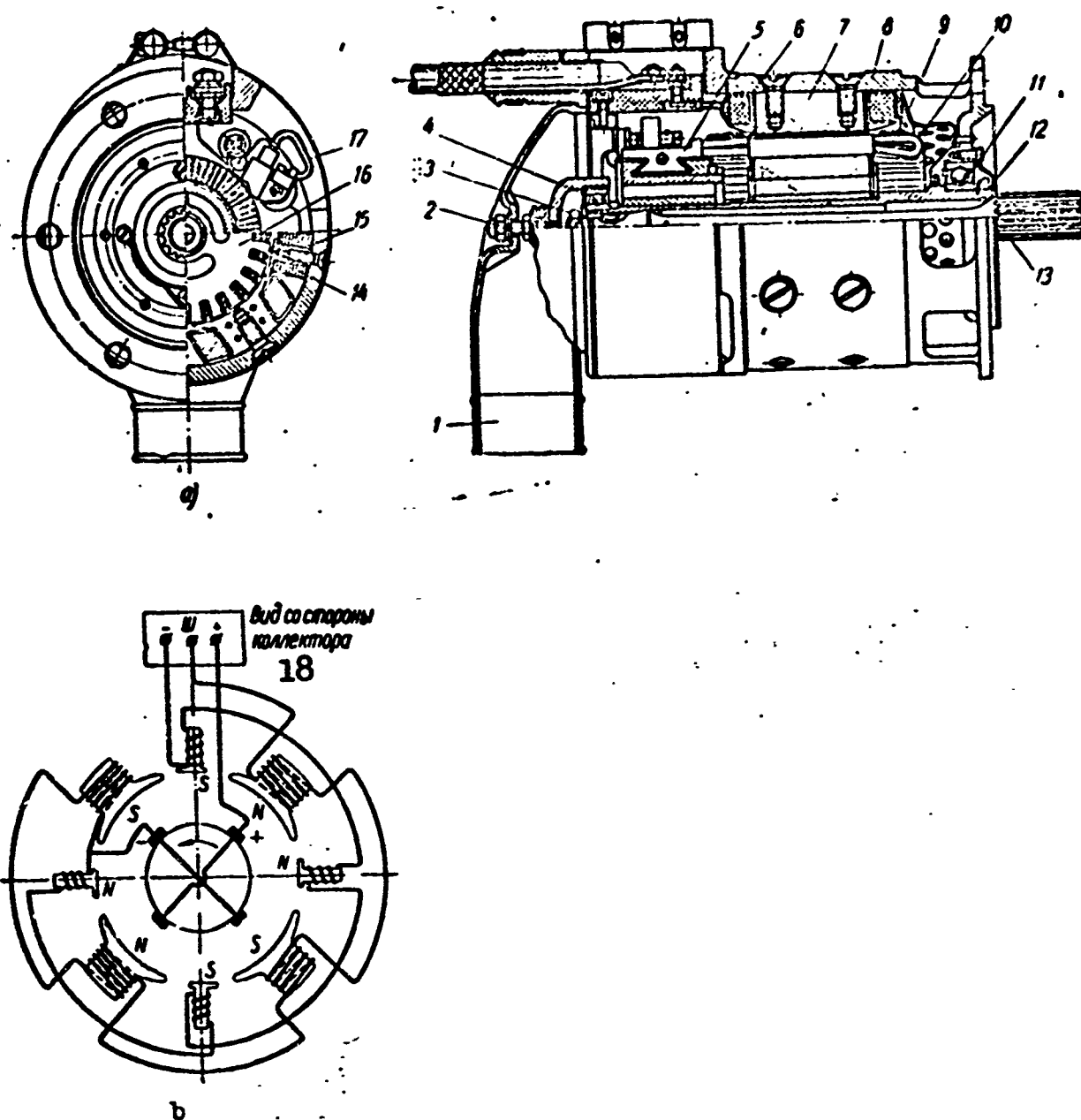


Fig. 6.7. Construction (a) and wiring diagram (b) of GSR-3000 generator with full complement of commutating poles. 1) Cap; 2) cap mounting; 3) flexible-shaft mounting; 4) bearing; 5) commutator; 6) field winding; 7) poles; 8) housing (mono-block); 9) protective guard; 10) armature winding; 11) bearing; 12) hollow shaft; 13) flexible shaft; 14) commutating-pole winding; 15) commutating pole; 16) armature; 17) brush-holder; 18) view from commutator.

ture winding. The number of equalizers that will maintain the equipotential points on a lap winding will equal

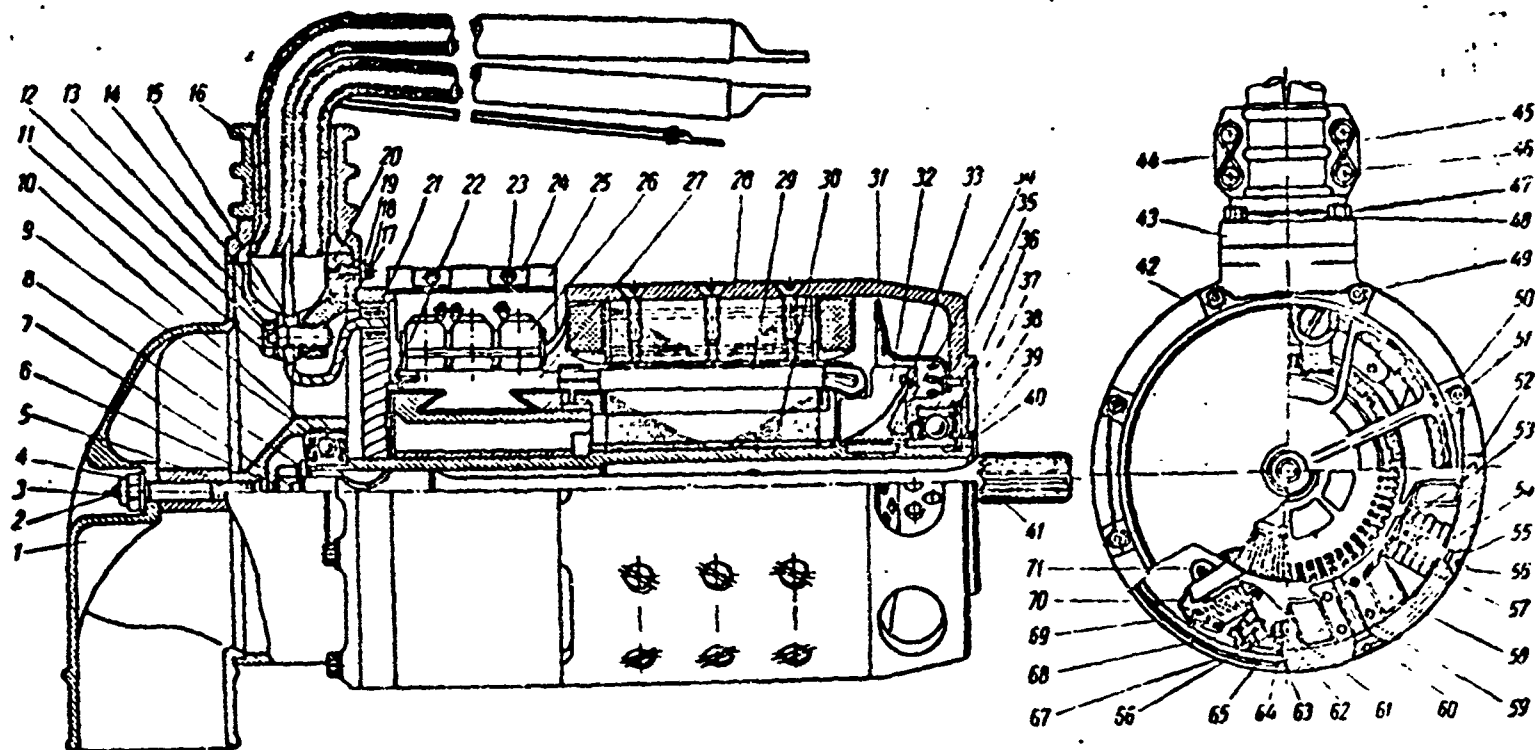


Fig. 6.8. Construction of 9-kw generator with full complement of commutating poles. 1) Cap; 2) bolt; 3) self-locking nut; 4) washer; 5) sleeve; 6) nut; 7) locking tab; 8) washer; 9) ball bearing; 10) key; 11) bolt; 12) locking tab; 13) laminated-fabric gasket; 14) lead; 15) flexible bus; 16) rubber cushion; 17) screw; 18) screw; 19) washer; 20) terminal panel; 21) ring (interbrush connection); 22) equalizers; 23) screw; 24) shaft; 25) protective strip; 26) brushes; 27) commutator; 28) frame; 29) armature; 30) hollow shaft; 31) guard; 32) fan; 33) key; 34) washer; 35) ball bearing; 36) trap; 37) snap ring; 38) spacer; 39) locking tab; 40) nut; 41) flexible shaft; 42) guard; 43) nipple; 44) clamp; 45) washer; 46) screw; 47) bolt; 48) washer; 49) bolt; 50) washer; 51) bolt; 52) pin; 53) commutating pole; 54) brass gasket; 55) screw; 56) commutating-pole winding; 57) laminated-fabric gasket; 58) field winding; 59) main pole; 60) screw; 61) nut; 62) washer; 63) screw; 64) laminated-fabric sleeve; 65) mica washer; 66) micanite cover; 67) micanite insert; 68) screw; 69) spring; 70) lever; 71) brushholder.

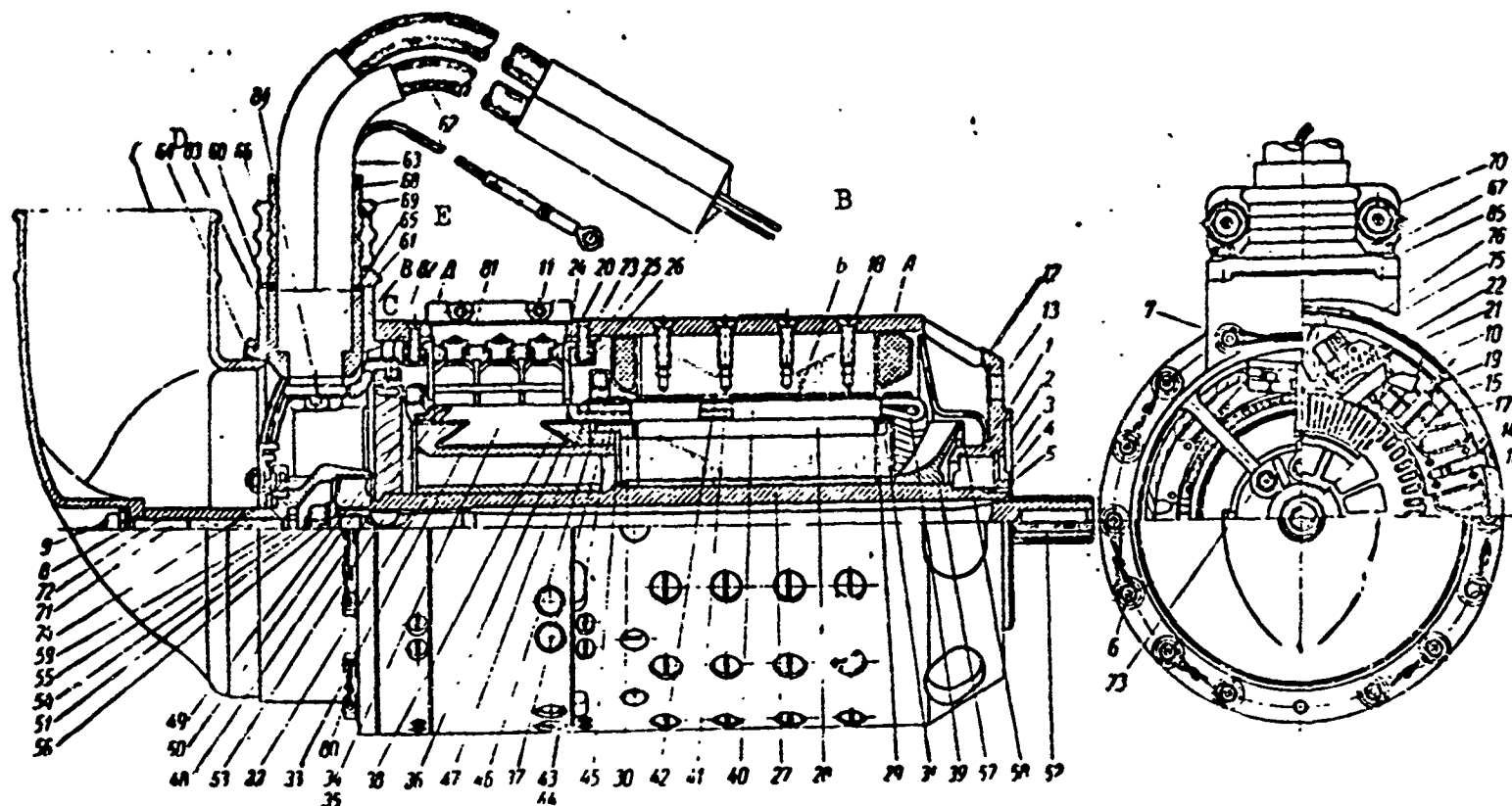


Fig. 6.9. Construction of 18-kw generator. A) Housing with poles, windings, and brushholders; B) armature (with winding and commutator); C) housing with terminal leads; D) intake; E) protective strip. 1) No. 140806 ball bearing; 2) snap ring; 3) spacer; 4) locking tab; 5) special nut; 6 and 7) bolts; 8) washer; 9) self-locking washer; 10) brushes (unit); 11) screw; 12) frame; 13) protective grill; 14) main pole; 15) commutating pole; 16) field winding; 17) commutating-pole windings; 18) screw; 19) diamagnetic insert; 20) brushholder; 21) cylindrical coil spring; 22) lever; 23) screw; 24) insulating insert; 25) insulating sleeve; 26) nut; 27) hollow shaft; 28) steel assembly; 29) insulating sheet; 30 and 31) backup washers; 32) spider; 33) commutator sleeve; 34) commutator segment; 35) insulating insert; 36) backup washer; 37) nut; 38) insulating cone; 39) armature winding; 40 and 41) inserts; 42) wedge; 43) mica strip; 44) insulation; 45) insert; 46) insulation; 47) band; 48) copper pin; 49) equalizer ring; 50) insert; 51) No. 30804 ball bearing; 52) spring (shaft); 53) key; 54) washer; 55) nut; 56) locking tab; 57) fan; 58) brass disk; 59) guard; 60) plastic pad (block); 61) tip; 62) conductor; 63) vinyl tube; 64) shunt-winding lead; 65) rubber gasket; 66) nipple; 67) bolt; 68) sheet rubber; 69) clamp; 70 and 71) bolts; 72) sleeve; 73) screw; 74) terminal

strip; 75) bolt; 76) locking tab; 80) washer; 81) insert; 82) inter-brush connection; 83) bolt; 84) locking tab; 85) washer.

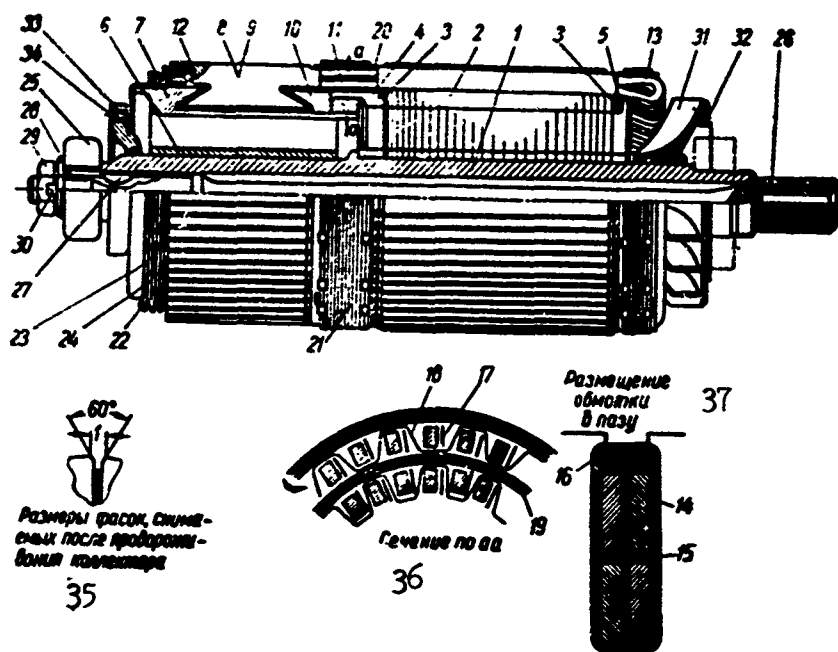


Fig. 6.10. Construction of armature for 18-kw generator. 1) Hollow shaft; 2) steel assembly; 3) insulating sheet; 4) backup washer; 5) backup washer; 6) spider; 7) commutator sleeve; 8) commutator segment; 9) insulating insert; 10) backup washer; 11) nut; 12) insulating cone; 13) armature winding; 14) insert; 15) insert between tiers; 16) wedge; 17) mica strip; 18) insulation; 19) insert; 20) insulation; 21) banding; 22) copper pin; 23) equalizer circuit; 24) insert; 25) ball bearings; 26) spring; 27) key; 28) washer; 29) nut; 30) locking tab; 31) fan; 32) brass disk; 33) flange; 34) gland packing; 35) dimensions of bevels made after commutator grooves have been cut; 36) section through AA; 37) arrangement of winding in slot.

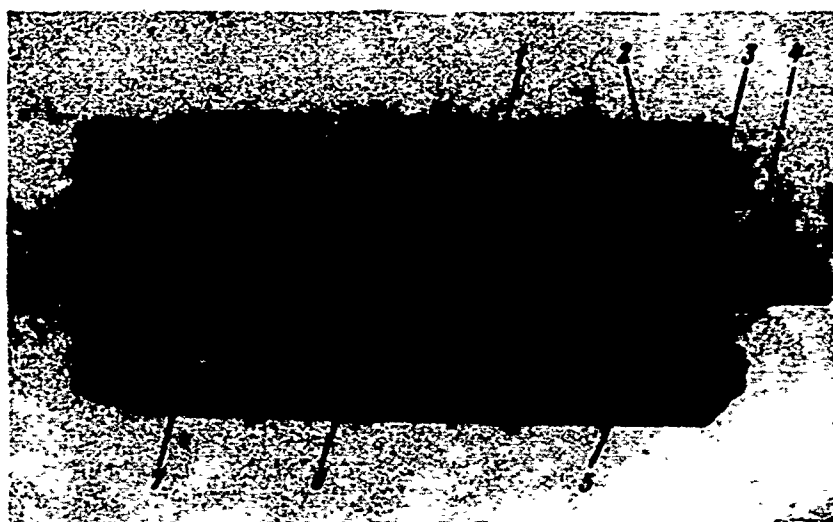


Fig. 6.11. Aircraft-generator armature; 1) Armature winding; 2) commutator segment; 3) ventilation duct; 4) hollow shaft; 5) commutator; 6) armature core; 7) banding [Callouts 1 and 7 appear to have been interchanged].

$$n_{yp} = \frac{K}{a},$$

where  $K$  is the number of collector segments;  $a$  is the number of pairs of parallel armature-winding circuits.

If the full number of equalizers were to be used, the machine would become heavier and more complicated. As experience has shown, we can limit ourselves to a considerable smaller number of equalizers, in particular:

$$n_{yp} \approx (0,15 + 0,3) \frac{K}{a},$$

where the first number corresponds to low-power generators (6-9 kw) and the second to generators of 18-30 kw power.

The equalizers are made in the form of copper rings whose faces are soldered to the commutator segments. Electro Karton [cardboard] inserts are used to insulate the rings. The cross-sectional area of all equalizers may be taken to equal 10-15% of the cross section of all armature-winding conductors. The cross-sectional area of a connecting ring normally equals 50-60% of the armature-winding conductor cross section.

Figure 6.12 shows an equalizer-connection circuit for an 18-kw generator.

For high-power heavy-duty aircraft generators, it may prove useful to use a "frog-leg" winding, which combines the characteristics of the armature winding and a complete equalizer system.

In modern aircraft generators, the slot insulation is made 0.2 mm thick on each side.

Armature-winding mounting. The armature winding is prevented from moving radially with the aid of wedges in the active zone and wire or hollow cylindrical banding at the end section.

For high speeds, hollow steel thin-walled cylinders are used in



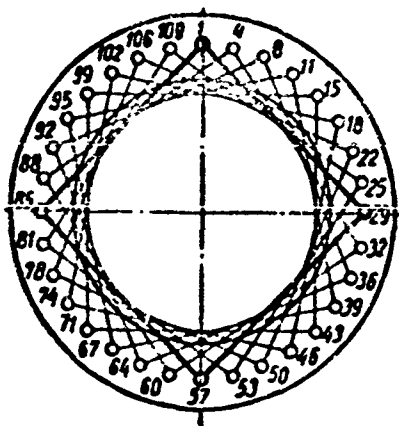


Fig. 6.12. Equalizer-circuit for commutator of aircraft generator.

place of wire banding; the cylinders are fitted over the end sections of the winding. As a rule, wire banding is of the single-layer type and does not exceed 10-15 mm in width. A nonmagnetic wire 0.5 mm in diameter with a yield point  $\sigma_s = 180 \text{ kg/mm}^2$  is used

for banding purposes. The banding is fastened by means of tin clips 0.3 mm thick or

by means of clips formed from tinned strip copper. In aircraft machines, the banding clips are made from Type M1 tinned strip copper which is  $h = 0.2 \text{ mm}$  thick and  $b = 5 \text{ mm}$  wide. In special cases, clip thickness may be reduced to 0.1 mm.

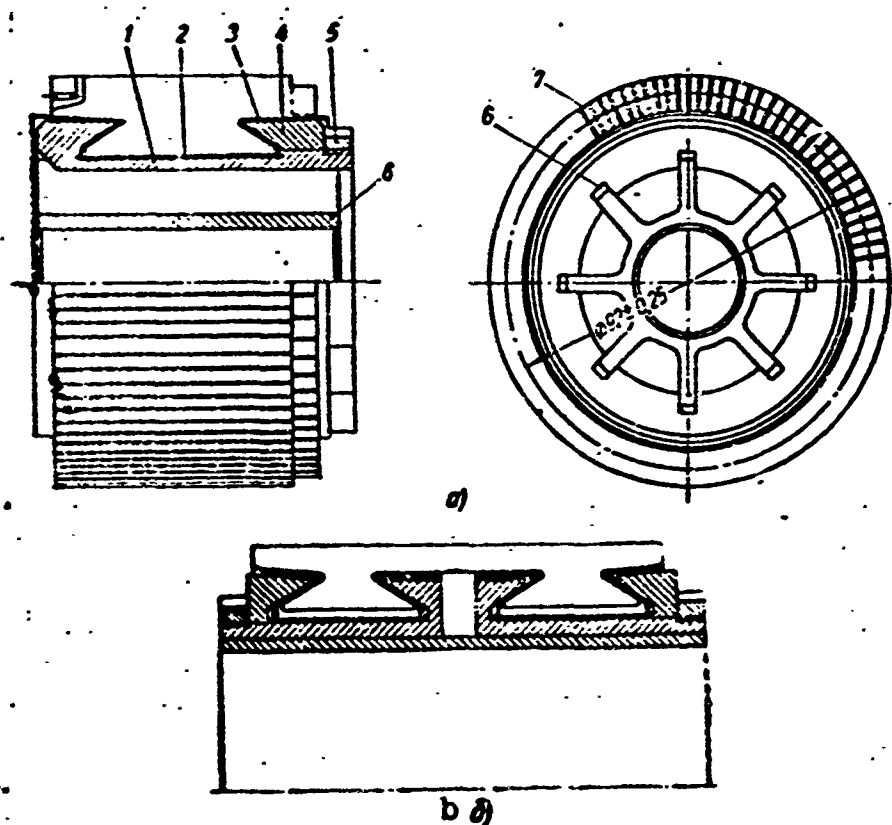


Fig. 6.13. Aircraft-generator commutator. a) Normal construction. 1) Steel sleeve; 2 and 3) insulation; 4) backup washer; 5) nut; 6) spider; 7) commutator segment; b) double dovetail mounting.

The commutator. The commutator is the most critical element in a

direct-current machine and to a considerable degree determines the conditions necessary for sparkless commutation.

Commutators are classified into five groups by structure: cylindrical commutators pressed into plastic; cylindrical commutators with segments attached by means of dovetailing and conical snap washers; cylindrical commutators with segments attached by means of locking rings; combination cylindrical commutators in which locking rings are used in addition to washers; and disk commutators whose segments are attached with the aid of a locking ring.

Cylindrical commutators using dovetails are classified by method of attaching the segments into arch and clamped types.

In arch-type commutators, only the dovetails are under pressure, while in clamped commutators, the overhung ends of the commutator segments are also held. As a result of this compression, barrel-type bending of the segments is prevented; this is an especially dangerous phenomenon in long and high-speed commutators.

The choice of commutator type is dictated by the speed and current. As a rule, aircraft generators employ cylindrical arch-type commutators consisting of copper-cadmium segments of trapezoidal cross section separated by inserts of solid micanite or mica and assembled into a hollow cylinder.

The commutator attachment fittings consist of two steel beveled washers held by tiebolts or a retainer nut. The commutator segments of direct-current aircraft machines are normally assembled on a steel sleeve (Fig. 6.13a) and fastened by means of a backup washer and nut. The backup washers are insulated from the segments by means of micanite insulating segments.

The commutator attachment fittings should provide a given degree of compression on the insulation between the commutator segments under

all operating conditions in order to prevent radial displacement of the insulation owing to centrifugal forces; they should keep the working surface cylindrical, and maintain plasticity in the axial direction to permit temperature variations and to maintain the cylindrical shape of the surface.

In order to impart the required solidity to the commutator and to test its mechanical strength, the unit is speeded up to an excess speed  $n = 1.45n_{\max}$  while heated to a temperature of  $200-250^{\circ}$ . Commutator runout is of great importance to sparkless commutator operation; in this connection, maximum permissible values of runout have been developed empirically; for aircraft direct-current generators, runout should not exceed 0.025 mm with  $D_k = 60-100$  mm and 0.03 mm with  $D_k = 100-125$  mm.

Finally, the commutator spider ribs should coincide with the armature-core ribs in order to decrease the aerodynamic resistance offered to the stream of cooling air.

For the neutral plane to be properly positioned it is necessary for the armature-slot axis to coincide with the axis of the intersegment insulation, or to be displaced by not more than 0.5 mm. The direction of displacement depends on the direction of rotation and machine operating mode (generator or motor). For series GSR generators, the slot axis can be displaced with respect to the intersegment insulation by 0.5 mm to the right, looking away from the commutator.

The armature winding is connected to the commutator by soldering or welding. Slots are milled into each collector segment. The length and width is determined by the dimensions of the armature wire to be connected and the method used to attach the wire to the commutator segment (by the permissible current density in the contact). If the armature conductors are soldered to the commutator plate, a hard sol-

der is used. Argon welding is frequently used in aircraft machines as it provides reliable contact between the armature winding and the commutator during operation and does not damage the armature-conductor insulation during welding.

In high-power aircraft generators in especially severe service, specially designed commutators are used with double dovetail mounting; this provides reliable commutator operation at considerable temperatures (Fig. 6.13b).

In order to reduce the amount of labor needed to manufacture the commutator and its cost, the number of commutator segments should be reduced to a minimum. In this case, however, we cannot exceed the permissible armature voltage ripple ( $k/p > 3$ ) or the permissible average voltage between neighboring commutator segments, i.e.,

$$U_{k, \text{cp}} = \frac{2U_{\text{nom}} p}{k} < 20 \quad \text{or} \quad \frac{k}{p} > 0.1 U_{\text{nom}}.$$

An upper bound to the number of commutator segments is imposed by the peripheral speed ( $v_k < 50\text{--}60$  m/sec) and the minimum permissible commutator pitch ( $\tau_k > 3$  mm).

Frame and guards. The frame of a direct-current machine acts as a part of the magnetic circuit; it is made of type 10 steel or armco steel.

Frame design will depend on machine function. Generators use a flange-type frame in the form of a single unit, including the guard on the prime mover side. The frame is rolled from armco sheet steel, welded and then annealed, while the frame is welded to the housing and then subjected to heat treatment. The longitudinal frame seam is located along the main-pole axis, which reduces its effect on the frame flux distribution.

It is desirable to use seamless tubing in place of welded armco

sheet-steel frames; substitution of the seamless tubing will reduce consumption of material, simplify production, and raise frame quality.

The joining of frame and flange into one integral unit (monoblock) increases mechanical strength, decreases the number of fittings and machine size, but somewhat complicates processing.

Holes are drilled through the end of the guard for stud bolts which are used to attach the generator to the aircraft engine. There are ports in the frame on the drive side to permit escape of cooling air; they also give access to the generator mounting. At the center of the housing there are holes used to attach the main and commutating poles. To prevent foreign substances from penetrating within the generator, the ports are provided with a cover that is attached to the guard face.

The guards on the commutator end (Fig. 6.14) are made from AL9 aluminum alloy. The guard structure should be strong and should provide access to the brushes and commutators; access is through ports in the guard; the aluminum-alloy brushholder is mounted in the spaces between the ports. A sleeve of type 45 steel is press fitted into the guard; the outside bearing ring is located in this sleeve, which provides a reliable fit for the bearing, which is especially important where the bearing is replaced during assembly or operation, since if there were no steel sleeve, there would be wear on the seating surface.

The guard is attached to the housing with the aid of a seating collar and pin, and is attached to the housing by means of alloy-steel bolts.

Guards can be attached to the frame by means of outside or inside locks. In the first case, the guard covers the frame, while in the second case, on the other hand, the frame covers the guard. As a rule,

internal locking is used in aircraft generators.

Poles and field windings. In medium- and high-power direct-current machines, removable main and commutating poles are used. As a rule, the number of commutating poles equals the number of main poles. In general-purpose bipolar machines of 1-3 kw power and in aircraft machines of up to 25 kw power, a half complement of commutating poles is frequently employed.

The main poles are permeated by a constant flux and they thus can be made solid, from one piece of steel. In this case, however, the pole pieces should be made of 0.5 to 2.0 mm thick sheet steel in order to reduce additional pulsation losses at the surface.

From the manufacturing point of view, it proves desirable to assemble the entire main (laminated) pole from steel sheets placed perpendicular to the shaft axis (Fig. 6.15). Another advantage of the laminated pole is improved magnetic-field response time, which is important in the presence of transience. The layer of surface oxidation also serves as adequate insulation for the laminations; the laminations are held together by rivets or study bolts.

Aircraft machines normally employ rivets; their diameter is chosen with an eye to the fact that the number of rivets per pole should be at least four, while the rivet diameter should be at least 3 mm.

The pole is attached to the frame by screws or bolts. There are two methods of attaching poles to the frame; by drilling holes in the pole core (for low- and medium-power machines) and by drilling a special steel rod located in the pole core (for high-power machines).

The asymmetric shape of the pole piece (see Fig. 6.15) is caused by the fact that where a half complement of commutating poles is used, the main poles are not arranged uniformly around the frame. The distance between the axes of main poles having a commutating pole located

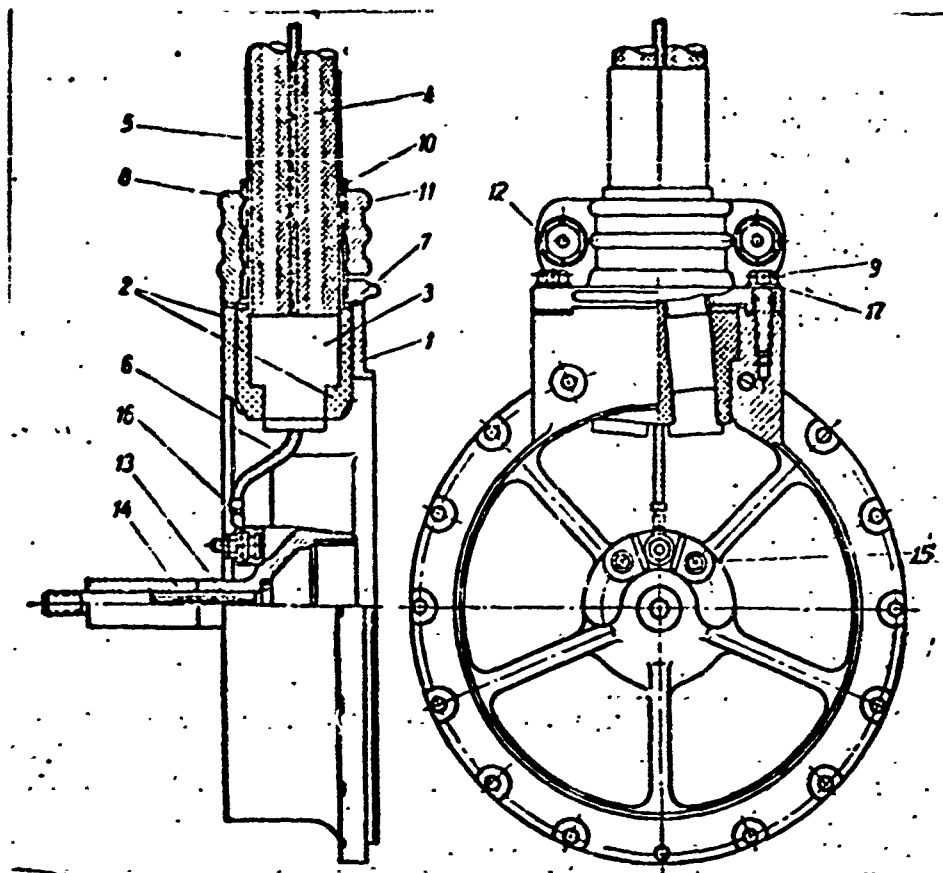


Fig. 5.14. Guard of 18-kw generator as seen from the commutator. 1) Guard; 2) plastic cushion; 3) tip; 4) conductor; 5) vinyl tube; 6) shunt-winding lead; 7) rubber gasket; 8) nipple; 9) bolt; 10) sheet rubber; 11) clamp; 12 and 13) bolts; 14) sleeve; 15) screw; 16) terminal strip; 17) washer.

between them will always be greater than the distance between the axes of main poles not having a commutating pole. At the same time, the pole pitch at the gap remains the same, equaling  $\tau = \pi D / 2p$ .

The pole surface facing the housing should be manufactured to correspond with the inside frame diameter, while the pole-piece profile should follow the design data strictly.

The commutating poles are made from armco steel. The core of the commutating pole is attached to the frame by means of screws, as are the main poles. The asymmetric arrangement of the commutating pole pieces when a half complement is used results from the attempt to decrease the commutating-pole leakage flux.

The field windings of direct-current machines are stationary and

are located on the main and commutating poles. Depending on the excitation method used, the machine will have a parallel (shunt) or sequential (series) field winding or, finally, both a parallel and a se-

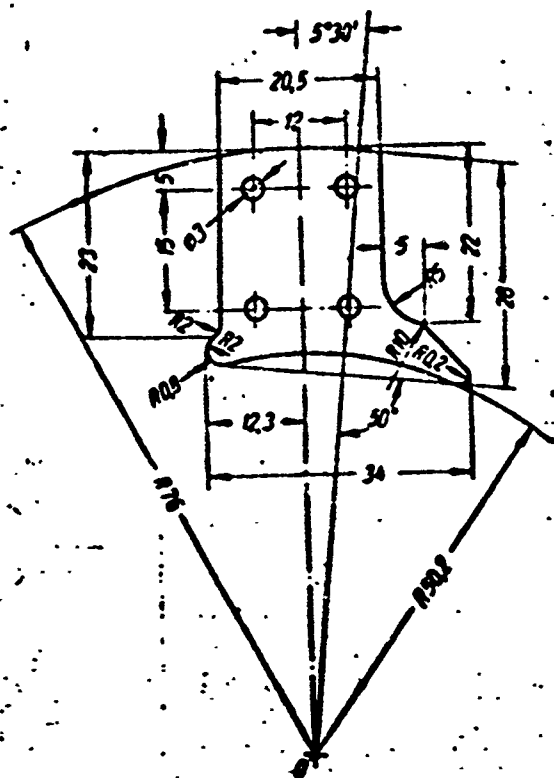


Fig. 6.15. Pole lamination for a generator with half complement of commutating poles.

ries field winding (machines using compound excitation). Machines of more than 3 kw power are usually provided with field windings located on the commutating poles and connected in series into the armature circuit.

Machines subject to a wide range of speed variations and operating under difficult commutation conditions are also provided with compensating field windings placed in the pole pieces of the main poles and also connected in series into the armature circuit.

From the structural viewpoint, there are two types of field winding: concentrated coil windings (wire or ribbon) and distributed windings.

Concentrated windings are normally used to excite main and commu-



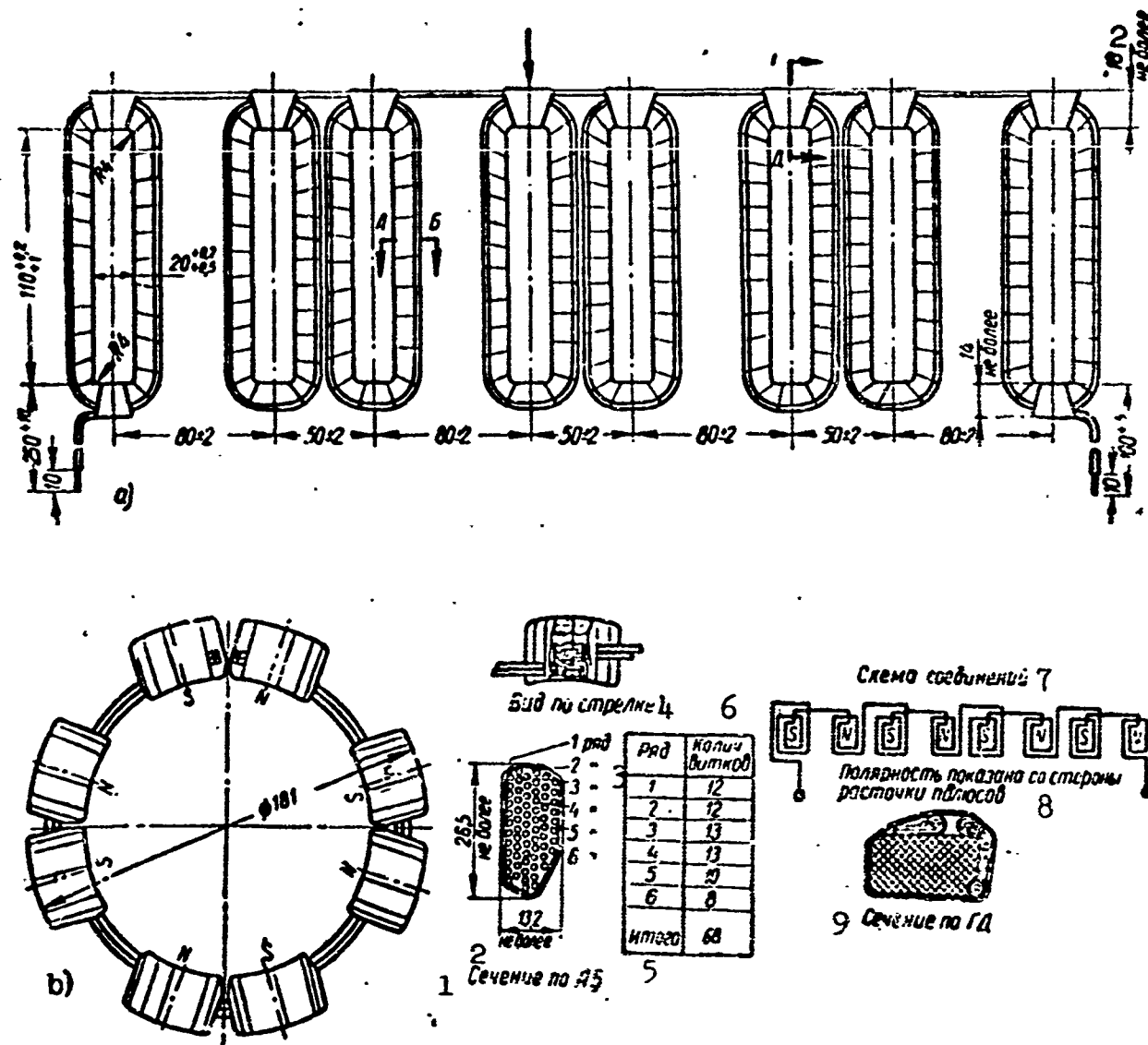


Fig. 6.16. Main-pole field windings and their wiring diagram. 1) Section through AB; 2) no more than; 3) tier; 4) view along arrow; 5) total; 6) number of turns; 7) wiring diagram; 8) polarity is shown looking from pole bore; 9) section through GD.

tating poles. Distributed windings are used for compensation, and in rare special cases to excite the main poles.

Flexible wire coils wound from insulated types PEV-2 or PEM-2 wire are used for the main poles of aircraft machines. The coils are insulated by a single-layer half cover of 0.06-mm thick varnish silk and a single-layer half cover of insulating tape 0.18 thick and 16-20 mm wide. The coils are connected together by means of Type PShchNDO flexible insulated copper conductor, while Type MGShDOLK flexible copper insulated conductor is used for the leads.

The drawings of Fig. 6.16 clearly show the wiring diagram and construction of the field coils for the main poles of an eight-pole aircraft generator.

Wire or ribbon coils may be used for the commutating poles of aircraft machines. As a rule, ribbon coils are used; they are wound from uninsulated copper wire of rectangular cross section bent on the high edge. Figure 6.17 shows the wiring diagram and construction of the commutating-pole windings for an eight-pole machine using a half complement of commutating poles.

The winding turns are insulated by a half covering of 0.06-mm thick varnished silk. Strips of cardboard 0.1 mm thick are placed between the turns.

The side surfaces of the poles are coated with No. 302 varnish and a single layer of 0.1-mm thick cardboard is glued to them.

The windings are dipped in an oily cresol varnish and dried, which improves their moisture resistance.

In order to decrease the leakage flux at the commutating poles, the windings are placed as close as possible to the armature surface.

The compensating windings are made in distributed form. A turn of a compensating winding consists of two straight insulated conductors of round or rectangular cross section, connected together by uninsulated arcs of strip copper.

Shafts. Two types of shafts are made for aircraft electrical machines:

- 1) Shafts for high-speed machines, which form a single unit with the rotor and which are loaded by a distributed load due to their own weight, the unidirectional force of magnetic attraction, and the transmitted torque. These shafts have a central cylindrical section (barrel) and end sections (shanks) of varying cross section. Shafts of

these types are used for synchronous nonsalient pole generators.

2) Shafts with a concentrated load due to the weight of the rotor, the unidirectional force of magnetic attraction, and the transmitted torque, which are sometimes also loaded by a force applied to the free end of the shaft (gear transmission, clutch). This type of shaft is used for direct-current machines. Shafts of the latter type are stepped so that the core, commutator, fan, etc. can be fitted independently.

In order to increase mechanical strength and reduce processing cost, it is desirable to decrease the number of steps and use only the minimum difference between step diameters.

Keyways under the armature core are normally replaced by knurling the shaft by means of toothed rollers, the shaft being polished before and after knurling.

Shafts of general-purpose electrical machines of up to 120 mm in diameter are usually made from Type st. 45 rolled steel in accordance with GOST V1050-52. The shafts of aircraft electrical generators and critical motors are made from 30KhGSA rolled steel.

The shafts of aircraft generators are driven from the aircraft-engine crankshaft through a reducing gear and friction shock-absorbing devices, elastic couplings, or flexible shafts. Since generators have a speed-variation range of 3000-10,000 rpm, a reducing gear with a gear ratio of 1.5-3.0 is used.

Owing to the nonuniform operation of the aircraft-engine prime mover and the nonuniform moment of resistance of certain mechanisms, the shafts of direct- and alternating-current aircraft generators are connected to the aircraft engines through friction slip clutches (for generators of up to 1.5 kw power) or the aid of a double (rigid and flexible) shaft (for generators of 3 kw power or more). Friction

clutches are normally adjusted for three or four times the rated torque. For torques greater than the clutch tensioning torque, the clutch will slip and protect the generator shaft against twisting.

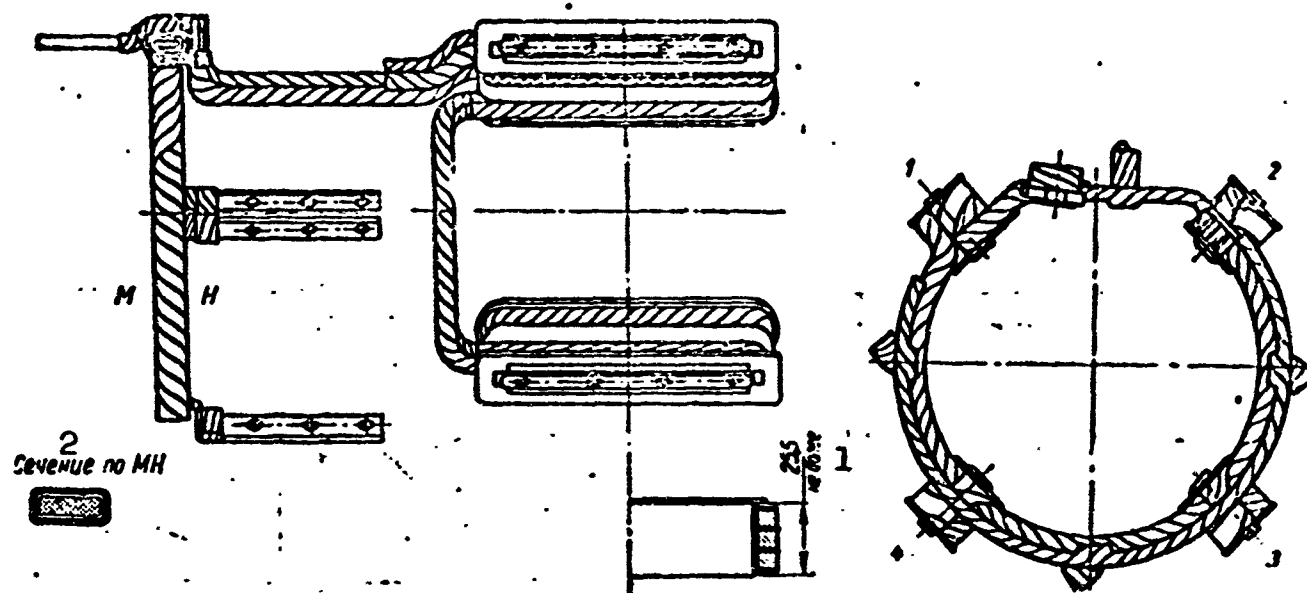


Fig. 6.17. Excitation winding of commutating poles. 1) No more than; 2) section through MN.

The utilization of a double-shaft system, where an external hollow rigid shaft installed on bearings carries the weight of the armature, while an inside flexible shaft transmits the torque to the outside hollow shaft from the commutator end, provides conditions such that oscillations in the drive-engine torque or in mechanism moment of resistance will be absorbed to a considerable degree by the flexible shaft. The machine armature will then operate with the permissible degree of operating nonuniformity.

This is especially important for the case in which the generator is driven by a piston aircraft engine. Even where jet aircraft engines are used to drive the generator, so that there is no pulsating torque, the generator must be protected against torsional oscillation.

Bearings. Aircraft electrical machines use rolling-friction bearings almost exclusively; the important advantages of such bearings are: small size and low weight, low friction losses and little wear,

simplicity of servicing and economy of lubricants, and the possibility of carrying considerable axial loads.

Almost all types of bearings have found application in electrical machine design. In aircraft electrical machine design, it is usual to employ single-row radial ball bearings consisting of an outer and inner steel race, balls, snap ring, and protector rings.

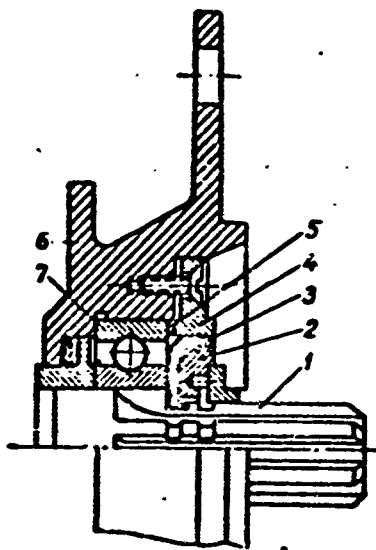


Fig. 6.18. Oil protective device of series GS generators.  
1) Shaft; 2) nut; 3) packing; 4) flange; 5) packing; 6) guard; 7) bearings.

Bearing seating. Various methods are used to install ball bearings on a shaft and in the housing, depending on the type, power, and function of the machine. Enclosed ball bearings are used in GSR-9000, a No. 180504 at the commutator end, and a No. 180506 at the drive end; they have two easily removable steel protector rings each, one on each side of the bearing; rubber washers are placed between them for packing.

Figures 6.6, 6.7, and 6.8 show standard methods for seating enclosed ball bearings in a direct-current aircraft generator at

the commutator end and at the drive end. The inner bearing race is fitted tightly over the rotating shaft, while the outer races are fitted into bearing shields so that they can move. To provide for axial temperature expansion of the shaft (shaft play) and to compensate for manufacturing and assembly tolerances on parts, one of the bearings fixes the shaft position while the other permits axial motion of the shaft.

Lubrication. The basic requirement for a lubricant used in aircraft electrical machines is that it operate satisfactorily under temperatures varying from  $-50$  to  $+100^{\circ}$  or more. Special lubricant grades

are used for these purposes, in particular, GSA sperm-oil base lubricant and the new OKB 122-7 lubricant used for the GSR generator series.

Oil protective devices for series GSR generators are shown in Figs. 6.6, 6.7, and 6.8; Fig. 6.18 shows the oil protective device for series GS generators.

## 6.2. ARMATURE REACTION

Characteristics of armature reaction in aircraft generators. The armature reaction, i.e., the effect of the armature magnetizing force on the field-winding magnetizing force, is considerably stronger in aircraft generators than in general-purpose generators. This is explained by the fact that in aircraft generators the relative armature magnetizing force is higher at the initial rotation speed than in general-purpose machines, i.e.,

$$\left(\frac{F_a}{F_f}\right)_{\text{as}} > \left(\frac{F_a}{F_f}\right)_{\text{adm}}$$

In addition, at high speeds and with the voltage across the generator terminals constant, the magnetic flux drops; as a result the magnetizing force at the poles (the excitation current) will also decrease as the speed increases, while at the same time the armature magnetizing force remains unchanged (we assume the machine is in rated operation). Thus, at the maximum speed

$$\left(\frac{F_a}{F_f}\right)_{\text{as}} \gg \left(\frac{F_a}{F_f}\right)_{\text{adm}}$$

As we know,

$$F_f = \pm F_{\text{ad}} + F_{\text{qd}} \pm F_{\text{ac}} \quad (6.6)$$

where  $F_{\text{ad}}$  is the magnetizing force due to the direct-axis reaction, produced by the direct-axis armature-current component (it appears when the brushes are shifted);  $F_{\text{qd}}$  is the magnetizing force due to the quadrature-axis reaction, produced by the demagnetizing effect of the

quadrature-axis component of the armature current;  $F_{k.s}$  is the magnetizing force due to the commutating sections (the commutation reaction), caused by the effect on the main field of current variations in the short-circuited sections of the armature.

As a rule, the brushes are located in the neutral plane, and the direct-axis armature reaction equals zero, i.e.,  $F_{yad} = 0$ , and

$$F_s = F_{a,d} \pm F_{k.c} \quad (6.7)$$

The demagnetizing action of the armature quadrature-axis reaction, as is known, equals zero for the linear sections of the no-load characteristic, i.e., in regions of low and very high saturation. In low-saturation regions, consequently (short-circuit operation at rated current),  $F_{yag} = 0$  and the armature-reaction magnetizing force reduces to the commutation reaction

$$F_s = \pm F_{k.c} = \pm b_{k.c} A. \quad (6.8)$$

The "plus" sign corresponds to slow commutation with the main field being weakened; the "minus" sign corresponds to fast commutation with the main field reinforced.

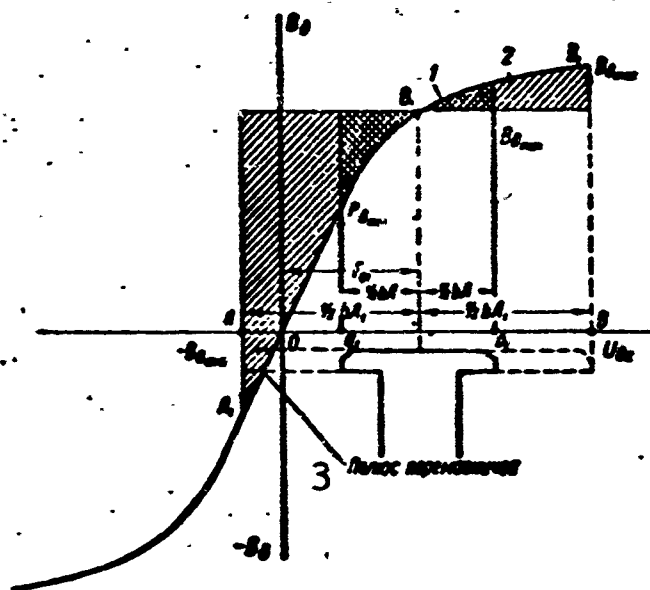


Fig. 6.19. No-load transition curve. 1) General-purpose machine,  $F'_{yag} < 1$ ; 2) aircraft machine,  $F'_{yag} > 1$ ; 3) pole reversed magnetically.

Here  $b_{k.z}$  is the width of the commutation zone, cm;  $A$  is the linear load, amp/cm;  $a$  is a coefficient equal roughly to 0.35.

Thus, for a 12-kw generator,  $A = 380$  amp/cm,  $F_{yaq} \approx 350$  ampere-turns, and  $b_{k.z} \approx 1.3$  cm; consequently,  $F_{k.s} = 0.35 \times 380 \times 1.3 \approx 260$  ampere-turns, i.e.,  $F_{k.s}$  is comparable in value to  $F_{yaq}$  and it cannot be neglected, especially at maximum speeds. For purely straight-line commutation, the commutation reaction  $F_{k.s} = 0$ .

For large relative armature reactions, where

$$0.5\pi A > F_0 = 0.8k_1 \delta B_1 k_r \quad (6.9)$$

the magnetic field in the machine air gap will change its sign, i.e., it will become "reverse." The phenomenon of field "reversal" in the air gap is especially well defined in direct-current aircraft machines (generators and motors) operating with overloads and at high speeds where the excitation field is weak ( $F_0$  small). In such a case, the sign of the field will prove to be reversed for nearly half the pole, and the true neutral plane will be displaced by nearly 90 electrical degrees with respect to the normal neutral plane.

Figure 6.19 shows the no-load transition curve  $A_1 E_1 B_1$ , that at the same time characterizes the distribution of magnetic induction in the machine air gap.

The hatched region of width  $a_1 b_1$  corresponds to a general-purpose direct-current machine for which the phenomenon of magnetic reversal in the air gap does not occur in rated operation ( $0.5 \pi A < F_{01}$ ).

The hatched region of width  $AB$  corresponds to direct-current aircraft machines, where field reversal in the gap can frequently be allowed even in rated operation ( $0.5 \pi A > F_{01}$ ). In this case, a part of the pole piece ( $OA$ ) will be subject to a magnetic reversal, i.e., it will be affected by a field of opposite sign.

The relative magnetizing force due to the quadrature armature re-



action will be

$$\dot{F}_{a,1} = \frac{0.5\pi A}{F_{01}} = \frac{bA}{1.6k_{s1}b k_s B_s} < 1 \quad (6.10)$$

for general-purpose machines, and

$$\dot{F}_{a,1} = \frac{bA}{1.6k_{s1}b B_s} > 1 \quad (6.11)$$

for aircraft machines.

Figure 6.20 shows the field pattern in the air gap for an aircraft generator in the absence of commutating poles and at high speed (series GS generator), with the brushes located in the neutral plane.

A peculiarity of the field pattern in the air gap of the aircraft machine is the appearance of the hatched area characterizing the part of the flux that demagnetizes the machine, changing the polarity of the poles and sharply displacing the true neutral plane.

In machines with conductive excitation, the size of the air gap has a considerable effect on the machine characteristic curve. It is desirable to increase the air gap in order to reduce the distortion of the field in the air gap due to the armature reaction and to reduce surface losses. This, however, increases the reluctance of the magnetic circuit, thus necessitating an increase in the excitation magnetizing force in order to keep the flux constant. This results in increased machine dimensions and losses. It has been established in general electrical-machine design practice that permissible field distortion will occur when the ratio

$$\frac{U_s + U_a}{0.5\pi A} = k_s \approx 1.2.$$

Since

$$U_s = 0.8\pi B_s \quad \text{and} \quad U_a = k_a U_s,$$

we obtain an expression for the minimum air gap

$$b = \frac{k_a \pi}{1.6(1 + k_a) k_s} \frac{A_s}{B_s}. \quad (6.12)$$

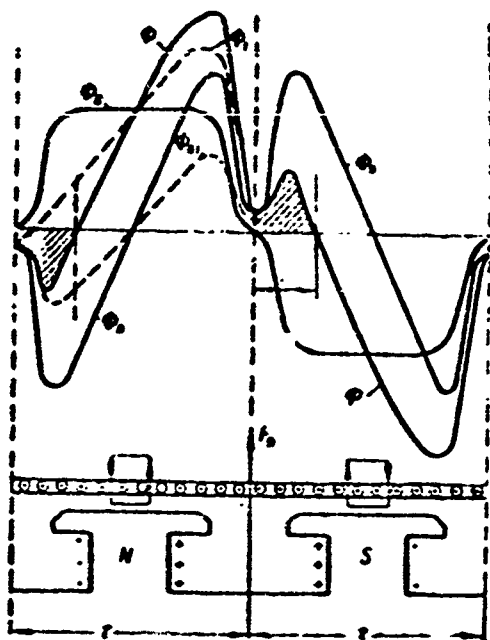


Fig. 6.20. Air-gap field curves for an aircraft generator without commutating poles.  $\Phi_0$ ) No-load flux;  $\Phi_{ya}$  and  $\Phi$ ) armature-reaction flux and flux under load; the dashed lines show the same fluxes for a general-purpose machine.

If the pole-span coefficient  $\alpha = 0.68$ , the air-gap coefficient  $k\delta = 1.15$  and  $k_{ya} = 1.12$ , we find that

$$\delta \geq \frac{0.45}{1+k_s} \frac{A\tau}{B_s} \text{ cm.} \quad (6.13)$$

In direct-current aircraft machines, the air gap is made considerably smaller than Expression (6.13) would require in order to reduce the size of the machine. Thus, a greater air-gap field distortion due to armature reaction is permitted than for general-purpose machines. In 6-18 kw aircraft generators,  $k_{ya} \approx 0.62$  and

$$\delta \approx \frac{0.23}{1+k_s} \frac{A\tau}{B_s} \approx 0.2 \frac{A\tau}{B_s} \text{ cm.} \quad (6.14)$$

In aircraft motors, taking the speed-regulation conditions into account, we take

$$\delta \approx 0.25 \frac{A\tau}{B_s} \text{ cm.} \quad (6.15)$$

In compensated machines, where there is no field distortion due to the armature reaction, the size of the air gap may be obtained from structural considerations by the formula

$$\delta_{\min} \geq 0.01 + \frac{\sqrt{Dl}}{500} \text{ cm.} \quad (6.16)$$

where  $D$  and  $l$  are given in centimeters.

Armature-reaction calculations. The effect of the armature magnetizing force must be considered in determining the excitation magnetizing force under load. The direct-axis component per pole of the armature magnetizing force is found from the formula

$$F_{ad} = cA \frac{D}{D_k} = c \frac{NI_a}{2a\pi D_k} = c \frac{N'I_a}{\pi D_k}, \quad (6.17)$$

where  $c$  is the brush shift along the commutator away from the normal neutral plane, cm;  $D$  and  $D_k$  are the armature and commutator diameters, cm;  $2a$  is the number of parallel circuits in the armature winding;  $N$  and  $N' = N/2a$  is the total number of armature conductors and the number of conductors in one armature circuit;  $I_{ya}$  is the armature current.

Where commutating poles are present, the brushes are normally set at the normal neutral plane and, consequently,  $c = 0$ . Even in this case, however, there will always be some brush shift due to brush wear and as a result of inaccurate installation. In direct-current aircraft machines, the linear load is considerable and thus even for a 1-2 mm brush shift, the direct-axis armature reaction may have a considerable influence on the main field, especially at high speeds. Thus, when  $A = 450$  amp/cm and  $c = 0.2$  cm, the direct-axis reaction will be  $F_{yad} = 90$  ampere-turns.

If we neglect the effect of the quadrature-axis armature magnetizing force outside the pole arc, the per-pole quadrature-axis armature magnetizing-force component will be determined, when  $c = 0$ , by the equation

$$F_{aq} = \alpha A = bA = b \frac{N'I_a}{\pi D} = \alpha \frac{N'I_a}{2p}, \quad (6.18)$$

where  $\tau$  and  $b$  are the pole pitch and width of the pole piece, cm;  $\alpha = b/\tau$  is the pole-span coefficient.

When the machine is under load, the air-gap induction will decrease to a value  $B_n$  owing to the effect of the quadrature-axis armature reaction; this value is less than the no-load induction  $B_\delta$ . The air-gap flux  $\phi_0$  will then decrease by a amount proportional to the difference of the hatched areas  $S_1$  and  $S_2$  (Fig. 6.21), i.e.,  $\Delta B =$

$$= B_{\delta} - B_n \text{ and}$$

$$\Delta\Phi = \Phi_0 - \Phi_n = \Delta B \cdot b \cdot l \equiv \Delta B \cdot b \cdot A = S_1 - S_2. \quad (6.19)$$

The demagnetizing effect of the quadrature-axis armature reaction  $F_{yaq}$  is normally calculated graphically.

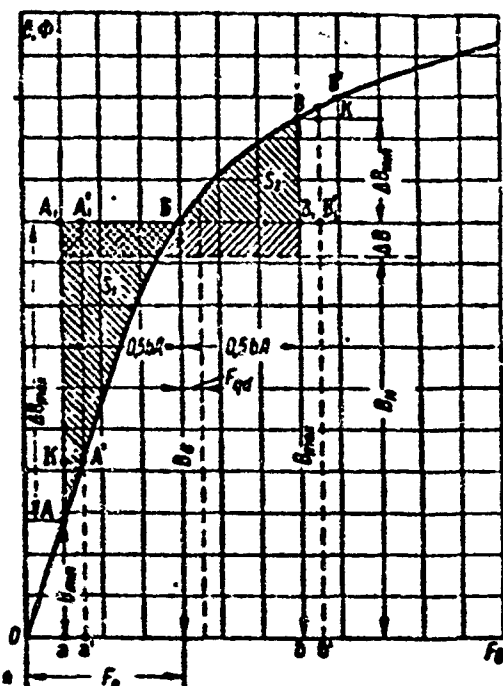


Fig. 6.21. Determination of the demagnetizing effect due to the quadrature-axis armature reaction.

To do this, we superpose the transition no-load curve ABB on the pole face, laying off to both sides of the pole axis half the quadrature-axis armature-magnetizing force component and then moving the curve quadrilateral aABb to the right until the curved triangle  $S'_1 = A'A'_1B$  becomes equal in area to  $S'_2 = BB'B'_1$ .

The displacement along the x-axis thus obtained will be measured in ampere-turns and will give the per-pole value of  $F_{qd}$ .

The flux bounded by the line  $a'A'B'b'$  and corresponding to the pole magnetizing force  $F_{01} + F_{qd}$  will equal the no-load flux, since it is obtained on the assumption that the additional pole magnetizing force  $F_{qd}$  cancels the demagnetizing effect of the quadrature-axis reaction. In other words, the area of  $a'A'B'b'$  is greater than the area of aABb by the area difference  $S_1 - S_2$ , i.e.,

$$\begin{aligned} \Delta B \cdot b \cdot A &= S_1 - S_2 = a'A'B'b' - \\ &- aABb = AA'A'_1A_1 + B_1BB'B'_1 = \\ &= (\Delta B_{\max} - 0.5AK)F_{qd} + (\Delta B_{\min} + \\ &+ 0.5B'K)F_{qd}. \end{aligned}$$

Neglecting the difference  $0.5(\overline{AK} - \overline{B'K})F_{qd}$ , we find that  $\Delta B \cdot b \cdot A \approx (\Delta B_{\max} + \Delta B_{\min})F_{qd}$  and, finally,

$$F_{qd} \approx \frac{\Delta B}{\Delta B_{\max} + \Delta B_{\min}} b \cdot A. \quad (6.20)$$

The approximate value of  $F_{qd}$  may be found by a graph-analytical method, taking account of (6.20) and using the equation

$$\begin{aligned} F_{qd} &\approx \Delta \Phi \frac{b \cdot A}{\Phi_{\max} - \Phi_{\min}} = \\ &= \frac{\Delta \Phi \cdot b \cdot A}{\Delta \Phi_{\max} + \Delta \Phi_{\min}}, \end{aligned} \quad (6.21)$$

where

$$\begin{aligned} \Delta \Phi &= \Delta B \cdot b \cdot l = B_g \cdot b \cdot l - \\ &- B_a \cdot b \cdot l = \Phi_0 - \Phi_a \end{aligned}$$

is the decrease in the useful air-gap flux owing to the effect of the quadrature-axis armature reaction; it may be found if we use a planimeter to find the areas of the curved triangles  $S_1$  and  $S_2$ ; then

$$\Delta \Phi = \Delta B \cdot b \cdot l = \frac{S_1 - S_2}{b \cdot A} b \cdot l, \quad (6.22)$$

either by the approximate quadrature formula

$$\Delta \Phi = \frac{(\Phi_0 - \Phi_{\min}) - (\Phi_{\max} - \Phi_0)}{6} = \frac{\Delta \Phi_{\max} - \Delta \Phi_{\min}}{6},$$

or

$$\Delta \Phi = \Phi_0 - \Phi_a = \Phi_0 - \frac{\Phi_{\min} + 4\Phi_0 + \Phi_{\max}}{6}. \quad (6.23)$$

If we take (6.21) and (6.23) into account, the final expression for the additional magnetizing force per pole will be

$$F_{qd} = \frac{b \cdot A}{6} \frac{\Delta \Phi_{\max} - \Delta \Phi_{\min}}{\Delta \Phi_{\max} + \Delta \Phi_{\min}} = \frac{b \cdot A}{6} \frac{\Delta B_{\max} - \Delta B_{\min}}{\Delta B_{\max} + \Delta B_{\min}}. \quad (6.24)$$

The methods shown for finding  $\Delta \Phi$  and  $F_{qd}$  will give satisfactory results for relatively low values of the quadrature-axis armature reaction ( $0.5b \cdot A < F_{O1}$ ).

Under overload conditions, which can occur both at  $n_{\min}$  and  $n_{\max}$ , where the pole magnetizing force expended in the air gap and teeth ( $F_{O1}$ ) is relatively small, it always turns out that  $0.5b \cdot A \gg F_{O1}$ .

In this case, the methods shown for finding the demagnetizing ef-

fect of the quadrature-axis armature reaction is not accurate enough, and we suggest that the following method be used.

Construct the no-load transition curve or the approximate no-load curve (by substituting  $F_0$  for  $F_{01}$ , Fig. 6.22). This curve will at the same time represent the distribution of magnetic induction in the air gap along the armature circumference. The pole arc is represented in this case by the segment  $\overline{a_1 b_1}$ ; the field under the leading edge of the pole piece will change in sign, i.e., will be "reversed."

The magnitude of the opposite-sign flux will be proportional to the area of the curved triangle  $A_1 a_1 0$  with base  $a_1 0$ ; allowing for the effect of the quadrature-axis armature reaction, the useful flux in the air gap will be proportional to the area  $\phi_1 B_1 b_1$  which, using the notation of Fig. 6.22, can be represented as

$$\text{area } \phi_1 B_1 b_1 = 2F_0 \frac{\phi_{a \min} + 4\phi_{a1} + \phi_{a \max}}{6}$$

The mean air-gap flux, allowing for the quadrature-axis armature reaction can be found by dividing this last expression by the length of the pole arc, which equals  $\overline{a_1 b_1} = bA$ , i.e.,

$$\phi_a = \frac{2F_0}{b \cdot A} \frac{\phi_{a \min} + 4\phi_{a1} + \phi_{a \max}}{6} \quad (6.25)$$

The decrease in the flux owing to the quadrature-axis armature reaction will be, in absolute and relative units respectively,

$$\Delta\phi = \phi_0 - \phi_a = \phi_0 \left( 1 - \frac{1}{6F'_{aq}} \frac{\phi_{a \min} + 4\phi_{a1} + \phi_{a \max}}{\phi_0} \right) \quad (6.26)$$

and

$$\frac{\Delta\phi}{\phi_0} = 1 - \frac{1}{F'_{aq}} \frac{\phi_{a \min} + 4\phi_{a1} + \phi_{a \max}}{6} \quad (6.27)$$

where

$$F'_{aq} = \frac{0.5b \cdot A}{F_0}$$

Using (6.26) and (6.27), we can construct the relationship

$$\Delta\Phi(\Delta\Phi) = f(F_{aq}).$$

from the no-load curve.

In order to compensate for the effect of the quadrature-axis armature reaction  $F_{yaq}$ , it is necessary to increase the excitation by  $F_{qd}$ , so that the additional flux produced will equal the flux decrease  $\Delta\Phi$  due to  $F_{yaq}$ . This last condition will be satisfied if  $b_1 B_1 B_2 b_2$ ,

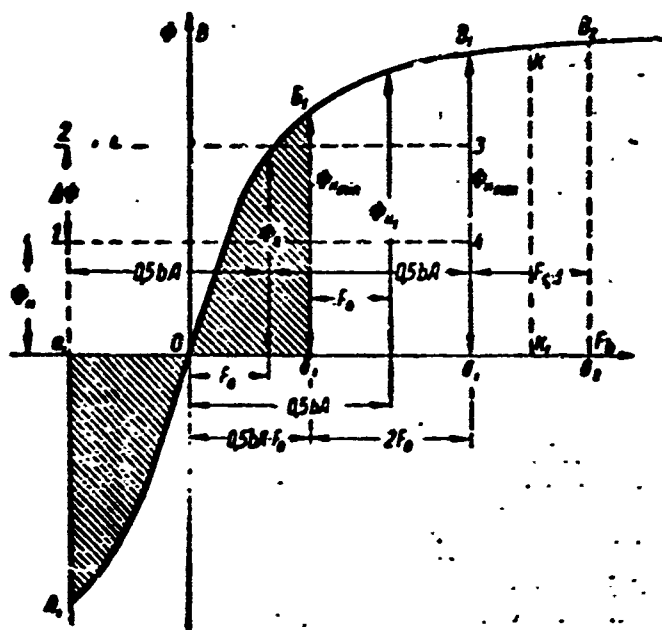


Fig. 6.22. Determination of  $F_{qd}$  when  $0.5bA > F_{01}$ .

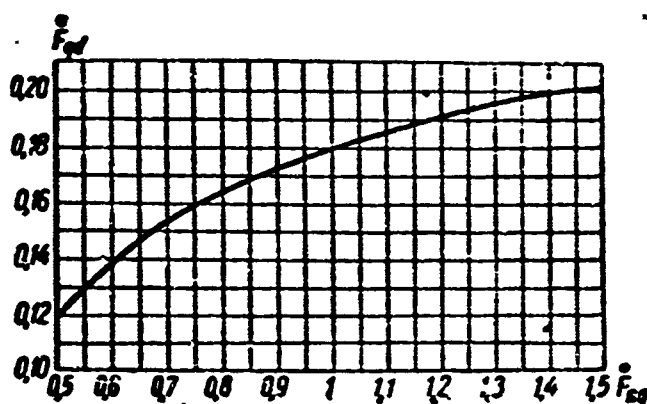


Fig. 6.23. Demagnetizing component of quadrature-axis armature reaction in relative units,  
 $F_{qd} = f(F_{yaq})$ .

with base  $b_1 b_2$ , is equal in area to  $\Delta\Phi bA$ , i.e.,

$$F_{qd} \approx \frac{\Delta \Phi \cdot b \cdot A}{\Phi_{n \max}} = bA \left( \frac{\Phi_0}{\Phi_{n \max}} - \frac{1}{6F'_{nq}} \frac{\Phi_{n \min} + 4\Phi_{n1} + \Phi_{n \max}}{\Phi_{n \max}} \right).$$

whence

$$\Delta \Phi \cdot b \cdot A = F_{qd} \frac{B_1 b_1 + 4KK_1 + B_2 b_2}{6} \approx F_{qd} \Phi_{n \max}. \quad (6.28)$$

The demagnetizing effect of the quadrature-axis armature reaction can be determined by using the analytical expression for the no-load curve.

Allowing for the compensation of the quadrature-axis armature reaction, the air-gap flux under load should equal the no-load flux. This is brought about by an increase in the excitation magnetizing force to  $F'_0 = F_0 + F_{qd}$ , i.e.,

$$\frac{1}{bA} \int_{F'_0 - 0.5bA}^{F'_0 + 0.5bA} \Phi dF = \Phi_0 \quad (6.29)$$

Approximating the no-load curve, for example, by the hyperbolic tangent in the form

$$\text{and} \quad \left. \begin{aligned} \Phi &= a \operatorname{th} BF + d \\ \Phi_0 &= a \operatorname{th} BF_0 + d. \end{aligned} \right\} \quad (6.30)$$

after evaluating the integral and reducing the constants a and d, we can obtain

$$\text{and} \quad \left. \begin{aligned} \frac{a}{BbA} \ln \frac{\operatorname{ch} B(F'_0 + 0.5bA)}{\operatorname{ch} B(F'_0 - 0.5bA)} + d &= a \operatorname{th} BF_0 + d \\ \ln \frac{\operatorname{ch} B(F'_0 + 0.5bA)}{\operatorname{ch} B(F'_0 - 0.5bA)} &= BbA \operatorname{th} BF_0 \end{aligned} \right\} \quad (6.31)$$

Since

$$\operatorname{ch} x = \frac{e^x + e^{-x}}{2} = \frac{\exp x + \exp(-x)}{2}.$$

Expression (6.31) may be written in exponential form



$$\frac{\exp B (F'_0 + 0.5bA) + \exp [-B (F'_0 + 0.5bA)]}{\exp B (F'_0 - 0.5bA) + \exp [-B (F'_0 - 0.5bA)]} = \exp BbA \tanh BF_0 = \exp K, \quad (6.32)$$

where  $K = BbA \tanh BF_0$  is known from the machine design calculations.

The magnitude of  $F'_0$ , i.e., the magnetizing force for which the flux under load equals the no-load flux, is found after manipulation of Expression (6.32) (see §6.3) as

$$F'_0 = \frac{1}{2B} \ln \frac{\exp BbA (\tanh BF_0 + 1) - 1}{\exp BbA - \exp BbA \tanh BF_0}. \quad (6.33)$$

Thus, the excitation magnetizing force that will compensate for the quadrature-axis armature reaction will equal

$$F_{qd} = F'_0 - F_0 \quad (6.34)$$

It should be noted that when  $F_{qd}$  is calculated from the no-load curve rather than the transition curve, the resulting values are somewhat high.

Figure 6.23 shows the functions  $\bar{F}_{qd}^* = f(\bar{F}_{ya}^*)$  for the normalized no-load curve of an aircraft generator. Using these curves, it is possible to find the ampere turns required to compensate for the quadrature-axis armature reaction rapidly and with sufficient accuracy.

### 6.3. CHARACTERISTICS OF DIRECT-CURRENT AIRCRAFT GENERATORS

In Chapter 3, we presented the general considerations that apply to the characteristics of direct- and alternating-current generators. In this section, we shall consider the special features of direct-current aircraft-generator characteristics.

#### No-Load Characteristic

$E = f(I_v)$  with  $R_n = \infty$ ,  $I = 0$ , and  $n = \text{const.}$

Figure 6.24 gives the normalized relative no-load characteristic for direct-current aircraft generators; the curves have been plotted from data obtained during tests of 3, 6, 9, 12, and 18 kw generators.

The relative characteristic curve shown for aircraft generators

resembles the relative characteristic curve for synchronous machines.

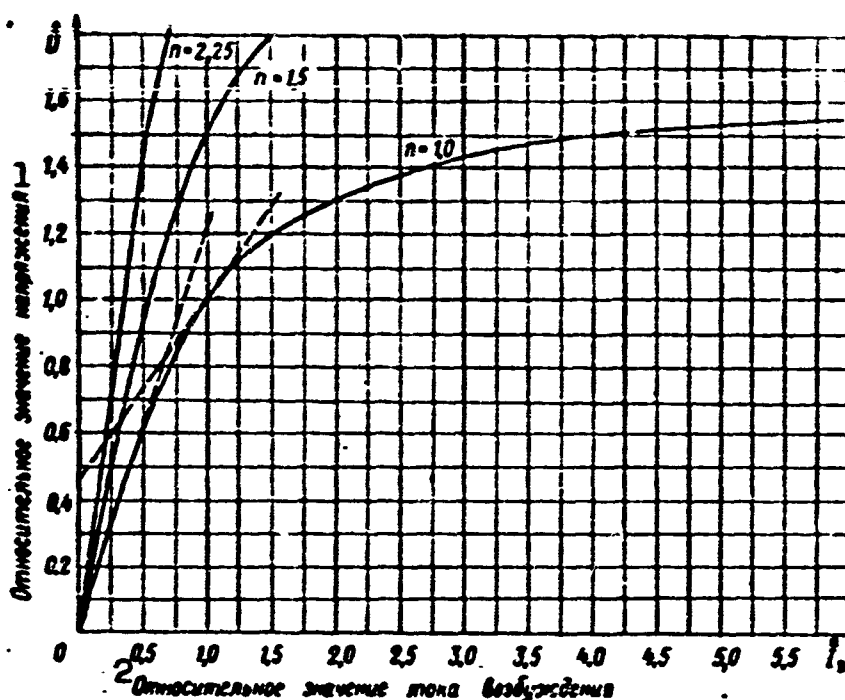


Fig. 6.24. Normalized relative no-load curve for direct-current aircraft generators at various speeds. 1) Relative voltage; 2) relative excitation current.

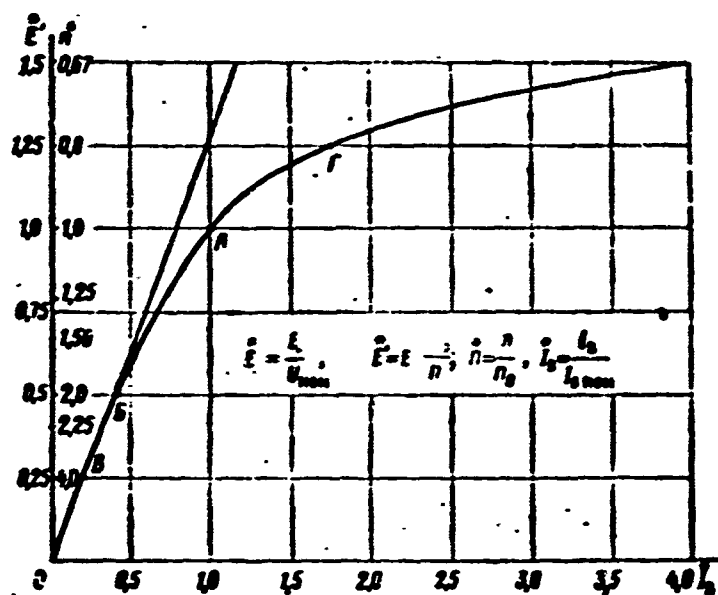


Fig. 6.25. Reduced normalized relative no-load characteristic for direct-current aircraft generators.

Actual no-load curves for aircraft generators depart from the normalized curve by  $\pm 10\%$ .

With a change in generator speed, the voltage across the generator terminals will be held constant automatically with the aid of a

voltage regulator, i.e.,

$$U = E - R_a I_a = kn\Phi - R_a I_a = \text{const.}$$

Where independent excitation is not used, for a machine under no load

$$U = E - R_a I_{a0} \approx E = kn\Phi = \text{const.}$$

Consequently, where a voltage regulator is used the machine flux will vary and will be inversely proportional to the change in speed:

$$\Phi \approx \frac{U}{kn} = \frac{\text{const}}{n},$$

i.e., in aircraft direct-current generators operating at changing speeds with a constant voltage across the terminals, the degree of saturation will fluctuate between wide limits.

If the speed increases, and the flux (excitation current) remains unchanged, the voltage will increase and the magnetic-circuit saturation of the machine ( $\Phi = E/kn = \text{const}$ ) will then remain unchanged, since the emf will also change appropriately as the speed increases.

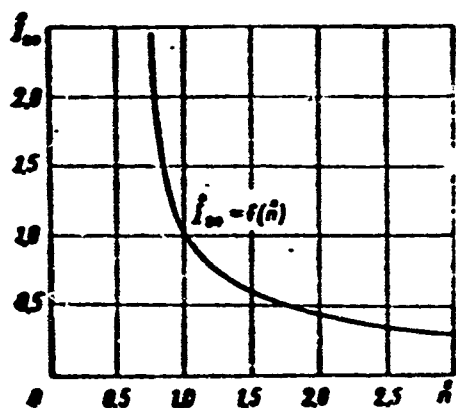


Fig. 6.26. Relative no-load current as a function of speed.

As we have already noted, for generators running with variable speed, it is possible to plot a family of no-load curves, each corresponding to a particular rotational speed. It is possible, however, to represent the entire family of curves by one reduced curve (Fig. 6.25) if we construct the function

$$E' = E \frac{n_0}{n} = f(i_a).$$

It is easily seen that in relative units the function

$$\dot{E} = \dot{E} \frac{n_0}{n} = f(\dot{i}_a)$$

corresponds to the curve  $n = 1$  on Fig. 6.24 if we take as the initial

TABLE 6.2

## Magnetic and Circuit Coefficients

1 Номинальная мощность $P_{\text{ном}}$ в кВт	2 Коэффициенты при $n_{\text{нач}}$			3 Коэффициенты при $n_{\text{max}}$		
	$k_s$	$k_{o.n}$	$k_n$	$k_s$	$k_{o.n}$	$k_n$
1	1,34	0,60	2,50	1,05	0,18	1,22
3	1,32	0,65	2,86	—	—	—
6	1,30	0,62	2,64	—	—	—
9	1,20	0,50	2,00	—	—	—
12	1,12	0,36	1,56	—	—	—
18	1,09	0,38	1,61	—	—	—

1) Rated power  $P_{\text{nom}}$ , kw; 2) coefficients at  $n_{\text{nach}}$ ; 3) coefficients at  $n_{\text{max}}$ .

speed the initial rotational speed  $n_0 = n_{\text{nach}} (n_{\text{min}})$ . Consequently, this curve will also be the reduced relative no-load characteristic curve for any speed.

At a speed higher than the initial speed ( $n_{\text{nach}}$ ), then A corresponding to the nominal voltage will be shifted nearer to the origin. There will be a unique position on the curve corresponding to each speed. The curve  $\bar{E}' = f(\bar{I}_V)$  clearly represents the excitation magnetizing force as a function of the speed at constant voltage.

Making use of the reduced normalized relative no-load curve, we can plot the relative no-load excitation current as a function of the speed (Fig. 6.26), i.e.,

$$\bar{I}_m = f(n).$$

Using coefficients, (3.120)–(3.122) were used to analyze the magnetization curve. Table 6.2 gives the values of the coefficients  $k_s$ ,  $k_n$ , and  $k_{o.n}$  for certain types of direct-current aircraft generators.

#### External Characteristic in the Absence of Voltage Regulator

$U = f(i)$  with  $R_V = \text{const}$  and  $I_V \neq \text{const}$  for various values of the parameter  $n$ .

For the case given, the voltage across the generator terminals

will be a function of the armature current and the speed, i.e.,  $U = f(I_{ya}, n)$ . Practically speaking, the magnetic circuit cannot be saturated, since the flux remains constant while the rise in voltage is nearly proportional to the increase in speed.

In a generator using shunt excitation, the following factors will cause the voltage to vary while the speed remains constant:

- a) the voltage drop across the armature winding, which is nearly proportional to the load, and the drop across the sliding contact;
- b) the effect of the quadrature- and direct-axis armature reactions, the field due to the commutating poles, and the reaction due to short-circuited armature sections;
- c) the variation in the excitation current  $I_v$  resulting from voltage variations across the terminals of the excitation circuit (in machines using independent excitation,  $I_v = \text{const}$ ).

Figure 6.27 shows external generator characteristics for three different speeds.

Where no voltage regulator is used, the machine will operate stably until a bend of a curve is reached, i.e., until low-current values corresponding to points B are reached; unstable operation commences between points B and C. Three limiting current values can be seen on the external characteristic curve: the rated, critical, and short-circuit currents. The maximum current for a given speed, the so-called critical current  $I_{kr}$ , depends on machine saturation, brush position, commutation conditions, winding temperature, and the resistance of the excitation circuit.

In aircraft generators, the commutation conditions and winding temperatures have a very great effect on the critical-current value. As the speed increases, commutation conditions are worsened and sparking at the brushes increases for the same value of low current.

As sparking increases, the voltage drop across the brush transfer contact rises, and since it is high, relatively speaking, for the low voltages used in aircraft generators, this will lead to a considerable decrease in the critical current.

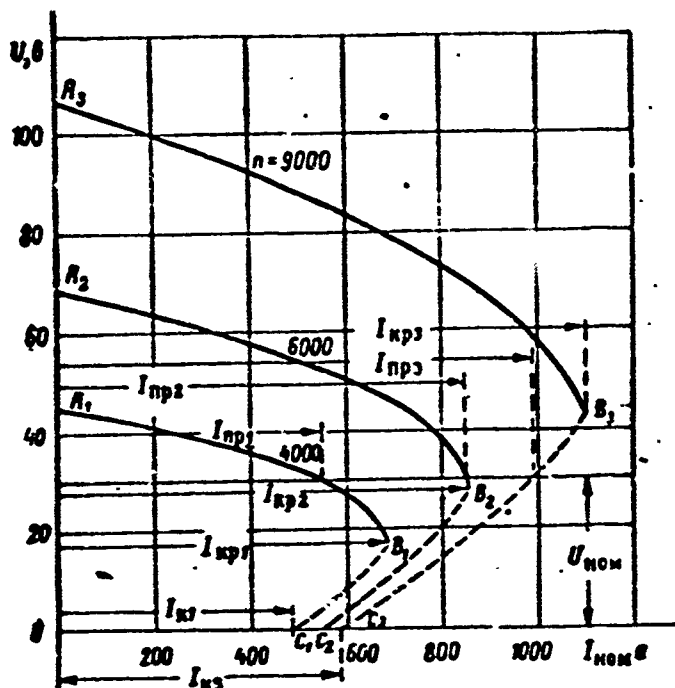


Fig. 6.27. Natural external characteristics for a 12-kw aircraft generator at various speeds.

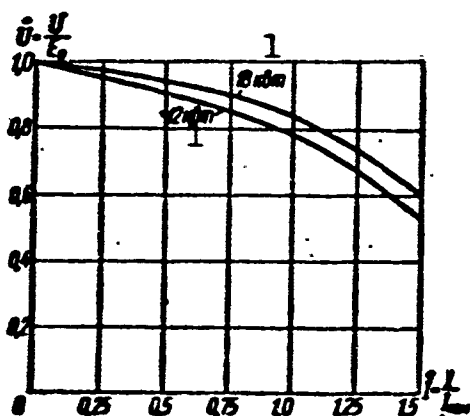


Fig. 6.28. External characteristics for aircraft generators, relative units, at initial speed.  
1) kw.

The same effect is produced by the increase in winding resistances that result from temperature rises.

As the speed increases, the current  $I_{kr}$  rises and as a result there is an increase in the stable portion of the characteristic curve (AB).

As a rule, the steady short-circuit current  $I_k$  is small; it is determined by the magnitude of the emf due to residual

magnetism and by the speed.

For the sake of example, we have shown in Fig. 6.28 the external

characteristics for 12 and 18 kw aircraft generators in relative units.

### The External Characteristic in the Presence of a Voltage Regulator

In this case, the voltage across the generator terminals is held constant at the no-load value until the so-called limiting load current  $I_{pr}$ . The voltage remains constant owing to the fact that the resistance in the excitation circuit is automatically varied in appropriate fashion.

For the limiting current  $I_{pr}$ , the resistance in the excitation circuit will have its minimum value, which equals the sum of the cold field-winding resistance  $R_{v.kh}$  and the minimum regulator-circuit resistance  $R_r \min$

$$R_{s \min} = R_{s.r} + R_{p \min} \quad (6.35)$$

In aircraft carbon regulators, the resistance of the compressed carbon stack, i.e., the minimum regulator resistance, equals  $R_r \min \approx 1.5$  ohms for a carbon stack of  $P_{u.s} = 90$  watts power while  $R_r \min \approx 0.7$  ohms where  $P_{u.s} = 180$  watts.

If the load resistance is reduced so that the armature current exceeds  $I_{pr}$ , the regulator ceases to hold the voltage constant and the machine begins to operate on the natural section of the external characteristic curve: operation is stable up to points B and unstable from points B to points C.

Under no-load conditions, the maximum excitation-circuit resistance will be

$$R_{s \max} = R_{s.r} + R_{p \max} \quad (6.36)$$

where  $R_r \max$  and  $R_r \min$  are the maximum and minimum regulator resistances;  $R_{v.g}$  is the field-winding resistance (hot value).

The external characteristic may be used to find the limiting generator current  $I_{pr}$  that the machine can deliver at rated voltage and a

given speed:

$$I_{np} = \frac{U_{nom}}{R_{\Sigma min}} = \frac{U_{nom}}{R_{\Sigma a} + R_{\Sigma min}} \quad (6.37)$$

The limiting current and, consequently, the overload performance of a machine goes up as the speed increases provided they are not limited by commutation heating conditions (see Fig. 6.27).

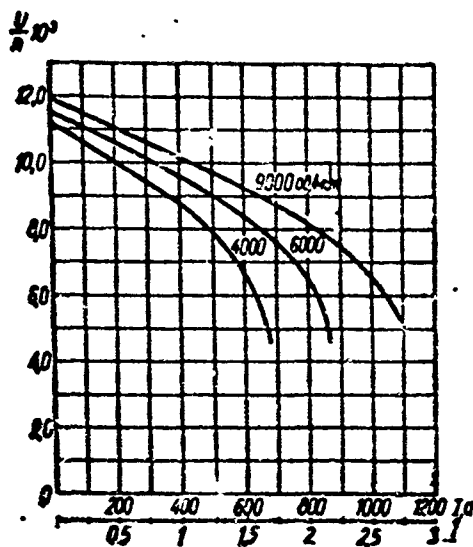


Fig. 6.29. Relative external characteristic curves. 1) rpm.

For series GS generators, the limiting-current ratio will have roughly the following values:  $I_{pr}/I_{nom} = 2.2-2.5$  at  $n_{min} = 3800$  rpm and  $3.2-3.6$  at  $n_{max} = 5900$  rpm.

Thus, as the speed increases from 3800 to 5900 rpm, i.e., by a factor of 1.53, the limiting current rises by about 50%.

In modern 9-18 kw aircraft generators, this ratio will have lower values, and at the initial speed will be

$$\frac{I_{np}}{I_{nom}} \approx 1.8, \quad \frac{I_{np}}{I_{nom}} \approx 1.7$$

$$\text{and } \frac{I_k}{I_{nom}} \approx 1.2.$$

At the maximum speed (9000 rpm)

$$\frac{I_{np}}{I_{nom}} \approx 2.75, \quad \frac{I_{np}}{I_{nom}} \approx 2.7$$

$$\text{and } \frac{I_k}{I_{nom}} \approx 1.45.$$

As the speed increases by a factor  $n_{max}/n_{min} = 2.25$ , the critical current will rise by about 50%, the limiting current by about 60%, and the short-circuit current by about 20%.

Figure 6.29 gives typical relative external characteristics for modern aircraft generators at various speeds, i.e., it shows the function



$$\frac{U}{n} = f(i).$$

Curves plotted for different speeds do not coincide and the difference will be greater the higher the relative low current. This results from the fact that speed fluctuations are accompanied by variations in machine saturation and commutation conditions such that the voltage drop in the machine for the same armature current will be greater at lower speeds. Thus, it is not possible to plot a single reduced external characteristic for all speeds in analogy to the method used for the no-load function  $\bar{E} = f(\bar{I}_v)$ .

### Regulation Characteristic

$I_v = f(I)$  for various values of the parameter  $\underline{n}$  with  $U = \text{const.}$

Figure 6.30 shows relative regulation characteristics for aircraft generators.

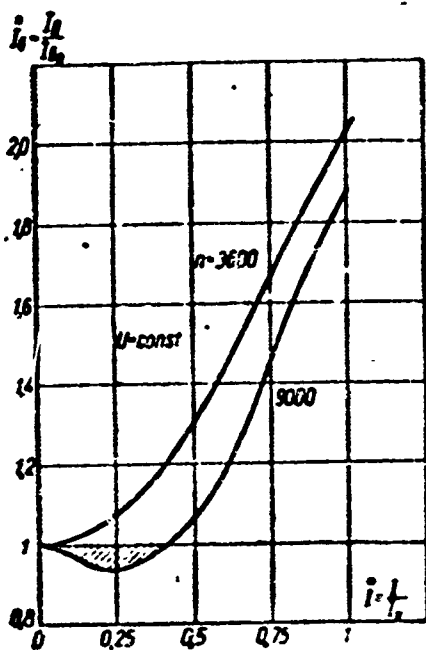


Fig. 6.30. Regulation characteristics of aircraft generator with half-complement of commutating poles for various speeds (relative units).

Regulation characteristics for direct-current aircraft generators with a half complement of commutating poles show a "dip" at the maximum speed.

If the regulation characteristic has a "dip" at high speeds ( $n_{kh}/n_{nach} > 2$ ), i.e., if for a low current in the range  $(0.15-0.5)I_{nom}$ , the excitation current is lower than the no-load current, the generator will be unstable when operated in parallel with other generators or a storage battery: it will have a tendency to self-oscillation at high speeds.

A dip may appear in the regulation characteristic of a generator at high speeds owing to the magnetizing

effect of the commutating poles and the commutation currents in a short-circuited section.

In fact, at the lowest speed, where the magnetic system is saturated, the magnetizing effect of a commutating pole and of the commutation currents, which are proportional to the load current, will be small in comparison with the magnetizing force due to the main poles. At high speeds, the main-pole magnetizing force will drop sharply, while the magnetizing forces due to the commutating poles,  $F_k$ , and the commutation currents  $F_{k.s}$  remain constant (the flux  $\phi_k$  will rise owing to the decreased reluctance of the commutating-pole circuit).

As a result, the relative influence of the commutating-pole magnetizing force and the commutation-current magnetizing force will increase, and where the armature currents are low a drop in excitation current will result. With a further increase in the load current, the excitation magnetizing force will rise more rapidly and  $F_k$  than  $F_{k.s}$ , and the curve will turn upward.

In order to obtain stable operation from a generator that has a "dip" in its regulation characteristic, we can make use of well-known methods for increasing parallel-operation stability (for obtaining artificial stability), i.e., equalizing connections may be used between generators operating in parallel, or stabilizing transformers may be employed.

It is better, however, to increase the natural parallel-operation stability, i.e., to eliminate the dip in the regulation characteristic; this may be done by appropriate adjustment of the machine magnetic system (the main and commutating poles) and by the use of a full complement of commutating poles.

For the reasons discussed above, it is not possible to construct a single reduced regulation characteristic applicable for all speeds;

for each speed it is necessary to plot an individual regulation characteristic, or to find it experimentally.

### Operating or Speed Characteristic

$I_v = f(n)$  with  $U = \text{const}$ ,  $R_n = \text{const}$  and, consequently,  $I = \text{const}$ .

As a rule, operating characteristics are found with the machine heated up, with a constant load resistance and under no-load conditions. Figure 6.31 shows typical operating characteristics for an aircraft generator over the working speed range, i.e., from 4000 to 9000 rpm.

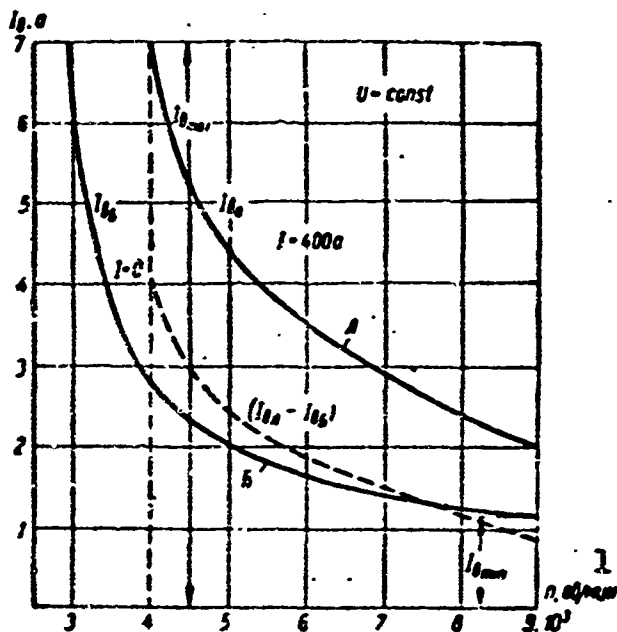


Fig. 6.31. Operating characteristic of aircraft generator. 1) rpm.

The speed range from 0 to  $n_{\text{nach}}$  is called the self-excitation region. Within this range, the field due to residual magnetism causes the generator voltage to rise with increasing speed and excitation current to some specific value, after which the voltage regulator begins to act; as the speed continues to rise, the regulator decreases the excitation current to the degree necessary to

hold the voltage across the generator terminal constant.

The minimum speed at which the generator can develop rated voltage is called the initial speed. There will be a difference between the initial speed under no-load conditions and the initial speed at rated load.

It is clear that the initial no-load speed will be lower than the initial speed at rated load.

A distinction is made between the initial speed with the minimum regulator resistance present in the excitation circuit and the initial speed in the absence of the regulator. Where there is no regulator resistance in the excitation circuit, the generator will develop the rated voltage or rated power at a lower initial speed.

As a rule, the initial speed is 10-12% more with no regulator than the initial speed in the presence of a regulator.

For practical purposes we are clearly interested in the initial speed at rated load, allowing for the regulator resistance. The voltage regulator should provide constant voltage in all rated generator modes, by changing the excitation current over a range extending from  $I_{V \max}$  at initial speed and rated current to  $I_{V \min}$  at maximum speed without load. The part of the range over which the excitation current varies, the wider will be the range of variation in the voltage-regulator resistance, which complicates the regulation problem. As a rule,  $I_{V \max}/I_{V \min} = 4.5-5.5$  with  $n_{\max}/n_{\min} = 2.25$ .

Figure 6.32 shows relative operating characteristics under no-load conditions and under rated load, i.e.,  $\dot{I}_V = f(\dot{n})$  at  $I = 0$  and  $I = 400$  amp, as well as the relative excitation current going to compensate for the effect of the load (armature reaction and voltage drop in the armature circuit), i.e.,

$$\frac{I_{0A} - I_{0E}}{(I_{0A} - I_{0E})_{\text{at } n=1000}} = f(\dot{n}).$$

An analysis of the curves given leads us to the following conclusions.

1. Under no-load conditions, the excitation current would be reduced by a factor of 2.5 from the initial value as the speed increases by a factor of 2.25, while at rated load, there will be a 3.5-fold drop in the excitation current for the same speed increase.

2. As the speed rises, the excitation current will drop relatively more under load than the no-load excitation current does. This is explained by the fact that as the speed increases, the magnetic saturation decreases and, consequently, there is a sharp drop in the demagnetizing effect of the quadrature-axis armature reaction.

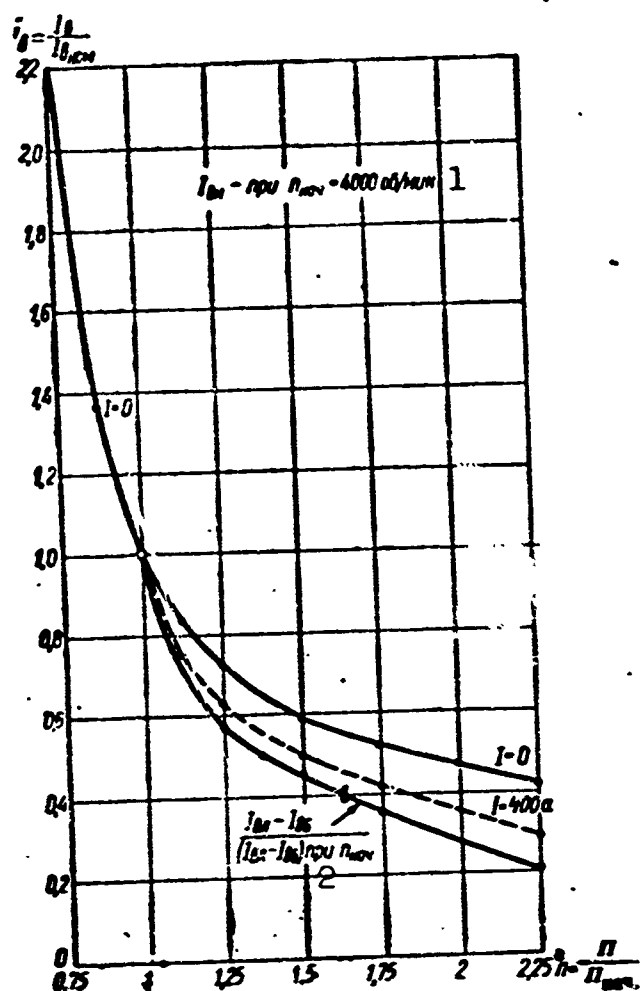


Fig. 6.32. Operating characteristic in relative units. 1) rpm; 2) at.

3. The excitation current going to compensate for the voltage drop across the armature resistance and for the quadrature-axis armature reaction will drop to 20% of its initial value, i.e., by roughly a factor of 5, as the speed increases by a factor of 2.25.

4. There is a sharp drop in the excitation current with increasing speed on the initial portion of the characteristic curves, where there is considerable magnetic-system saturation. At low saturations, the magnitude of the excitation current will be nearly linear in character, and will be determined solely by the magnetic potential drop across the air gap and the voltage drop across the armature resistance.

Generator emf as a Function of Speed Under No-Load Conditions

$$E = U_0 = f(n) \text{ with } R_v = \text{const and } I = 0.$$

This characteristic is of practical interest for aircraft generators, since it represents the initial section of the operating charac-

teristic before the voltage regulator comes into operation, i.e., the self-excitation zone.

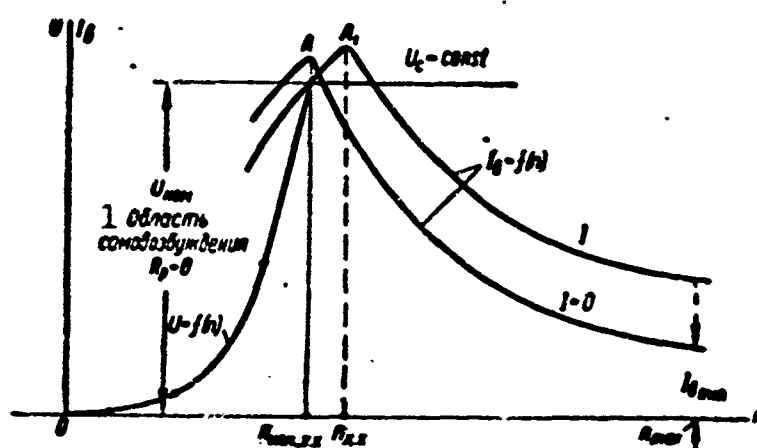


Fig. 6.33. Generator emf and excitation current as a function of speed. 1, Self-excitation region.

In independently excited machines the no-load generator emf with the brushes at the neutral plane will increase in proportion to the speed, i.e.,  $\Phi = \text{const}$  and  $E = k n \Phi \propto n$ .

With the brushes shifted away from the neutral plane, the currents in the commutating sections will affect the main machine field, destroying the straight-line nature of the  $E$  vs.  $n$  curve.

In machines using shunt excitation the function  $E = f(n)$  is non-linear, since with the excitation-circuit resistance unchanged, the excitation current will rise in proportion to the voltage across the generator terminals while the armature emf of a self-excited generator will change more rapidly with a change in speed than is the case in an independently excited generator. In this case, the  $E = f(n)$  curve will consist in three sections (Fig. 6.33). At low speeds, the generator emf produced by the residual-magnetism field is small and consequently, the excitation current is also small. In this case, the machine flux is nearly constant and the generator emf will vary in proportion to the speed, i.e., at low speeds the characteristic  $E = f(n)$  will be linear in nature.

After some specific critical speed is reached, the effect of the excitation current increases noticeably and the generator emf rises sharply as the speed and excitation current increase; as a result, the characteristic curve comes nearly quadratic.

With a further rise in speed, the excitation current increases so much that the magnetic system begins to be saturated. When this happens, further increases in excitation current are accompanied by almost no rise in machine flux.

### Analytical Expression of Characteristic Curves

It is difficult to express characteristic curves analytically, since the relationship between magnetizing force and induction, upon which all characteristics are based, is nonlinear. In many cases, however, in order to generalize investigations it is desirable to have an analytical expression for the characteristics, even if it is only approximate. To do this, we use some well-known method to approximate the saturation curve, e.g., a hyperbolic tangent of the form (6.30)

$$\Phi = a \tanh BF + d,$$

where  $a$ ,  $B$ , and  $d$  are constants;  $F = w_v I_v = w_v (U/R_v)$  is the excitation magnetizing force per pole.

The constants  $a$ ,  $B$ , and  $d$  are found on the basis of the following considerations. In the absence of excitation current,  $F = 0$  and the flux  $\Phi$  equals the residual flux  $\Phi_{ost}$ , i.e.,

$$\Phi = \Phi_{ost} = a \tanh 0 + d = d. \quad (6.38)$$

At maximum excitation current  $F_{max}$ , the flux reaches its maximum  $\Phi_{max}$ , and the saturation curve will run almost parallel to the x-axis. In this case, the expression

$$\Phi_{max} = a \tanh BF_{max} + d \approx a + d = \Phi_{ost} \quad (6.39)$$

will hold. This occurs when  $\tanh BF_{max} = 1$ , i.e., when  $BF \geq 3$ , since  $\tanh 3 \approx 0.995$ .

Consequently, on the basis of (6.39), the constant  $a$  will equal

$$a = \Phi_{\max} - \Phi_{\text{oct}} \quad (6.40)$$

and the equation for the flux will take the form

$$\Phi = (\Phi_{\max} - \Phi_{\text{oct}}) \text{th } BF + \Phi_{\text{oct}}. \quad (6.41)$$

Then the equation for the no-load characteristic will be written as

$$E = k n \Phi = k n [\Phi_{\text{oct}} + (\Phi_{\max} - \Phi_{\text{oct}}) \text{th } BF] \quad (6.42)$$

or

$$E = E_{\text{oct}} + E'_{\max} \text{th } BF, \quad (6.43)$$

where  $E_{\text{ost}} = k n \Phi_{\text{ost}}$  is the voltage due to residual magnetism;

$$E'_{\max} = k n a = k n (\Phi_{\max} - \Phi_{\text{oct}}) = E_{\max} - E_{\text{oct}}.$$

$k = (p/a_1)(N/60) 10^{-8}$  is a structural coefficient.

If we make use of the normalized no-load curve in relative units over the  $\frac{E}{E_{\max}} = 0-3$  range and neglect residual magnetization, the missing coefficient  $B$  can be found in the following way.

With  $\frac{E}{E_{\max}} = 1$  and  $\frac{I}{I_{\max}} = 1$

$$\frac{E}{E_{\max}} = \frac{E'}{E'_{\max}} \text{th } BF = 1.$$

Taking  $\frac{E}{E_{\max}} = 1.43$  with  $\frac{I}{I_{\max}} = 3.0$  we find that

$$1.43 \text{th } B = 1, \text{ th } B = 0.7, \text{ th } B = 0.87.$$

Thus, the equation for the normalized no-load curve of the aircraft generator will be

$$\frac{E}{E_{\max}} \approx 1.43 \text{th } 0.87 \frac{I}{I_{\max}}. \quad (6.44)$$

Expression (6.44) can easily be refined if we allow for the residual magnetization. In like manner, we can determine the coefficients for other excitation-current variation limits.

### External Characteristic

The way in which the voltage across the generator terminals depends on the load current is represented by the expression

$$U = E - E_r = k n \Phi - R_a I_a. \quad (6.45)$$



With the brushes positioned arbitrarily, the flux  $\Phi$  in the air gap will depend on the excitation current, the direct- and quadrature-axis armature reaction, the commutating-pole field, and the currents in the commutating sections. For a separately excited machine, the excitation current can be assumed to be constant, while with shunt excitation, the excitation resistance remains constant while the excitation current  $I_V = U/R_V$  turns out to be a function of the voltage across the terminals of the machine. In this latter case, the analysis becomes quite a bit more complicated.

External characteristic with separate excitation,  $I_V = \text{const.}$  We use a well-known method for determining the additional excitation ampere-turns needed to compensate for the demagnetizing effect of the quadrature-axis armature reaction in order to allow for the effect of this reaction.

Using the notation of Fig. 6.19 and Expression (6.29) we can represent the mean flux in the air gap, allowing for the effect of the quadrature-axis armature reaction, as

$$\Phi = \frac{1}{bA} \int_{F-0.5bA}^{F+0.5bA} \Phi dF$$

or, allowing for (6.30), as

$$\Phi = \frac{1}{bA} \int_{F-0.5bA}^{F+0.5bA} [a \operatorname{th} BF + d] dF. \quad (6.46)$$

Since

$$\int \operatorname{th} BF dF = \frac{1}{B} \ln \operatorname{ch} BF + K_1,$$

where  $K_1$  is a constant of integration, following some simple manipulations we obtain the following expression:

$$\Phi = \frac{a}{BbA} \ln \frac{\operatorname{ch} B(F+0.5bA)}{\operatorname{ch} B(F-0.5bA)} + d. \quad (6.47)$$

Taking the direct-axis armature reaction into account,

$$\Phi = \frac{a}{BbA} \ln \frac{\operatorname{ch} B(F + 0.5bA \mp F_d)}{\operatorname{ch} B(F - 0.5bA \mp F_d)} + d. \quad (6.48)$$

In the general case, the direct-axis field  $F_d$  may have a "minus" or "plus" sign. Now, making use of (6.45) and (6.48), we can write the equation for the external characteristic:

$$U = kn \left[ \frac{a}{BbA} \ln \frac{\operatorname{ch} B(F' + 0.5bA)}{\operatorname{ch} B(F' - 0.5bA)} + d \right] - R_a I_a, \quad (6.49)$$

where for brevity we let  $F' = F \mp F_d$ .

When the armature reaction is completely compensated or under no-load conditions, Eqs. (6.47) and (6.49) will become ambiguous; the ambiguity may be removed, however, and then

$$U_0 = \lim_{I_a \rightarrow 0} kn (a \operatorname{th} BF + d) = E_0 \quad (6.50)$$

under no-load conditions

$$\text{and} \quad U = kn [a \operatorname{th} B(F \mp F_d) + d] - R_a I_a \quad (6.51)$$

where the armature reaction is completely compensated.

External characteristic with dependent shunt excitation. We shall consider two cases:

a) the machine is compensated and there is no quadrature-axis armature reaction;

b) the machine is not compensated and the quadrature-axis armature reaction must be considered.

For the purposes of the study it is assumed that the brushes are located at the neutral plane, commutation is linear, and there is one commutating pole for every two main poles.

In the first case, on the basis of (6.30) and the assumption that  $d = \Phi_{\text{ost}} = 0$ , the machine emf as a function of load current will be

$$E = kn\Phi = kna \operatorname{th} BF = E_{\text{max}} \operatorname{th} B \frac{E - R_a I_a}{R_a} \quad (6.52)$$

where

$$F = w_p I_a = w_p \frac{U}{R_a} = w_p \frac{E - R_a I_a}{R_a}.$$

The voltage across the generator terminals will then be

$$U = E - R_a I_a = E_{\max} \operatorname{th} \mu U - R_a I_a. \quad (6.53)$$

where  $\mu = B(w_p/F_v) = \text{const.}$

Since

$$\operatorname{th} x = \frac{e^{2x} - 1}{e^{2x} + 1} \text{ and } e^x = \sum_{k=0}^{\infty} \frac{x^k}{k!},$$

we find on the basis of (6.53) that

$$U + R_a I_a = E_{\max} \operatorname{th} \mu U = E_{\max} \frac{e^{2\mu U} - 1}{e^{2\mu U} + 1}. \quad (6.54)$$

On the basis of the value of  $2\mu U$  and the accuracy of the calculation, we select the number of terms ( $k$ ) to be used from the infinite series. Here it is necessary to remember that the order of the finite equation used to determine the voltage  $U$  will equal the number of turns in the series.

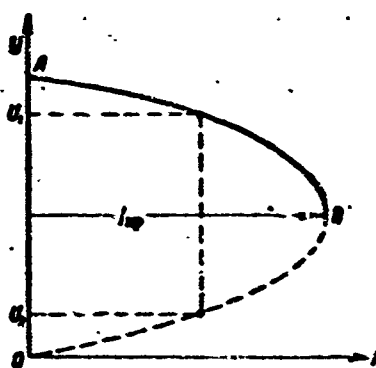


Fig. 6.34. External characteristic of aircraft generator in relative units (simplified).

If  $2\mu U < 0.75$  and the permissible error is 10%, we may take  $k = 2$ . In this case, we obtain a quadratic equation of the type

$$\left. \begin{aligned} \frac{U + R_a I_a}{E_{\max}} &= \frac{\mu U}{1 + \mu U} \\ U^2 + a_1 U + a_0 &= 0, \end{aligned} \right\} \quad (6.55)$$

and

where

$$\begin{aligned} e_1 &= R_s I_s - \left( E_{\max} - \frac{R_s}{Bw_s} \right) = R_s I_s - 2\gamma, \\ e_0 &= \frac{R_s R_s}{Bw_s} I_s, \\ \gamma &= 0.5 \left( E_{\max} - \frac{R_s}{Bw_s} \right). \end{aligned}$$

Solving the quadratic equation, we obtain

$$U_{1,2} = \gamma - 0.5 R_s I_s \pm \sqrt{(\gamma - 0.5 R_s I_s)^2 - \frac{R_s R_s}{Bw_s} I_s} \quad (6.56)$$

where

$$\gamma = \text{const. for } n = \text{const.}$$

Thus, the external characteristic, i.e., the function  $U = f(I_{ya})$ , may be represented like an equation of the form

$$\begin{aligned} U_{1,2} &= 0.5 \left( E_{\max} - \frac{R_s}{Bw_s} - R_s I_s \right) \pm \\ &\pm \sqrt{\frac{1}{4} \left( E_{\max} - \frac{R_s}{Bw_s} - R_s I_s \right)^2 - \frac{R_s R_s}{Bw_s} I_s}. \end{aligned} \quad (6.57)$$

Two voltages will correspond to each load-current value: one of them ( $U_1$ ) will lie on the stable section of the external characteristic, and the other ( $U_2$ ) on the unstable portion (Fig. 6.34).

The critical-current value will occur when

$$U_1 = U_2 = \gamma - 0.5 R_s I_{sp} = 0.5 \left[ E_{\max} - \left( R_s I_{sp} + \frac{R_s}{Bw_s} \right) \right],$$

or the expression under the radical equals zero, i.e.,

$$\begin{aligned} \sqrt{(\gamma - 0.5 R_s I_{sp})^2 - \frac{R_s R_s}{Bw_s} I_{sp}} &= 0, \\ I_{sp}^2 - 4 I_{sp} \frac{\gamma + \frac{R_s}{Bw_s}}{R_s} + 4 \frac{\gamma^2}{R_s^2} &= 0 \end{aligned}$$

and

$$I_{sp} = \frac{2}{R_s} \left[ \left( \gamma + \frac{R_s}{Bw_s} \right) \pm \sqrt{\left( \frac{R_s}{Bw_s} \right)^2 + 2\gamma \frac{R_s}{Bw_s}} \right]$$

or after substituting the value  $2\gamma = E_{\max} - (R_s/Bw_s)$ ,

$$I_{ap} = \frac{1}{R_s} \left[ E_{max} \pm 2 \sqrt{E_{max} \frac{R_s}{B \omega_s}} \right]. \quad (6.58)$$

The way in which the load current depends on the voltage across the generator terminals is of practical interest. Equation (6.56) can be represented as follows:

$$(U_1 - 1 + 0.5 R_s I_a)^2 = (1 - 0.5 R_s I_a)^2 - \frac{R_s I_a}{S_1}$$

and, solving it for  $I_{ya}$ , we find that

$$I_a = \frac{U_1}{R_s} \frac{E_{max} - \left( U_1 + \frac{1}{B_1} \right)}{U_1 + \frac{1}{B_1}} = \frac{U_1}{R_s} \left( \frac{E_{max}}{U_1 + \frac{1}{B_1}} - 1 \right). \quad (6.59)$$

Equations (6.55)-(6.59) were obtained on the assumption that  $2B_1 U < 0.75$ . If, however,  $1 < 2B_1 U < 2$ , it is necessary to use a value of  $k = 3$ , and in this case the external characteristic will take the form of a cubic equation in canonical form, i.e.,

$$\left. \begin{aligned} \frac{U + R_s I_a}{E_{max}} &= \frac{B_1 U + (B_1 U)^2}{1 + B_1 U + (B_1 U)^2} \\ U^3 + \alpha_2 U^2 + \alpha_1 U + \alpha_0 &= 0, \end{aligned} \right\} \quad (6.60)$$

and

where

$$\begin{aligned} \alpha_2 &= B_1^{-1} + R_s I_a - E_{max}, \\ \alpha_1 &= B_1^{-1} (B_1^{-1} + R_s I_a - E_{max}) = B_1^{-1} \alpha_2, \\ \alpha_0 &= B_1^{-2} R_s I_a. \end{aligned}$$

The coefficients  $\alpha_2$ ,  $\alpha_1$ , and  $\alpha_0$  are functions of the load current and speed. At constant speed, the external characteristic can be plotted from Eq. (6.60)

For an uncompensated machine with brushes located in the neutral plane, linear computation, and  $2p$  commutating poles, the air-gap flux, emf, and voltage will be [considering (6.47) and taking  $\underline{d}$  equal to zero]

$$\Phi = \frac{\Phi_{max}}{B b A} \ln \frac{\operatorname{ch} [B_1 (E - R_s I_a) + 0.5 B b A]}{\operatorname{ch} [B_1 (E - R_s I_a) - 0.5 B b A]} \quad (6.61)$$

and

$$E = \frac{E_{\max}}{BbA} \ln \frac{\operatorname{ch}(B_1 U + 0.5BbA)}{\operatorname{ch}(B_1 U - 0.5BbA)} \quad (6.62)$$

where

$$B_1 = B \frac{U_0}{R_0}, \quad \Phi_{\max} - \Phi_{\text{oct}} = a \approx \Phi_{\max}.$$

Since  $\cosh x = 0.5(e^x + e^{-x})$ , this last expression may be written as

$$\ln \frac{e^{B_1 U + \mu} + e^{-B_1 U - \mu}}{e^{B_1 U - \mu} + e^{-B_1 U + \mu}} = \frac{2\mu U}{E_{\max}} - \frac{2\mu R_0 I_0}{E_{\max}} = \mu_1 U - \mu_2 \quad (6.63)$$

where

$$\mu = 0.5BbA, \quad \mu_1 = \frac{2\mu}{E_{\max}} \text{ and } \mu_2 = \frac{2\mu R_0 I_0}{E_{\max}}.$$

Removing the element containing  $U$  from (6.63) and eliminating the logarithm, i.e., writing

$$\frac{A_1^2 e^{2B_1 U} + 1}{e^{2B_1 U} + A_1^2} = A_2 e^{\mu_1 U}, \quad (6.64)$$

where

$$A_1 = e^{\mu} = e^{0.5BbA} = f(I_0)$$

and

$$A_2 = e^{-\frac{BbAR_0 I_0}{E_{\max}}} = f(I_0^2, n),$$

we find

$$A_1^2 (A_2 e^{\mu_1 U} - e^{2B_1 U}) + A_2 e^{(2B_1 + \mu_1)U} = 1$$

or

$$A_1^2 \left[ A_2 \sum_{k=0}^{\infty} \frac{(\mu_1 U)^k}{k!} - \sum_{k=0}^{\infty} \frac{(2B_1 U)^k}{k!} \right] + A_2 \sum_{k=0}^{\infty} \frac{[(2B_1 + \mu_1)U]^k}{k!} - 1 = 0. \quad (6.65)$$

Since the expression  $(2B_1 + \mu_1)U$  is usually greater than unity, it is necessary to take at least 4-5 terms of the infinite series.

If we take four terms of the infinite series, we will obtain a cubic equation in canonical form:

$$U^3 + \alpha_2 U^2 + \alpha_1 U + \alpha_0 = 0, \quad (6.66)$$

where  $\alpha_2$ ,  $\alpha_1$ , and  $\alpha_0$  are functions of the load current and the speed.

Letting  $n = \text{const}$ , we can calculate the external characteristic for the uncompensated machine with dependent shunt excitation.

### Regulation Characteristic

Solving Eq. (6.49) for the excitation magnetizing force, we obtain the function  $F = f(I_{ya})$  with  $U = \text{const}$  and  $n = \text{const}$ , i.e., the regulation characteristic.

To do this we represent Eq. (6.49) in the form

$$\ln \frac{\text{ch}[B(F \mp F_d + 0.5bA)]}{\text{ch}[B(F \mp F_d - 0.5bA)]} = BbA \frac{U + R_a I_a - knd}{E_{\max}} \quad (6.67)$$

or, for brevity, let

$$\ln \frac{\text{ch}(BF' + 0.5bAB)}{\text{ch}(BF' - 0.5bAB)} = \ln \frac{\text{ch}(BF' + \mu)}{\text{ch}(BF' - \mu)} = \beta, \quad (6.68)$$

where

$$\beta = BbA \frac{U + R_a I_a - E_{\text{occ}}}{E_{\max}} = \mu_1 (U + R_a I_a - E_{\text{occ}}) = f(I_a, n),$$

while considering that

$$\frac{\text{ch}(BF' + \mu)}{\text{ch}(BF' - \mu)} = \frac{e^{BF'} e^{\mu} + e^{-BF'} e^{-\mu}}{e^{BF'} e^{-\mu} + e^{-BF'} e^{\mu}}, \quad (6.69)$$

and letting  $e^{\mu} = A_1$ , we may use (6.68) to find that

$$\ln \frac{A_1 e^{BF'} + A_1^{-1} e^{-BF'}}{A_1^{-1} e^{BF'} + A_1 e^{-BF'}} = \beta$$

or

$$\ln \frac{A_1^2 e^{2BF'} + 1}{e^{2BF'} + A_1^2} = \beta. \quad (6.70)$$

We eliminate the logarithm and isolate the expression containing  $F'$ , i.e.,

$$\frac{A_1^2 e^{2BF'} + 1}{e^{2BF'} + A_1^2} = e^{\beta} \quad (6.71)$$

and

$$e^{2\beta F} = \frac{A_1^2 e^\beta - 1}{A_1^2 - e^\beta}. \quad (6.72)$$

Taking the logarithm of (6.72), we obtain the equation for the regulation characteristic in the form

$$F = \frac{1}{2B} \ln \frac{A_1^2 e^\beta - 1}{A_1^2 - e^\beta} \pm F_d. \quad (6.73)$$

Substituting the value of  $A_1$  into (6.73), taking the values of  $\mu$  and  $\beta$ , and going over to exponential forms, we finally obtain

$$F = \frac{1}{2B} \frac{\exp\left(1 + \frac{U + R_s I_s - E_{oct}}{E_{oct}}\right) BbA - 1}{\exp BbA - \exp \frac{U + R_s I_s - E_{oct}}{E_{oct}} BbA} \pm F_d. \quad (6.74)$$

Above we have shown that  $\Phi_{ost} = d$ ,  $\Phi_{max} - \Phi_{ost} = a$ ,

$$E'_{max} = kna, E_{max} = E_{max} - E_{oct},$$

$$E_{oct} = knd \text{ and } E_{max} = kn\Phi_{max}.$$

If we use the simplified expression for the no-load curve, on the assumption that  $\Phi_{ost} = d = 0$ , we obtain

$$F = \frac{1}{2B} \ln \frac{\exp\left(\frac{U + R_s I_s}{E_{max}} BbA\right) - \exp(-BbA)}{1 - \exp\left(\frac{U + R_s I_s}{E_{max}} - 1\right) BbA} \pm F_d = I_s w_r. \quad (6.75)$$

Expressions (6.74) and (6.75) apply to self-excited machines. For machines using self-excitation, the excitation current equals

$$I_s = \frac{U}{R_s} = \frac{F_s}{w_s},$$

from which, using (6.75), we can find the total resistance in the excitation circuit.

#### 6.4. DIRECT-CURRENT COMMUTATION

The maximum load for electrical-machine commutators is determined not only by the temperature rise, but in many cases by the requirement for sparkless operation of the sliding contact as well.



Major difficulties are involved in the study of commutation and the practical attainment of sparkless machine operation, since many different phenomena - electromagnetic, mechanical, physical, and chemical - are involved.

The effect of mechanical and physical-chemical factors on spark formation is especially great for aircraft commutator-type machines, which operate in the presence of severe vibration and sharply varying ambient-medium parameters.

From the practical viewpoint, the problem of commutation has been solved for general-purpose electrical commutator machines. At the same time, further study of this problem is required for commutator machines operating under severe conditions: direct-current aircraft machines used at high altitudes and high flight speeds, high-speed motors with a wide range of speed adjustment, motors used for intermittent duty with a large number of cycles, etc.

The classical theory of commutation, based on the assumption that the brush transfer-contact resistance is proportional to the area covered, i.e., that there is only contact conductance in the transition layer, has become suspect owing to several experiments and theoretical investigations carried out by Soviet authors (M.F. Karasev, O.B. Bron, etc.). So far, however, we still do not have a generally accepted theory of commutation which, in accordance with the latest studies, could yield an engineering design method for obtaining sparkless operation of commutator machines.

The fundamentals of the classical theory of commutation have been covered in the general course in electrical machines. In the present study, we consider only certain problems associated with special features of aircraft commutator machines and commutation calculations.

In order to decrease weight and size, aircraft electrical ma-

chines are made with high linear loads, high peripheral speeds, and relatively small air gaps; this results in considerable distortion of the magnetic field in the air gap, and increase in the mean reactive emf in a short-circuited section ( $e_r$ ), and intense vibration.

The field distortion and associated sharp shift in the true neutral plane causes the commutating section to enter a zone in which the armature-reaction field can act; this field induces an emf  $e_{yaq}$  in the commutating section that corresponds with  $e_r$ .

Since the mean values of  $e_{yaq}$  and  $e_r$  are proportional to the speed, commutation conditions are impaired as the speed increases, especially when we consider that vibration and jolting also increase.

We recall that in aircraft machines, the specific pressure on a brush can reach 400-700 g/cm<sup>2</sup>, i.e., it is 2-3 times greater than the normally acceptable specific pressures, which results in some decrease in the transfer-contact resistance and, consequently, in an increase in the current through the short-circuited section and impairment of commutation conditions.

In aircraft electrical machines, there will always be an induced transformer emf

$$e_t = -\frac{d\Phi}{dt} \cdot 10^{-8},$$

where  $t$  is the variation time of the excitation flux;  $\Phi$  is the excitation flux provided by the main poles.

The transformer emf appears as a result of the continuous variation in the main flux, which is a consequence of the regulation of generator voltage and motor speed.

If we also consider the variation in ambient-medium parameters during high-altitude and high-speed flights, it becomes clear that aircraft electrical machines operate under severe commutation condi-

tions.

It follows from what we have said that commutation problems should be given especial attention in machine design and manufacture.

As we know from the general course, the instantaneous current in a short-circuited section, on the basis of the classical commutation theory, is found from the equation

$$i_x = 2i_a \frac{0.5 - \tau}{1 + K_r \tau (1 - \tau)} + \frac{\sum e}{R} (1 - \tau) \tau, \quad (6.76)$$

where  $\sum e = -L \frac{di}{dt} + e_x + e_{s,r} + e_r$  is the sum of the emf's acting in the short-circuited section;  $\tau = t/T$  is the relative commutation time;  $K_r = (2r_k + r)/R$  is the relative resistance of the section,  $r$ , and of the risers,  $r_k$ ;  $R$  is the transfer-contact resistance;  $i_{ya}$  is the instantaneous current in a parallel circuit of the armature winding.

Depending on the value of  $\sum e$ , we can have: resistance commutation, where  $\sum e = 0$ , delayed commutation, where  $\sum e < 0$ , and accelerated commutation, where  $\sum e > 0$ .

Accelerated commutation is the most favorable, since in this case the current density at the trailing edge of the brush (which runs under poorer conditions, from the vibration viewpoint, than the leading edge) will be less and, consequently, the brush will leave the commutator segment (opening a circuit with self-induction) at a lower current density.

Assuming uniform (linear) variation of the current in the short-circuited section (straight-line commutation), we find the mean reactive emf in the form

$$e_p = \frac{4\Omega}{\delta_m} \omega^2 v i_a = \omega^2 c i_a, \quad (6.77)$$

i.e., the mean value of the reactive emf is directly proportional to the armature current  $i_{ya}$ , the speed  $v$ , and the square of the number of

turns  $w^2$  in the short-circuited section.

On the basis of the classical theory of commutation, the factor responsible for sparking is the excessive current density at the trailing edge of the brush which results from the addition to the working current of the additional current  $i_k$  due to the reactive emf. As we know, in the trailing portion of the brush, the working and additional currents have the same direction, i.e.,  $i_2 = i_{ya} + i_k$ ; this accounts for the tendency to form an external commutating emf  $e_k$  that would compensate  $e_r$  throughout the entire commutation cycle.

It is clear that this can occur only where the curve representing the commutating emf is the mirror image of the reactive-emf curve. Since this cannot actually occur, the basic cause of sparking must be considered to be the presence of the uncompensated parts of  $e_r$  ( $\Delta e = e_r - e_k$  in Fig. 6.35); as has been shown, they rise as the number of turns, the load, and the speed increase. This accounts for the tendency to limit  $e_r$  to the minimum possible value, which also leads to a decrease in  $\Delta e$  (below it is shown that this is not so).

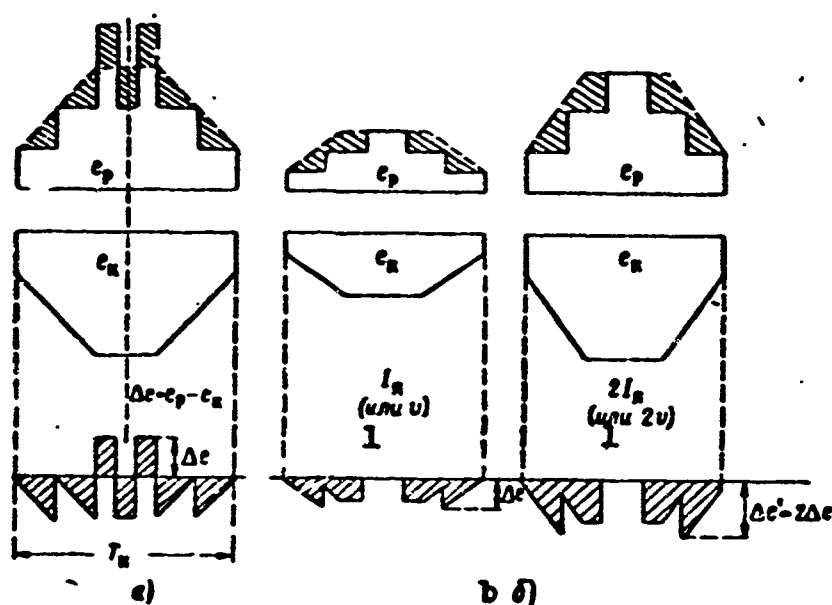


Fig. 6.35. Curves for reactance and commutation emf's. a) Uncompensated parts of emf; b) effect of current  $I_{ya}$  or speed  $v$  on magnitude of uncompensated portion of emf  $\Delta e$ . 1) Or.

Although the classical theory of commutation is based on the assumption that there is purely contact conductance in the brush contact, the latest investigations have established that more complicated phenomena occur: ion processes, spark processes (due to contact vibrations), and electrolysis of the thin layer of moisture that precipitates on the commutator surface. Current can flow between brush and commutator by way of contact conductance, ion conductance, and electronic emission.

In brushes carrying currents of less than 3 amp, contact conductance predominates, and the classical theory of commutation is applicable.

The processes occurring in brushes carrying more than 3 amp are basically of ionic nature, and the classical theory of commutation is inapplicable.

#### The Nature of the Sliding Contact

Even well-adjusted brushes and an outstandingly well-made commutator will not provide a perfect match between the commutator and the brush surface owing to brush play in the brushholder and the inevita-

ble roughness of the commutator, the differing thermal coefficients of expansion of the brushes and commutator, and vibration in the mechanical structure.

As a result, at any instant in time, the contact surface between brush and commutator consists of three parts, as it were: a zone of direct contact - the mechanical contact, the zone filled with a conducting layer of copper-graphite dust, and a zone containing a thin layer of air (Fig. 6.36).

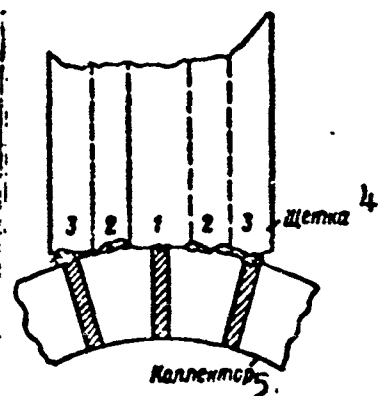


Fig. 6.36. Illustrative diagram of sliding contact. 1) Zone of direct contact; 2) conducting layer of copper-carbon dust; 3) air gap; 4) brush; 5) commutator.

The zones vary continuously both in magnitude and their location at the brush surface.

Thus there are three ways for a current to flow through a sliding contact: through the direct contact; through the conducting layer of copper dust, and through the thin air p.

The current density at the contact points reaches values of several thousand amps/cm<sup>2</sup> with mean current densities of 10-30 amp/cm<sup>2</sup>. As a result of the great current density, some of the contact points become red hot, and others white hot. As we know, at red heat, there will be a flow of positive ions from anode to cathode (Fig. 6.37); the acceleration of the ions will be greater the higher the voltage applied to the electrodes (commutator-brushes). In addition, electrons are emitted from the cathode at white heat.

Thus, in a brush contact we observe thermal ionization at red-hot points and thermal emission of electrons at white-hot points.

At some definite speed (determined by the voltage) of the positive ions, burst ionization will appear. In this case, the stream of electrons from the cathode ionizes the gases lying between the electrodes, forming an electric arc.

The transport of electricity by positive ions is accompanied by anodic vaporization of matter. Since the vaporization temperature of copper (about 2400°) is lower than the vaporization temperature of carbon (about 4000°), copper emits far more ions than carbon, i.e., anodic vaporization at the commutator is greater than anodic vaporization at a brush. In addition, spark and arc discharges occur at the sliding commutator contact as a result of the closing and opening of commutator-section circuits.

As we know, vibration of a contact in an electrical circuit is accompanied by sparking at times of contact closure and by arcing at

times of contact opening (not visible at low voltages).

Since the opening of a contact is accompanied by an arc only when the voltage and current exceed specified values (Fig. 6.38), two regimes and zones are possible: pure spark discharges and spark and arc discharges. Spark and arc discharges are accompanied by directional transport of matter.

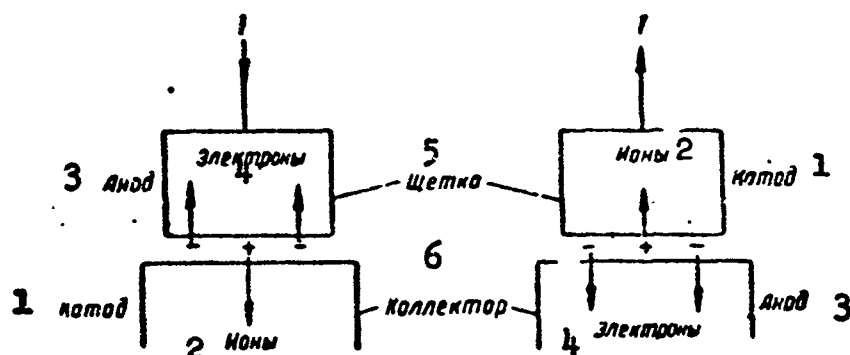


Fig. 6.37. Direction of anodic vaporization and electron emission as a function of brush polarity (current direction). 1) Cathode; 2) ion; 3) anode; 4) electron; 5) brush; 6) commutator.

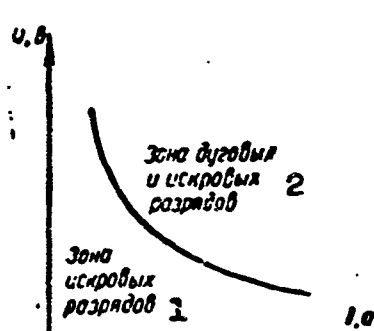


Fig. 6.38. Transition boundary between spark-discharge zone and arc-discharge zone. 1) Spark-discharge zone; 2) arc-and-spark discharge zone.

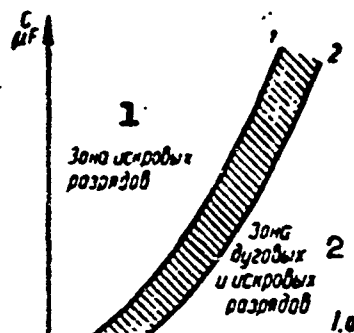


Fig. 6.39. Zone of minimum brush and commutator wear. 1) Spark-discharge zone; 2) arc-and-spark discharge zone.

In the presence of a spark discharge, the temperature of the electrodes does not increase, and matter is transported from anode to cathode, as in the case of anodic vaporization by positive ions. In an

arc discharge, there occur temperature rises and matter is transported from cathode to anode resulting in thermal destruction of the cathode.

If the electrical circuit operates in the zone of arc and spark discharges, a region can also exist in which matter is transported from anode to cathode by spark and from cathode to anode by arc in roughly equal amounts (Fig. 6.39).

It is clear that for operation in the zone to the left of 1, matter will be transported to the cathode, while for the operation in the zone to the right of 2, transported matter to the anode will predominate.

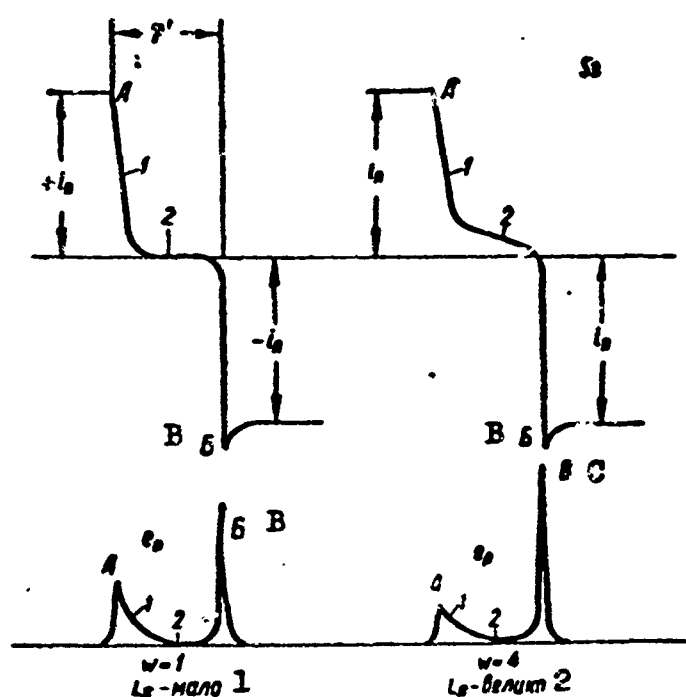


Fig. 6.40. Curves for current and reactance emf of commutation section. A) Section closure; B) section opening. a) Low inductance,  $w = 1$ ; b) high inductance,  $w = 4$ .

Transport due to spark and arc discharges in a sliding contact will depend on many factors, including the characteristics of the commutation circuit, the brush material, and the properties of the medium between the brush and commutator.

We can state that in the general case current can flow through a



sliding commutator contact in three parallel modes: using the contact conductance, anodic vaporization, and spark or arc discharge.

In accordance with what has been said, we should consider the problem of minimum electrical wear on brushes and commutator (zone 1-2).

Phenomena occurring in a commutation section. M.F. Karasev, generalizing studies of K.I. Shenfer, S.B. Yuditskiy, O.G. Vagner, O.S. Yelokhin, and others, has used models, a cathode-ray oscilloscope, and a peak voltmeter to study the nature of the commutation process in a short-circuited section and the way in which  $e_r$  depends on  $i_{ya}$ ,  $w$ ,  $n$ , etc.

It follows from the experimental curves of Fig. 6.40 that: a) in a commutation section there is no smooth variation in current, voltage, and contact resistance ( $r_1$  and  $r_2$ ), i.e., there is almost no resistance commutation; b) in the general case, the commutation process consists of two quite different phenomena: a rapid decrease in the current to zero at the instant the section is closed (A) and an abrupt rise in the current in the opposite direction when the section is opened (B); these events are accompanied by corresponding voltage spikes.

Thus, commutation is a discontinuous rather than a continuous process, and consists of two basically different phenomena accompanying section closure and opening.

Experimental results agree with the physical picture of the ionic-electronic nature of the sliding contact.

#### Effect of Various Factors on $e_{r \max}$

Effect of load current (Fig. 6.41). The function  $e_{r \max} = f(i_{ya})$  displays abrupt variations, i.e., at low currents  $e_{r \max}$  increases slowly, and at some critical current in the section ( $i_{kr}$ ) it rises sharply to a maximum value, and then remains constant with further

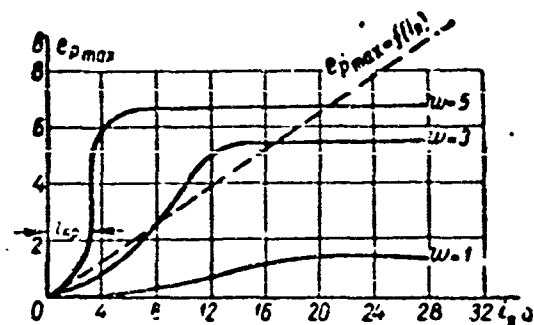


Fig. 6.41. Quantity  $e_{r \max}$  as a function of load current for various numbers of commutation-section turns with a copper-graphite MG brush. The dashed line shows the way in which  $e_{r \max}$  depends on  $I_a$  according to the classical theory.

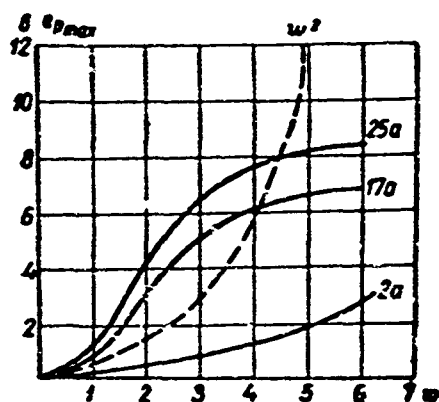


Fig. 6.42. Quantity  $e_{r \max}$  as a function of number of turns in section with  $n$  and  $I$  constant. The dashed line shows the function  $e_{r \max} = f(w)$  according to the classical theory.

increases in current. The abruptly changing function  $e_{r \max} = f(I_a)$  indicates the ionic nature of the sliding contact.

The sharp increase in  $e_{r \max}$  when the critical current is reached is explained by the fact that an ionized region is formed under the trailing edge of the brush, and the current in the section will vary sharply in magnitude; as a result, a peak reactance emf will appear. A further increase in

the current will not increase the peak reactance emf, but will only increase its base width, indicating that there is an expansion of the ionized region under the brush.

Thus, contact conductance predominates on the section of low subcritical currents, while ionization occurs when the critical current is reached and the contact conductance loses its importance. For currents above the critical value, the ionization rate increases; as we know, however, this is not accompanied by an increase in the voltage between the electrodes.

Effect of the number of turns. Despite the classical theory, the function  $e_{r \max} = f(w)$  (Fig. 6.42) is not parabolic in nature in the general form. For a current of less than critical value (contact conductance),  $e_{r \max} = f(w)$  will be parabolic, while for currents above  $I_{kr}$ , the bend in

the curve  $e_{r \max} = f(w)$  will change sharply, and at low values  $w$ ,  $e_{r \max} \equiv w$ . Where the number of turns is large,  $e_{r \max}$  is nearly in-

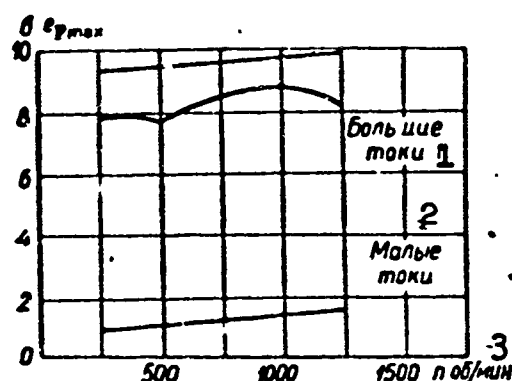


Fig. 6.43. The quantity  $e_{r \max}$  as a function of speed for small and large currents. 1) Large currents; 2) small currents; 3) rpm.

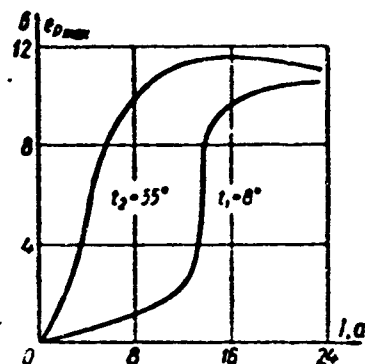


Fig. 6.44. Quantity  $e_{r \max}$  as a function of load current for various contact-layer temperatures.

dependent of  $w$ .

It has been found that the higher the inductance  $L$  of the section the lower the currents at which the "parabolic" relationship commences to cease to apply. This is explained by the fact that the factor responsible for the ionization is the electromagnetic energy of the section, which is proportional to the inductance and, consequently, when the inductance increases, less current is needed to trigger ionization.

The quantity  $e_{r \max}$  can characterize vaporization to some degree only in the initial stage of the ionic process in the brush contact. The quantity  $e_{r \max}$  is characteristic of brush quality, rather than its degree of vaporization. The degree of sparking and its intensity is characterized by the ratio of currents  $i/i_{kr}$ ; specifically when  $i/i_{kr} \leq 1$ , there is no sparking, while sparking is observed when  $i/i_{kr} > 1$ .

Effect of speed. For currents below the critical value, the function  $e_{r \max} = f(n)$  (Fig. 6.43) will vary in accordance with the conc?

sions of classical commutation theory, i.e.,  $e_{r \max} = n$ , while for currents exceeding the critical value, where there is contact ionization,  $e_{r \max}$  will be nearly independent of the speed.

Effect of contact-layer temperature (Fig. 6.44). The higher the temperature in the commutator contact layer, the lower the value of load current at which ionization will commence in the contact layer and the higher the value of  $e_{r \max}$ . Thus, with an increase in commutator temperature there will be a drop in the value of the critical current, i.e., the ionization triggering current and, consequently, all other conditions being equal the spark formation will commence at lower load values.

Role of the commutating poles. In classical commutation theory, the commutating poles are considered as a device designed to compensate for the reactance emf. Here it is assumed that once compensation occurs, it will not be disturbed by variations in armature speed; in practice, this is not the case, since it is impossible to obtain perfect compensation owing to the difference in the shapes of the  $e_k$  and  $e_r$  curves. As we know, the magnetizing force due to the commutating-pole windings equals the sum of the armature magnetizing force in the commutation zone and the magnetizing force needed to form the commutating-pole flux. A series of experiments were carried out in order to find the influence of the commutating poles; the results are given below.

An analysis of the oscillograms of Fig. 6.45 shows that in machines with commutating poles, the current distribution between the trailing and leading portions of the brush is automatically kept unchanged under load variations, i.e.,

$$\frac{i_2}{i_1} \approx \text{const.}$$

Thus, series connection of the commutating-pole windings does not compensate the reactance emf, but does keep the current distribution between the trailing and leading regions of the brush unchanged.

By varying the excitation of a commutating pole, it is possible to transfer the current-takeoff process from the trailing region of the brush to the leading region, and to change the current distribution to values favoring commutation ( $i_2 \approx 0.6-0.7 i_{ya}$ ). It is possible to shift the current takeoff function completely to the leading portion of the brush and even to make  $i_2$  negative (Fig. 6.46).

Consequently, the commutating poles can transfer a considerable portion of the current takeoff function to the leading region of the brush, which operates under less severe vibration; there is automatic adjustment of the given (favorable) current distribution, i.e., the ratio  $i_2/i_1 = \text{const}$ , but it is not possible to eliminate sparking if the electromagnetic energy of the section proves to be excessive. This means that brush sparking is not caused by the fact that the  $e_k$  and  $e_r$  curves do not cancel each other out ( $e_k$  and  $e_r$  have nothing in common), but by the fact that an excessive load is permitted for a given brush quality, and sparkless commutation is impossible. The degree of sparking depends on the brush-contact operating regime, in the sense of the distribution of current between the leading and trailing parts. We may draw several conclusions from the preceding discussion.

1. At small loads, we basically have contact conductance in the brush contact through the points of contact.
2. When the critical current is reached, the trailing edge of the brush is abruptly ionized and the curves characterizing commutation experience a sharp change in form.
3. The current and emf curves indicate that the commutation process contains two time-delimited processes - section closure and open-

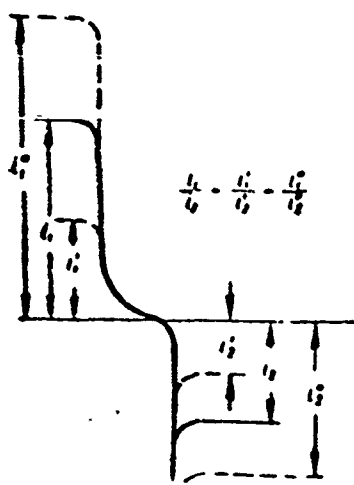


Fig. 6.45. Ratio of current in leading part of brush  $i_k$  to current in trailing part of brush  $i_2$  as a function of load.

ing, which correspond to drops in currents and the corresponding reactance-voltage peaks.

In actual machines (rather than models) these processes are less well defined owing to the superposition of extraneous influences, but they can always be observed.

4. It has been noted that the quantity  $e_{r \max}$  corresponds to the voltage across the electric arc. Since various grades of brush will have differing values of arc voltage, the value of  $e_{r \max}$  will also be different for different brush grades.

5. When ionization begins at the critical current, sparking cannot be noticed. The existence of brush-contact ionization at the crit-

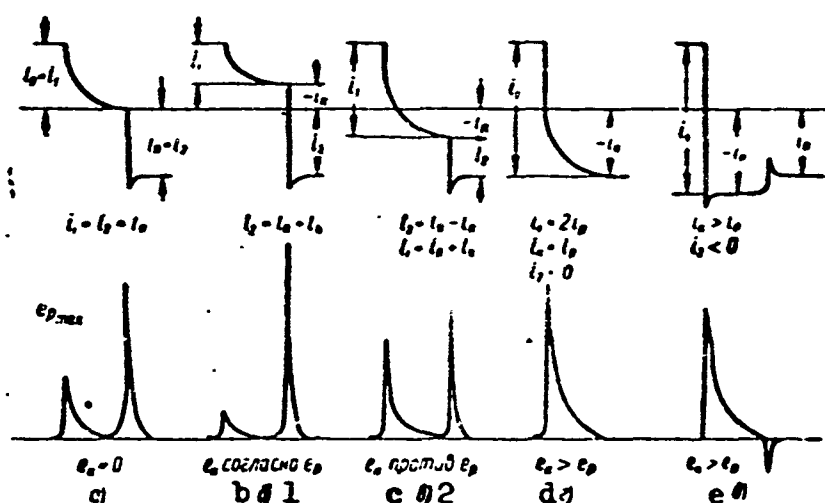


Fig. 6.46. Curves for current and reactance emf as a function of degree of excitation of commutating poles (d.p.). a) Commutating poles not excited,  $e_k = 0$ , delayed commutation; b) commutating poles excited, but  $e_k$  and  $e_r$  have same direction - commutation greatly delayed; c) commutating poles excited and  $e_k$  opposite in direction to  $e_r$ ; d) commutating poles overexcited and  $e_k > e_r$ , trailing edge of brush carries no current, commutation accelerated; e) commutating poles considerably overexcited, reactance emf at trailing edge of brush changes sign.

ical current can be verified by the abrupt variation in brush-contact conductance owing to the effect of temperature variation.

Experiments have shown that noticeable sparking at the brushes appears when the load current is two or three times the critical value, i.e., when the ionization rate reaches some specific value.

It is possible to conclude that spark formation in sliding contacts of commutator machines appears as the result of a vigorous ionization, and that is determined by the electromagnetic energy of the section, all other conditions being equal.

For a given value of section electromagnetic energy, the appearance of noticeable sparking is affected by numerous factors that decrease the critical-current value (brush quality, condition of the rubbing surfaces, parameters of the ambient medium) and increase the ratio  $1/i_{kr}$ , which characterizes the ionization rate.

The basic data of the classical commutation theory have long ago been shown to be inadequate. In view of the complexity of commutation phenomena, however, it is only within the past decade that a new picture of the nature of the sliding contact has been formed. Unfortunately, there so far is no mathematical solution for the commutation problem that takes account of the ionic processes involved. It is necessary to accumulate further experimental materials from models and actual machines. We should take note of the analytical commutation theory of O.G. Wagner, which is based on the constant voltage drop at the brushes, and the theory of I.S. Yelokhin, based on the constant contact resistance of the leading and trailing brush edges. Both of these theories give good agreement with experimental data for special cases; they do not take into account all of the phenomena involving commutation, however, and cannot be accepted as a general theory of commutation.

The classical commutation theory will be used henceforth, since it permits examination of commutation with the utilization of a large body of experimental material.

A considerable improvement in commutation can be obtained by proper choice of commutation zone and commutator, brushes, and brush holding device, active-layer geometry and winding circuit, as well as by the utilization of commutating poles and compensating windings.

### Commutation Zone

The commutation zone, i.e., the length of the arc along the armature circumference on which commutating sections are located, is determined by the dimensions of the commutator and brushes, as well as by the type of armature winding.

The width of the commutation zone may be found from the equation

$$b_{k,z} = b'_{shch} + \tau'_k \left( n_s + \epsilon - \frac{a}{p} \right), \quad (6.78)$$

where  $b'_{shch} = b_{shch}(D/D_k)$  and  $\tau'_k = \tau_k(D/D_k)$  are the brush width and commutator pitch in terms of the armature circumference;  $\epsilon = K/(2p - y_1)$  is the decrease or increase in the winding pitch;  $n_s = K/z_p$  is the number of elementary slots in a single slot;  $z_p$  and  $K$  are the number of armature slots and commutator segments;  $y_1$  is the coil pitch.

The commutation zone should not exceed the pole spacing, i.e.,

$$b_{k,z} < \tau - b = \tau(1 - a) = b_{k,z} + 2t_{k,z}, \quad (6.79)$$

where  $t_{k,z}$  is the distance between the edge of a main pole and the end of the commutation zone (Fig. 6.47).

This last expression may be written as

$$b_{k,z} = k_{k,z}(\tau - b) = k_{k,z}(1 - a)\tau. \quad (6.80)$$

In selecting the permissible width of the commutation zone, we must consider that an increase in the ratio  $k_{k,z} = b_{k,z}/(\tau - b)$ , i.e., a decrease in  $t_{k,z}$ , will impair the electromagnetic processes in the



commutation zone, since the commutation section will enter a region in which the main-pole leakage fluxes will have a harmful effect; a decrease in the  $k_{k.z}$  ratio, i.e., an increase in  $t_{k.z}$ , favors the commutation process but leads to a decrease in  $\alpha$  and a corresponding increase in machine size and weight.

The two requirements are contradictory and we select the maximum commutation-zone width for which commutation is satisfactory, i.e., the main-pole leakage fluxes take on permissible values in the leading and trailing portions of the commutation zone.

In general-purpose machines, the distance between the edge of the main pole and the end of the commutation zone normally equals

$$t_{k.s} = (0.25 + 0.35)(1 - \alpha)\tau. \quad (6.81)$$

Taking (6.79) and (6.81) into account, we find that

$$k_{k.s} = \frac{b_{k.s}}{\tau - b} = 1 - \frac{2t_{k.s}}{(1 - \alpha)\tau} \approx 0.5 + 0.3, \quad (6.82)$$

i.e., in general-purpose machines the commutation zone amounts to (50-30)% of the interpole space, and  $b_{k.z} = (0.5 - 0.3) \times (\tau - b)$ .

In aircraft machines using commutating poles

$$t_{k.s} \approx (0.05 + 0.2)(1 - \alpha)\tau \quad (6.83)$$

consequently,

$$k_{k.s} = 1 - \frac{2t_{k.s}}{(1 - \alpha)\tau} \approx 0.9 + 0.6. \quad (6.84)$$

In the absence of commutating poles

$$t_{k.s} \approx (0 + 0.075)(1 - \alpha)\tau$$

and

$$k_{k.s} \approx 1.0 + 0.85. \quad (6.85)$$

If  $b_{k.z}$  is expressed in pole-pitch fractions, the width of the commutation zone for a general-purpose direct-current machine will equal  $b_{k.z} \approx (0.1 - 0.15)\tau$ , while in aircraft generators it will reach values of  $b_{k.z} \approx (0.2 - 0.25)\tau$ . In aircraft machines, the commutation

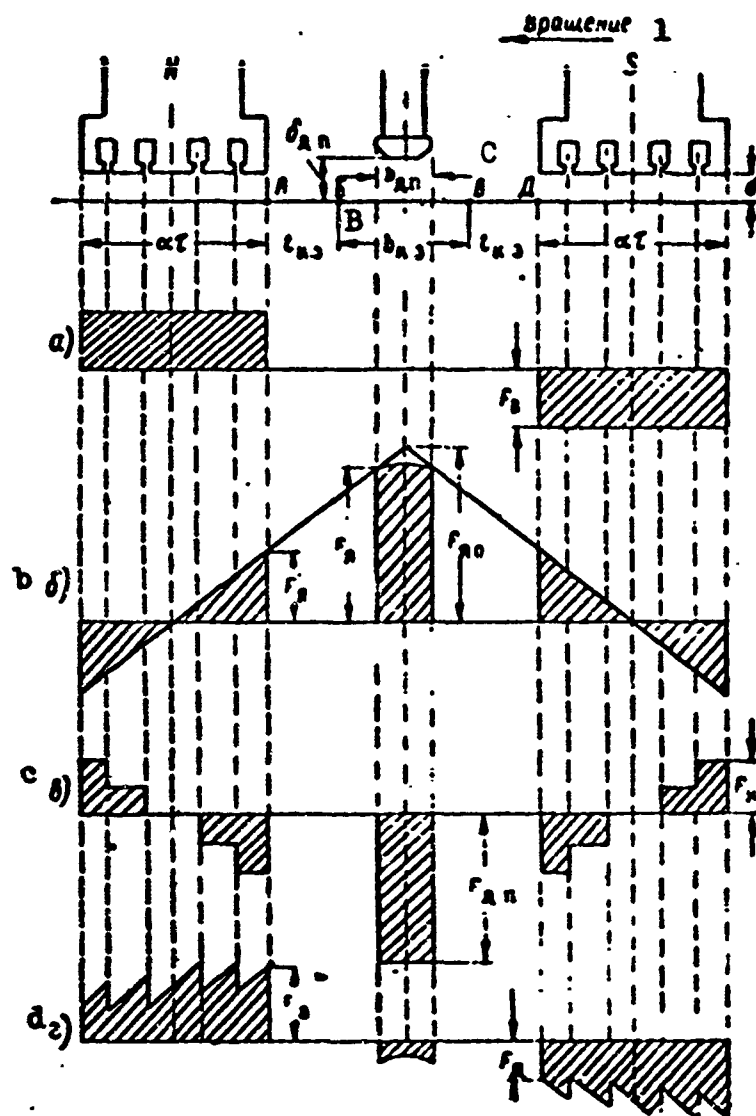


Fig. 6.47. Simplified drawing of magnetizing force in compensated aircraft generator. 1) Direction of rotation.

zone is increased in the attempt to reduce commutator length. As a matter of fact, for constant current density,  $j_{shch} = \text{const}$ ; the cross section under the brush remains constant, i.e.,

$$S_m = b_m l_m = \frac{l}{j_m} = \text{const.}$$

If  $D_k$  and  $\tau_k$  are constant, the commutation zone can be expanded by increasing  $b_{shch}$  and, consequently, reducing the active length of the commutator.

The width of a brush and the active length of the commutator, de-

pending on the magnitude of the commutation zone, will equal

$$\left. \begin{aligned} b_m &= b_{x,0} - i_x \left( n_s + z - \frac{z}{p} \right) = b_{x,0} - \beta, \\ l_x &= n_k l_m = n_k \frac{S_m}{b_m} = \frac{n_k S_m}{b_{x,0} - \beta} \frac{D}{D_k}, \end{aligned} \right\} \quad (6.86)$$

where

$$\beta = i_x \left( n_s + z - \frac{z}{p} \right) = \text{const.}$$

$n_k$  is the number of brushes per pole.

It must be remembered that shortening of the commutator by expansion of the commutation zone (by increasing  $b_{shch}$ ) leads to increased commutator heating. Actually, the temperature drop at the commutator surface will be determined by the equation

$$\theta_x = \frac{A_x}{\alpha_x},$$

where

$$A_x = \frac{P_x}{\pi D_k l'_x} = \frac{l \Delta U_m + P_{r,x}}{\pi D_k l'_x} \text{ [watt/cm}^2\text{]} \quad (6.87)$$

is the heat-transfer rate;

$$\alpha_x = \alpha_0 + \alpha_1 \sqrt{v_x} \text{ [watt/cm}^2 \text{ } ^\circ\text{C]} \quad (6.88)$$

is the heat-transfer coefficient for the commutator surface; here

$$l'_x = l_x + b n_k + a_1 \text{ [cm]} \quad (6.89)$$

is the total commutator length (Fig. 6.48);

$$P_x = P_{e,x} + P_{r,x} \text{ [watts]}$$

are the total commutator losses;

$$P_{e,x} = l \Delta U_m \text{ [watts]}$$

are the electrical losses at the commutator;

$$P_{r,x} = 9.81 S_x v_x P_{shch} \text{ [watts]}$$

are the brush friction losses ( $P_{shch}$  is the brush pressure).

Since where  $v_k$  and  $D_k$  are constant in value,  $P_k$  and  $\alpha_k$  do not depend on brush width, since

$$l_k = n_k \frac{S_m}{b_m} \text{ and } S_m = \text{const},$$

the temperature drop at the commutator will be

$$\theta_k = \frac{P_k}{\pi D_k a_k} \frac{b_m}{n_k S_m \left( 1 + b_m \frac{a_1 + b n_k}{n_k S_m} \right)}. \quad (6.90)$$

i.e., it rises with an increase in the brush width  $b_{shch}$  and, consequently, in the commutation zone  $b_{k.z.}$ . Thus, the increase in commutation-zone width is also limited by commutator heating.

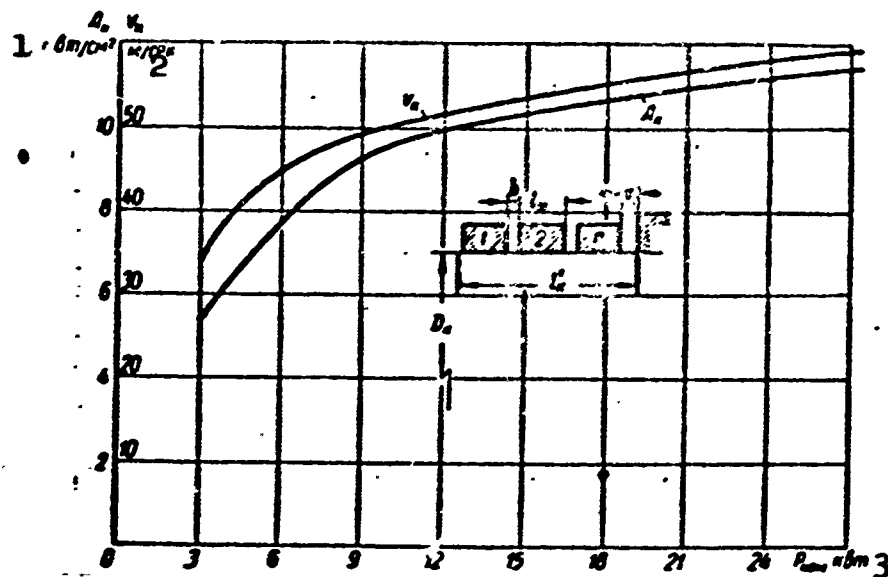


Fig. 6.48. Heat-transfer rate  $A_k$  and peripheral speed  $V_k$  for aircraft-generator commutators. 1) Watts/cm<sup>2</sup>; 2) m/sec; 3) kw.

A commutation section located in the commutation zone on the arc  $\overline{BB}$  is subject to the action of the main-pole leakage fluxes. If a magnetizing force  $F_A$  acts at point A (see Fig. 6.47), it will form a field with induction at point B where the leading part of the short-circuited section is located.

$$B_B = 1.25 \frac{F_A}{\sqrt{r_{A0}^2 + l^2}}.$$

Similarly, at the trailing portion of the section (point C) the main-pole leakage field  $B_B$  acts as a result of the magnetizing force  $F_D$ , i.e.,

$$B_B = 1.25 \frac{F_D}{\sqrt{r_{D0}^2 + l^2}}.$$

The fields  $B_E$  and  $B_B$  induce an emf in the short-circuited section that has the same direction as  $e_r$ , and which impairs commutation conditions.

By the measure of the degree to which commutation processes are worsened in the commutation zone owing to the main-pole leakage fluxes, we may use the ratio of the leakage magnetic induction in the commutation zone  $B_E$  and  $B_B$  to the maximum commutating-pole induction  $B_{k \max}$ .

The permissible values of the ratios  $B_E/B_{k \max}$  and  $B_B/B_{k \max}$  will depend on the magnitude of  $e_r$  for the commutating section, brush quality, the voltage between adjacent commutator segments, the rigidity of the structure, and machining quality.

#### Determining Commutator Dimensions

For a given commutator active surface or total brush cross section  $S_k = 2pn_k S_{shch}$ , the commutator may be made in two versions: a)  $D_k$  small,  $l'_k$  large; b)  $D_k$  large,  $l'_k$  small.

In the first case, the friction losses will be reduced, since  $P_{t.k} \equiv D_k(v_k)$  and commutation conditions will be improved. Here, however, cooling conditions are impaired, since  $\alpha_k$  depends on  $\sqrt{D_k}$ , and there will be an increase in excitation-current fluctuations due to shifts in the neutral plane that will be observed during operation. Here the commutation zone  $b_{k.z} \equiv D/D_k$  will be increased, since the ratio  $D/D_k$  will increase. This will prove harmful as long as the brush width and commutator pitch remain unchanged. If, however, the commutator diameter is decreased to some specific limit, there may be a corresponding decrease in brush width and commutator pitch, i.e., the ratio  $b_{shch}/\tau_k$  will remain unchanged. In this case, as the expression

$$\begin{aligned} \delta_{\omega} &= \frac{D}{D_k} \tau_k \left[ \frac{b_m}{\tau_k} + \left( n_s + s - \frac{e}{p} \right) \right] = \\ &= \frac{\omega D}{K} \left[ \frac{b_m}{\tau_k} + \left( n_s + s - \frac{e}{p} \right) \right]. \end{aligned} \quad (6.91)$$

shows clearly, the commutation zone remains unchanged since

$$\pi D_z = K \tau_k, \quad D_z = \frac{K \tau_k}{\pi} \quad \text{and} \quad \frac{D_z}{\tau_k} = \frac{K}{\pi}.$$

Thus,  $b_{k.z}$  does not depend on the commutator diameter provided by  $b_{shch}/\tau_k = \text{const.}$

By reducing the commutator diameter we decrease the commutator losses, which is especially important in aircraft machines, where they are large. In aircraft generators the commutator diameter normally equals the armature diameter, while in direct-current general-purpose machines, it is less than the armature diameter.

The shorter the brush, the more reliably an individual brush makes contact and the better the cooling. The number of brush bolts will always be taken equal to the number of poles. In contrast to general-purpose machines where the brushes are staggered in order to reduce commutator wear, in aircraft machines they are placed in a single row in order to reduce the axial lengths of the commutator.

Optimum commutator dimensions. It is of practical interest to determine the minimum surface or minimum volume of a commutator for a given temperature rise  $\vartheta_k$  and active commutator surface  $S_k = 2\pi n_k S_{shch} \times \times \text{cm}^2$ . The commutator temperature rise may be represented by the equation

$$\vartheta_k = \frac{P_k}{S_{k,z} \alpha_k} = \frac{P_{a,k} + P_{r,k}}{\pi D_z l'_k \alpha_k}. \quad (6.92)$$

In this case, the total heat-exchange surface of the commutator will be

$$S_{k,z} = \pi D_z l'_k = \frac{1.5 U_m + k \tau_k}{\alpha_k (z_0 + z_1 \sqrt{\vartheta_k})} = f(\vartheta_k). \quad (6.93)$$

The commutator volume is

$$Q_k = \frac{\pi D_z^2 l'_k}{4} = S_{k,z} \frac{D_z}{4} = \frac{P_{a,k} + P_{r,k}}{1.5 \alpha_k} \frac{60 \vartheta_k}{4 \pi n_k} \quad (6.94)$$

or, taking  $\alpha_k$  into account,

$$Q_k = \frac{15v_k}{\pi n} \frac{I\Delta U_m + k_1 v_k}{\theta_k (\alpha_0 + \alpha_1 \sqrt{v_k})} \quad (6.95)$$

where

$$\begin{aligned} P_{r,k} &= k_1 v_k \\ k_1 &= 9.81 S_k P_m v_m \approx 19.6 p n_k S_m P_m v_m \\ v_k &= \frac{\pi D_k n}{60} \\ \alpha_k &= \alpha_0 + \alpha_1 \sqrt{v_k} \end{aligned}$$

Taking the derivative of (6.93) with respect to  $v_k$ , we can obtain the commutator speed and diameter for which the value of  $S_{p,k}$  will be a minimum, while by taking the derivative of (6.95) with respect to  $v_k$  and assuming  $n = \text{const}$ , we can find the commutator speed and diameter for which the commutator volume will be at a minimum (on the assumption that  $v_k$  is increased by increasing  $D_k$ ).

#### Current Density Under a Brush

The permissible current density under the brushes is determined from the heating conditions for the brush and commutator.

Substituting into (6.92) the active commutator surface and the armature current, i.e.,  $S_k = 2pl_k b_{shch}$  and  $I = pl_k b_{shch} j_{shch}$ , we obtain

$$\theta = \frac{9.81 v_k (2pl_k b_m) P_m v_m + \Delta U_m (pl_k b_m) j_m}{\pi D_k j_k \alpha_k} \quad (6.96)$$

and then, since  $\alpha_k = \alpha_0 + \alpha_1 \sqrt{v_k}$ , the current density at the brush will equal

$$j_m = \frac{v_k}{\Delta U_m} \left( \frac{\pi D_k}{2p} \frac{j_k}{l_k} \frac{2\theta_k}{b_m} \frac{\alpha_0 + \alpha_1 \sqrt{v_k}}{v_k} - 19.62 P_m v_m \right)$$

or

$$j_m = \frac{v_k}{\Delta U_m} \left[ \frac{60}{pn} \frac{j_k}{l_k} \frac{\theta_k}{b_m} (\alpha_0 + \alpha_1 \sqrt{v_k}) - 19.62 P_m v_m \right] \quad (6.97)$$

Thus, the permissible current density under the brushes will rise with increases in the permissible temperature rise  $\theta_k$ , the commutator

peripheral speed  $v_k$ , and the ratio  $l'_k/l_k$ , as well as with decreases in the brush width, brush pressure  $P_{shch}$ , and voltage drop across the sliding contact  $\Delta U_{shch}$ .

#### 6.5. THE SLIDING CONTACT AT HIGH ALTITUDES

The condition of the sliding contact between brush and commutator determines the reliability of commutator-machine operation.

The carbon brush is widely used in electrical-machine design owing to the fact that it possesses two noteworthy properties: low coefficient of friction and low contact resistance. Metals that have low contact resistances cannot be used without lubrication, while all types of lubricants, with the exception of graphite, are poor conductors and impair the contact.

Brushes may be made in almost any form and in any combination with powdered metals, which makes it possible to manufacture them with various characteristics and to use them under different conditions. Under normal sea-level operating conditions, brush wear owing to electrical and mechanical factors proceeds relatively slowly. Wear owing to the phenomenon of commutation is more important than are mechanical factors. This is confirmed by the fact that brushes wear considerably more rapidly at a commutator than at slip rings.

The brushes of aircraft electrical machines should provide almost "dark" commutation (1-1/4 units on the scale) under all rated operating conditions, allowing for variations in temperature, pressure, humidity, and air composition; they should have relatively low losses at high peripheral commutative speeds; there should be only slight wear during high-altitude flights; and they should withstand the intense vibration of the aircraft engine.

These requirements are satisfied by the electrically engraved Type A brushes used in GS-series generators of 0.35-1.5 kw power and



TABLE 6.3

The Basic Parameters of Brushes for Aircraft Electrical Machines

1 Обозна- чение	2 Плотность тока $j_{sh}$ в а/см <sup>2</sup>	3 Давление на щетку $P_{sh}$ в г	4 Скорость коллектора $v_k$ в м/сек	5 Падение напряже- ния $\Delta U_{sh}$ в в	6 Удельное сопротив- ление $\rho$ , ом/мм <sup>2</sup>	7 Кoeffици- ент трения $\mu_{sh}$	8 Износ за 50 час. мм	9 Твердость по Шору, °
15 МГС-6	15	250	15	2,0	3-15	0,25	0,25	—
15 МГС-7	27	600	55	1,6-2,4	3-10	0,20	0,35	14÷25
15 МГС-8	28	600	55	2,0-2,8	6-16	0,20	0,50	11÷21
15 МГС-12	—	—	—	1,0	He 60- acc 5	0,16	0,50	15÷25
А-8	15	250	15	0,7-1,7	2,5-10,5	0,20	0,20	26÷35
А-12	24	600	15	1,6	2,5-10,5	0,17	0,25	—
А-16	15	400	40	2,3	24-40	0,25	0,15	40÷60
А-29	24	500	40	3,5	10-17	0,22	0,20	—

1) Designation; 2) current density; 3) pressure on brush; 4) commutator speed; 5) voltage drop; 6) resistivity; 7) coefficient of friction; 8) wear in 50 hr; 9) Shore hardness; 10)  $j_{shch}$ , amp/cm<sup>2</sup>; 11)  $P_{shch}$ , g; 12)  $v_k$ , m/sec; 13)  $\Delta U_{shch}$ , v; 14)  $\rho$ , ohm/mm<sup>2</sup>; 15) MGS; 16) no more than 5.

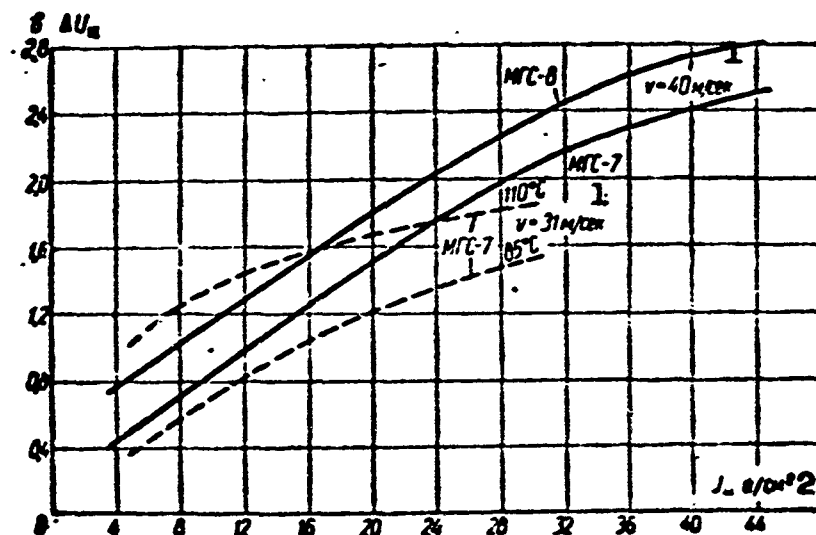


Fig. 6.49. Volt-ampere characteristic for high-altitude MGS brushes. The dashed line gives experimental curves for  $v = 31$  m/sec, and the solid lines represent averaged data for  $v = 40$  m/sec. 1) m/sec; 2) amp/cm<sup>2</sup>.

the Type MGS high-altitude copper-graphite brushes used in high-power generator series. The basic characteristics of these brushes are shown in Table 6.3.

Figure 6.49 shows the volt-ampere characteristic of MGS brushes.

It is clear that the steeper the volt-ampere characteristic of a brush, the wider will be the range of current densities under the brush for which the voltage drop will remain constant, and the smoother machine commutation will be. The voltage drop or contact resistance depends on the specific pressure of the brush, the ambient parameters, and the commutation conditions.

As brush resistivity increases, the voltage drop decreases. With increasing flight altitude, the contact resistance and contact voltage drop will rise, and at altitudes of about 20 km will have roughly (at the working current densities) twice their ground-level values.

Brush construction. As a rule, the current-carrying lead of the brush cable is attached to the brush with the aid of a special fitting, or is soldered on. Under high-temperature conditions, solder is not reliable while if the fitting is used without soldering, there will be a considerable increase in the contact resistance between the brush and the brush-cable lead, causing additional heating of the brush. In addition, this type of mounting is not reliable in the presence of vibration.

For aircraft brushes, it is worth using a "calked" connection; here the brush cable is inserted in a drilled and tapped hole in the brush which is then filled under pressure with a copper-graphite powder containing up to 30% silver so as to fill the space between brush and cable.

Brush installation. For two-way rotation, the brushes are installed radially, while for rotation in one direction, they are in-

clined to the direction of rotation of the commutator. The brushes will operate more stably if they are located at an angle to the commutator. In this case, the friction forces appearing between brush and commutator reduce the force with which the spring presses the brush against the ring. As a result, the contact operates more smoothly, and friction losses between brush and ring are reduced.

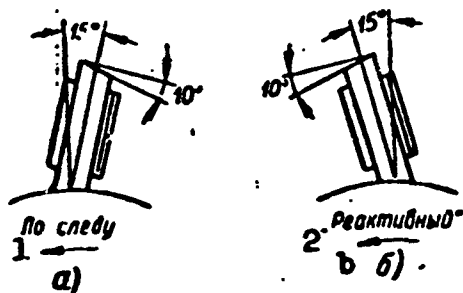


Fig. 6.50. Arrangement of brushes at commutator. a) Trailing brush; b) leading brush. 1) With rotation; 2) "reaction."

As shown in Fig. 6.50, there are two possible ways of installing brushes: inclined in the direction of rotation "trailing," and inclined against the direction of rotation "leading." Brushes mounted in the second manner are called reaction brushes and bare brushholders are called reaction brushholders.

The purpose of the  $10^\circ$  brush bevel is to form a component of force in the direction of rotation due to the brush-spring pressure. In this case, the brushholder and the forward (leading) side of the ring form a damper that presses the brush against the commutator and ring. As experience has shown, "trailing" brushes provide more stable commutation under speed variations. With a reaction brushholder, as the speed increases, a tendency is observed for the current at the leading edge of the brush to increase.

In machines designed for reversible operation, the brushes must be installed radially with respect to the commutator.

Brushholder. Proper brushholder construction plays an important part in good commutation. An unsuccessful brushholder design leads to brush vibration, which causes sparking.

Figures 6.8 and 6.10 show some brushholder designs used in various aircraft electrical machines.

In all cases it is necessary to see that the gap between brush and ring does not exceed 0.2-0.3 mm, and that the commutator runout does not exceed 0.02-0.03 mm.

The sliding commutator contact under high-altitude conditions.

During high-altitude flights ( $H > 6$  km), there is increased wear on normal carbon brushes and severe commutator wear. At altitudes  $H > 6$  km, the brushes are found to wear out completely within 7 hr, while when  $H > 10$  km, they wear out within 1-3 hr. Here the working brush length wears away in (30-60) min.

Increased brush wear is accompanied by more vigorous spark formation, loud friction noises, intense formation of carbon dust and, finally, generator failure; this rapidly drains the storage battery that supplies the electrical system of the flying craft and makes it necessary to land, since brushes cannot be changed in flight.

The rapid brush wear is caused by the increased coefficient of friction between brush and commutator, which depends on the atmospheric content of moisture and oxygen by weight, as well as on brush temperature. The lower the moisture and oxygen contents and the higher the brush temperature, the greater the coefficient of friction and the greater the rate of brush wear.

The main cause for rapid brush wear is insufficient air moisture content at high altitudes.

There is an intermediate layer between brush and commutator - a jacket of water and gas - that acts as a lubricant during operation. After a certain period of operation, however, a dark deposit usually forms on the commutator surface; it consists of a 0.05-0.06 micron thick film of cupric oxide and graphite, called "varnish" by men in the field.

Copper combines with oxygen to form the cupric oxide, while the

graphite layer is produced by transport of brush material. The surface film absorbs water vapor and oxygen from the air, forming a water-gas shell that acts as a lubricant between the brushes and commutator. We thus have semifluid friction, with a low coefficient of friction and little brush wear. The important element in the lubricating layer is the moisture, which is practically absent at high altitudes, since the amount of saturated water vapor in the atmosphere decreases sharply with altitude: at a height of 6 km, there is about 15 times less moisture and at 10 km about 360 times less moisture than at sea level.

As investigations have shown, at altitudes up to 3 km (where the amount of water vapor amounts to about  $3.25 \text{ g/m}^3$  and a pressure of 3 mm Hg) brush wear reaches 1.0 mm over a 100-hr period, which is quite acceptable. As the amount of water vapor decreases, i.e., the pressure drops below 3 mm Hg, brush wear rises sharply and at altitudes above 6 km, where the atmospheric moisture content drops sharply, brush wear reaches unacceptable values.

Thus, at altitudes of the order of 6-8 km, brush wear reaches (5-10) mm per hour, while the commutator wear is 0.1 mm per hour, while at altitudes above 8-9 km, where there is almost no moisture in the atmosphere, brush wear reaches 22 mm. It is clear that a generator will rapidly fail under such conditions.

Figure 6.51 shows the effect of saturated water-vapor pressure on the coefficient of friction for various brush temperatures.

Analysis of the data indicates that as the temperature rises, the coefficient of friction goes up considerably if the pressure of saturated water vapor remains unchanged. At high temperatures, the coefficient of friction depends little on the atmospheric vapor content, i.e., at high temperatures the coefficient of friction will be high even in the presence of considerable quantities of vapor. For a water

vapor pressure of less than 5 mm Hg with  $t_{shch} = 80^{\circ}$ , there will be almost no wear on the brushes.

Here we can also see that the pressure of dry oxygen affects the brush coefficient of friction; when brushes operate in an atmosphere of dry oxygen, the coefficient of friction increases from 0.15-0.2 at a pressure of about 160 mm (at sea level) to 0.75 at a pressure of 10 mm (an altitude of 24 km).

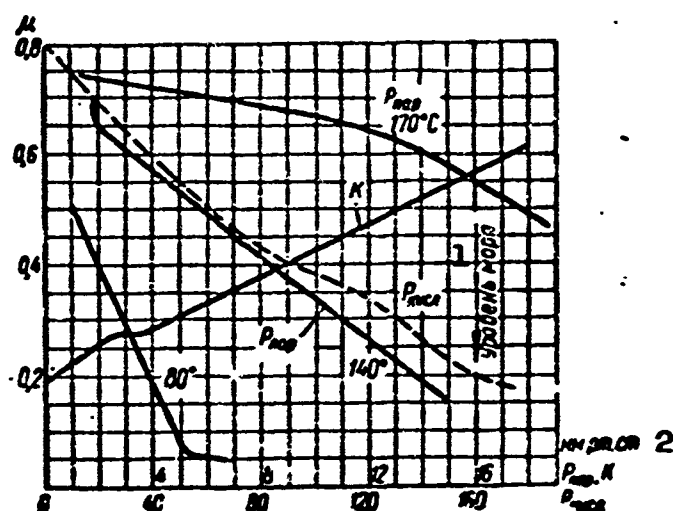


Fig. 6.51. Coefficient of friction for copper-carbon brushes as a function of water-vapor and oxygen pressure. Spring pressure  $R_{shch} = 770 \text{ g/cm}^2$ ;  $K$  is the brush wear in an atmosphere of dry oxygen. 1) Sea level; 2) mm Hg,  $P_{par}$ ;  $K_{kisl}$ .

The brush wear K in an atmosphere of dry hydrogen at a pressure of 160 mm Hg (corresponding to ground conditions) is quite large (0.5 mm per hour). At pressures of 120 mm (1-2 km) or less, the amount of brush wear becomes unacceptable. At a dry-oxygen pressure of 20 mm Hg ( $H \approx 15$  km), the coefficient of friction is nearly triple the ground-level value, while brush wear increases by roughly a factor of 30. The data given show that the atmospheric oxygen content has a noticeable effect on the coefficient of friction and brush wear. Relia-

ble operation of a sliding contact is not obtained, however, if the dry-oxygen pressure is held constant (160 mm Hg).

Thus, at an altitude  $H > 6$  km, the water and gas jackets at the commutator surface, which decrease friction, cease to be effective. In the absence of a lubricating shell between commutator and brushes, the friction between the unlubricated surfaces increases many times, brush wear reaches 5-10 mm per hour, rather than 0.1-0.5 mm in 50 hr, while the commutator wears at a rate of 0.05-0.01 mm per hour.

As pressure-chamber studies have shown, the protective shell vanishes more rapidly the lower atmospheric pressure, the higher the speed of the cooling air, and the greater the commutator temperature.

The commutator temperature is produced by commutator friction and contact-resistance losses.

As brush wear increases, friction losses rise by a factor of 3-4, resulting in increased commutator temperature and, consequently, increased brush wear. As a result the "shell" vanishes and the layer of oxide on the commutator is ground off. At high altitudes, this layer forms far more slowly than at the earth's surface.

The elimination of the oxide layer - the varnish - reduces the contact resistance between brush and commutator. With slip rings, this has a positive effect, since the contact losses are reduced, but for a commutator the effect is negative, since the commutation currents increase and, consequently, commutation is impaired and the contact losses may become greater than on the ground. This situation will always occur in aircraft generators.

Thus, impairment of commutation at high altitudes is a consequence of high brush wear, rather than its cause, as had been supposed earlier. It is clear that poor commutation also facilitates further brush wear.

Rapid brush wear creates conditions suitable for further increase in wear owing to increased commutator temperature and impaired commutation.

Brush wear may be reduced by improving lubrication between commutator and brush by employing brushes impregnated with a special compound that is held for a long period of time at temperatures of up to  $150-300^{\circ}$ ; by reducing commutator and brush temperature by improving machine ventilation and commutation, and decreasing "current" and pressure loads on brushes (here we do not recommend an increased in forced-air ventilation of the commutator contact surface); and by improving commutator lubrication by adding moisture to the air.

By impregnating the brushes with grease, their service life can be increased by a factor of 100, extending it to hundreds of hours.

High-altitude brushes should be impregnated with a heat-resistant compound that can form a lubricating layer under high-altitude conditions. Zinc iodide and lead iodide are used as impregnating substances. They ensure normal brush wear, but are insufficiently heat-resistant. Graphite brushes with admixtures of calcium sulfate or barium oxide operate satisfactorily. Brushes made from graphite, copper, and sulfur briquetted at a pressure of  $60-70 \text{ kg/cm}^2$  have given good performance.

Rapid brush wear is only observed in generators. It does not occur in motors or converters, since the thermal loads are lighter and the operating periods shorter (the high-altitude performance of brushes becomes an acute problem for these machines as well at high altitudes).

Adding moisture to the cooling air improves brush operating conditions. Where there is a large amount of moisture at the commutator, however, a water layer forms between brush and collector and we have fluid friction. In this case, the coefficient of friction is small,



but the drop at the brushes rises sharply, since the water film acts as a dielectric and it will increase the contact resistance.

Thus, there exists an optimum amount of moisture that provides good commutation at the commutator. This consideration is important where a machine is cooled by injecting water into the cooling-air stream.

## 6.6. COMMUTATING POLES AND COMPENSATING WINDINGS

In direct-current aircraft machines with field "reversal" it is impossible for practical reasons to form a commutating field by shifting the brushes, since in this case the short-circuited section would enter the armature-reaction field, which exceeds the commutating field, and commutation conditions would be impaired. In addition, a direct-axis component of the demagnetizing armature reaction would appear, requiring an increase in the volume of the field winding and impairing the starting characteristics of electric motors.

In motors running under constant load without field reversal, commutation may be improved by shifting the brushes in the direction opposite to that in which the armature rotates. In direct-current aircraft machines of 3-kw power or more, it is necessary to use commutating poles.

As we have already said, there are half as many or exactly as many commutating poles as main poles, and they are usually as long as the main poles.

The utilization of commutating poles makes it possible to increase the linear machine load and the magnitude of  $e_p$ , which in the last analysis reduces machine weight and size and also increases reliability. Commutating poles are designed so as to provide accelerated commutation, i.e., so as to shift current takeoff to the leading edge of the brush.

## Effect of Commutating-Pole Magnetizing Force on the Main Field

Below we shall discuss the effect of commutating-pole magnetizing forces on the main pole of the machine running at fixed and variable speeds, and with full and half complements of poles.

Full complement of commutating poles. If the brushes are set at the neutral plane, where a full complement of commutating poles is used, their field will be superimposed on the field of the main poles so that in half the armature core and in half the yoke the fields will add and in the other halves they will subtract (Fig. 6.52). In addi-

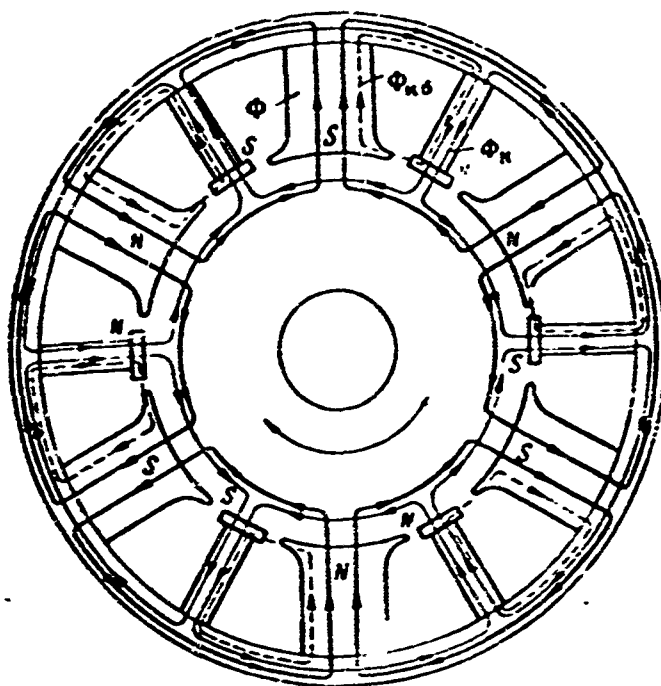


Fig. 6.52. Magnetic system of machine with full complement of commutating poles.

tion, the commutating-pole leakage flux  $\Phi_{k\sigma}$  will also flow through the main poles. At the same time, the magnitude of the field in the air gap will remain unchanged.

Owing to saturation, the decline of the main field in half the armature core and half the yoke will not be compensated by the strengthening of the main field in the other half of the armature core and the other half of the yoke, and the over-all main field will be

weakened. Thus, the commutating-pole field reduces the main field and increases the voltage drop, which is taken into account in determining the main-pole magnetizing force by means of a corresponding increase in the main-pole excitation magnetizing force by an amount  $F_{kd}$  that corresponds to the demagnetizing effect of the commutating poles. The value of  $F_{kd}$  clearly rises with increasing magnetic-circuit saturation.

If the brushes are shifted away from the true neutral plane in the direction of armature rotation, the commutating-pole field will weaken the main field in generator air gaps and intensify it for motors (Fig. 6.53). If the brushes are shifted against the rotation the opposite phenomenon will occur.

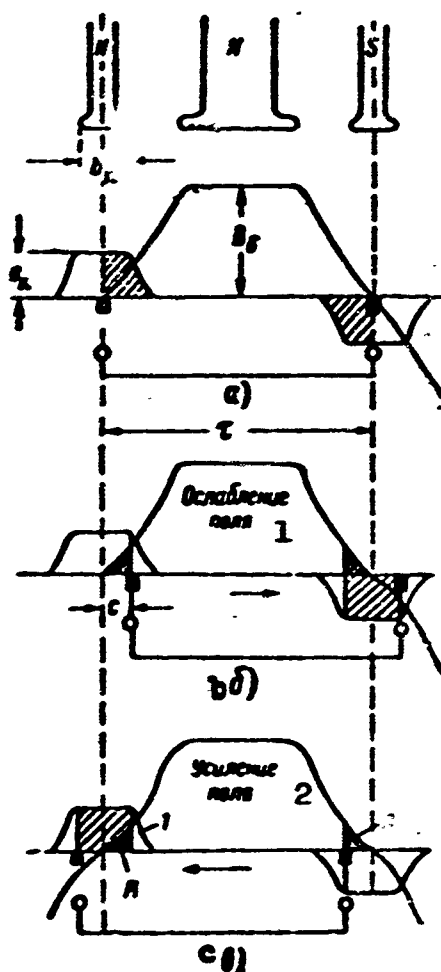


Fig. 6.53. Effect of brush shift, full complement of commutating poles. a) Hatched areas cancel; б) main field reduced by amount of hatched areas; в) main field reduced by hatched areas A and strengthened by hatched commutating-field quadrilateral. 1) Field weakened; 2) field strengthened.

The flux  $\phi_g$  in the air gap between brushes may be determined, allowing for the brush shift with  $2c < b_k$ , from the equation

$$\phi_g = \phi - \phi_k \frac{2c}{b_k}, \quad (6.96)$$

where  $\phi_k$  is the commutating-pole flux;  $\phi$  is the main-pole flux, neglecting the commutating-pole flux.

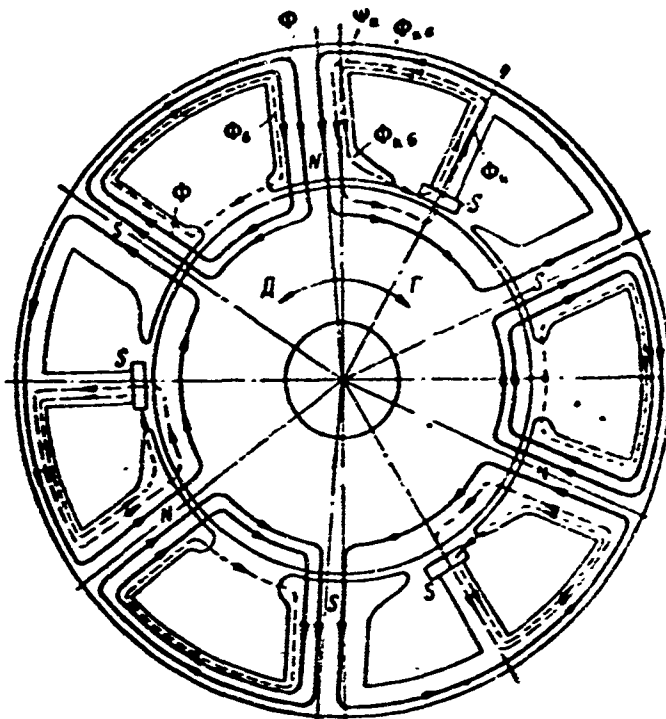


Fig. 6.54. Magnetic system of machine with half complement of commutating poles.

The "minus" sign applies to a brush shift in the direction of armature rotation for a generator and against the direction of rotation for a motor.

In machines with commutating poles, the brushes are normally set at the true neutral plane. In this case, however, there is a brush shift owing to inaccurate installation of brushholders and displacement of the brush axis when it wears.

Thus, there is some compounding action of the commutating poles when a full complement is used and the brushes are set at the neutral plane.

Half complement of commutating poles. If the brushes are at the neutral plane, when a half complement of commutating poles is used, the main and commutating fields will be superposed not only in the armature core and yoke, but also in the armature teeth and main-pole core (Fig. 6.54).

In contrast to magnetic systems using a full complement of commutating poles, in this case the commutating field increases the induction in certain parts of the armature core and the yoke without decreasing it in other portions. Main poles differing in polarity from the commutating poles will have increased induction, since the main and commutating fields will be additive in them. The effect of the commutating field is stronger the greater the saturation of the magnetic system.

In addition with a half complement of commutating poles and brushes located at the neutral plane, the commutating field has a direct influence on the main field in the air which is not observed to be the case where a full complement of commutating poles is used.

A flux  $\phi + \phi_k$  from the main north pole N enters the armature for the length of a pole pitch (Fig. 6.55).

At the same time, one-half the commutating-pole flux ( $0.5\phi_k$ ) from the armature enters the commutating pole for the same pole pitch.

Thus, the resultant flux in the air gap under the north pole will turn out to equal  $\phi_\delta = \phi + \phi_k - 0.5\phi'_k = \phi + 0.5\phi_k$ .

A flux  $\phi$  enters the main south pole S from the armature for the length of the next pole pitch, and a flux  $0.5\phi_k$  enters the commutating pole for the same length. Consequently, the resultant flux in the air gap under the south pole will also equal  $\phi_\delta = \phi + 0.5\phi_k$ .

Consequently, with a half complement of commutating poles and brushes located at the neutral plane, the commutating field will in-

tensify the main field at all poles to exactly the same degree.

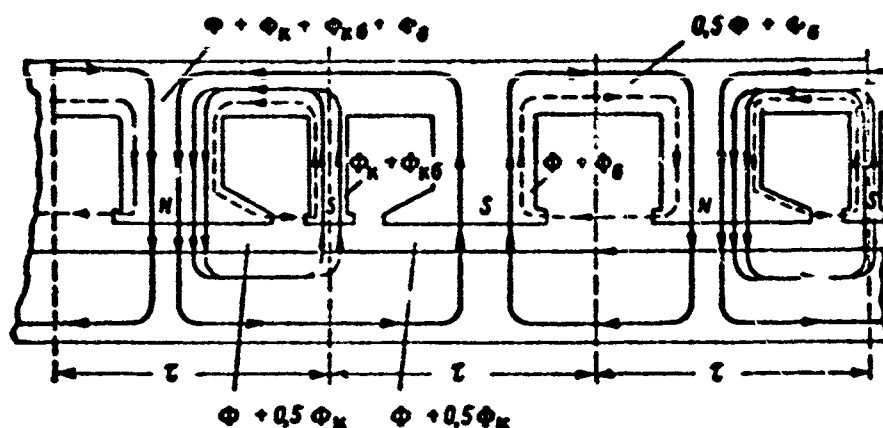


Fig. 6.55. Diagram showing flux distribution in air gap of direct-current machine with half complement of commutating poles.

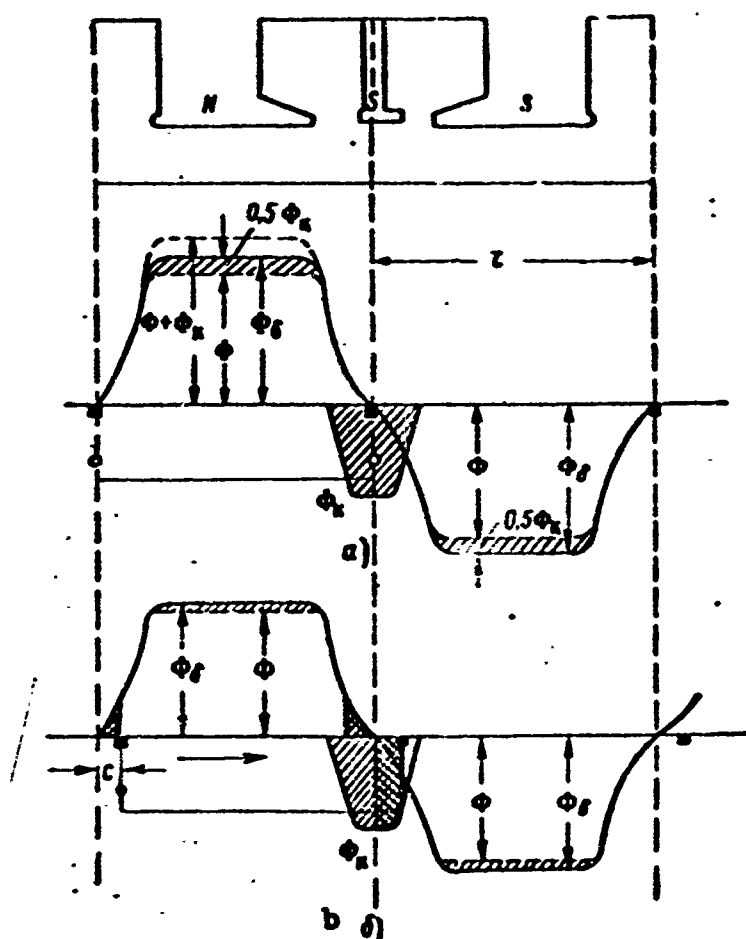


Fig. 6.56. Effect of brush shift with half complement of commutating poles. a) Main field intensified by half of commutating-pole field (hatched section of main field); b) main field weakened (cross-hatched areas).

If the brushes are shifted away from the normal neutral plane in the direction of rotation of the generator armature (Fig. 6.56), the

influence of the commutating-pole field on the main field is reduced and will reach zero when the brushes are shifted by about  $c = 0.5b_k$ , where  $b_k$  is the width of the commutating-pole piece.

The magnitude of the flux in the air gap between the brushes will be, in this case,

$$\Phi_s = \Phi + 0.5\Phi_k \left(1 - \frac{2c}{b_k}\right) \quad (6.99)$$

for a brush shift  $c = 0-0.5b_k$  and

$$\Phi_\delta = \Phi$$

for a brush shift  $c > b_k$ .

When the brushes are shifted in a direction opposite to that in which the generator armature rotates, the field of the main pole of like polarity is strengthened owing to  $\Phi_k$ , while the degree to which the field of the unlike main pole is weakened by the commutating field, is reduced, i.e., the main field of the generator is strengthened as a whole to a value  $\Phi_\delta = \Phi + \Phi_k$ , i.e., by  $0.5\Phi_k$ . The magnitude of the flux in the air gap in the brushes is represented by the same formula, but with a "plus" sign within the parentheses, i.e.,

$$\Phi_s = \Phi + 0.5\Phi_k \left(1 + \frac{2c}{b_k}\right). \quad (6.100)$$

When the machine is operated as a motor, the opposite phenomenon occurs: when the brushes are shifted in the direction of rotation of the armature, the main field will be strengthened, while when the brushes are shifted against the direction of armature rotation, the main field will be weakened.

Thus, with a half complement of commutating poles, a brush shift basically has the same effect as when a full complement is used.

#### Effect of Commutating-Pole Magnetizing Forces on the Main Field in the Presence of Speed Variations

Where the load current is constant, the commutating-pole flux is

nearly independent of speed. An increase in speed reduces the reluctance of the commutating-pole magnetic circuit with the magnetizing force constant in magnitude which leads to some increase in  $\Phi_k$  and  $\Phi_{k0}$ . This fact may be of importance at high magnetic-circuit saturations where there is a broad speed-variation range.

As has already been shown, with the brushes of the neutral plane, the commutating field strengthens the main field in the air gap only where there is a half complement of commutating poles; in this case

$$\Phi_i = \Phi \left( 1 + 0,5 \frac{\Phi_k}{\Phi} \right) = \gamma'_k \Phi, \quad (6.101)$$

where

$$\gamma'_k = 1 + 0,5 \frac{\Phi_k}{\Phi}.$$

With the emf and load current constant, the flux in the air gap should vary in inverse proportion to the speed. Consequently, when the speed varies the last equation may be represented as

$$\Phi_i = \Phi \frac{n_{min}}{n_{max}} \left( 1 + 0,5 \frac{\Phi_k}{\Phi} \frac{n_{max}}{n_{min}} \right) = \gamma'_k \frac{n_{min}}{n_{max}} \Phi, \quad (6.102)$$

where  $\Phi$  is the main-pole flux neglecting  $\Phi_k$  for  $n_{min}$

$$\gamma_k = 1 + 0,5 \frac{\Phi_k}{\Phi} \frac{n_{max}}{n_{min}} \quad (6.103)$$

is a coefficient characterizing the degree of main-field compounding with speed variation. If at minimum speed the ratio  $\Phi_k/\Phi = 0.2$  and  $\gamma_k = 1.1$ , then with a speed increase by a factor of 2.5, the compounding coefficient will increase to  $\gamma_k = 1.25$ .

Thus, with the half complement of commutating poles, an increase in speed, while leaving the magnitude of the commutating-pole flux nearly unchanged, will increase the degree to which it affects the main field.

#### The Effect of Commutating-Section Magnetizing Forces on the Main Field

If the commutating poles are overexcited,  $e_k > e_r$ , and additional



currents will flow in the commutating sections that accelerate commutation. Where the commutating poles are underexcited ( $e_k < e_r$ ), delayed commutation is observed.

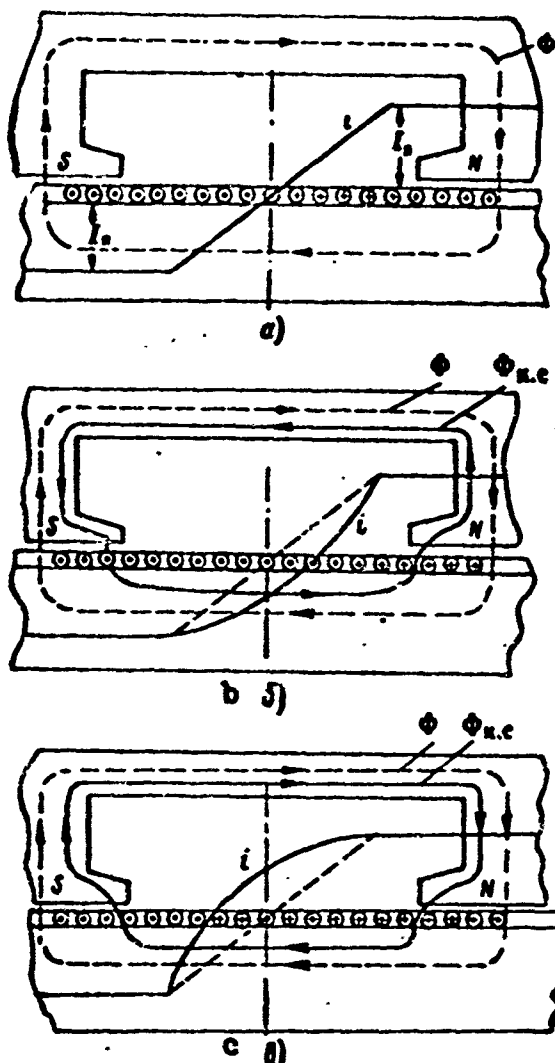


Fig. 6.57. Effect of commutating-section field on main field. a) Straight-line commutation,  $\Phi_{k.s}$  has no effect on main field; b) delayed commutation,  $\Phi_{k.s}$  reduces main field; c) accelerated commutation,  $\Phi_{k.s}$  intensifies main field.

cited section;  $w_{ya}$  is the number of turns in one parallel armature circuit;  $\beta = b_{shch}/\tau_k$  is the ratio of the brush width to the commutator pitch;  $l$  is the armature length;  $R_k$  is the total brush-contact resistance;  $\tau$  is the pole pitch;  $p$  is the number of pole pairs;  $\delta' = k_\delta \delta$  is the design air gap;  $\lambda$  is the conductivity, equal to 5-7;  $D_k$  is the

The commutation currents form a direct-axis field that intensifies or weakens the main field, i.e., they form a commutation reaction.

The magnetizing forces due to the commutating sections reinforce the main field in a generator where there is accelerated commutation (Fig. 6.57c) and reduce it (Fig. 6.57b) where there is delayed commutation (in motors, this situation is exactly the opposite).

The magnetizing forces of the commutating sections may be found, in approximation, from the equation

$$F_{k.c} = k_{k.c} I_a n_k^2, \quad (6.104)$$

where

$$k_{k.c} \approx 4.15 \cdot 10^{-3} \frac{F^2}{\beta} w_{ya} n_k \sqrt{\frac{b_m}{D_k} \frac{n_k}{\lambda} \left( \frac{l}{R_k} \right)^2}$$

$I_a$  is the armature current;  $n_k$  is the number of turns in the short-cir-

commutator diameter;  $\underline{n}$  is the speed.

The commutating-section flux is

$$\Phi_{u.c} = \frac{F_{u.c}}{R_{u.c}} \quad (6.105)$$

The resultant flux in the air gap may be represented by the expression

$$\Phi_s = \Phi \pm \Phi_{u.c} \text{ and } \Phi_s = \Phi \pm 0,5 \Phi_u + \Phi_{u.c} \quad (6.106)$$

for a full and half complement of commutating poles.

Making use of (6.104) and (6.106), we can write an expression for the resultant flux in the gap in the presence of speed variations:

$$\begin{aligned} \Phi_s &= \Phi \frac{n_{min}}{n_{max}} \pm \Phi_{u.c} \left( \frac{n_{max}}{n_{min}} \right)^{\frac{2}{3}} = \\ &= \Phi \frac{n_{min}}{n_{max}} \left[ 1 \pm \frac{\Phi_{u.c}}{\Phi} \left( \frac{n_{max}}{n_{min}} \right)^{\frac{5}{3}} \right] \end{aligned} \quad (6.107)$$

for a full complement of commutating poles and

$$\begin{aligned} \Phi_s &= \Phi \frac{n_{min}}{n_{max}} \left[ 1 \pm \frac{\Phi_{u.c}}{\Phi} \left( \frac{n_{max}}{n_{min}} \right)^{\frac{5}{3}} + \right. \\ &\quad \left. + 0,5 \frac{\Phi_u}{\Phi} \left( \frac{n_{max}}{n_{min}} \right) \right] = \gamma_s \frac{n_{min}}{n_{max}} \Phi \end{aligned} \quad (6.108)$$

for a half complement.

In relative units, the resultant flux is

$$\dot{\Phi}_s = \frac{1}{\dot{n}} \left( 1 \pm \dot{\Phi}_{u.c} \dot{n}^{\frac{5}{3}} + 0,5 \dot{\Phi}_u \dot{n} \right) = \frac{\gamma_s}{\dot{n}}, \quad (6.109)$$

where the compounding coefficient for the first and second cases will be, respectively,

$$\left. \begin{aligned} \gamma_s &= 1 \pm \dot{\Phi}_{u.c} (\dot{n})^{\frac{5}{3}} \\ \gamma_s &= 1 \pm \dot{\Phi}_{u.c} (\dot{n})^{\frac{5}{3}} + 0,5 \dot{\Phi}_u \dot{n} \end{aligned} \right\} \quad (6.110)$$

and

It follows from these last equations, that with overexcitation of the commutating poles (a "plus" sign in front of  $\Phi_{k.s}$ ) and with the brushes located at the neutral plane, the main field would be rein-

forced with increasing speed and load current owing to the effect of the commutating-section magnetizing forces; where there are  $p$  commutating poles, there is also the additional direct influence of the commutating-pole field. The effect of speed and the degree of compounding for the commutating-section field is especially important.

Thus, for example, for  $n_{\min} = 3600$  rpm and rated current,  $\Phi_k^* = 0.2$  and  $\Phi_{k.s}^* = 0.05$ .

With  $n = 3600$  rpm, the compounding coefficient will equal  $\gamma_k = 1 + 0.05 + 0.5 \cdot 0.2 = 1.15$  with  $p$  commutating poles, while  $\gamma_k = 1.05$  where there are  $2p$  commutating poles.

Where  $n = 9000$  rpm, i.e., when  $\dot{n} = 2.5$ :

$\gamma_k = 1 + 0.05(2.5)^{\frac{2}{3}} + 0.5 \cdot 0.2 \cdot 2.5 \approx 1.477$  for a half complement of commutating poles;  
 $\gamma_k = 1 + 0.05(2.5)^{\frac{2}{3}} \approx 1.227$  for a full complement of commutating poles.

The air-gap flux will be  $\Phi_\delta^* = 1.15$  or  $1.05$  with  $n = 3600$  rpm while  $\Phi_\delta^* = 0.59$  or  $0.49$  with  $n = 9000$  rpm, i.e., as the speed increases by a factor of 2.5, the flux is reduced to 59% (49%) rather than to 40% under the influence of compounding by the commutating poles and commutating sections.

#### Commutating-Pole Saturation Curve

The flux in the commutating-pole core and in part of the yolk core (Fig. 6.55) will equal the sum of the commutating-pole fluxes in the air gap  $\Phi_k$  and the commutating-pole leakage flux  $\Phi_{k\sigma}$ , i.e.,  $\Phi_{k.m} = \Phi_k + \Phi_{k\sigma}$  and  $\Phi_k = \Phi_{k.m} - \Phi_{k\sigma}$ .

Figure 6.58a shows the way in which the flux in the commutating-pole core depends on the load current, i.e., the function  $\Phi_{k.m} = f(I_{ya})$ .

We may assume in first approximation that the leakage flux will vary as a function of load current in accordance with the straight line  $OK_1$ .

Let us find the effect of commutating-pole saturation and leakage on the commutating-pole flux in the air gap. Its saturation curve, i.e., the line representing the air-gap flux at the commutating pole as a function of its magnetizing force should be linear (the line  $OK_2$ ) by the conditions required for good commutation. At some specific

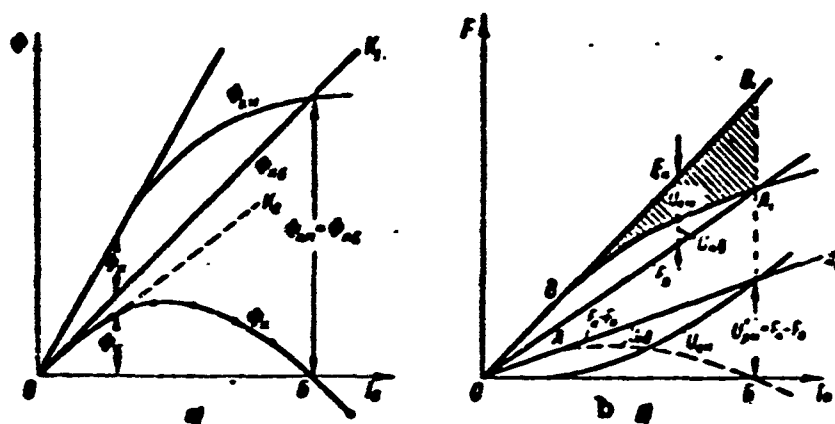


Fig. 6.58. Magnetization of commutating pole allowing for saturation and leakage fluxes. a) Commutating-pole flux curves; b) curves for magnetizing force and magnetic-potential drops.

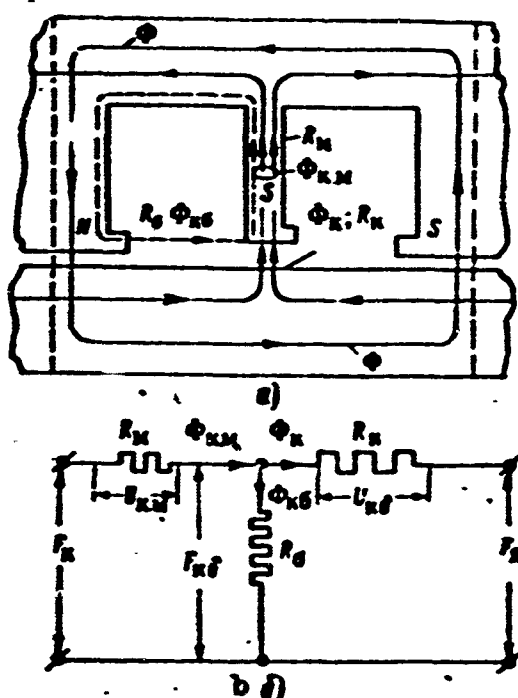


Fig. 6.59. Equivalent circuit of commutating pole. a) Magnetic circuit; b) equivalent circuit.

load, however (above the rated value), the commutating-pole saturation curve will usually depart from a straight line in the direction of the x-axis. The curve will bend rapidly, since the air-gap magnetizing force will form a small part of the over-all magnetizing force. The saturation curve intersects the x-axis at the load value ( $OB$ ) such that the flux in the core becomes equal to the leakage flux  $\Phi_{k.m} = \Phi_{k0}$ , and this can only occur when the flux in the gap  $\Phi_k$  equals zero. This means that

at some specific load, the commutating-pole field can change sign and,

consequently, increase the reactance emf, i.e., hamper commutation.

This phenomenon will become clear if we consider Fig. 6.58b, where lines  $OB_1$  and  $OA_1$ , respectively, represent the commutating-pole magnetizing force  $F_k$  and the armature magnetizing force  $F_{ya}$  as functions of load current. It is clear that the difference  $F_k - F_{ya} = f(I_{ya})$  - the line  $OA'_1$  - represents the commutating-pole magnetizing force needed to force the flux through the commutating-pole magnetic circuit, i.e.,

$$F_k - F_{ya} = f(I_{ya}) = U_{k.m} + U_{k\delta} \quad (6.111)$$

The drop in the iron magnetic potential in the commutating-pole air gap is represented by the curves  $U_{k.m} = f(I_{ya})$  and  $U_{k\delta} = f(I_{ya})$ .

As the load current increases, the magnetic-potential drop in the iron rises, while it falls in the air gap. A decrease in the magnetic-potential drop across the air gap to zero indicates that the useful flux  $\phi_k$  has vanished. Physically, this means that as the load current increases, the leakage flux  $\phi_{k\sigma}$  rises while the useful flux  $\phi_k$  diminishes, and when  $\phi_{k.m} = \phi_{k\sigma}$ , the useful flux becomes equal to zero. With a further increase in load current, the leakage flux reverses the polarity of the commutating pole. It is clear that the lower the relative value of the leakage flux, i.e., the smaller the leakage coefficient  $k_{k\sigma}$  of the commutating pole and the lower the saturation of its magnetic circuit, the less well-defined this phenomenon will be, and the better the commutation under overloads.

Let us find an analytical solution for the phenomenon under consideration.

If we use the notation of Fig. 6.59a, it is possible to obtain the equivalent commutating-pole circuit of Fig. 6.59b. In accordance with the equivalent circuit, the equation for the magnetic-potential drop along the main commutating-pole circuit may be written in the

following form:

$$F_a - F_s = \Phi_a R_a + \Phi_{a,s} R_s. \quad (6.112)$$

Since

$$F_a = I_a n_a, \quad A = \frac{2 I_a w_a}{\pi D}$$

and

$$F_s = 0.5 A \tau = \frac{I_a w_a}{2p},$$

we find that

$$\begin{aligned} I_a \left( n_a - \frac{w_a}{2p} \right) &= \\ &= \Phi_a R_a + (\Phi_a + \Phi_{a,s}) R_s. \end{aligned} \quad (6.113)$$

It follows from (6.113) that the flux in the commutating-pole air gap will equal

$$\Phi_s = \frac{I_a k_F - \Phi_{a,s} R_s}{R_s + R_a} = I_a \frac{1}{1 + \frac{R_s}{R_a}} \left( \frac{k_F}{R_a} - \gamma_s \right), \quad (6.114)$$

where

$$k_F = n_a - \frac{w_a}{2p} = \text{const} \quad \text{and} \quad \gamma_s = \frac{\Phi_{a,s}}{I_a} \approx \text{const}.$$

As the load increases,  $\gamma_s$  drops somewhat, while it increases with increasing speed, since in the first case circuit saturation rises, while in the second case it drops.

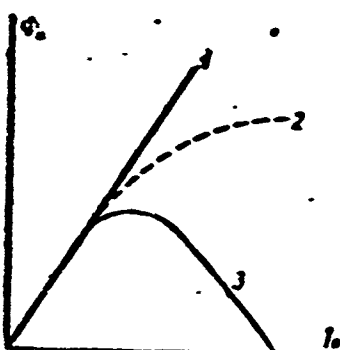


Fig. 6.60. Saturation curves for commutating pole.

The commutation emf will be

$$e_s = k_s \Phi_s = \frac{k_s I_a}{1 + \frac{R_s}{R_a}} \left( \frac{k_F}{R_a} - \gamma_s \right). \quad (6.115)$$

where

$$k_s = 4 n_a f \tau S_a^{-1} 10^{-8} \quad \text{and} \quad S_a = \frac{\Phi_s}{B_a}.$$

Since  $e_r = k_r I_{ya}$ , the degree of commutating-pole excitation will be determined by the expression

$$\xi_k = \frac{e_k}{e_p} = \frac{k_k \Phi_k}{k_p I_a} = k_{k,p} \frac{\Phi_k}{I_a} = \frac{k_{k,p}}{1 + \frac{R_k}{R_m}} \left( \frac{k_F}{R_k} - \gamma_\sigma \right), \quad (6.116)$$

where

$$k_p = \frac{4n_k w_k l' l_a}{p 10^6} \text{ and } k_{k,p} = \frac{\tau p}{w_k \lambda S_k} = \text{const.}$$

The reluctance of the leakage-flux circuit  $R_\sigma$  and the reluctance of the commutating-pole air gap  $R_k$  may be considered to be roughly constant and independent of the load current, while the reluctance of the main circuit  $R_m$  rises with increasing load current.

In view of what we have said, the following conclusions may be drawn from Eq. (6.116).

1. In the absence of saturation of the commutating-pole magnetic circuit, i.e., where  $R_m = \text{const}$ , the flux  $\Phi_k$  will increase in proportion to the load current (curve 1 of Fig. 6.60).

2. Where the commutating-pole magnetic circuit is saturated and there is no leakage ( $\Phi_{k\sigma} = 0$  and  $\gamma_\sigma = 0$ ), the flux variation will follow curve 2.

3. Where there is saturation of the commutating-pole magnetic circuit, and we take the leakage flux into account, the functions  $\Phi_k = f(I_{ya})$  and  $e_k = f(I_{ya})$  will lose their linear character, and may become equal to zero under the influence of the leakage flux and may even take on negative values (curve 3). Thus, where  $\gamma_\sigma = k_F/R_m$ , the flux  $\Phi_k = 0$ , while in  $\gamma_\sigma > k_F/R_m$ , the flux will have a negative sign at  $\Phi_k < 0$ .

4. If the commutation (commutating pole) is adjusted for rated load current, then in the presence of overloads, where  $R_m$  rises, the commutating pole will prove to be underexcited, and delayed commutation will occur.

5. The larger the ratio  $R_k/R_m$ , i.e., the larger the air gap under

the commutating pole, the smaller will be the effect of magnetic-circuit saturation, which has a favorable effect on overload commutation, and reduces the effect of the commutating-pole field on the main field at high speeds.

6. The larger the leakage flux ( $\gamma_g$ ), the greater the influence of magnetic-circuit saturation, which has an unfavorable effect on commutation under overloads.

In aircraft machines, the air gap  $\delta_k$  under a commutating pole is usually small and the leakage large, which also has an unfavorable effect on commutation in the presence of overloads; commutation becomes delayed. Thus, saturation of the commutating-pole magnetic circuit and leakage lead to delayed commutation.

#### Design of Commutating Poles

Induction in a commutating-pole gap. The mean reactance emf in a commutating section does not depend on the number of commutating poles, and equals

$$e_p = 2n_s \frac{A}{100} \frac{v}{100} \frac{i}{100} \lambda \quad (6.117)$$

Here  $\lambda = 5-7$  is a coefficient for the mean specific permeance of the commutating section;  $v$  is the armature speed, m/sec.

The emf induced in the commutating section by the quadrature-axis armature field,  $e_{yaq}$ , depends on the number of commutating poles.

If we neglect the magnetic drop in the iron of the transverse circuit, then with a full complement of commutating poles and  $l \neq l_k$ ,

$$e_{s,q} \approx 2.5 \frac{n_s}{1-s} \frac{A}{100} \frac{v}{100} \frac{l-l_k}{100} \quad (6.118)$$

With a half complement of commutating poles, one side of the commutating section will be located in an uncompensated quadrature-axis armature field, and on our assumptions, a total emf



$$e_{aq} \approx 2,5 \frac{n_k}{1-s} \frac{A}{100} \frac{v}{100} \frac{1-0,5l_k}{100}. \quad (6.119)$$

will be induced in it.

If  $\underline{l} = l_k$ , which, as a rule, will always be the case, with a full complement of commutating poles,  $e_{yaq} = 0$ , while with a half complement of commutating poles,

$$e_{aq} \approx 1,25 \frac{n_k}{1-s} \frac{A}{100} \frac{v}{100} \frac{l}{100}. \quad (6.120)$$

The emf induced in the commutating section by the commutating-pole field will depend on the number of poles.

With a full complement of commutating poles

$$e_k = 2n_k \frac{B_r}{100} \frac{v}{100} \frac{l_k}{100}. \quad (6.121)$$

With a half complement of commutating poles, one side of the commutating section will come under the influence of the commutating pole and, consequently,

$$e_k = n_k \frac{B_r}{100} \frac{v}{100} \frac{l_k}{100}. \quad (6.122)$$

In view of what we have said, the value of  $B_k$  is determined from the condition  $e_k \geq e_r + e_{yaq}$ : with a full set of commutating poles and  $\underline{l} = l_k$ ,  $e_k = e_r$  and

$$B_k \geq \lambda A. \quad (6.123)$$

With a half set of commutating poles and  $\underline{l} = l_k$ ,  $e_k = e_r + e_{yaq}$  and

$$B'_k = \lambda A \rho_r \quad (6.124)$$

$$\rho_r = \frac{B'_k}{B_k} = 2 + \frac{1,25}{1-s} \frac{l}{\lambda}. \quad (6.125)$$

With a half complement, the induction in a commutating-pole gap increases by more than a factor of 2.

In order to obtain accelerated commutation, the gap induction is increased by 10-15%. In this case

$$B_s = (1,1 + 1,15) \lambda A \quad (6.126)$$

and

$$B_s = (1,1 + 1,15) \lambda A p_s. \quad (6.127)$$

Commutating-pole magnetizing forces. With a full complement of commutating poles, the magnetizing force per pole is

$$F_s = 0,5F_s + F_{\alpha s}. \quad (6.128)$$

where  $F_{Ok}$  is the magnetizing force required to form the magnetic flux in the commutating-pole air gap;  $0,5F_{ya} = 0,5\tau A$  is the maximum armature magnetizing force with the brushes set at the neutral plane.

The magnetizing force due to all commutating poles is

$$\sum F_s = 2p(0,5F_s + F_{\alpha s}). \quad (6.129)$$

With a half complement of commutating poles, the magnetizing force per pole is

$$F'_s = 0,5F_s + F'_{\alpha s} \quad (6.130)$$

while the magnetizing force due to all commutating poles is

$$\sum F'_s = p(0,5F_s + F'_{\alpha s}). \quad (6.131)$$

The ratio of the half- and full-complement commutating-pole magnetizing forces equals

$$\beta_s = \frac{\sum F'_s}{\sum F_s} = 0,5 \frac{1 + 2 \frac{F'_{\alpha s}}{\tau A}}{1 + 2 \frac{F_{\alpha s}}{\tau A}}. \quad (6.132)$$

Consequently, the problem reduces to determining  $F'_{Ok}$  and  $F_{Ok}$ . The magnetizing force required to form the commutating-pole flux for the full and half complements will equal, respectively,

$$F_{\alpha s} = 0,8\lambda_s B_s k_{s s} = (1,1 + 1,15) 0,8\lambda A z_s k_{s s}, \quad (6.133)$$

$$F'_{\alpha s} = 0,8\lambda'_s B'_s k'_{s s} \left(1 + 0,5 \frac{\gamma'_s}{\gamma_s} \frac{l_s}{l_p}\right) \approx (0,88 + 0,92) \lambda A z'_s k'_{s s} \gamma_s, \quad (6.134)$$

where

$$\gamma_s = 1 + 0,5 \frac{\gamma'_s}{\gamma_s} \frac{l_s}{l_p}.$$

The air gap  $\delta_k$  under a commutating pole is usually somewhat larger than the gap  $\delta$  under a main pole, amounting in aircraft machines to

$$\delta_k \approx \delta + (0.1 + 0.2) [\mu\mu].$$

A moderate increase in the commutating-pole air gap leads to improved commutation conditions, since this increases the linearity of the commutating-pole magnetic characteristic and reduces the effect of the toothed armature shape on pulsation of the induction  $B_k$ .

The inequality

$$k'_{s\kappa} = 1 + \frac{U'_{cr,\kappa}}{U'_{s\kappa}} > k_{s\kappa} = 1 + \frac{U_{cr,\kappa}}{U_{s\kappa}},$$

holds for the commutating-pole magnetic-circuit coefficients since with a half complement of commutating poles the flux  $\Phi_k$  is added to the main flux in the armature core and teeth as well as in the main poles and yoke.

If we assume that the length of the air gaps under the commutating poles is identical in both cases, we will have the ratio

$$\frac{F'_{0\kappa}}{F_{0\kappa}} = \gamma_{\kappa} \rho_{\kappa} \frac{k'_{s\kappa}}{k_{s\kappa}}. \quad (6.135)$$

In view of what has been said, we may write the ratio of the magnetizing force due to all commutating poles as

$$\rho_{\kappa} = \frac{\sum F'_{\kappa}}{\sum F_{\kappa}} \approx 0.5 \frac{1 + 1.8 \rho_{\kappa} k'_{s\kappa} \gamma_{\kappa} \frac{\delta'_{\kappa}}{\tau}}{1 + 1.8 \lambda k_{s\kappa} \frac{\delta_{\kappa}}{\tau}}. \quad (6.136)$$

If in this case we let

$$\frac{k'_{s\kappa}}{k_{s\kappa}} = 1.1, \rho_{\kappa} = \frac{B'_{\kappa}}{B_{\kappa}} = 2.6, \lambda = 6, k_{s\kappa} = 1.1 \text{ and } \gamma_{\kappa} = 1.3,$$

we then find that  $F'_{0\kappa}/F_{0\kappa} \approx 3.7$ , while with  $\delta'_{\kappa}/\tau = 0.015-0.025$

$$\rho_{\kappa} = \frac{\sum F'_{\kappa}}{\sum F_{\kappa}} = 0.705 \div 0.81.$$

For aircraft generators, we may assume that on the average  $\beta_k \approx 0.75$ . Thus, the required magnetizing force for all commutating poles turns out to be less for a half complement than for a full complement, especially with an increase in the relative air gap  $\delta'/\delta'_k$  and the permeance  $\lambda$ .

The decrease in the total commutating-pole magnetizing force for a half complement occurs owing to the fact that the armature reaction is compensated only at half the commutating poles.

For a half complement of commutating poles, the magnetizing force of one commutating pole increases by a factor of  $2\beta_k \approx 1.5$  times and there is a corresponding increase in the leakage flux. The leakage coefficient in this case decreases, however, since the useful commutating-pole flux in the gap rises still more, by a factor of  $\rho_k \approx 2.6$ .

Thus

$$k'_{\sigma k} \approx \frac{2\beta_k}{\rho_k} k_{\sigma k} \approx 0.6 k_{\sigma k}, \quad (6.137)$$

while the cross-section ratio for the commutating-pole core is

$$\frac{S'_{k.m}}{S_{k.m}} = \frac{\Phi'_{k.m}}{\Phi_{k.m}} = \frac{\Phi'_k k'_{\sigma k}}{\Phi_k k_{\sigma k}} \approx 2\beta_k. \quad (6.138)$$

Consequently,  $S'_{k.m} > S_{k.m}$ , i.e.,  $l'_{sr.k} > l_{sr.k}$  as well; this means that the cross section of the core and the mean length of the commutating-pole winding are greater for a half complement of commutating poles, i.e., in this case both the decrease in armature and core weight and the reduction in commutating-pole copper losses will be negligible.

#### Compensating Windings

A compensating winding is normally used together with commutating poles to compensate the quadrature-axis armature reaction within the limits of the pole piece. The presence of a compensating winding re-

sults in a situation in which the air-gap magnetic field remains practically unchanged when the machine goes from no-load to load conditions.

This fact makes it possible to increase the average voltage per segment by 25% under no-load conditions, and to reduce the air gap.

The linear load on the compensation winding should equal the linear armature load  $A_{k.o} = A$  or

$$\frac{N' I}{2p} = \frac{N_{k.o} J}{a\tau}, \quad (6.139)$$

so that the number of compensating-winding bars per pole will be

$$N_{k.o} = \frac{N'}{2p} a = \frac{N}{4ap} a \quad (6.140)$$

and the compensating-winding cross section will be

$$S_{k.o} = \frac{I}{J_{k.o}}. \quad (6.141)$$

Effect of compensation on generator characteristics. Aircraft direct-current generators of 6 kw power or more are sometimes made in compensated form, especially where there is a wide range of speed variation. As we know, the armature magnetizing force is compensated with the aid of a winding placed in slots in the main pole pieces.

The compensating winding is connected in series into the machine armature circuit, and is located on the pole quadrature axis, i.e., it is rotated through  $90^\circ$  with respect to the field-winding axis and coincides with the axis of the commutating-pole winding. Figure 6.61 shows air-gap field curves for various methods of armature magnetizing-force compensation.

Figure 6.61a shows field curves for a compensated machine not using commutating poles; here the compensating-winding magnetizing force is so chosen as to compensate the armature magnetizing force and form a commutating field in the commutation zone. In this case the result-

ant air-gap field (curve 3) is sharply distorted and the induction in the pole pieces may change sign.

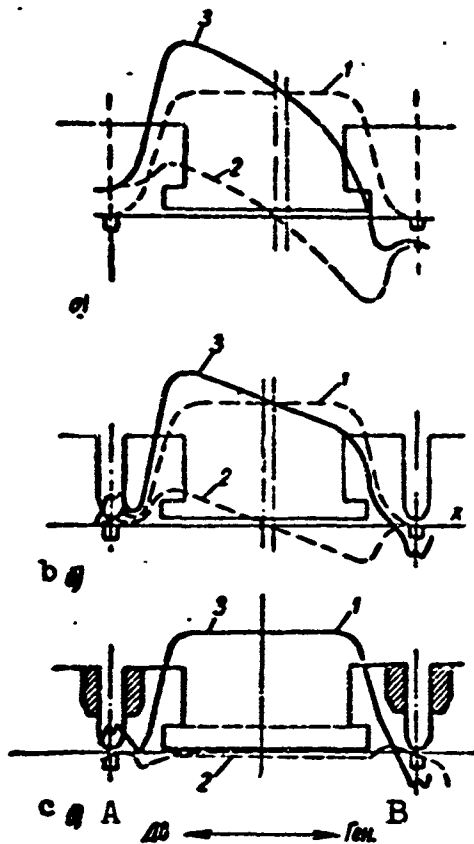


Fig. 6.61. Field curves for compensated generator. A) Motor; B) generator.

Figure 6.61b shows field curves for compensated machines using unexcited commutating poles, i.e., commutating poles without windings. Here the compensating-winding magnetizing force also exceeds the armature magnetizing force and equals

$$F_{c.o.} = kF_a = 0.5kA, \quad (6.142)$$

so that it equals zero on the pole axis while at a distance of  $0.5\alpha\tau$  away from the axis, i.e., at a pole edge, it amounts to

$$F_{c.o.} - F_a = 0.5(k-2)\tau A \approx 0.325\tau A,$$

if  $k = 1.3$  and  $\alpha = 0.65$ .

The resultant magnetizing force is directed opposite to the armature magnetizing force and forms a transverse field opposite in direction to the armature field (curve 2). Out-

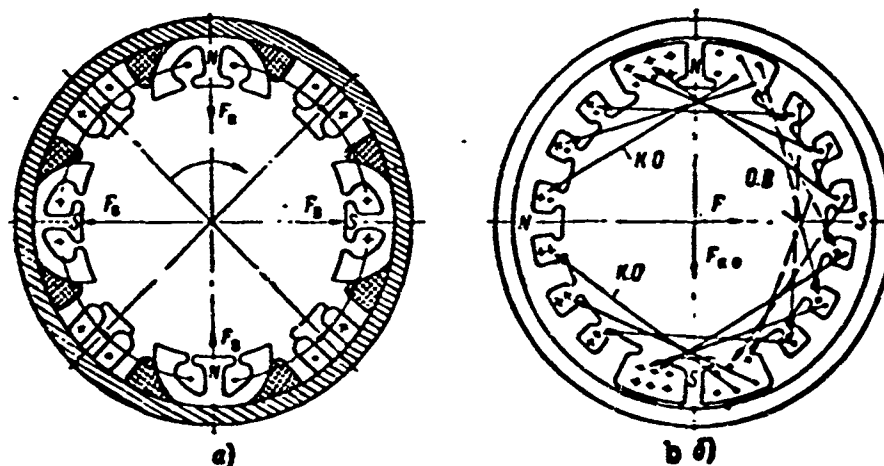


Fig. 6.62. Structural diagram of 9-kw compensated aircraft generator. a) Salient-pole construction; b) nonsalient-pole construction.

side the limits of the main pole, the transverse-field curve drops rapidly, since the reluctance presented to the transverse flux rises while the magnetizing-force difference  $F_{k.o} - F_{ya}$  decreases.

Figure 6.61c gives field curves for a compensated machine using excited commutating poles. In this case, compensation of the armature magnetizing force over the length of the pole arc is used as the basis for selecting the magnetizing force  $F_{k.o}$ ; the remaining portion of the armature magnetizing force is compensated by the commutating-pole winding.

Comparing the curves of Fig. 6.61, we see that the best results are given by the last method of compensation, which provides nearly constant field shape in the gap under all load conditions with minimum consumption of copper.

The number of compensating-winding slots does not depend on the number of armature slots. It is desirable, for structural reasons, to have one or two bars in each slot. The slots normally are of the closed or half-closed type.

Compensated direct-current generators may differ structurally, for example, as shown in Fig. 6.62.

The advantages of machines using distributed field windings and a compensating winding (Fig. 6.62b) are excellent commutation characteristics, minimum losses, and less departure from the neutral plane. At the same time, they are poorer from the viewpoint of weight than salient-pole generators, whose field and compensating windings are of the concentrated type. Compensated generators with salient poles are roughly 10% lighter than compensated generators with nonsalient poles; thus aircraft compensated generators are made with salient poles.

Figure 6.63 shows the efficiency curve and external characteristic for a compensated aircraft generator.

It follows from these curves that as the machine goes from no load to rated load, the voltage drops by only 20%, while the efficiency of a 6-kw generator reaches 80%.

Thus, a compensated generator has higher efficiency and a flatter external characteristic than an uncompensated machine.

In general-purpose direct-current machines, compensating windings are used when  $P_{\text{nom}} n \geq 350,000$ . In view of the wide range of speed variation characteristic of aircraft generators, we can recommend that they be of the compensated type when  $P_{\text{nom}} n > 100,000$ , where  $P_{\text{nom}}$  is given in kilowatts, and  $n$  in revolutions per minute.

Despite their more complicated construction, compensated machines offer several important advantages. The compensating winding, which eliminates the effect of the quadrature-axis armature reaction, helps to increase the maximum and critical armature currents and, consequently, to improve the overload performance of the generator. As experience has shown, compensated machines make it possible to increase  $I_{\text{kr}}$  and  $I_{\text{pr}}$  by roughly 25% (see Fig. 6.64), and, consequently, to develop higher power for short periods of time.

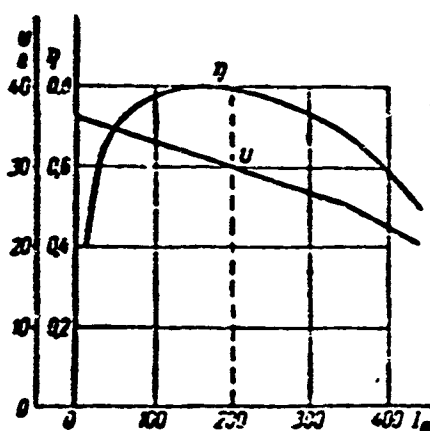


Fig. 6.63. External characteristic and efficiency curve of aircraft direct-current compensated generator, 6 kw power.

In this connection, we should take note of several special features characterizing the operation of direct-current compensated aircraft generators.

1. Under all operating conditions, the air-gap magnetic field remains nearly the same as under no-load conditions; under all operating conditions, including overload and short circuit, commutation conditions are considerably improved and the voltage between commutator segments may be



increased to the maximum value.

2. The air gap may be decreased to the minimum value permitted by mechanical-strength considerations, in view of the absence of magnetic-field distortion in the air gap under load; this makes it possible to reduce the dimensions of the field winding and to decrease the excitation power, which is important not only with respect to increased efficiency and decreased heating, but also with respect to decreased power and size of the voltage regulator.

3. The dimensions of the commutating-pole winding are sharply reduced, since in designing them we need only consider the uncompensated portion of the armature reaction.

If in accordance with (6.142) the compensating-winding magnetizing force equals

$$F_{\Sigma 0} = 0.5\pi A,$$

then an amount

$$F_k' = 0.5\pi A(1-\alpha).$$

is used for the commutating pole.

As a rule,  $\alpha \approx 0.65$  and, consequently,

$$\text{and } \left. \begin{aligned} F_{\Sigma 0} &\approx 0.325\pi A \\ F_k' &\approx 0.175\pi A \end{aligned} \right\} \quad (6.143)$$

i.e., the compensation of the armature magnetizing force  $F_{ya}$  is due 65% to the compensating winding and 35% to the commutating-pole winding.

We recall that in addition the commutating-pole magnetizing force should form a commutating field, so that the magnetizing force for the commutating-pole winding equals

$$F_k = F_k' + F_k'' = 0.5\pi A(1-\alpha) + 0.8B_k \xi_k. \quad (6.144)$$

where  $F_k''$  is the magnetizing force required to form the induction at

the commutating pole.

To what we have said we should add that the commutating-pole leakage flux for a compensated machine is reduced by 30-40% ( $k_{k\sigma} = 3-4$  in comparison with  $k_{k\sigma} = 4-5$  for uncompensated machines).

4. The linear load and peripheral speed of the armature may be increased, which cancels any possible increase in machine size and weight due to the utilization of the compensating winding.

5. Operating stability at high speeds and small loads is increased owing to the fact that the regulation characteristic becomes an ascending curve.

6. The phenomenon of magnetic pole reversal at high speeds is eliminated, since the magnetic field in the gap is not distorted by the load.

7. The range over which the excitation currents vary is decreased and, consequently, the machine is less sensitive to increases in the resistance of the field-winding circuit.

8. Additional losses in the armature core, brush contact, and short-circuited sections are reduced owing to improved commutation; in addition, excitation losses are reduced.

Thus the total losses in the machine are reduced for high speeds and small air gaps, while efficiency rises.

To provide a comparison, we have shown in Fig. 6.64 experimentally obtained external characteristics for compensated and uncompensated generators of exactly the same power, running at  $n = 2500$  rpm with series resistances in the excitation circuit of  $r_v = 1.0$  and  $0.25$  ohms.

An analysis of these curves shows that a compensated generator has a maximum load that is greater than that for an uncompensated generator by a factor of  $260/200 = 1.3$  where  $r_v = 0.25$  ohm, and by  $200/$

/100 = 2.0 where  $r_v = 1.0$  ohm. This is especially important when sudden load variations are encountered, a case in which certain generators fail, or when large motors are started.

A compensated machine will develop a high critical current at low voltage, which is important in the presence of large overloads or short circuits, where the voltage regulator does not work and the voltage drops. As a result, the generator will have very high output in all types of operation, even under emergency conditions.

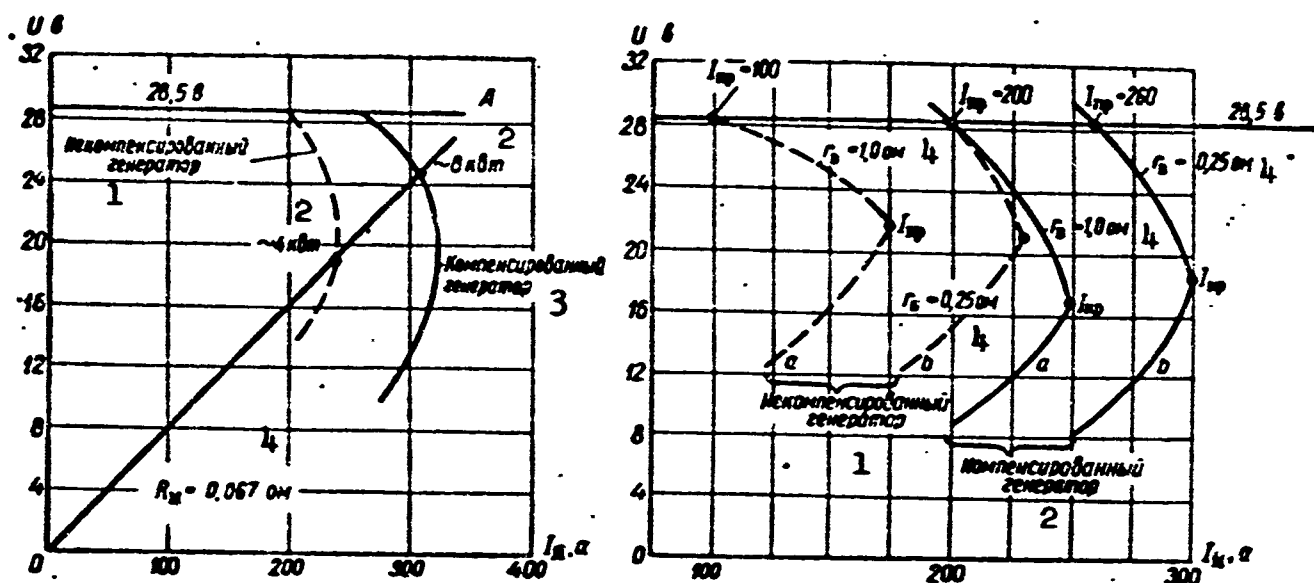


Fig. 6.64. Comparison of external characteristics for compensated and uncompensated direct-current aircraft generators. 1) Uncompensated generator; 2) kw; 3) compensated generator; 4) ohms.

A change in the series resistance in the excitation circuit from 1.0 to 0.25 ohm in an uncompensated generator causes the load current to change by a factor of 2 (from 100 to 200 amp), while in the compensated generator it only changes by a factor of 1.3 (from 200 to 260 amp). This means that a change in the excitation-circuit resistance in compensated machines has less effect on the armature current than in uncompensated machines.

It also follows from Fig. 6.64 that with constant load resistance (line OA)  $R_n = 0.067$  ohm, the compensated machine develops twice the power (8 kw as against 4 kw) of the uncompensated machine. Thus, a

change in excitation-circuit resistance and a decrease in voltage have less effect on the power delivered by compensated generators, i.e., these machines are more stable and have greater operating reliability. The existing notion that compensated generators are heavier and have higher losses is baseless.

The number of turns and conductor cross section for compensating and commutating-pole windings equal the number of turns and cross section of the commutating-pole winding in an uncompensated machine (given the simplifying condition that the current density is the same in all windings); the mean turn length for the compensating winding is roughly 40-50% greater than the mean turn length for the commutating-pole winding. As a result, the weight of copper, voltage drop, and losses rise by about 20-25%.

The increased losses and weight of copper, as well as the voltage drop in the armature circuit due to the utilization of the compensating winding are balanced:

a) by a nearly two-fold decrease in weight and losses in the field winding (the field winding weighs roughly 2.5 times more than the commutating-pole winding, since the current density in the commutating-pole winding is roughly 2.2-2.4 times that in the field winding);

b) by a decrease in the voltage drop at the sliding contact owing to improved commutation (this does not completely compensate, however, for the increased voltage drop in the armature circuit);

c) by excitation losses - the losses in the field winding and regulator decrease by roughly a factor of 2, which compensates for the increased armature-circuit losses.

On the whole, the total copper weight and copper losses are lower in compensated machines than in uncompensated machines; the voltage

drop is somewhat greater in compensated machines.

In 9-kw or larger direct-current aircraft machines it is desirable to use a compensating winding when  $n_{\max}/n_{\min} \geq 2$ , despite the structural complications involved.

## 6.7. STARTER-GENERATORS

Various methods are used to start aircraft engines.

In order to start piston engines, it is necessary to impart to the crankshaft a minimum starting speed  $n$  that will overcome the static moment of resistance  $M_s$ .

In order to start turbojet engines, the compressor must be brought up to the speed  $n_1$  needed to begin turbine operation, and then turbine rotation must be followed for some period of time. As a rule, the turbine begins to operate at a speed  $n_1 = 900$ -1200 rpm, while the turbine must be assisted until a speed  $n_2 = 1200$ -1500 rpm is reached.

A 3-7 kw direct-current electric motor with series excitation is usually used to start modern piston aircraft engines of 1000-2000 horsepower. For direct starting of a piston engine of about 1000 horsepower, an electric motor is needed with a starting power  $P_{\text{nom}} = 3.7$  kw at a starting speed of  $n_p = 60$  rpm, weighing about 15 kg together with a 70 amp-hr storage battery weighing 70 kg. The starting period is 3-5 sec long. A direct-action starter consists of an electric motor and reducing gear.

In order to reduce the dimensions of the electric motor and storage battery, indirect or combination starters are used. In indirect starters (inertia starters), the aircraft engine is started by a flywheel first brought up to speed by a high-speed electric motor, which is disconnected when the aircraft engine starts. In combination starters, both a flywheel previously brought up to speed and an electric motor are used.

Since with inertia starters, an electric motor brings the fly-wheel up to rated speed within 10-15 sec, the power of the electric motor and the storage-battery capacity are considerably reduced.

Inertia starters are considerably lighter and less efficient than direct-acting starters. A combination-type starter has higher efficiency for the same weight.

Modern turbojet engines are usually started by means of direct-acting electric starters consisting of a compound-wound 3-7 kw electric motor and a reducing gear. The starting process is automatic: the electric motor is connected to the line through a limiting resistance (in order to decrease the torque of the electric motor for the first 1-2 sec after it is connected in order to avoid dynamic overloads on the mechanism); the limiting resistance is cut out 3-4 sec after the beginning of the starting process. After the limiting resistance has been disconnected, the electric motor develops full torque and gradually picks up speed; it starts the engine within no more than 25-30 sec.

The rated power of the electric motor is determined by the requirement that maximum power be developed at the speed  $n_1$  at which fuel is supplied and the turbine begins to operate, i.e.,

$$P_2 = 1.02 \frac{M_1 n_1}{\eta_r} \mu, \quad (6.145)$$

where  $M_1 = M_{s \max}$  is the motor moment of resistance at  $n_1$ ;  $\eta_r$  is the reducing-gear efficiency;  $\mu$  is a coefficient that takes into account the relationship between the moment of inertia and moment of resistance of the engine being started; for a starting period of 25-30 sec, it equals 1.3-1.5.

Figure 6.65 gives characteristic curves for a jet engine, i.e., it shows the moment of resistance as a function of speed,  $M_s = f(n)$ ;

it also shows the mechanical characteristic curve for the electric starter, i.e., the torque as a function of the speed,  $M' = f(n)$ .

At the speed  $n_1$  corresponding to the beginning of turbine operation, the moment of resistance of the aircraft engine is at its maximum and the electric starter should develop its maximum power. At the speed  $n_2$ , the electric starter ceases to help the turbine and cuts out.

The excess torque  $M' - M_s = J(d\omega/dt)$  determines the acceleration of the shaft and the length of the starting period.

The ratio  $M'_1/M_{s \max}$  is determined by the given length of the starting period, i.e., the time required to reach the speed  $n_2$  at which the starter cuts out. As a rule  $M'_1 \approx (1.5-2)M_{s \max}$ .

In recent years, aircraft generators installed on the engines to be started, and called starter-generators, have come into use for direct starting of turbojet engines.

The utilization of starter-generators reduces the size and weight of the starting system, since it eliminates the special starting electric motor, although there is a resulting complication in the control system.

Starter-generators use shunt or compound excitation; in the starting mode they operate as motors, while after the starting process has been concluded, they operate as generators.

The powers of a machine in the generator and motor modes are related by the expression

$$\frac{P_{st}}{P_g} = \frac{n_{st}}{n_g} i_g k_p \quad (6.146)$$

where  $P_g$  is the generator power at the initial rotational speed  $n_g$ ;  $P_{st}$  is the power in the starter mode at a speed  $n_{st} = n_1$ ;  $i_g = n_g/n_D$  is the gear ratio between generator and jet engine;  $k_p$  is the overload

coefficient in the starter mode (allowing for the short-time nature of machine operation in this mode).

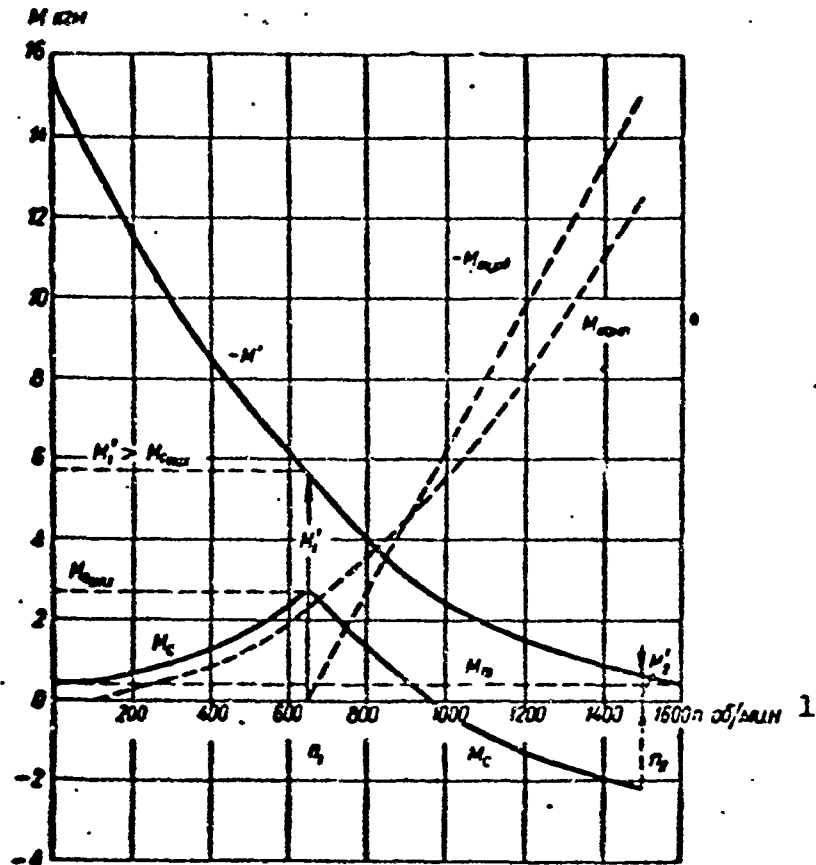


Fig. 6.65. Characteristics of jet engine and electric starter drawing its power from storage battery.  $M_{komp}$ ) Moment of resistance of compressor and turbine at rest;  $M_{tr}$ ) moment of friction of engine;  $M_{turb}$ ) torque developed by turbine. 1) rpm.

If we let  $n_g = 3800$  rpm,  $n_1 = 700-800$  rpm, and  $k_p = 1.5$ , then

$$\frac{P_{st}}{P_r} \leq 0.3i_r.$$

Thus, 9-24 kw aircraft generators may develop 2.7-7.0 kw in the starter mode with a gear ratio  $i_g = 1$ . Here the machine will be very close to short-circuit operation ( $k_p = 1.5$ ), i.e., it will run under unfavorable conditions.

In order to increase generator power in the starter mode, it is necessary to increase the gear ratio, making it greater than unity



(for operation in the generator mode, however, it should be less than unity). This problem is solved by the use of two-speed reducing gears: one speed ( $i_g < 1$ ) is used for generator operation and the other ( $i_{st} > 1$ ) for starter operation.

The maximum electromagnetic power developed by the armature in the motor (starter) mode is determined from the expression

$$\frac{dP_e}{dI} = \frac{d}{dI} \left[ (E_b - \Delta U_m) I - I^2 \sum R \right] = 0,$$

whence

$$I_{max} = \frac{E_b - \Delta U_m}{2 \sum R} = 0.5 I_k$$

and

$$P_{e,max} = \frac{E_b^2}{4R_t} \frac{(1 - \Delta \dot{U}_m)^2}{\xi_R} = \frac{P_{cr,max}}{\eta_e} = \frac{P_{cr}}{\eta_e}, \quad (6.147)$$

where

$$\sum R = R_s \left( 1 + \frac{R_b}{R_s} + \frac{R_{ap}}{R_s} \right) = \xi_R R_s$$

is the total circuit resistance for the storage battery ( $R_b$ ), connecting leads ( $R_{pr}$ ), and machine armature ( $R_{ya}$ );  $\Delta \dot{U}_{shch}^* = \Delta U_{shch} / E_b$  is the relative voltage drop at the brushes;  $\eta_e$  is the electrical efficiency of the motor;  $E_b$  is the storage-battery emf;  $I_{max}$  is the maximum machine current, equal to one-half the short-circuit current  $I_k$ .

If we take into account the fact that the total machine armature resistances

$$R_a = \frac{\Delta U_a}{I_{nom}} = \Delta \dot{U}_a \frac{I_{nom}}{P_r},$$

the relationship between the power developed by the machine in the starter mode and in the generator mode will then be

$$\frac{P_{cr}}{P_r} = \frac{\eta_e}{\xi_R} \frac{1}{\Delta \dot{U}_a} \left( \frac{E_b}{U_{nom}} \right)^2 \left( \frac{1 - \Delta \dot{U}_m}{2} \right)^2, \quad (6.148)$$

where  $\Delta \dot{U}_{ya}^* = \Delta U_{ya} / U_{nom}$  is the relative total voltage drop in the machine armature.

An analysis of the last equation shows that the larger the relative voltage drop at the brushes and the relative voltage drop across the armature resistance, the less power the generator will develop in the starter mode. If the voltage across the starter-generator terminals is raised during starting (by connecting two storage batteries in series),  $\Delta \dot{U}_{shch}^*$  and  $\Delta \dot{U}_{ya}^*$  will decrease and, consequently, the power developed in the starter mode will increase; for the same storage-battery characteristics, higher-power generators will develop relatively large amounts of power in starter operation, since as the rated power rises, the quantity  $\Delta \dot{U}_{ya}^*$  decreases while  $\eta_e$  increases.

Taking  $U_{nom} = 28.5$  v,  $E'_b = 24$  v,

$$\Delta \dot{U}_m = 0.063, \Delta \dot{U}_s = 0.1 + 0.15,$$

$$\eta_e = 0.9 \text{ and } \xi_R = 1 + \frac{R_b}{R_a} + \frac{R_{sp}}{R_a} = 2 + 3,$$

we obtain the relationship

$$\frac{P_{st}}{P_r} \approx 0.65 + 0.3.$$

In the Soviet Union, aircraft generators of 6 kw or more are produced in the form of starter-generators.

#### Choosing an Electric Starter for a Jet Engine

The choice of electric starter is dictated by the machine heating specification and the length of the starting period, which are determined, respectively, from the characteristic curves  $I = \varphi_1(t)$  and  $n = \varphi_2(t)$  using the balance-of-moments equation

$$M' - M_c = J \frac{\pi}{30} \frac{dn}{dt} \quad (6.149)$$

and the known starter characteristic  $M = \varphi_3(I)$ , where  $M_s$  is the moment of resistance of the aircraft engine in starting;  $M'$  is the torque applied by the electric starter to the shaft of the aircraft engine;  $J$  is the moment of inertia of the aircraft-engine rotor (the moment of

inertia of the electrical-machine rotor and the reducing gear are neglected).

To solve the nonlinear differential equation (6.149), we need to know the starter mechanical characteristic  $n = f_1(M)$ , the aircraft-engine characteristic  $M_s = f(n)$ , and the system moment of inertia  $J$ . The functions  $n = f_1(M)$  and  $M = \varphi_3(I)$  can only be plotted for an actual electric starter, however; thus the final choice of a starter cannot be made unless we first know some of its characteristics.

In making a preliminary choice of an electric starter, we start with the jet-engine characteristic  $M_s = f(n)$  and the length of the starting period (the number of attempts at starting, the intervals between attempts, the speed  $n_2$  at which the starter drops out, and the time  $t_2$ ).

The moment of resistance of the jet engine equals

$$M_s = M_{s_{max}} + M_{s_0} - M_{s_{red}} \quad (6.150)$$

The mechanical characteristic of the electric starter, referred to the engine shaft, should provide the acceleration needed to permit the starter drop-out speed  $n_2$  to be reached within the given time interval.

This last condition can be satisfied if the reduced starter torque at the speed  $n_1$  at which the turbine begins to operate exceeds the maximum moment of resistance of the jet engine  $M_{s_{max}}$  by an amount determined by the predetermined starting interval. As a rule,  $M'_1 = 1.5-3.0 M_{s_{max}}$ .

The gear ratio for the reducing gear (between the electric starter and the jet engine) is selected on the basis of the requirement that

$$M'_1 > M_{s_{max}} \text{ and } M'_2 > M_{red}$$

where  $M_{red}$  is the moment due to losses in the reducing gear at the speed corresponding to starter drop-out.

It is necessary for  $M'$  to be considerably larger than  $M_g$ , i.e., there must be a large amount of excess torque when the starting process begins (before  $n_1$  is reached) in order to reduce the length of the starting period.

An electric starter operates with large armature currents and high magnetic-circuit saturations; thus in determining  $n = f_1(M)$  and  $M = \varphi_3(I)$ , the magnetic-circuit saturation and armature reaction are taken into account. In addition, it is necessary to allow for the variation in voltage across the storage-battery terminals owing to variation in current and capacity.

The electric-starter characteristics  $M = \varphi_3(I)$  and  $n = f_1(M)$  are found from the expressions

$$M = k_M I \Phi$$

and

$$n = \frac{U - \Delta U_m}{k_E \Phi} - \frac{R_a I}{k_E \Phi}, \quad (6.151)$$

where

$$k_M \approx \frac{pN}{9.81 \cdot 2\pi a},$$

$$k_E = \frac{pN}{60a} \cdot 10^{-3},$$

$N$  and  $a$  are the number of conductors and number of pairs of parallel circuits in the armature winding;  $p$  is the number of pole pairs;  $\Phi$  is the resultant magnetic flux in the gap.

#### Series Resistance in the Armature Circuit

In order to permit the starter shaft to engage the engine shaft smoothly at the beginning of the starting process, the acceleration of the electric-motor shaft is limited to about  $d\omega/dt \approx 0.3$  per  $\text{sec}^2$ . In order to obtain the desired shaft acceleration at the beginning of the starting process, a series resistance  $R_{dob}$  is connected into the arma-

ture circuit; it is later shorted out.

The value of the series resistance is determined on the assumption that the dynamic moment and, consequently, the acceleration during the first stage of the starting process are roughly constant. Actually, it may be assumed that during the first stage of its starting the moment of resistance roughly equals the friction moment, i.e.,

$$M_e \approx M_m \approx \text{const};$$

the armature current, flux, and torque of the electric motor are roughly constant, since the speed and, consequently, the back emf are small, i.e.,

$$I = \text{const}, \Phi \approx \text{const} \text{ and } M' \approx \text{const}.$$

Thus

$$M' - M_e = J \frac{d\omega}{dt} \approx \text{const} \text{ and } \frac{d\omega}{dt} \approx \text{const}.$$

Knowing  $M' = M_s + J(d\omega/dt)$ , we use the curve  $M' = f(I)$  to find the armature current  $I_{ya1}$  that corresponds to the first stage of the starting process.

Then the series resistance in the armature for a given acceleration will be

$$R_{\text{ser}} = \frac{U_s - \Delta U_m - R_a I_{a1}}{I_{a1}} \quad (6.152)$$

while the speed at the end of the first stage of starting will equal

$$\omega_1 = t_1 \frac{d\omega}{dt} \approx 0.3t.$$

where  $t_1$  is the duration of the first stage of the starting process.

Figure 6.66 shows a general view and the construction of the Type STG-12T compensated starter-generator.

Series GSR-ST starter-generators differ from series GSR generators only in that they use compound excitation. The series field winding, used only in the starter mode, is used to improve the starting

characteristics of the machine in starter operation. In order to increase the speed at the end of the starting process (with a slight decrease in torque), the machine is subsequently switched automatically to series excitation (Fig. 6.67). We note that the starter-generators are somewhat larger and heavier (by 10-20%) than the corresponding generators.

A starter-generator is connected to the aircraft engine through a multiratio reducing gear, which automatically shifts from the gear ratio  $i_2$  in motor operation to the gear ratio  $i_g = 0.8$  in generator operation.

In motor operation, the optimum gear ratio ( $i_2 \approx 1-1.7$ ) is determined experimentally. If the gear ratio  $i_2$  is increased, there will be a reduction in the amount of electric power consumed by each start, but the duration of the starting period will then be increased and the speed (revolutions) to which the electric motor accompanies the aircraft-engine turbine will be reduced. As a result, the temperature of the gas in the exhaust nozzle of the aircraft-engine turbine will exceed the permissible value.

Figure 6.68 shows the wiring diagram for a GSR-ST-6000A starter-generator.

With this circuit:

- two starter-generators can be started alternately with the aid of one Type AVP-1VD automatic timer;
- the starting apparatus cannot operate when the given starter-generator is running in the generator mode;
- one starter-generator cannot be started while the other is operating as a motor;
- the automatic timer will reset freely, i.e., without operating the starting apparatus, if the supply voltage should be cut off during

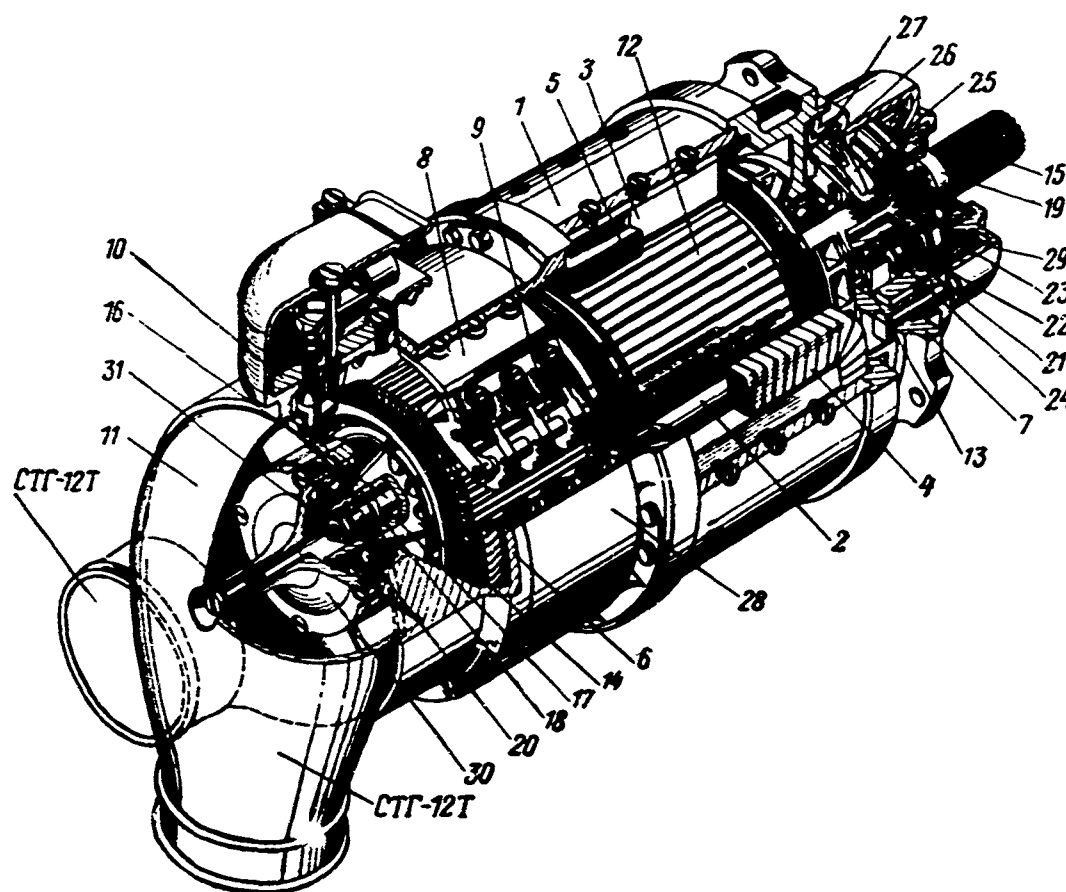
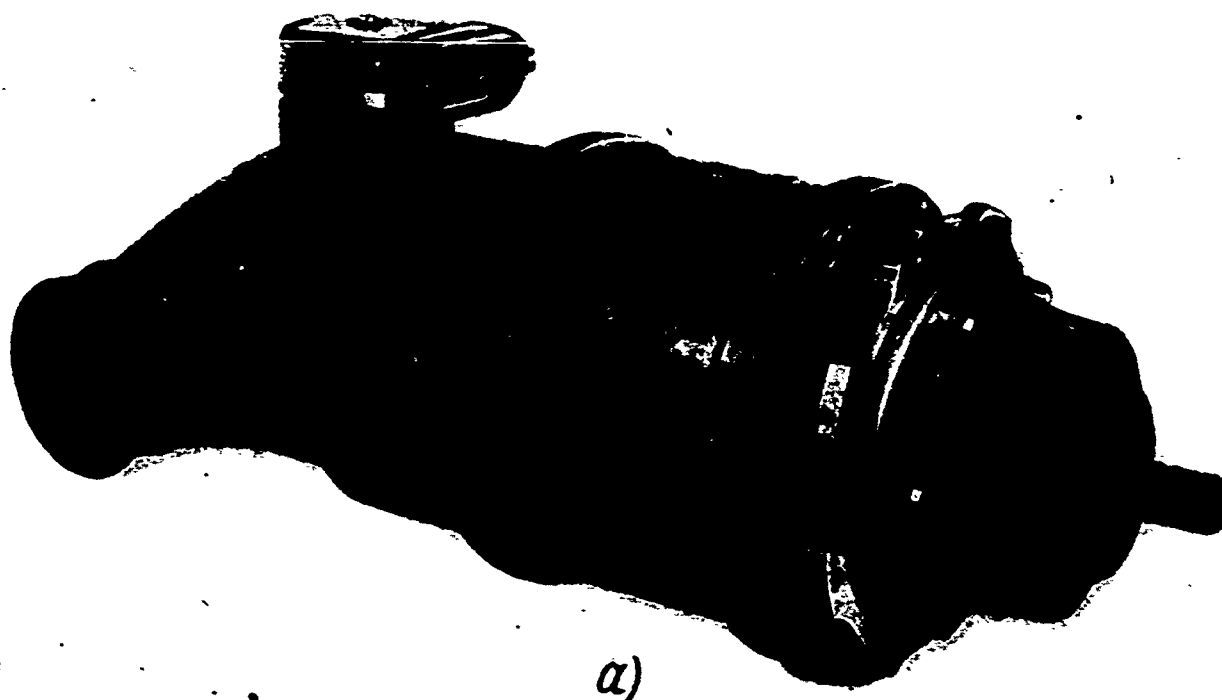


Fig. 6.66. Type STG-12T 12-kw compensated starter-generator. a) Overall view; b) construction. 1) Frame; 2) main pole; 3) commutating pole; 4) field winding; 5) commutating-pole winding; 6) guard; 7) front

guard; 8) brushholder; 9) brush; 10) panel; 11) cap with duct, 12) armature; 13) hollow shaft; 14) hub; 15) flexible drive sleeve; 16) roller-type free-wheeling clutch; 17) steel roller; 18) laminated-fabric spacer; 19) satellite carrier; 20) ball bearings; 21) planet gears; 22) ring gear; 23 and 24) separators; 25) dog; 26) spiral spring; 27) ratchet wheel; 28) protective strip; 29) reducing-gear housing; 30) flange; 31) nut.

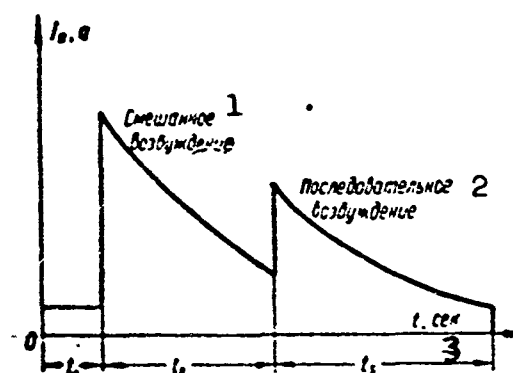


Fig. 6.67. Typical oscillogram for current drawn on a uncompensated starter-generator in the course of a starting cycle. 1) Compound excitation; 2) series excitation; 3) sec.

the starting process and then reappear.

Fig. 6.68. Wiring diagram for two starter-generators with starting and control apparatus: AVP-1VD automatic timer, R-25A carbon voltage regulator, RP-2 normally-closed contacts, MR-2, RP-3 and RL-9Sh relays, D-5TR electric motor, KM-50D and KM-200D contactors, and DMR-400 reverse-current relay. 1) Battery; 2) switch; 3) generator; 4) main positive bus; 5) start; 6) equalizing bus; 7) to ignition.





[List of Transliterated Symbols]

473	НОМ = nom = nominal'nyy = rated
473	д.п = d.p = dopolnitel'nyy polyus = commutating pole
473	к.о = k.o = kompensatsionnaya obmotka
473	В = v = возбuzhdeniye = excitation
473	щ = shch = shchetka = brush (shchetochnyy)
474	н = n = nagruzka = load
475	ГСК = GSK [Type Designation]
475	ГСН = GSN [Type Designation]
475	ГСП = GSR [Type Designation]
476	к = k = kollektor = commutator
476	я = ya = yakor' = armature
476	В = v = vol'ty = volts
476	э = e = elektromagnitnyy = electromagnetic
476	ср = sr = sredniy = average
476	з.п = z.p = zapolneniye, pazy = fill factor, slots
479	кг = kg [kilograms]
484	Ш = Sh = shina = bus
488	ур = ur = uravnitel'nyy = equalizing
491	к = k = kollektor = commutator
499	ГОСТ = GOST = Gosudarstvennyy obshchesoyuznyy standart = All-Union State Standard
502	ав = av = aviatsionnyy = aircraft
502	общ = obshch = obshchego primeneniya = general-purpose
502	к.с = k.s = kommutiruyushchiye seksii = commutating sections
503	к.з = k.z = kommutatsionnaya zona = commutation zone
505	з = z = [zubets = tooth]

512 th = tanh  
 512 ch = cosh  
 516 наш = nach = nachal'nyy = initial  
 516 о.н = o.n = otnositel'noye nasyshcheniye = relative saturation  
 517 кр = kr = kriticheskiy = critical  
 518 пр = pr = predel'nyy = limiting  
 519 х = kh = kholodnyy = cold  
 519 р = r = regulyator = regulator  
 519 у.с = u.s = ugol'nyy stolb = carbon stack  
 519 в.г = v.g = возбuzhdeniye, goryacheye = excitation, hot  
 520 к = k = korotkogo zamykaniya = short-circuit  
 524 при = pri = for  
 527 ост = ost = ostatochnyy = residual  
 538 р = r = reaktivnyy = reactive  
 538 т = t = transformatornyy = transformer  
 555 т = t = treniye = friction  
 566 пар = par = para = vapor  
 566 кисл = kisl = kislorod = oxygen  
 587 ст = st = stator = stator  
 589 к.о = k.o = kompensatsionnaya obmotka = compensation winding  
 590 Дв = Dv = dvigatel' = motor  
 590 Ген = Gen = generator = generator  
 590 О.В = O.V = obmotka возбuzhdeniya = excitation winding  
 597 с = s = soprotivleniye = resistance  
 597 п = p = puskovoy = starting  
 599 ст = st = starter = starter  
 599 г = g = generator = generator  
 599 п = p = peregruzka = overload

600       комп = komp = kompressor = compressor  
600       тр = tr = treniye = friction  
600       турб = turb = turbina = turbine  
600       кгм = kg-m  
601       б = b = batareya = battery  
601       пр = pr = provod = lead  
601       э = e = elektricheskiy = electric  
603       ред = red = reduktor = reduction gear  
604       доб = dob = dobavochnyy = series  
609       АВП-ІВД = AVP-1VD  
          Р-25А = R-25A  
609       РП-2 = RP-2  
609       МР-2 = MR-2  
609       РП-3 = RP-3  
609       РЛ-9Ш = RL-9Sh  
609       Д5ТР = D5TR  
609       КМ-50Д = KM-50D  
609       КМ-200Д = KM-200D  
609       ДМР-400 = DMR-400

## Chapter 7

### PARALLEL OPERATION OF AIRCRAFT GENERATORS

#### 7.1. GENERAL INFORMATION ON PARALLEL OPERATION

As a rule, alternating- and direct-current electrical machines are operated together by connecting them in parallel; a series connection is used only in special circuits and shall not be considered here.

As is well known, parallel operation of electric generators increases the reliability of the electrical system, since when some of the generators fail, the remaining generators provide electric power to the most important units; it makes it possible in independent electrical systems to start and supply motors having more power than a generator taken separately; and the installed capacity required for stand-by purposes is reduced.

At the same time, parallel operation of electrical machines requires that especial care be taken in establishing connections, that the loads (resistive and reactive) be distributed between generators operating in parallel in proportion to their rated powers, etc.

All of this requires the utilization of additional automatic equipment for connecting generators into the line and maintaining proper operation with the parallel connection.

The problem of parallel operation of synchronous machines and entire power systems has been solved for general-purpose installations, while the problem of parallel operation of aircraft generators has as yet not been solved completely.

Parallel-operation conditions are considerably more complicated for aircraft generators than for stationary generators which operate with identical prime-mover and generator power, with constant prime-mover speed, with the speeds of all prime movers proportional to the line frequency, with negligible accelerations (during variation of prime-mover speed), and with the prime mover controlled by generator operating conditions.

Parallel operation in aircraft power systems is characterized by a generator power amounting to 1-2% of the engine power as well as by the variable engine speed (speed variation range of 3:1 or more), by the difference in speeds of system engines, by high accelerations occurring with changes in prime-mover speed (an engine picks up speed at a rate of over 2000 rpm per second), and by the fact that engine regulation does not depend on generator operating conditions.

The following three cases of parallel operation of alternating-current aircraft generators should be studied:

- parallel operation of constant-frequency generators driven through a coupling with a continuously variable gear ratio;
- parallel operation of variable-frequency generators driven directly by a main aircraft engine;
- parallel operation of stabilized-frequency generators driven by direct-current electric motors (converters).

Here we shall not consider parallel operation of synchronous generators with independent drive, since their operation is similar to that of general-purpose generators.

In Chapter 1, it was shown that there are two alternating-current aircraft electrical power systems: the constant-frequency system and the variable-frequency system.

In the first system, generator speed is held constant while in

the second system all generators turn at the same speed, but this speed may vary within wide limits.

Here we shall consider conditions for parallel operation of generators in a constant-frequency system. Certain features of parallel generator operation in a variable-frequency system will be considered later.

In the general course on electrical machinery it was established that two basic types of operation are possible with paralleled synchronous machines: a) joint operation of a generator and a line of comparable power, where a change in excitation of one generator affects the line voltage and, consequently, to keep the line voltage constant it is necessary to make appropriate changes in the excitation of the other paralleled generators;

b) operation of a generator into a line of nearly infinite power, or a change in operation of one generator (variation in excitation or load) has no effect on line voltage.

In aircraft electrical systems, from two to eight identical generators are operated in parallel. Since the line voltage is held constant automatically with the aid of regulators, it may be assumed that with the exception of the dependence on the number of generators operating in parallel, each generator operates under the second set of conditions, i.e., as if it were operating into a line of infinite power. Here we neglect any possible delay in regulator operation, which may be of importance in the study of transient phenomena.

Thus we shall henceforth assume that parallel operation of aircraft generators takes place under conditions of constant line voltage. This assumption cannot be made in studying processes of switching to parallel operation, especially for converters, since such switching is accompanied by a brief drop in line voltage.

As we know from the general course, in order to transfer a resistive load from one generator to another, it is necessary to use the drive-motor power regulator to cause the generator whose load is to be increased to lead. The more heavily loaded generator operates with an internal shift angle  $\theta_1$  (the angle between the machine quadrature axis and the high-voltage vector) greater than the value of the similar angle  $\theta$  for other identically loaded paralleled generators. The generator excitation is varied only by changing the magnitude and phase of the current; in this case, the real load remains unchanged.

From the viewpoint of minimum system losses, the most sensible method is parallel operation of generators such that the real and reactive loads are distributed among them in proportion to their rated powers. For aircraft electrical systems, this means operation of all generators with identical loads and identical power factors.

Figure 7.1 shows a circuit for parallel operation of three-phase synchronous generators driven through a constant-speed transmission.

For voltage regulation, each generator is provided with a voltage regulator RN while a power regulator RM is provided for regulation of the speed (real load). When the generator operates independently, the voltage regulator and power regulator maintain the given frequency and alternating-current line voltage under variations in load and cooling-medium temperature.

Stable operation is ensured by the fact that the regulators have inherent static stability, i.e., a descending speed vs. real load curve and a descending voltage vs. total load curve. For parallel generator operation, a real-load distributor RAN is added to the power regulator, and a reactive-load distributor RRN to the voltage regulator; the switching circuits and operating principles of these devices will be described below.



For proper and efficient operation of an alternating-current electrical system it is necessary for the reactive and real loads to be distributed among the paralleled generators in proportion to their rated capacities. In this case all of the paralleled generators will

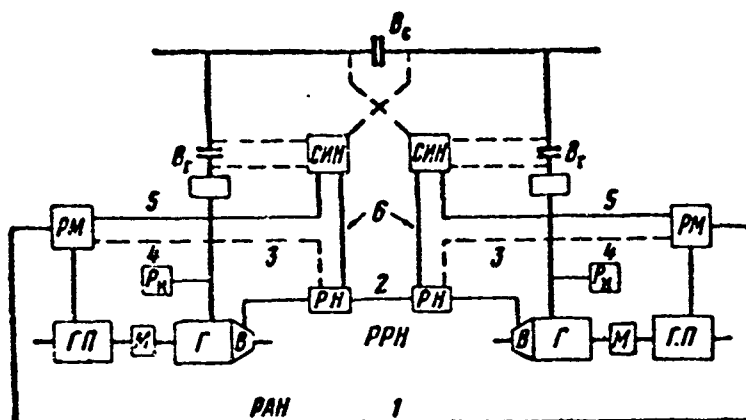


Fig. 7.1. Diagram showing parallel operation of three-phase generators. G) Generator; V) exciter; GP) hydraulic drive mechanism; M) free-wheeling clutch; RM and RN) power and voltage regulators; SIN) synchronizing device;  $R_N$ ) overvoltage relay;  $V_G$  and  $V_S$ ) generator and line switches; RAN and RRN [1 and 2]) real and reactance load distributors; 3 and 4) reactance- and real-load signals; 5 and 6) speed and voltage corrections.

have the same power factor equal to the load power factor, and the system will have a power rating equal to the sum of the power ratings of the generators entering into the system for minimum system losses.

When the uniform distribution of real or reactive load is upset, the system cannot deliver rated power, since the permissible maximum system power is reached when one of the generators carries its rated load, while the remaining generators will be underloaded.

The circuits used for distribution of reactive and real loads in aircraft electrical systems take the form of voltage-regulating and generator-speed-regulating devices which act to eliminate the load unbalance between paralleled generators and thus provide minimum decreases in voltage and frequency (speed) with increasing load.

## 7.2. DISTRIBUTION OF REACTANCE LOAD

A reactance-load distributor (Fig. 7.2) consists of current

transformers TT whose primaries are connected into one of the generator phases and whose secondaries are connected into the primaries of the coupling transformers of the voltage-regulator circuit; the coupling transformers TS whose primaries are connected to the voltage regulators and whose secondaries are connected to the three-phase line; and the circuits (Fig. 7.3) used to connect the current-transformer secondaries into the coupling-transformer primaries and which form the circuit of the reaction-power distributor.

Operation of reaction-load distributor. When the generators are loaded in proportion to their power ratings, currents proportional to the load will flow through the secondaries of all the current transformers. Where the generators have the same power rating, the effec-

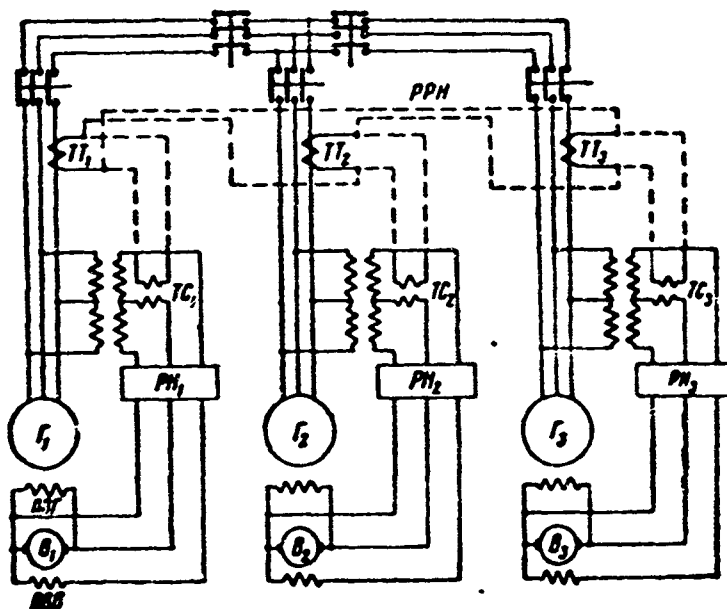


Fig. 7.2. Basic circuit for distribution of reactance load among three-phase paralleled generators.

tive currents will be the same for each of them, i.e.,

$$I_1 = I_2 = \dots = I_n$$

If load currents proportional to the power ratings flow in all the paralleled generators, there will be no current in the primaries of the coupling transformers, and a voltage proportional to the line

voltage will be applied to the voltage-regulator inputs. If for any reason the load current in one of the paralleled generators rises in comparison with the load current in the remaining generators, a reactive equalizing current will appear in the circuit of the reactive-load equalizer. The voltage drop due to the equalizing current in the coupling-transformer secondary circuit combines with the input voltage of the voltage regulator, changing its magnitude so that the resulting change in excitation current tends to reduce the additional voltage due to the reactive current to zero.

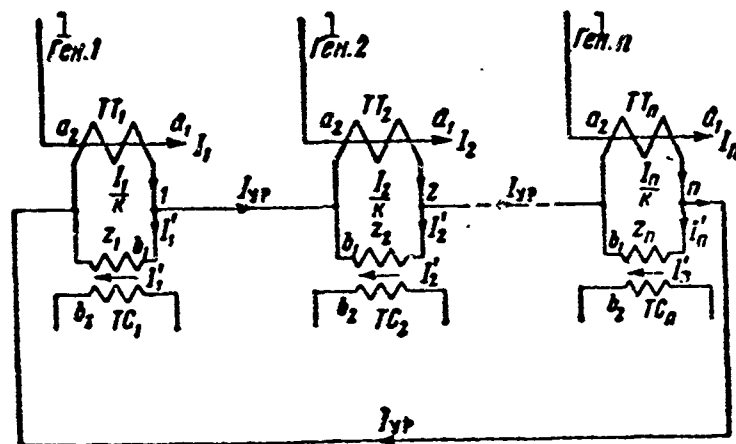


Fig. 7.3. Reaction-load distributor (RRN).  $a_1$  and  $a_2$ ) TT primaries and secondaries;  $b_1$  and  $b_2$ ) TS primaries and secondaries;  $I_1, I_2, \dots, I_n$ ) generator currents in windings  $a_1$ ;  $I_1/k, I_2/k, \dots, I_n/k$ ) currents in windings  $a_2$ ;  $I'_1, I'_2, \dots, I'_n$ ) currents in windings  $b_1$ ;  $I_{ur}$ ) equalizing current in RRN circuit;  $z_1, z_2, \dots, z_n$ ) impedances; 1) generator.

Thus the system, decreasing the equalizing current, ensures proportional distribution of the reactive load with the rated voltage unchanged.

The signal applied to the voltage-regulator input consists of two

parts: a main part proportional to the line voltage, and a correction that is proportional to the reactive component of the current in the coupling-transformer secondary circuit.

If we assume that the paralleled generators, exciters, and regulators have absolutely identical characteristics, identical signals proportional to the line voltage will appear at the input of all voltage regulators when a change in system operation occurs and the magnitudes and phases of the currents in all the generators will vary identically. In this case, there will be no second signal from the reactive-power distributor.

Under actual conditions, the characteristics of the generators, exciters, and regulators will not be identical, and a current will flow in each coupling transformer that will vary the excitation so as to bring about a uniform distribution of the reactive load; when load uniformity has been achieved, the currents cease to flow.

The effect of the reactive components of the currents in the secondary circuit of a coupling transformer on the voltage of the nth generator may be found by using the equation

$$U_n = U_{on} - B_1 I'_n \sin \alpha = U_{on} - B_1 I'_{rn} \quad (7.1)$$

where  $U_n$  is the voltage of the nth generator;  $U_{on}$  is the reference or rated voltage of the nth generator;  $I'_n$  is the current in the coupling-transformer primary;  $\alpha$  is the phase angle by which the coupling-transformer current lags behind the generator voltage;  $I'_n \sin \alpha = I'_{rn}$  is the reactive component of the coupling-transformer current;  $B_1$  is a coefficient of proportionality, assumed to be constant over the working regulator range.

With a uniform distribution of the reactive load among the paralleled generators,  $I_1 = I_2 = \dots = I_n = I_g/n$  where  $I_g$  is the total line current. If for any reason the load on one of the generators (1) be-

comes different from that on the others,  $I_1 \neq I_s/n$ , and an equalizing current  $I_{ur}$  will begin to flow in the circuit of the reactive-load equalizer, while currents  $I'_1, I'_2, \dots, I'_n$  begin to flow in the coupling-transformer primaries.

In this case, when  $I_1 > I_s/n$ , the following equations will hold for elements 1 and  $n$  of the circuit of Fig. 7.3:

$$\frac{I_1}{k} = I'_1 + I'_{yp}; \quad (7.2)$$

$$\frac{I_n}{k} = I'_n + I'_{yp}; \quad (7.3)$$

$$\frac{I_1 - I_n}{k} = I'_1 - I'_n, \quad (7.4)$$

where  $k$  is the current ratio for the current transformers.

If we let  $Z_1 = Z_2 = \dots = Z_n$  be the [vector] impedances of the coupling-transformer primaries, then neglecting the connecting-wire resistances we can use the second Kirchhoff law to write an expression for the circuit consisting of all the coupling-transformer primaries:

$$\dot{I}'_1 Z_1 + \dot{I}'_2 Z_2 + \dots + \dot{I}'_n Z_n = 0. \quad (7.5)$$

Since  $Z_1 = Z_2 = \dots = Z_n$ , we find from (7.5) that

$$\dot{I}'_1 + \dot{I}'_2 + \dots + \dot{I}'_n = \sum_{i=1}^n \dot{I}'_i = 0$$

or

$$\dot{I}'_1 + (n-1)\dot{I}'_n = 0,$$

since  $\dot{I}'_2 = \dot{I}'_3 = \dots = \dot{I}'_n$  by hypothesis.

Then

$$\dot{I}'_1 = -\dot{I}'_n (n-1) \quad (7.6)$$

and

$$\frac{I_1 - I_n}{k} = -\dot{I}'_n - \dot{I}'_n (n-1) = -\dot{I}'_n,$$

i.e.,

$$\dot{I}'_n = -\frac{I_1 - I_n}{nk} = -\frac{\Delta I}{nk}. \quad (7.7)$$

Substituting the expression for  $\dot{I}_n'$  into (7.6) we find

$$\dot{I}_1' = \frac{n-1}{nk} \Delta I = \frac{n-1}{nk} (\Delta I_a + j \Delta I_p). \quad (7.8)$$

The vector difference in the load currents  $\dot{I}_1 - \dot{I}_n = \Delta \dot{I}$  contains a real component  $\Delta I_a$  and a reactive component  $\Delta I_p$ ; consequently, the currents in the coupling-transformer primaries will also contain real and reactive components, i.e.,

$$I_{a1}' = \frac{n-1}{nk} \Delta I_a \text{ and } I_{p1}' = \frac{n-1}{nk} \Delta I_p, \quad (7.9)$$

and taking (7.6) into account, we also have

$$I_{an}' = -\frac{1}{nk} \Delta I_a \text{ and } I_{pn}' = -\frac{1}{nk} \Delta I_p. \quad (7.9a)$$

Under normal operating conditions, i.e., where the real load components are uniformly distributed, only the reactive load components will affect the voltage regulator; their difference will equal

$$\Delta I_p = I_1 \sin \varphi_1 - I_n \sin \varphi_n \quad (7.10)$$

and, consequently, the reactive component of the coupling-transformer primary current, in view of (7.9) and (7.10), will be

$$I_{p1}' = \frac{n-1}{nk} (I_1 \sin \varphi_1 - I_n \sin \varphi_n) \quad (7.11)$$

for the first generator, and

$$I_{pn}' = -\frac{1}{nk} (I_1 \sin \varphi_1 - I_n \sin \varphi_n) \quad (7.12)$$

for the nth generator.

When  $I_1 = I_n$  and  $\varphi_1 = \varphi_n$ , the currents  $I_{r1}'$  and  $I_{rn}'$  in the coupling-transformer primaries will vanish, and the signal appearing at the voltage-regulator input will be proportional to the line voltage alone.

On the basis of (7.1), (7.11), and (7.12) we can obtain an expression for the voltage at the terminals of the generator (1) under study, as well as for all the remaining generators

$$U_1 = U_{01} - k_1 \frac{n-1}{n} (I_1 \sin \varphi_1 - I_n \sin \varphi_n), \quad (7.13)$$

$$U_n = U_{0n} + \frac{n-1}{n} (I_1 \sin \varphi_1 - I_n \sin \varphi_n). \quad (7.14)$$

The quantity  $k_1 = B_1/k$ , which characterizes the resultant effect of the reactive-load distributor, may be found experimentally. To do this, we need to find the way in which the voltage across the terminals of the investigated independently operating generator depends on the reactive load, i.e., we have to plot the external characteristic under an inductive load. In this case, the ratio  $k_1 = B_1/k$  will equal the tangent of the external-characteristic slope angle with the sign reversed, i.e.,  $k_1 = -\tan \alpha_1$ . As a rule,  $k_1 \approx 0.1$  in relative units, i.e., as the current varies from zero to the rated value (with  $\cos \varphi = 0$ ), the system voltage drops by  $\Delta U = k_1 U_0 \approx 21$  v with  $U_0 = 208$  v.

Equations (7.13) and (7.14) may be used to study reactive-load distribution systems under various system operating conditions.

#### Power Utilization Factor for Electrical System

As we have already shown, with a nonuniform distribution of reactive load, there is a decrease in the degree to which the installed generator capacity of an electrical system is used. While one of  $n$  paralleled generators is underloaded owing to regulator error, the remaining  $(n-1)$  generators carry rated load. In order to determine the utilization factor, it is necessary to subtract (7.14) from (7.13), making use of the fact that the voltages of all  $n$  generators are equal

$$0 = U_{01} - U_{0n} - k_1 (I_1 \sin \varphi_1 - I_n \sin \varphi_n)$$

and

$$I_1 \sin \varphi_1 - I_n \sin \varphi_n = \frac{U_{01} - U_{0n}}{k_1} = -\frac{\Delta U}{k_1}, \quad (7.15)$$

where

$$k_1 = \frac{B_1}{k} \text{ and } \Delta U = U_{01} - U_{0n}.$$

whence

$$I_1 \sin \varphi_1 = I_n \sin \varphi_n - \frac{\Delta U}{k_1} \quad (7.16)$$

If we use a relative system of units with  $I_n$  taken as unity,

$$\begin{aligned} \dot{I}_1 \sin \varphi_1 &= \sin \varphi_n - \frac{\Delta \dot{U}}{k_1}, \\ \Delta \dot{U} &= \frac{\Delta U}{I_n}. \end{aligned} \quad (7.17)$$

The reactive load (current) for all current-consuming devices will equal

$$I_c \sin \varphi = I_1 \sin \varphi_1 + I_n (n-1) \sin \varphi_n$$

or, in relative units,

$$\dot{I}_c \sin \varphi = \dot{I}_1 \sin \varphi_1 + (n-1) \sin \varphi_n. \quad (7.18)$$

On the basis of (7.17) and (7.18), we obtain the relative reactive power

$$\dot{Q} = \frac{Q}{U_c I_n} = \dot{I}_c \sin \varphi = n \sin \varphi_n - \frac{\Delta \dot{U}}{k_1}, \quad (7.19)$$

where  $I_s$  is the total line current and  $\dot{I}_s^* = I_s / I_n$  is its relative value.

On the assumption that the real loads on all generators are equal, we may write

$$\dot{P} = \frac{P}{U_c I_n} = \dot{I}_c \cos \varphi = n \cos \varphi. \quad (7.20)$$

The total relative system power is

$$\dot{S} = \dot{P} + j\dot{Q} = n \left[ \cos \varphi + j \left( \sin \varphi_n - \frac{\Delta \dot{U}}{nk_1} \right) \right] \quad (7.21)$$

and

$$|\dot{S}| = \sqrt{\dot{P}^2 + \dot{Q}^2} = n \sqrt{\cos^2 \varphi + \left( \sin \varphi_n - \frac{\Delta \dot{U}}{nk_1} \right)^2}, \quad (7.21a)$$

if we neglect the variation in system voltage, which does not exceed 0.5-0.6%.



The relative system available power or, in other words, the system power utilization factor is defined in relative units by dividing Expression (7.21a) by the number of paralleled generators, i.e.,

$$k_{uc} = \sqrt{\cos^2 \varphi + \left( \sin \varphi_n - \frac{\Delta \dot{U}}{nk_1} \right)^2} = \frac{|\dot{S}|}{n}. \quad (7.22)$$

Analysis of (7.22) shows that the decrease in system power, i.e., its utilization factor, depends on the system power factor, the coefficient  $k_1$ , and the shift in the regulator setting ( $\Delta \dot{U}^*$ ).

The smaller the coefficient  $k_1$  and the larger the number  $n$  of paralleled generators, the less effect a shift in regulator settings will have and, consequently, the higher the system utilization factor

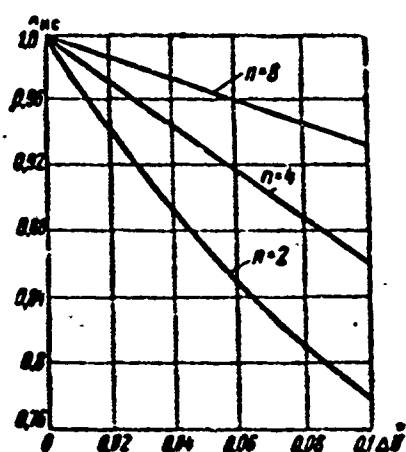


Fig. 7.4. System power utilization factor.

will be. In order to increase the system power utilization factor in the presence of regulator errors, it is desirable to make the coefficient  $k_1$  as large as possible, i.e., to obtain maximum slope of the external characteristic under an inductive load. This may produce fluctuations in the voltage-regulation system, however, owing to the presence of an unsteady current unbal-

ance. In view of this,  $k_1$  is given the largest possible value consistent with stable voltage regulation.

Thus, for example, the setting of one of the voltage regulators is shifted below the rated value by  $\Delta \dot{U}^* = 0.01, 0.025, 0.05$ , and  $0.1$ , while the remaining voltage regulators are set at the rated value. Here, using the normal value for aircraft systems of  $\cos \varphi = 0.75$  and  $\sin \varphi = 0.661$ , and the experimental value  $k_1 = 0.106$ , we can find the system power utilization factor from (7.22). The results of a calculation with  $n = 2-8$  are shown in Fig. 7.4.

A fault in a generator excitation system may produce an extremely high generator voltage — an overvoltage — or may decrease the voltage to the amount determined by the residual magnetism, producing underexcitation.

Overvoltage may be a consequence of: short circuits within the exciter, damage to the voltage regulator, damage to the reactive-load distributor, regulator errors, or broken wires between regulator and distributor. Undervoltage may be a consequence of: a break in the generator excitation circuit or exciter excitation circuit, or a faulty voltage regulator.

An extended period of overexcitation will lead to system overvoltage and, consequently, to increased power consumption and damage to certain power-consuming devices; to increased excitation and reactive currents (and, therefore, to increased exciter and generator temperatures); to loss of synchronism, i.e., to large fluctuations in currents and moments in all generators and to line-voltage ripple that is somewhat greater in relative value than the rated figure.

An extended period of undirect citation or complete loss of excitation will lead to a decrease in system voltage and, as a consequence, to interruption of normal operation of current-consuming devices; to faulty generator operation in the reactive mode, characterized by the drawing of large amounts of reactive current from the line and a drop in the real power to 0.25 times the nominal value (in this case, the generator may go out of synchronism); to an increase in excitation current and reactive current in the properly operating generators and exciters of the system and, consequently, to an excessive increase in their temperatures; to loss of synchronism, i.e., to large fluctuations of currents and moments in all system generators and to a relative line-voltage ripple that is somewhat above the nominal value.

System voltage and the equalizing reactive current in the presence of a malfunction in the excitation system of one of the paralleled generators may be determined analytically and used in designing the electrical system and its protective devices.

### 7.3. REAL-LOAD DISTRIBUTION

Distribution of real load among paralleled generators is based on precise regulation of drive-motor speed.

In aircraft electrical systems, the generators are normally driven by the main aircraft engines, whose speeds are determined solely by flight conditions and are independent of generator operation. Thus real-load distribution is accomplished by regulating the speed of the hydraulic drive mechanism, which is the element directly driving the generator.

The operating principle of the hydraulic clutch has been described already: by changing the position of a "floating" ring, it is possible to maintain constant speed of the hydraulic drive-mechanism output shaft, which is connected to the generator shaft, under variations in the speed of the hydraulic drive-mechanism input shaft, which is connected to the aircraft-engine shaft.

The angle of inclination of the "floating" plate is varied with the aid of the power regulator. The real-power regulator should react to variation in speed (variation in real load) of the individual generators.

The speed (frequency) stabilization device should meet the following technical requirements:

1. The given device should be designed to provide constant frequency and the possibility of parallel operation.

In order to maintain synchronism, it is necessary for the generator axes to be shifted by less than 80 electrical degrees, which is

equivalent to a shift of up to 20 mechanical degrees for a machine in which  $2p = 8$  and up to  $26^\circ$  where  $2p = 6$ .

For proper distribution of loads among the generators, their axes should be shifted by no more than 1-2 mechanical degrees.

2. Real power is distributed among paralleled generators by automatic speed regulation, which provides uniform distribution of torque among the generators. Here the regulator should maintain the following speeds and frequencies under load variations:

$P_n, \%$	1	0	100	120
$n, f, \%$	2	$105 \pm 1$	$100 \pm 1$	$95 \pm 1$

1)  $P_n, \%$ ; 2)  $\underline{n}$  and  $\underline{f}, \%$ .

#### Arrangement and Operation of Speed-Regulation Circuit

Figure 7.5 shows the basic circuit used for real-power regulation with paralleled alternating-current aircraft generators, while Fig. 7.6 shows the basic circuit of the active-power regulator. It consists of two main sections: the regulator itself (tachometer generator and servomotor) and a vector-sensing circuit that applies an impulse to the regulator that is proportional to the generator real power.

The regulator control signal is obtained from a three-phase permanent-magnet tachometer generator TG, which is actuated by the driven shaft of the drive mechanism through bevel gearing.

The alternating voltage of the tachometer generator, which is proportional to the speed, is rectified and applied through a series-connected variable resistor  $R_4$  to the control winding of the regulator  $K_1$ . The solenoid armature of control windings  $K_1$  and  $K_2$  is connected mechanically to the hydraulic-transmission three-way valve 1 and the spring 3 that provides preliminary valve displacement.

Under steady conditions, the force due to the current in control

winding  $K_1$  is balanced by the spring tension, and the valve "floats" freely at the neutral position.

Any change in the angular velocity of the drive-mechanism driven shaft (owing to variation in load or in the angular velocity of the drive shaft) causes a brief change in the current through control winding  $K_1$ ; the temporary equilibrium of the valve is destroyed, and it forces oil into the servodrive mechanism which changes the position (inclination) of the movable plate.

In this case, the direction of the force acting on the valve and the change in plate inclination will be such that the initial angular velocity of the driven shaft will be reestablished. When the normal speed has been reestablished, the control valve 4 of the servodrive mechanism returns to the neutral position. Thus the speed is continuously regulated with the aid of a servomotor with electromagnetic control. The rheostat  $R_5$ , located on the flight engineer's instrument panel, may be used to set the speed that should be maintained by the regulator.

For proper parallel operation of synchronous generators it is necessary for the generator speeds to increase as the load increases. This is accomplished with the aid of the vector-sensing circuit.

Arrangement and operation of vector-sensing circuit. Generator phase voltage is applied to an autotransformer AT. The center tap of the autotransformer secondary is connected to two identical transformers  $T_1$  and  $T_2$  at the common point a.

The voltages from the transformers ( $T_1$  and  $T_2$ ) are rectified by means of selenium rectifiers ( $V_1$  and  $V_2$ ) which are so interconnected that the rectified voltages subtract, and the voltage difference is applied to control winding  $K_2$ . Winding  $K_2$  is wound concentrically on the core with the main control winding  $K_1$ . Since the secondary volt-



in opposition (identical);  $C_1$  and  $C_2$ ) capacitors (identical);  $R_1$ ) fixed resistor;  $R_2$  and  $R_3$ ) variable resistors;  $K_2$ ) control winding reacting to generator real loads; TG) tachometer generator;  $V_3$ ) three-phase rectifier for TG;  $R_4$  and  $R_5$ ) variable resistors for TG;  $K_1$ ) control winding reacting to generator speed; A) servomotor with electromagnetic control. 1) Three-way valve of hydraulic transmission; 2) electromagnetic slide valve; 3) tensioning spring; 4) servodrive; 5) control valve; 6) clutch; 7) vector-sensing circuit; 8) regulator; 9) servomotor; 10) oil; 11) outlet; 12) inlet; 13) steady operation; 14) tensioning spring;  $K_3$ ) protective winding of centrifugal switch TsV.

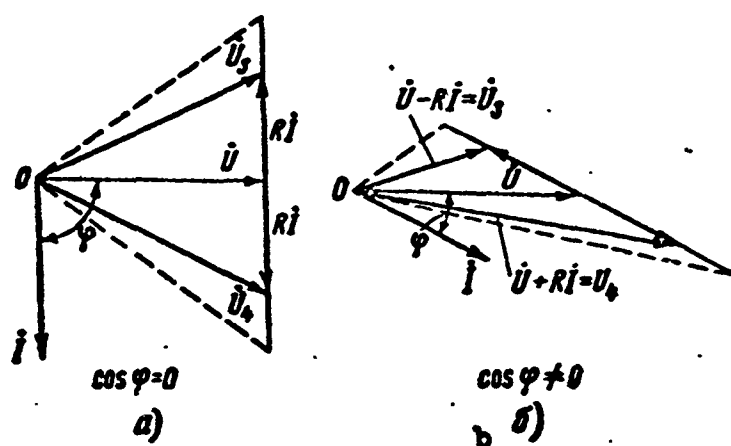


Fig. 7.7. Voltage diagram for vector-sensing circuit. a)  $\cos \varphi = 0$  — output voltages identical; b)  $\cos \varphi \neq 0$  — output voltages differ.

ages  $U_3$  and  $U_4$  are equal and also are opposite in sign after rectification, the current in control winding  $K_2$  will equal zero.

If we now insert resistance  $R_1$  between points A and A' and apply across it a voltage proportional to the load current from the current transformer  $T_3$ , the voltages  $U_3$  and  $U_4$  will equal, respectively, the sum and difference of the voltage vector  $U$  and the drop across resistor  $R_1$ , i.e.,

$$\dot{U}_3 = \dot{U} + R_1 i \text{ and } \dot{U}_4 = \dot{U} - R_1 i.$$

Following rectification, the voltage difference  $U_3 - U_4$  will no longer equal zero and the current flowing in winding  $K_2$  will be proportional to the voltage difference

$$\dot{U}_3 - \dot{U}_4 = (\dot{U} + R_1 i) - (\dot{U} - R_1 i).$$

Thus, in the presence of a load the signal corresponding to the

generator voltage is increased or decreased by a signal proportional to the load current, and a current will flow in control winding  $K_2$ ; a filter ( $C_1$ ,  $C_2$ , and  $R_2$ ) is used to smooth the ripple in this current.

Winding  $K_2$  is so connected that in the presence of a load on the generator, the direction of the flux will coincide with the axis of the flux produced by  $K_1$ , i.e., it has the same effect on the servomotor as an increase in shaft speed.

When the circuit of control winding  $K_1$  is interrupted, the generator can reach its maximum (dangerous) speed. The centrifugal switch TsV is provided to prevent the machine from racing; at a predetermined speed ( $n \approx 1.15n_{\text{nom}}$ ) it connects in the winding  $K_3$ , which replaces the faulty winding  $K_1$ ; it draws its power from the direct-current system.

A generator tends to lose speed under a heavy load and gains speed under a light load; as a result, loads are distributed uniformly. With such a system of regulating division of loads among generators, system frequency will drop by 5% in going from no load to rated load.

It is clear from the vector diagrams of Fig. 7.7 that the circuit reacts only to variations in real power.

Results of hydraulic-transmission tests. A system using two 30-kw generators,  $\cos \varphi = 0.75$  and  $f = 400$  cps, were tested with aircraft engines of 450 horsepower each.

The generators with exciters weigh 35.4 kg each, corresponding to a wave-to-power ratio of 0.885 kg/kva or 1.18 kg/kw. The hydraulic transmission weighed 25 kg, the regulators and auxiliary mechanisms 40.8 kg, and the tachometer generators 1.4 kg. Thus a complete set weighed 67.2 kg with a driven-shaft speed variation range of 2700 to 7000 rpm. The tests showed that the generators came into synchronism rapidly and operated stably, with the rotors connected while their



axes were 180 electrical degrees apart, when the engines ran at different speeds, and when one of the engines was accelerated at a rate of 1700 rpm per second.

### Basic Equations

With a uniform distribution of the active load among the paralleled generators, there will be no current in the connecting wires. If for any reason the active load on one generator increases in comparison with the load on the others, a current will appear in the circuit; its magnitude and direction should ensure restoration of the uniform active-load division among the generators through its action on the slide valves of all  $n$  hydraulic drive mechanisms.

The following equations hold for the output voltages of the vector-sensing circuits (Fig. 7.8):

$$\left. \begin{aligned} E_{a1} &= B_2 I_1 \cos \varphi_1 \\ &\dots \dots \dots \\ E_{an} &= B_2 I_n \cos \varphi_n \end{aligned} \right\} \quad (7.23)$$

Here the  $E_{a1}$ ,  $E_{a2}$ , ...,  $E_{an}$  are the output voltages of the vector-sensing circuits;  $B_2$  is a coefficient of proportionality for the vector-sensing circuits;  $\varphi_1$ ,  $\varphi_2$ , ...,  $\varphi_n$  are the angles by which the load currents  $I_1$ ,  $I_2$ , ...,  $I_n$  lag behind the voltage.

The circuit of Fig. 7.8a may be converted to the circuit of Fig. 7.8b, for which the relationship

$$I_{a1} = \frac{n-1}{n} \frac{E_{a1} - E_{an}}{R_{02}} = \frac{n-1}{n} \frac{\Delta E}{R_{02}}, \quad (7.24)$$

holds; here  $R_{02}$  is the resistance of the second control winding.

Taking (7.23 and 7.24) into account, we obtain

$$I_{a1} = \frac{n-1}{n} \frac{B_2}{R_{02}} (I_1 \cos \varphi_1 - I_n \cos \varphi_n). \quad (7.25)$$

For an independent generator operating into an individual load, the frequency will be nearly directly proportional to the voltage drop

across the terminals of the second control winding, which is a linear function of the voltage  $E_a$ , i.e.,

$$f = f_0 - \beta U_a = f_0 - \beta I_a R_{a2}, \quad (7.26)$$

where  $f_0$  is the frequency level or the reference frequency of the setting, i.e., the frequency determined solely by the first control winding (the generator no-load frequency);  $U_a$  and  $I_a$  are the voltage drop and current for the second control winding (static-stability winding).

This expression can be applied to each of the paralleled machines; consequently, in view of (7.25), we can write an expression for all of the generators

$$\begin{aligned} f &= f_{01} - \beta I_{a1} R_{a2} = f_{01} - K_2 \frac{n-1}{n} (I_1 \cos \varphi_1 - I_n \cos \varphi_n), \\ &\dots \dots \dots \\ f &= f_{0n} - \beta I_{an} R_{a2} = f_{0n} + \frac{K_2}{n} (I_1 \cos \varphi_1 - I_n \cos \varphi_n), \end{aligned} \quad (7.27)$$

where  $K_2 = \beta B_2$  and  $I_n = -I_1/(n-1)$  for the  $n$ th generator.

The constant  $K_2$  may be found experimentally for an independently operating generator for which the speed characteristic, i.e., the function  $f = \varphi(I)$ , has been plotted. The constant  $K_2$  is the tangent of the velocity-characteristic slope with the sign reversed, i.e.,

$$K_2 = -\operatorname{tg} \alpha_2.$$

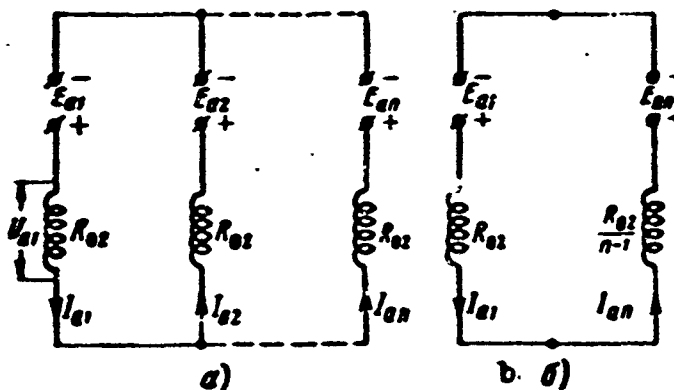


Fig. 7.8. Circuit of real-load equalizer. a) Basic; b) equivalent.

As a rule, in relative units  $K_2 = 0.05$ ; this means that at a nominal system frequency of 400 cps, the frequency will drop by  $\Delta f =$

$$= K_2 f_0 = 0.05 \cdot 400 = 20 \text{ cps with variation from no load to rated load.}$$

By using a rheostat in the circuit of the second control winding (static-stability winding) it is possible to change the slope of the velocity characteristic, i.e., the quantity  $K_2$  (in practical terms, over the range  $K_2 = 0.16-0.04$ ). Consequently, the vector-sensing circuit will operate so that as the real load increases, generator speed will decrease.

Experience gained in operating an independent generator without a vector-sensing device has shown that the speed (frequency) of the generator drops somewhat as the real load increases. This means that the first control winding itself introduces some degree of static stability. As the load rises from no load to the rated value, the frequency will always drop by several cycles per second (where  $f_0 = 400$  cps); in this connection, we may assume that when the static-stability winding circuit is interrupted  $K_2 \approx 0$  (i.e., the static stability of the first control winding is neglected).

We note that the voltage equations (7.13) and (7.14) are similar to the frequency equations (7.27).

#### Electrical-System Power Utilization Factor

The utilization of electrical-system rated power decreases where there is nonuniform division of the real power among paralleled generators. Power losses due to disturbance of speed-regulator settings (level) may be determined as in the case of disturbances to voltage-regulator settings.

Thus, considering that all paralleled generators in a system have the same frequency, we find from (7.27) that

$$0 = f_{\alpha} - f_{\alpha} - K_2 (I_1 \cos \varphi_1 - I_n \cos \varphi_n)$$

or

$$I_1 \cos \varphi_1 - I_n \cos \varphi_n = \frac{f_{01} - f_{0n}}{K_2} = -\frac{\Delta f}{K_2} \quad (7.28)$$

(normally,  $f_{0n} > f_{01}$  and  $\Delta f$  has a "minus" sign).

In relative units

$$\dot{I}_1 \cos \varphi_1 = \cos \varphi_n - \frac{\Delta \dot{f}}{K_2}, \quad (7.29)$$

where

$$\Delta \dot{f} = \frac{\Delta f}{I_n} \text{ and } \dot{I}_1 = \frac{I_1}{I_n}.$$

The active load (current) for all current-consuming devices equals

$$I_c \cos \varphi = I_1 \cos \varphi_1 + I_n (n-1) \cos \varphi_n,$$

or, in relative units,

$$\dot{P} = \dot{I}_c \cos \varphi = \dot{I}_1 \cos \varphi_1 + (n-1) \cos \varphi_n. \quad (7.30)$$

Making use of (7.29) and (7.30) we find

that

$$\dot{P} = \dot{I}_c \cos \varphi = n \cos \varphi_n - \frac{\Delta \dot{f}_1}{K_2}.$$

The total relative power for the system

is

$$\begin{aligned} \dot{S} &= \dot{P} + j\dot{Q} = \\ &= n \left[ \left( \cos \varphi_n - \frac{\Delta \dot{f}}{nK_2} \right) + j \sin \varphi \right]. \end{aligned} \quad (7.31)$$

provided we neglect the small variation in system voltage.

The absolute value of the total relative power will equal

$$|\dot{S}| = n \sqrt{\sin^2 \varphi + \left( \cos \varphi_n - \frac{\Delta \dot{f}}{nK_2} \right)^2}. \quad (7.32)$$

The system power utilization factor is

$$k_{ue} = \frac{|\dot{S}|}{n} = \sqrt{\sin^2 \varphi + \left( \cos \varphi_n - \frac{\Delta \dot{f}}{nK_2} \right)^2}. \quad (7.33)$$

Figure 7.9 shows the function

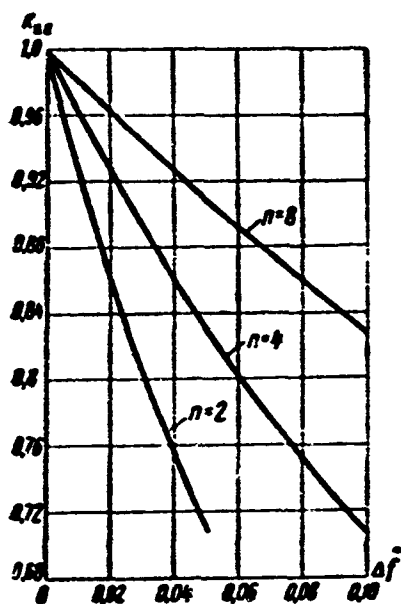


Fig. 7.9. Electrical-system power utilization factor as a function of frequency unbalance.

$$k_{sa} = \varphi(\Delta f) \text{ for } \cos \varphi = 0.75 \text{ or } K_s = 0.05,$$

from which it follows that the greater the number of generators operating in parallel, the less effect disturbance of the speed-regulator settings will have.

If we permit a decrease of 10% in the utilization ( $k_{ia} \approx 0.9$ ), we can permit a deviation from power-regulator settings of 1.5% when  $n = 2$  or 2.5% with  $n = 4$  and 5.5% at  $n = 8$ .

#### 7.4. CONNECTION FOR PARALLEL OPERATION

The process of connecting synchronous machines for parallel operation is called synchronization. The problem is to maintain synchronism after connection with minimum equalizing current and minimum excess-power surge at the instant of connection.

If the rules for connecting synchronous machines for parallel operation are violated, equalizing-current surges and excess-moment surges will appear.

Where frequencies are equal and phases coincide, but voltage differences exist, an equalizing current will appear, equal to

$$I_{np} = \frac{E_r - U_c}{(R_r + R_d) + j(\tau_r + x_d)}$$

or when  $R_g \ll x_g$  and  $R_s \ll x_s$

$$I_{np} = -j \frac{E_r - U_c}{x_{dr} + x_{dc}}, \quad (7.34)$$

i.e., the equalizing current is basically reactive in nature. The direction of the equalizing current is such that the machine field is reinforced when the voltage is too low and the machine field is weakened when the voltage is too high, so that the voltage remains the same across the line terminals.

When the voltages are equal but the frequencies or phases do not correspond, a pulsation in the voltage difference will occur and a real current component will appear that alternately places a real-

power load on the line and the connected machine.

The voltage pulsation (ripple) occurs within the double-voltage range and the instantaneous values can be represented by the equation

$$\begin{aligned}\Delta u = u_e - e_r &= \sqrt{2}E (\sin \omega_1 t - \sin \omega_2 t) = \\ &= 2\sqrt{2}E \sin \frac{\omega_1 - \omega_2}{2} \cos \frac{\omega_1 + \omega_2}{2},\end{aligned}\quad (7.35)$$

where  $\omega_1$  and  $\omega_2$  are the line and generator angular frequencies;  $U_g = E_g = E$  is the effective line voltage.

Two main types of machine synchronization are known: precise synchronization, where the machines are connected to the line when voltages and frequencies are equal and the excited generator running without load and the line are in phase; and self-synchronization, where an unexcited synchronous machine is connected to the line when the rotor reaches subsynchronous speed.

Precise synchronization and self-synchronization may be initiated manually, semiautomatically, or automatically. In aircraft electrical systems, it makes sense to use an automatic or semiautomatic system for precise synchronization or self-synchronization.

### Precise Synchronization

Two systems are used in practice for aircraft electrical systems:

a) the automatic system, in which the exciting generator is brought into synchronism with the aid of a synchronizer and then connected into the line;

b) the semiautomatic system, in which the exciting generator is brought into synchronism with the aid of a synchronizer and kept in this condition until it is connected into the line manually.

Figures 7.10 and 7.11 show one semiautomatic synchronization system used with aircraft generators.

Here differential selsyns are used to bring the generator automatically to within range of the synchronous speed, after which the

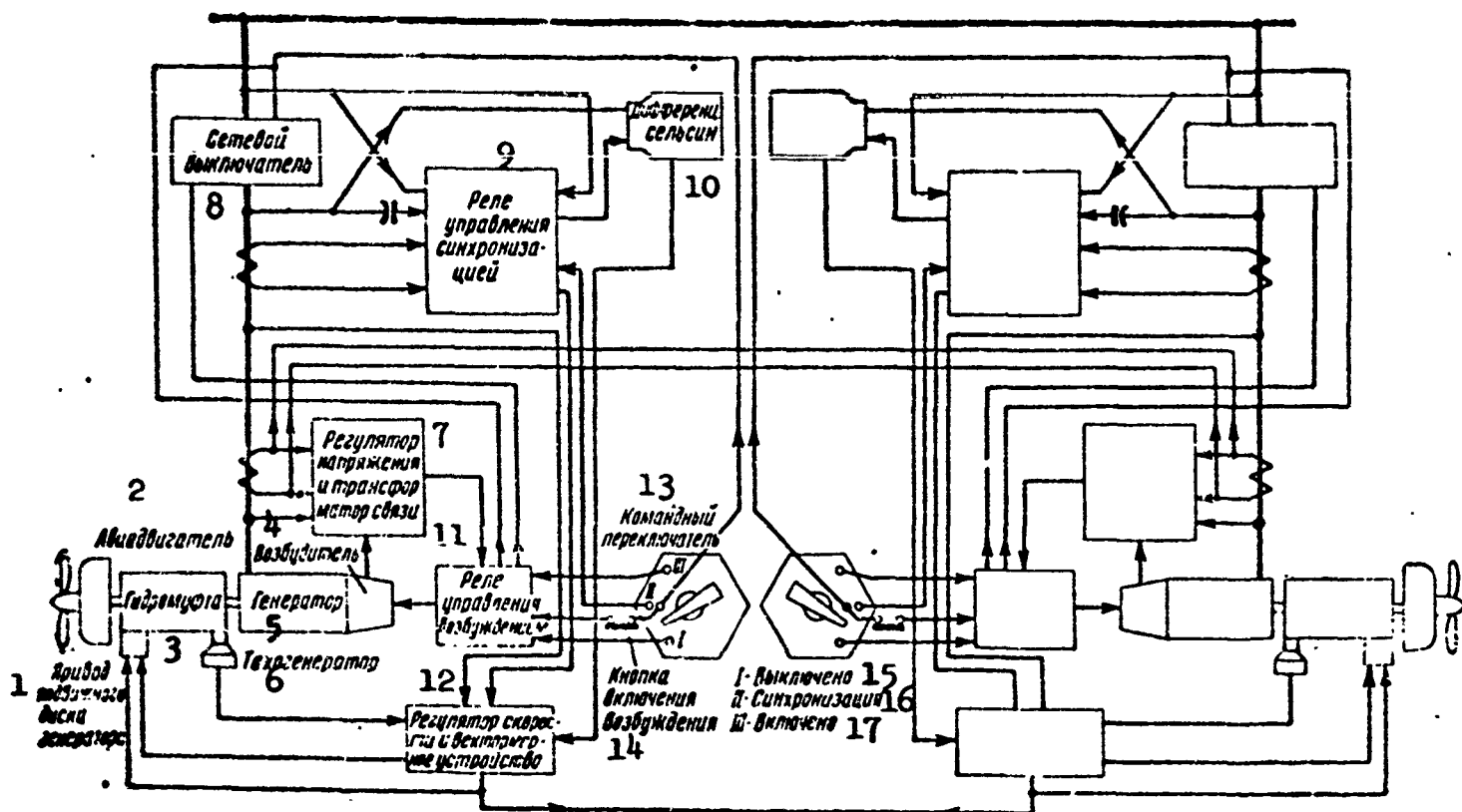


Fig. 7.10. Block diagram for semiautomatic synchronization of three-phase aircraft generators. 1) Drive mechanism for generator variable-inclination plate; 2) aircraft engine; 3) hydraulic clutch; 4) exciter; 5) generator; 6) tachometer generator; 7) voltage regulator and coupling transformer; 8) selenium rectifier; 9) synchronization control relay; 10) differential selsyn; 11) excitation control relay; 12) speed regulator and a vector-sensing device; 13) command switch; 14) excitation connect button; 15) I - disconnected; 16) II - synchronization; 17) III - connected.

real-load distribution is used to bring the generator into synchronism, and the machine is connected manually into the line.

Operating sequence for synchronizing device of Fig. 7.11. If it is necessary to connect generator  $G_1$  for parallel operation with generator  $G_2$ , which is carrying a specific load, the following operations must be carried out.

Initially, generator  $G_1$  is not excited, the command switch KP is set to position I-I, line contactor K is disconnected and pilot light SL is lit, the contacts of the synchronizing relay RS are open, and the vector-sensing circuit is connected as a real-load distributor (i.e., resistor  $R_1$  of the VMU is connected across the current trans-

former  $T_3$ ).

In the connection process, the command switch is set to position II-II ("ready") and the generator is excited by pushing button 15; winding RS is then excited with generator voltage, RS switches the vector-sensing device VMU to synchronizer operation, and applies line voltage to the stator of the differential selsyn DS. The selsyn rotor, which is always connected to the generator stator, derives its power from the generator excitation.

Thus, the generator voltage is applied across the input auto-transformer of the VMU, while line voltage is applied across control winding  $K_2$  and, consequently, the VMU reacts to the difference between the generator and line voltages (sensing both magnitude and phase). Line voltage at frequency  $f_1$  is applied to the DS stator, and generator voltage at frequency  $f_2$  to the rotor; consequently, the DS reacts to the difference in frequencies.

We recall that the RS excitation winding and the DS rotor are excited by the generator and, consequently, excitation will only occur when the generator is excited.

In the "ready" position, the synchronizing device operates as follows: the DS rotor, running at a speed corresponding to the difference between the line and generator frequencies  $(f_2 - f_1) = \Delta f$ , acts through a reducing gear to move the lever of the frequency-control rheostat ( $R_n$ ) at a speed proportional to the difference between the generator and line frequencies so as to reduce this difference, i.e., so as to bring the generator frequency to the line frequency. Roughly 2 seconds after KP has been set to the "ready" position, the frequency difference becomes so small (0.5%) that the vector-sensing device may be brought into synchronism; this device electrically controls the constant-speed hydraulic drive mechanism by changing the



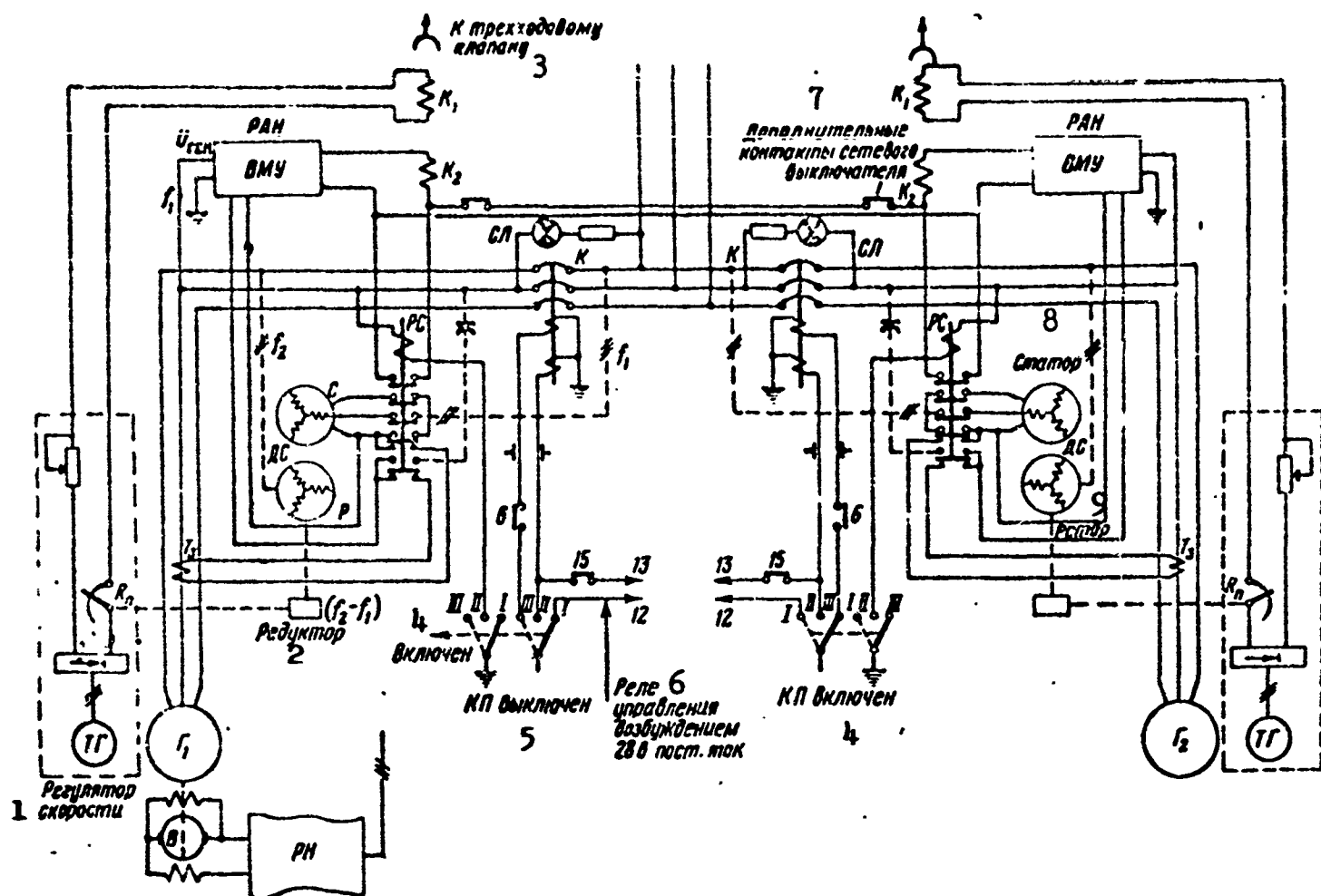


Fig. 7.11. Basic circuit used for semiautomatic synchronization of three-phase aircraft generators. RS) Synchronization relay; DS) differential selsyn; VMU) vector-sensing device; KP) command switch. 1) Speed regulator; 2) reducing gear; 3) to three-way valve; 4) connected; 5) disconnected; 6) excitation control relay, 28 v DC; 7) additional line-switch contacts; 8) stator; 9) rotor.

slope of the floating plate. The latter reduces the clutch output-shaft speed until the difference in the voltages at the main contacts of line contactor K, i.e., the difference between the generator and line voltages, is very small and the synchronization light goes out.

When synchronism is reached, KP shifts to the position III-III ("connected"); then the auxiliary contacts are used to close line contactor K, and the generator is connected to the line; the synchronization relay opens and the transformer is connected across the VMU input, i.e., the VMU takes over the normal functions of a real-load distributor.

An advantage of precise synchronization is the possibility of limiting the equalizing-current and transfer-power surges to the desired magnitude. A drawback of automatic precise synchronization is the complexity of the synchronization apparatus and the fact that manual synchronization requires highly skilled personnel. Precise synchronization, especially in the presence of system frequency and voltage fluctuations, requires a relatively long period of time, which tends to cause accidents under emergency conditions.

In addition, if faulty connections are made with the method of precise synchronization, the current and transfer-power surges may exceed those occurring under some synchronization. There are numerous examples of failure of large generators and transformers in high-power electrical systems owing to erroneous connections when the method of precise synchronization was used.

Improper connection of an excited synchronous machine ( $\theta = \pi$ ) may produce current surges reaching values of

$$I_{pp\max} = \frac{1.8 \cdot 2 \sqrt{2} E_d'}{x_d'' + x_d'' + x_{c.s.}} \quad (7.36)$$

Here  $x_d''$  and  $x_{d2}''$  are the subtransient direct-axis inductive reactances of the generator and the system;  $x_{s.p}$  is the inductive reactance of the connecting lines between generator and system;  $E_d''$  is the subtransient emf.

For machines whose power is comparable with the system power

$$x_d'' \approx x_{d2}''$$

and

$$I_{pp\max} = \frac{3.6 \sqrt{2} E_d'}{2x_d'' + x_{c.s.}} \approx \frac{1.8 \sqrt{2} E_d'}{x_d''} = I_{n.72}, \quad (7.37)$$

i.e., the equalizing current roughly equals the maximum asymmetric short-circuit current.

For machines whose power is considerably less than the line power, i.e., when a connection is made to a high-power system,  $x_{d2}'' \rightarrow 0$  and

$$I_{\text{eq}} \approx 2I_{\text{sc}}$$

i.e., the equalizing current is close in value to twice the maximum asymmetric short-circuit current.

When an excited machine is connected into the line, it may develop a generator power exceeding the rated value by a factor of 4-6, while when an unexcited machine is connected to the line, there will be no synchronous moment owing to the absence of rotor flux.

### Self-synchronization

Self-synchronization of synchronous machines, i.e., connection of an unexcited synchronous machine into the system at subsynchronous speed offers several important advantages, which also make this a desirable method for aircraft electrical systems.

The basic drawback of the self-synchronization system is the large equalizing-current surge that occurs when the unexcited generator is connected and the brief drop in system voltage.

The basic advantage in self-synchronization lies in its simplicity, provided no errors appear, in its reliability, the low weight of the control apparatus, the rapid response of the system, and the possibility of making a connection in the presence of severe voltage dips.

There are also two systems used in practice for aircraft electrical systems:

a) automatic self-synchronization, where the synchronizing device brings the unexcited generator to subsynchronous speed, connects it to the line, and applies excitation;

b) semiautomatic self-synchronization in which the synchronizing

device connects the generator into the line and applies excitation after the speed has been brought to the subsynchronous value manually.

A frequency-difference relay is used for semiautomatic and automatic self-synchronization; it is operated by the residual generator voltage. It has two windings; line voltage is applied to one and generator voltage to the other. The windings are connected in opposition, and a slippage of the order of 2% operates the relay, so that the generator is connected to the line.

The possibility of using self-synchronization is determined by the permissible equalizing-current surge, the possibility of pulling the machine into synchronism, and the magnitude of the system voltage dip.

Equalizing-current surge with self-synchronization. A periodic current component calculated for the generator direct-axis transient inductive reactance that does not exceed 3.5 times the rated machine current at the instant the unexcited generator is connected is a permissible value on power systems of the Soviet Union. For low-power synchronous machines and, in particular, for aircraft machines with short service lives, this quantity may safely be increased to a factor of 5 or even more.

We use  $x'_d$  in the calculations, rather than  $x''_d$ , since the subtransient current is so rapidly damped that, as measurements have shown, it has no mechanical effect on the armature winding.

The direct-axis transient inductive reactance of a machine also determines the permissible current surge.

In view of the fact that aircraft generators normally are connected to a line of comparable power, the current surge with self-synchronization cannot be more than quadruple the rated value, which is quite acceptable.

Transient currents (with self-synchronization). Let us connect an unexcited synchronous machine to the line when its rotor is turning with a slip  $s$  with respect to the synchronous speed of the field that determines the line frequency. In order to avoid insulation breakdown due to overvoltage, the field winding is short-circuited or connected across a low resistance at the instant of connection. Here free current components that follow an exponential damping law will appear in the stator and rotor windings.

The free current in a rotor with a short-circuited winding dies out with a time constant  $T'_d$ . If the rotor winding is connected across a resistance, the current will be damped considerably more rapidly. The magnetic field formed by the free rotor current turns together with the rotor and induces a periodically damped current in the stator winding at a frequency  $f(1 - s)$ .

The transient phenomena that occur when an unexcited synchronous machine is connected to the line are in many ways similar to the transient phenomena that accompany an abrupt short circuit (Fig. 7.12).

In the most unfavorable case, the following currents flow in the stator winding.

A forced periodic current with the line frequency  $f$  that depends for its magnitude on the slip  $s$  and that decreases as the slip is reduced. At the synchronous speed, where  $s = 0$ , the forced periodic current reaches its minimum value, which is determined by the synchronous reactance  $x_d$  and the corresponding sustained short-circuit current. Owing to the magnetic and electrical asymmetry of the rotor, the amplitude of the forced stator-current component will pulsate at twice the slip frequency  $2fs$ .

The periodically damped current, which has a frequency  $f(1 - s)$

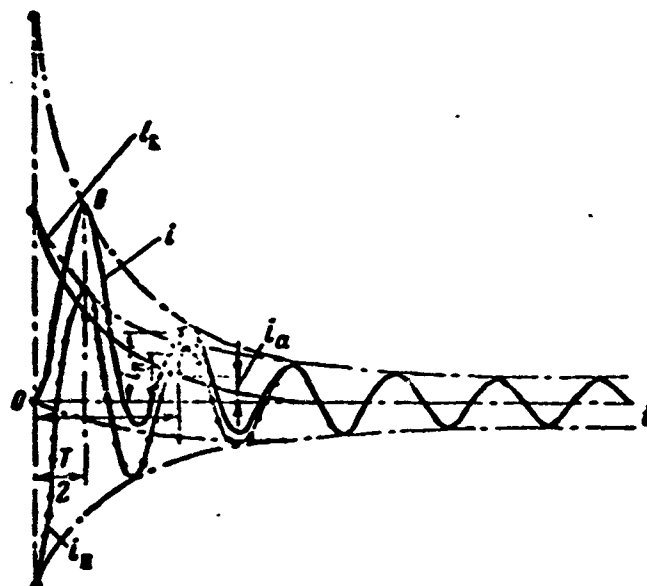


Fig. 7.12. Transient currents in armature winding.  $i_p$ ) Periodic component;  $i_{ap}$ ) aperiodic component;  $i = i_p + i_{ap}$ ) total transient current.

and is induced in the stator winding by the free rotor current, is damped by a time constant  $T'_d$ .

The sum of the forced and transient damped stator currents will give the resultant periodic stator current.

The free aperiodic current, which is similar to the aperiodic abrupt-short circuit current, dies away rapidly with a time constant  $T_a$  and forms a spatially fixed field that cuts the closed field winding, inducing an alternating current in it with frequency  $f(1 - s)$ .

The slip  $s$  is taken to be positive when the rotor lags behind the field set up by the line.

The initial free aperiodic current appearing in the field winding and, consequently, the transient periodic armature-current component will depend on the relative positions of the field-winding axis and the flux at the instant of connection. At an unfavorable instant, when the energy of the magnetic field is at a maximum, the aperiodic current will be at a maximum while at another moment separated from

the first by an angle  $\pi/2$ , there will be no such current.

In the first case, the initial armature current will take on its maximum value, while in the second case it will be at a minimum and will equal the sum of the aperiodic component and the forced periodic component. The maximum initial value of the aperiodic armature-current component is determined by the transient inductive reactance  $x'_d$ .

If the machine has short-circuited loops (damper windings), a subtransient current component will also appear that is damped rapidly with a time constant  $T''_d$ . In this case, the maximum period armature-current component is determined by the subtransient inductive reactance  $x''_d$ .

A full damper cage is used in single-phase aircraft machines; the magnitude of the free rotor current and the maximum initial armature current will therefore depend little on the instant at which the machine is connected into the line. In addition, the forced-current pulsation due to slip will be smoothed considerably.

#### Conditions for Pulling into Synchronism

When an excited generator is connected into the line, the following rotational moments act on its shaft:

a) the synchronous moment due to interaction of the excitation field and the quadrature-axis armature magnetizing-force component

$$M_e = \frac{E_d U}{x_d} \sin \theta = I_{x_d} U \sin \theta;$$

b) the reactive moment due to magnetic-system asymmetry

$$M_p = \frac{U^2}{2x_d} (k - 1) \sin 2\theta;$$

c) the asynchronous moment due to interaction of the excitation field and currents in short-circuited loops of the secondary circuit when the rotor is running asynchronously

$$M_{sc} = p \frac{\omega_c - \omega}{\omega_c}$$

or

$$M_{sc} = -\frac{p}{\omega_c} \frac{d\theta}{dt} = D \frac{d\theta}{dt};$$

the maximum value of the asynchronous moment equals  $0.5-0.6 M_{nom}$  in the absence of a damper cage and  $M_{as} = M_{nom}$  where there is a damper cage; it is important to note that the asynchronous moment reaches its maximum at low slip  $s = 0.2-0.3\%$ , while at a slip of  $2-3\%$ , it is reduced by roughly a factor of 10, and becomes too small to pull the machine into synchronism;

d) the torque developed by the prime mover  $M_{dv}$  (in converters, the torque developed by the direct-current motor);

e) the moment of resistance due to forces of mechanical friction,  $M_{tr}$ ;

f) the dynamic moment due to inertial forces appearing during variations in rotor speed,

$$M_j = \frac{J}{p} \frac{d^2\theta}{dt^2}.$$

In the equations given,  $x_d$  and  $x_q$  are the direct- and quadrature-axis synchronous reactances;  $J$  is the moment of inertia of the rotating parts;  $p$  is the number of pole pairs;

$$k = \frac{x_d}{x_q}.$$

The equilibrium-of-moments condition for asynchronous rotation may be represented in approximate form by an equation of the general type

$$M_{sp} = M_{as} - M_{rp} = \pm (M_e + M_p + M_{sc} + M_j)$$

or

$$M_{sp} = \pm \left[ \frac{E_d U}{x_d} \sin \theta + \frac{U^2}{2x_d} (k - 1) \sin 2\theta + D \frac{d\theta}{dt} + \frac{J}{p} \frac{d^2\theta}{dt^2} \right]. \quad (7.38)$$



For uniform rotation with constant slip,  $M_J = 0$  and

$$M_{sp} = \pm \left( k_c \sin \theta + k_R \sin 2\theta + D \frac{d\theta}{dt} \right), \quad (7.39)$$

where

$$k_c = \frac{E_d U}{x_d}, \quad k_R = \frac{U^2}{2x_d} (k - 1).$$

When an unexcited machine is connected into line, i.e., in the absence of excitation, the synchronous moment will equal zero and

$$M_{sp} = \pm \left( k_p \sin 2\theta + D \frac{d\theta}{dt} + \frac{J}{p} \frac{d^2\theta}{dt^2} \right). \quad (7.40)$$

If the power of the prime mover is used solely to overcome mechanical losses in rotation ( $M_{dv} - M_{tr} = 0$ ), there will be no acceleration of the rotor as a result of the prime-mover torque. In this case, where the rotor speed  $n_r$  is less than the synchronous speed of the field  $n$ , the sum of the moments  $M_r + M_{as}$  will have a positive sign, and the rotor will be accelerated up to the synchronous speed; where  $n_r > n$ , the moment  $M_r + M_{as}$  will have a negative sign, and the rotor speed will be reduced to the synchronous speed.

At subsynchronous speed, the rotor may be pulled into synchronism by either the reactive moment, where the machine is not excited, or by the synchronous moment, where excitation has been supplied to the machine.

At subsynchronous speed, the asynchronous motor is close to zero for all practical purposes.

Experiments have shown that the reactive moment  $M_r$  will always be adequate to pull the rotor into synchronism even for synchronous machines with nonsalient poles, where  $M_r$  is small.

When an unexcited machine is connected in by the method of self-synchronization, the reactive moment acting on the rotor after damping of the free current components in the stator and rotor will equal (ne-

glecting the stator-winding resistance)

$$\begin{aligned} \dot{M}_p = & \frac{U^2}{2x_d} \left\{ (k-i) \sin 2\theta - \left( \frac{x_d}{x_q} - i \right) \frac{sT_d'}{1+(sT_d')^2} \times \right. \\ & \times \left[ 1 + V \sqrt{1+(sT_d')^2} \sin \left( 2\theta - \arctg \frac{1}{sT_d'} \right) \right] - \\ & \left. - k \left( \frac{x_q}{x_d} - 1 \right) \left[ 1 - V \sqrt{1+(sT_d')^2} \sin \left( 2\theta - \arctg \frac{1}{sT_d'} \right) \right] \right\}, \quad (7.41) \end{aligned}$$

where  $T_d'$  is the time constant for a transient in the direct-axis circuit, equal on the average to  $T_d' \approx 0.01$  sec.

For aircraft generators,  $\dot{x}_d^*$ ,  $\dot{x}_q^*$ ,  $\dot{x}_d'^*$ , and  $\dot{x}_q'^*$  equal approximately

$$\begin{aligned} \dot{x}_d^* &= 1.0 \div 1.4; \quad \dot{x}_q^* = 0.55 \div 0.7; \\ \dot{x}_d'^* &= 0.15 \div 0.2; \quad \dot{x}_q'^* = \dot{x}_q^*; \quad k = \frac{x_d}{x_q} \approx 2.0. \end{aligned}$$

If excitation current is applied to the rotor winding at the same time the stator winding is connected to the line, then in addition to the reactive moment  $M_r'$ , a synchronous moment  $M_s'$  will appear in the generator; it will increase in time in accordance with the exponential function

$$M_s' = M_{s,cr} \left( 1 - e^{-\frac{t}{T_d'}} \right). \quad (7.42)$$

The instant the rotor reaches the synchronous speed, the moment  $M_s'$  is able to attain a magnitude that ensures reliable pulling into synchronism under any conditions.

If the machine is pulled into synchronism by the reactive moment before excitation is applied, two cases may occur:

a) incorrect self-synchronization, where the excitation polarity is such that the rotor must turn through 180 electrical degrees and will produce a transient-current surge when excitation is applied together with considerable fluctuation;

b) proper self-synchronization, where the excitation polarity is such that the rotor maintains its synchronous position and the appli-

cation of excitation current does not produce a noticeable transient-current surge.

In view of what we have said, it is desirable in self-synchronization to apply excitation before the machine is pulled into synchronism by the reactive moment. In this case, both the time occupied by the transient and the magnitude of surge currents will be reduced.

As studies of self-synchronization in aircraft generators have shown, the closer the machine is to the subsynchronous speed at the instant of connection, i.e., the less the slip, the shorter the transient. It may be assumed that with self-synchronization it is desirable to connect a synchronous machine into the line of a slip  $s < \pm 3\%$ ; successful and safe self-synchronization is also possible when  $s = \pm 10\%$ , however.

Excess torque on the machine shaft at the subsynchronous speed has a negative effect on self-synchronization. If at the instant of self-synchronization  $M_{vr} > 0$ , i.e., the prime mover develops excess torque, it may prove to be greater than the asynchronous moment developed by the machine and self-synchronization will be hampered.

In single-phase aircraft generators, a powerful damper cage is normally used, and this moment is considerable. This facilitates self-synchronization.

At the instant an unexcited generator is connected into the line, the line voltage will drop; the drop will be greater the higher the relative power of the machine being connected. Where the connected generator has a power equal to the line power, the voltage may drop by 10-40%.

The line voltage will rapidly be restored, since the current in the connected generator will drop rapidly; if, however, electric motors or other current-consuming devices having instantaneous under-

voltage protective devices are connected to the line, they may be turned off when the generator is connected in. This must be taken into account in selecting types of protective devices.

The literature indicates that with self-synchronization, system power should be at least 5 times the power of the machine being connected. This is a baseless assertion.

Experiments carried out by the author for aircraft machines have shown that self-synchronization of two synchronous machines of comparable or equal power is completely possible.

The resistance in the generator field-winding circuit plays a positive role in synchronous-machine self-synchronization; by increasing the resistance, the length of the transient can be reduced.

We may draw the following conclusions from what has been said.

1. Two machines of equal power may be paralleled by the method of self-synchronization.

2. It is desirable to connect an unexcited generator into the line at minimum slip, although reliable self-synchronization is also possible where  $s = \pm 10\%$ .

3. It is desirable to connect a generator when there is steady asynchronous rotation, and the prime-mover excess torque equals zero.

4. Excitation should be applied before the machine is pulled into synchronism; this should be done at minimum possible slip ( $s \leq 0.5\%$ ), however.

5. In order to speed up the self-synchronization process, reduce the duration of transience, and reduce the danger of field-winding breakdown due to overvoltage, it is desirable to connect the field winding across an absorbing resistor at the instant the generator is connected into the line.

## 7.5. PARALLEL OPERATION OF CONVERTERS

In combination electrical systems, the alternating-current supply is frequently centralized. In this case, several converters of relatively high power are installed; they are operated in parallel. Parallel operation of aircraft converters is complicated by the fact that they should maintain an assigned voltage level and alternating-current line frequency under direct-current line-voltage fluctuations of  $\pm 10\%$  of the nominal value, under loads varying from zero to rated value, and over a broad range of ambient temperature variations.

The general requirements for systems of paralleled synchronous generators also apply with full force to converters using synchronous generators.

Figure 7.13 shows the basic circuit for parallel operation of two three-phase synchronous converters. The diagram shows the connection of the power regulators RM and real-load distributor RAN, voltage regulator RN, and reactive-load distributor RRN.

For an independently operating converter, the frequency regulator and voltage regulator, which may take various forms, keep the frequency and voltage of the alternating current line nearly constant under variations in load, direct-current line voltage, and cooling-medium temperature. Departure of AC frequency and voltage from rated values can be reduced to  $\pm 0.05$  for frequency, and  $\pm 1\%$  or less for voltage.

The power and voltage regulators are statically stable, i.e., the speed (frequency) and voltage for the alternating-current line decrease, respectively, with increases in the generator real and reactive loads.

Let us consider the principle on which the parallel-operation circuit action is based, without investigating the voltage regulator

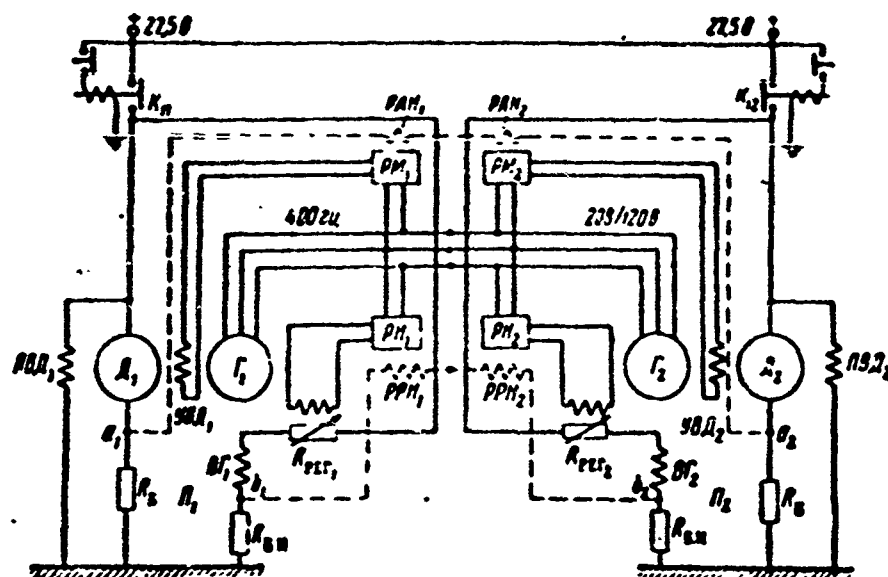


Fig. 7.13. Basic circuit for parallel operation of two aircraft converters. RM and RN) Power and voltage regulators; RAN and RRN) real- and reactive-load distributor; VG) generator excitation; PVD and UVD) constant and controlled motor excitation;  $R_{reg}$ ) regulator resistance;  $R_b$  and  $R_{b.n}$ ) motor and generator ballast resistors.

or frequency (power) regulator.

Real-load distribution. In parallel operation of synchronous converters, in addition to the power regulator there is a real-load distributor RAN, which consists of a special winding (control winding) located on the frequency regulator saturable reactor, and connected to points  $a_1 a_2$  (Figs. 7.13 and 7.14).

This last element reacts to the difference in the currents of the direct-current drive motors of the paralleled converters.

If the real load is distributed uniformly between the drive motors of the paralleled converters, there will be no current in the RAN circuit (between points  $a_1$  and  $a_2$ ), but if the real load on converter  $P_1$  rises in comparison with the load on  $P_2$ , the voltage at point  $a_1$  equal to  $U_{a1} = I_1 R_b$ , will exceed the voltage at point  $a_2$ , which equals  $U_{a2} = I_2 R_b$ .

The difference in currents

$$U_{a1} - U_{a2} = (I_1 - I_2) R_b = I_1 - I_2$$

in the RAN circuit (between points  $a_1$  and  $a_2$ ) will cause an equalizing current  $I_{ur}$  to flow; it will equal

$$I_{ur} = \frac{U_{a1} - U_{a2}}{2R_y} = (I_1 - I_2) \frac{R_6}{2R_y}. \quad (7.43)$$

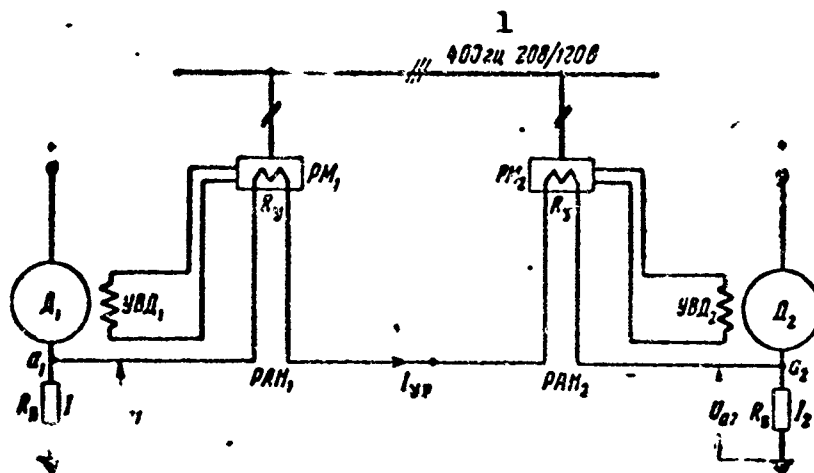


Fig. 7.14. Real-load distribution circuit.  
1) cps.

The RAN equalizing current acts on the power regulators so as to increase excitation current in the overloaded motor, and to decrease the excitation current in the underloaded motor so that the speed of the overloaded motor will drop somewhat and that of the underloaded motor will rise.

The speed of the overloaded motor will decrease and the speed of the underloaded motor will rise until the operating angles of the synchronous generators become nearly equal and, consequently, the real loads are distributed uniformly between them. It should be noted that this method for distributing real load between parallel generators is an indirect method. In essence, it is the direct-current drive motors that are being uniformly loaded.

If the function  $\eta = f(P_g)$  has identical values for all paralleled converters, the uniform distribution of real load will coincide with uniform loading of the drive motors.

Reactive-load distribution. For uniform distribution of reactive

load between paralleled generators, a reactive-load distributor RRN is added to the voltage regulator. The distributor consists of a spe-

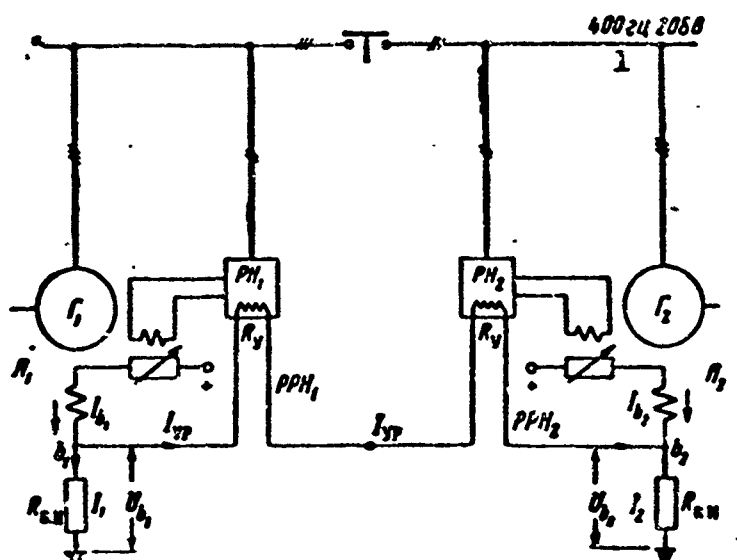


Fig. 7.15. Reactive-load distribution circuit. 1) cps.

cial (control) winding located on the saturable reactor of the voltage regulator. The series-connected control windings are connected to points  $b_1$  and  $b_2$  (Fig. 7.15).

Real-load distributors react to the difference in excitation currents of the paralleled generators. With uniform reactive-load distribution, the generator excitation currents are identical, the voltage drops across all generator ballast resistors are identical, and there is no current in the RRN circuit. If the real loads are distributed identically, while the reactive load on the first generator is greater than that on the second generator, the voltage drop across the ballast resistor of the first generator will be greater than for the second generator, i.e.,  $U_{b1} > U_{b2}$ . As a result, an equalizing current will flow and will increase the excitation of the second generator and reduce the excitation of the first generator.

#### Connecting Converters for Parallel Operation

Synchronous converters are connected for parallel operation as





The synchronizing transformer is made with a separate magnetic circuit so that the primaries will not be linked magnetically.

The synchronization-transformer primary consists of two identical opposing windings. Line voltage (or voltage from  $P_2$ ) is applied to one winding, and voltage from converter  $P_1$  to the other. Thus, the flux in the transformer core is determined by the difference in the magnetizing forces of the opposed windings, i.e.,

$$\begin{aligned}\Phi &= \frac{F_1 - F_2}{R_m} = \Phi_1 - \Phi_2 = \frac{w_1}{R_m} (i_1 - i_2) = \\ &= \gamma \left( \frac{U_{1m} \sin \omega_1 t}{\frac{r + j\omega_1 L}{r + j\omega_2 L}} - U_{2m} \sin \omega_2 t \right).\end{aligned}\quad (7.44)$$

If we assume that  $r \ll \omega_2 L$  and  $r \ll \omega_1 L$  (the latter is the case at subsynchronous speed), then

$$\Phi = \gamma \left( \frac{\omega_2}{\omega_1} U_{1m} \sin \omega_1 t - U_{2m} \sin \omega_2 t \right), \quad (7.45)$$

where

$$\gamma = \frac{1.25 \sqrt{2} w_1}{Z_2 R_m}, \quad \Phi_1 = \gamma \frac{\omega_2}{\omega_1} U_{1m} \sin \omega_1 t, \quad \Phi_2 = \gamma U_{2m} \sin \omega_2 t,$$

$R_m$  is the reluctance of the ST core, which is assumed to be constant (the core is lightly saturated);  $w_1$  is the number of turns in each transformer primary;  $Z_2 = r + j\omega L$  is the impedance of the primary connected to the line.

Two emf's are induced in the transformer secondary; they differ in magnitude and frequency:

$$e_1 = 4.44 \cdot 10^{-8} \omega_2 f_1 \Phi_1 = 4.44 \cdot 10^{-8} \omega_2 f_1 \gamma \frac{\omega_2}{\omega_1} U_{1m} \sin \omega_1 t,$$

i.e.,

$$\left. \begin{aligned}e_1 &= \gamma_1 U_{1m} f_2 \sin \omega_1 t \\ e_2 &= \gamma_1 U_{2m} f_2 \sin \omega_2 t.\end{aligned} \right\} \quad (7.46)$$

and similarly

The beat voltage equal to the difference of the emf's is applied to the rectifier:

$$e = e_1 - e_2 = \gamma_1 f_2 (\dot{U}_{1m} \sin \omega_1 t - \dot{U}_{2m} \sin \omega_2 t), \quad (7.47)$$

this voltage will equal zero only where the phases, frequencies, and line voltages are the same for converter  $P_2$  and converter  $P_1$ .

When converter  $P_1$  is connected to the line of converter  $P_2$ , the synchronization system works in the following way.

In the initial position of the "start" switch, contactors  $K_{11}$  and  $K_{12}$  are open, while the contacts of relay RS are closed. The "start" switch is used to actuate contactor  $K_{11}$  of the drive motor, which has two additional contacts that:

- a) connect the drive motor to the direct-current line — the motor starts to run;
- b) apply full voltage to the generator field winding — the generator is excited;
- c) close the excitation-winding circuit of the synchronization relay; the contacts of this relay open until DC voltage is applied to the OVK.

In this position, the converter, as in independent operation, reaches nearly the synchronous speed with the aid of the frequency regulator and reaches rated voltage with the aid of the voltage regulator. Depending on the converter power, the process of attaining rated voltage and a frequency near the rated value requires 1-2 sec.

The real- and reactive-load distributors are disconnected in this case. The direct-current circuit of the synchronization rectifier VS is completed by contacts of  $K_{11}$  and current flows through it to keep the contacts of the synchronization relay RS open. The current in the VS circuit will flow until the voltage of converter  $P_1$  becomes synchronized with the voltage of converter  $P_2$ .

When a working degree of synchronism is reached, the current in the relay excitation-winding circuit goes to zero, and the relay con-

tacts close the circuit of the excitation winding of generator contactor  $K_{21}$ , which connects the generator into the line and cuts in the real- and reactive-power distributors. Thus, the process of starting and synchronizing is completely automatic, with the sole manual of operation being the pushing of the "start" button.

The automatic synchronization system has the following drawbacks:

- the excitation-winding circuit OVR of the relay may be open-circuited or the OVK and OVR circuits may be connected simultaneously, which when  $K_{11}$  is actuated will cause the excited converter  $P_1$  to be connected by contactor  $K_{12}$  to the line without synchronization when the speed is quite far from the synchronous speed (as a result there will be large current and moment fluctuations);

- circuit complication and increased control-apparatus weight;

- more time required for synchronization in the presence of frequency and line-voltage fluctuations.

When it is operating properly, the advantages of the system lie in the reduced equalizing current, interchange power, and line-voltage fluctuations.

Figure 7.17 shows the basic circuit for parallel operation of two three-phase aircraft converters with automatic self-synchronization. In contrast to the circuit of Fig. 7.16, there is no synchronization transformer here, and converter  $P_1$  is connected into the line with the aid of the time-delay relay RVV.

The self-synchronization circuit operates as follows.

With the "start" button in the initial position, the contacts of contactors  $K_{11}$  and relay RVV are open. The "start" button is used to actuate contactor  $K_{11}$  and start the motor. At the same time, voltage is applied to the excitation winding of relay RVV<sub>1</sub> and the excitation winding of contactor  $K_{21}$ , which connects the unexcited generator into

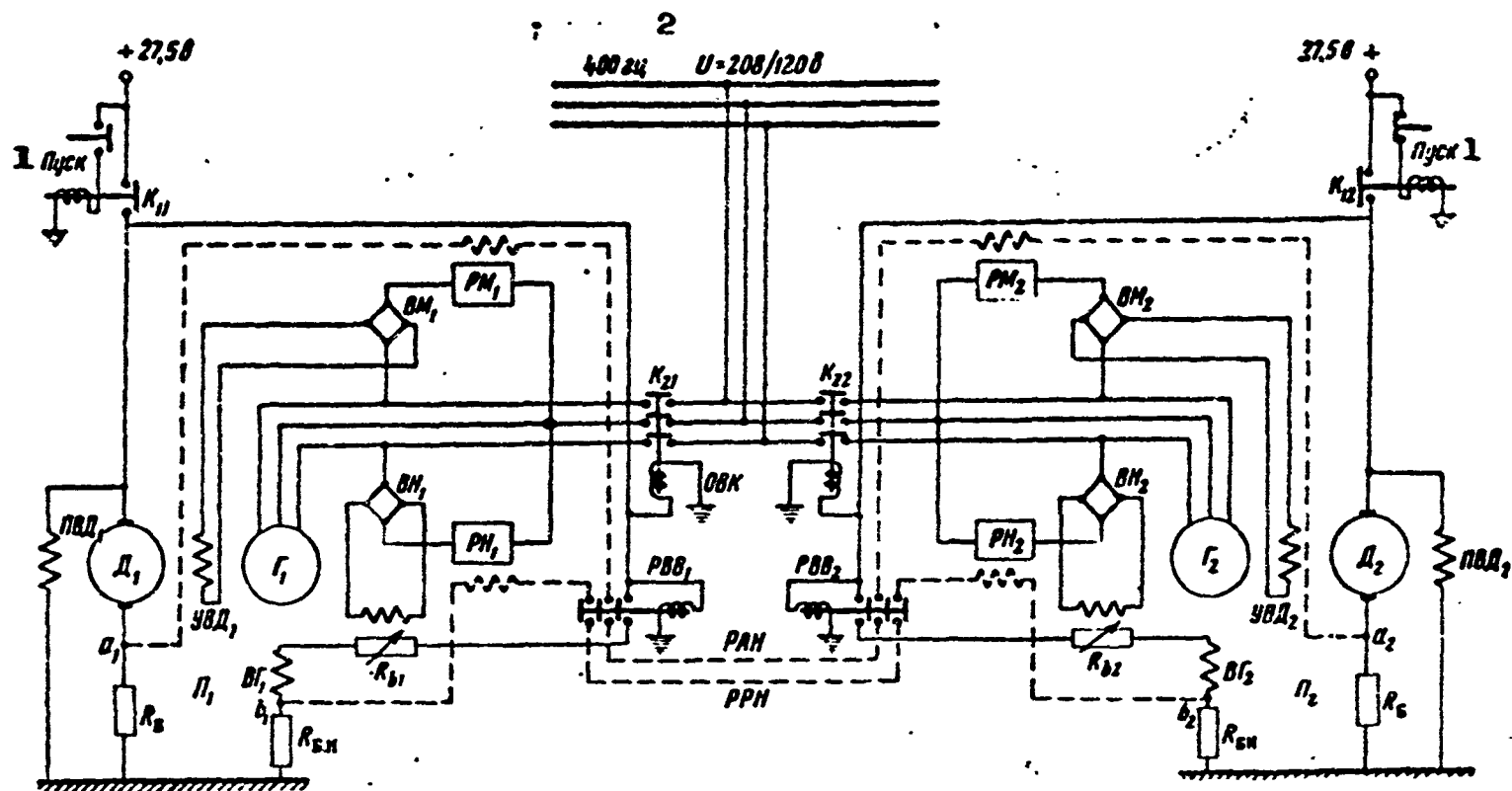


Fig. 7.17. Basic circuit for parallel operation of converters with self-synchronization. RVV) Time-delay relay; 1) start; 2) cps.

the line. In this position, the speed regulator is receiving the line voltage, and it attempts to bring the converter up to synchronous speed. The voltage regulator is also under line voltage, but it has no effect on the voltage of the  $P_1$  generator, since its excitation circuit is open (RVV has not operated).

After a certain time interval, relay  $RVV_1$  operates, its contacts supply excitation to the  $P_1$  generator and cut in the real- and reactive-load distributors.

The  $RVV_1$  time delay determines the time at which excitation is supplied to the generator; the delay should be chosen on the basis of the consideration discussed above.

Figure 7.18 gives as an example oscillograms showing connection of a three-phase converter for parallel operation with the two synchronization methods.

The results of the oscillographic study of the various ways of connecting three-phase aircraft converters of identical power for parallel operation are shown in Table 7.1.

The data given show that the best results are obtained with automatic precise synchronization; this method requires relatively complicated equipment, however. The self-synchronization method may be recommended for aircraft generators; in this case, it is desirable to cut in the excitation at minimum slip.

The division of loads between two converters after they have been connected for parallel operation is shown in Table 7.2; here one-half of the load on converter  $P_2$  in independent operation is taken as 100%.

The table shows clearly that the power regulator provides uniform load division between the motors and as a consequence, less accurate

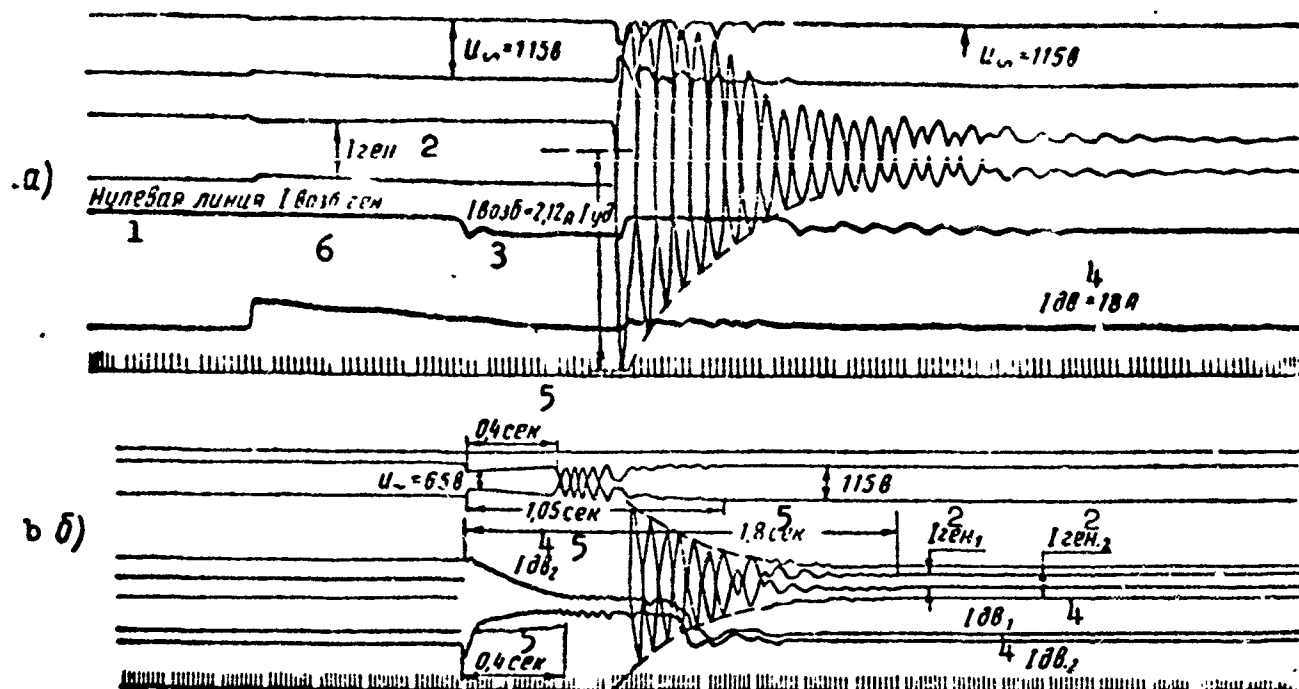


Fig. 7.18. Oscillograms showing three-phase aircraft converter connected for parallel operation. a) Excited generator connected at  $f = 390$  cps; b) self-synchronization system used for connection. 1) Zero line; 2) generator; 3) excitation; 4) motor; 5) sec; 6) excited generator.

TABLE 7.1

Various Methods of Synchronization

1 Способ включения	2 Скольжение при вклю- чении %		5 Максимальный ток при включении а		6 Снижение напряже- ния в	7 Время успокое- ния сек.
	3 гене- рато- ра	4 воз- буж- дения	3 генератора	4 возбуждения		
8 Включение возбужденного генератора	2,5	—	$(4 \div 9) I_{ном}$	—	$(0,26 \div 0,22) U_{ном}$	$1,3 \div 1,6$
9 Включение невозбужден- ного генерато- ра (самосинхро- низация)	5	3,5	$(2,5 \div 3) I_{ном}$	$(5 \div 6) I_{в.ном}$	$0,57 U_{ном}$	1,8
	—	1,0	—	$(4 \div 4,5) I_{в.ном}$	$0,62 U_{ном}$	1,4
10 Точная син- хронизация	0,3	—	$1,6 I_{ном}$	—	$U_{ном}$	0,74
	0,75	—	$2,2 I_{ном}$	—	—	—

1) Method of connection; 2) slip at connection, %; 3) generator; 4) excitation; 5) maximum current at connection, amp; 6) voltage dip, v; 7) settling time, sec; 8) connection of excited generator; 9) connection of unexcited generator (self-synchronization); 10) precise synchronization.

load division between the generators. A motor load variation range of 3% corresponds to a generator load variation range of 12% ( $\pm 6\%$ ).

TABLE 7.2

Distribution of Converter Load

		1 Бортовая		2 Сеть переменного тока				
		$U$ В	$I$ %	$U$ В	$f$ Гц	$I$ %	$\cos \varphi$	$P$ %
3 Автономная работа преобразователя $\Pi_2$		26,9	100	209	398	100	0,69	100
4 Параллельная работа преобразователей	$\Pi_2$	26,8	125	209	398	109,5	0,69	106
	$\Pi_1$	26,8	122	209	398	90,5	0,72	94

1) Aircraft electrical system; 2) alternating-current line; 3) independent operation of converter  $P_2$ ; 4) parallel operation of converters.

#### 7.6. PARALLEL OPERATION OF VARIABLE-FREQUENCY GENERATORS

Alternating-current aircraft generators can also be operated in parallel when they are driven directly by the aircraft engine with no speed conversion.

Figure 7.19 shows a circuit for parallel operation of aircraft variable-frequency generators suggested and constructed by A.F. Fedoseyev.

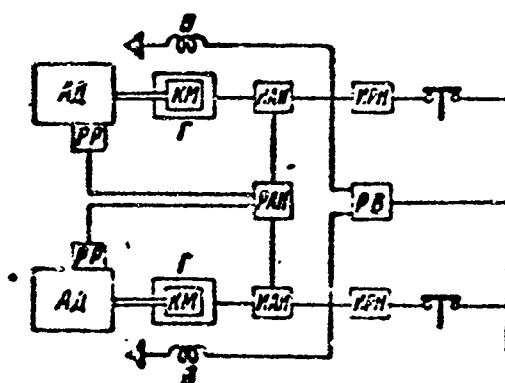


Fig. 7.19. Block diagram for parallel operation of variable-frequency generators. AD) Aircraft engine; KM) combination coupling built into generator; G) generator; V) generator field winding; IAN and IRN) real- and reactive-load measuring devices; RAN) real-load regulator; RV)



excitation regulator; RR) aircraft-engine control.

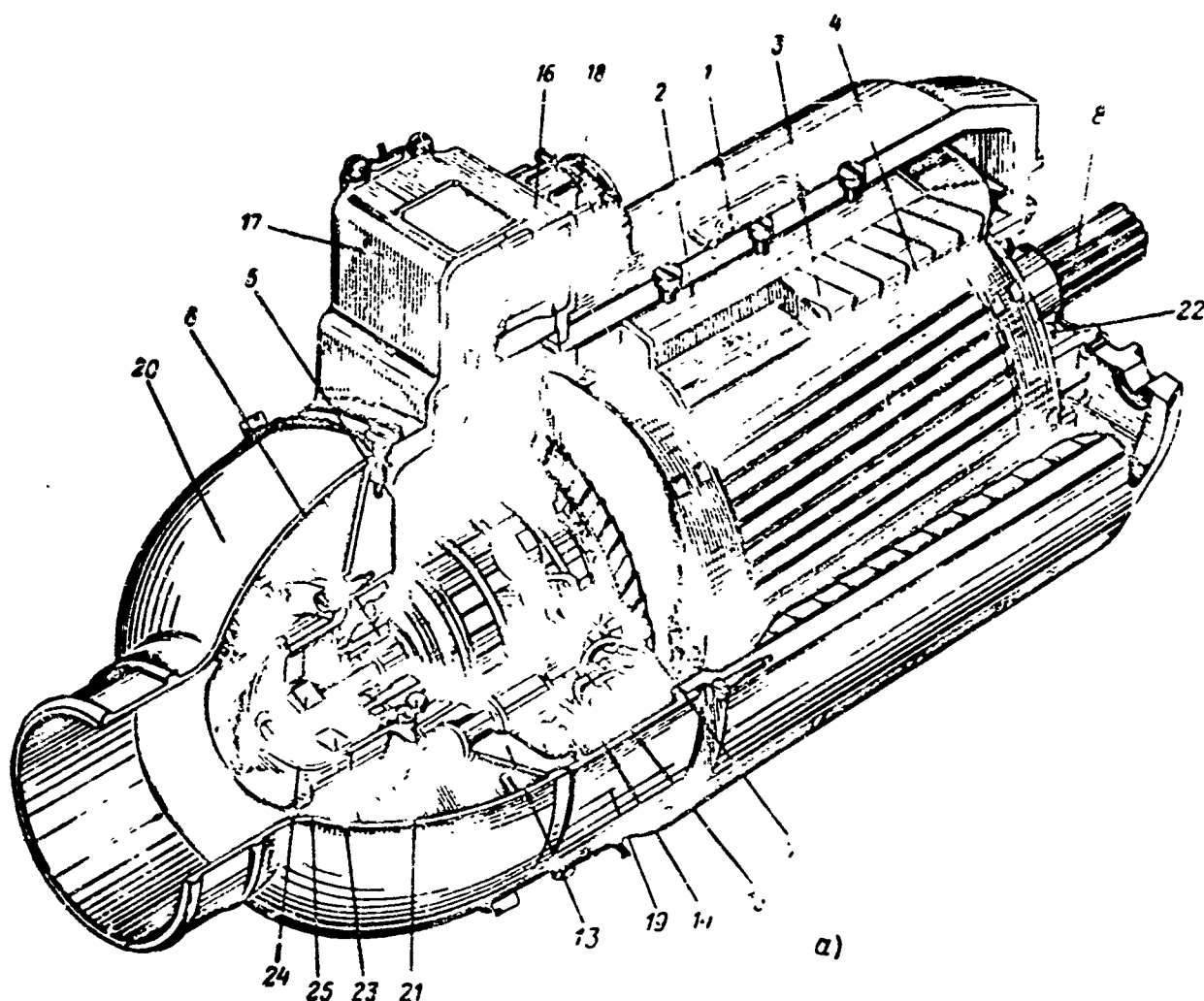


Fig. 7.20a. Construction of three-phase aircraft generator with external poles and built-in combination coupling. a) Generator. 1) Frame; 2) pole; 3) field coil; 4) armature; 5) slip rings; 6) hollow shaft; 7) hub; 8) drive shaft; 13) guard; 14) brushholder; 15) brush; 16) panel; 17) terminal-strip cover; 18) nipple nut; 19) blind flanged section; 20) cap; 21 and 22) ball bearings; 23) tachometer-generator stator; 24) tachometer-generator rotor; 25) tachometer-generator housing.

The generators are operated in parallel with the aid of the combination coupling KM, built into the hollow generator shaft (Fig.

7.20). It performs the following operations:

a) provides a rigid coupling between the generator and drive-motor shafts in the basic synchronous mode of the prime mover, i.e., on the synchronous-motor speed ( $n_{dv} = n_s$ ) and the generator power are below the maximum values ( $P_n < P_{g \max}$ );

b) operates as an asynchronous coupling with slip  $s$  when the mo-

tor speed is below the synchronous value and the generator develops a maximum power determined by the friction clutch (in this mode, the friction clutch, as usual, absorbs an amount of power proportional to the slip, thus reducing generator efficiency);

c) runs free, i.e., disconnects the generator shaft from the motor shaft when  $n_{dv} < n_s$ ; in this mode, the generator operates as a synchronous condenser, generating no real power but supplying magnetizing current (reactive power) to the line.

The combination coupling consists of three elements: a free-wheeling coupling (wedge, roller, or spring), a friction clutch, and a mechanical ball-type torque regulator.

As we know, a free-release coupling (free-running coupling) permits the generator armature to rotate in one direction only: when  $n_{dv} < n_s$ , the generator is disconnected. When the generator power reaches the specific maximum value  $P_{g \max}$ , the friction clutch begins to slip, preventing a further increase in generator power; the difference in the powers, proportional to the slip  $s$ , is absorbed by the friction clutch.

When  $n_{dv} > n_s$ , the friction clutch slips continuously, and losses are developed in it.

The job of the mechanical power regulator is to activate the friction clutch when the generator reaches the maximum power.

Clearly,  $P_{g \max}$  is not determined by the generator parameters, but by the friction-clutch adjustment.

The system operates so that the automatic generator real-power regulator affects the speed of the prime movers so that their average speed remains unchanged and is determined by flight conditions. At the same time, the speeds of the individual motors (their mutual synchronization) are equalized.

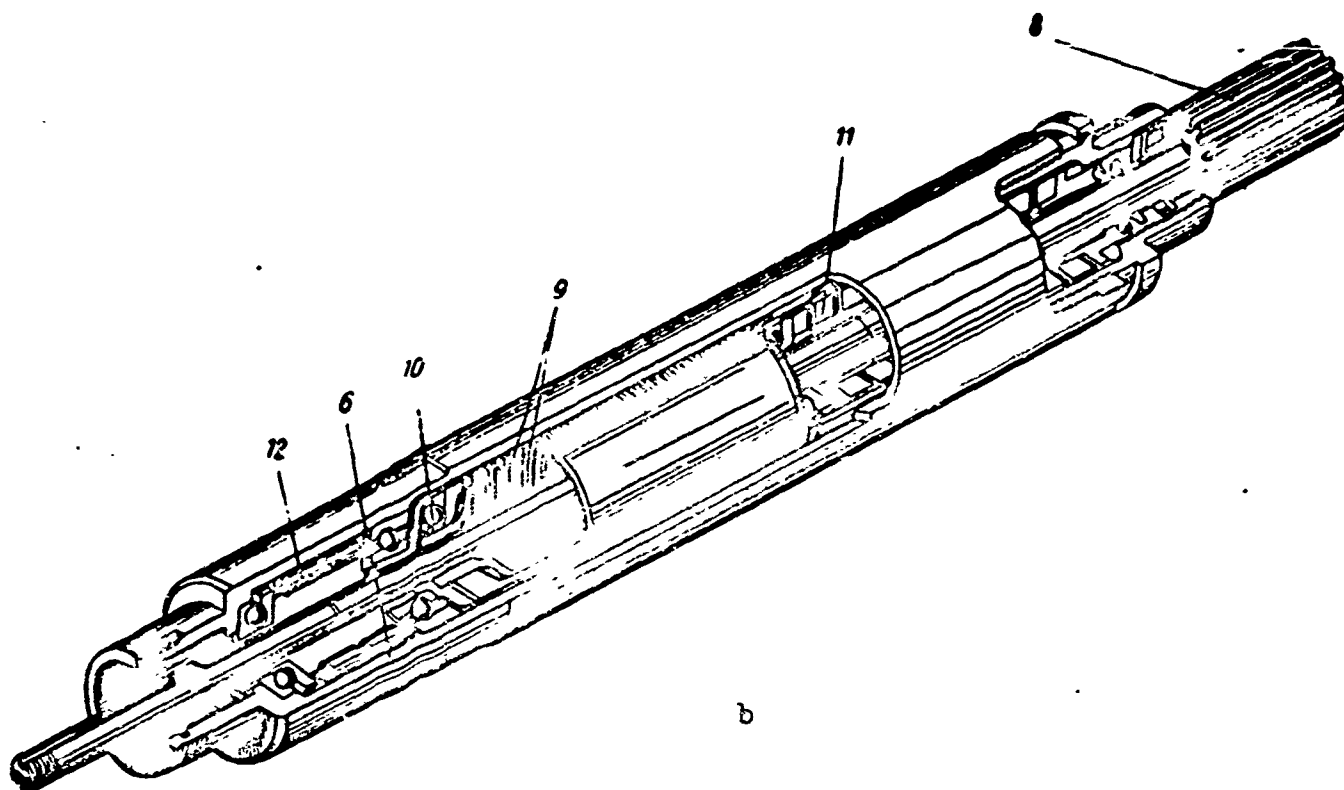


Fig. 7.20b. Construction of three-phase aircraft generator with external poles and built-in combination coupling. b) Combination coupling. 9) Friction disks; 10) ball-type regulator; 11) spring; 12) free-wheeling clutch proper.

Owing to the difference in the speeds of the individual engines, cases may arise in the process of regulation in which the individual generators operate in the asynchronous-coupling and free-running modes; here, however, synchronism will be maintained and the system will not separate. In the asynchronous mode, the coupling operates intermittently and at low slip so that the energy losses are small and system efficiency high.

Proper distribution of the real load is accomplished with the aid of the active-load regulators RAN, which act on the aircraft-engine operating control RR so as to establish identical speeds. The reactive load is distributed by the excitation regulator RV. Where the RR works with a high degree of accuracy, the engines are maintained at the same speed and there is no need for a power regulator.

## 7.7. PARALLEL OPERATION OF DIRECT-CURRENT GENERATORS

In studying parallel operation, the following problems are considered:

- connection and disconnection conditions for the machines;
- methods of shifting load from one generator to another;
- division of loads between paralleled generators in the presence of external-circuit load variations;
- point of connection of voltage regulator;
- system stability under parallel operation.

The fundamentals of the theory of parallel direct-current generator operation have been covered in the general course of electrical machines. Here we shall consider some special features of aircraft-generator parallel operation.

Aircraft direct-current electrical systems normally consist of two-eight generators of the same type and power. They must operate stably with full utilization of the installed generator capacity under sharp variations in prime-mover speed and at various speeds (3600-9000 rpm).

As we know, with minimum system losses, generator power will be used completely if the load is divided among the generators in proportion to their rated powers.

Paralleled aircraft generators of identical power may be considered to be operating satisfactorily when the load is divided uniformly to within  $\pm 10\%$  under all operating conditions, there is no vibration of the undercurrent-relay contact, and the line voltage fluctuates within a  $\pm 2\%$  range.

As operating experience has shown, the problem of satisfactory parallel operation of aircraft generators still requires work.

The quality of parallel generator operation is determined by the

characteristics of the generators, voltage regulators, and the line. For proportional distribution of the load and stable parallel operation, the generator external characteristics should be similar and descending.

In practice, the external characteristics of generators of identical power and type will differ from each other owing to inevitable manufacturing variations. The most important are: air-gap variation over a  $\pm 10\%$  range, variation in magnetic properties of magnetic-circuit iron over a  $\pm 5\%$  range, the  $\pm 5\%$  tolerance for armature-circuit winding resistances, fluctuation of the brush voltage drop to 0.5 v, departure of brush position from the normal neutral plane.

Two cases of parallel operation can be distinguished:

a) parallel operation of a generator into a line having many times the power of the machine under study, where it may be assumed that  $U = \text{const}$  and  $R_g \approx 0$ ;

b) parallel operation of generators of comparable power, where the line voltage depends on the emf of the machine under study.

In either case, the machines may operate in accordance with their natural characteristic or automatic voltage regulation may be used. For aircraft purposes, parallel operation is accompanied by automatic voltage regulation. In order to clarify the physical nature of the phenomenon, however, we shall first consider parallel operation of  $n$  generators without automatic voltage regulation, for shunt-excited generators.

For parallel operation of a generator into a high-power line, the current in the  $k$ th generator will equal

$$I_k = \frac{E_k - U}{R_k};$$

the load (line) current will be

$$I_k = \frac{U}{R_k},$$

where  $E_k$  is the emf of the  $k$ th generator;  $R_k$  is the total resistance for the  $k$ th generator (between busses);  $I_s$  is the line current, which considerably exceeds  $I_k$ ;  $R_s$  is the total load (line) resistance; then

$$R_s \ll R_k,$$

and the line voltage  $U$  is nearly independent of the generator current  $I_k$ .

#### Parallel Operation of Generators of Identical Power

Figure 7.21 shows in simplified form the presently accepted system used aboard aircraft to connect generators for parallel operation (with automatic voltage regulation).

If we do not consider the effect of the voltage regulators, the circuit of Fig. 7.21 may be simplified further to the form shown in Fig. 7.22.

In analyzing  $n$  paralleled generators, the method of node voltages may be used to replace them with a single generator having an equivalent resistance between terminals and busses of

$$R_e = \left( \sum_1^n \frac{1}{R_k} \right)^{-1} \quad (7.48)$$

and an equivalent voltage at the terminals of

$$U_s = R_e \sum_1^n \frac{U_k}{R_k}. \quad (7.49)$$

where  $U_k$  is the voltage across the terminals of the  $k$ th generator;  $R_k = R''_k + R'_k$  is the resistance of the  $k$ th generator from the generator terminals to the busses;  $R''_k$  is the resistance of the  $k$ th-generator circuit from the positive generator terminal to the positive bus ("plus" resistance);  $R'_k$  is the same quantity measured from the negative generator terminal to the negative bus ("minus" or ballast

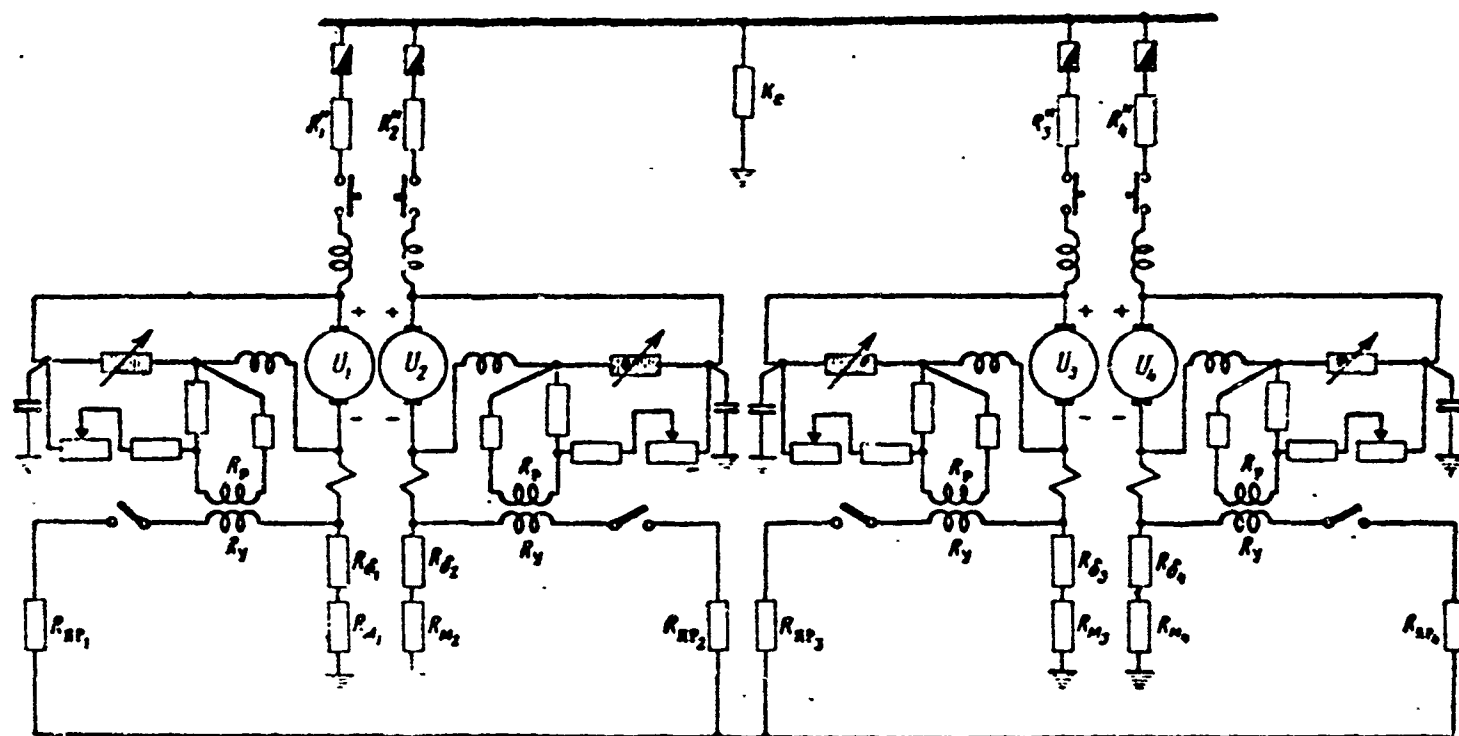


Fig. 7.21. Diagram for parallel operation of four direct-current aircraft generators.

resistance).

Using the node-voltage method and the notation of Fig. 7.22, we can write the basic relationships for parallel operation.

The voltage at the busses will be

$$U = U_e \frac{R_c}{R_c + R_0}. \quad (7.50)$$

The total system current (line current) is

$$I_c = \sum_1^n I_k = \frac{U_e}{R_c} = \frac{U_e}{R_c + R_0}. \quad (7.51)$$

If we take the least favorable condition for parallel operation, where  $U_k > U_e$ , the current in the  $k$ th generator will equal

$$I_k = \frac{U_k - U}{R_k} = \frac{U_k(R_c + R_0) - U_e R_c}{R_k(R_c + R_0)}. \quad (7.52)$$

The current  $I_k$  can be considered to consist of the average current  $I_{gr} = I_s/n$  and the unbalanced current  $I_{qk}$ , which is absorbed by the remaining  $(n - 1)$  generators of the system without entering the line, i.e.,

$$I_k = \frac{I_c}{n} + I_{qk}.$$

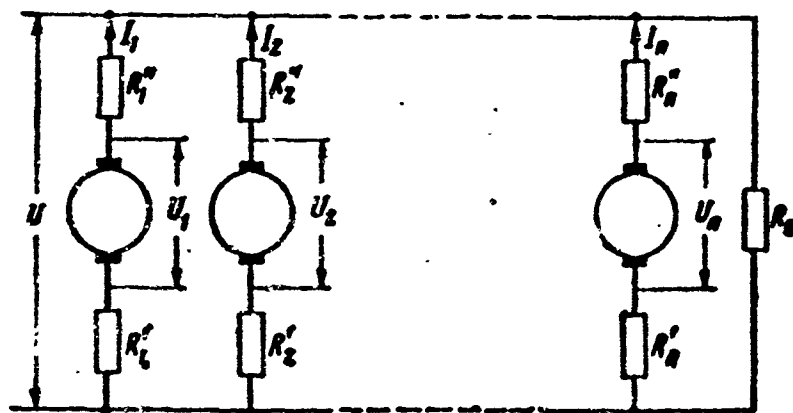


Fig. 7.22. Basic circuit for parallel operation of  $n$  generators without voltage regulators.

and thus the unbalanced current will be



$$I_{qk} = I_k - \frac{I_c}{n} = \frac{U_k}{R_k} - \frac{U_0(nR_c + R_k)}{nR_k(R_c + R_0)}. \quad (7.53)$$

The nonuniformity of current distribution between the paralleled generators or the degree of overload on the overexcited generator may be found by using the overload coefficient, defined as the ratio

$$k_k = \frac{I_{qk}n}{I_c} = 1 + \frac{I_{qk}}{I_c}n = n \frac{R_c \Delta U_k + R_0 U_k}{R_k U_0}, \quad (7.54)$$

where

$$\Delta U_k = U_k - U_0.$$

Thus, proper load distribution occurs for equal voltages ( $U_k - U_0 = \Delta U_k = 0$ ) and equal resistances  $nR_c = R_k$ .

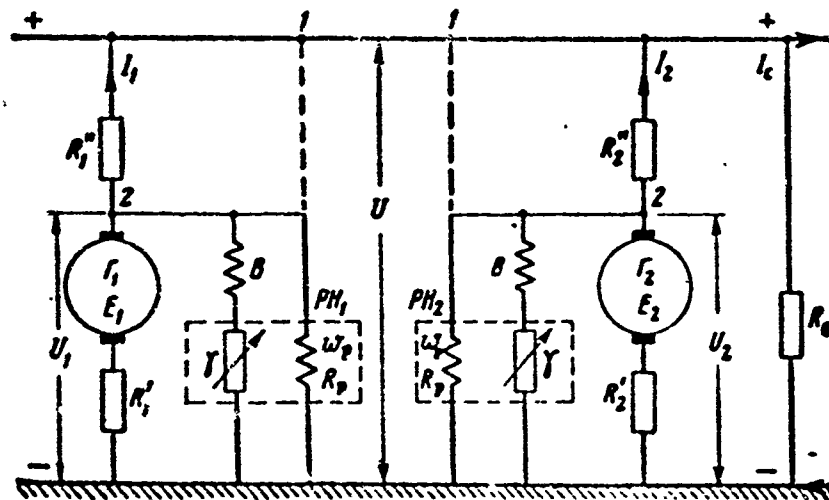


Fig. 7.23. Location of voltage regulators. V) Excitation winding;  $\gamma$ ) variable resistance of regulator in excitation-winding circuit; RN) voltage regulator;  $w_p$ ) regulator working winding;  $R_p$ ) resistance of regulator working winding.

For the special case in which  $R_1 = R_2 = \dots = R_n = R$ , Expressions (7.48)-(7.53) will be simplified:

$$R_0 = \frac{R}{n}; \quad (7.55)$$

$$U_0 = \frac{1}{n} \sum_1^n U_k; \quad (7.56)$$

$$U = \frac{R_c}{R + nR_c} \sum_1^n U_k; \quad (7.57)$$

$$I_c = \frac{1}{R + nR_c} \sum_1^n U_k; \quad (7.58)$$

$$I_k = \frac{(nU_k - \sum_1^n U_k) R_c + U_k R}{R(R + nR_c)}; \quad (7.59)$$

$$I_{\Sigma} = \frac{nU_k - \sum_1^n U_k}{nR} = \frac{U_k - \frac{1}{n} \sum_1^n U_k}{R}; \quad (7.60)$$

$$k_0 = n \frac{R_c (nU_k - \sum_1^n U_k) + RU_k}{R \sum_1^n U_k}. \quad (7.61)$$

Analysis of (7.52) shows that the expression

$$\frac{U_k}{U_0} = \frac{R_c}{R_c + R_0} \quad (7.62)$$

corresponds to no load on the  $k$ th machine ( $I_k = 0$ ) and, consequently, it will go over to motor operation when

$$\frac{U_k}{U_0} < \frac{R_c}{R_c + R_0}$$

and to generator operation when

$$\frac{U_k}{U_0} > \frac{R_c}{R_c + R_0}.$$

If we assume the load resistance to be constant ( $R_0 = \text{const}$ ), then, as follows from (7.53), the division of current (load) among the generators will depend on the excitation of the generators, allowing for the armature reactions, i.e., the distribution will depend on the values

$$U_1, U_2, \dots, U_k, \dots, U_n.$$

With variation in the machine excitation  $U_k$ , the generator currents and line voltage will also vary, as we can see from (7.50) and (7.52). If we want to maintain the line voltage  $U$  constant, in distributing the loads, it is necessary to vary the generator excitation so as to keep the numerator of (7.50) constant, i.e.,

$$U_0 = R_c \sum_1^n \frac{U_k}{R_k} = \text{const.}$$

With a uniform division of current among the paralleled genera-

tors, the unbalanced current  $I_q = 0$  and the relative overload factor  $k_p = 1$ . In this case, we find from (7.53) and (7.54) the necessary condition for uniform load distribution; it takes the form

$$\frac{U_k}{U_e} = \frac{R_k + nR_e}{n(R_e + R_k)}. \quad (7.63)$$

When  $R_e = R/n$  this means that  $U_k = U_e = 1/n \sum_1^n U_k$ .

#### Parallel Operation of Generators with Voltage Regulators

In order to maintain the voltage constant under variations in load, speed, and temperature, aircraft generators are provided with voltage regulators. Consequently, parallel operation occurs under artificial external-characteristic conditions. Below we shall consider problems of voltage-regulator location, equalizing-winding function, and load distribution among paralleled generators.

Location of voltage regulators. Regulators may be connected either to generator collecting busses [at points 1 (Fig. 7.23)] or directly across generator terminals [points 2 (Fig. 7.23)].

The following expressions hold for the first case:

$$\left. \begin{aligned} I_e = I_1 + I_2 &= \frac{U}{R_e} = \frac{U_1 - U}{R_1} + \frac{U_2 - U}{R_2}, \\ \frac{I_1}{I_2} &= \frac{U_1 - U}{U_2 - U} \frac{R_2}{R_1}, \\ \text{and} \quad \frac{U_1}{R_1} + \frac{U_2}{R_2} &= U \left( \frac{1}{R_e} + \frac{1}{R_1} + \frac{1}{R_2} \right), \end{aligned} \right\} \quad (7.64)$$

where  $U$  is the bus voltage;  $U_1$  and  $U_2$  are the generator-terminal voltages;  $R_1$  and  $R_2$  are the resistances from the generator pole to the bus;  $R_e$  is the load resistance.

It follows from (7.64) that the distribution of the common load  $I_g$  depends on  $U_1$  and  $U_2$  when  $U = \text{const}$ ,  $R_1$  and  $R_2 = \text{const}$ .

For the load to be distributed evenly, it is necessary for  $U_1 = U_2$  when  $R_1 = R_2$ . The regulators are connected to the collecting

busses, however, and, consequently, they react to the voltage deviation at the busses and act so as to keep  $U = \text{const}$ . Thus, when  $U = \text{const}$ ,  $R_g$ ,  $R''_1$ , and  $R''_2 = \text{const}$ , we will have the inequality  $U_1 \neq U_2$  and the equation  $U_1 R''_2 = U_2 R''_1 = \text{const}$  will hold, i.e., the load will be distributed arbitrarily, since the last equation is satisfied by any values of  $U_1$  and  $U_2$ .

In the second case, where the regulators are connected to the generator terminals, the current ratio will equal

$$\frac{I_1}{I_2} = \frac{U_1 - U}{U_2 - U} \frac{R''_2}{R''_1} = \frac{R''_2 I_c + \Delta U}{R''_1 I_c - \Delta U} \quad (7.65)$$

where

$$\Delta U = U_1 - U_2$$

and

$$U = U_1 - (I_c - I_2) R''_1 = \frac{R''_1 U_2 + R''_2 U_1 - R''_1 R''_2 I_c}{R''_1 + R''_2}.$$

Since in the case given the regulators hold the voltages  $U_1$  and  $U_2$  constant, when the values of  $I_g$ ,  $R''_1$ , and  $R''_2$  remain unchanged, the ratio of the currents will have a quite definite value.

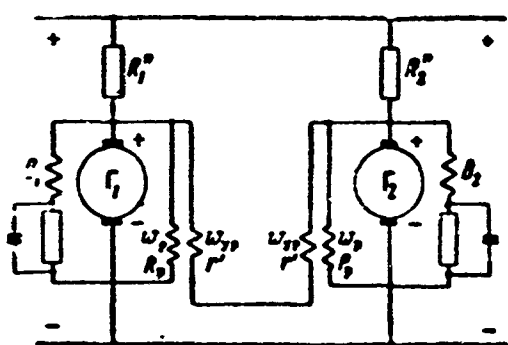


Fig. 7.24. Basic circuit for parallel operation of two generators using vibrator-type voltage regulators.

For a uniform current distribution, i.e.,  $I_1 = I_2 = 0.5 I_g$ , it is necessary to ensure that the equations  $R''_1 = R''_2 = R''$  and  $U_1 = U_2$  hold.

In this case

$$\frac{U}{U_1} = \frac{2R_c}{R'' + 2R_c} \quad (7.66)$$

It follows from (7.66) that when the load increases ( $R_g$  decreases) the line voltage will drop if  $U_1 = \text{const}$ . Consequently, for proper load distribution, the voltage regulators must be connected to the generator terminals and not to the collecting busses.

Function of equalizer winding. Equalizer windings are designed for automatic equalization of voltage in paralleled generators. They usually have a small number of turns  $w_{ur}$  and are located on the same electromagnet core of the regulator as the working winding.

The equalizer circuit, consisting of the equalizing windings ( $r'$ ) and connecting wires ( $r_0$ ) may be connected between the positive generator terminals (Fig. 7.24) or between the negative generator terminals (Fig. 7.25).

In the first case, the resistance between the positive generator terminal and the bus  $R''$  is used as a ballast resistance, and the required voltage drop is created across this resistance when the generator current flows.

In the second case, the special ballast resistor  $R'$  is connected into the negative side of the machine circuit.

The equalizer circuit is connected to the positive terminals in low-power generators using vibrator regulators and to the negative terminals in medium- and high-power generators using carbon or magnetic regulators.

In order to clarify the process of voltage equalization, let us consider parallel operation of two generators with the voltage regulators of Fig. 7.25 where  $E_1 > E_2$ .

For the case under consideration, with  $R'_1 = R'_2$  the potential at point  $a_2$  will be higher than the potential at  $a_1$ , since  $I_1 > I_2$  and the voltage drop across the ballast resistor  $R'_1$  will be greater than across  $R'_2$ . Since the voltage drops in the ballast resistances are not the same, a current  $I_{ur}$  will flow in the equalizing circuit. The magnetizing force due to the current flowing in the equalizing windings is added to the magnetizing force produced by the regulator working winding in the first generator and subtracted from the magnetizing

force produced by the working winding of the regulator in the second generator.

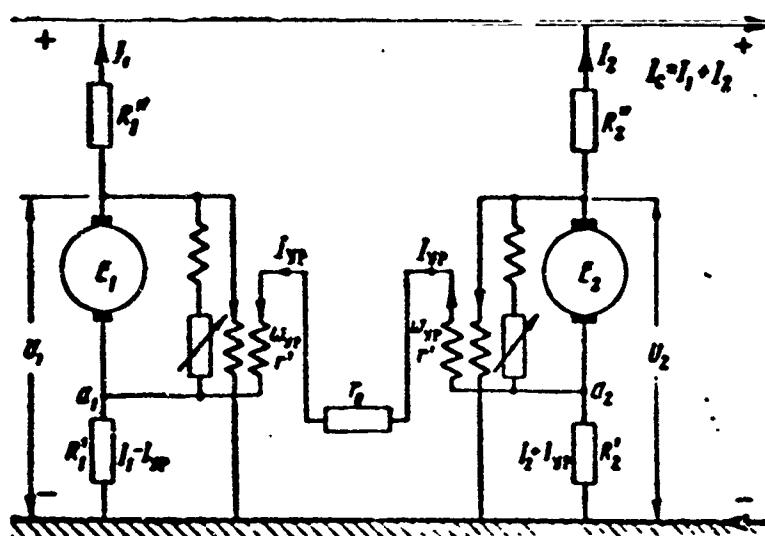


Fig. 7.25. Basic circuit for parallel operation of two generators with carbon voltage regulators.

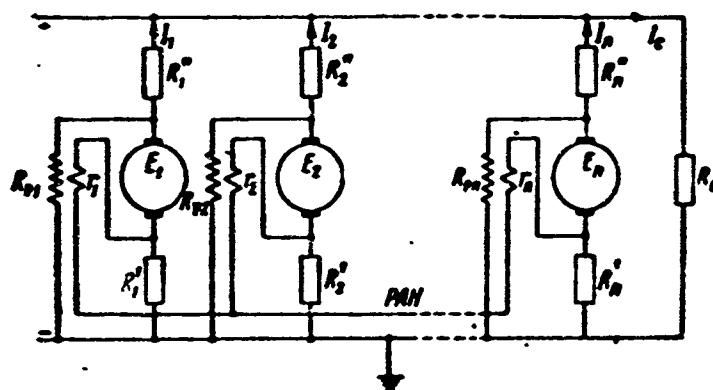


Fig. 7.26. Basic circuit for parallel operation of  $n$  identical direct-current generators provided with voltage regulators.

As a result, the voltage of the first generator drops while the voltage of the second generator rises. Thus, the currents flowing in the equalizing connections act to balance the generator voltages.

The magnetizing forces due to the regulator-electromagnet windings for the overexcited and underexcited generators may be represented by the following expressions:

$$\left. \begin{aligned} F_{p1} &= \frac{E_1}{R_p} w_p = \frac{U_1}{R_p} w_p + I_{yp} w_{yp} \\ F_{p2} &= \frac{E_2}{R_p} w_p = \frac{U_2}{R_p} w_p - I_{yp} w_{yp} \end{aligned} \right\} \quad (7.67)$$

where  $w_p$  and  $R_p$  are the number of turns and resistance of the electromagnet windings of the voltage regulators;  $w_{ur}$  and  $I_{ur}$  are the number of turns and current for the equalizing winding;  $U_1$  and  $U_2$  are the voltages at the generator terminal with the equalizing circuit connected and a load current  $I_s = I_1 + I_2$ ;  $E_1$  and  $E_2$  are the voltages at the generator terminals under no-load conditions with the equalizing circuit disconnected.

Where the generator parameters are identical, we find from (7.67) that

$$U_1 = E_1 - r_r I_n$$

and

$$U_2 = E_2 + r_r I_n$$

where  $r_r = R_p (w_{ur}/w_p)$  is the reduced resistance for the regulator working winding.

In this case, the current in the equalizing circuit will be

$$I_n = \frac{I_1 R_1' - I_2 R_2'}{R_1' + R_2' + 2r}, \quad (7.68)$$

where  $2r = 2r' + r_0$  is the total resistance in the equalizing circuit.

Load distribution. The presence of the voltage regulators and equalizing circuits complicates the solution of the problem at hand.

On the basis of the loop-current method, we may write  $2n$  equations for the circuit of Fig. 7.26 giving the generator currents  $I$  and the equalizer-circuit current  $I_{ur}$  in the form

$$\begin{aligned} (E_1 - r_{p1} I_{yp1}) - R_1' I_1 - R_1' (I_1 - I_{yp1}) = \\ = (E_2 - r_{p2} I_{yp2}) - R_2' I_2 - R_2' (I_2 - I_{yp2}) \end{aligned} \quad (7.69)$$

or

$$\left. \begin{aligned} I_{yp1}(r_{p1} - K_1) - I_{ypk}(r_{pk} - K_k) + I_1 R_1 - I_k R_k &= E_1 - E_k = \Delta E_{1k}, \\ (k=2+n) \\ I_{yp1}(r_1 + R_1) - I_{ypk}(r_k + R_k) - I_1 R_1 + I_k R_k &= 0, \\ (k=2+n), \end{aligned} \right\} \quad (7.70)$$

where  $R_1 = R''_1 + R'_1$  and  $R_k = R''_k + R'_k$  are the total resistances (in the positive and negative sections) for the circuits of the first and kth generators.

The current in the equalizing circuit and the current in the kth generator are determined from the expressions

$$\text{and} \quad \left. \begin{aligned} I_{ypk} &= \frac{D_k}{D} \\ I_k &= \frac{D_{n+k}}{D}, \end{aligned} \right\} \quad (7.71)$$

where  $D$  is the determinant of System (7.70);  $D_k$  is a determinant of order  $2n$  obtained by substituting the column for the right sides of the equations for the coefficients of the kth column of determinant  $D$ ;  $D_{n+k}$  is a determinant obtained by substituting the column for the right sides of the equations for the coefficients of the  $(n+k)$ th column in determinant  $D$ .

The unbalanced current in the kth generator due to the remaining  $(n-1)$  generators, in view of the fact that  $I_s = \sum_{k=1}^n I_k$ , will be

$$I_{u_k} = I_k - \frac{I_s}{n} = \frac{D_{n+k}}{D} - \frac{1}{nD} \sum_{k=1}^n D_{n+k} \quad (7.72)$$

Using (7.71) and (7.72), we can obtain the load distribution among n paralleled generators in general form, i.e., for any system mismatch conditions.

Of practical interest, however, is the special case in which the no-load voltages of all generators, except for one, are equal, i.e.,

$$E_1 \cong E_2 = E_3 = \dots = E_n = E.$$

If for the sake of simplifying the analysis of the last case we



assume that for "plus" resistances

$$R_1' \neq R_2' = R_3' = \dots = R_n' = R',$$

for "minus" resistances

$$R_1' \neq R_2' = R_3' = \dots = R_n' = R',$$

for the total resistances

$$R_1 \neq R_2 = R_3 = \dots = R_n = R,$$

for the equalizing-winding resistances

$$r_1' = r_2' = \dots = r_n' = r'$$

and for the reduced resistances of the regulator working winding

$$r_{p1} = r_{p2} = \dots = r_{pn} = r_p$$

the problem will then reduce to parallel operation of two generators of different power (Fig. 7.27).

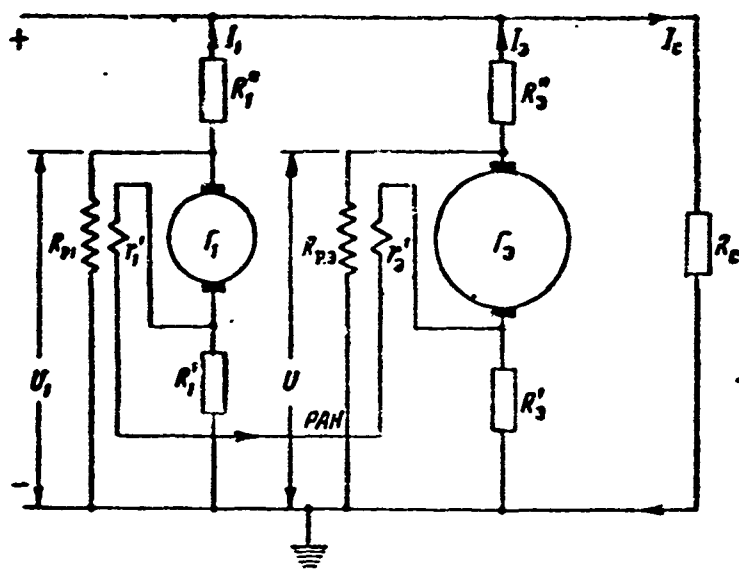


Fig. 7.27. Basic circuit for parallel operation of two generators of different power.

In this case, one generator  $G_1$  has a power  $P_1$ , a voltage  $E_1$ , a current  $I_1$ , and resistances  $R''_1$ ,  $R'_1$ ,  $R$ ,  $r'_1 = r'$ , and  $r_{r1} = r_r = R_r(w_{ur}/w_r)$ ; the other, equivalent generator  $G_e$  has a power corresponding to those of the  $(n - 1)$  generators of the system, and is characterized by the fact that for this machine all system resistances are decreased by a factor of  $(n - 1)$  while the current rises by a factor

of  $(n - 1)$ .

Thus, for the equivalent generator the following relationships hold:

the current in the equivalent generator is

$$I_s = (n-1)I;$$

the resistances of the equivalent generator are

$$R_s = \frac{R}{n-1}, \quad K_s = \frac{R''}{n-1}, \quad R'_s = \frac{R'}{n-1};$$

the resistances of the equivalent regulator working winding are

$$R_{p,s} = \frac{R_p}{n-1}, \quad r_{p,s} = R_{p,s} \frac{w_{yp}}{w_p} = \frac{R_p}{n-1} \frac{w_{yp}}{w_p} = \frac{r_p}{n-1}$$

while the resistance of the equivalent equalizing winding is

$$r'_s = \frac{r'}{n-1}.$$

The regulator voltage adjustment equations, which characterize the load distribution, will then be

$$U_1 = E_1 - r_p I_{yp} \text{ and } U_s = E_s + r_p I_{yp} \quad (7.73)$$

where  $U_e$  and  $E_e$  are the equivalent-generator voltages under load and at no load.

Considering the assumptions made, we obtain on the basis of (7.70) the following system of equations:

$$\left. \begin{aligned} I_{yp1}(n-1)(r_p - R'_s) + I_{yp1}(r_p - R') + \\ + I_1(n-1)R_1 - (I_e - I_1)R = (n-1)\Delta E, \\ I_{yp1}(n-1)(r' + R'_s) + I_{yp1}(r' + R') - \\ - I_1(n-1)K_1 + (I_e - I_1)R' = 0, \end{aligned} \right\} \quad (7.74)$$

where we take into account the fact that  $I_{ur1} = -\sum_2^n I_{urk}$  and  $I_s - I_1 = \sum_2^n I_k$ .

Making use of the equivalent-generator parameters in accordance with the notation of Fig. 7.27, we may represent (7.74) as follows:

$$I_{yp1}(nr_{p,s} - R'_s - R'_s) + I_1(R_1 + R_s) - I_e R_s = \Delta E,$$

$$I_{yp1}(nr'_s + R'_1 + R'_s) - I_1(R'_1 + R'_s) + I_c R'_s = 0.$$

Solving the last equation for  $I_{ur1}$  and  $I_1$ , we obtain, following simple manipulations,

$$\left. \begin{aligned} I_{yp1} &= \frac{\rho(R'_1 + R'_s)}{n(r_{ps} + r_s)} \frac{\Delta E + I_c(R'_s - R'_1)}{\rho(R'_1 + R'_s) + R'_1 + R'_s} \\ I_1 &= \frac{\Delta E + I_c(\rho R'_s + R'_s)}{\rho(R'_1 + R'_s) + R'_1 + R'_s} \end{aligned} \right\} \quad (7.75)$$

where

$$\varepsilon = \frac{n(r_{ps} + r'_s)}{nr'_s + R'_1 + R'_s} = \frac{n(r_p + r')}{nr' + R'_1(n-1) + R'}.$$

Finally, the current unbalance for generator  $G_1$ , equaling

$$\begin{aligned} I_{q1} &= I_1 - (I_c/n) = -I_{q0}, \text{ will be} \\ I_{q1} &= \frac{\Delta E - \frac{I_c}{n}(\rho \Delta R' + \Delta R'')}{\rho(R'_1 + R'_s) + R'_1 + R'_s}. \end{aligned} \quad (7.76)$$

If we assume that  $R''_1 = R''_2 = \dots = R''_n = R''$  and  $R'_1 = R'_2 = \dots = R'_n = R'$ , then  $\Delta R'' = R''_1 - R'' = 0$ ,  $\Delta R' = R'_1 - R' = 0$ , and

$$I_{q1} = \frac{\Delta E}{nR''} \frac{n-1}{1 + \frac{R' r_p + r'}{R' R' + r'}}. \quad (7.77)$$

It follows from this last expression that the greater the number of paralleled generators, the greater the current unbalance (all other conditions being equal).

Consequently, the greater the number of paralleled generators, the more accurate the voltage-regulator adjustments must be (the smaller the value of  $\Delta E$ ) for  $I_{q1}$  not to exceed the permissible value.

The resistances  $R''$  and  $R'$  may be neglected in comparison with  $r'$ , since, as a rule,  $r' \gg R''$  and  $R'$ .

In addition, we may assume that

$$R'_1 + R'_s \approx nR'_1/(n-1), \quad k_1 + k_s \approx \frac{nR'_1}{n-1}, \quad \frac{\Delta R'}{R'} = \frac{\Delta R''}{R''}$$

and

$$\frac{\Delta R' + \Delta R''}{R_1} \approx \frac{\Delta R'}{\bar{R}_1},$$

and then Expression (7.76) will be simplified, taking the form

$$I_{q1} \approx \frac{n-1}{n I_1} \left( \frac{\Delta E}{R_1} - \frac{I_c}{n} \frac{\Delta R'}{R_1} \gamma_1 \right), \quad (7.78)$$

where

$$\gamma_1 = 1 + \frac{R_1'}{R_1} \frac{r_p}{r'} \approx 1 + 0.4 \frac{r_p}{r'}.$$

The degree to which the overexcited generator is overloaded, in normal operation, may be found from the relative-overload factor

$$k_n = \frac{I_{c, \text{nom}} + n I_q}{I_{c, \text{nom}}} = 1 + n \frac{I_q}{I_{c, \text{nom}}},$$

whence for an arbitrary line load  $I_s$

$$k_n = i_c + \frac{n-1}{\gamma_1} \left( \frac{\Delta E}{R_1} - \frac{I_c}{n} \frac{\Delta R'}{R_1} \gamma_1 \right) \frac{1}{I_{c, \text{nom}}}, \quad (7.79)$$

where

$$i_c = \frac{I_c}{I_{c, \text{nom}}}.$$

By using (7.79) it is possible to establish the relative permissible voltage unbalance ( $\Delta E/U_{\text{nom}}$ ) and the relative permissible resistance unbalance ( $\Delta R''/R''$  and  $\Delta R'/R'$ ) on the basis of the given generator relative overload factor.

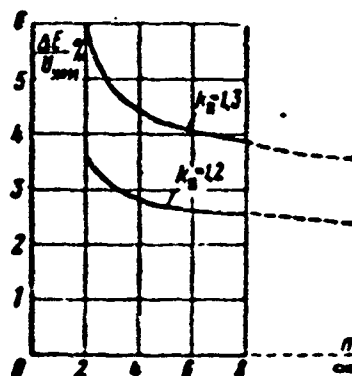


Fig. 7.28. Percent voltage mismatch as a function of number of paralleled generators and generator overload coefficient.

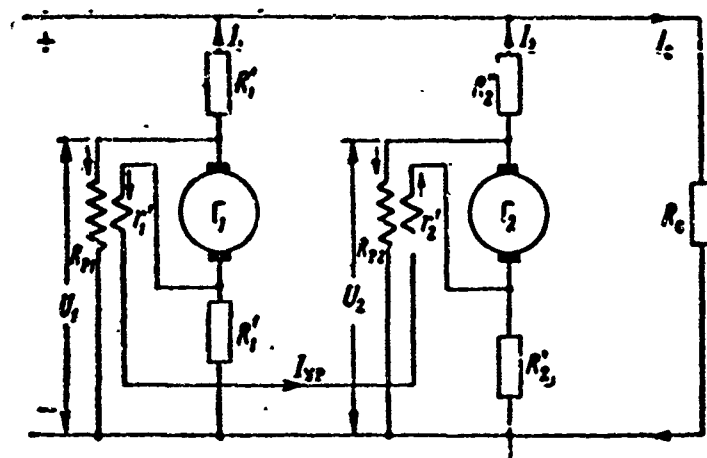


Fig. 7.29. Basic circuit for parallel operation of two generators of identical power.

The relative voltage unbalance may be represented as

$$\frac{\Delta E}{U_{\text{nom}}} = \frac{R_1 I_{\text{nom}}}{U_{\text{nom}}} \gamma_1 \left[ (k_z - \dot{I}_c) \frac{n}{n-1} + \dot{I}_c \frac{\Delta R'}{R_1'} \right], \quad (7.80)$$

where  $U_{\text{nom}}$  and  $I_{\text{nom}}$  are the rated voltages and currents for the generator.

Figure 7.28 shows the functions

$$\frac{\Delta E}{U_{\text{nom}}} = f(n)$$

when

$$\frac{R_1''}{R'} = \frac{R_1'}{R'} = 0.9$$

(corresponding to  $\Delta R''/R'' = \Delta R'/R' = -0.1$ ) and  $I_{\text{nom}} R_1/U_{\text{nom}} = 0.048$ ; the curves show that the larger the number of paralleled generators, the more accurately the voltage regulators must work for a given degree of overload ( $k_p$ ).

For the other special case of two paralleled generators of identical power (Fig. 7.29), we use Expressions (7.75) and (7.76), making the substitutions  $n = 2$ ,  $R''_e = R''_2$ ,  $R'_e = R'_2$ ,  $r'_e = r'$ , and  $r_{r.e} = r_r$ , and find that

$$\left. \begin{aligned} I_0 &= \frac{\Delta E - 0.5I_c(\rho \Delta R' + \Delta R'')}{\rho(R_1' + R_2') + R_1 + R_2} \\ I_1 &= \frac{k}{2} + I_0 \\ I_2 &= 0.5I_c - I_0 \end{aligned} \right\} \quad (7.81)$$

and

where

$$\rho = 2 \frac{r' + r''}{2r' + R_1' + R_2'}.$$

As (7.81) shows clearly, uniform distribution of a load among paralleled generators can occur only when  $I_0 = 0$ , which takes place when

$$\Delta E = 0, \Delta R' = R_1' - R_2' = 0 \text{ and } \Delta R'' = R_1'' - R_2'' = 0.$$

Thus, the proper division of current among paralleled generators may be upset when any of the following are out of balance: the regulator adjustment voltages, the resistances of the "plus" sections of the generator circuits, or the ballast ("minus") resistances.

Inequality of regulator adjustment voltages will cause a potential difference  $\Delta E$  to appear between generators; this difference will be maintained by the regulators. The result will be: in accurate regulator adjustment, voltage fluctuations that will be tolerated by the regulators, divergence in regulator characteristics, deterioration of regulator adjustment during service, and poor temperature compensation.

Differences in generator-circuit pole resistances ( $\Delta R \neq 0$ ) can occur owing to: manufacturing tolerances or elements forming the plus-section resistance (relay windings, measuring instruments, connecting wires); unequal contact resistances; nonuniform impairment of contact condition during operation; and cooling conditions that differ. Unbalanced currents appear as a result of this lack of equality.

The effect of contact resistances is large, since the "plus" re-

distances are measured in thousandths of an ohm.

Differences in ballast resistances ( $\Delta R' \neq 0$ ) appear for the same reasons as differences in the plus resistances.

Let us investigate the factors that disturb parallel operation of two generators of identical power.

1. Effect of regulator adjustment voltage unbalance. Let us assume that  $E_1 > E_2$  with  $R''_1 = R''_2 = R''$  and  $R'_1 = R'_2 = R'$ , i.e.,  $\Delta R'' = 0$ ,  $\Delta R' = 0$ ; we can then find the unbalanced current in the form

$$I_{q1} = -I_{q2} = \frac{\Delta E}{2R'' \left(1 + \frac{R'}{R''} \frac{r_p + r'}{r' + R'}\right)}. \quad (7.82)$$

Thus, the unbalanced current depends solely on the regulator adjustment-voltage inequality, and does not depend on the load current. This also occurs under no-load conditions, where one generator operates as a motor with a current  $I_q$  while the other generator supplies the first machine.

If we open the equalizing circuit,

$$I_{q0} = \frac{\Delta E}{2R''}. \quad (7.83)$$

As a rule,  $R''$  is so chosen that the voltage drop across it with rated current does not exceed some definite percent  $\xi$  of the nominal voltage, i.e.,

$$R'' I_{nom} = \xi U_{nom} \text{ and } R'' = \xi \frac{U_{nom}}{I_{nom}}.$$

Thus, in the absence of an equalizing circuit

$$I_{q0} = \frac{0.5}{\xi} \frac{\Delta E}{U_{nom}} I_{nom},$$

while if we assume that  $\Delta E = 0.02 U_{nom}$  and  $\xi = 0.02$ , then  $I_{q0} = 0.5 I_{nom}$  and the current difference  $I_{10} - I_{20} = 2 I_{q0} = I_{nom}$ , i.e., the unbalance-current ratio

$$\frac{I_{q0}}{I_q} = 1 + \frac{R'}{R''} \frac{r_p + r'}{r' + R'} > 1.$$

shows that the equalizer circuit reduces the unbalanced current and, consequently, equalizes the voltages and currents for paralleled generators.

2. Effect of inequality of resistances of cross sections. Let us assume that  $\Delta E = 0$ ,  $R'_1 = R'_2 = R'$ , and  $R''_1 \neq R''_2$ . In this case,  $\Delta R' = 0$ ,  $\Delta R'' \neq 0$  and the unbalanced current

$$I_q = -\frac{I_c}{2(R'_1 + R'_2)} \frac{\Delta R''}{1 + \frac{2R'}{R'_1 + R'_2} \frac{r_p + r'}{R' + r'}} \quad (7.84)$$

is a linear function of load current.

If we disconnect the equalizing circuit, then

$$I_{q0} = -I_c \frac{\Delta R''}{2(R'_1 + R'_2)} \quad (7.85)$$

with  $R''_1 + R''_2 \approx 2\xi(I_{\text{nom}}/U_{\text{nom}})$ , we find that

$$I_{q0} \approx -\frac{I_c}{4\xi} \frac{I_{\text{nom}} \Delta R''}{U_{\text{nom}}}$$

Assuming that  $I_{\text{nom}} \Delta R''/U_{\text{nom}} = 0.01$  and  $\xi = 0.02$ , we find that

$$I_{q0} \approx -0.125 I_s.$$

The unbalance-current ratio

$$\frac{I_{q0}}{I_q} = 1 + \frac{2R'}{R'_1 + R'_2} \frac{r_p + r'}{R' + r'} \quad (7.86)$$

shows that the equalizing circuit decreases the unbalanced current in this case as well.

The load-current ratios in the absence and in the presence of the equalizing circuit equal, respectively,

$$\left. \begin{aligned} \frac{I_{10}}{I_{20}} &= \frac{0.5I_c + I_{q0}}{0.5I_c - I_{q0}} = \frac{R'_2}{R'_1}, \\ \frac{I_1}{I_2} &= \frac{0.5I_c + I_q}{0.5I_c - I_q} = \frac{R'_2}{R'_1} \end{aligned} \right\} \quad (7.87)$$

where, when  $R''_2/R''_1 > 1$ ,



$$\bar{\gamma} = \frac{1 + \frac{R'}{R_2} \frac{r_D + r'}{R' + r'}}{1 + \frac{R'}{R_1} \frac{r_D + r'}{R' + r'}} < 1.$$

It follows from (7.87) that in the absence of the equalizing circuit, the generator loads will be distributed in inverse proportion to the distances of the positive generator-circuit sections, while when the equalizer circuit is present, the load distribution depends less on the ratio  $R''_2/R''_1$ .

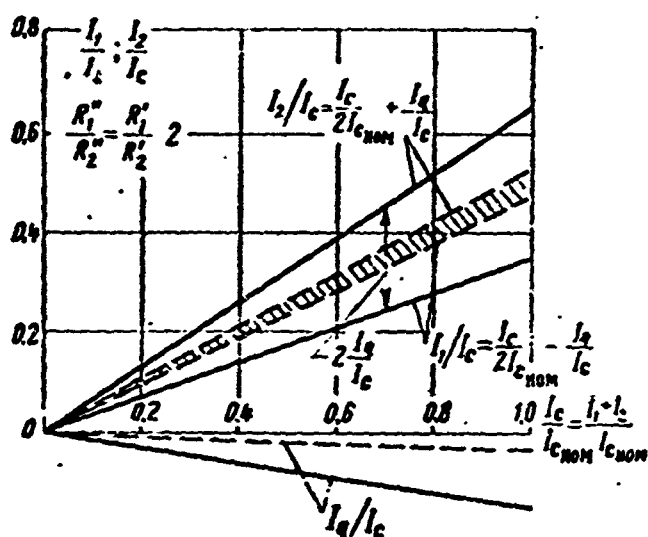


Fig. 7.30. Distribution of current between two paralleled generators of identical power as a function of load. a) Solid lines  $R''_1 = R''_2$  and  $R'_1/R'_2 = 2$ ; b) broken lines  $R'_1 = R'_2$  and  $R''_1/R''_2 = 2$ .

The last statement is a consequence of the fact that the current in the equalizing circuit decreases the voltage at the loaded generator and increases the voltage at the underloaded generator.

Thus, lack of equality between the resistances of the positive generator-circuit sections has little effect on load distribution.

3. Effect of unequal ballast resistances. Let us assume that  $\Delta E = 0$ ,  $R''_1 = R''_2$ , and  $R'_1 \neq R'_2$ . In this case,  $\Delta R'' = R''_1 - R'' = 0$ , and  $\Delta R' = R'_1 - R'_2 \neq 0$ , and the unbalanced current

$$[I]_q = -\frac{I_c}{2(R'_1 + R'_2)} \frac{\Delta R''}{1 + \frac{R''}{R'_1 + R'_2} \frac{2r' + R'_1 + R'_2}{r_p + r'}} \quad (7.88)$$

is a linear function of load current.

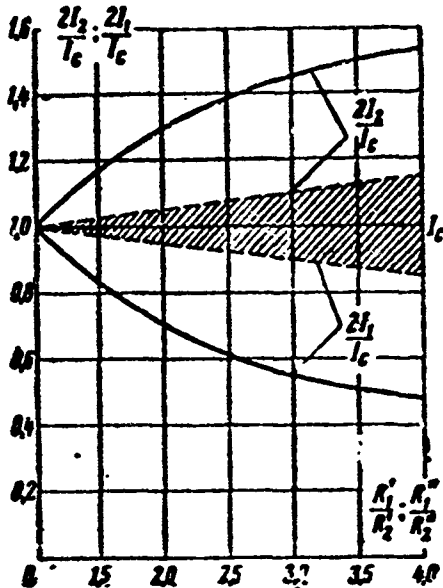


Fig. 7.31. Distribution of constant rated load ( $I_s = \text{const}$ ) between two paralleled generators of identical power as a function of ballast-resistance ratio  $R'_1/R'_2$  (solid lines) and "plus" resistance ratio  $R''_1/R''_2$  (dashed lines).

As we can see by comparing (7.84) and (7.88), when  $\Delta R' = \Delta R''$ , the unbalanced currents will not be equal,  $I''_q < I'_q$ , since  $\frac{r_p + r'}{R' + r'} > \frac{r' + 0.5(R'_1 + R'_2)}{r_p + r'}$ , i.e., ballast (minus) resistance unbalance has a greater influence on load-current distribution than "plus" resistance unbalance.

The load-current ratio is

$$\frac{I_1}{I_2} = \frac{I_c + 2I'_q}{I_c - 2I'_q} = \frac{R'_2}{R'_1} \tau, \quad (7.89)$$

where when  $R'_2/R'_1 > 1$ , the ratio

$$\tau = \frac{1 + \frac{R''}{R'_2} \frac{r' + 0.5(R'_1 + R'_2)}{r_p + r'}}{1 + \frac{R''}{R'_1} \frac{r' + 0.5(R'_1 + R'_2)}{r_p + r'}} < 1.$$

In the absence of an equalizer circuit, ballast-resistance inequality will

have no effect on the load-current distribution, since  $I_{q0} = 0$ . At the same time, when an equalizing circuit is present and  $\Delta R' \neq 0$ , an unbalanced current will appear ( $I_q > 0$ ) and, consequently, in the presence of ballast-resistance unbalances, equalizing windings aggravate load-distribution nonuniformity.

In view of this, it is necessary to ensure precise equality of the ballast (minus) resistances.

Figure 7.30 and 7.31 show several curves in relative form, characterizing the distribution of current between two paralleled generators of identical power as a function of load (with the resistance ra-

tio unchanged) and of resistance ratio (with the load unchanged) when  $\Delta E = 0$ .

Manu-  
script  
Page  
No.

[List of Transliterated Symbols]

613	PH = RN = regulyator napryazheniya = voltage regulator
613	PM = RM = regulyator moshchnosti = power regulator
613	PAH = RAN = raspredeliteľ aktivnoy nagruzki = real-load distributor
613	PPH = RRN + raspredeliteľ reaktivnoy nagruzki = reactive-load distributor
613	$\Gamma$ = G = generator = generator
613	B = V = vozbuditel' = exciter
613	ITI = GP = gidroprivod = hydraulic drive mechanism
613	M = M = mufta = clutch
613	CMH = SIN = sinkhroniziruyushcheye ustroystvo = synchronizing unit
613	P = R = rele = relay
613	B = V = vyklyuchatel' = switch (with subscripts g and s)
613	r = g = generator = generator
613	c = s = set' = line
615	TT = TT = transformator toka = current transformer
615	TC = TS = transformator svyazi = coupling transformer
619	a = a = aktivnyy = active, real
619	p = r = reaktivnyy = reactive
622	uc = is = ispol'zovaniye = utilization
626	T = T = transformator = transformer
626	B = V = vypryamitel' = rectifier
627	AT = AT = avtotransformator = autotransformer
627	TI = TG = takhogenerator = tachometer generator

627 ЦВ = ТсВ = tsentrobezchnyy vyklyuchatel' = centrifugal switch  
 627 К = К = katushka = coil, winding  
 629 НОМ = ном = nominal'nyy = rated  
 633 И = и = ispol'zovaniye = utilization  
 634 УР = ур = uravnitel'nyy = equalizing  
 636 КП = КР = komandnyy pereklyuchatel' = command switch  
 636 К = К = kontaktor = contactor  
 636 СЛ = СЛ = signal'naya lampa = pilot light  
 636 РС = РС = rele sinkhronizatsii = synchronizing relay  
 636 ВМУ = ВМУ = vektornoye ustroystvo = vector-sensing device  
 637 ДС = ДС = differentsial'nyy sel'sin = differential selsyn  
 639 С.П = С.П = soyedinitel'nyy provod = connecting line  
 639 К = к = korotkogo zamykaniya = short-circuit  
 639 УД = уд = udarnyy = maximum-asymmetry  
 643 П = п = periodicheskiy = periodic  
 643 АП = ап = aperiodicheskiy = aperiodic  
 644 С = с = sinkhronnyy = synchronous  
 645 АС = ас = asinkhronnyy = asynchronous, induction  
 645 ДВ = дв = dvigatel' = mover, motor  
 645 ТР = тр = treniye = friction  
 645 ВР = вр = vrashchatel'nyy = rotational  
 645 Р = р = reaktivnyy = reactive  
 647 УСТ = уст = ustanovivshiysya = steady-state  
 651 ВГ = ВГ = возбуждениe генератора = generator excitation  
 651 ПВД = ПВД = postoyannoye возбуждениe двигателя = constant  
 651 УВД = УВД = upravlyayemoye возбуждениe двигателя = controlled motor excitation  
 651 РР = рег = regulyator = regulator

651         $\delta = b = \text{ballastnyy} = \text{ballast}$   
 652         $\hat{0} = v = \text{volts}$   
 654        CT = ST = sinkhroniziruyushchiy transformator = synchroni-  
           zing transformer  
 654        BC = VS = vyklyuchatel' sinkhronizatsii = synchronization  
           switch  
 654        PC = RS = rele sinkhronizatsii = synchronization relay  
 654        OBP = OVR = obmotka возбуждения реле = relay synchroni-  
           zation winding  
 654        OBK = OVK = obmotka возбуждения контактора = contactor  
           excitation winding  
 655         $m = m = \text{magnitnyy} = \text{magnetic}$   
 657        PBB = RVV = rele s vyderzhkoy vremeni = time-delay relay  
 661         $\Pi = P = \text{preobrazovatel'} = \text{converter}$   
 661         $\text{14} = \text{cycles/sec}$   
 661        AИ = AD = aviatsionnyy dvigatel' = aircraft engine  
 661        KM = KM = kombinirovannaya mufta = combination coupling  
 661        B = V = возбуждение = excitation  
 661        ИАИ - ИАН = izmeritel' aktivnoy nagruzki = real-load meas-  
           uring device  
 661        ИРП = ИРН = izmeritel' reaktivnoy nagruzki = reactive-load  
           measuring device  
 661        PB = RV = regul'yator возбуждения = excitation regulator  
 661        PP = RR = regul'yator rezhima = control  
 667         $\mathfrak{z} = e = \text{ekvivalentnyy} = \text{equivalent}$   
 670         $n = p = \text{peregruzka} = \text{overload}$   
 676         $p = r = \text{rabochiy} = \text{working}$

## REFERENCES

1. Alekseyev, A.Ye., Konstruktsiya elektricheskikh mashin. [Design of Electric Machines], Gosenergoizdat, 1949.
2. Al'per, N.Ya., Generatory induktornogo tipa [Induction Generators], VEP [Herald of the Electrical Industry], 1957, No. 8.
3. Bertinov, A.I. and Rizink, G.A., Proyektirovaniye aviatsionnykh elektricheskikh mashin postoyannogo toka [Design of Direct-Current Aircraft Electric Machines, 1958.
4. Vinogradov, N.V., Tekhnologiya proizvodsta elektricheskikh mashin [Production Technology of Electric Machines], Gosenergoizdat, 1954.
5. Volotdin, V.P. and Spitsyn, M.L., Generatory vysokoy chastoty [High-Frequency Generators], ONTI [United Scientific and Technical Publishing Houses], 1935.
6. Yermolin, N.P., Raschet malomoshchnykh kollektornykh mashin [Design of Low-Power Commutator Machines], Gosenergoizdat, 1955.
7. Kanter, A.S., Postoyannyye magnity [Permanent Magnets], Gostekhizdat, 1938.
8. Kostenko, M.P., Elektricheskiye mashiny. Spetsial'naya chast' [Electric Machines. Special Section], Gosenergoizdat [State Publishing House of Literature on Power Engineering], 1949.
9. Kostenko, M.P. and Piotrovskiy, L.M., Elektricheskiye mashiny, chast' I [Electric Machines, Part I], Gosenergoizdat, 1957, Part II, Gosenergoizdat, 1958.
10. Kulebakin, V.S., Morozovskiy, V.T. and Sindeyev, I.M., Elek-

trosnabzheniye samoletov [Aircraft Electrical Equipment], Oborongiz, 1956.

11. Osnovy elektrooborudovaniya samoletov i avtomashin. Pod redaktsiyey A.N. Larianova [Fundamentals of Aircraft and Motor Vehicle Engines. Edited by A.N. Larionov], Gosenergoizdat, 1955.
12. Petrov, G.N., Elektricheskiye mashiny [Electrical Machines], part I, Gosenergoizdat, 1956, part II, Gosenergoizdat, 1947 [sic].
13. Postnikov, I.M., Proyektirovaniye elektricheskikh mashin [Design of Electrical Machines], DTVU [unlisted], 1952.
14. Proyektirovaniye elektricheskikh mashin. Pod redaktsiyey P.S. Sergeyeva [Design of Electrical Machines. Edited by P.S. Sergeyev], Gosenergoizdat, 1956.
15. Soroker, T.G., O raschete sinkhronnykh mashin s postoyannymi magnitami [The Design of Synchronous Machines With Permanent Magnets], VEP [unlisted], 1940, No. 2.
16. Soroker, T.G., O rasseyanii postoyannykh magnetov [Dissipation of Permanent Magnets], Bulletin, VEI, 1940, No. 4.
17. Walker, J.H., High-Frequency Alternators, The Journal of the Institution of Electrical Engineers, 1946, No. 31, Vol. 93, part II.
18. Brainard, Maurice W., Synchronous Machines with Rotating Permanent-Magnet Fields, Transactions AIEE, August, 1952.
19. Scott, Dale H., Effects of Terminal Voltage, Load Current and Minimum Rotor Speed on the Weight of D.C. Aircraft Generators, Transactions AIEE, September, 1952.
20. Martin, Cecil G., Study of Aircraft Cooling Systems for Rotating Electric Equipment, Transactions AIEE, July, 1952.

# DISTRIBUTION LIST

DEPARTMENT OF DEFENSE	Nr. Copies	MAJOR AIR COMMANDS	Nr. Copies
		SAC	1
		AFSC	
		SCFDD	1
		DDC	20
		TDBTL	5
		TDBDP	2
		TDCS	1
HEADQUARTERS USAF		TDEPO (Smith)	1
		TDEWG (Kroggel)	1
AFCIN-3D2	1	AEDC (AEY)	1
ARL (ARB)	1	AFFTC (FTF)	1
		AFWL (WLF)	1
		ASD (ASFA)	2
		BSD (BSF)	1
		ESD (ESY)	1
		SSD (SSF)	2
OTHER AGENCIES			
CIA	1		
NSA	6		
DIA	4		
AID	2		
OTS	2		
AEC	2		
PWS	1		
NASA (ATSS-T)	1		
ARMY (FSTC)	3		
NAVY	3		
NAFEC	1		
RAND	1		
PGE	12		
SPECTRUM	1		